Zhaoqing Yang
Andrea Copping *Editors*

Marine Renewable Energy

Resource Characterization and Physical Effects

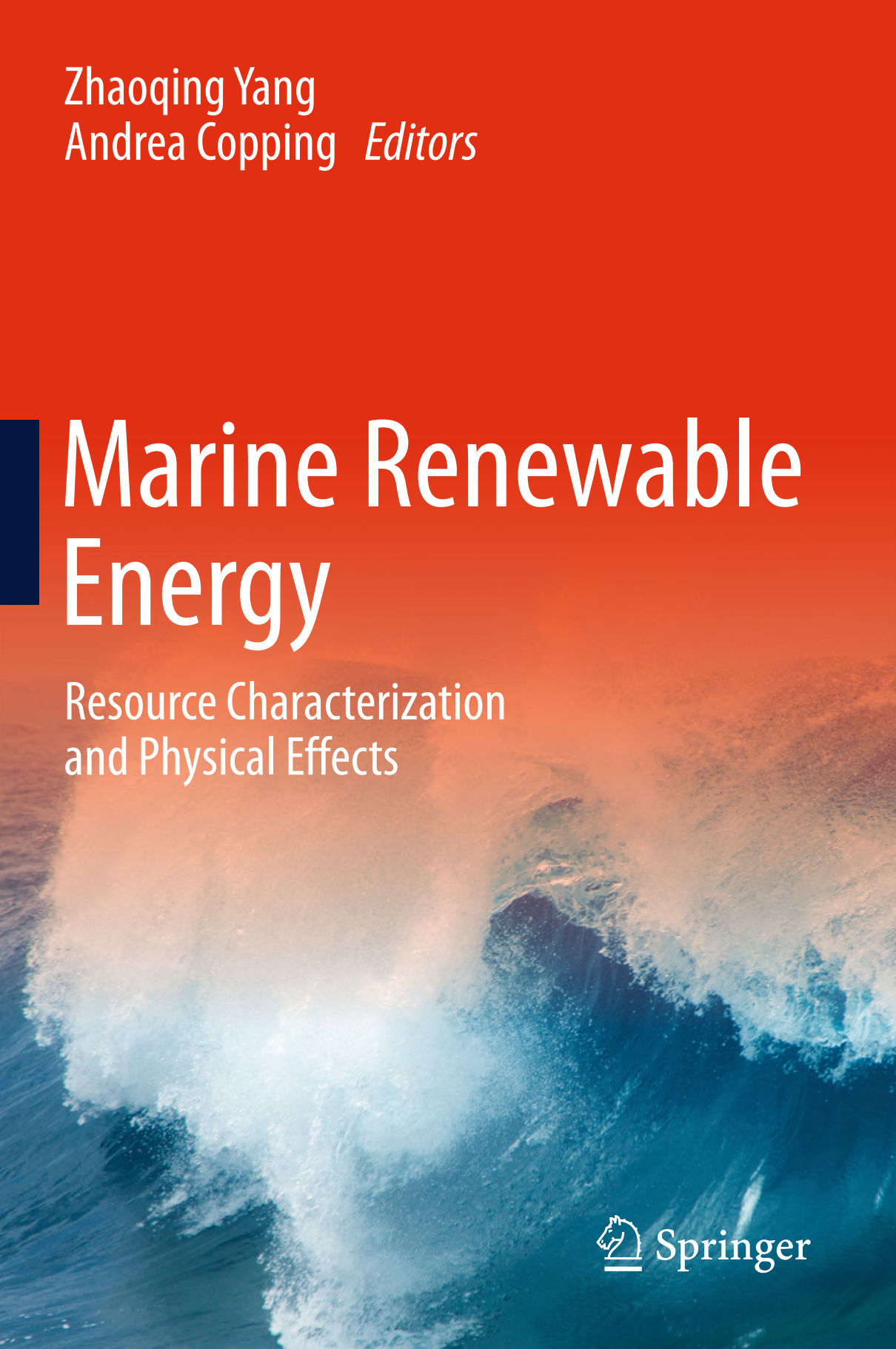

Springer

Marine Renewable Energy

Zhaoqing Yang · Andrea Copping
Editors

Marine Renewable Energy

Resource Characterization and Physical Effects

Springer

Editors
Zhaoqing Yang
Marine Sciences Laboratory, Pacific Northwest National Laboratory
Seattle, WA
USA

Andrea Copping
Marine Sciences Laboratory, Pacific Northwest National Laboratory
Seattle, WA
USA

ISBN 978-3-319-53534-0 ISBN 978-3-319-53536-4 (eBook)
DOI 10.1007/978-3-319-53536-4

Library of Congress Control Number: 2017932430

Printed on acid-free paper

This Springer imprint is published by Springer Nature
The registered company is Springer International Publishing AG
The registered company address is: Gewerbestrasse 11, 6330 Cham, Switzerland

Preface

Facing the Challenges of Resource Characterization and Physical System Effects of Marine Renewable Energy Development

Many nations have expanded their national energy portfolio to ameliorate the effects of climate change and to ensure the security and certainty of energy availability. These efforts have led to scrutiny of marine renewable energy (MRE) as one of several viable new renewable energy sources. In addition to the need to prove the reliability and efficiency of current and wave energy converters, effective siting and operation of MRE devices requires detailed and accurate characterization of the tidal stream, ocean current, and wave resource, as well as assessments of the potential risk to the physical marine environment from MRE development.

The desire to understand the many challenges to characterizing marine energy resources and the effects of energy extraction on physical systems motivated the compilation of the chapters in this book, which represent research and review efforts that address these two important topics. Chapters Wave Energy Assessments: Quantifying the Resource and Understanding the Uncertainty through Marine Hydrokinetic Energy in the Gulf Stream Off North Carolina: An Assessment Using Observations and Ocean Circulation Models address resource characterization of wave, tidal stream, and ocean current energy using laboratory experiments, field measurements, and numerical models. Chapters Effects of Tidal Stream Energy Extraction on Water Exchange and Transport Timescales through Planning and Management Frameworks for Renewable Ocean Energy cover topics related to the effects of energy extraction on physical systems, such as water exchange in coastal estuaries and bays, sediment transport, underwater noise, and marine spatial planning for MRE development.

In many parts of the world, harvesting wave energy seems very promising because of the very large potential resource located near many coastlines. Chapters Wave Energy Assessments: Quantifying the Resource and Understanding the Uncertainty through Analyses of Wave Scattering and Absorption Produced by WEC Arrays: Physical/Numerical Experiments and Model Assessment are devoted

to techniques and methodologies for wave resource characterization. In Chap. Wave Energy Assessments: Quantifying the Resource and Understanding the Uncertainty, Robertson provides an overview of wave resource characterization and assessment using field measurements and numerical modeling approaches. The popular state-of-the-art, third-generation, phase-average spectral wave models that are suitable for wave resource characterization are reviewed by model framework, physical processes, computational requirements, and their applications to wave resource assessment at global, regional, and local scales. Techniques and methodologies for conducting baseline and high-fidelity resource assessments are presented, and the challenges of predicting extreme sea states and the uncertainty associated with wave resource characterization are discussed. The International Electrotechnical Commission (IEC) Technical Specification (TS) for wave resource characterization is also described in the chapter. The six parameters recommended by the IEC for characterizing wave energy resources are described—omnidirectional wave power, significant wave height, energy period, spectral width, direction of maximum directionally resolved wave power, and the directionality coefficient.

The Atlantic coast of Europe has some of the highest wave power resources in the world. In Chap. Wave Energy Resources Along the European Atlantic coast, Gleizon et al. present a joint effort by several European countries, including the UK, Portugal, France, Spain, and Ireland, to estimate the potential wave energy resource along the European Atlantic coast. Long-term hindcasts with high-resolution spectral wave models can greatly improve the accuracy of wave resource characterization and reduce the uncertainty associated with those estimates. A unique numerical modeling approach used in their study combines the regional-scale spectral wave model WaveWatch III (WWIII) for the continental shelf with high-resolution and the unstructured-grid Simulating WAves Nearshore (SWAN) model for the nearshore regions. Specifically, wave resource characterization was conducted based on 7-year high-resolution spectral wave hindcasts at five distinct coastal regions: Scotland (UK), Ireland, France, Galicia (Spain), and Portugal. Spatial and temporal variabilities in the wave climate are discussed. This study provides detailed information about the wave resource along the European Atlantic coast to help identify optimal areas for pilot-scale tests and commercial-scale development of wave energy converters (WECs).

While phase-averaged spectral wave models are commonly used in wave resource characterization, laboratory experiments and phase-resolving models enable the investigation of the dynamic interactions between WEC arrays and wave fields. In Chap. Analyses of Wave Scattering and Absorption Produced by WEC Arrays: Physical/Numerical Experiments and Model Assessment, Ozkan-Haller et al. evaluate the wave scattering and absorption induced by WEC arrays through laboratory and numerical experiments. The experimental study described was carried out with 1:33-scale commercial WECs under different array configurations subject to a range of regular waves and random sea states. Numerical experiments were carried out with the phase-resolving model WAMIT and the phase-averaged SWAN model. Model validations were conducted using data collected from the laboratory study. Their study results suggest that the environmental effects of WEC

arrays can be minimized by designing WECs to operate optimally when the significant wave energy lies at periods near, or larger than, the period of peak energy extraction.

Chapters Hydrokinetic Tidal Energy Resource Assessments Using Numerical Models through Wave-Tide Interactions in Ocean Renewable Energy focus on tidal stream resource characterization and wave–tide interactions. Chapter Hydrokinetic Tidal Energy Resource Assessments Using Numerical Models by Haas et al. and Chap. Tidal Energy Resource Measurements by Thomson et al. present methodologies and techniques for tidal stream energy resource assessment and include case study examples from modeling and measurement perspectives, respectively. Both chapters discuss the importance of incorporating standards recommended by the IEC TS in the process of tidal energy resource characterization. These IEC standards include model grid resolution, bathymetric resolution, number of tidal constituents for the open boundary condition, measurement and simulation periods, and impacts of energy extraction.

In Chap. Hydrokinetic Tidal Energy Resource Assessments Using Numerical Models, Haas et al. provide clear definitions for theoretical, technical, and practical resources at different scales of resource assessment. Concepts and modeling approaches for tidal energy resource assessment at individual turbine, regional, and project scales are discussed in detail. Finally, model results from a case study in the Piscataqua River, located between the border of Maine and New Hampshire (USA), illustrate the processes of tidal resource assessment at turbine, project, and regional scales using the Regional Ocean Modeling System.

In Chap. Tidal Energy Resource Measurements, Thomson et al. address tidal energy assessments conducted using analytical and numerical models that should be complemented by information from field measurements, especially at large regional scales. High-quality field measurements can be used to characterize current spatial and temporal variations and site-specific tidal resource assessment, as well as to validate models that are used for tidal resource assessment at various scales. A full suite of parameters that can be obtained from field measurements, such as tidal harmonic constituents, turbulence spectra and intensity, current histograms, lateral shear and current asymmetry, power density, and annual energy production, are noted, and their application to resource assessment is described. In a case study in Admiralty Inlet of Puget Sound in Washington State (USA), the authors demonstrate that field measurements collected at high sampling frequencies and over long periods of time are required to resolve stochastic and deterministic components of tidal currents.

High wave and tidal energy resources may coexist in some coastal regions, such as the seas of the northwest European continental shelf, the Gulf of Alaska, New Zealand, northwest Australia, and the Atlantic seaboard of Argentina. In these coastal regions, wave–tide interaction may be an important factor in resource characterization. In Chap. Wave-Tide Interactions in Ocean Renewable Energy, Hashemi and Lewis evaluate the potential effects of wave–tide interactions on resource characterization using simple analytical methods and coupled wave–tidal modeling techniques. Their study shows that tidal stream energy resources may be

reduced due to wave–tide interactions under extreme wave conditions, and wave properties may be altered as a result of wave–tide interactions. The authors recommend that wave–tide interactions be considered in either wave or tidal stream resource assessment in regions where high wave and tidal energy exist.

Chapters Use of Global Satellite Altimeter and Drifter Data for Ocean Current Resource Characterization through Marine Hydrokinetic Energy in the Gulf Stream Off North Carolina: An Assessment Using Observations and Ocean Circulation Models address the current state of the science and research on ocean current energy. Unlike waves and tides, which propagate in a form of gravity waves, strong ocean currents are mainly generated by wind and the Coriolis force, which result in "western intensification," a phenomenon occurring along the western boundaries of large-scale open-ocean basins. In Chap. Use of Global Satellite Altimeter and Drifter Data for Ocean Current Resource Characterization, Tseng et al. examine the large-scale ocean current resource using long-term global satellite altimeter data and SVP drifter data. They quantify averaged surface velocities in the global oceans based on long-term data sets and evaluate long-term-averaged velocity maximums in the four strongest western boundary currents (WBCs): the Agulhas Current in the Indian Ocean, the Gulf Stream in the Atlantic Ocean, and the Mindanao Current and the Kuroshio Current in the Pacific Ocean. Specific locations of the velocity maximums for these four WBCs are identified, and the temporal variability influenced by monsoon winds and the El Niño Southern Oscillation are investigated. Further detailed analysis is conducted to evaluate potential sites for ocean current power generation in the North Pacific, South China Sea, and Oceania, based on a set of criteria including current speed and frequency, water depth, and distance from the shore.

Meyer et al. examine the potential for energy extraction from the Agulhas Current along South Africa's East Coast in Chap. Mapping the Ocean Current Strength and Persistence in the Agulhas to Inform Marine Energy Development using an integrated approach that combines state-of-the-art satellite remote sensing, predictive modeling, and in situ observation techniques. They evaluate two specific locations, one at mid-shelf and one at offshore, for potential ocean current power generation. Current spatial and temporal variability and power density at these two potential sites are analyzed. Meyer et al. show that data generated from these combined methodologies can provide useful insight into the unique challenges encountered in resource assessment for the Agulhas Current. Finally, considerations of the technical challenges for energy extraction from the Agulhas Current and potential environment impacts are discussed.

Chapters Ocean Current Energy Resource Assessment for the Gulf Stream System: The Florida Current and Marine Hydrokinetic Energy in the Gulf Stream Off North Carolina: An Assessment Using Observations and Ocean Circulation Models are two companion chapters about resource assessment in the Gulf Stream, each focusing on different geographic locations and different methodologies. In Chap. Ocean Current Energy Resource Assessment for the Gulf Stream System: The Florida Current, Haas et al. evaluate the theoretical resource in the Florida Current portion of the Gulf Stream System, based on idealized and realistic

numerical model simulations using the Hybrid Coordinate Ocean Model. Their study indicates that while the mean power in the Florida Current was found to be over 22 GW, extraction of only 5 GW of power from the Florida Current would require deployments of thousands of turbines under undisturbed flow assumption. In their study, Haas et al. demonstrate the importance of incorporating the additional dissipation due to the presence of turbines in model simulations for ocean current resource assessment, the result of which is a smaller level of technically extractable power.

In Chap. Marine Hydrokinetic Energy in the Gulf Stream Off North Carolina: An Assessment Using Observations and Ocean Circulation Models, Lowcher et al. assess the theoretical energy resource in the portion of Gulf Stream off the North Carolina Coast, based on a combination of observations and numerical model simulations. Current observation data were collected from moored and shipboard acoustic Doppler current profilers as well as from high-resolution ocean surface-current radars. Model simulations were generated from a high-resolution regional ocean circulation model for the Mid- and South Atlantic Bight. While it is challenging to accurately predict the high-frequency variability in spatial and temporal scales, the model estimates are in good agreement with the observed mean currents. Annual power density along three transects off the North Carolina Coast was calculated based on model outputs.

Chapters Effects of Tidal Stream Energy Extraction on Water Exchange and Transport Timescales and The Impact of Marine Renewable Energy Extraction on Sediment Dynamics address the effects of MRE extraction on physical ocean processes, such as water exchange and sediment transport. In Chap. Effects of Tidal Stream Energy Extraction on Water Exchange and Transport Timescales, Yang and Wang review the concept of transport timescales and numerical models for assessing tidal energy potential and its effect on volume flux and flushing time. Model results from idealized and realistic case studies show that the change in flushing time is linearly correlated with the volume flux reduction when the change in volume flux is small, but with a greater rate of change. Their study demonstrates the importance of using three-dimensional models in tidal stream energy resource assessment, as well as the importance of using flushing time as a transport timescale to quantify the effect of tidal energy extraction on transport processes.

In Chap. The Impact of Marine Renewable Energy Extraction on Sediment Dynamics, Neill et al. provide a detailed review of sediment dynamics and sediment transport processes in coastal and estuarine systems due to tidal current, wave action, or their combined effect. Impacts on morphodynamics of offshore sand banks as a result of tidal stream energy extraction, and on beach erosion and replenishment due to wave energy conversion are explored. The scale of impacts resulting from MRE extraction on sediment transport processes and coastal morphodynamics under extreme wave and storm, compared to scales of natural variability, is discussed.

Like other anthropogenic sources of sound, underwater noise can act as a stressor to marine animals in the marine environment and is an inevitable byproduct of energy generation. Chapters Assessing the Impacts of Marine-Hydrokinetic

Energy (MHK) Device Noise on Marine Systems by Using Underwater Acoustic Models as Enabling Tools and Challenges to Characterization of Sound Produced by Marine Energy Converters address the issue of underwater noise on the marine environment. In Chap. Assessing the Impacts of Marine-Hydrokinetic Energy (MHK) Device Noise on Marine Systems by Using Underwater Acoustic Models as Enabling Tools, Etter provides a comprehensive review of the theory of underwater acoustics and describes the background noise fields arising from natural and anthropogenic sounds as well as from MRE devices. A suite of underwater acoustic models is evaluated, and potential applications of different models toward understanding the impact of anthropogenic noise induced by MRE devices on the marine environment are discussed.

In Chap. Challenges to Characterization of Sound Produced by Marine Energy Converters, Polagye discusses the challenges of characterizing underwater noise generated by MRE devices and the role of field measurements in quantifying acoustic emissions from MRE devices and arrays. Specifically, this chapter addresses the factors influencing sound generation by an MRE device, methods for distinguishing device sound from ambient noise, and masking of the device sound by flow noise. Field measurements of spectrograms and annotated periodograms from a WEC are presented to illustrate these challenges. Potential solutions to overcome these challenges are also discussed.

Marine spatial planning (MSP) is a relatively new approach to analyzing and allocating parts of marine spaces for specific uses or objectives in order to achieve ecological, economic, and social objectives. In Chap. Planning and Management Frameworks for Renewable Ocean Energy, O'Hagan provides an overview of how the requirements of the ocean energy sector are taken into account when designing marine planning systems, how scientific information is reflected in the process, and the tools used to implement MSP. The chapter also identifies how possible or currently experienced conflicts between different sectors or users are managed. The chapter concludes with a section on the key limiting factors to implementation of MSP.

This book presents only part of the ongoing effort to enhance our understanding of the challenges of and barriers to MRE development. By no means does it cover every aspect of resource characterization and physical system effects in MRE development. We hope this book will serve as a useful tool to researchers, industry, and members of the general public who are interested in understanding the current state of the science in MRE development, especially the challenges and approaches to improving resource characterization and reducing system effects.

Finally, we thank the chapter authors for their hard work and contributions to the book, and the many reviewers for their valuable comments and input that improved the quality of the chapters. We also thank Ms. Susan Ennor of Pacific Northwest National Laboratory for technical editing of all of the chapters.

Pacific Northwest National Laboratory
Seattle, WA, USA

Zhaoqing Yang
Andrea Copping

Contents

About the Editors

Dr. Zhaoqing Yang is a chief scientist for coastal ocean modeling at the US Department of Energy's Pacific Northwest National Laboratory (PNNL) and a distinguished faculty fellow in the Department of Civil and Environmental Engineering at the University of Washington in Seattle, Washington. Dr. Yang's research covers broad areas related to coastal hydrodynamics and transport processes using advanced numerical models. His recent research has focused on marine renewable energy resource assessment and the impacts of extreme events and anthropogenic disturbances on coastal infrastructure and ecosystems. Dr. Yang leads PNNL's modeling effort on wave and tidal energy resource characterization as well as associated environmental impact assessment. He holds a Ph.D. in Physical Oceanography from the School of Marine Sciences at the College of William and Mary. Dr. Yang is a member of the Journal of Renewable Energy Editorial Board and served on the National Academy of Sciences—National Research Council's Committee on Marine and Hydrokinetic Energy Assessment.

Dr. Andrea Copping is a senior research scientist and program manager for Pacific Northwest National Laboratory (PNNL) and a distinguished faculty fellow in the School of Marine and Environmental Affairs at the University of Washington in Seattle, Washington. Dr. Copping's research focuses on the environmental effects of development of wave and tidal energy and offshore wind installations, and the role that these effects play in technology development and project initiation across the nation. Andrea leads international projects under International Energy Agency agreements on the environmental effects of marine energy development (Annex IV) and of wind (WREN) that share environmental effects information in order to benefit from progress made around the world. Prior to joining PNNL, Dr. Copping was the associate director of the Washington Sea Grant Program. Although trained as a blue water biological oceanographer, Andrea has spent most of her professional career examining the interactions of humans and the marine environment. Andrea holds a Ph.D. in Biological Oceanography from the University of Washington. Dr. Copping is an associate editor of the Coastal Management Journal, and on the Editorial Board of the International Journal of Marine Energy.

Wave Energy Assessments: Quantifying the Resource and Understanding the Uncertainty

Bryson Robertson

Introduction

Raw wave energy and the associated potential power production from wave energy converters hold great promise as an abundant, carbon-neutral source of electricity generation for generations to come. The International Energy Agencies (IEA) Ocean Energy Systems (OES) (OES 2015) estimates that the global wave resource could provide up to 29,500 TWh of carbon-neutral electrical energy annually through the use of wave energy conversion (WEC) technologies. Substantial efforts are being made to understand coastal and offshore wave energy resources, expand methods to quantify and characterize the measurements, and provide wave energy companies with the necessary knowledge to design WEC technologies (Cornett and Zhang 2008; Dunnett and Wallace 2009; Kim et al. 2012; Reikard et al. 2015; Robertson et al. 2013; Hiles et al. 2014).

Highly resolved and accurate assessments of the gross wave resource are required for the wave energy industry to mature and begin to provide power to electrical grids. Wave resource assessments are the foundation for the architectural design of a wave energy converter (WEC), a project developer's unit cost calculations, a utility's reserve costing plans, and for a regulator's cost-benefit analyses of large-scale WEC activities. The importance of the resource assessment in providing an accurate and precise representation cannot be overstated.

Wave energy can be described as a concentration and moving reservoir of solar energy. As the world heats differentially from incoming solar irradiance, air masses heat and cool, moving air from high pressure to low pressure areas, thereby creating wind. When this wind blows over vast stretches of unobstructed ocean fetch, waves are generated. If the wind blows with sufficient speed, over a large enough fetch and

B. Robertson (✉)
Institute for Integrated Energy Systems, University of Victoria, Victoria, Canada
e-mail: bryson@uvic.ca

Z. Yang and A. Copping (eds.), *Marine Renewable Energy*,
DOI 10.1007/978-3-319-53536-4_1

for extended portions of time, ocean swells develop. The longer and harder the wind blows, over increasing fetches, the more the wave height and wave period increase. Once generated, ocean swells are able to propagate vast distances with negligible dissipation or dependence on the wind that generated them. As a result, ocean waves arriving at any shoreline globally are the culmination of the local wind conditions, as well as the hysteresis effect of hundreds of storms across the millions of square kilometers of surrounding ocean. As a result, ocean swells are moving reservoirs of concentrated wind and solar energy. The stores feature high power density and are well predicted. Excluding tidal energy resources, ocean waves are the most energy dense form of renewable energy sources. For example, solar energy flux is measured in kilowatts per square meter and reaches a maximum of 1 kW/m^2 at high noon on the equator, while relatively benign regular wave sea state of 2-m wave height with a ten second period features ~20 kW/m of wave energy flux (Falnes 2002; DNV 2010).

The goal of this chapter is to provide an introduction to the vast, complex, and engaging research area of wave resource assessments. The objectives, methods, and outcomes of various wave resource methodologies will be discussed. The intricacies of a resource assessment and the implications for final WEC power production will be quantified. Recommendations and further work in future research avenues will be presented as the topics are discussed and analyzed; a brief introduction to extreme wave analysis and the siting of future WEC farms is included. Ultimately, the goal of this chapter is to provide an overview of the present state of the art in wave resource assessment methodologies, recommendations for best practices, and help illuminate the true nature of this vast resource for future renewable energy generation.

Wave Data Sources

The development and accuracy of a robust wave resource assessment methodology rely intrinsically on the input data sources. Hence, the collection of high-resolution observations, or measurements, of the wave conditions and a detailed and validated numerical model is of utmost importance. As will be shown throughout this chapter, the present level of the accuracy and robustness of the resource assessment is limited by the availability of necessary data sources; however, as the industry evolves over time, more data will be collected and the resource assessment methodology will become increasingly robust and accurate.

Wave Measurements

Waves are generally either directly measured, through deployed in situ measurement devices, or remotely measured through backscatter and Doppler shifts by

radar and satellites. As noted, the most common direct measurement of wave conditions is through the deployment of in situ wave measurement devices; generally moored wave buoys, seafloor-mounted acoustic measurement devices, or statically mounted wave poles.

Wave buoys float on the ocean surface and follow the three-dimensional varying ocean surface over time. Wave buoys are deployed across the globe and provide continuous measurements of wave conditions to metrological organizations, shipping traffic, and recreational ocean users such as surfers. Buoys can either be permanently moored or free-floating measurement devices. Moored buoys provide a clean consistent record of wave conditions at a specific location, with depths ranging from 10 s to 1000 s of meters. However, buoys are susceptible to breaking wave loading and are unsuitable for shallow water deployments where breaking waves are expected. Through detailed analysis of the recorded buoy accelerations, the buoys' heave (vertical motion) and horizontal movements can be calculated and are generally presented as a time-dependent Heave-Northing-Easting record. Using the same input data, a representation of the incoming directional wave spectrum is created (a detailed explanation of directional wave spectra is presented later).

Increasingly common for shallow water applications with breaking waves, seafloor-mounted devices can take acoustic measurements of the water surface and record the orbital velocities of particles near the surface and/or the time-varying water pressure. Single-point-of-measurement pressure devices provide a time-history of the sea surface elevation but provide no details about the directionality of the incoming waves. Acoustic measurement devices featuring multiple acoustic beams will recreate the full incoming wave spectra through detailed analysis of these multiple beam time-histories. Measurements derived from seafloor-mounted devices provide extremely precise measurement of the sea surface but are generally limited in application to shallow water locations. Point measurements from wave buoys or acoustic measurement devices are widely understood, and their deployments are easily achieved. However, they provide limited knowledge of the spatial variability in the resource.

Remote measurements from aircraft, satellites, or tall coastal structures are better suited for giving larger spatial distributions of the wave field. The resulting measurements of the sea surface from these remote methods are developed through detailed analysis of the radar backscatter or recorded imagery pixel intensity. As a result, wave measurements obtained using remote methods generally lack the high level of precision and accuracy that in situ measurements provide and are generally of shorter duration than existing in situ measurements.

The suitability of a certain wave measurement technique depends on the goal of the measurement campaign; each method has advantages and disadvantages. For the wave energy industry, the current standard is wave buoys—primarily due to their ease of deployment and the availability of long-term data sets.

It is important to note that a wave measurement sample is only one realization of the underlying spectrum; slight variations in timing, frequency bands, and record length will result in variations in the final spectrum. Direct measurement of wave conditions, from wave buoys, acoustic wave and current (AWAC) profilers, radar,

etc., are not without systematic biases and random errors. Each measurement platform and technique includes a range of inherent assumptions in the recreation of the sea state, and, if possible, these assumptions should be quantified prior to their detailed use for wave resource assessments. For example, the Joint WMO-IOC Technical Commission for Oceanography and Marine Meteorology (JCOMM) (JCOMM 2014) provides a database of buoy intercomparisons and quantifies the accuracy of measurements for permanent wave buoys around the globe. The results from the JCOMM project and other similar studies (Robertson et al. 2015) provide the necessary quantitative information to help correct and improve the accuracy of wave measurement records. These sorts of analyses should be performed in parallel with numerical model development to ensure final numerical model validation is compared against the most accurate measurements of wave conditions possible.

Numerical Wave Models

Wave measurements from buoys, satellites, or radars are not wholly sufficient for characterizing wave conditions across an area of interest. Robust wave resource assessments require detailed knowledge of wave conditions across significant spatial areas and over long time frames. Numerical wave propagation models provide the bulk of the data required for a wave resource assessment because they provide the necessary temporal and spatial scope to allow for a detailed understanding of the wave climate. A wide range of numerical models is available for simulating surface wave processes, based on different physical formulations, assumptions, and numerical frameworks. Wave models can be divided into two major categories: phase-resolving models and phase-averaged models.

Phase-resolving models are based on fundamental wave equations that involve rigorous approximations. The propagation and evolution of each phase-resolved wave must be computed on a grid with a resolution finer than the wavelength. Phase-resolving models solve for the water surface elevation and account for the horizontal and vertical flow velocity. These types of models are suitable for resolving radiation and diffraction over 10 s of kilometers or short time periods (Hiles et al. 2014) but are too computationally expensive for large-scale or long-term analyses.

Phase-averaged spectral models compute the evolution of the wave spectrum in space and time, based on the wave energy balance equation, and are currently the only practical models for assessing large-scale wave resources (i.e., ocean basin scale). The oceanographic community has developed many spectral wave models, and recent wave resource assessment is almost exclusively based on third-generation (3G) version of these models. The most popular 3G wave models are the Wave Action Model (WAM) (WAMDI 1988), WAVEWATCH III (WWIII) (Tolman 2014), Simulating WAves Nearshore (SWAN) (SWAN 2006), TOMAWAC (Benoit et al. 1996), and MIKE-21 SW (DHI 2012).

The 3G wave models resolve the nonlinear interactions through the spectral wave action density (N) equation (Eq. 1) and balance the equation across the full frequency and direction domain (Tolman 2014). Wave action density is defined as wave energy density divided by frequency of occurrence $(N = E/\sigma)$. Action density is conserved in the presence of ambient current, whereas energy density (E, to be discussed in detail later) is not, hence the use of action density (SWAN 2006). The evolution of the wave spectrum is calculated by implicitly solving the action balance equation (Eq. 1) to predict wave conditions across a computational grid.

$$\frac{\partial N}{\partial t} + \frac{\partial (C_{g,x} + U)N}{\partial x} + \frac{\partial (C_{g,y} + V)N}{\partial y} + \frac{\partial C_{g,\sigma} N}{\partial \sigma} + \frac{\partial C_{g,\vartheta} N}{\partial \vartheta} = S/\sigma \qquad (1)$$

The wave action density evolves as a function of time (t), distance (shown in the Cartesian coordinates (x, y)), depth and current induced refraction (θ), and frequency (σ). Frequency-shifting is related to the Doppler effect and is due to the presence of ambient current. Relative frequency (σ) is due to variation in depths and currents; C_g denotes the wave action propagation speed in (x, y, σ, and θ) space (see Eq. (9)); U and V are the depth-averaged current velocities in (x, y) space, while S denotes the generation and dissipation terms within the model.

Each model is dependent on a computational spatial grid, a series of nodes and cells that define the geographic space over which the model will compute the propagation and evolution of the wave action density. Grids are either fixed size (or "structured") or variable size (or "unstructured").

Structured grids can either be uniform rectilinear or curvilinear quadrilateral grids. Rectilinear grids are based on uniform-distributed nodes, and the cell dimensions are based on Cartesian coordinates. Curvilinear grids are also based on uniform cell discretization but are based on spherical coordinates to better represent the spherical nature of the planet. Given that these are both types of quadrilateral grids, four cells are required to meet at internal nodes within structured grids.

Unstructured grids allow for variable resolution in the grid spacing and cell shape. Unstructured grids can be combination of triangles and quadrilaterals, a so-called hybrid grid. The goal of an unstructured grid is to improve grid resolution in spatial areas of interest, while reducing the computational overhead.

WAM

WAM—the first 3G spectral wave model to be widely adopted—is one of the most well-tested wave models and is widely used internationally, especially in the European wave modeling communities. Developed by the WAMDI Group (1988), WAM simulates spectra of random wind-generated waves by solving the action density equation, including nonlinear wave–wave interactions. It has since been further developed by different organizations but without a centrally maintained version. WAM has proven to be reliable for deep-water open-ocean applications

over regular grids, yet it does not contain the necessary shallow water physics for application in depth-limited locations.

WAM was the first operational wave model to be fully coupled to an atmospheric model and later to an ocean circulation model. This work was carried out at the European Centre for Medium-Range Weather Forecasts (ECMWF). Further documentation on the current ECMWF WAM model can be found in (ECMWF 2013). Coupling to a hydrodynamic model was first carried in the PRO-WAM version, and a recent version of WAM (4.5.4) was also made available as part of the MyWave project (http://mywave.github.io/WAM/). For additional detail, see chapter "Wave Energy Resources Along the European Atlantic Coast".

WWIII

WWIII is a popular wave model for global analyses and is continually developed by the Marine Modeling and Analysis Branch at the National Centers for Environmental Prediction and by an international team of developers. Similar to WAM, WWIII solves the random phase spectral action density balance equation. The current version 4.18 of WWIII, which is available to the public, allows for various grid options and physics packages. WWIII generally uses an explicit numerical scheme to solve the governing equation on traditional structured rectilinear or curvilinear grids. Hence, the model run time-step is constrained by the Courant–Friedrichs–Lewis (CFL) stability criteria (CFL $\leq$ 1), which simply states that wave energy may not travel more than one geographic computational grid cell per time-step. Further documentation on the current WWIII model can be found in (Tolman 2014).

WWIII and WAM are excellent examples of wave models suited for global wave resource assessments; they are able to provide the necessary long-term hindcasts of wave conditions, over large spatial domains, with sufficient resolution to precisely and accurately quantify the wave resources. These sorts of standardized meteorological office wave products provide an excellent resource for identifying geographical regions that have sufficient wave energy transport resources for future development. However, when attempting to identify specific locations for deployment and assessment of the wave resource, additional spatial resolution in the model computational grid and resolution within the model wave parameter output are required. For these applications, nested or multigrid WAM or WW3 models could be employed, or boundary conditions from a global model could be used within models specifically designed for coastal applications, such as SWAN, TOMAWAC, or MIKE-21 SW. Note that both WAM and WWIII have current and in-development model implementations that have all of the necessary physics and numerical schemes to handle coastal applications.

SWAN

The basic scientific philosophy of SWAN is identical to that of WAM, but with applications for shallow water. SWAN is an open-source wave model that was developed at the Delft University of Technology and was built as an extension of the 3G WAM model. The fundamental difference between SWAN and WWIII/WAM is the numerical scheme used to solve the spectral action balance equation. SWAN only uses an implicit formulation, which allows for larger computational time-steps and efficient simulations of high spatial resolution areas (<1 km). Designed to simulate the propagation of waves in shallow nearshore areas (depth <½ wavelength), SWAN is often applied for wave resource assessments (Ruehl 2013; Dykes et al. 2002; Rusu and Soares 2009; Choi et al. 2009; Robertson et al. 2014). As an example of the generation and dissipation terms, noted in Eq. 1 and expanded in Eq. 2, SWAN breaks the *S* term down to account for input by wind (S_{in}), triad and quadruplet nonlinear wave-wave interactions (S_{nl}), and wave dissipation through white-capping (S_{wc}). In shallow water, *S* includes the effects of bottom friction (S_{bf}) and shoaling-induced breaking (S_{br}) (SWAN 2006).

$$S = S_{in} + S_{nl} + S_{wc} + S_{bf} + S_{br} \tag{2}$$

SWAN can solve the steady form of the action balance equation by running in the stationary mode, which greatly reduces computational requirements and run times, yet should only be applied when the model domain is sufficiently small (~100 km). Further documentation of the base SWAN model is available online (Tolman 2014).

TOMAWAC

TOMAWAC is the coastal wave propagation sub-module of the commercial integrated TELEMAC modeling system (Telemac-Mascaret 2015). TOMAWAC/TELEMAC is managed and developed by Artelia, BundesAnstalt fur Wasserbau, Centre d'Etudes Techniques Maritimes at Fluviales, Daresbury Laboratory, and Electricité de France R&D and HR Wallingford. TELEMAC is a modeling tool used for free-surface flows; it is based on a finite element method and can be solved over both structured and unstructured grids. Similar to SWAN, TOMAWAC models the sea states by solving the balance equation of the action density directional spectrum.

MIKE-21 SW

MIKE-21 SW is the spectral wave modeling sub-module of the MIKE-21 suite (DHI 2016), developed by DHI International. MIKE-21 SW is also a 3G spectral

wind-wave model and based on a cell-centered finite volume formulation. The time integration is performed using a fractional step approach where a multi-sequence explicit method is applied for wave propagation (DHI 2012). MIKE-21 can be formulated as either a fully directional spectral formulation or a parametric formulation. It includes shallow water physics and works on both structured and unstructured grids.

The use of localized coastal wave models, such as SWAN, TOMAWAC, or MIKE-21, allows wave energy developers to run high-resolution, long-term hindcasts of wave conditions without having access to significant high-powered computing resources. SWAN, TOMAWAC, and MIKE-21 SW are not constrained to run on structured computational girds; they are able to run on unstructured computational grids that have more flexibility on grid resolution and format. Depending on the application, these models still rely on global wave models, or in situ instruments, for spatially invariant wave and wind boundary conditions. If the model domain is larger than 10 s of kilometers, it is suggested that wind forcing fields should be included in the local model to more accurately recreate locally generated wind seas and, hence, improve the representation of the true sea surface conditions.

Table 1 provides a quick overview of the main characteristics of the models discussed. Global and regional wave models are still models and do not exactly replicate the true sea conditions. Models are known to underpredict extreme wave conditions, overpredict low-energy wave conditions, and provide a smoother representation of wave conditions. In contrast to wave measurements, which are a single realization of the underlying wave spectrum, wave models provide an estimate of the underlying spectrum. Hence, it is nearly impossible to get a zero root mean square error (RMSE) between a measurement and a model. Regardless, data from an in situ measurement device should be thoroughly checked for errors and consistent biases. Any model used for wave resource assessment should be validated against numerous independent wave measurements prior to use, preferably measurements obtained using calibrated wave measurement devices (JCOMM 2014).

Table 1 Overview of wave model and characteristics

Model	General application	Solver	Method	Grid	Source
WAM	Global	Explicit	Finite difference	Structured	Open source
WWIII	Global/coastal	Explicit/implicit	Finite difference	Structured/ unstructured	Open source
SWAN	Coastal	Implicit	Finite difference	Structured/ unstructured	Open source
TOMAWAC	Coastal	Implicit	Finite element	Structured/ unstructured	Open source
MIKE 21	Coastal	Explicit	Finite volume	Structured/ unstructured	Commercial

Analyzing and Quantifying the Resource

Over the past decade, significant effort has been expended on analyzing the data from wave models and wave measurement instruments to quantify the magnitude and distribution of wave energy resources around the world. A nonexhaustive review of published literature indicated the availability of wave resource assessments in the contiguous United States (EPRI 2011; Lenee-Bluhm et al. 2011; Dallman and Neary 2014), Hawaii (Stopa et al. 2011), Australia (Hughes and Heap 2010; Hemer and Griffin 2010), Canada (Hiles et al. 2014), (Robertson et al. 2014), (Cornett 2006), Chile (Monardez et al. 2008), Africa (Sierra et al. 2016), and across the European Union (Smith et al. 2012; Rusu and Soares 2012; Rute Bento et al. 2016; Liberti et al. 2013; Ayat 2013; Folley and Whittaker 2009). In the majority of the noted studies, a numerical wave model was validated against wave buoys and was subsequently used to quantify the characteristics of the long-term wave climate.

Precisely quantifying the multi-dimensional characteristics of wave conditions is more complex than for other renewable forms of energy, i.e., wind, tidal, or solar resources. Generally, wind, solar, and tidal resource can be described using a single variable—wind speed, solar irradiation, or water speed, respectively. In contrast, wave energy transport is a multivariable problem and can only be quantified, at a very minimum, through detailed knowledge of both the significant wave height (H_{m0}) and the wave energy period (T_e) parameters. This added dimension significantly complicates wave resource assessments and necessitates both a high-resolution wave data set and a detailed understanding of all of the influencing variables.

Wave Spectra and Characteristic Parameterizations

Under the assumption that the sea surface elevation is a stationary and Gaussian process, the short-term (<30 min) characteristics of a single sea state can be characterized, at any particular point in time or space, by a directional variance density wave spectrum, which is more commonly referred to as a *directional wave spectrum*. A sample directional wave spectrum is presented in Fig. 1; the directional wave spectrum plots the sea surface variance density (E_{ij}) over a range of wave frequencies (i) and directions (j). As shown, the frequency component of the variance density is represented by concentric rings showing the reducing frequency/increasing wave period values as the rings approach the center. The direction that the variance density is *arriving from* is represented by the respective angles, with 0° generally representing a swell traveling from the north to the south and 270° generally representing a swell traveling from the west to the east. The magnitude of the variance density for each direction and frequency is represented by the color-intensity map.

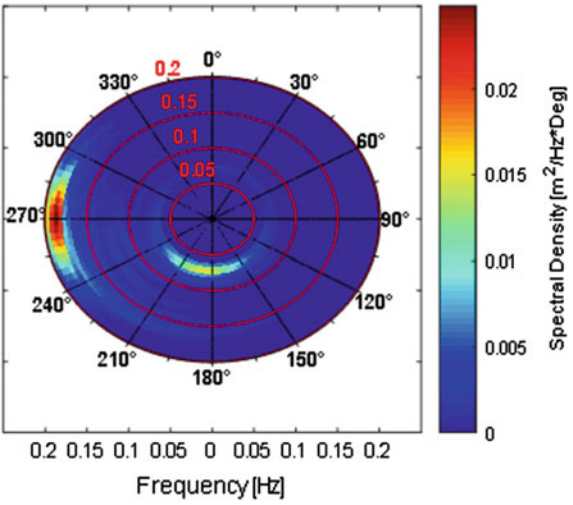

Fig. 1 Directional spectral variance density spectrum

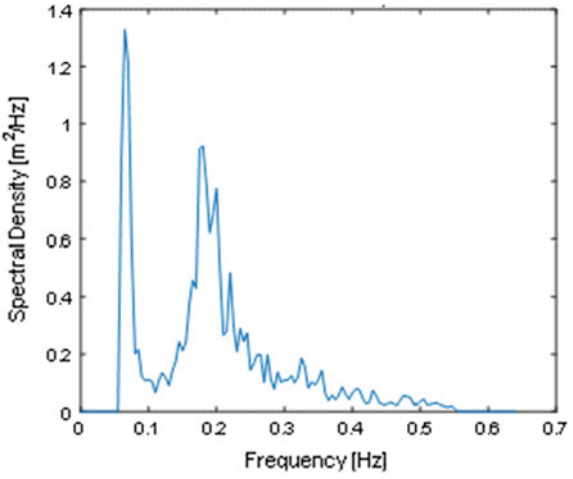

Fig. 2 Nondirectional spectral variance density spectrum

Older wave measurement buoys and fixed in situ instruments, such as pressure sensors, are generally unable to measure the directional content of the variance density spectrum and often only report the *nondirectional variance density spectrum*. A sample nondirectional variance density spectrum is shown in Fig. 2 for the same sea state used in Fig. 1. The nondirectional spectrum can be easily generated from the directional wave spectrum by simply integrating all of the directional components (θ) of the variance density within a single frequency band, as shown in Eq. (3):

$$E_i = \sum_j E_{ij} \Delta\theta \tag{3}$$

When quantifying the long-term wave resource at a location of interest, the use of the full directional wave spectrum is exceedingly cumbersome, impractical, and

does not allow for quick comparative exercises. For example, a 10-year numerical hindcast of wave conditions at a single location would involve ~87,600 hourly directional wave spectra. It is necessary to parameterize these data into simplified metrics that provide the necessary level of detail for the sea state and are tractable when quantifying the wave climate. This parameterization process inherently introduces uncertainty to the wave resource assessment but is required to keep the wave climate data manageable for both WEC developers and policymakers.

The two dominant parameters used for wave resource assessments are the significant wave height (H_{m0}), also known as the zero-moment wave height, and the energy period (T_e). The significant wave height is used to characterize the wave height of a given sea state and, historically, was calculated as the average value for the highest third of waves from a time-series zero-up or zero-down crossing analysis. In the frequency-domain, and more conventionally, it is calculated using the zeroth spectral moment of the wave spectrum, according to Eq. (4). This also equates to the variance or the square root of the standard deviation of the sea surface elevation.

$$H_{m0} = 4\sqrt{m_0} \tag{4}$$

where the spectral moment of nth order, m_n, uses Eq. (5) when calculating from the nondirectional variance density spectrum using:

$$m_n = \sum_i f_i^n E_i \Delta f \tag{5}$$

where Δf is the frequency increment and f_i^n is the ith frequency to the nth power.

The energy period is the variance-weighted mean period from the directional or nondirectional variance density spectrum. The energy period is calculated using moments of the wave spectrum according to Eq. (6):

$$T_e = \frac{m_{-1}}{m_0} \tag{6}$$

It is still common to see wave resource assessment uses the peak period (T_p) and peak direction (θ_p) to quantify the periodicity and directionality of the wave climate. The peak period and direction correspond to the wave frequency and direction, which feature the maximum variance density; for example in Fig. 2, T_p is 11.4 s while T_e is 7.2 s. The peak period and direction are independent of the distribution of the variance density across the frequency and direction axis and are prone to chaotic behavior. As a result, the energy period has become the preferred metric for characterizing the periodicity of the wave condition, while θ_{Jmax} is specified by the International Electrotechnical Commission (IEC) for directionality (θ_{Jmax} is discussed on the next page). If shape of the wave spectrum follows a known spectral shape, the transform from T_p to T_e can be easily calculated. See Table 2 for a Pierson–Moskowitz spectral shape. For more detail about the impact of energy values, see (Cahill and Lewis 2014) and (Goda 2009).

Table 2 Pierson–Moskowitz spectrum $T_p - T_e$ transform

Peak period	2	3	4	5	6	7	8	9	10	11	12	13	14	15	16	17	18	19
Energy period	1.8	2.6	3.4	4.3	5.1	6.0	6.9	7.7	8.6	9.4	10.3	11.1	12.0	12.9	13.7	14.6	15.4	16.3

An additional wave spectrum parameter often cited is the spectral width. The spectral width characterizes the distribution of the variance density along the frequency axis. Saulnier et al. (Saulnier et al. 2011) review different published spectral width formulations and found that Eq. (7), which defines the spectral width as the standard deviation of the period variance density normalized by the energy period, provides a robust representation of the width.

$$\epsilon_0 = \sqrt{\frac{m_0 m_{-2}}{m_{-1}^2} - 1} \tag{7}$$

The most commonly cited energy parameter is the omnidirectional wave energy transport (J). The omnidirectional wave energy transport provides a measure of the time-averaged energy flux, through an envisioned vertical cylinder of unit diameter extending from the sea floor to the surface, and is the power per meter of wave front that WECs are attempting to capture. It is calculated using:

$$J = \rho g \sum_i c_{g,i} E_i \, \Delta f \Delta \theta \tag{8}$$

where

$$c_{g,i} = \frac{\pi f_i}{k_i} \left(1 + \frac{2k_i h}{\sinh 2k_i h} \right) \tag{9}$$

where ρ is water density, g is gravity, k_i is the wave number at the ith frequency, c_g is the group velocity, and h is the mean water depth. The wave number is calculated as $2\pi/L$.

The parameters noted thus far are common, standardized oceanographic and marine wave condition parameterizations. Moving beyond these parameters and identifying parameters of interest and necessity to the wave energy community, the IEC works with international experts to develop baseline standards for wave, tidal, and water resource assessments, under the Technical Committee-114 identifier (Piche et al. 2015; International Electrotechnical Commission T C 114 2015). Based on the cumulative scientific knowledge about wave resource assessments, and first published by Lenee-Bluhm et al. (2011), the IEC has included three additional parameters for wave resource assessments in their current technical specification: the directional wave energy transport, the direction of the directionally resolved wave energy transport, and the directionality coefficient.

Resolving the directional components of the omnidirectional wave energy transport requires a measure of the time-averaged energy flux through the same envisioned vertical plane of unit width, extending from the sea floor to the surface, but with its normal vector parallel with direction, θ. This directionally resolved wave energy transport is the sum of the contributions of each component, with a positive component in direction θ and is calculated as follows:

$$J_\theta = \rho g \sum_{i,j} c_{g,i} E_{ij} \Delta f \Delta\theta \cos\left(\theta - \theta_j\right) \delta \quad \begin{cases} \delta = 1, & \cos\left(\theta - \theta_j\right) \geq 0 \\ \delta = 0, & \cos\left(\theta - \theta_j\right) < 0 \end{cases} \tag{10}$$

When assessing the directionality of a sea state, the IEC specification recommends using the direction of maximum directionally resolved wave energy transport (θ_{Jmax}), which corresponds to the maximum value of J_θ.

Finally, the directionality coefficient is a characteristic measure of the directional spreading of wave energy transport. It is the ratio of the maximum directionally resolved wave energy transport to the omnidirectional wave energy transport (see Eq. (11)).

$$d = \frac{J_{\theta_{Jmax}}}{J} \tag{11}$$

Baseline Resource Assessment

Over the past couple of decades, numerous methodologies have been presented to perform a baseline wave resource assessment—an assessment that provides both the necessary information about the wave resource and sufficient detail for the development of WEC technologies. International wave energy experts are collaborating with the IEC to develop technical specifications that outline a robust and consistent method for performing baseline wave resource assessments. The technical specifications are consistently updated, generally based on published academic research, and can be purchased from IEC (International Electrotechnical Commission T C 114 2015).

As noted in the numerical wave models section, one of the major advantages of numerical wave models is their ability to quantify the spatial distribution of wave resources and characteristic metrics. The resulting maps (example shown in Fig. 3) allow for the identification of prospective locations of interest and further investigation. If the prospective location does not have a direct measurement of the resource (through one of the methods presented in the wave measurements section), researchers have been using measure–correlate–predict (MCP) (Phillips et al. 2008) or triple-collocation methods (Robertson et al. 2015) to provide an improved assessment of the resource.

The primary metric used to quantify the wave climate at a prospective wave energy deployment location is a bivariate histogram of H_{m0} and T_e. The histogram illustrates the mean annual occurrence and annual energy contribution of specific wave conditions from a long-term hindcast. A sample histogram is shown in Fig. 4. The values in each bin represent the mean number of hours in a year that a particular wave sea state occurs, while the color scale represents the percentage contribution of each condition bin to the annual omnidirectional wave energy transport (J). The histogram is generally parameterized at a resolution of 0.5 m and

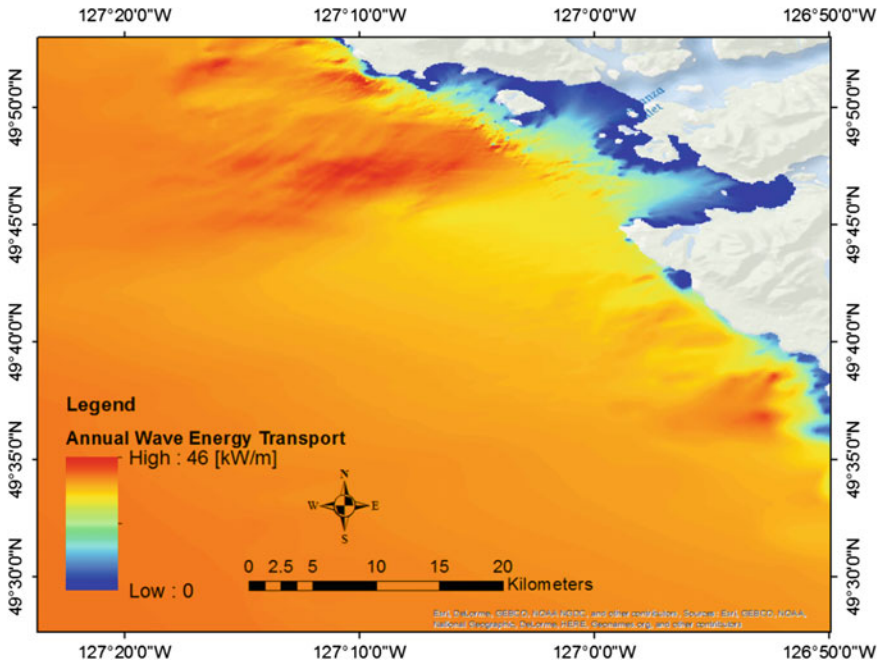

Fig. 3 Mean annual wave energy transport (J) in the Canadian Pacific

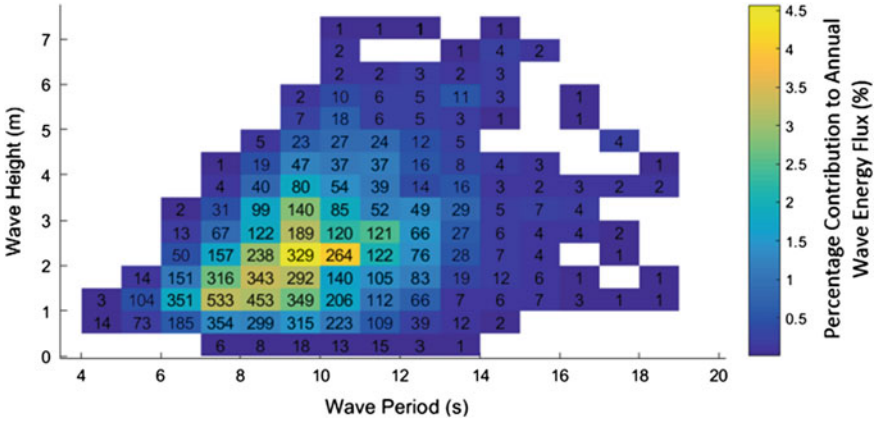

Fig. 4 Wave bivariate histogram for Amphitrite Bank, Canada. Numbers indicate the number of hours each year, while the contour *colors* indicate the percentage of total energy within that sea state

1 s, respectively. However, the discretization of H_{m0} and T_e space into specific bins changes between authors and locations (Liberti et al. 2013; Mackay et al. 2010).

The histogram provides a simple, tractable representation of the annual wave climate, allowing for quick analyses of the wave climate, and comparison between prospective sites. For example, the details included in Fig. 4 illustrate that the most frequent sea state (H_{m0}: 1.25 m, T_e: 8.5 s) does not provide the highest annual wave energy contribution (H_{m0}: 1.75 m, T_e: 9.5 s). These characteristics are easily extracted from the histogram and, from the point of view of the WEC developer, indicate the need for a detailed optimization of device architecture to maximize WEC performance under the most frequent or most energetic wave conditions (Bailey et al. 2016).

Complementing the histogram and providing details about the directional distribution of the mean annual wave climate is a directional wave rose. The rose discretizes the magnitude of the parameter of interest across differing directions and can be modified to present the distribution of significant wave heights, energy period, omnidirectional wave energy, or any of the baseline wave parameters previously presented. Figure 5 provides an example of the directional distribution of omnidirectional wave energy.

Wave histograms and wave roses provide simple tractable representations of wave climate, yet they provide no details about the temporal variability of the wave parameters, i.e., how does the parameter vary by seasonal, monthly, and hourly time

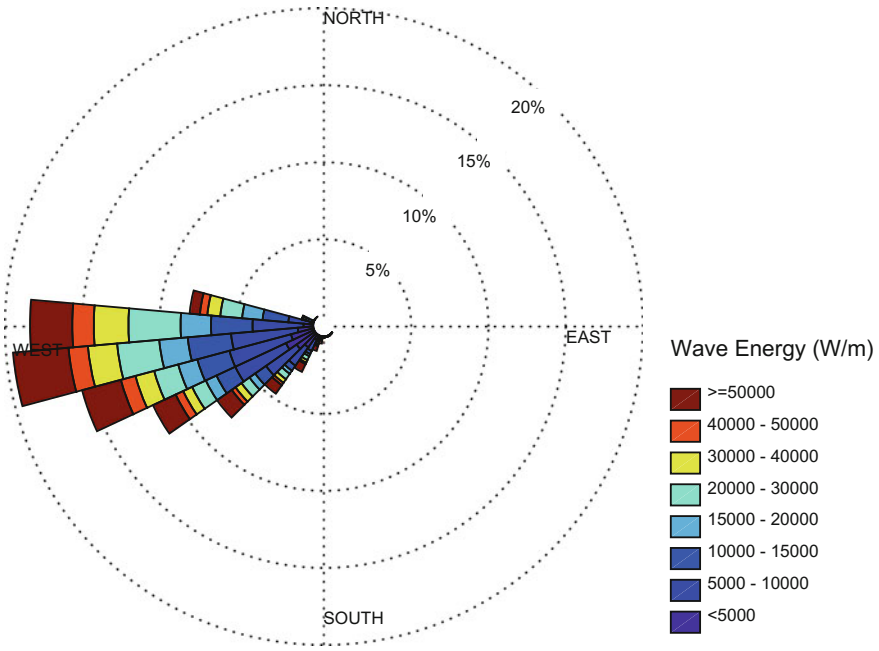

Fig. 5 Directional wave rose

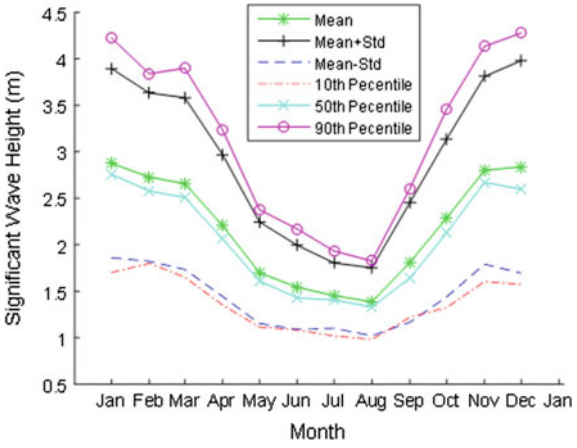

Fig. 6 Monthly variability of significant wave height

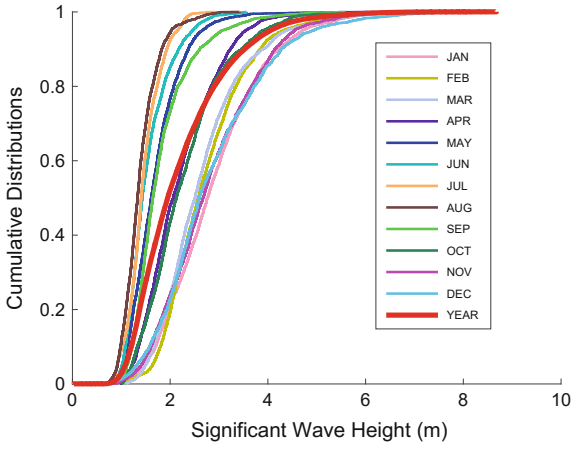

Fig. 7 Cumulative distribution function for significant wave height

frames? The interannual or monthly variation in wave parameters is easily represented by a simple line plot, generally presented in conjunction with the mean ± single standard deviation and various percentiles, as shown in Fig. 6. For this location, the November–February period is extremely active, showing 90th percentile significant wave heights of ~4.0 m, while during the May–August period, the mean wave height is just 1.6 m.

A cumulative distribution function (CDF) is another frequently used presentation technique for temporally varying parameters. The CDF allows the assessment to provide a simple representation of the distributions of wave parameters across the differing months. Figure 7 shows that the 98th percentile significant wave height in December is ~6 m but only 1.9 m in July.

The monthly variability plots in Figs. 5 and 6 detail the interannual variation, but they provide no details about the short hourly or daily time scales. While numerous

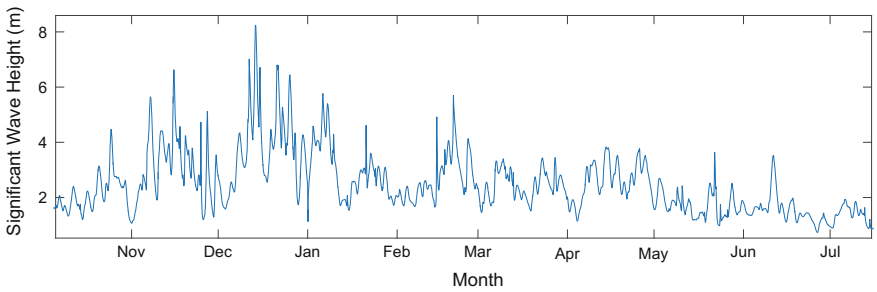

Fig. 8 Hourly variation of significant wave height in Western Canada

methods exist for presenting these data, it is often most illuminating to simply view a time-history of the relevant parameters, as shown in Fig. 8.

Finally, if suitably extensive data sets are available, it is important to ensure that the reference data period used for all of the analysis is representative of the long-term wave climate and that the data set was not extracted during a period of low/high wave activity due to a natural or anthropogenic climatic variability. For example, Mackay et al. (2010) show that the North Atlantic Oscillation can greatly affect the results of a wave resource assessment if only 5 years of hindcast data are used, and they illustrate that use of 20 years of hindcast data greatly reduces these effects. The IEC Technical Specification currently recommends a minimum of 10 years (International Electrotechnical Commission T C 114 2015).

Higher Fidelity Resource Assessments

As the wave energy industry develops, there is a clear and distinct need to provide higher fidelity resource assessments and reduce the associated uncertainty. The IEC Technical Specification suggests a methodology that will undoubtedly provide the *necessary* data for an assessment, particularly when assessing the gross mean annual energy production. However, evidence indicates that the resulting data set may be *insufficient* to mitigate uncertainty in the hour-to-hour variability in the final WEC power production (Robertson et al. 2015, 2016). Hence, higher fidelity assessment methods are being developed to reduce the uncertainty in the resource characteristics and parameterizations. However, these improvement methods need to continue to create results that are easily relayed to those with a less intimate understanding of wave dynamics.

Prior to detailing these improved methods, it is illustrative to revisit the baseline parameterization of a full directional wave spectrum into a few representative parameters. This process inherently introduces significant uncertainty in the resulting wave resources assessment. The parameterization of the directional wave energy spectrum into significant wave height and energy period parameters

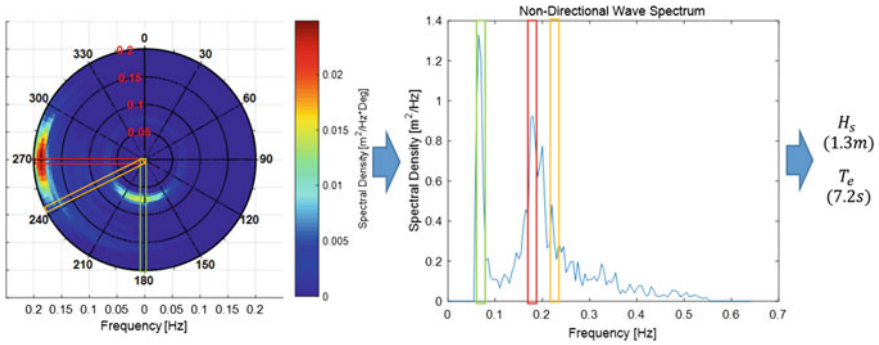

Fig. 9 Parameterization of directional variance density spectra

removes all details about the variance density distribution across the frequency and direction axes. As Fig. 9 illustrates, directional variance density information is lost when using a nondirectional wave spectrum, and the frequency variance density information is lost when using basic parameters. The colored boxes in Fig. 9 indicate individual wave systems in the various representations.

As a result of this information loss, it is commonly assumed that any wave condition, drawn from any histogram bin, can be represented with a single-peaked spectrum with a Joint North Sea Wave Project (JONSWAP) or Pierson–Moskowitz (PM) spectrum with an equivalent H_{m0} and T_e value (Hiles et al. 2014; Lenee-Bluhm et al. 2011; Rusu and Soares 2012; Babarit et al. 2012; Iglesias and Carballo 2011; van Nieuwkoop et al. 2013). The generalized JONSWAP spectral form is presented in Eq. (12):

$$E(f) = \alpha g^2 (2\pi)^{-4} f^{-5} \exp\left[-\frac{5}{4}\left(\frac{f}{f_{peak}}\right)^{-4}\right] \gamma^{\exp\left[-\frac{1}{2}\left(\frac{f/f_{peak}-1}{\varphi}\right)^2\right]} \tag{12}$$

where α is calculated so that $\int S(f)\,df = H_{mo}^2/16$ (Brodtkorb et al. 2000), φ is a peak-width parameter ($\varphi = 0.07$ for $f \leq f_{peak}$ and $\varphi = 0.09$ for $f > f_{peak}$), and γ is a peak-enhancement factor. For a standard JONSWAP spectrum $\gamma = 3.3$, while $\gamma = 1$ for a PM spectrum.

A simple method for increasing resource assessment fidelity is to quantify the "best-fit" peak-enhancement factor, γ, for each histogram bin. The resulting γ value will improve the representation of the wave spectrum with limited nontractable increases in the characterization parameters.

However, as shown in Fig. 10, a reconstructed spectrum, even with a "best-fit" JONSWAP spectral shape based on wave buoy H_{m0} and T_e measurements, can still vary dramatically from the original measured wave spectrum. It is apparent that the discrepancy is primarily due to the assumption of a single-peaked wave spectrum. This assumption results in two significant uncertainty sources: firstly, the peak value of the variance density spectrum will be erroneous, and secondly, variance

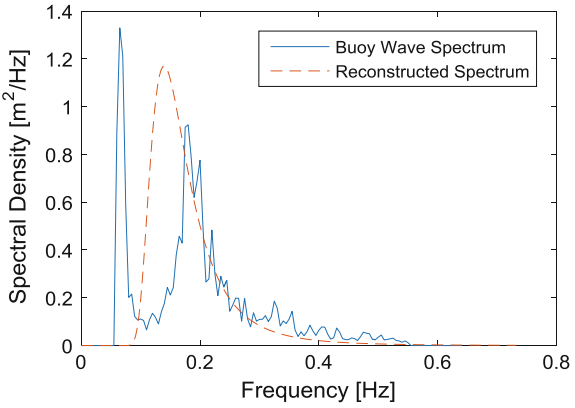

Fig. 10 Comparison of measured and histogram equivalent variance densities spectra

density will be misappropriated across the frequency axis. The incorrect representation of the peak variance density results from all of the variance density being constrained to a single spectral peak. If two or three peaks exist, as shown in Fig. 10, all of the variance density will be assigned to the single priority peak. Compounding these uncertainties, the energy period is a variance-weighted mean of frequency-domain variance density, and not a physical component of the spectrum, so the location of the peak variance density will generally fall between subsequent variance density peaks. Expanding this analysis to a fully directional variance density spectrum, a similar misappropriation of variance density in the directional space will result from an assumed single-peaked wave spectrum with θ_{Jmax} direction.

While there are bimodal (double-peaked) analytical spectral shapes (Ochi and Hubble 1976; Torsethaugen and Haver 2004), they generally require five to six descriptive parameters for each wave condition and are thus extremely cumbersome to handle and nontractable to the general audience.

The predominance of multi-peaked wave spectra is heavily dependent on location, so relative uncertainties associated with single-peaked assumptions are not homogeneous. For example, locations that are fetch constrained will generally result in single-peaked spectra and minimal uncertainty under the single-peaked assumption. However, locations that have vast geographic fetches will experience multi-peaked wave systems more commonly. For example, the west coast of Canada experiences multi-peaked wave systems 67% of the year (Robertson et al. 2016), and the shape and distribution of the variance density can vary dramatically (Fig. 11).

More recently, numerical wave models are using a spectral-partitioning method to improve the representation of the sea state. Spectral partitioning separates the directional wave spectrum and represents each variance density peak, or wave system, individually. The current version of WWIII and the upcoming release of SWAN have built-in spectral-partitioning algorithms to assist with this effort. Wave spectral partitioning has been used in oceanography for over two decades as a

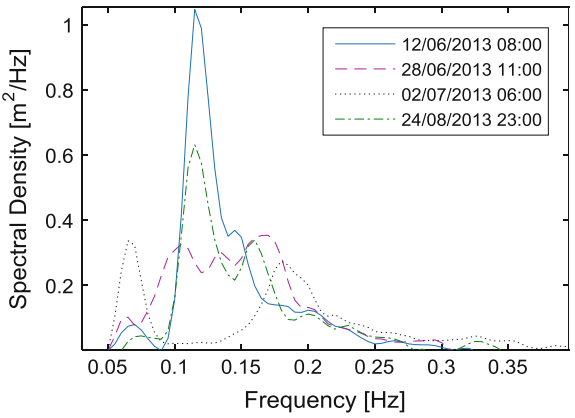

Fig. 11 Variation in nondirectional spectral shapes within single histogram bin (measured by the Amphitrite Bank buoy off the west coast of Canada (WCWI 2016))

post-processing technique to add fidelity to sea state characterizations (Boukhanovsky and Soares 2009; Gerling 1991; Hanson and Phillips 2001; Portilla et al. 2009). The technique has only recently been applied within the wave energy sector (Robertson et al. 2016; Kerbiriou et al. 2007).

The spectral-partitioning method uses the complete directional wave spectrum and incrementally increases a threshold variance density value to find regions of lower variance density (troughs) between two higher variance density areas (peaks). Once a trough is found, the peaks are separated and defined as separate partitions. These separate partitions are recursively searched to find additional troughs. Once all of the partitions are located, a series of filters is applied to determine the discrete wave systems. Gerling recommended that the ratio of discrete peak frequencies needs to be greater than 1.25, the difference between peak directions greater than 20°, and the wave mode weights greater than a factor of 10 in order to be classified as a distinct and separate spectral partition (Gerling 1991). Through the spectral-partitioning process, the variance-weighted T_e or the peak-related T_p both provide a sufficient representation of the frequency distribution of wave energy around the single peak.

Using the same data used to create the histogram in Figs. 4 and 12 provides the histograms for the primary, secondary, and tertiary wave systems. Several important details about the wave climate can be identified in these partitioned histograms: (1) the full range of incoming wave conditions is represented (Fig. 12 correctly identifies waves at 22.5 s, while Fig. 4 has a maximum period of 18.5 s); (2) fidelity in large significant wave height sea conditions is increased by separating the maximum variance density for individual wave systems (represented by system-specific significant wave height); and (3) both the most frequent and most energetic wave individual wave system occurs at lower wave heights. Given that many WEC technologies maximize power generation within narrow wave height and energy period bandwidths, the noted changes in maximum wave height, wave period, and most frequent sea states may alter the physical WEC design and associated dynamics for WECs to be deployed at the location of study.

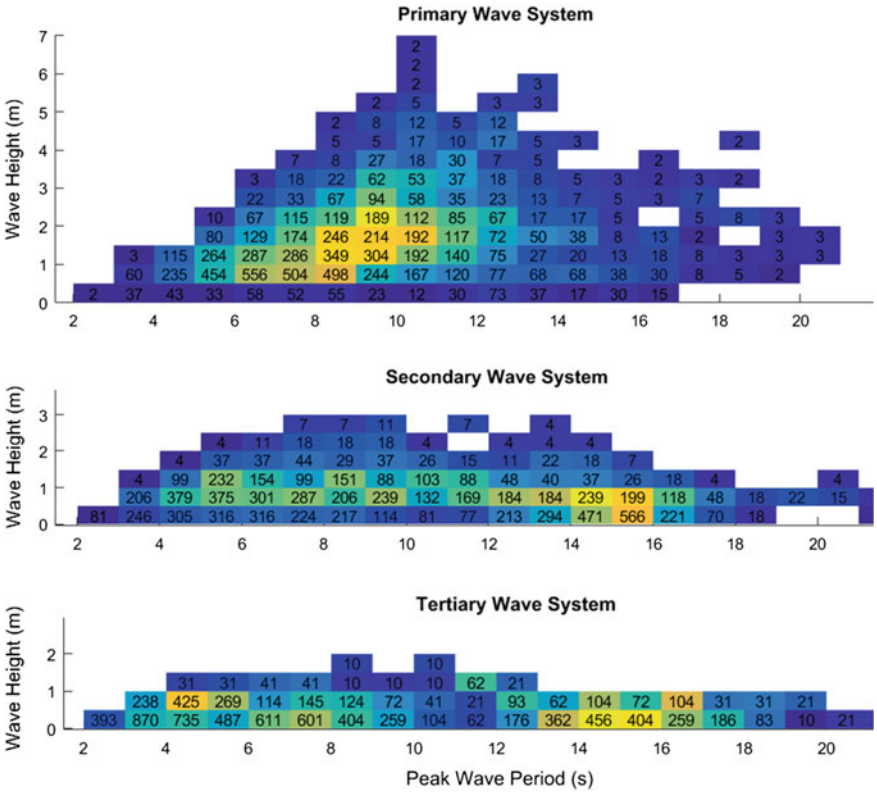

Fig. 12 Primary, secondary, and tertiary wave histogram resulting from spectral partitioning of the directional wave spectrum. Note that the total number of hours is greater than the annual total; this is due to the dominance of multi-peaked conditions in the presented location

Extreme Wave Analysis

Extreme wave conditions are a major cause of concern for developers of WECs and many other ocean users. However, they are often omitted from wave resource assessments because of limited buoy data sets in the region of interest and the current inability of numerical models to accurately recreate extreme wave events. The conditions captured by the IEC-recommended 10-year wave condition database will likely not provide a complete description of all extreme wave conditions; conditions that dominate the structural design, survivability, and true cost of a WEC. (Note that quantifying extreme waves is beyond the scope of the current IEC Technical Specification). Additionally, the accuracy of wave measurements in extreme waves, derived from buoys, satellites, and models remains uncertain, and this is an active area of research by the JCOMM (2014). Quantifying the statistical magnitude and recurrence of extreme wave conditions is a very necessary aspect of determining the suitability of a prospective location for deployment of a WEC.

The statistical analysis of extreme wave conditions is a vast and complex area of study. For a complete investigation and description of extreme value theory, interested readers are directed to (Goda 2009; Coles et al. 2001), and (Vanem and Bitner-Gregersen 2015). To provide an introduction to extreme value analysis and its application in wave resource assessments, two methods are presented here: a univariate peak-over-threshold method and a bivariate inverse first-order reliability method (IFORM).

One of the most fundamental requirements of any extreme wave analysis is that the records must be statistically independent and identically distributed (Holthuijsen 2007). A common method of fulfilling this requirement and allowing for the statistical prediction of extreme wave heights is the univariate peak-over-threshold (POT) extreme value analysis. The POT approach sets a significant wave height threshold and only uses the maximum wave height within this threshold exceedance time period. This method helps satisfy the independence and identical distribution requirements by only using the maximum value from each storm or extreme event. The threshold must be set high enough to ensure independence between samples, yet low enough to ensure the number of samples is sufficient to ensure the resulting statistical distribution fit is statistically robust. It is important to use a sufficiently long data set to allow for proper threshold limits and still allow for robust fitting. Once a suitable "extreme" value data set is generated, a generalized Pareto distribution is recommended as the most appropriate distribution for the POT approach (Coles et al. 2001). Based on the resulting distribution, the return period of a certain significant wave height can then be calculated using Eq. (13):

$$RP_{\underline{H}_{s,peak} > H_{s,peak}} = \frac{\Delta T_{storm}}{1 - P\left(H_{s,peak}\right)_{threshold}} \tag{13}$$

where $RP_{\underline{H}_{s,peak} > H_{s,peak}}$ is the return period (RP) of a significant wave height above a defined value and ΔT_{storm} is the characteristic time between storm events. $P\left(H_{s,peak}\right)_{threshold}$ represents the exceedance probability for a certain wave height from the generalized Pareto distribution (Holthuijsen 2007). The POT methodology allows the resource assessment to present the maximum value for a single wave parameter at specified return periods; for example, the maximum 50-year significant wave height at the La Perouse Bank off the Canadian West Coast is ~11.7 m (NOAA 2016).

However, as frequently noted in this chapter, wave parameters are not independent. The significant wave height and the energy period are, at the very least, intrinsically linked and need to be statistically resolved together to provide accurate representations of extreme wave conditions. Hence, conditional environmental contours of extreme conditions are required to quantify the bivariate distribution of extreme conditions, at specified return periods.

A commonly applied method of developing extreme value environmental contours is the IFORM. For a thorough discussion of the IFORM, readers are directed to (Vanem and Bitner-Gregersen 2015) and (Winterstein et al. 1993; Eckert-Gallup

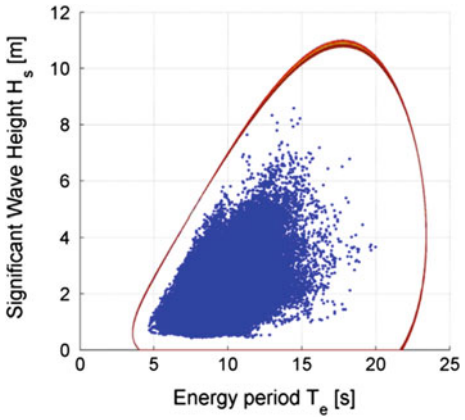

Fig. 13 100-year extreme environmental contour for Humboldt Bay buoy (NDBC 46212) (Eckert-Gallup et al. 2016)

et al. 2016; Veritas 2010). The IFORM initially determines the probability distribution of significant wave height, using all available data. The data set is binned, according to significant wave height values, and individual probability distributions are fitted to the bin-specific energy period data (DetNorskeVeritas suggests using T_p). Thus, the joint probability of significant wave height and energy period within specific bins can be quantified.

A probability contour is defined in standard normal space based on the desired return period. A Rosenblatt (Haver and Winterstein 2010; Vanem and Bitner-Gregersen 2012) or Nataf (Silva-Gonzlez et al. 2013) transformation is used with the joint-probability distribution to transform the contour back into the original parameter space. The fitted joint-probability distributions allow extrapolation of return periods beyond the measured data. An example 10-year return period environmental contour for wave conditions off the west coast of the United States is presented in Fig. 13.

The inclusion of an extreme wave analysis into a high-fidelity wave resource assessment provides WEC technology and project developers with the necessary quantified data to ensure the structural design and survivability of the WEC architecture is suitable for the proposed location. Without detailed extreme value analyses, the risks associated with WEC technology failure are significantly and unnecessarily increased. Different WEC architectures will have differing responses to the extreme sea state energy period; therefore, it is worth noting that the most energetic sea state may not be the most destructive.

Quantifying Environmental Factors

Resolving the temporal and spatial attributes of wave conditions is undoubtedly the primary objective of wave resource assessments, but a host of additional environmental parameters are coupled with these measured wave conditions. The driving

forces behind a 1 m significant wave height with 10 s energy period can vary dramatically. These wave conditions could be driven by locally generated winds or a distant storm combined with local current effects. Without detailed knowledge of local environmental conditions, these conditions cannot be differentiated, despite their significant effect of on the final energy production of WECs.

Relevant environmental parameters include, but are not limited to, local wind speed and direction, tidal current magnitude and direction, and water depth variation. The performance of various WEC architectures will be susceptible to differing environmental conditions. For example, tidal currents can dramatically reduce the dynamic motion of specific WEC moorings and associated power output (Ortiz et al. 2015). Deep draft devices will be most affected by currents, while devices with significant above-water windage will be vulnerable to changes in local wind direction and speed. The inclusion of environmental parameters in the wave resource assessment will help mitigate uncertainty risks in WEC performance estimates in the location of interest.

Traditionally, the assessment of wave and environmental conditions has been conducted as two parallel, independent processes. For example, Zheng et al. (2013), Fusco et al. (2010), and Stoutenburg et al. (2010) all completed independent assessments of wind and wave resources to identify possible priority deployment locations for combined wind-wave converter farms and quantified the reduction in resulting power variability. In reality, these two energy resources are intrinsically linked, and the parallel processes do not provide WEC developers with the necessary data to assist in the design of WEC technologies or help mitigate the uncertainties in final power production estimates.

While a deterministic representation of all combinations of wave, wind, current, and water depth would be ideal, the resulting set of wave and environmental conditions would be immense and too cumbersome for WEC performance assessments. To provide a representation of all of the combinations within individual histogram bins, Bailey et al. (2016) aggregated all wind and tidal conditions within the histogram bin framework and developed a stochastic probability distribution for each environmental parameter. As an example, Fig. 14 presents the measured tidal current speed at Amphitrite Bank (WCWI 2016) within the 1.25 m and 8.5 s histogram bin. A stochastic gamma distribution with shape ($a = 2.49$) and scale ($b = 98.91$) minimized the RMSE between the measured data and stochastic distribution. A similar procedure was used for all other parameters and provided a stochastic representation of wave and environmental parameters.

Bailey et al.'s procedure provides a method for quantifying the distributions of wind speeds and directions, current speeds and directions, and variations in tidal water levels within the existing histogram baseline resource assessment methodology, but numerous additional methods are available. The representation of environmental conditions continues to be an active area of research in wave energy resource assessments and requires further work to improve our characterization of environmental conditions, while reducing the resulting set of defining parameters.

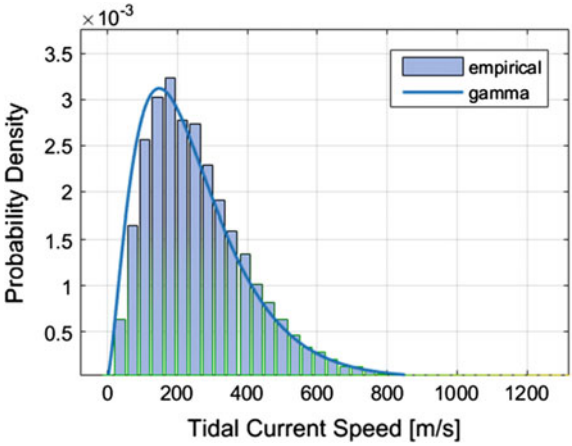

Fig. 14 Probability density function for tidal current speeds at Amphitrite Bank

Impact of Resource Assessment Methodology on WEC Power Production Estimates

In the previous sections, we detailed a baseline wave resource assessment methodology and a number of higher resolution methods. Each method has associated strengths and weaknesses, and the methodology should be adapted according to local wave conditions with the ultimate goal of reducing uncertainty on the true magnitude and distribution of the wave characteristics. From the point of view of WEC architecture or the wave energy project developer, it is arguably more important to understand the impact of the various resource assessment methodologies on the final power production estimates and associated uncertainty than the values presented in the resource assessment. These uncertainties will have a significant impact on the financial viability of the project, power production variability, requirements for grid connection infrastructure, and backup electrical generation.

Prior to presenting results about the impact, it must be well understood that most WEC architectures are designed to respond to specific wave conditions, and the power production impact of resource mischaracterization is heavily dependent on the proposed WEC architecture. This WEC-dependence effect is illustrated by the work of Saulnier et al. (2011). They investigated six different formulations of spectral width (see Eq. (9)) with both a single degree of freedom (DOF) axis-symmetric point absorber and the 6 DOF Système Autonome Electrique de Récupération de l'Energie des Vagues (SEAREV) WEC (Babarit 2005). The best parameterization of spectral width was found to be dependent on the WEC used, yet they suggested ϵ_0 provided a robust estimate for both WECs. This result was confirmed by Hiles et al. (2015), who used the WaveBob-inspired self-reacting point absorber (Beatty et al. 2007) to explore the dependence on a high-order spectral width formulations, ϵ_2 (Saulnier et al. 2011). They found this specific

spectral width formulation to be dependent on frequency-domain cut-off boundaries in the Fourier transformation, and this was inconsistent between different models and buoys—thus resulting in more uncertainty in the final WEC power production than the standard baseline methodology.

With this WEC-dependence in mind, the remaining portion of this section will use a WaveBob-inspired self-reacting point absorber (SRPA) to provide a quantitative comparison between differing resource assessment methods. WaveBob is a two-body axisymmetric point absorber and the pre-commercial wave energy company closed its doors in 2013 (Beatty et al. 2007). The WEC architecture continues to be an active research platform (Beatty 2016).

Robertson et al. (2016) assessed the impact of spectral shape on wave energy production using the WaveBob platform. The results showed that the assumption of a single-peaked JONSWAP or PM spectral shape resulted in significant variation in power output (up to 244%), when compared to the power production derived from the full directional representation of the wave spectrum. However, on an annual basis, the mean power production deviation was limited to just 4.1%, indicating that the assumption of a single-peaked spectrum is suitable for annual predictions but greatly reduces the hour-to-hour variability on the WEC power production—an important differentiation. Using a "best-fit" spectral shape formulation and a single-peaked spectrum, they found negligible differences in both annual and hourly power production.

Eliminating the assumption of a single-peaked wave spectrum and applying a spectral-partitioning algorithm, Robertson et al. (2014) estimated that spectral partitioning reduces WEC power production estimate uncertainty to below 20% (when compared with the production from the measured full directional spectrum). Figure 15 illustrates the WaveBob power production under an assumed single-peaked wave spectrum and the summation of the power production from the two dominant partitioned peaks. It is immediately evident that the baseline resource

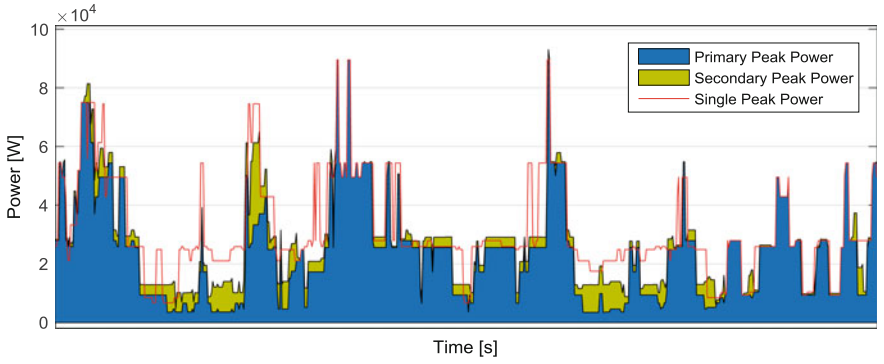

Fig. 15 WEC power production from the assumed single-peaked spectrum and a stacked power production time series from the primary and secondary peaks (discretized using a spectral-partitioning algorithm)

assessment methodology both overpredicts the WEC power production and underpredicts the power variability.

Bailey et al. (2016) assessed the impact of additional environmental conditions on the power performance, again using the WaveBob device. The wave and environmental conditions were directly measured by an in situ wave measurement buoy. They developed stochastic representations of the environmental conditions, within the 1.25 m and 8.5 s histogram bin and conducted a detailed Monte Carlo experiment of ~12,000 simulations. When compared with results from a baseline resource assessment, environmental conditions were found to have a significant effect on final power production. Specifically, they noted that the relative directional difference between the primary wave direction and ambient current direction would significantly affect the performance of the device (a 90° difference would reduce the mean power output by 7.2%). Wave directional spread and the speed of the ambient current were also shown to play a role in adding uncertainty to the final performance of a WEC. Their study concluded that additional environmental conditions should be included in future wave energy resource assessments, rather than focusing solely on wave conditions.

Site Identification for WEC Deployments

Wave resource assessments are conducted with two major goals in mind: 1) provide the necessary quantitative data to identify optimal sites for future WEC deployments and 2) provide an accurate and reliable assessment of wave and environmental conditions at the identified location.

Determining the best locations for future WEC deployment requires a consistent and easily repeatable methodology that exposes technical, environmental, and political constraints. In this section, analyses will focus on the technical constraints of the identification process; the environmental and political aspects are left for later chapters and authors. Examples of technical constraints include the magnitude of the wave energy resource, distance to existing electrical infrastructure, water depth, and probability of extreme wave conditions. Examples of environmental and political aspects include biological species identification, marine protected areas, commercial fishing, or military use areas. The relative impact of the technical aspects are acknowledged to be dependent on the local industry, political landscape, and WEC architecture of choice. Nevertheless, a baseline methodology and procedural framework are valuable for providing guidance for global efforts to identify optimal deployment locations for individual WECs and future WEC farms.

The proposed identification methodology sequentially filters the wave resource assessment data until only regions that satisfy a series of constraints are identified. First, given the high costs associated with procurement and laying of seafloor electrical cables, up to ~USD $1.7 M/km (Kim et al. 2012), it is unlikely that WEC deployment in the far-offshore region will be financially viable initially (Dykes et al. 2002). The added operating and maintenance costs associated with deep water

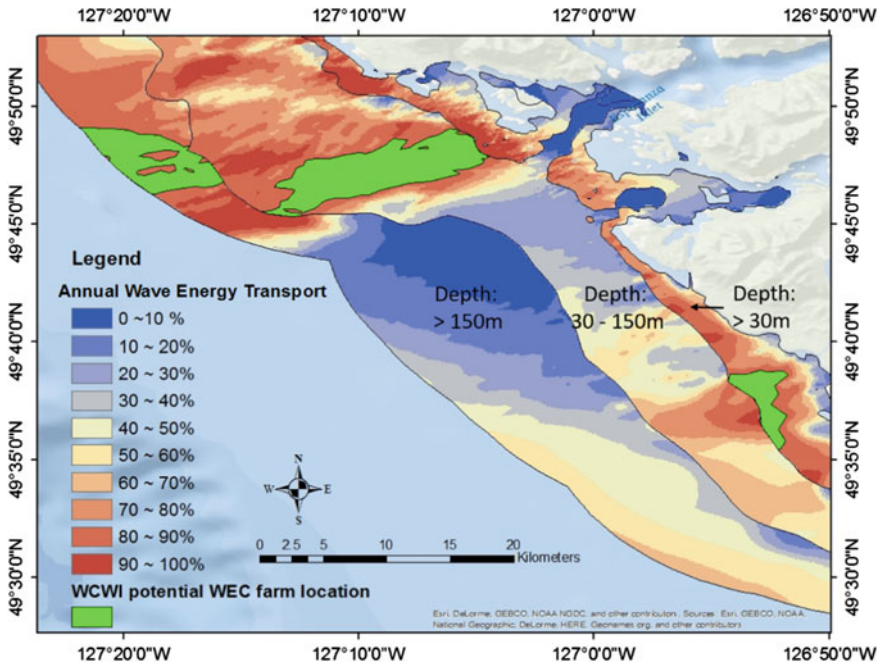

Fig. 16 Possible WEC farm deployment locations on the west coast of Canada. Green identifies farm locations; the *color* map provide percentile wave energy transport; and the depths regions are noted

and far flung sites make these sites increasingly unattractive. Under this constraint, the a priori application of a maximum offshore deployment distance (say, 15 km) greatly reduces the computational effort associated with detailed statistical analysis of the wave climate and wave resource characteristics.

Within the resulting 15 km coastal region, water depth has been used as a proxy for the differing WEC operating and energy extraction principles and fiscal suitability (Boelen et al. 2010). Under this broad generalization, the global suite of WEC architectures can be categorized by their operating depths, and the 15-km-wide coastal region can be divided into distinct depth-correlated regions. The use of this depth/WEC architecture proxy allows the optimal deployment site within each region to be identified. For illustration purposes, Fig. 16 used 0–0 m, 30–150 m, and greater than 150-m-depth regions for characterizing WEC operating depths and as a proxy for WEC architectures.

Within each of these regions, the spatial distribution and magnitude of nearshore wave energy vary dramatically because of bathymetric and coastal topographic features. Ranking the omnidirectional wave energy transport (J) values associated with each computational grid point in each depth region allows for the identification of percentile-based wave energy transport values. For example, Robertson et al. (2002) only used the 90th percentile of wave energy transport grid nodes in their

Table 3 Statistics for identified prospective WEC farm locations

Water depth (m)	Farm area (km^2)	Mean J (kW/m)	Distance to shore (km)	Water depth (m)
0–30	8	35.42	3.26	16.88
30–150	33	39.03	7.58	41.03
>150	19	36.72	13.17	175.96

siting exercise. The analysis will identify not only the value for the 90th percentile wave energy transport, but also the associated spatial area and coast-parallel length. The area and length can be used as secondary proxies for the maximum number of individual WEC deployments within the farm and the rated generation capacity of the farm. Figure 16 illustrates the WEC farm locations identified for the three depth regions off the west coast of Canada, while Table 3 presents the details associated with the differing locations. Note that the annual wave energy transport percentile ranking values in Fig. 16 are depth-region dependent and cannot be compared across regions. In this example, and contrary to conventional wisdom, the deepest site does not have the highest mean wave energy transport and the highest potential for electricity generation. The middle depth site has the highest mean annual wave energy transport and features the largest spatial area and a moderate depth for mooring configurations. The statistics presented in Table 3 provide the baseline information required to help WEC technology and project developers objectively assess the suitability and comparative performance of prospective deployment locations.

The proposed methodology provides a first-pass and rough estimate of prospective WEC deployment sites and the rated capacity of the associated WEC farms. This allows for quick side-by-side comparisons of the costs vs generation potential for potential future WEC farm deployment locations. Note that this method does not take into account the impact of the actual WEC or WEC farm on the ambient wave climate, and, depending on the WEC and number of WECs deployed, will generally result in an overestimation of WEC power production. The modeling of WEC farms is an active area of research (Ruehl 2013; Luczko et al. 2016; Folley and Whittaker 2011) and, undoubtedly, will result in the development of numerical models that can optimize farm layouts and maximize power production for a specific site.

Additional fidelity can be added to the siting methodology through numerous mechanisms. If a specific WEC and associated performance matrix are available, the site can be identified through a percentile analysis of WEC power production, rather than the suggested bulk omnidirectional wave energy transport metric. If multiple prospective sites are identified, the application of an extreme wave analysis will identify the respective probabilities of large and destructive wave events within the prospective regions and provide quantitative technical data for use in filtering unsuitable locations.

Conclusions

Wave energy holds great promise as an abundant, carbon-neutral source of electrical generation. The IEA OES estimates that the annual global wave resource could provide up to 29,500 TWh of electricity (OES 2015). With this energetic climate, there is an opportunity to generate significant quantities of renewable electricity through the use of WEC technologies (Cornett and Zhang 2008; Dunnett and Wallace 2009; Kim et al. 2012; Reikard et al. 2015; Robertson et al. 2013; Hiles et al. 2014). To properly quantify the opportunity for wave energy, a robust and repeatable methodology of quantifying the wave resource is paramount.

The collection of accurate and high-resolution measurements of the wave conditions is a precursor to any resource assessment methodology. Traditionally, measurements of wave condition have been captured through moored wave measurement buoys or seafloor-mounted acoustic measurement devices. Recently, satellite and other remote measurement techniques are becoming increasingly accurate and provide an interesting opportunity for making future spatially expansive measurements. Beyond measurements, a wide variety of numerical models is available to provide the necessary long-term representation of historical sea states over large domains. Large-scale global simulations of wave conditions are generally conducted using WAM or WWIII, while coastal models, such as SWAN and TOMAWAC, are commonly used to provide the additional depth-influenced fidelity at specific sites of interest. All of the models described are 3G models, solve the action balance equation (Eq. 1), and are under constant revision by international experts, whose constant shared objective is to produce better hindcasted realizations of measured wave events.

A wave resource assessment provides a quantitative summary of wave conditions at a prospective WEC deployment site over a period of years. Using decades of full directional wave spectra, a detailed assessment must parameterize the thousands of directional wave spectra into a tractable and tangible baseline parametric representation, while minimizing the uncertainties associated with the parametric representation. The parameterization process inherently discards detailed knowledge of the incoming waves, thereby introducing uncertainty into the final resource assessment. However, it is not feasible to calculate WEC performance estimates in every measured wave spectrum; the actual wave observations have to be condensed to a finite population of cases as represented by the recorded parameter sets. This compromise between accuracy and tractability results in a variety of proposed methods.

The IEC works with international wave energy experts to develop technical standards and specifications to specify a baseline methodology for assessing a wave resource. These methods provide an excellent representation of the wave climate and the necessary detail to predict the mean annual energy production from a WEC. However, the current recommended methodology introduces ambiguity in the estimation of the wave resource and may not provide sufficient detail to resolve the temporal variability within the resulting WEC power production. The requirement

to include additional resource assessment methods, including novel spectral width, spectral shape, and spectral partitioning, would provide additional descriptions of the wave climate with minimal additional descriptive parameters. Extreme wave analysis is a developing field within the wave energy community and benefits greatly from a long history of studies within the oceanographic and naval architecture fields. A univariate POT method and IFORM joint probability were described to provide an introduction to extreme value theory.

An often overlooked aspect of wave resource assessments is the assessment of the environmental conditions concurrent with measurement of the waves. While waves are the main excitation and driving force for WEC power, the impact of local winds, currents, and tides should not be overlooked. In concert with measuring and assessing the wave resource, measurements should be collected for as many additional environmental parameters as possible. Uncertainty in wave measurements, wave model results, and the resource assessment methodology is directly correlated to final WEC power production uncertainty. For the SRPA example, baseline wave resource assessments were shown to overpredict WEC power production and underestimate the temporal variability of the resulting power. These inaccuracies may result in an underprediction of both WEC power production variability and the structural loads to which the WEC will be exposed during operation. Improved wave resource assessment methodologies are constantly evolving in parallel with the maturation of the wave energy industry and access to high-powered computing resources. Therefore, future iterations of the IEC specifications are expected to include the higher fidelity metrics presented in this chapter and are an excellent resource for first-stage assessments.

References

Ayat, B. (2013). Wave power atlas of Eastern Mediterranean and Aegean Seas. *Energy, 54,* 251–262.

Babarit, A. (2005). Optimisation hydrodynamique et controle optimal d'un recuperateur de l'energie des vagues," L'Ecole Centrale de Nantes et l'Universite de Nantes.

Babarit, A., Hals, J., Muliawan, M. J., Kurniawan, A., Moan, T., & Krokstad, J. (2012). Numerical benchmarking study of a selection of wave energy converters. *Renewable Energy, 41,* 44–63.

Bailey, H., Robertson, B., Buckham, B. J. (2016). Optimizing wecs for canadian waters.

Bailey, H., Robertson, B., & Buckham, B. (2016). Quantifying and discritizing the uncertainty in power production estimates of a Wave Energy Converter. In *Marine Energy Technology Symposium (METS)*, pp. 4–6.

Beatty, S. (2016). Experimental comparison of self-reacting point absorber WEC designs.

Beatty, S. J., Buckham, B., & Wild, P. (2007). Modeling, design and testing of a two-body heaving wave energy converter. In *Proceedings of the International Society of Offshore and Polar Engineers, ISOPE 2007, Lisbon Portugal*.

Benoit, M., Marcos, F., & Becq, F. (1996). Development of a third generation shallow-water wave model with unstructured spatial meshing. In *Proceedings of the 25th International Conference Coastal Engineering* (pp. 465–478).

Boelen, M. A., Bishop, I., & Pettit, C. (2010). Selecting offshore renewable energy futures for victoria. *Ekscentar, 13,* 63–67.

Boukhanovsky, A. V., & Soares, C. Guedes. (2009). Modelling of multipeaked directional wave spectra. *Applied Ocean Research, 31*(2), 132–141.

Brodtkorb, P. A., Johannesson, P., Lindgren, G., Rychlik, I., & Rydacn, J. (2000). WAFO—a Matlab toolbox for analysis of random waves and loads. In *Proceedings of the 10th International Offshore and Polar Engineering Conference*, Vol. 3, pp. 343–350.

Cahill, B., & Lewis, A. W. (2014). Wave period ratios and the calculation of wave power. In *2nd Marine Energy Technology Symposium*, pp. 1–10.

Choi, J., Lim, C. H., Lee, J. I., & Yoon, S. B. (2009). Evolution of waves and currents over a submerged laboratory shoal. *Coastal Engineering, 56*(3), 297–312.

Coles, S., Bawa, J., Trenner, L., & Dorazio, P. (2001). *An introduction to statistical modeling of extreme values* (Vol. 208). Springer.

Cornett, A. (2006). *Inventory of Canada's marine renewable energy resources.* National Research Council—Canadian Hydraulics Centre, Ottawa, K1A 0R6, Canada, Report.

Cornett, A., & Zhang, J. (2008). Nearshore wave energy resources, Western Vancouver Island, B. C. Canadian Hydraulics Centre, Report.

Dallman, A., & Neary, V. (2014). Initial characterization of the wave resource at several high energy U.S. Sites. In *2nd Marine Energy Technology Symposium* (Vol. 3, pp. 1–7).

DHI. (2012). Mike 21 Spectral Waves FM—Short Description.

DHI. (2016). MIKE, Powered by DHI, 2016. Retrieved August 12, 2016, from https://www.mikepoweredbydhi.com/.

DNV. (2010). DNV-RP-C205: Environmental conditions and environmental loads. *Norw. DetNorskeVeritas*.

Dunnett, D., & Wallace, J. S. (2009). Electricity generation from wave power in Canada. *Renewable Energy, 34*(1), 179–195.

Dykes, J. D., Hsu, Y. L., & Rogers, W. E. (2002). The development of an operational SWAN model for NGLI. In *Ocean. '02 MTS/IEEE* (Vol. 2, pp. 859–866).

Eckert-Gallup, A. C., Sallaberry, C. J., Dallman, A. R., & Neary, V. S. (2016). Application of principal component analysis (PCA) and improved joint probability distributions to the inverse first-order reliability method (I-FORM) for predicting extreme sea states. *Ocean Engineering, 112,* 307–319.

ECMWF. (2013). Part VII : ECMWF Wave Model IFS DOCUMENTATION—PART VII : ECMWF WAVE MODEL.

EPRI. (2011). EPRI USA Waters Wave Resource Assessment, 2011.

Falnes, J. (2002). *Ocean waves and oscillating systems: Linear interactions including wave energy extraction*. Cambridge University Press.

Folley, M., & Whittaker, T. J. T. (2009). Analysis of the nearshore wave energy resource. *Renewable Energy, 34*(7), 1709–1715.

Folley, M., & Whittaker, T. (2011). The adequacy of phase-averaged models for modelling wave farms. In *ASME 2011 30th International Conference on Ocean, Offshore and Arctic Engineering*, pp. 663–671.

Fusco, F., Nolan, G., & Ringwood, J. V. (2010). Variability reduction through optimal combination of wind/wave resources—An Irish case study. *Energy, 35*(1), 314–325.

Gerling, T. W. (1991). Partitioning sequences and arrays of directional ocean wave spectra into component wave systems. *Journal of Atmospheric and Oceanic Technology, 9,* 444–458.

Goda, Y. (2009). Random seas and design of maritime structures. In *Advanced Series* on *Ocean Engineering* (Vol. 33, p. 708). World Scientific.

Hanson, J. L., & Phillips, O. M. (2001). Automated analysis of ocean surface directional wave spectra. *Journal of Atmospheric and Oceanic Technology, 18*(2), 277–293.

Haver, S., & Winterstein, S. R. (2010). Environmental contour lines—a method for estimating long term extremes by a short term analysis. *Transactions of the Society of Naval Architects and Marine Engineers, 116*(October), 116–127.

Hemer, M. A., & Griffin, D. A. (2010). The wave energy resource along Australia's Southern margin *Jounal of Renewable Sustainable Energy*, *2*(4).

Hiles, C. E., Buckham, B. J., Wild, P., & Robertson, B. (2014). Wave energy resources near Hot Springs Cove, Canada. *Renewable Energy, 71,* 598–608.

Hiles, C., David, A., Guitierrez, D. A., Beatty, S., Buckham, B., & Bc, V. (2015). A case study on the matrix approach to WEC performance characterization. In *European Wave and Tidal Energy Conference*.

Holthuijsen, L. H. (2007). *Waves in oceanic and coastal waters*. Cambridge University Press.

Hughes, M. G., & Heap, A. D. (2010). National-scale wave energy resource assessment for Australia. *Renewable Energy, 35*(8), 1783–1791.

Iglesias, G., & Carballo, R. (2011). Choosing the site for the first wave farm in a region: a case study in the Galician Southwest (Spain). *Energy, 36*(9), 5525–5531.

International Electrotechnical Commission T C 114. (2015). IEC TS 62600-100 Technicial Specification—Part 101: Wave energy resource assessment and characterization. Standard, 2015.

JCOMM. (2014). Joint WMO-IOC technical commission for oceanography and marine meteorology wave measurement evaluation and test. Retrieved from http://www.jcomm.info/index.php?option=com_content&view=article&id=62.

Kerbiriou, M., Prevosto, M., Maisondieu, C., Clement, A., & Babarit, A. (2007). Influence of Sea-States description on wave energy production assessment. In *European Wave and Tidal Energy Conference*.

Kim, C.-K., Toft, J. E., Papenfus, M., Verutes, G., Guerry, A. D., Ruckelshaus, M. H., et al. (2012). Catching the right wave: Evaluating wave energy resources and potential compatibility with existing marine and coastal uses. *PLoS ONE, 7*(11), e47598.

Lenee-Bluhm, P., Paasch, R., & Özkan-Haller, H. T. (2011). Characterizing the wave energy resource of the US Pacific Northwest. *Renewable Energy, 36*(8), 2106–2119.

Liberti, L., Carillo, A., & Sannino, G. (2013). Wave energy resource assessment in the Mediterranean, the Italian perspective. *Renewable Energy, 50,* 938–949.

Luczko, E., Bailey, H., Robertson, B., Hiles, C., Buckham, B. (2016). Assimilating a time-domain representation of a wave energy converter into a spectral wave model. In *International Conference on Offshore Mechanics and Arctic Engineering*, 1–10.

Mackay, E. B. L., Bahaj, A. S., & Challenor, P. G. (2010a). Uncertainty in wave energy resource assessment. Part 1: Historic data. *Renewable Energy, 35*(8), 1792–1808.

Mackay, E. B. L., Bahaj, A. S., & Challenor, P. G. (2010b). Uncertainty in wave energy resource assessment. Part 2: Variability and predictability. *Renewable Energy, 35*(8), 1809–1819.

Monardez, P., Acuña, H., & Scott, D. (2008). Evaluation of the potential of wave energy in Chile. *Omae, 2008–57887,* 1–9.

NOAA. (2016). Station 46206- La Perouse Bank. http://www.ndbc.noaa.gov/station_page.php?station=46206.

Ochi, M. K., & Hubble, E. N. (1976). On six-parameter wave spectra. In *Proceedings of the 15th International Conference on Coastal Engineering*, Vol. 1, pp. 301–328.

OES. (2015). Ocean Energy Systems: Annual Report 2015.

Ortiz, J. P., Bailey, H., Buckham, B., & Crawford, C. (2015). Surrogate based design of a mooring system for a self-reacting point absorber. In *Proceedings of the International Offshore* and *Polar Engineering Conference*, pp. 936–943.

Phillips, J., Cruz, J., Holbrow, R., Parkes, J., & Rawlinson-Smith, R. (2008). Defining the long-term wave resource at wave hub: The role of measurements and models. In *ASME 2008 27th International Conference on Offshore Mechanics and Arctic Engineering*, pp. 645–652.

Piche, S., Cornett, A., Baker, S., & Nistor, I. (2015). Validation of the IEC technical specification for wave energy resource assessment. In *European Wave and Tidal Energy Conference*, 2015, p. 10.

Portilla, J., Ocampo-Torres, F. J., & Monbaliu, J. (2009). Spectral partitioning and identification of wind sea and swell. *Journal of Atmospheric and Oceanic Technology, 26*(1), 107–122.

Reikard, G., Robertson, B., Buckham, B., Bidlot, J.-R., & Hiles, C. (2015). Simulating and forecasting ocean wave energy in western Canada. *Ocean Engineering, 103,* 223–236.

Robertson, B., Hiles, C., & Buckham, B. (2013). Characterizing the Nearshore wave energy resource on the West Coast of Vancouver Island. *Renewable Energy*.

Robertson, B., Hiles, C., & Buckham, B. (2014a). Characterizing the near shore wave energy resource on the west coast of Vancouver Island, Canada. *Renewable Energy, 71,* 665–678.

Robertson, B., Bailey, H., Clancy, D., Ortiz, J., & Buckham, B. (2014). Influence of wave resource assessment methods of wave power production estimates. In *International Conference on Ocean Energy*, pp. 1–19.

Robertson, B., Lin, Y., & Buckham, B. (2015). Application of triple collocation technique to wave resource assessments and wave energy converter energy production. In *14th Workshop on Wave Hindcasting and Forecasting* (p. 23).

Robertson, B., Clancy, D., Bailey, H., & Buckham, B. (2015). *Improved energy production estimates from wave energy converters through spectral partitioning of wave conditions* (p. 8). International Society of Offshore and Polar Engineers.

Robertson, B., Bailey, H., Clancy, D., Ortiz, J., & Buckham, B. (2016). Influence of wave resource assessment methodology on wave energy production estimates. *Renewable Energy, 86,* 1145–1160.

Ruehl, K. (2013). Development of SNL-SWAN. In *European Wave and Tidal*.

Rusu, E., & Soares, C. Guedes. (2009). "Numerical modelling to estimate the spatial distribution of the wave energy in the Portuguese nearshore". *Renewable Energy, 34*(6), 1501–1516.

Rusu, L., & Soares, C. G. (2012). Wave energy assessments in the Azores islands. *Renewable Energy, 45,* 183–196.

Rute Bento, A., Rusu, E., Martinho, P., & Guedes Soares, C. (2016). Assessment of the changes induced by a wave energy farm in the nearshore wave conditions. *Computers & Geosciences*.

Saulnier, J. B., Clment, A., Falco, A. F. D. O., Pontes, T., Prevosto, M., & Ricci, P. (2011). Wave groupiness and spectral bandwidth as relevant parameters for the performance assessment of wave energy converters. *Ocean Engineering, 38*(1), 130–147.

Sierra, J. P., Martín, C., Mösso, C., Mestres, M., & Jebbad, R. (2016). Wave energy potential along the Atlantic coast of Morocco. *Renewable Energy, 96,* 20–32.

Silva-Gonzlez, F., Heredia-Zavoni, E., & Montes-Iturrizaga, R. (2013). Development of environmental contours using Nataf distribution model. *Ocean Engineering, 58,* 27–34.

Smith, H. C. M., Pearce, C., & Millar, D. L. (2012). Further analysis of change in nearshore wave climate due to an offshore wave farm: An enhanced case study for the Wave Hub site. *Renewable Energy, 40*(1), 51–64.

Stopa, J. E., Cheung, K. F., & Chen, Y.-L. (2011). Assessment of wave energy resources in Hawaii. *Renewable Energy, 36*(2), 554–567.

Stoutenburg, E. D., Jenkins, N., & Jacobson, M. Z. (2010). Power output variations of co-located offshore wind turbines and wave energy converters in California. *Renewable Energy, 35*(12), 2781–2791.

SWAN. (2006). SWAN scientific and technical documentation. Delft University of Technology, The Netherlands, Computer Program 41.01A, 2006.

Telemac-Mascaret. (2015). Open TELEMAC-MASCARET, 2015. Retrieved March 31, 2016, from http://www.opentelemac.org/.

Tolman, H. L. (2014). User manual and system documentation of WAVEWATCH III version 4.18.

Torsethaugen, K., & Haver, S. (2004). Simplified double peak spectral model for ocean waves. In *Proceedings of the International Offshore and Polar Engineering Conference*, pp. 76–84.

van Nieuwkoop, J. C. C., Smith, H. C. M., Smith, G. H., & Johanning, L. (2013). Wave resource assessment along the Cornish coast (UK) from a 23-year hindcast dataset validated against buoy measurements. *Renewable Energy, 58,* 1–14.

Vanem, E., & Bitner-Gregersen, E. M. (2012). Stochastic modelling of long-term trends in the wave climate and its potential impact on ship structural loads. *Applied Ocean Research, 37,* 235–248.

Vanem, E., & Bitner-Gregersen, E. M. (2015). Alternative environmental contours for marine structural design—a comparison study. *Journal of Offshore Mechanics and Arctic Engineering, 137*(5), 51601.

Veritas, D. N. (2010). Environmental conditions and environmental loads. *Dnv*, 9–123.

WAMDI. (1988). The WAM model—A third generation ocean wave prediction model. *Journal of Physical Oceanography, 18*(12), 1775–1810.

WCWI. (2016). WCWI Wave Measurement Buoys: Amphitrite Bank, 2016. http://www.uvic.ca/research/projects/wcwi/research/buoy-information/beverley/index.php.

Winterstein, S. R., Ude, T. C., Cornell, C. A., Bjerager, P. , & Haver, S. (1993). Environmental parameters for extreme response: Inverse FORM with omission factors. In *Proceedings of the 6th International Conference on Structural Safety and Reliability, Innsbruck, Austria*.

Zheng, C. W., Pan, J., & Li, J. X. (2013). Assessing the China Sea wind energy and wave energy resources from 1988 to 2009. *Ocean Engineering, 65,* 39–48.

Wave Energy Resources Along the European Atlantic Coast

Philippe Gleizon, Francisco Campuzano, Pablo Carracedo, André Martinez, Jamie Goggins, Reduan Atan and Stephen Nash

Introduction

Requirements for reducing industrial carbon dioxide emissions, together with the depletion of fossil fuel reserves and the need for more secure energy, drive governments and energy industries to diversify their energy sources and consider more sustainable resources. Renewable energy has become a credible alternative to fossil fuels for meeting the increasing energy demand of industrialised societies. Most renewable energy already produced is from hydraulic, wind, and solar power. In contrast, marine energy represents a tiny proportion of current energy production. Yet, the Atlantic Coast of Europe has one of the most important marine renewable energy resources in the world in terms of tidal range such as in the Severn Estuary (UK) or Saint-Michel Bay (France), tidal stream such as in the Pentland Firth (UK) or near Alderney Island (UK/France), and waves.

Conscious of Europe's abundant renewable energy resources, the European Commission has adopted a proactive attitude to encourage, promote, and develop

P. Gleizon (✉)
Environmental Research Institute, University of the Highlands and Islands, Thurso, UK
e-mail: Philippe.Gleizon@uhi.ac.uk

F. Campuzano
Maretec, Instituto Superior Técnico, Universidade de Lisboa, Avenida Rovisco Pais, Lisbon, Portugal

P. Carracedo
Meteogalicia, San Lazaro S/N, Santiago de Compostela, Spain

A. Martinez
EIGSI, 26 rue Vaux de Foletier, La Rochelle, France

J. Goggins · R. Atan · S. Nash
College of Engineering and Informatics and Marine Renewable Energy Ireland Research Centre, National University of Ireland, Galway, Ireland

Z. Yang and A. Copping (eds.), *Marine Renewable Energy*,
DOI 10.1007/978-3-319-53536-4_2

Table 1 Targets of renewable energy source (RES) as a percentage of gross final consumption, and marine energy contribution (installed capacity and gross electricity generation) for the five Atlantic European countries in 2020 and 2015 (NREAP 2010)

	Target—2020			Target—2015		Installed—2014	
	% RES (S_{2020})	Capacity (MW)	Energy (GWh)	Capacity (MW)	Energy (GWh)	Capacity (MW)	Energy (GWh)
France	23	380	1150	302	789	240	414
Ireland	16	500	1533	0	0	0	0
Portugal	31	250	437	60	75	1	0.026
Spain	20	100	220	0	0	0	0
UK	15	1300	3950	0	0	3	2

the production of energy from these resources. The European Union Renewable Energy Directive has set a binding target to all member states of providing 20% of energy supply with renewable energy by 2020 and at least 27% by 2030 (European Commission 2015). Each European country has proposed a National Renewable Energy Action Plan (NREAP 2010) submitted under the Article 4 of Renewable Energy Directive 2009/28/EC, setting their national targets for renewable energy in accordance with their national energy consumption rates and available resources and aligning them with the European targets. Note that the National Renewable Energy Action Plan (NREAP 2010) gives a comprehensive strategy but does not differentiate between the different types of marine energy, and they encompass other marine energy sources such as thermal or osmotic energy.

Table 1 summarises for each of the five Atlantic European countries the targets for the contribution of energy production from renewable sources as a percentage of gross final energy consumption (S_{2020}), and the projected installed capacity and electricity generation of marine energy for 2015 and 2020. Although it has the lowest S_{2020}, the United Kingdom (UK) has the most ambitious targets for marine resource development of the five countries. It plans to increase its capacity by 1300 MW within 5 years. This target is considered achievable because of the abundance of the combined marine energy resources of tidal range, tidal stream, and waves. France already had some marine energy capacity because of the tidal power plant in La Rance estuary. The plant has been operating since 1967 and has a capacity of 240 MW. Portugal developed the first commercial wave site at Aguçadoura (near Porto), which unfortunately was short-lived because of a bearing problem on the first generation of Pelamis attenuators, and has been operating a pilot Oscillating Water Column plant on the Island of Pico (Azores) since 2006. The installed marine capacity in 2015 has not yet been reported, but progress towards targets can be estimated from the 2014 capacity reported to the European Commission (Table 1).

The current contribution of marine energy in the renewable energy scheme remains limited compared to other renewable sectors. Tidal energy is geographically constrained to few sites where available energy is sufficient to make the sites

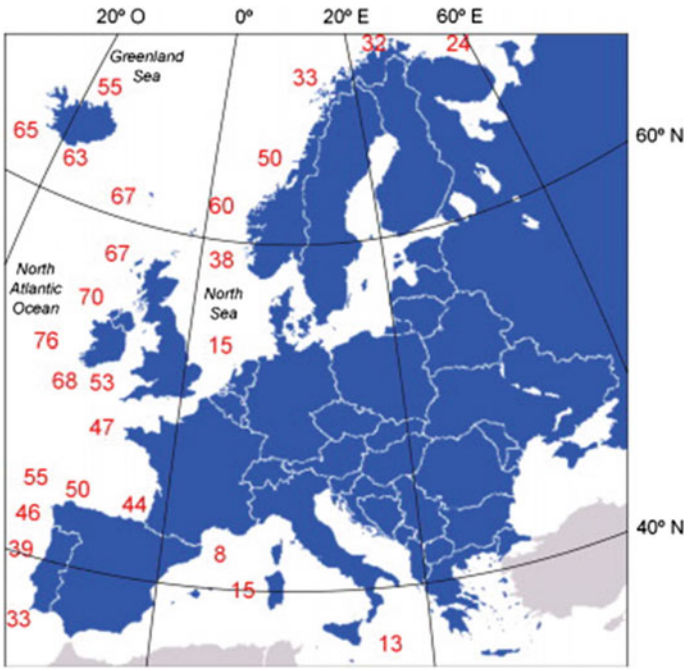

Fig. 1 Estimated annual mean power distribution in Europe (Lopez et al. 2013)

profitable. Conversely, the wave resource is more widely distributed and is therefore a promising source of energy, but the distribution of wave activity depends largely on the fetch and is mainly concentrated between 30° and 70° north and south latitudes (Barstow et al. 2008, 2009). A bulk estimate of the annual wave power distribution in Europe shows that it can reach up to 76 kW/m off the western coast of Ireland (Fig. 1). However, the commercial development of this source of energy is likely to be one of the latest due to (1) its relatively recent technological development and therefore the relative lack of tried and tested engineering solutions and (2) the uncertainty of resource availability mainly because of the inherent unpredictability of long-term wind and therefore wave climate. Therefore, a thorough evaluation of the resources is essential to assessing the energy yield of a potential site.

The transnational project EnergyMare was commissioned to investigate the potential of marine renewable resources along the European Atlantic Coast, to test innovative monitoring techniques and to promote the development of test sites. Through a collaborative partnership, existing computing and monitoring resources have been combined to produce a comprehensive picture of the wave resources on the European Atlantic shelf that provides both a holistic description of the wave climate and detailed maps of sites of potential interest.

Fig. 2 Atlantic Europe general view

The European coastline shows an irregular outline in the most exposed regions of western Scotland (UK), western Ireland, Bretagne (France), and Galicia (Spain) (Fig. 2). These regions are characterised by rocky shores and a succession of cliffs, rock outcrops, and sandy bays. These coastal features reveal the presence of high wave activity on a geology dominated by igneous or metamorphic rocks (May and Hansom 2003). In addition, there are more than 700 islands around Scotland, most of them distributed in three major archipelagos—the Shetlands, Orkneys, and Hebrides. The coast of Galicia is also irregular, featuring the presence of numerous headlands and rías (inlets), such as the Rías Baixas in the west. It is more open than the Scottish Coast and features longer stretches of sandy bays. Except in the Lisbon–Setubal area, the Portuguese coastline is more linear, but the bathymetry

Fig. 3 Bathymetry offshore the Portuguese coast (Fig. 2 *red inset*)

reveals the presence of three sets of submarine canyons near the coast: Nazaré Canyon, Lisbon and Setubal Canyons, and St. Vincente Canyon (Fig. 3). The bathymetry near the canyons deepens quickly from 50 m on the continental shelf to more than 300 m at the bottom of the canyon (e.g. Nazaré Canyon). Although they generally have very minor impacts on wind waves, under specific swell conditions, these canyons create conditions for occasional giant local waves (30 m) well known to surfers.

These coastal and bathymetric irregularities can influence the wave patterns near the coast and consequently introduce small-scale variability in wave energy distribution. Getting refined estimates at the areas of interest is therefore of prime interest for the wave industry, stakeholders, and regulators.

A description of wave resources can be obtained from long-term hindcasts of spectral wave models and can be supported by monitoring data. Third-generation spectral models have become the state of the art in wave modelling. Few of these models have emerged from the same fundamental equations and processes. The most common are the WAve Model (WAM), WaveWatch III, Simulating WAves Nearshore (SWAN) model, TELEMAC-based Operational Model Addressing Wave Action Computation (TOMAWAC), and MIKE21-SW. A more comprehensive description of these models is given in a previous chapter by Robertson (2016).

The first comprehensive description of wave energy resources in Europe was provided by the Wave Energy Resource Atlas (WERATLAS) project (Pontes 1998)

funded by the JOULE/THERMIE programme. The WAM was used to calculate the wave parameters, significant wave height H_s, mean wave energy period T_e, peak period T_p, mean direction θ_m, and energy flux per unit crest length P_w over the European continental shelf (49°W–45°E; 26.5°N–73°N). The values were calculated based on 85 data points of which 41 were in the Atlantic Ocean. Data collection, analysis, and interpretation were performed over the period from 1987 to 1994 for the Atlantic Ocean. WERATLAS gave the first wave hindcast at a synoptic scale but on a coarse grid (Pontes 1998; Pontes et al. 1998). The planning and development of energy sites requires finer characterisation of the wave energy to optimise the cost/benefits by selecting the most appropriate devices and array layouts. In particular, a finer wave resource characterisation could be needed in the presence of irregular coastline or complex bathymetry, which can affect the wave characteristics over short distances.

To complete a fine-resolution assessment of the wave resources at a local scale, state-of-the-art wave models were applied on unstructured or high-resolution structured meshes (see Bertotti and Cavaleri 2012). Venugopal and Nemalidinne (2015) set the spectral wave module MIKE21-SW of the MIKE21 modelling suite (DHI 2007) on an unstructured grid over the UK/Scotland waters, with fine-resolution characterisation down to 0.0005 square degrees in the Orkneys and Pentland Firth waters. The boundary conditions for this model were taken from predictions of a large-scale MIKE21-SW model extending over the North Atlantic Ocean and the North Sea (10°N–70°N and 75°W–10°E). The UK model was run for short periods during 2011 and 2012, and it was successfully validated against wave buoy data recorded at five locations around Scotland. The validation produced correlation coefficients that were higher than 0.96, for the significant wave height. The spatial distribution of the mean significant wave height and wave power around Scotland was found to be consistent with the atlas of UK renewable energy (ABP MER 2008), but with a much higher resolution, because the maps from the atlas are based on a 12 km model grid resolution in coastal areas. The wave power distribution was lowest on the eastern coasts of Scotland and highest on the western coasts, where the mean was estimated to be between 40 to 45 kW/m and the maximum values were estimated to be up to 650 kW/m near the Hebrides and Shetlands shores during January–December 2010.

Guillou and Chapalain (2015) implemented the nearshore spectral wave model SWAN on an unstructured mesh over the Sea of Iroise, in western Brittany, France, with the cell edges varying from 10 km offshore to less than 300 m nearshore. The wave power was averaged over a 7-year (2004–2011) hindcast modelling period. This regional wave model was driven by three-hour time interval wind data at a spatial resolution of 10 km obtained from Météo-France's meteorological model ALADIN, and wave components (significant wave height, peak period, peak direction, and spreading) predicted by a regional run of the large-scale spectral wave model WaveWatch III with a spatial resolution of 18 km and a temporal resolution of 3 h. The validation of the model predictions against nine wave buoy measurements gave values of Pearson correlation coefficient between 0.88 and 0.98 for the significant wave height and between 0.5 and 0.78 for the peak period.

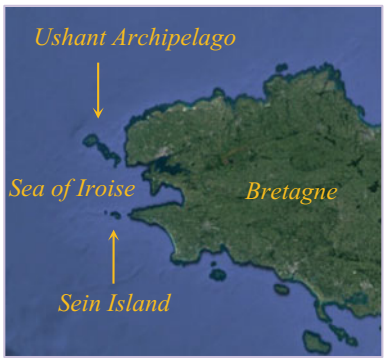

Fig. 4 Brittany (Fig. 2 *white inset*)

The annual mean wave power near the coast showed a strong variability around 20 kW/m, influenced by the shadowing effect of the Ushant Archipelago in the north and Sein Island in the south (see Fig. 4). Seasonal variations show a marked difference between the summer months when wave activity is consistently low, and winter months when wave activity is high on average but less consistent from one year to another. In a parallel study, Guillou (2015) investigated the difference between the third-generation spectral wave models SWAN and TOMAWAC, using the same grid, input data, period of simulation, and the most accurate parameterisation for both models. The comparison between these two models revealed that SWAN gives lower estimates of mean wave power in offshore waters than TOMAWAC but similar estimates in onshore waters. The comparable results for the significant wave height in offshore waters suggest that the main difference could be due to the computational methods used for wave period or the energy propagation.

Iglesias et al. (2009) investigated the wave energy potential in Galicia using the nearshore spectral wave model SWAN (Booij et al. 1999) on a 200 × 200 m grid. The open boundary conditions were provided by a large-scale WAM (18°N–69°N and 60°W–9°W) with a coarser resolution of 0.25° (approx. 30 km). The model was run over the period from 1996 to 2005 to derive a hindcast for the wave climate and wave power at various sections of the Galician coast (for locations, see Figs. 2, 13, and 15g)—Costa de la Muerte (Iglesias and Carballo 2009), Cape San Adrian to Cape Ortega (Iglesias et al. 2009), and Estaca de Bares area (Iglesias and Carballo 2010c). The model was extended to the north coast of Spain to the Asturias coastal region (Iglesias and Carballo 2010a) and the Bay of Biscay (Iglesias and Carballo 2010b). These fine-scale models applied near an irregular coastline and in the presence of a highly variable bathymetry showed that the wave energy potential can be doubled or halved over distances of only few kilometres, due to refraction, shoaling, bottom friction, sheltering, and diffraction from islands and headlands.

These studies emphasise the variety of spectral wave models and their range of applications. Although all of these third-generation spectral models use the same fundamental formulation to represent wave propagation—here the spectral action balance equation—they may differ in their numerical techniques or their

representation of source–sink terms, for instance, for the wind input, whitecapping, or nonlinear wave–wave interactions (WISE Group 2007).

The existing wave models, developed by the EnergyMare project partners, used primarily WaveWatch III and SWAN, which were combined to provide a holistic view and a detailed description of the wave resources along the Atlantic Coast. In the next section, the commonalities and differences of the relevant spectral wave models are presented, with an emphasis on WaveWatch III and SWAN. This introduces a more specific description of each model and its validation against monitoring data when applicable. In the last section, the spatial distribution and temporal variability of wave energy resources across areas of the European Atlantic coastal waters, based on medium-/long-term hindcast, are presented in term of resource availability and risk to installations.

Spectral Wave Modelling

Overview of Models

The third-generation spectral wave models, developed in the late 1980s, allow for free development of the wave spectrum without any specific shape constraint. In particular, they include the energy transfer between resonant frequencies from quadruplet wave–wave nonlinear interactions (Haselmann 1962).

The so-called progressive wave models, such as WAM (WAMDI Group 1988) or WaveWatch III (Tollman 1990), are suitable for modelling wind waves in deep seas; they proved to be less accurate in coastal waters for reasons that are presented later. The SWAN model was specifically designed based on the initial WAM source code to improve wave prediction capability nearshore (Booij et al. 1999), but it is less suitable for modelling waves in the open ocean. From this point of view, estimating the wave energy resource both on synoptic and local scales can be challenging and may require a combination of the different models.

WAM

The first spectral wave model WAM was developed by the so-called WAMDI Group (WAMDI Group 1988) and is still operated by the European Centre for Medium-Range Weather Forecasts (ECMWF), which provides wave hindcast data over the global ocean and on nested domains such as the North Atlantic Ocean. The action density balance Eq. (1) is solved by a two-time level fully implicit integration scheme (Hersbach and Janssen 1999):

$$\frac{\partial N}{\partial t} + \overrightarrow{\nabla_{\vec{x}}} \cdot \left(\left(\overrightarrow{c_g} + \vec{U} \right) \cdot N \right) + \frac{\partial c_\sigma N}{\partial \sigma} + \frac{\partial c_\theta N}{\partial \theta} = \frac{S_{tot}}{\sigma} \quad (1)$$

where $N(\vec{x}, t; \sigma, \theta)$ is the action density defined from the energy density $E(\vec{x}, t; \sigma, \theta)$ by $N = \frac{E}{\sigma}$ and depends on space $\vec{x}$, time t, frequency σ, and direction θ; $\overrightarrow{c_g}$ is the group velocity in the physical space; $\vec{U}$ represents a current velocity; c_σ and c_θ are the wave propagation velocity components in the spectral space, for frequency and direction, respectively; and S_{tot} encompasses all of the source/sink terms.

Besides the quadruplet wave–wave nonlinear transfer, the source/sink terms include whitecapping, bottom friction, duration, and fetch-limited growth from wind friction, which also takes into account the effect of wind gustiness and air density. Wave generation includes both linear (Cavaleri and Malanotte-Rizzoli 1981) and exponential growth (Komen et al. 1984) caused by wind stress. The model is operated on regular meshgrid. The WAM model proved to be reliable for deep water and therefore the open ocean, but the absence of shallow-water processes, such as depth-induced breaking or triad nonlinear wave interactions (Booij et al. 1999), made the model less accurate nearshore, in spite of late implementation of a depth-controlled algorithm for maximum wave energy and frequency down shifting. The impact of currents on waves is often minimal except in shallow nearshore areas, in particular inside the entrance of bays and harbours where tidal currents can be strong (Yang and Wang 2015).

WaveWatch III

Soon after WAM became operational, the National Oceanic and Atmospheric Administration (NOAA) developed the spectral wave model WaveWatch III to account for wave–current interactions in unsteady conditions (Tolman 1990). The main difference between the WAM and the WaveWatch III model is their numerical technique. Due to their complexity, the numerical schemes used by WaveWatch III cannot be detailed but, in summary, it calculates the solution of the action density balance Eq. (1) using a time-splitting approach. Four different time steps are used:

- a global time step in which the entire solution is propagated, which includes winds and currents;
- a time step for spatial propagation; this time step is adjusted on the wave frequencies to ensure numerical stability and optimise the computing time;
- a time step for the intra-spectral propagation; and
- a time step to integrate the source terms, giving more accurate calculations for rapidly changing wind and wave conditions.

The default numerical scheme for wave propagation in WaveWatch III is the ULTIMATE QUICKEST scheme (Leonard 1979, 1991) implemented both for the physical space and for the directional space (θ-space). In the frequency space

(σ-space), the scheme is adapted to take into account variable grid spacing, and a first-order upwind scheme is used for the lowest and highest wave numbers. These numerical techniques result in a more accurate replication of peak values and give a better representation of rapidly changing wind and wave conditions. Until recently, WaveWatch III could only be implemented on rectangular grids, but the newest version 4.18 can be set up on an unstructured grid (Roland 2009).

SWAN

The spectral wave model SWAN was developed from WAM to improve the accuracy of spectral wave modelling in the nearshore zone. Therefore, it uses the same scientific background and equations, but includes additional functionality such as triad wave–wave nonlinear interactions and depth-induced wave breaking (Booij et al. 1999). Recently, SWAN has also been designed to run on unstructured grids, which provide a more suitable resolution nearshore especially in the presence of irregular coastlines (Zijlema 2010).

The option of implementing SWAN on either structured or unstructured meshgrid has been a major improvement to the model. Unstructured meshgrids were essentially used in finite element models such as TOMAWAC (Robertson 2016). Tuomi et al. (2014) tested the response of a spectral wave model (WAM) on a structured grid over an archipelago in the Gulf of Bothnia (Baltic Sea). They demonstrated that the model overestimated the wave energy propagating through the archipelago mainly because of slight inaccuracies in the representation of refraction and dissipation effects. The predictions are improved by using finer grids but at considerable expense of computing time. Unstructured grids allow for fine-resolution mapping nearshore and a better representation of convoluted coastlines, resulting in improved predictions as shown in the wave resource assessments of Robertson et al. (2014, 2016) conducted on the western coast of Vancouver Island, Canada. Implicit schemes are generally used with unstructured grid to avoid stability restrictions imposed by the Courant–Friedrichs-Lewy criterion. For the equation discretisation, SWAN uses an implicit Euler scheme solved by a three-direction sweep Gauss–Seidel relaxation technique to ensure a convergence of the solution for all grid points (Zijlema 2010). To avoid instability problems, the model does not allow triangular elements that have an angle wider than 143°.

Different numerical schemes are used for discretising the equations, depending on the type of simulation, node location, and user choice. First, a fully implicit first-order upwind scheme, which is robust and unconditionally stable but introduces numerical diffusion, was implemented (Booij et al. 1999). This scheme provided an accurate enough solution for wave propagation in the geographical space, but the spectral space required higher accuracy. More advanced schemes were introduced to improve the accuracy. For instance, nonstationary computations use the Stelling and Leendertse scheme (Stelling and Leendertse 1992), except next to boundary nodes where the first-order upwind scheme applies. The Stelling and

Leendertse scheme is known to have such a small numerical diffusion that it can generate a so-called garden sprinkler effect due to spectral resolution over large grid intervals. To counteract that effect without increasing the numerical diffusion too much, a diffusion tensor can be added to the propagation equation (Booij and Holthuijsen 1987; Tolman 2002). In a more recent development, limiters were introduced to reduce local errors due to excessive transfer of energy in the spectral propagation by refraction or frequency shifting where the bathymetry representation is too coarse (Dietrich et al. 2013).

Model Set-up and ValidationModel Set-up and Validation

To obtain wave statistics along the European Atlantic Coast, wave hindcast modelling was carried out using WaveWatch III and SWAN over five distinct coastal zones: Scotland (UK), Ireland, France, Galicia (Spain), and Portugal.

Scotland

The irregular coastline of Scotland and the presence of archipelagos required that the model be run over an unstructured grid to provide good nearshore resolution without affecting computing time too much and to represent more accurately the attenuation of wave energy through the archipelagos (Tuomi et al. 2014). The hindcast was therefore performed by running SWAN on an unstructured mesh extending from 10° to 0°W and from 56° to 62°N (Fig. 5). The grid has

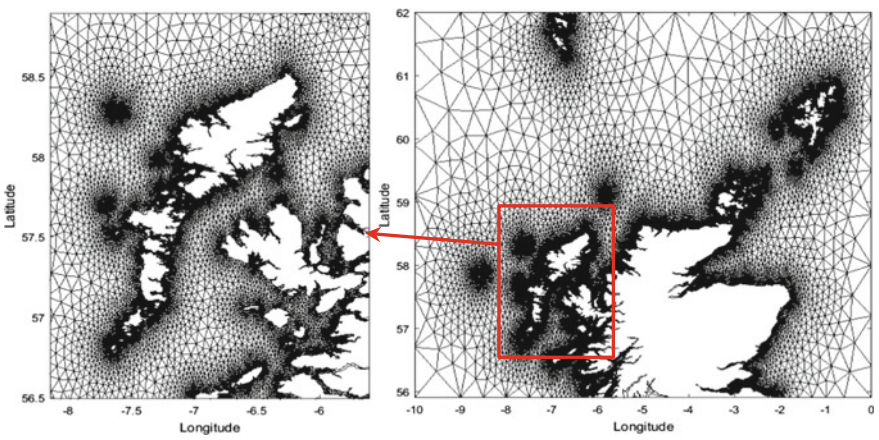

Fig. 5 Meshgrid for the Scotland wave model for the entire domain (*right*) and a detailed view of the Hebrides Islands (*left*)

approximately 48,000 nodes and more than 83,000 elements with a minimum edge of ~ 50 m. The model was run with a time interval of 3 h over a 10-year period (2004–2014).

The bathymetry was obtained from three different sources and at three different resolutions:

- SeaZone—1 arc second, for coastal areas and around archipelagos where the grid has the finest resolution;
- SeaZone—30 arc seconds, for nearshore areas covering most of the Scottish shelf; and
- GEBCO (General Bathymetric Chart of the Oceans)—1 arc minute, for the remaining offshore areas mainly near the northern, north-western, and eastern boundaries where the grid is coarser.

The bathymetry data were then averaged over the Voronoï cells related to the grid and integrated with the model.

Wind forcing uses 10 m elevation wind obtained from ECMWF reanalysis data on a 0.75° grid interval and 3-hour time interval. Sensitivity tests performed using the National Aeronautics and Space Administration's Modern Era Retrospective-analysis for Research and Applications (MERRA) reanalysis wind data at the same elevation but with finer spatial (0.5°) and temporal (1-hour) resolution did not show much difference in the model results. However, the use of this fine-resolution data significantly increased the computational time, so the simulations were carried out using wind forcing from ECMWF wind data.

As presented by Gleizon and Woolf (2013) and Gleizon and Murray (2014), swells can travel long distances and influence wave energy even in the centre of the domain of a model of that scale. Wave boundary conditions were obtained from the predictions of a large-scale model (WaveWatch III) covering the North Atlantic basin and were specified as two-dimensional energy density spectra.

In addition to wave generation by wind forcing, the parameterisation of the model included other source/sink processes: triad and quadruplet wave–wave nonlinear interaction; bottom friction using a JONSWAP (Joint North Sea Wave Project) formulation with a constant friction coefficient of 0.038 m^2s^{-3}, which can be applied both for wind waves and for swell conditions (Hasselmann et al. 1973); whitecapping using a nonlinear saturation-based formulation (Van der Westhuysen et al. 2007); and wave breaking. However, sensitivity tests showed that these effects are minor compared to the generation by wind forcing and the boundary conditions.

The development of the model was supported by extensive wave monitoring data in the early 2010s. The locations, monitoring periods, and responsible institutions for the control of the wave buoys are listed in Table 2 and depicted in Fig. 6. The moored buoy K7, maintained by the UK Met Office, has been the longest operating buoy in the area and is part of a national meteorological surveillance network.

More accessible are the historical data from the Centre for Environment, Fisheries and Aquaculture Science (CEFAS) WaveNet directional waverider buoys. WaveNet is a strategic wave monitoring network for the UK. North of Scotland,

Table 2 Wave monitoring period and location

Source	Location	Period	Long.	Lat.
ERI	Brim Ness	02/13–08/13	3.75°W	58.63°N
	Dunnet Bay	12/12–08/13	3.44°W	58.64°N
	Pentland F	01/12–07/12	3.28°W	58.68°N
	Wick	01/12–07/12	2.79°W	58.46°N
LCC	Bragar	10/11–09/12	6.91°W	58.43°N
	Siadar	10/11–09/12	6.72°W	58.50°N
CEFAS (WaveNet)	South Uist	02/09–05/12	7.91°W	57.29°N
	Moray F.	08/08–09/12	3.33°W	57.97°N
	Dounreay	10/97–05/01	3.75°W	58.59°N
Met Office	K7 buoy	04/92–11/01	4.50°W	60.70°N

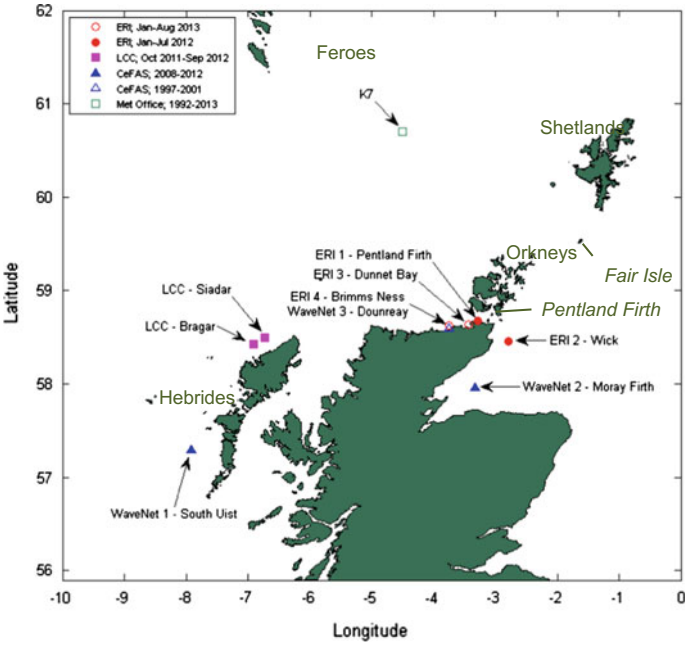

Fig. 6 Wave buoy locations

only three buoys were deployed from the late 1990s up to today; they are in the West Hebrides (WMO ID: 62048; referred here as South Uist), Moray Firth (WMO ID: 62046), and Dounreay (decommissioned in 2001).

Complementary wave data were provided by Lews Castle College (LCC)[1] who deployed directional Datawell waverider buoys MKIII off the north-east of Lewis

[1]University of the Highlands and Islands.

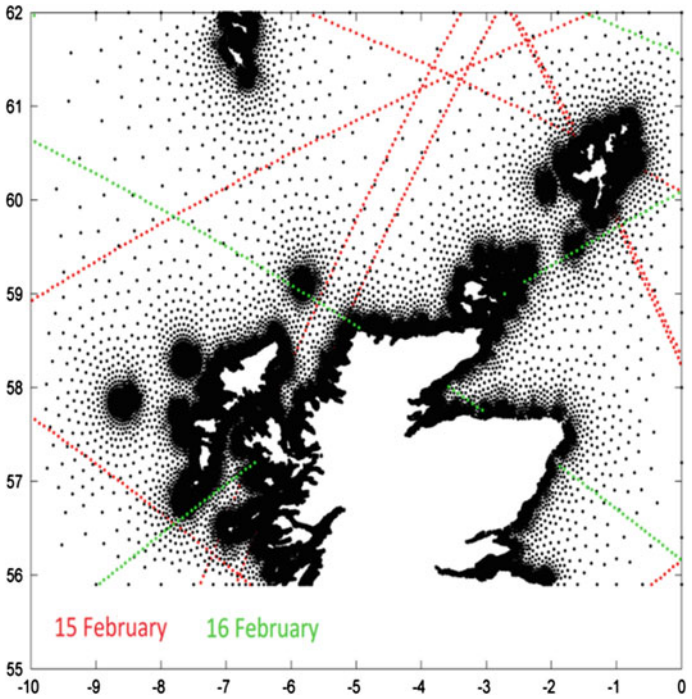

Fig. 7 Satellite altimeter passes on 15 and 16 February 2011. The black dots indicate the model grid nodes

Island (Outer Hebrides) in 2011/12 at Bragar and Siadar. The records gave a range of statistical and spectral data.

Finally, the Environmental Research Institute (ERI)[2] deployed directional buoys MKIII for 6-month periods in 2012/13 at four different locations along the northern coast of Scotland: Brim Ness, Dunnet Bay, Pentland Firth, and Wick.

In addition to wave buoys, wave data were obtained from the CERSAT (Centre d'Expertise et de Recherche Satellitaire) database of the IFREMER (Institut Français de Recherche pour l'Exploitation de la Mer). The CERSAT database provides processed altimetry data collected from operational altimeter satellites (Piollé and Croizé-Fillon 2012). For the purpose of model validation, altimetry data for 15⁻16 February 2011 were downloaded from the database. These data, recorded by four altimeter satellites (ERS2, ENVISAT-GDR, Jason-1, Jason-2) during 11 passes during that period, give good coverage of the model domain (Fig. 7) that is complementary to the wave buoy data, in particular for offshore locations.

The model predictions are in a good agreement with monitoring data, as revealed by the coefficient of determination R^2 values, which are between 0.81 and 0.91 for

[2]University of the Highlands and Islands.

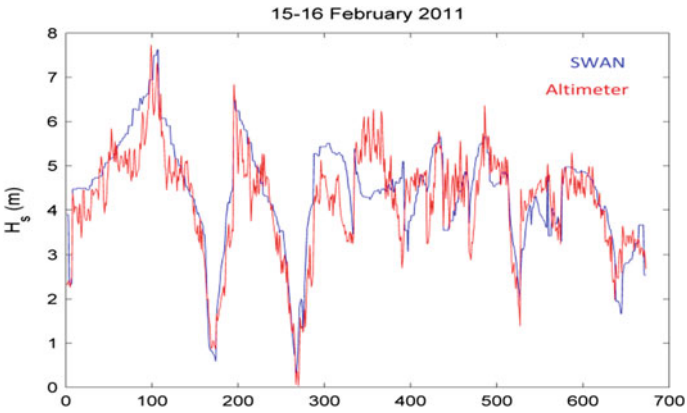

Fig. 8 Comparison of predicted significant wave height with altimetry data on 15–16 February 2011

the significant wave height and between 0.6 and 0.79 for the mean period (Gleizon and Murray 2014).

The validation against altimetry data is more complex because the relevant model results must be extracted to coincide with time and space with the satellite passes. It was nonetheless possible to get a comparison with 681 points during two days of satellite passes (15–16 February 2011) that shows a good replication of observed significant wave height (Fig. 8).

Ireland

The SWAN model was implemented on a regular grid with a grid interval of 0.05° (~ 5.5 km in latitude and ~ 3.3 km longitude). The domain covers a large area around Ireland and over the Atlantic Ocean from 20°E to 3°E, and 50°N to 59°N (Fig. 9). The bathymetry with a resolution of 1 arc minute was obtained from the NOAA Centers for Environmental Information. The wind forcing was provided by ECMWF Era-Interim data with a spatial resolution of 0.5 degrees and a time interval of 6 h. The wave boundary conditions were obtained from global Wave-Watch III model data at 6-hour time interval, provided by the Fleet Numerical Meteorology and Oceanography Center. The model was run with a time interval of 1 h over a 7-year period (2008–2014).

Model calibration process involved a substantial number of sensitivity tests on model parameters, such as wind input, wave growth formulations, whitecapping, and bottom friction coefficients. The modelled output was compared to available data collected from four wave buoys off the Irish western coast (Fig. 9). The model calibrations show good correlation with monitoring data; the coefficient of determination R^2 value is 0.9 for the significant wave height Hs and the R^2 value is 0.8 for the mean period Tz at almost all four sites (Atan et al. 2015).

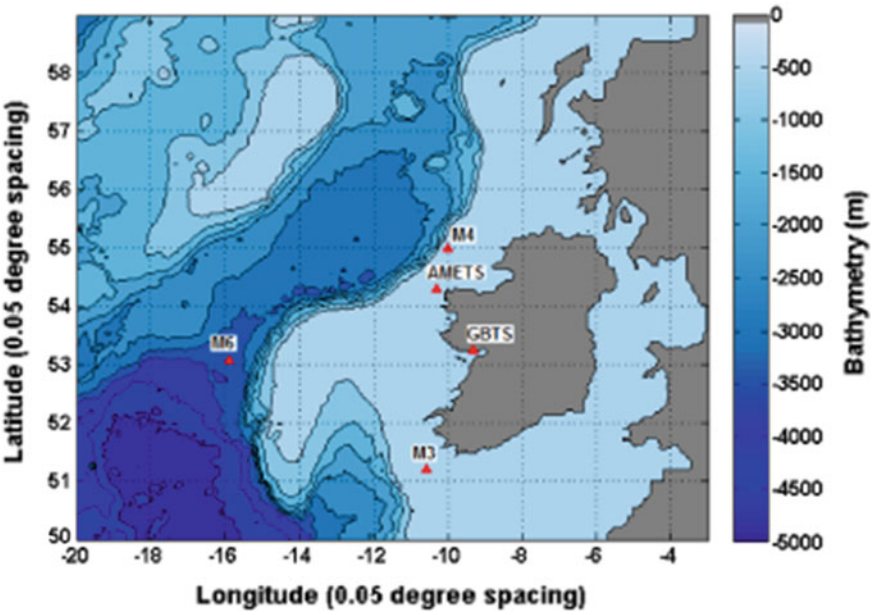

Fig. 9 Irish model domain and wave buoy locations

France

The wave hindcast along the French coast was imported from the Previmer database. The hindcast was initially carried out by WaveWatch III over nine fine-resolution (200 m) regular grids covering the French coast from Dover Strait to the Bay of Biscay with a time interval of 1 h (Fig. 10). These grids were nested in a larger model domain extending from 10°W to 12°E and from 43°N to 58°N with a coarser grid resolution (4 km) and time interval (3 h). Wave hindcasts were obtained for a 7-year period, from 2008 to 2014.

The validation of the model predictions was done on a routine basis using data from Météo-France, CEREMA (Centre D'Étude et D'Expertise sur les Risques, L'Environnement, la Mobilité et l'Aménagement), ports and harbours for coastal validation, and IFREMER altimetry data for offshore validation. The models are also used to provide near-real-time forecasts of sea state.

Galicia

The spectral wave model SWAN was applied on a high-resolution unstructured grid along the Galician coast to provide near-real-time wave forecast. The modelling domain extends up to 40 km offshore. The grid has a resolution from 100 m near the

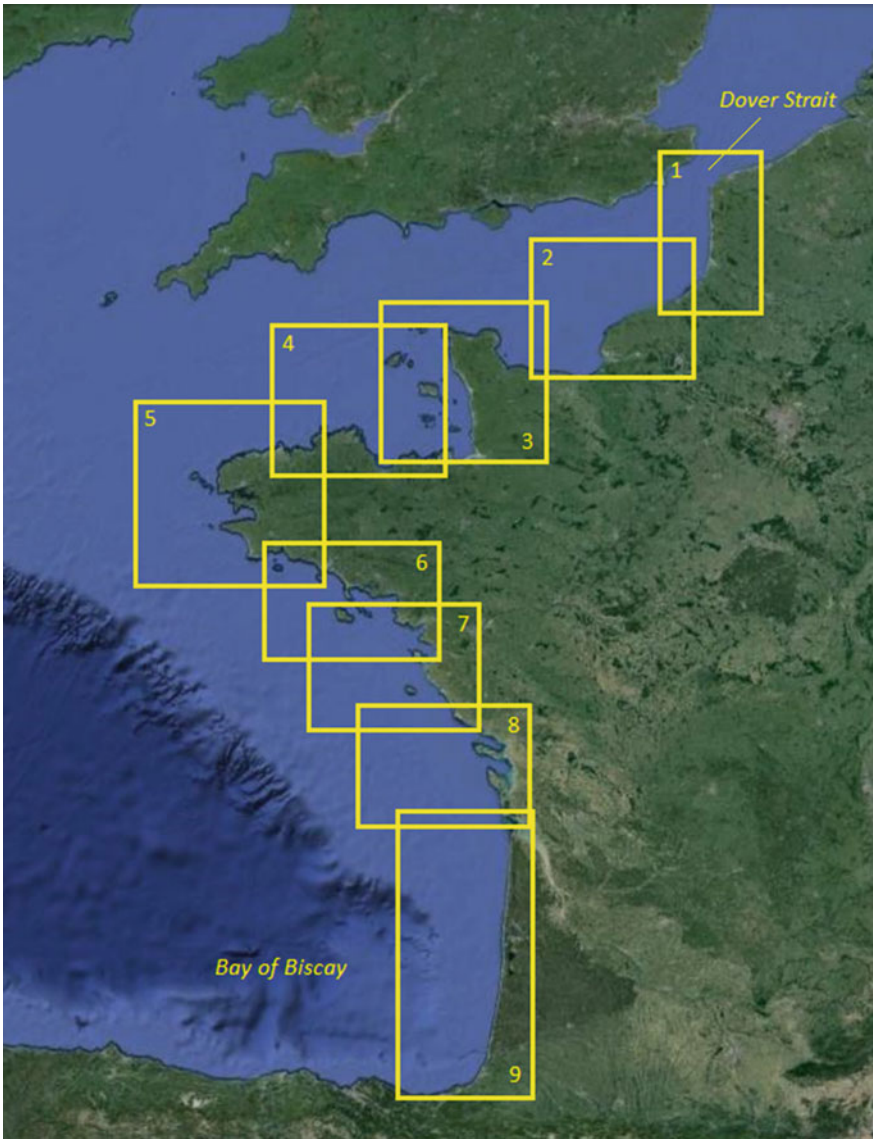

Fig. 10 Sub-domains of the wave hindcast along the French Atlantic Coast

coast up to 8 km offshore (Fig. 11). The bathymetry was obtained from digitalisation of nautical charts made by Meteogalicia and InTeCMar (Institutotecnoloxico para o Control do Mediomariño). These data were filtered and interpolated to the unstructured mesh to provide the model with a high-resolution bathymetry.

The model provided a 42-year period wave hindcast, from 1958 to 2000. This extended period allowed for determining wave height for different return periods

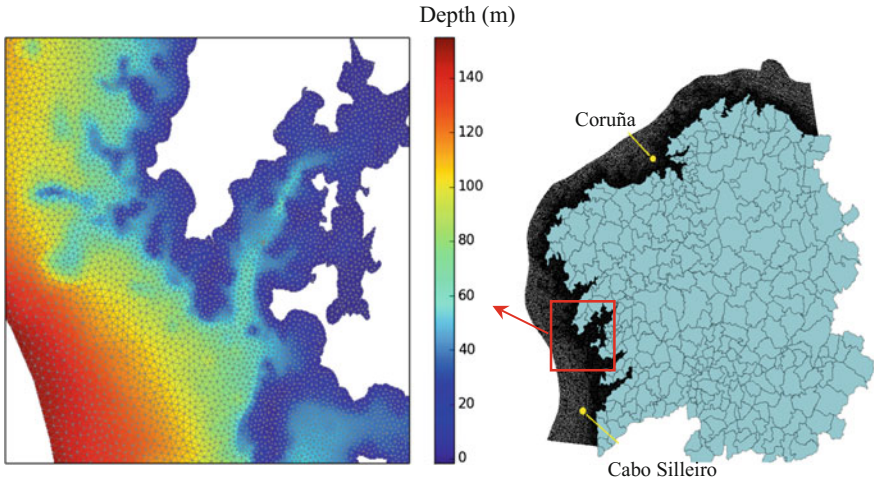

Fig. 11 Meshgrid of Galician model for the entire domain (*right*) and a detailed view of the Rias Baixas area (*right*)

(2, 10, 25, 50, and 100 years), which can be used, for instance, for evaluating the risk to installations.

Because the model only covers a narrow band along the coast, it is primarily driven by the boundary conditions. Wave boundary conditions were obtained from a 6-hour interval hindcast from the HIPOCAS (Hindcast of Dynamic Processes of the Ocean and Coastal Areas of Europe) project (Guedes Soares et al. 2002). The model was validated against wave buoy data recorded by Puertos del Estado during February 2013 at two locations: Cabo Silleiro and Coruña (see Fig. 11). It showed close predictions of the model with the data, for both significant wave height and peak period (Gleizon et al. 2015).

Portugal

The NOAA WaveWatch III v3.14 model was used to assess wave energy along the Portuguese coast. The model was applied on three nested grids (Fig. 12):

- a large-scale domain covering the North Atlantic Ocean (NAt) with a grid resolution of 0.5 degree;
- a continental-scale domain covering the south-west part of Europe (SWE) and extending from 23°W to 0°W and 33°N to 48°N with a grid resolution of 0.25 degree; and
- a coastal domain covering the Portuguese continental coast (PCC) and extending from 11.8°W to 7.4°W and 35.6°N to 42.8°N with a grid resolution of 0.05 degree.

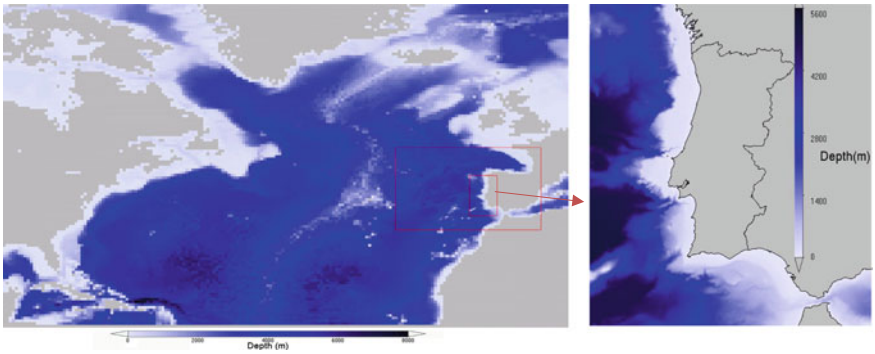

Fig. 12 Domains of the WaveWatch III models for the Portuguese coastal application. Nested models are indicated by the *red boxes*

Different sources of bathymetric data were combined to populate the various nested models with appropriate resolution. The EMODNet (European Marine Observation and Data Network[3]) hydrographic portal provided fine-resolution bathymetry of 7.5 arc seconds, in particular for the nested models, and was completed by 30-arc second resolution global bathymetry data SRTM30_PLUS (Becker et al. 2009) without EMODNet data.

The wave energy resource was evaluated using a hindcast covering the period from 2000 to 2010. The National Centers for Environmental Prediction (NCEP) FNL Operational Model Global Tropospheric Analyses (NCEP/NWS/NOAA/U.S. Department of Commerce 2000) was used to feed the wave models with wind intensities and directions from July 1999 on a time interval of 6 h and over a grid resolution of 1 degree. The wave boundary conditions for the SWE and PCC models were simply given by the larger scale models, NAt and SWE, respectively.

The SWE and PCC model hindcasts were validated against eight wave buoy stations distributed along the western coast of the Iberian Peninsula. The location of the wave buoys and validation results for significant wave heights and mean periods are summarised in Fig. 13 and Table 3.

The coefficients of determination R^2 show a good correlation between predicted and measured values for the significant wave height (H_S); values fell between 0.89 and 0.92, except near the southern coast at the stations of Faro and Cadiz where they have lower values around 0.8. The mean period generally shows less good correlation—the R^2 values fell between 0.61 and 0.75 at most locations and were 0.2 and 0.31 at the southernmost stations of Faro and Cadiz, respectively. However, considering that areas of interest for the wave energy resources are mainly from the central to northern part of Portugal, the model was deemed sufficiently accurate for estimating the resource along this coast.

[3][http://www.emodnet-hydrography.eu].

Fig. 13 Wave monitoring stations on the western Iberian Peninsula

Table 3 Monitoring stations along the western Iberian Peninsula coast and coefficients of determination R^2 for the significant wave height (H_S) and mean wave periods (T_m). The subscript near the station names indicates the institution providing the data: (a) Puertos del Estado (Spain) and (b) Instituto Hidrográfico (Portugal)

Station Name	Domain	Latitude	Longitude	Period	R^2	
					H_S	T_m
Estaca de Bares[a]	SWE	44.06°N	7.62°W	Jan 02–Dec 09	0.92	0.75
Cabo de Peñas[a]	SWE	43.73°N	6.19°W	Jan 02–Dec 09	0.89	0.71
Villano-Sisargas[a]	SWE	43.49°N	9.21°W	Jan 02–Dec 09	0.90	0.74
Silleiro[a]	PCC	42.12°N	9.40°W	Jan 02–Dec 09	0.91	0.69
Leixões[b]	PCC	41.18°N	8.70°W	Jan 08–Dec 09	0.91	0.61
Sines[b]	PCC	37.92°N	8.92°W	Jan 08–Dec 09	0.90	0.61
Faro[b]	PCC	36.90°N	7.90°W	Jan 08–Dec 09	0.80	0.20
Cadiz[a]	SWE	36.84°N	6.98°W	Jan 08–Dec 09	0.79	0.31

Wave Resource Assessment

Spatial Distribution

The North Atlantic weather system is largely governed by the so-called North Atlantic Oscillation, which is characterised by the presence of westerly winds (Fig. 14) and a recurring pattern of weather conditions coupled with the Gulf Stream system, with occasional influence of influx of cold weather from the north (Arctic) or the east (Siberia).

This particular weather system generates swells that build over long fetch distances and travel more than 3000 km before reaching the exposed European coasts. Figure 15 shows the distribution of mean significant wave height, from a WaveWatch III hindcast averaged over a 10-year period. Wave activity and resources along the European Atlantic Coast were characterised by significant wave height (H_S), direction (θ), peak period (T_P), and power per metre of wave crest (P).

The wave climate of the North Atlantic is one of the most energetic of the planet's oceans, particularly in the northern hemisphere and in its approach to the north-western European coast of Ireland and Scotland (Atan et al. 2016). The mean available wave power flux reaches 70 kW/m near the western coast of Ireland and Scotland and approximately 45 kW/h in Galicia at the north-western tip of the Iberian Peninsula (Fig. 16).

This hindcast gives an overview of the wave climate over the North Atlantic basin, but the exploitation of wave energy requires a finer characterisation of wave resources in coastal areas, in particular near irregular coastlines.

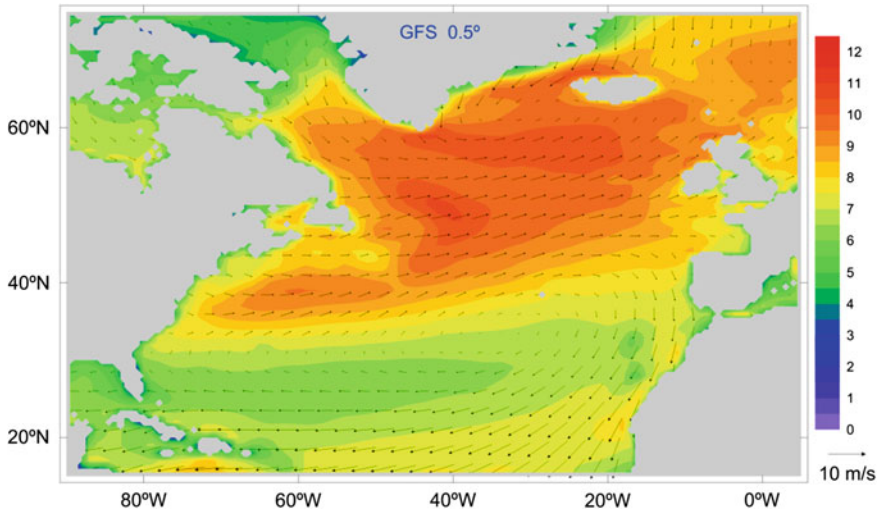

Fig. 14 Mean wind speed modulus (m/s) and direction over the North Atlantic

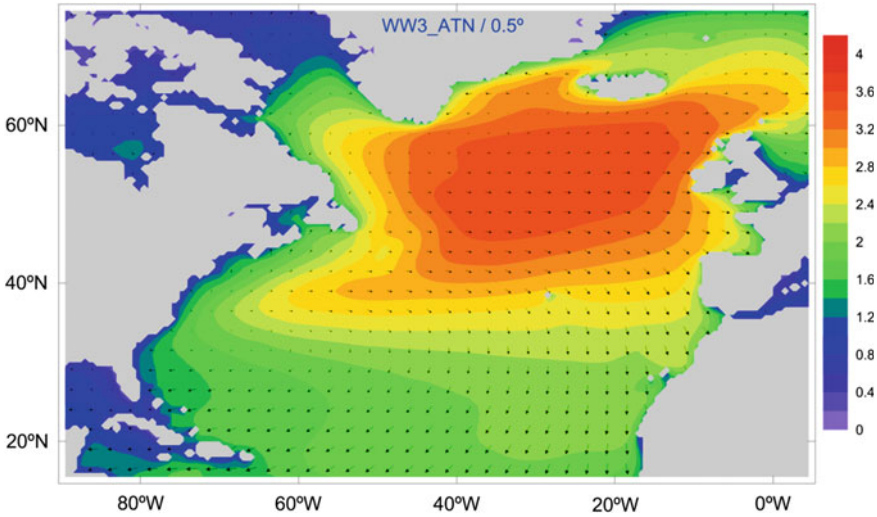

Fig. 15 Mean significant wave height (m) and direction over the North Atlantic

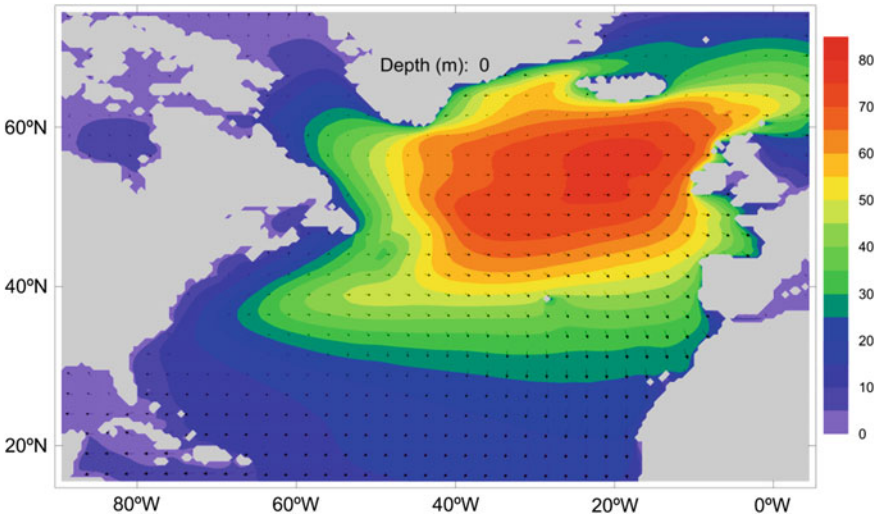

Fig. 16 Mean wave power density (kW/m) and wave direction over the North Atlantic

Annual and seasonal averages were determined from a 7-year period, 2008–2014. Presented as an atlas of fine-resolution maps, the hindcast shows the variability of the resource at local scale and provides a holistic view of the wave climate along the European Atlantic Coast (Figs. 17 and 18). In addition, the 99 percentile wave height (H_{99}) was estimated throughout the modelling period, as an indicator of peak wave activity and therefore potential risk to marine energy installations.

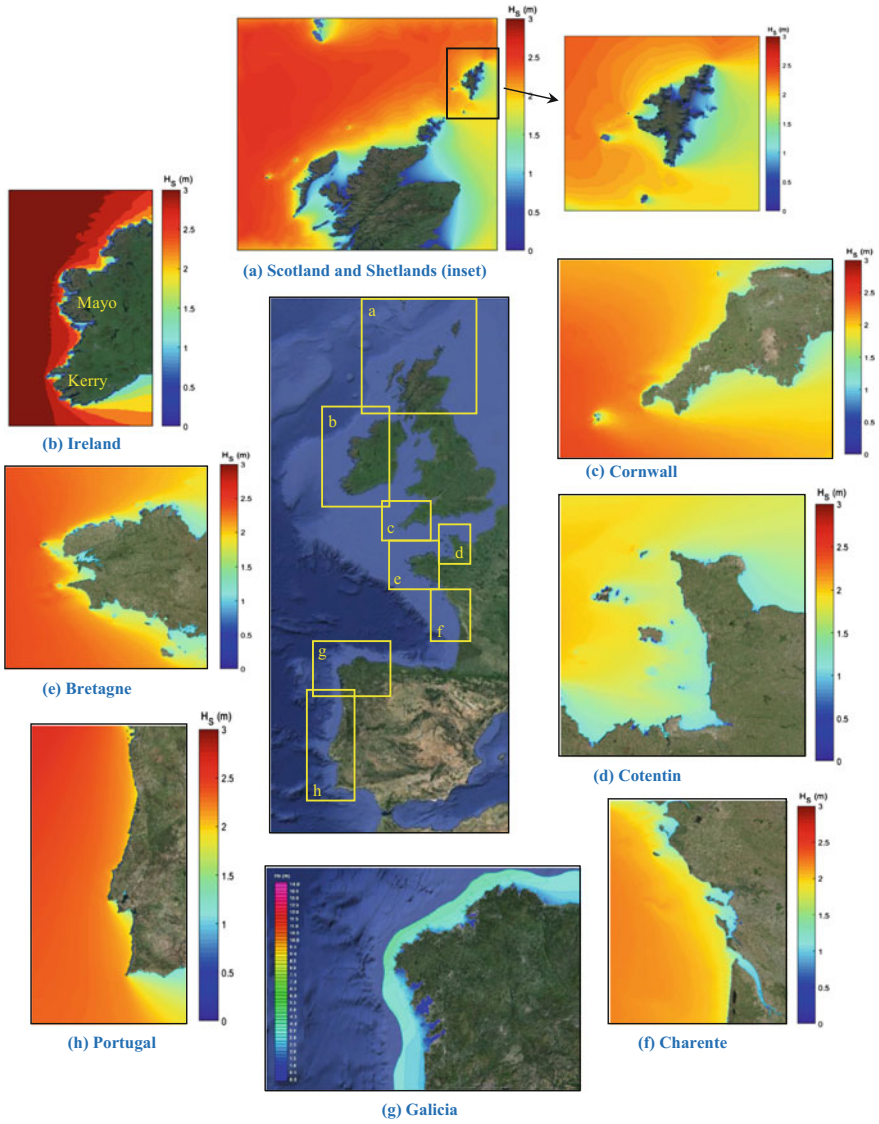

Fig. 17 Mean significant wave height along the European Atlantic Coast

Around Scotland, waves are higher on the western coast (Fig. 17a). This is mainly due to the predominance of westerly and south-westerly winds combined with longer fetches on the North Atlantic side, which induce strong swells near western Scotland. Nearer to the coasts, the wave height can present a more unequal

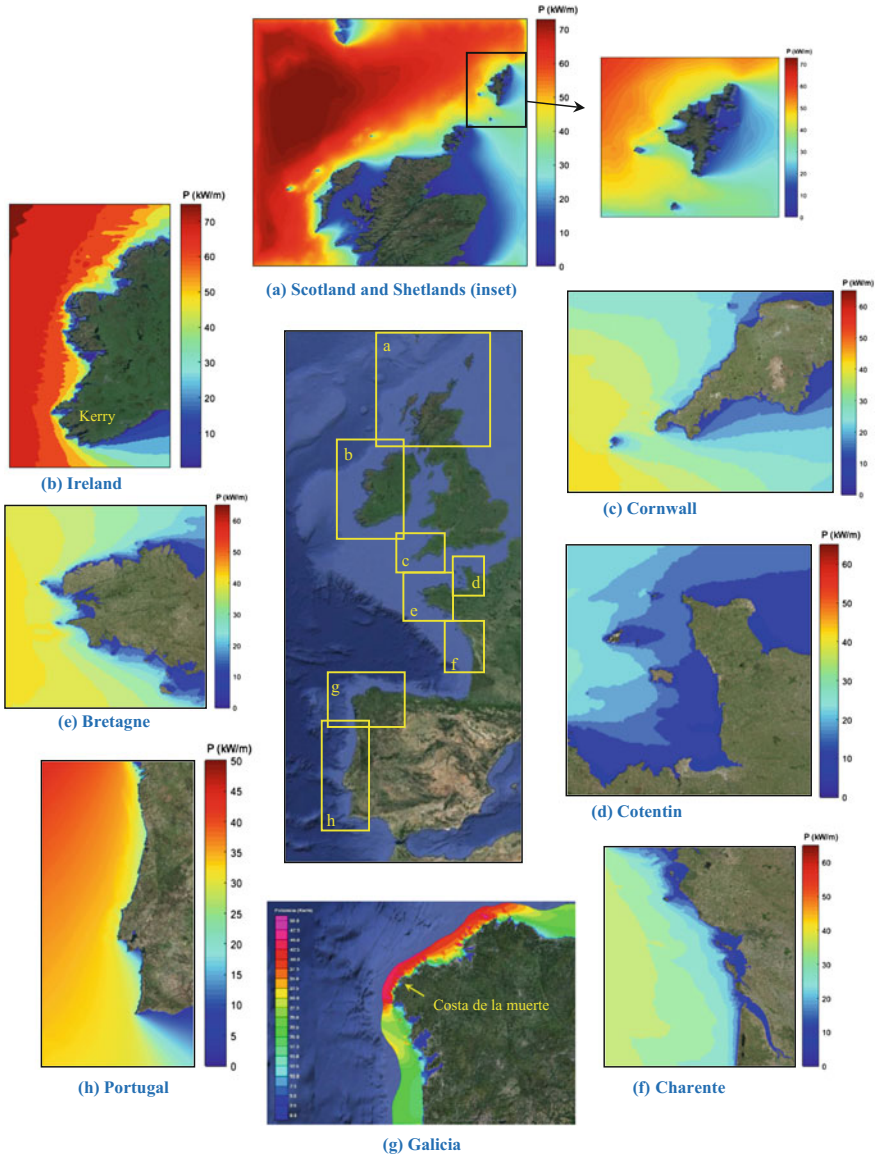

Fig. 18 Mean wave power density along the European Atlantic Coast

distribution depending on the bathymetry, coastal configuration, and presence of islands, as shown for instance around the Shetland Islands (Fig. 17a). The western coast of Ireland is more frontally exposed to North Atlantic swells and experiences

the highest wave activity in Europe. The mean significant wave height reaches values up to 3 m near its westernmost headlands of counties Mayo and Kerry (Fig. 17b). In comparison, lesser wave activity occurs at lower latitudes where wave heights reach mean values between 2 and 2.5 m near the most exposed headlands of Cornwall, Bretagne, and Galicia, and along the northern to central part of the Portuguese coast. The maps also reveal the variability in wave height distribution over relatively short distances in the presence of islands, as observed for instance around the Shetland Islands, Cotentin, or Bretagne (Fig. 17a, d, and e respectively). Although these local variations in wave height may appear small, they can have a more significant impact on available wave power that is proportional to the square of the significant wave height. The implication of these wave pattern irregularities on the wave power is examined in power density maps for the same areas (Fig. 18). The power density P is calculated from the significant wave height H_S and the wave energy period T_e by:

$$P = \frac{\rho g^2}{64\pi} H_S^2 T_e \tag{2}$$

where ρ and g represent the seawater density and gravity acceleration, respectively. This simplified expression uses deep-water approximation (see Nielsen 2009), which fits well most of the modelled domain and all of the locations considered hereafter.

Near the coast, the wave power density tends to concentrate near unsheltered headlands such as the northern tip of the Shetland Islands (Fig. 18a), the westernmost headlands of Kerry County (Fig. 18b), or at Costa de la Muerte in Galicia (Fig. 18g). The fine grid resolution along Galicia shows that the wave power density can vary substantially over short distances (few 10 s of kilometres) near irregular shores. It can be observed that the mean wave power distribution depends on latitude, but probably more significantly on exposure to open waters. As evidence, the highest wave power in European coastal waters was found off the western coasts of Ireland and was estimated to be between 50 and 65 kW/m, except within sheltered bay areas (Fig. 18b).

A comparison of wave characteristics and resources was undertaken at 12 locations distributed over a fair geographical spread along the coast, from the Shetland Islands in the north to the southernmost Portuguese headland of Cabo de São Vincente (Fig. 19 and Table 4). Most of these locations were selected to coincide with the proximity of existing or potential test or energy sites.

The mean values of H_S, H_{99}, T_P, and P were estimated at each location. The depth and exposure to Atlantic swells were variable. The deepest locations were at Kerry, Pontevedra, Belmullet, and Nazaré because of their proximity to the continental shelf slope or to a canyon (Nazaré). Table 4 corroborates the previous observations that wave activity is related to latitude and exposure. The 99 percentile of wave height, H_{99}, is approximately 2.5 to 3 times higher than H_S, but these are

Fig. 19 Selected locations for wave resource variability study

annual averages. Direct observations suggest that this ratio may be dependent on interannual or seasonal variability, in particular with a distinct split between winter and summer months.

Seasonal and Interannual Variability

The seasonal variability is determined for each simulated year by separating and analysing the hindcast data into four seasons: winter (December of previous year to February of current year), spring (March to May), summer (June to August), and

Table 4 Wave annual statistics

Location	Latitude	Longitude	D (m)	H_S (m)	H_{99} (m)	T_P (s)	P (kW/m)
Shetlands	60.56°N	1.58°W	78	2.50	7.48	10.8	40.12
Orkneys	58.98°N	3.40°W	54	2.15	5.93	10.5	28.70
Hebrides	58.37°N	6.67°W	30	2.48	6.40	11.1	39.11
Belmullet	54.28°N	10.28°W	89	3.09	7.80	10.6	61.88
Kerry	51.20°N	10.60°W	155	3.13	8.04	10.6	64.52
Cotentin	49.75°N	1.92°W	53	1.20	3.50	6.0	5.33
Bretagne	48.03°N	4.91°W	46	2.20	5.88	10.0	34.12
Landes	44.03°N	1.44°W	38	1.74	5.06	10.5	21.89
Estaca de Bares	44.06°N	7.62°W	46	1.80	5.43	8.7	34.34
Pontevedra	42.12°N	9.40°W	105	1.54	5.96	8.3	29.54
Nazaré	39.59°N	9.12°W	88	1.92	5.32	10.6	24.1
SãoVincente	37.01°N	8.99°W	61	1.90	5.34	10.6	23.1

autumn (September to November). The seasonal average is simply obtained by taking the average of the relevant seasonal values over the period of simulation.

The seasonal variability shows a clear predominance of wave activity during the winter months (Table 5). The difference between summer and winter months appears to be slightly more pronounced in the upper latitudes. A comparison between the different locations, for instance Kerry and Cotentin, highlights the influence of exposure to Atlantic waters on wave resource, but there is no evidence that this exposure could affect the seasonal variability by reducing or enhancing the difference of activity between winter and summer months.

Depending on the weather system, the wave climate has not only a seasonal variability but also an interannual and geographical variability. Figure 20 compares the interannual and seasonal variations of H_S, H_{99}, and P from 2008 to 2014 at three different locations: the Shetlands, Belmullet, and Bretagne. The wave power density clearly shows the consistent seasonal contrast between summer and winter at all locations. The interannual wave activity during spring and autumn months is more variable. For instance, during autumn 2014, H_{99} is high in comparison with H_S for equivalent periods, in particular during winter. This is the signature of peak wave activity over short periods of time.

The geographical difference in wave activity is highlighted by the winter interannual variability. In Bretagne, the highest wave activity is noted during winters 2013 and 2014. In comparison, it is significantly lower during winters 2011 and 2012. Conversely, at the uppermost latitude of the Shetlands, the highest wave activity was noted during winters 2011 and 2012, and it diminished during winters 2013 and 2014. Finally, the interannual and seasonal wave resource estimates at Belmullet appear to be more consistent throughout the period studied, exhibiting a marked lower activity during summer.

Table 5 Wave seasonal statistics

Locations	Hs (m)				H_{99} (m)				Tp (s)				P (kW/m)			
	Sp	Su	Au	Wi	Sp	Su	Au	Wi	Sp	Su	Au	Wi	Sp	Su	Au	Wi
Shetlands	2.55	1.39	2.51	3.55	5.46	3.88	6.95	8.88	10.9	9.0	11.1	12.3	36.2	9.6	37.0	78.3
Orkneys	2.26	1.09	2.24	3.04	4.59	3.23	5.76	6.72	10.7	8.8	10.7	11.9	27.3	5.9	27.7	54.4
Hebrides	2.65	1.34	2.47	3.47	5.14	3.18	6.29	7.57	11.2	8.9	11.2	12.9	39.2	7.9	34.8	75.2
Belmullet	2.87	2.09	3.35	4.07	6.84	4.72	7.63	8.78	10.5	8.9	11.0	12.1	49.9	20.7	66.9	111.3
Kerry	2.92	2.11	3.33	4.22	7.33	4.75	7.90	9.15	10.4	9.0	11.0	12.1	51.7	20.8	68.2	121.6
Cotentin	1.06	0.97	1.22	1.45	2.97	2.65	3.46	3.52	6.0	5.4	6.0	7.1	4.2	2.9	5.6	8.1
Bretagne	1.99	1.62	2.28	3.04	5.19	3.76	5.73	6.4	10.1	8.5	10.5	12.0	25.4	12.7	37.0	64.1
Landes	1.63	1.25	1.74	2.40	4.61	2.86	4.71	5.53	10.7	9.0	11.1	12.5	18.6	7.9	23.4	43.6
Nazaré	2.22	1.43	1.58	2.47	5.41	3.15	4.31	6.28	11.5	9.0	9.7	12.0	31.0	9.5	14.1	42.1
São Vincente	2.20	1.41	1.54	2.46	5.63	2.95	4.00	6.12	11.7	8.9	9.7	12.1	30.6	8.4	12.6	41.2

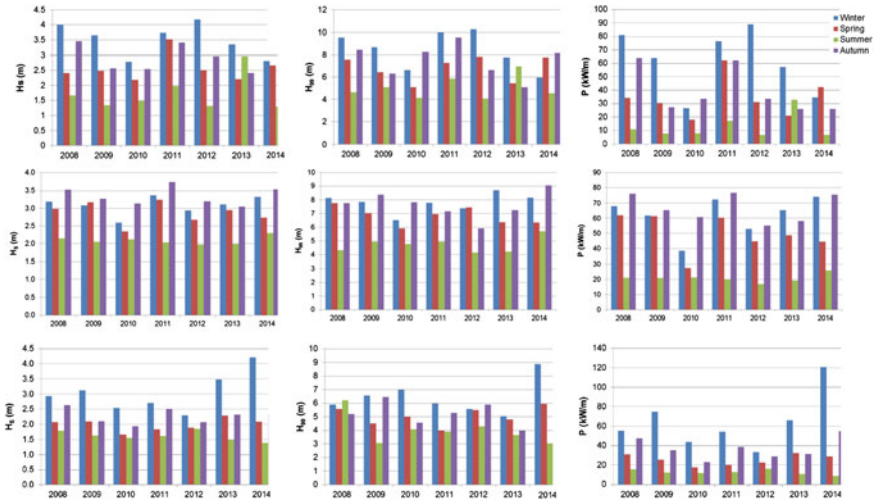

Fig. 20 Interannual variations of H_S (first column graphs), H_{99} (second column), and P (third column) at Shetland (*top row*), Belmullet (*middle row*), and Bretagne (*bottom row*)

No clear interannual trend can be derived from these estimates. The seasonal variability and differences between the selected locations suggest that the local wave climate is sensitive to mesoscale wind variations (~ 1000 km) over relatively short periods of time.

Summary and Discussion

The wave resources along the European Atlantic Coast are characterised using a 7-year hindcast of high-resolution spectral wave models. The modelling domains cover almost the entire European coast from the Shetland Islands in the north to the Portuguese Algarve region in the south, except for Asturias and Cantabria on the northern coast of Spain. The extent and resolution of the models can provide detailed maps of the resource for energy site developers, regulators, and/or potential users and at the same time provide a holistic description of the resource in Europe.

The high-resolution maps show that in coastal areas the wave power can vary significantly over short distances, in particular in the presence of irregular coastlines such as in Galicia, Bretagne, and Ireland, or in the vicinity of islands and archipelagos such as those in Scotland, Cotentin, or Charente. The resource can therefore only be accurately estimated using a fine-resolution grid. Tuomi et al. (2014) showed that inappropriate grid resolution can result in insufficient attenuation of waves in archipelagos and therefore in overestimating the resource. Most spectral wave models can now operate on unstructured meshes, which should be used around complex coastlines.

The wave characteristics and power density were compared at various locations selected near sites of potential interest and fairly distributed along the coastline. The comparisons showed that the wave resource depends essentially on the latitude, but perhaps more importantly on the exposure to Atlantic open waters. Located between 51°N and 55°N and frontally exposed to the North Atlantic, western Ireland has the highest wave energy resource in Europe. The annual average power density at Belmullet (north-west) and Kerry (south-west) has been estimated to be between 60 and 65 kW/m. At these locations, the wave height 99 percentile, which can be used as an indicator of peak wave activity and therefore of potential risk to installations and maintenance operations, can reach 8.5 to 9 metres during the winter months. Annual averaged peak wave periods are estimated to be between 10 and 11 s at most of the selected locations.

The seasonal variability shows a clear and consistent difference between summer (lowest wave activity) and winter (highest wave activity) at all locations. However, no clear trend emerges in the interannual variability. From the investigated locations, the most consistent interannual wave activity was found at Belmullet.

This study provides a detailed description of wave resources along the European Atlantic Coast that investigates both their spatial distribution and temporal variability using hindcast modelling. However, the energy yield of a marine energy site does not only depend on the availability of the resource. Other factors that may influence energy yield include the array layout that can optimise or reduce the resource at a local level, the morphology of the seabed that may change, for instance with accretion or erosion of sediments in sandy areas, or simply affect the local wave patterns by inducing wave breaking, refraction and shoaling, or the local hydrodynamic conditions related, for instance, to tidal currents and water levels.

In addition, wave resources are uncertain because of their inherent unpredictability over the medium to long term, which itself depends on meteorological unpredictability and long-term uncertainties caused by climate change. Statistics from hindcast modelling probably provide the closest evaluation of the resource, which need to be regularly re-evaluated to adjust for longer term changes.

Acknowledgements This work was funded by the European Regional Development Fund under the EnergyMare project of the Atlantic Area Programme.

The authors are grateful to INCAT (Ingeniería Civil de Atlàntico) for post-processing the model output data and for producing maps of wave height and wave power along the Galician coast, and to Thibault Coulombier and Camille Letretel for their help in providing additional data related to the French coast.

References

ABP MER. (2008). Atlas of UK marine renewable energy resources: Atlas pages. A strategic environmental assessment report, Department for Business Entreprise and Regulatory Reform.

Atan, R., Goggins, J., Hartnett, M., Agostinho, P., & Nash, S. (2016). Assessment of wave characteristics and resource variability at a 1/4-scale wave energy site in Galway Bay using waverider and high frequency radar (CODAR) data. *Ocean Engineering, 117,* 272–291.

Atan, R., Goggins, J., & Nash, S. (2015). A preliminary assessment of the wave characteristics at the Atlantic Marine Energy Test Site (AMETS) using SWAN. In *Proceedings of the 11th European Wave and Tidal Energy Conference*, Nantes, France.

Barstow, S., Mollison, D., & Cruz, J. (2008). The wave energy resource. In Cruz, J. (Ed.), *Ocean wave energy* (pp. 40). Springer.

Barstow, S., Mørk, G., Lønseth, L., & Mathisen J. P. (2009). WorldWaves wave energy resource assessments for the deep ocean to the coast. In *Proceedings of the 8th European Wave and Tidal Energy Conference*, Uppsala, Sweden (pp. 149–159).

Becker, J. J., Sandwell, D. T., Smith, W. H. F., Braud, J., Binder, B., Depner, J., et al. (2009). Global bathymetry and elevation data at 30 arc seconds resolution: SRTM30_PLUS. *Marine Geodesy, 32*(4), 355–371.

Bertotti, L., & Cavaleri, L. (2012). Modelling waves at Orkney coastal locations. *Journal of Marine Systems, 96–97,* 116–121.

Booij, N., & Holthuijsen, L. H. (1987). Propagation of ocean waves in discrete spectral wave models. *Journal of Computational Physics, 68*(2), 307–326.

Booij, N., RisR, C., & Holthuijsen, L. H. (1999). A third generation model for coastal regions. Part I: model description and validation. *Journal of Geophysical Research, 104*(C4), 7649–7666.

Cavaleri, L., & Malanotte-Rizzoli, P. (1981). Wind wave prediction in shallow water. Theory and applications. *Journal of Geophysical Research, 86C11*, 10961–10973.

DHI. (2007). *MIKE21 SW—Spectral waves FM module User guide*. Denmark: Scientific Document, Danish Hydraulic Institute.

Dietrich, J. C., Ziljema, M., Allier, P. E., Holthuijsen, L. H., Booij, N., Meixner, J. D., et al. (2013). Limiters for spectral propagation velocities in SWAN. *Ocean Modelling, 70,* 85–102.

European Commission. (2015). Renewable energy progress report, Report from the commission to the European parliament, the council, the European economic and social committee and the committee of the regions, SWD (2015), p. 117.

Gleizon, P., Campuzano F. J., Carracedo García, P., Gomez B., & Martinez, A. (2015). Wave energy mapping along the European Atlantic coast. In *Proceedings of the 11th European Wave and Tidal Energy Conference*, Nantes, France.

Gleizon, P., & Murray, A. (2014). Modelling wave energy in archipelagos—Case of northern Scotland. In *Proceedings of the 2nd Environmental Interactions of Marine Renewable Energy Technologies*, Stornoway, United Kingdom.

Gleizon, P., & Woolf, D. (2013). Wave energy assessment in Scotland. In *Proceedings of the 10th European Wave and Tidal Energy Conference*, Aalborg, Denmark.

Guedes Soares, C., Weisse, R., Carretero, J. C., & Alvarez, E. (2002). A 40 years hindcast of wind, sea level and waves in European waters. In *Proceedings of the 21st International Conference on Offshore Mechanics and Arctic Engineering (OMAE 2002)*, Oslo, Norway.

Guillou, N. (2015). Evaluation of wave energy potential in the Sea of Iroise with two spectral models. *Ocean Engineering, 106,* 141–151.

Guillou, N., & Chapalain, G. (2015). Numerical modelling of nearshore wave energy resource in the Sea of Iroise. *Renewable Energy, 83,* 942–953.

Hasselmann, K. (1962). On the nonlinear energy transfer in a gravity-wave spectrum—Part I. General Theory. *Journal of Fluid Mechanics, 12,* 481–500.

Hasselmann, K., Barnett, T. P., Bouws, E., Carlson, H., Cartwright D. E., Enke, K., et al. (1973). Measurements of wind-wave growth and swell decayduring the Joint North Sea Wave Project (JONSWAP), Deutschen Hydrographischen Zeitschrift, Suppl. A(8) n° 12, pp. 95.

Hersbach, H., & Janssen, P. A. E. M. (1999). Improvement of the short-fetch behavior in the wave ocean model (WAM). *Journal of Atmospheric and Oceanic Technology, 16,* 884–892.

Iglesias, G., & Carballo, R. (2009). Wave energy potential along the Death Coast (Spain). *Energy, 34,* 1963–1975.

Iglesias, G., & Carballo, R. (2010a). Offshore and inshore wave energy assessment: Asturias (N Spain). *Energy, 35,* 1964–1972.

Iglesias, G., & Carballo, R. (2010b). Wave energy and nearshore hot spots: The case of the SE Bay of Biscay. *Renewable Energy, 35,* 2490–2500.

Iglesias, G., & Carballo, R. (2010c). Wave energy resource in the Estaca de Bares area (Spain). *Renewable Energy, 35,* 1574–1594.

Iglesias, G., Lopez, M., Carballo, R., Castro, A., Fraguela, J. A., & Frigaard, P. (2009). Wave energy potential in Galicia (NW Spain). *Renewable Energy, 34,* 2323–2333.

Komen, G. J., Hasselmann, S., & Hasselmann, K. (1984). On the existence of a fully developed wind-sea spectrum. *Journal of Physical Oceanography, 14,* 1271–1285.

Leonard, B. P. (1979). A stable an accurate convective modelling procedure based on quadratic upstream interpolation. *Computer Methods in Applied Mechanics and Engineering, 18,* 17–74.

Leonard, B. P. (1991). The ULTIMATE conservative difference scheme applied to unsteady one-dimensional advection. *Computer Methods in Applied Mechanics and Engineering, 88,* 59–98.

Lopez, I., Andreu, J., Ceballos, S., Martínez de Alegría, I., & Kortabarria, I. (2013). Review of wave energy technologies and the necessary power-equipment. *Renewable and Sustainable Energy Reviews, 27,* 413–434.

May, V. J., Hansom, J. D. (2003). Coastal geomorphology of Great Britain, Geological Conservation Review Series (Vol. 28, pp. 754). ISBN 1 86107 484 0.

NCEP/NWS/NOAA/U.S. Department of Commerce. (2000). NCEP FNL Operational Model Global Tropospheric Analyses, continuing from July 1999, Research Data Archive at the National Center for Atmospheric Research, Computational and Information Systems Laboratory, Boulder, Colorado. Retrieved February 11, 2015, from http://dx.doi.org/10.5065/D6M043C6.

Nielsen, P. (2009). *Coastal and Estuarine processes, advanced series on ocean engineering* (Vol. 29). World Scientific.

NREAP (National Renewable Energy Action Plan). (2010). http://ec.europa.eu/energy/en/topics/renewable-energy/national-action-plans.

Piollé, J. F., Croizé-Fillon, D. (2012). Operation of CERSAT data centre. Ifremer report 13/2 213 213.

Pontes, M. T. (1998). Assessing the European wave energy resource. *Journal of Offshore Mechanics and Artic Engineering, 120*(4), 226–231.

Pontes, M. T., Athanassoulis, G. A., Barstow, S., Bertotti, L., Cavaleri, L., Holmes, B., et al. (1998). The European wave energy resource. In *Proceedings of the 3rd European Wave Energy Conference*, Patras, Greece.

Robertson, B. (2017). Wave energy assessments: quantifying the resource and understanding the uncertainty. In Z. Yang & A. Copping (Ed.), *Marine renewable energy: Resource characterization, practical energy harvest and effects on physical systems*. Springer.

Robertson, B., Hiles, C., & Buckham, B. (2014). Characterizing the near shore wave energy resource on the west coast of Vancouver Island. *Canada, Renewable Energy, 71,* 665–678.

Robertson, B., Hiles, C., Luczko, E., & Buckham, B. (2016). Quantifying wave power and wave energy converter array production potential. *International Journal of Marine Energy, 14,* 143–160.

Roland, A. (2009) *Development of WWM II: Spectral wave modelling on unstructured meshes*, Ph. D. thesis, Technische University at Darmstadt, Institute of Hydraulic and Water Resources Engineering.

Stelling, G. S., & Leendertse J. J. (1992). Approximation of convective processes by cyclic AOI methods. In *Proceedings of 2nd International Conference on Estuarine and Coastal Modelling*, ASCE Tampa, Florida (pp. 771–782).

Tolman, H. L. (1990). A third-generation model for wind waves on slowly varying, unsteady, and inhomogeneous depths and currents. *Journal of Physical Oceanography, 21,* 782–797.

Tolman, H. L. (2002). Alleviating the garden sprinkler effect in wind wave models. *Ocean Modelling, 4,* 269–289.

Tuomi, L., Pettersson, H., Fortelius, C., Tikka, K., & Björkqvist, Kahma K. K. (2014). Wave modelling in archipelagos. *Coastal Engineering, 83,* 205–220.

Van der Westhuysen, A. J., Zijlema, M., & Battjes, J. A. (2007). Nonlinear saturation-based whitecapping dissipation in SWAN for deep and shallow water. *Coastal Engineering, 54,* 151–170.

Venugopal, V., & Nemalidinne, R. (2015). Wave resource assessment for Scottish waters using a large scale North Atlantic spectral wave model. *Renewable Energy, 76,* 503–525.

WAMDI group (1988) The WAM model—a third generation wave prediction model, Journal of Physical Oceanography, 18, 1775–1810.

WISE Group. (2007). Wave modeling—The state of the art. *Progress in Oceanography, 75*, 603–674.

Yang, Z., & Wang T. (2015). Modelling wave resource characterization using and unstructured grid coastal ocean model. In *Proceedings of the 11th European Wave and Tidal Energy Conference 2015*, Nantes, France.

Zijlema, M. (2010). Computation of wind-wave spectra in coastal waters with SWAN on unstructured grids. *Coastal Engineering, 57,* 267–277.

Analyses of Wave Scattering and Absorption Produced by WEC Arrays: Physical/Numerical Experiments and Model Assessment

H. Tuba Özkan-Haller, Merrick C. Haller, J. Cameron McNatt, Aaron Porter and Pukha Lenee-Bluhm

Introduction

The deployment of wave energy converters (WECs) on a commercial scale will necessitate the grouping of devices into arrays to minimize the costs of installation, mooring, maintenance, and electrical cabling for power delivery. The fundamental purpose of WECs is to remove energy from the waves, so they necessarily decrease the wave height in their lee, i.e., they cast a wave shadow. In general, WECs not only capture energy but also redistribute it through the processes of radiation and scattering. The near-field effects of the shadowing and redistribution can have significant implications for the design and performance of WEC arrays (e.g., Beels et al. 2010; Borgarino et al. 2012; Nihous 2012; Babarit 2013; de Andrés et al. 2014; Kara 2016; Sinha et al. 2016). In addition, the far-field effects may extend to the nearshore region (e.g., Millar et al. 2007; Beels et al. 2010; Palha et al. 2010; Smith et al. 2012), where wave-driven currents and sediment transport are the dominant physical processes and are potentially affected by the offshore WEC array

H. Tuba Özkan-Haller (✉)
College of Earth, Ocean, and Atmospheric Sciences, Oregon State University, Corvallis, USA
e-mail: ozkan@coas.oregonstate.edu

M.C. Haller
School of Civil and Construction Engineering, Oregon State University, Corvallis, USA

J. Cameron McNatt
Mocean Energy, Edinburgh, UK

A. Porter
Coast and Harbor Engineering, Edmonds, WA, USA

P. Lenee-Bluhm
Columbia Power Technologies, Corvallis, OR, USA

Z. Yang and A. Copping (eds.), *Marine Renewable Energy*,
DOI 10.1007/978-3-319-53536-4_3

(Rusu and Guedes Soares 2013; Gonzalez-Santamaria et al. 2013; Abanades et al. 2014a and 2014b; Mendoza et al. 2014; O'Dea et al. 2015). Far-field effects may also impact commercial and recreational activities, or ecological processes.

The wave energy industry is still in its nascent stage. Diverse proposed WEC technologies exist, and several field testing sites for wave energy technology have been developed around the world. Comprehensive reviews of WEC technologies can be found in Falcão (2010) and Babarit et al. (2012). Point absorber WECs extract wave energy when wave momentum is transferred to the mechanical motions of the device, which is subsequently converted to other forms of energy. However, the process is not simple—some wave energy is reflected off of the device and additional radiated waves are generated by WEC motion (for reviews of numerical simulation methods, see Li and Yu 2012 and Day et al. 2015). This can lead to a very complex wave field with short-scale variability in the region of the WEC array (e.g., Chatjigeorgiou 2011; Borgarino et al. 2012; McNatt et al. 2013). However, the far field is generally smoothed by the process of wave diffraction and the decay of scattered/radiated waves, and the length scales of variability increase in the far field.

A large number of WEC array studies are performed analytically or computationally. Computational methods are necessary because they underlie the predictive tools used to design WEC arrays and to estimate the nearshore impacts of wave farms at field scales. To gain confidence in these computational tools, they need to be validated with experimental data. To date, only a handful of WEC array experiments have been performed in the laboratory, and WEC array data at the field scale do not yet exist.

Different WEC technologies—including the Salter Duck (Payne et al. 2008), the Manchester Bobber (Alexandre et al. 2009; Weller et al. 2010), the Savonius rotor (Tutar and Veci 2016), oscillating water columns (OWCs; Ashton et al. 2009; Folley and Whittaker 2013; Iturrioz et al. 2014), bottom-pitching WECs (Flocard and Finnigan 2010), and the wave overtopping device WaveCat (Fernandez et al. 2012)—have recently been tested in the laboratory. The study reported here concerns arrays of point absorber WECs (Columbia Power "Manta"); preliminary results were reported by Haller et al. (2011) and Porter et al. (2012).

Much of the previous experimental work was concerned primarily with the energy capture performance of individual WECs and WEC arrays, as opposed to analysis of the wave field changes induced by WEC arrays. Alexandre et al. (2009) presented observations of induced changes in the wave spectrum in the lee of WEC arrays using a set of three wave gages. Their WEC array experiments were at a small scale (1:67) but involved a substantial number of WECs (5×1 and 5×2 arrays) and a single-input Bretschneider wave spectrum. Weller et al. (2010) provided additional data from the same facility with an additional WEC array configuration (3×4). That work focused on WEC power capture and WEC array interaction factors but did not analyze the wave field changes.

Ashton et al. (2009) performed WEC array experiments at a larger scale (1:20) with three different array configurations (1 WEC, 2 × 1 and 3 × 2 WEC arrays). They used six wave gages spaced within and around the WEC arrays, and they noted differences between the measured WEC power capture and the wave power deficit measured in the WEC array wave shadow. In fact, in the case of the 3 × 2 WEC array, a wave power surplus was observed in the downstream wave gage. However, this result is likely an effect of their wave gages being in the near field of the WEC array where the wave field is highly variable at short scales; hence, the wave shadow is much harder to resolve and is not representative of the far-field wave shadow. Ashton et al. (2009) also noted difficulties with analyzing monochromatic wave conditions, again due to high spatial variability. Very recently, Stratigaki et al. (2015) presented a database of laboratory observations of the wave field modification induced by a large 5 × 5 rectilinear array of heaving WECs ("WECwakes" project).

Finally, field data derived from a single WEC field deployment were published by Eriksson et al. (2007) and Waters et al. (2007, 2011). The deployment involved a floating buoy of 3 m diameter attached to a linear generator and installed at the 25-m depth near Lysekil, Sweden. These data concern device performance as a function of wave conditions.

Here, we report on a comprehensive set of laboratory tests that analyze the near- and far-field modifications due to the presence of an array of five-point absorber WECs. The set of experiments described here is most similar to the set used by Ashton et al. (2009), in that they were performed with WEC arrays of one/three/five devices (here at the 1:33 scale) under both regular monochromatic and fully directional random wave conditions. The key differences in the present work are a significant increase in the available instrumentation for wave observations and a significantly larger suite of tested wave conditions. Further, this work describes two prediction strategies, the phase-resolving model WAMIT (see WAMIT, Inc. 2000) and the phase-averaged Simulating WAves Nearshore (SWAN) model (Booij et al. 1999), and compares them to the wave observations. Results reveal the fidelity of each model and help to frame their appropriate future implementation and uses for WEC array modeling. Additionally, the experimental and model data contribute to the description of the WEC-induced wave field and inform effective WEC array design.

This chapter begins with a review of the laboratory experiments (section "WEC Array Laboratory Experiments"), including details about the wave conditions, WEC devices, instrumentation, and observational strategies for the determination of absorbed wave power. In section "Numerical Modeling," we discuss the two wave modeling strategies, giving special attention to the wave power extraction formulations. Model results and comparisons to wave observations are given in section "Results." In section "Discussion," we discuss further model simulations and their implications for the SWAN model WEC formulation with regard to the capability of simulating wave shadows induced by WEC arrays.

WEC Array Laboratory Experiments

Laboratory experiments were conducted at Oregon State University (OSU) in collaboration with Columbia Power Technologies, Inc. (CPT). The experiments were conducted in the Hinsdale Wave Research Laboratory, used 1:33 scale versions of the CPT "Manta" device (version 3.1), and included an extensive matrix of incident wave conditions and WEC array configurations. Array configurations of one, three, and five devices were moored inside the Tsunami Wave Basin (TWB), and incident wave conditions consisted of a range of regular monochromatic and random spectral sea states. Many of the spectral sea states also included directional spreading.

The TWB is 48.8 m long and 26.5 m wide. It has a directional wavemaker consisting 29. 2 m wide, piston-type wave paddles that are individually controlled. During the experiments, a crushed rock beach (1:12 slope) was installed opposite the wavemaker for wave dissipation, and the still water depth was maintained at 1.37 m on average.

Incident Wave Conditions

Experimental wave conditions included normally incident and oblique regular waves and long- and short-crested irregular waves. The laboratory-scale wave heights and periods were devised from targeted field-scale conditions and Froude scaling. The field-scale monochromatic wave periods ranged from 5.2 to 16 s (laboratory scale 0.9–2.8 s) and field-scale heights from 1 to 5 m (laboratory scale 3–15 cm). Most wave conditions were normally incident (with respect to the wavemaker as well as the WECs), but a limited set of regular monochromatic wave conditions was generated at 22.5 degrees incidence. Table 1 summarizes all of the tested regular wave conditions. This analysis focuses on the field-scale wave heights of 2 m (6 cm) because those runs contain the widest variety of wave periods and WEC array configurations. Most of the regular wave trials contained 50 waves. However, early in the experiment, some wave tests were conducted with only 12 waves.

Irregular wave conditions were intended to simulate sea state climatology at different potential WEC array installation sites. Seven target sea states were chosen and are listed in Table 1 (lower portion). They consist of five Oregon sea states (Oregon 1–5) ranked in the order of increasing wave power and a target Hawaii and Ireland sea state. The five Oregon sea states roughly span the climatology observed in 13 years of wave data derived from National Data Buoy Center Station 46050 (NDBC Stonewall Banks). The Hawaiian sea state is at a relatively shorter wave period and was derived from NDBC 51202. The Ireland sea state is of relatively higher energy and was derived from the M4 buoy. The Oregon storm conditions were derived from a peak-over-threshold extreme wave analysis of the NDBC

Table 1 Experimental wave conditions (top panel). Regular wave conditions, all cases include both incident angles 0º and 22.5º except for "T = 6 (o)" which is oblique 22.5º only. Values in the table indicate the number of WECs (1, 3, or 5) (bottom panel). Laboratory-scale conditions for random sea states. 2* indicates a case tested only with 3 and 5 WEC configurations. UD indicates unidirectional cases; *s* refers to the directional spreading parameter

Regular waves—wave period (s)																					
H (cm)	T (sec)	0.9	1.0	1.1	1.2	1.3	1.4	1.5	1.6	1.7	1.8	1.9	2.0	2.1	2.2	2.3	2.4	2.5	2.6	2.7	2.8
	3		1		1		1		1		1		1		1		1		1	1	1
	6	1, 3, 5	1, 3, 5	1, 3, 5	1, 3, 5	1, 3, 5	1, 3, 5	1, 3, 5	1, 3, 5	1, 3, 5	1	1, 3, 5	1, 3, 5	1, 3, 5	1	1, 3, 5	1	1, 3, 5	1	1, 3, 5	1
	6(o)										3,5				3,5						3,5
	9		1, 3, 5		1, 3, 5	1, 3, 5	1, 3, 5		1, 3, 5				1, 3, 5						1, 3, 5		
	12					1, 3, 5	1, 3, 5		1, 3, 5				1, 3, 5						1, 3, 5		
	15					1, 3, 5	1, 3, 5		1, 3, 5				1, 3, 5						1, 3, 5		

Real seas target conditions					
Wave height	Peak period	Peak direction	Directional spreading	Sea state	WEC ARRAY
H_{mo} *(cm)*	T_p *(sec)*	$\theta_p{}^o$	s^1		
4.5	1.2, 1.6	0, 22.5	2*, 4, 10, UD	HI—Kaneohe, Oregon 1	1, 3, 5
7.6	1.4, 1.8, 2.2	0, 22.5	2*, 4, 10, UD	Oregon 2, 3, 4	1, 3, 5
10.6	1.6	0, 22.5	2*, 4, 10, UD	IR—M4 Buoy	1, 3, 5
13.6	2.2	0, 22.5	2*, 4, 10, UD	Oregon 5	1, 3, 5
30	2.6	0	UD	Oregon storm	1
45.2	2.6	0	2, UD	100-yr storm	1
45.2	2.6	22.5	UD	100-yr storm	1

46050 data. Note that in this chapter, we only analyze a subset of these sea states, but they are all listed here for completeness. The generated wave frequency spectrum used the Pierson–Moskowitz model with a range of different directional spreading factors representative of the NDBC 46050 data. The irregular wave run-times ranged from 313 to 540 s, which was longer than the run-times of regular waves in order to improve the statistical significance of the collected data.

Model WECs and WEC Arrays

Five experimental WECs were fabricated for the experiments. They were designed as scaled versions of the Columbia Power Manta 3.1, and each consists of three rigid bodies as shown in Fig. 1. The central body is composed of the main spar and a nacelle, and is designed to stay relatively stationary in heave due to the large damper tank at its base. Two identical fore and aft floats differ by a rotation of 90°, as attached. The fore and aft floats are free to move only in pitch with respect to the central body. Thus, the WECs are constrained to move in a total of eight degrees of freedom (DOF), one for each float (relative pitch) and six for the central body (surge, sway, heave, roll, pitch, and yaw).

Each float is connected to the top of the spar through a drive shaft, and model generators are actuated by the relative motion between each float and the spar. The

Fig. 1 Manta 3.1 WEC assembly

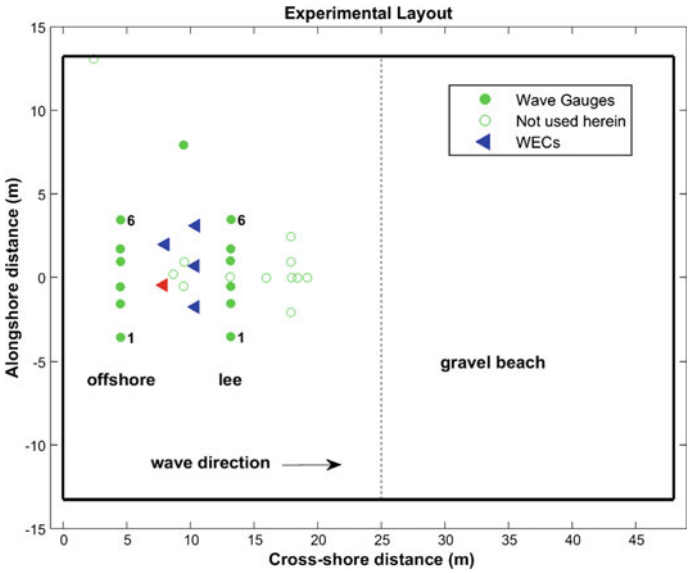

Fig. 2 Location of offshore and lee wave gage arrays (*filled green circles*), location of WECs for the single WEC experiments (*red triangle*), and locations of the 5-WEC experiments (combination of *red* and *blue triangles*)

generators were modeled using oil-filled rotary dashpots that were calibrated before deployment. A linear damping estimate was calculated via a least squares linear fit of measured torque to speed. Damping estimates for each dashpot were performed both pre- and post-experiment and were found to have changed significantly. Torque (the product of damping and rotational velocity) was not measured during the experiments, so for the power capture analysis the damping coefficients were assumed to trend linearly between the pre- and post-experiment values.

Three WEC configurations were tested—a single WEC and arrays of three and five WECs. The WEC arrangements are shown in Fig. 2. The mooring of each WEC was accomplished by running horizontal elastic lines between vertical stanchions and the damper tank of each WEC in a symmetrical three-point configuration. The elastic lines were selected to have a load/displacement curve that was similar to the field-scale mooring system design. At the laboratory scale, the WECs have a beam of 0.55 m (18 m at prototype) and the draft from the surface to its lowest point is 0.75 m.

Wave Instrumentation

The extensive set of instrumentation used during the experiments included 28 in situ instruments (wave gages and current meters) arranged in small arrays

designed to resolve the wave field offshore of the WEC array as well as in the immediate lee and far field of the WEC array. In addition, three acoustic Doppler velocimeters with co-located wave gages were arranged within the WEC array to capture near-field wave information. Because the near-field wave patterns were expected to be highly variable and difficult to measure in situ, a bi-static camera system was installed on the ceiling to attempt three-dimensional wave imaging through binocular stereovision techniques. Initial results from the analysis of those data are provided by Black and Haller (2013); here, we focus only on the observations offshore and in the lee of the WEC arrays. A schematic of the TWB coordinate system and the instrument and WEC locations is shown in Fig. 2. Wave gages were sampled at 50 Hz. More information about the experimental design and analysis procedures can be found in Rhinefrank et al. (2013).

Determination of the Relative Capture Width

A commercial motion-tracking system was installed on each of the WECs, and the motion data for the three rigid bodies composing each WEC (8 DOF) were used to estimate power capture. The system used a swarm (~90 total) of light-emitting diodes (LEDs) attached to lightweight rods on each of the three bodies composing the individual WECs. These active LEDs were tracked with a network of cameras installed on a frame above the tank. During wave action, the system of markers and cameras allowed the motion of each rigid body component to be tracked at 480 Hz. Subsequently, a zero-phase low-pass filter (50 Hz) was applied to the motion data, and the resulting signals were down-sampled to 50 Hz for analysis.

The velocity of the relative rotation of each float with respect to the spar, referred to as the generator speed, is needed to estimate the absorbed mechanical power; it was determined by differencing the relative rotation position signal and dividing by the 50 Hz time step. The signals were not de-trended for this calculation. The instantaneous mechanical power is calculated for each generator (fore and aft) as the product of the generator speed and the torque. The generator torque is calculated as the product of the estimated linear damping coefficient of the characterized generator and generator speed signal. The mean mechanical power of the fore and aft generators sum to the mean mechanical power of the total system. This procedure is used to calculate mean mechanical power in regular waves and real seas.

WEC performance is quantified as the mean mechanical power, normalized by the mean wave power incident across a width equal to the nominal WEC width (54.54 cm). This dimensionless performance parameter, used extensively in the WEC industry, is called the relative capture width (RCW) and can be thought of as the proportion of incident wave energy (in a crest length equal to the nominal WEC dimension) captured by the device. The power absorption characteristics of the experimental WEC were measured at individual frequencies across a range of regular wave conditions using the motion capture data. The resulting measured RCW is shown as the dashed line in Fig. 3. Data only exist for wave periods

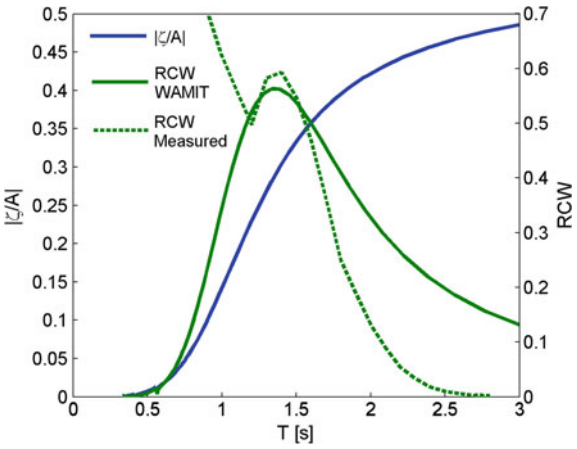

Fig. 3 Modeled WEC surge motion (*solid blue*) and the measured (*dashed green*) and WAMIT modeled (*solid green*) power absorption plotted versus wave period. The power absorption is plotted as the relative capture width (RCW), which is the ratio of the power absorbed by the device to the wave energy flux incident to its width

ranging from 0.9 to 2.7 s because they represent the extent of regular wave testing. The experimentally determined RCW curve demonstrates a peak near 1.4 s, and no power is absorbed for waves with periods longer than about 2 s. Additional analysis (not shown here) has extended the experimentally measured RCW to wave periods shorter than 0.9 s (see Rhinefrank et al. 2013). The extended experimental curve indicates increased RCW at even shorter wave periods. However, the extended RCW information has limited impact on the conditions analyzed here (see Table 1), which are composed of regular wave cases with the specific range of periods described by the RCW curve in Fig. 3 (0.9–2.7 s) and real sea state conditions that contain little or no energy at periods shorter than 0.9 s.

Numerical Modeling

When waves encounter WECs, portions of their energy are absorbed or scattered. A shadow region forms behind the devices but the diffraction process, acting over long distances shoreward, reduces the wave shadow by transmitting energy into the lee of the array. As a result, the wave field is modified both offshore of the array as well as in its lee. If the WECs are mobile in at least one degree of freedom (which most point absorber WECs are designed to be), the wave forces induce WEC motion, which generates additional wave motions (see Mei 2012 for a review). The feedback between the wave field and the WECs can, therefore, be quite complex, and the resulting combined wave field typically displays complex partial standing wave patterns. Such patterns also occur when a wave field interacts with isolated bathymetric features (for example, see Choi et al. 2009), and their prediction requires the consideration of wave-phase information. The partial standing wave patterns are known to be most pronounced for regular wave conditions and can be best captured using phase-resolving wave models. In contrast for random wave

conditions with directional spreading, the patterns are much less pronounced, and phase-averaged models can successfully predict the overall wave field (Choi et al. 2009).

To date, several types of models have been used to simulate wave–WEC interactions. The models range in complexity and vary in their ability to account for wave-phase information. In this chapter, we evaluate the performance of two such models. Specifically, we compare the performance of a phase-resolving and a phase-averaged model (WAMIT and SWAN, respectively) in the simulation of the experimental conditions. In addition, we use the phase-resolving model to analyze the impact of incident wave frequency on wave scattering and radiation from an individual WEC, and assess the applicability of either model for the variety of experimental wave conditions considered.

Phase-Resolved Linear Wave Theory—WAMIT

WAMIT is a state-of-the-art commercial boundary-element solver (WAMIT, Inc. 2000) that simulates linear hydrodynamic forces on immersed objects due to planar waves. It solves the standard linear wave-body boundary-value problem in the frequency domain. The assumptions underlying the model are that (1) the fluid is incompressible and inviscid; (2) the flow is irrotational and the velocity can be expressed as the gradient of a scalar velocity potential; (3) the wave height is small compared to the wavelength and water depth; and (4) the amplitudes of body motions are small compared to the size of the body. The latter two assumptions enable the use of linear wave (airy) theory. To find the solution to the boundary-value problem, WAMIT uses the boundary-element method, in which all body surfaces are represented as source or dipole functions that satisfy the governing equation (Laplace's equation for the velocity potential) and the free surface condition; the magnitudes of the dipole functions satisfy the no-penetration condition on all wetted surfaces.

Because WAMIT assumes linear waves, each frequency component can be treated independently and the velocity potential associated with each frequency component can be summed to describe the total fluid motion. All other variables of interest (i.e., flow velocities, surface elevation, and pressure fields) can be computed using the velocity potential and well-known linear wave theory formulations. Also, thanks to the assumption of linearity, the total velocity potential at a given frequency can be found as the superposition of the incident and scattered velocity potentials (ϕ_i and ϕ_s, respectively) and the radiation velocity potentials (ϕ_r^j) due to body motions in each degree of freedom, j. The scattered potential is the modification of the wave field due to the encounter with the device. The sum of the incident and scattered potentials is often referred to as the diffraction wave potential. The pressure field on the structure associated with the combination of the incident and scattered wave potentials is used to estimate the motion of the device,

and this motion results in the generation of radiated waves, described by the radiation velocity potentials, ϕ_r^j, associated with each degree of freedom of the device.

Spectral wave fields are considered by evaluating multiple wave components at given frequencies (ω) and directions (β), and associating an amplitude with the incident wave component as defined by an incident wave spectrum, $S_i(\omega, \beta)$. At a given frequency and direction, the magnitude of the incident wave amplitude is $|A| = \sqrt{2S_i(\omega, \beta)\Delta\omega\Delta\beta}$, where $\Delta\omega$ and $\Delta\beta$ are the bin widths at the given frequency and direction, respectively. For the phase of the incident wave components, random values are chosen from a uniform distribution between 0 and 2π. From the point spectrum, the bulk parameter of the zeroth-moment significant wave height can be computed as $H_s = 4\sqrt{\sum\sum S(\omega, \beta)\Delta\omega\Delta\beta}$.

To model the WEC array experiments described above, a geometric model of the physical WEC being tested is required. As an initial assessment, a simple cylinder was adopted as the geometry for the computational model. Although a cylinder is a very rough approximation of the physical model, the behavior of the cylinder can be controlled to closely mimic the WEC. First, the dimensions of the cylinder were chosen to match the approximate size of the physical model; the diameter of the cylinder is 0.6 m and the draft is 0.8 m. Second, the single degree-of-freedom mode of motion was chosen to be surge, because the surge motion of the cylinder most closely resembles the power-absorbing motion of the physical model WEC under consideration. In particular, the power absorption curve of the surging cylindrical WEC reproduces the important portions of the power absorption curve associated with the physical model WEC (see Fig. 3 for the comparison). Finally, a power take-off (PTO) damping for the computational model WEC was chosen (at 2000 kg/s), so that the peak absorbed power was of the same approximate magnitude and occurred at approximately the same frequency as in the physical model (Fig. 3).

The modeled wave field domain is the same size as the TWB. The water depth was fixed at 1.4 m throughout the domain. No effort was made to model the sloping beach, wave basin walls, or the wavemaker. Wave data from 21 wave gages are available for comparison. Comparisons are made directly at two sets of wave gages. The offshore set corresponds to the set of six gages that were between the WEC arrays and the wavemaker. The set of lee instruments corresponds to a line of six gages behind the WECs. The offshore and lee wave gages are numbered 1–6 from left to right facing the wavemaker. The wave gage and WEC positions are shown in Fig. 2.

Phase-Averaged Linear Wave Theory—SWAN

The SWAN model was designed to simulate the transformation of the wave action density spectrum over a variable bathymetry and ambient current field, as well as

the energy gain or loss of wave components due to mechanisms such as wind input and wave dissipation (Booij et al. 1999). Like WAMIT, SWAN is essentially based on linear wave theory; hence, a spectral sea can be represented as the sum of harmonic wave components at given frequencies and directions (although some empirical formulations can be included to account for nonlinear processes such as wave–wave interactions). In SWAN, all wave components are planar, and the wave action density of each wave component is considered through a conservation of action equation solved over a regular grid using finite difference methods (an unstructured grid option also exists; see Zijlema 2010). For the computation of wave action density, the relevant quantities are the magnitude of the planar wave component, or wave height, and its relative frequency and direction; the phase of the wave component is not considered.

The SWAN model has an option to include the representation of coastal structures, such as breakwaters or jetties (Ilic et al. 2007). However, in this standard option the structures are represented relatively simplistically using frequency-independent modifications of the wave action spectrum via reflection and transmission coefficients that must be pre-determined for the given structures. Further, the absence of wave-phase information precludes SWAN from providing a more realistic representation of the effect of immersed bodies on the wave field, because the reproduction of conditions with intersecting wave trains (that form partial standing wave patterns) would require knowledge of phase information associated with the wave components.

In this work, we are interested in improving the representation of immersed bodies in the SWAN model and implementing a representation of the WEC structure that includes information about the frequency-dependent nature of the energy absorption. This is achieved by using a nested-domain approach. For a situation involving multiple rows of WEC devices, the nested approach involves dividing the domain into multiple adjacent sub-domains separated by rows of WECs. SWAN is then used to propagate waves from the offshore boundary through the first sub-domain to the first row of WECs. The SWAN-produced wave spectra at the locations of the WECs are then manually altered given the experimentally determined, frequency-dependent RCW (Rhinefrank et al. 2013) associated with each WEC. The resulting alongshore-variable wave field then enters the next shoreward sub-domain, and the evolution of this wave field is computed using SWAN until the next row of devices is encountered. Similar frequency-dependent WEC formulations for spectral wave models were given by Alexandre et al. (2009) and Silverthorne and Folley (2013); however, they used theoretical RCW curves with limited (if any) comparisons to field observations. Chang et al. (2016) have incorporated the methodology we used here into the SWAN source code, which eliminates the need for nesting and external modification of the spectra.

Even though our implementation is an improvement over many preexisting representations of WECs in the SWAN model, it has several important shortcomings. In particular, wave field effects are accounted for only in the lee of the devices and are the result of only WEC power absorption. Hence, the implementation does not consider any scattered or radiated wave energy. Furthermore, no modification to

the wave direction in the shadow region is produced. Use of the diffraction formulation included in the SWAN model (Holthuijsen et al. 2003) can potentially remedy this latter shortcoming, but, given the phase-averaged nature of SWAN, this formulation only reproduces the modification to the group velocity associated with wave components and will still not produce a realistic phase-dependent diffraction pattern. Use of the diffraction formulation also comes at a significant computational cost that can lead to difficulties in achieving a desired spatial resolution. Despite these shortcomings, ascertaining the conditions under which this approximate treatment in SWAN is adequate to obtain a reasonable representation of the near-field wave field is of interest.

To model the experiments, the entire TWB is considered using the measured basin bathymetry (obtained using a mobile lidar system). Monochromatic wave cases are approximated with a very narrow spectral shape. To assess the model skill at reproducing the observed conditions, we consider a metric that is indicative of the overall reduction in wave power in the lee of the WECs. We define this power loss metric by considering the difference between the incident wave energy flux through an alongshore transect and the net wave energy flux integrated over the same alongshore distance in the lee of the WECs. The total alongshore distance considered for the power loss metric is the extent of the alongshore array of gages (see Fig. 2). For spectral sea comparisons, the energy flux computation requires integrating over frequency and direction.

Results

The results section is divided into two parts: In the first part, in order to elucidate the spatial scales of scattering and radiation induced by WECs and their dependence on incident wave frequency, WAMIT wave fields are compared to the experimental observations. This comparison also assesses the ability of the WAMIT model setup to simulate the overall experimental conditions. In the second part, the magnitude of the wave shadow simulated by the SWAN model with the experimentally determined RCW is compared to the wave shadow observations.

WAMIT-Data Comparisons

We begin our analysis with the cases involving 1 or 5 WECs subjected to regular wave conditions (Fig. 4) and spectral sea states (Fig. 5). To quantify the importance of the wave field changes induced by the WEC arrays, the observed wave heights are normalized by the measured incident wave height for each case. It should be noted that defining/measuring the incident wave height with the laboratory data introduces challenges due to the near-immediate presence of WEC-scattered waves offshore of the WECs. Here, for the incident wave height we take the average of all

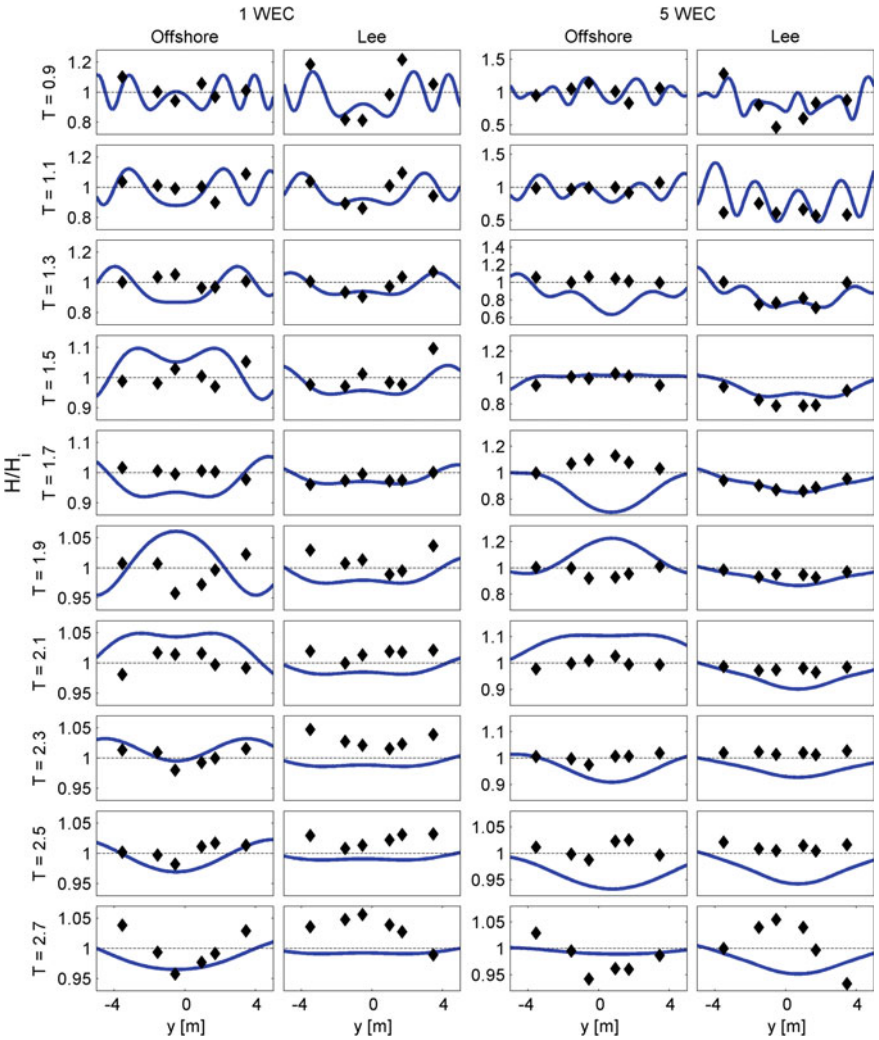

Fig. 4 WAMIT model results (*lines*) and observations (*black diamonds*) for the regular wave cases with 1 WEC (*columns 1 and 2*), and 5 WECs (*columns 3 and 4*). For each WEC array, the *left column* shows offshore data and the *right column* the lee data. Wave heights normalized by the average incident wave height (H/H_i) for different wave periods as indicated on the left-hand side of each row

of the wave height measurements at the offshore gage array, including the lone gage positioned at ~ [9, 8 m] (cross-shore, alongshore) about 5 m alongshore from the WEC array.

For the conditions involving wave periods of 0.9 and 1.1 s, the WAMIT results demonstrate that the near-field waves are highly variable spatially and are consistent

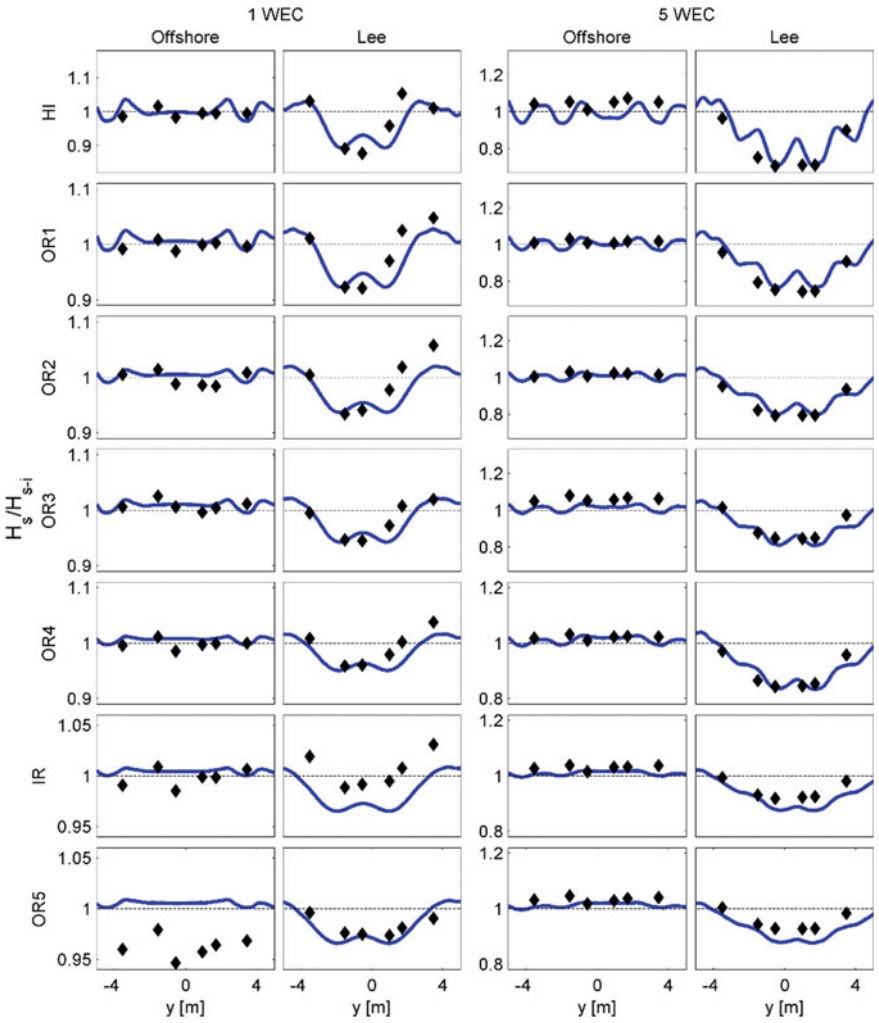

Fig. 5 Same as Fig. 4 but for spectral sea states. Sea states listed at the far *left*

with the well-known alongshore standing wave ridge pattern (see also Farley 2011 and McNatt et al. 2013). For these periods, the length scales of variability are short (~1 m) and the amplitude variability is relatively large (±20% change from incident wave height for 1 WEC and close to 50% for the 5 WEC cases), and multiple ridges are present within the observational arrays.

The full spatial standing wave ridge patterns simulated by WAMIT for the 1 WEC cases are also shown in Fig. 6 (left panels), in which the short-length scales of the wave height variation are very evident, especially for the shortest wave periods. The results show that the amplitude of the wave height ridge pattern is more

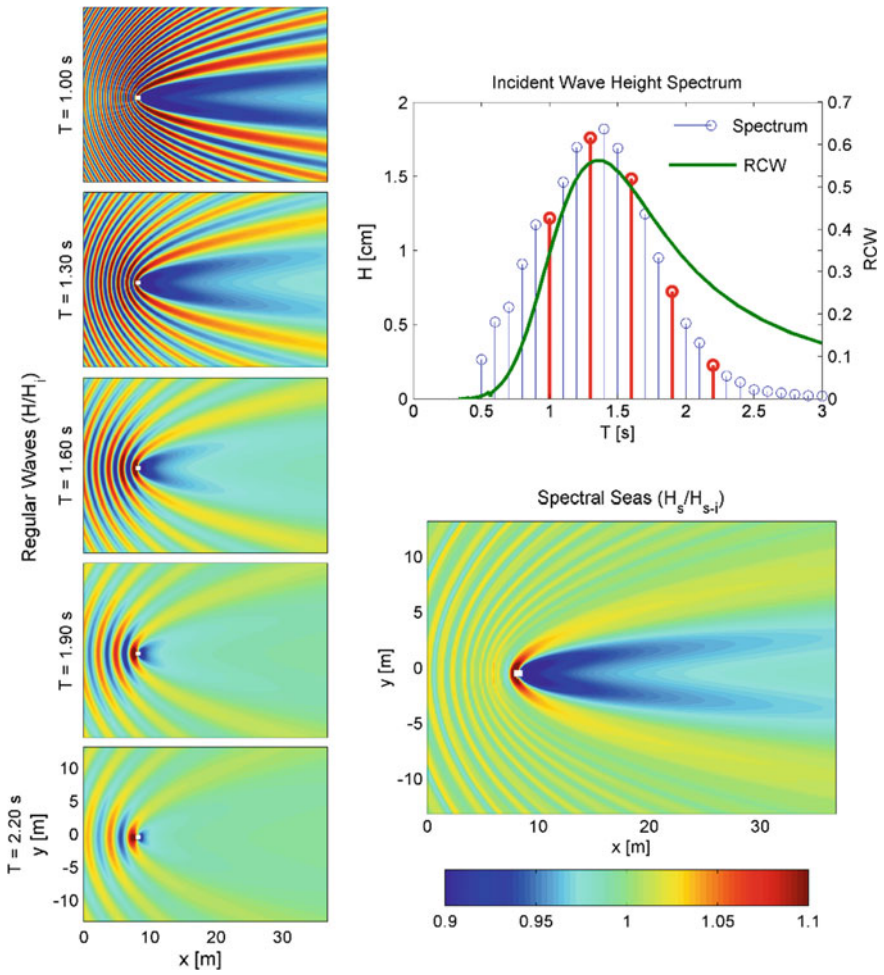

Fig. 6 (*Left panels*) Wave height modification (local wave height normalized by incident wave height) for different wave components (*top-right panel*) wave heights of individual components of the spectrum (*left panels* correspond to *red components*) with the modeled RCW curve, and (*bottom-right panel*) normalized significant wave height including all components ($T_p = 1.4$ s)

pronounced for short periods, which indicates that the reflected and radiated wave components are more important for short-period waves than for long-period waves. This is consistent with the device motion estimates produced by WAMIT (see Fig. 3), which indicate that the WEC functions as a wave follower (i.e., motion amplitude is more similar to the incident wave amplitude and phase coupling with the incident waves) for large periods (i.e., periods $\geq$ peak RCW). Hence, shorter incident waves are associated with more energetic radiated wave components. One ramification of the related redistribution of wave energy is that the shadow region is more pronounced for short-period waves.

The short-scale variability under regular wave conditions is clearly evident in the laboratory observations (Fig. 4). Of course, the observed ridge locations must have some sensitivities to the details of the WEC shape and response characteristics as well as to the finite drift of the WECs on their compliant moorings; hence, the partial standing wave pattern likely has some additional space/time variabilities beyond the WAMIT modeling capabilities as we have it configured here. Despite these shortcomings, the locations of the peaks and troughs of the ridges, as well as the magnitude of the wave height variability in the regular wave cases, are fairly well simulated by WAMIT. The short-scale variability is present in both of the alongshore arrays, in the lee as well as offshore of the WECs. The lee transect primarily demonstrates the wave shadow and an overall reduction in wave height directly behind the devices and provides evidence of corresponding ridges at alongshore distances from the edge of the WEC arrays (e.g., T = 0.9 s, 1/5 WEC lee array). The offshore data also show the effects of the scattering of wave energy from the WECs as well as the radiated waves due to WEC movement. The amplitude of wave height variability in the offshore array significantly decreases with wave period. The model results provide much-needed context for the observations given that the observations only sparsely sample the short-scale variability of the wave pattern.

The trend in the spatial structure in the lee of the WECs is that it smooths out (i.e., the spatial scales increase) for cases with longer wave periods and more resembles a simple wave shadow for which the wave height deficit signal also decreases for periods greater than 1.5 s. The results for the 1.3, 1.5, and 1.7 s periods show very good agreement (especially at the lee transect), but the measured transect is not wide enough to capture a full-standing wave pattern. The magnitude of the wave modification is not large, ±10%, for these cases. For even longer periods, the wave height modification at the lee transect is minimal (<5%, note the scale changes in the plots), and the length scales are large enough where no major oscillations are expected within the observational transect. The model/data disagreement appears to be larger for the longer wave periods, but it should be considered in the context of the small signal-to-noise ratio as wave period increases, the experimental uncertainties, and the necessary model approximations. In addition, the relative distance (distance divided by wavelength) between the WEC arrays and the lee transect is greater for the shorter waves, which may make the results somewhat less dependent on the details of the WEC geometry or the translation and movement of the individual WECs.

On the other hand, the general realism shown by the model data comparisons can be attributed to the accurate geometric size of the model WECs and their reasonable approximation of the power capture characteristics of the physical devices even though they are represented rather simplistically as moving cylinders. In general, it appears that phase-resolved, linear wave theory has some skills in modeling the wave field for both single and multiple WEC configurations, and that the predicted standing waves do indeed exist. Note that the correct interpretation of the peaks and troughs of the data transect would have been very difficult without having the phase-resolved computational model for context.

In spectral seas, the computational prediction and experimental data match well (Fig. 5) for both the 1-WEC and 5-WEC cases. Figure 6 (left panels and bottom-right panel) also illustrates the contributions of individual frequency components to the overall wave height variation for spectral seas. In the figure, the modifications to the wave field due to specific frequency components are shown along with the total resultant significant wave height spatial variability when the entire spectrum is considered (spectral peak at T = 1.4 s, top-right panel). Both figures demonstrate that, at the offshore gage array, the significant wave height is fairly uniform, and in the lee of the devices the structure of the wave shadow is fairly consistent for all sea states. The wave shadow is easily discerned in the both model and data, and the model appears to accurately capture the alongshore scale and magnitude. A few cases appear to show a vertical offset but an appropriate alongshore trend. We attribute this to the small signal-to-noise ratio of the wave shadow we have tried to capture here (wave height differences of the order 2–3% in some cases).

The spatial variation in wave height due to standing waves that is quite pronounced in the regular wave cases is smoothed when random waves are considered. This is because the wave components of differing frequencies that make up the random wave field are associated with standing wave ridge patterns with nodes that occur at differing locations. The significant wave height (shown in Figs. 5 and 6 bottom-right panel) is indicative of a composite of the spatial patterns associated with the individual wave components and therefore displays much less variability in space. This is especially evident at the offshore observational transect. At the lee transect, a wave shadow pattern exists in addition to the short-scale variability due to the standing wave ridge pattern. Although the locations of the nodes associated with the ridge patterns all vary with frequency at the lee transect, the wave shadows at different frequencies occur at mostly the same locations. As a consequence, the wave shadow effect is more pronounced for the random wave cases.

SWAN Data Comparisons

The SWAN simulations approximate only the formation of the shadow in the lee of the devices and cannot capture the nodal structure associated with the standing wave ridge pattern. This is primarily because of the phase-averaged nature of the model; hence, radiated waves are not simulated; only the extraction of wave energy due to the WECs and the associated reduction in the wave action density spectrum are considered. Therefore, we evaluate the ability of the SWAN simulations to reproduce the bulk description of the wave shadowing when a realistic device RCW curve is used. The wave shadow estimated by the model is taken as the net power deficit between the offshore and lee array locations as evidenced in the SWAN simulations. Because the wave propagation distance between the WECs and the lee array is short, this deficit is mostly (but not entirely) determined by the model spectral modifications applied at the WEC locations, which are directly determined

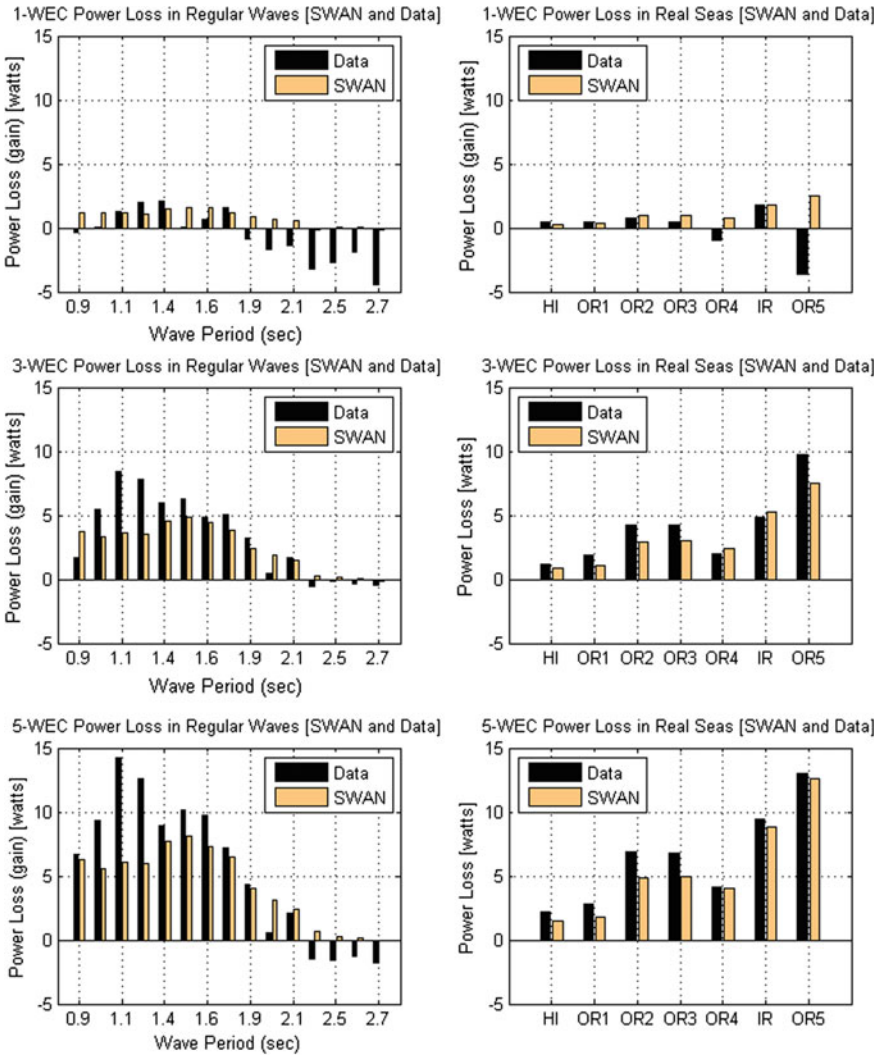

Fig. 7 Wave energy flux deficit measured by gage arrays (*black bars*) and SWAN-simulated (*tan bars*). Deficit is defined as the difference between the wave energy flux offshore and in the lee of the devices for 1-WEC (*top row*), 3-WEC (*middle row*), and 5-WEC (*bottom row*) arrays for regular wave cases (*left column*) and real sea states (*right column*)

from the experimental RCW curve developed from the WEC motion observations. In Fig. 7, the wave shadow estimated in the model is compared to the net difference between the observed wave energy flux crossing the offshore gage array and that crossing the lee wave gage array.

Immediately evident from Fig. 7 is that the SWAN data comparisons for real sea states (right column) are generally quite good. Also evident for both regular waves

and real seas (both columns) is the relative increase in the total power loss (wave shadow) moving from the 1-WEC (upper panels) and 3-WEC (middle panels) to the 5-WEC (lower panels) configurations. Thus, there is also an inherently corresponding increase in the signal-to-noise ratio of the power loss estimates with the increased number of WECs. For the regular wave cases (left column), there is an evident peak in the SWAN-simulated power loss around $T = 1.5$ s, which mimics the RCW curve that was used (see Fig. 3), as expected, and is independently confirmed from the observed wave shadow data here (also see Fig. 4).

We also note that the SWAN data comparisons for regular wave conditions need to be considered with care, especially for cases involving regular waves with short periods, because of the difficulties involved in using point observations to quantify the spatially, highly variable wave field either offshore or in the lee of the WECs (see Fig. 4). There is evidence of increased observed power loss at periods shorter than about 1.4 s (the peak of the RCW curve). However, the WAMIT results discussed in "WAMIT-data comparisons" suggest that reflected and radiated waves might play an increased role for these shorter periods, so that the power loss observed in the lee of the WECs cannot entirely be attributed to power absorption. Instead, wave power has been spatially redistributed. Given the reliance on only wave absorption information (via the RCW curve), the SWAN model cannot reproduce these more complex power redistribution effects.

There are also SWAN data discrepancies in the regular wave cases (left column) that involve periods longer than about 2 s. For these long-period cases, the SWAN simulations indicate no energy loss (or gain), but the observations suggest some energy gain. Again, the SWAN simulations correctly conform to the experimental RCW curve, and the SWAN data difference likely derives from the offshore wave scattering from the WECs. Specifically, if the majority of gages in the offshore array happened to be located in a valley of the partial standing wave pattern (see Fig. 6, left-bottom panel) and the lee array located in a lower amplitude wave shadow, as expected, the wave height differences between the observational arrays would lead to a negative power deficit (i.e., power gain).

Discussion

Next, we show results from simulations using the two models, explicitly keeping the model WEC power capture characteristics the same in both, so that we can illustrate how the scattering and radiation affect the ability of the SWAN model (with the associated WEC parameterization) to simulate the wave shadow. The results also demonstrate the impact of the scattering and radiated fields on the severity of the wave shadow, which has implications for the overall nearshore wave effects of WEC arrays.

The simulation conditions bookmark the range of scattering behavior seen in both the model and experimental results in the previous section. In particular, model results are obtained for two regular wave cases with $T = 1$ and $T = 2$ s and four

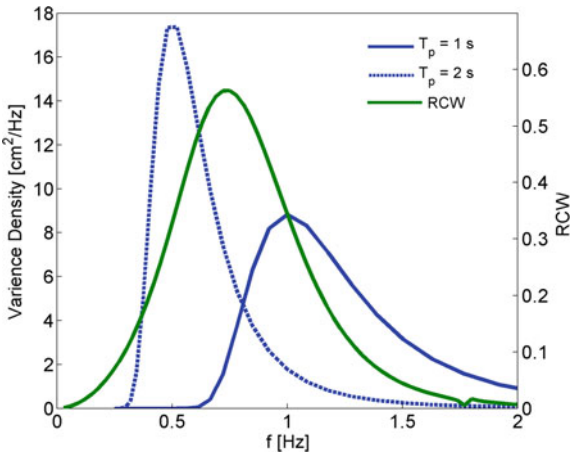

Fig. 8 Wave spectra (1-second peak period in *solid blue* and 2-second period in *dashed blue*) and WAMIT-computed RCW (*green line*, also shown in Fig. 3)

spectral seas cases—unidirectional waves and directionally spread seas both with $T_p = 1$ and $T_p = 2$ s. As can be seen in Fig. 8, the two wave periods chosen have nearly the same model RCW value of ~0.35. This enables a comparison of their differing scattered and radiated wave fields in a setting where the expected power capture is the same. All simulations have the same incident wave height, but the two different spectral peak periods have somewhat different spectral shapes that follow the Pierson–Moskowitz model (also shown in Fig. 8). Directional spreading (two cases) used a $\cos^{2s}$ distribution with a spreading parameter of $s = 10$.

All SWAN runs were carried out with and without the diffraction option, except for the regular wave $T = 2$ s case where convergence could not be attained for SWAN with diffraction (see missing panel in Fig. 9). To allow for a more direct comparison, the power capture characteristics are kept the same in both models by using the RCW performance curve computed by WAMIT (shown in Figs. 3 and 8) for the SWAN simulations.

To assess the utility of SWAN in estimating the wave shadow, we begin by analyzing the simulations involving regular waves (see top two rows in Fig. 9). Because the WEC model in SWAN is based solely on energy extraction, the SWAN results (with no diffraction effects) for both periods are identical. For these cases, the wave shadow produced by SWAN extends onshore as a narrow streak, and there is almost no recovery in wave height with distance to the lee of the WEC. In contrast, the WAMIT wave fields for the two periods are quite different from one another. The scattered and radiated wave components are more energetic for the shorter period case, as evidenced by the stronger standing wave ridge patterns. Because these scattering processes redistribute the wave energy spatially, the wave shadow is also clearly more pronounced for the shorter period case, even though the amount of energy extracted from the wave field is similar for both periods. When the diffraction option in SWAN is used, the shadow spreads alongshore more readily, as expected, and the resulting shadow region is little more similar to the

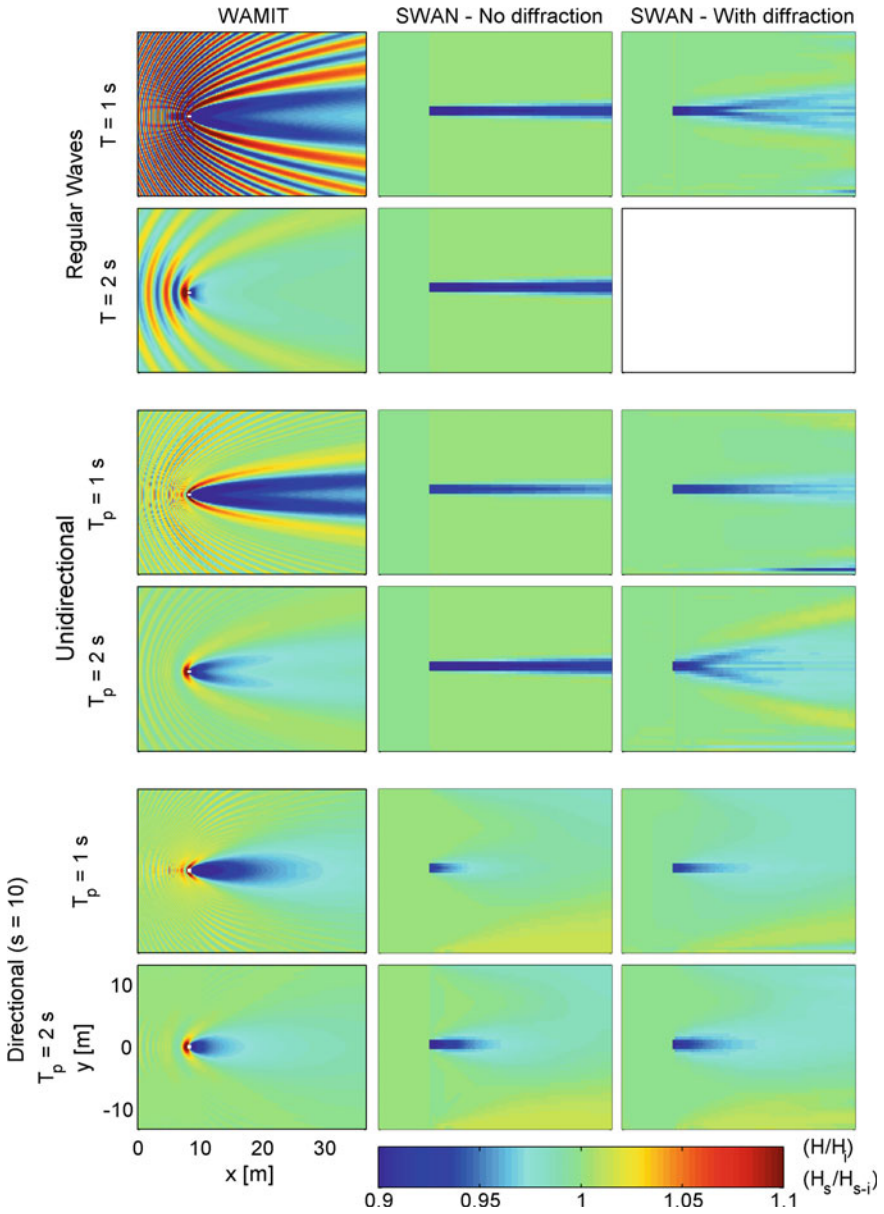

Fig. 9 WAMIT-SWAN wave field comparisons for regular waves (*rows 1 and 2*), unidirectional random waves (*rows 3 and 4*), and directionally spread random waves (*rows 5 and 6*). Each type has both 1-second and 2-second peak periods. The SWAN solution did not converge for T = 2 s regular waves w/diffraction

WAMIT results. However, the spatial variability related to the scattered and radiated waves is not reproduced.

In the previous section, we noted from Fig. 7 that the SWAN model consistently underestimated the observed wave shadow magnitude for regular wave conditions from 1.0 to 1.4 s, i.e., for waves with smaller periods than those of the peak (experimental) RCW. This under-prediction occurs because the wave shadow associated with these shorter period waves is only partially controlled by the amount of wave energy absorption by the WEC; it is also affected by the increased wave-scattering processes at these wave periods. Note that Beels et al. (2010) observed a similar phenomenon in their modeling of the Wave Dragon WEC. Specifically, they noted that the wave height reduction behind the device could not always be explained by energy absorption; it could instead be related to wave reflection. This is also supported by the WAMIT results in Fig. 9, which shows that the short-period cases consistently have a greater wave shadow magnitude than the longer period cases (for both regular and spectral sea states).

For wave periods around the RCW peak, the wave energy flux deficit shown in Fig. 7 indicates that the SWAN model could better represent the observed wave shadow. This is because at these periods, the wave shadow is most closely linked to the absorbed power. For even longer periods, for which the RCW is near zero, the experimental shadow observations are again dominated by the redistribution due to scattering processes, and the SWAN simulations do not produce wave shadows because there is no expected power capture at those wave periods.

For the unidirectional sea simulations (Fig. 9 middle panels), the shorter period WAMIT results display more spatial variability, a more pronounced shadow region, and a distinct wave amplification region in the shape of a parabola around the wave shadow. Similar to its performance in the regular wave cases, the SWAN model is not able to capture any of these features. In the WAMIT simulation, the wave height modification is less pronounced for the longer period case, and the standing wave ridge pattern offshore is almost absent. This is again due to the reduced scattering and radiation and also to the smoothing induced by the phase relationships between the set of wave periods present. Here, SWAN, considering spectral wave conditions and with the diffraction option, is better able to reproduce the wave height variability in the lee of the WEC as compared to SWAN performance in the regular wave case.

WAMIT results associated with the directionally spread seas results (bottom two rows in Fig. 9) show a much smoother wave height modification pattern, as would be expected in the presence of wave components from a variety of directions. Here, the results from the different periods are more similar, though the amplitude of the wave shadow is still larger for the short-period case. The effect of the diffraction option in the SWAN model is less important here, which is an expected result for directionally spread waves. Overall, the SWAN results for the longer peak period most closely resemble the WAMIT wave field, but only in the lee of the device. In general, the SWAN results for the directionally spread cases are a better match to the WAMIT results than those for either the unidirectional or regular wave cases.

Conclusions

In this chapter, we have presented results from a laboratory experiment conducted using an array of 1:33 scale WEC devices to ascertain the wave field modifications caused by the presence of the WECs. Further, two commonly used numerical models—the phase-resolving model WAMIT and the phase-averaged model SWAN—were applied to the conditions of the experiment and validated using the available observations. The SWAN simulations took into account the frequency-dependent nature of the wave energy absorption through a nested domain approach, whereby the spectra at the locations of the devices were altered based on preexisting knowledge of the power absorption curve leading to the simulated wave field modifications in the lee of the devices.

We found that the short-scale variability predicted by phase-resolving models such as WAMIT is indeed consistent with the observations from an array of wave gages both offshore and in the lee of the WECs. The short-scale variability is linked to a standing wave ridge pattern that arises because of wave scattering by the WEC device. The scattered waves are generated by scattering from the device and radiated waves generated by device motion. At short-wave periods, this high short-scale wave height variability complicates the interpretation of point observations. The issues arise either because the variability cannot be adequately resolved, or the observations are biased toward either ridges or valleys in the partial standing wave pattern.

Overall, the results indicate two things: First, the WEC parameterization we have used in the SWAN model can be effective at simulating the wave shadows induced by WEC arrays under conditions where the wave shadow is primarily controlled by the WEC power capture characteristics rather than by the redistribution of wave energy due to scattering and radiation. Generally speaking, these conditions occur when much of the wave energy lies at wave periods around the RCW peak period and higher when the RCW is still nonzero. The parameterization will underestimate the wave shadow when the significant energy lies below the RCW peak period, where scattering and radiation are of increased importance. The parameterization does not capture the partial standing wave field offshore of WEC arrays because it is caused by scattering and radiation and not power capture.

Second, the analysis of wave shadows induced by WECs using the WAMIT simulations has indicated that under similar power capture characteristics, it is possible to have significantly different wave shadows. Specifically, the WAMIT results demonstrate that the shorter period cases have shadows of larger magnitude and more complicated offshore structure, even when frequency and directional spreading are included. It is reasonable to argue that a characteristic potential environmental effect of WEC arrays is the amount of wave field modification induced by the presence of an array. Hence, these results indicate that even when the potential for wave energy capture is normalized for (i.e., similar power capture conditions), the environmental effects of WEC arrays (i.e., the wave shadow) are

reduced when WECs are designed to operate such that the expected wave climate lies on the longer period side of the WEC RCW curve.

Acknowledgements This work was supported by the US Department of Energy (Award #DE-EE0002658), Sandia National Laboratories, and Columbia Power Technologies under Research Subagreement NO. 2010-1698. Additional support came from the Oregon Wave Energy Trust through Award Number OIC-0911-109. We also wish to thank Ken Rhinefrank, Joe Prudell, Al Schacher, Erik Hammagren, Tim Maddux, and the staff of the Hinsdale Wave Research Laboratory for their help in the experimental effort.

References

Abanades, J., Greaves, D., & Iglesias, G. (2014a). Wave farm impact on the beach profile: A case study. *Coastal Engineering, 86,* 36–44.

Abanades, J., Greaves, D., & Iglesias, G. (2014b). Coastal defence through wave farms. *Coastal Engineering, 91,* 299–307.

Alexandre, A., Stallard, T., & Stansby, P. K. (2009). Transformation of wave spectra across a line of wave devices. *Proceedings of the 8th European Wave and Tidal Energy Conference* (*EWTEC 2009*).

Ashton, I. G. C., Johanning, L., & Linfoot, B. (2009). Measurement of the effect of power absorption in the lee of a wave energy converter. *Proceedings of OMAE 2009*, OMAE2009–79793.

Babarit, A., Hals, J., Muliawan, M. J., Kurniawan, A., Moan, T., & Krokstad, J. (2012). Numerical benchmarking study of a selection of wave energy converters. *Renewable Energy, 41,* 44–63.

Babarit, A. (2013). On the park effect in arrays of oscillating wave energy converters. *Renewable Energy, 58,* 68–78.

Beels, C., Troch, P., De Visch, K., Kofoed, J. P., & De Backer, G. (2010). Application of the time-dependent mild-slope equations for the simulation of wake effects in the lee of a farm of wave dragon wave energy converters. *Renewable Energy, 35,* 1644–1661.

Black, C., & Haller, M. C. (2013). *Analysis of waves in the near-field of wave energy converter arrays through stereo video, Abstract: OS11C-1657*. San Francisco, CA: AGU Fall Meeting.

Booij, N., Ris, R. C., & Holthuijsen, L. H. (1999). A third-generation wave model for coastal regions—1. Model description and validation. *Journal Geophysical Research, 104*(C4), 7649–7666.

Borgarino, B., Babarit, A., & Ferrant, P. (2012). Impact of wave interactions effects on energy absorption in large arrays of wave energy converters. *Ocean Engineering, 41,* 79–88.

Chang, G., Ruehl, K., Jones, C. A., Roberts, J., & Chartrand, C. (2016). Numerical modeling of the effects of wave energy converter characteristics on nearshore wave conditions. *Renewable Energy, 89,* 636–648.

Chatjigeorgiou, I. K. (2011). Three dimensional wave scattering by arrays of elliptical and circular cylinders. *Ocean Engineering, 38,* 1480–1494.

Choi, J, Lim, C. H., Lee, J. I. & Yoon S. B. (2009). Evolution of waves and currents over a submerged laboratory shoal. *Coastal Engineering*, Vol. 56, 297–312.

Day, A. H., Babarit, A., Fontaine, A., He, Y.-P., Kraskowski, M., Mirai, M., et al. (2015). *Ocean Engineering, 108,* 46–69.

De Andrés, A. D., Guanche, R., Meneses, L., Vidal, C., & Losada, I. J. (2014). Factors that influence array layout on wave energy farms. *Ocean Engineering, 82,* 32–41.

Eriksson, M., Waters, R., Svensson, O., Isberg, J., & Leijon, M. (2007). Wave power absorption: Experiments in open sea and simulation. *Journal of Applied Physics, 102,* 084910.

de Falcão, A. F. (2010). O., Wave energy utilization: A review of technologies. *Renewable and Sustainable Energy Reviews, 14,* 899–918.

Farley, F. J. M., (2011). Far-field theory of wave power capture by oscillating systems. *Philosophical Transactions of the Royal Society A:Mathematical, Physical and Engineering Sciences*, 370(1959), 278–287.

Fernandez, H., Iglesias, G., Carballo, R., Castro, A., Fraguela, J. A., Taveira-Pinto, F., et al. (2012). The new wave energy converter WaveCat: Concept and laboratory tests. *Marine Structures, 29,* 58–70.

Flocard, F., & Finnigan, T. D. (2010). Laboratory experiments on the power capture of pitching vertical cylinders in waves. *Ocean Engineering, 37,* 989–997.

Folley, M., & Whittaker, T. (2013). Validating a spectral-domain model of an OWC using physical model data. *International Journal of Marine Energy, 2,* 1–11.

Gonzalez-Santamaria, R., Zou, Q. P., & Pan, S. (2013). Impacts of a wave farm on waves, currents and coastal morphology in Southest England. *Estuaries and Coasts, 1,* 1–14.

Haller, M. C., Porter, A., Lenee-Bluhm, P., Rhinefrank, K., Hammagren, E., Özkan-Haller, T. & Newborn, D. (2011). Laboratory observations of waves in the vicinity of WEC-arrays. *Proceedings of European Wave and Tidal Energy Conference* (*EWTEC 2011*), Paper No. 419.

Holthuijsen, L., Herman, A. & Booij, N. (2003). Phase-decoupled refraction–diffraction for spectral wave models. *Coastal Engineering*, 49(4), 291–305.

Ilic, S., van der Westhuysen, A. J., Roelvink, J. A., & Chadwick, A. J. (2007). Multidirectional wave transformation around detached breakwaters. *Coastal Engineering, 54,* 775–789.

Iturrioz, A., Guanche, R., Armesto, J. A., Alves, M. A., Vidal, C., & Losada, I. J. (2014). Time-domain modeling of a fixed detached oscillating water column towards a floating multi-chamber device. *Ocean Engineering, 76,* 65–74.

Kara, F. (2016). Time domain prediction of power absorption from ocean waves with wave energy converter arrays. *Renewable Energy, 92,* 30–46.

Li, Y., & Yu, Y.-H. (2012). A synthesis of numerical methods for modeling wave energy converter-point absorbers. *Renewable and Sustainable Energy Reviews, 16,* 4352–4364.

McNatt, J. C., Venugopal, V., & Forehand, D. (2013). The cylindrical wave field of wave energy converters. *International Journal of Marine Energy, 3–4,* e26–e39.

Mei, C. C. (2012). Hydrodynamic principles of wave power extraction. *Philosophical Transactions of the Royal Society A, 370,* 208–234.

Mendoza, E., Silva, R., Zanuttigh, B., Angelelli, E., Andersen, T. L., Martinelli, L., et al. (2014). Beach response to wave energy converter farms acting as coastal defence. *Coastal Engineering, 87,* 97–111.

Millar, D. L., Smith, H. C. M., & Reeve, D. E. (2007). Modelling analysis of the sensitivity of shoreline change to a wave farm. *Ocean Engineering, 34*(5–6), 884–901.

Nihous, G. C. (2012). Wave power extraction by arbitrary arrays of non-diffracting oscillating water columns. *Ocean Engineering, 51,* 94–105.

O'Dea, A., Haller, M. C. & Özkan-Haller, H. T. (2015). The impact of wave energy converter arrays on wave-induced forcing in the surf zone. *Submitted to Renewable Energy*.

Palha, A., Mendes, L., Fortes, C. J., Brito-Melo, A., & Sarmento, A. (2010). The impact of wave energy farms in the shoreline wave climate: Portuguese pilot zone case study using Pelamis energy wave devices. *Renewable Energy, 35*(1), 62–77.

Payne, G. S., Taylor, J. R. M., Bruce, T., & Parkin, P. (2008). Assessment of boundary-element method for modelling a free-floating sloped wave energy device. Part 2: Experimental validation. *Ocean Engineering, 35,* 342–357.

Porter, A. K., Haller, M. C. & Lenee-Bluhm, P. (2012). Laboratory observations and numerical modeling of the effects of an array of wave energy converters. *Proceedings of 33rd ICCE 2012.* Santander, Spain, doi:10.9753/icce.v33.management.67.

Rhinefrank, K., et al. (2013). Benchmark Modeling of the Near-Field and Far-Field Wave Effects of Wave Energy Arrays, *Columbia Power Technologies Final Report*, DE-EE0002658, U.S. Dept. of Energy, www.osti.gov/servlets/purl/1060889/.

Rusu, E., & Guedes, C. (2013). Soares, Coastal impact induced by a Pelamis wave farm operating in the Portuguese nearshore. *Renewable Energy, 58,* 34–49.

Silverthorne, K. E. & Folley, M. (2013). A new numerical representation of wave energy converters in a spectral wave model. *Proceedings of the 10th European Wave and Tidal Energy Conference* (*EWTEC 2013*).

Sinha, A., Karmakar, D., & GuedesSoares, C. (2016). Performance of optimally tuned arrays of heaving point absorbers. *Renewable Energy, 92,* 517–531.

Smith, H. C. M., Pearce, C., & Millar, D. L. (2012). Further analysis of change in nearshore wave climate due to an offshore wave farm: an enhanced case study for the Wave Hub site. *Renewable Energy, 40*(1), 51–64.

Stratigaki, V., Troch, P., Stallard, T., Forehand, D., Folley, M., Kofoed, J. P., et al. (2015). Sea-state modification and heaving float interaction factors from physical modelling of arrays of wave energy converters. *Journal of Renewable and Sustainable Energy, 7,* 061705.

Tutar, M., & Veci, I. (2016). Performance analysis of a horizontal axis 3-bladed Savonius type wave turbine in an experimental wave flume (EWF). *Renewable Energy, 86,* 8–25.

WAMIT, Inc., (2000). WAMIT user manual version 6.0, 6.0PC, 5.3S. Available from www.wamit.com.

Waters, R., et al. (2007). Experimental results from sea trials of an offshore wave energy system. *Applied Physics Letters*, 90, 034105.

Waters, R., et al. (2011). Ocean wave energy absorption in response to wave period and amplitude —Offshore experiments on a wave energy converter. *IET Renewable Power Generation*, 5(6), 465–469.

Weller, S. D., Stallard, T. J. & Stansby, P. K. (2010). Experimental measurements of irregular wave interaction factors in closely spaced arrays. *IET Renewable Power Generation*, 4(6), 628–637.

Zijlema, M. (2010). Computation of wind-wave spectra in coastal waters with SWAN on unstructured grids. *Coastal Engineering*, 57(3), 267–277.

Hydrokinetic Tidal Energy Resource Assessments Using Numerical Models

Kevin Haas, Zafer Defne, Xiufeng Yang and Brittany Bruder

Introduction

A promising source of energy within the ocean is the tide, the rise (flood) and fall (ebb) of sea levels driven by the combined gravitational acceleration between the Earth, Moon, and Sun as well as the centrifugal acceleration from their rotation around each other. One estimate of total global energy resource for the ocean's tides is approximately 3.7 TW; however, only a fraction of this will be extractable (Arbic and Garrett 2010). Due to the high density of seawater, the energy density (>1 kW/m^2) in the ocean, particularly for tides, is generally quite high compared to other forms of renewable energy (Polagye and Thomson 2013).

The gravitational forces of celestial objects induce the tides on Earth; their periodic motion with respect to the Earth, combined with the Earth's own periodic motion, creates rhythmic motions of water bodies at known frequencies. Therefore, the tidal elevation (level of seawater relative to a mean tidal level) is frequently approximated as the superposition of various tidal constituents with known frequencies given as

K. Haas (✉)
Georgia Institute of Technology, Atlanta, USA
e-mail: khaas@gatech.edu

Z. Defne
United States Geological Survey, Woods Hole, USA

X. Yang
Chevron Energy Technology Company, Houston, USA

B. Bruder
University of Delaware, Newark, USA

Z. Yang and A. Copping (eds.), *Marine Renewable Energy*,
DOI 10.1007/978-3-319-53536-4_4

$$H = a_0 + \sum_{i=1}^{N} a_i \cos(\sigma_i t + \delta_i) \quad (1)$$

where H is the tidal water level, a_0 is the vertical offset, and a_i, σ_i, δ_i are the amplitude, angular frequency, and phase angle of the ith tidal constituents, respectively. The constituent frequencies range over different timescales (hours, months, years); but once the constituent amplitudes and phases are determined for a particular location, the tides are easy to predict. The spatial variability in the water level generates pressure gradients which drive tidal currents, often magnified in locations with flow constrictions such as inlets. A similar procedure can be followed for computing the tidal current constituents using complex amplitudes representing the vector components of the velocity from long-term-recorded time series. This predictability of the tides makes it attractive relative to other renewables which suffer from intermittency with low predictability of capacity such as wind and solar (Naksrisuk and Audomvongseree 2013). However, there are limits to the predictability of tidal power; atmospheric forcing may modify the currents, although large disturbances are typically rare and will only occasionally result in major modifications to the currents (Adcock et al. 2015). Of more concern is the observations that harmonic analysis has limitations for predicting strong tidal currents (e.g., Polagye et al. 2010 and Stock-Williams et al. 2013).

There are generally two different approaches for capturing tidal energy: either extracting the (1) potential or (2) kinetic energy. Capturing the potential energy is similar to classical hydropower where a barrier, also known as a tidal barrage, is constructed across an estuary. Alternatively, kinetic energy may be extracted from the tidal currents using hydrokinetic turbines, conceptually analogous to wind energy. Hydrokinetic turbines have some advantages over other forms of renewable energy as suggested by Yuce and Muratoglu (2015). Hydrokinetic turbines do not require water impoundment and therefore do not include the significant costs associated with the construction of dams. They are significantly smaller in scale than tidal barrages, requiring much smaller capital expenditures. They are typically deployed in arrays with many individual units much like wind farms, increasing system redundancy and resilience.

As with other forms of energy, resource assessments are necessary to determine the feasibility of hydrokinetic tidal energy for a particular region, to help with the project layout design and to ultimately provide the projected annual energy production (AEP). The methods for performing the resource assessments depend on both the desired scope (feasibility or design) as well as the project scale. To help clarify the types of resource assessments, the International Electrotechnical Commission (IEC) has defined a conceptual framework for assessing marine hydrokinetic resources (IEC 2013) which the United States Department of Energy has adopted (The National Research Council 2013). The overall assessment process is considered in three stages: theoretical, technical, and practical. The theoretical resource consists of the hydrokinetic energy available for conversion without consideration of any turbine properties. In essence, this is the power within the

undisturbed flow field. The technical resource is the amount of power that can be generated considering the particular technology to be utilized. This resource assessment will incorporate turbine efficiencies and interactions with the flow field and will be a fraction of the theoretical resource. Finally, the practical resource includes the additional constraints of turbine operation such as regulatory, environmental, economic, and life cycle constraints.

Performing a hydrokinetic tidal energy resource assessment requires an accurate determination of the tidal water levels and currents. While high-quality tidal elevation predictions are readily available, accurate tidal current predictions based on recorded data are scarce. Furthermore, proposed project sites may have spatially varying hydrodynamics and constituents; costly hydrodynamic measurements in a single location may not be adequate to assess the full hydrokinetic resource. In addition, arrays of devices will induce further complexity to existing hydrodynamics and alter the tidal constituents and the available energy resource, thereby restricting the use of direct observations of tidal currents for use in resource assessments. Therefore, due to the deterministic nature of tidal flows, numerical modeling of hydrodynamics with and without hydrokinetic tidal energy extraction provides a description of a site's resource resolved in both space and time.

The focus of this chapter is on performing numerical modeling resource assessments for in-stream tidal hydrokinetic turbine projects. Within this chapter, the following sections explain the different methodologies for using numerical models to determine the tidal energy resource at various stages and scales, beginning at the scale of an individual turbine, followed by feasibility assessments and ending with the final project assessment. The chapter concludes with examples of employing these methodologies as a case study.

Individual Turbine Assessments

To identify the resource available for an individual device, the theoretical power density in a free stream, P_t, is readily computed as a cube of the free stream velocity

$$P_t = \frac{1}{2}\rho V^3 \tag{2}$$

where ρ is the density of the fluid and V is the current speed. This equation can be modified to incorporate the efficiency of a turbine in producing electricity by adding the power coefficient C_p

$$P_d = \frac{1}{2}C_p\rho V^3 \tag{3}$$

where P_d is the technical power density. Sometimes, C_p is referred to as the performance coefficient and represents the mechanical shaft power rather than the

actual electrical power output efficiency. An upper efficiency bound for turbines in an unconstrained flow can be derived using actuator disk theory. The upper limit is formally referred as the Lanchester–Betz–Joukowsky limit; however, it is most frequently called the Betz limit (Betz 1920; Lanchester 1915; Juokowsky 1920). The theoretical limit was derived by applying conservation of mass, momentum, and energy for the volume of the flow passing through the turbine. The maximum power coefficient was determined to be 16/27 or 59.3%. This analysis was performed for wind turbines; however, it is generally accepted to apply for tidal energy, provided the turbine swept area is small relative to the channel depth and width (Blunden and Bahaj 2007).

The actual power output for a particular device must take into account several additional properties of the turbine. For horizontal axis turbines, the incoming current speed V needs to be the component of the velocity normal to the extraction plane whereas for the vertical axis turbines this is not an issue. In addition, neglecting turbulence is generally not significant if deploying near the free surface and away from any boundary layers and wake turbulence generated from upstream turbines or in-stream structures, e.g., bridge piers, as shown by Neary et al. (2013). However, if turbulence intensities are at or exceed 20%, power is underestimated by over 10%. This is the case at the RITE site at hub height for currents just above cut-in speed at 1 m/s; turbulence intensities were about 23% (Gunawan et al. 2014). In this case, not accounting for turbulence in the power equation could result in significant underestimation of AEP.

In addition to representing the turbine efficiencies, the power coefficient C_p also incorporates a minimum cut-in speed below which the turbine does not operate and a rated speed at which the turbine does not generate more power for higher current velocities. The power coefficient may be determined empirically using the method outlined by the IEC technical specification (TS) (IEC 2014). This specification provides a standardized methodology for measuring the incoming-free stream velocity along with the electrical power output of the turbine to be used for computing the power coefficient. Optimal efficiencies of tidal energy converters are generally lower than the Betz limit and are reported to be typically between 16 and 50% (Gorban et al. 2001 and Ben Elghali et al. 2007). However, the Betz limit no longer applies and may be exceeded under conditions with constrained flow or when using turbines with ducted intakes (e.g., Lawn 2003).

The actual power output for the turbine (P) is found by multiplying the power density by the swept area of the turbine, A_s

$$P = \frac{1}{2} C_p \rho V^3 A_s. \tag{4}$$

The turbine AEP is essentially the time integral of the power production of turbine over a year. However, the predicted AEP is generally computed based on the annual probability distribution of the current velocities in conjunction with the power curve. The probability distributions are derived using data from either model

simulations or long-term observations directly at the turbine location. The AEP is computed according to the following equation:

$$AEP = N_{\mathrm{h}} \sum_{i=1}^{N_{\mathrm{B}}} P_i(V_i) \cdot f_i(V_i) \tag{5}$$

where AEP is the expected annual power production in kWh, N_{h} is the number of hours for the year, N_{B} is the total number of velocity bins in the device power curve, $P_i(V_i)$ is the power in kW generated by the ith velocity bin, U_i is the mean current velocity in m/s of the ith bin, and $f_i(V_i)$ is the probability ith bin of the annual velocity probability distribution.

The AEP is a good aggregate measure of annual power production at a given site; however, it does not provide an adequate description of the power production on shorter timescales, particularly the degree of intermittency needed for full-fledged project design. For example, tidal flows at energetic sites which are dominated by the semidiurnal M_2 constituent will fluctuate with a primary period slightly greater than 12 h, leading to low velocities and hence no power generation during slack water times, about every 6 h. This leads to a substantial quarter-diurnal variation in the theoretical power as well as the turbine efficiency and thus technical turbine power output (Adcock et al. 2014).

Significant variability can also occur over the timescale of an individual tidal cycle. As an example, the tidal distortion, which is the inequality of the ebb to flood tide generated by different harmonic constituents or geometric features (Bruder et al. 2014), can lead to significant differences of the power produced by the turbines and again is dependent on the turbine characteristics (Bruder and Haas 2014). In particular, the tidal distortion is quantified by skewness, the degree of symmetry about the horizontal axis, taking into account the relative broadness and magnitudes of the peaks of flood and ebb currents and the asymmetry which is the degree of symmetry about the vertical axis, the relative duration of periods of increasing and decreasing velocity magnitudes. The degree of skewness and asymmetry is highly dependent on the relative phase between the M_2 and M_4 constituents. Bruder and Haas (2014) found that while the theoretical available power for a signal with or without distortion is similar, the technical power had up to 15% variations depending on the turbine properties. For highly skewed time series, because peak flood and ebb velocities will be very different, it is important to have a broad operating range for the turbine whereas this is less important for asymmetric time series.

For locations where the lunar and solar semi-diurnal constituents (M_2 and S_2) are significant, the superposition of these two constituents leads to a beating of the tidal signal producing a roughly two-week cycle of large (spring) and small (neap) tides (Adcock et al. 2015). This causes a significant variability in the power output of tidal turbines over the spring/neap cycle (Adcock and Draper 2014).

Generally speaking, any location will have multiple tidal constituents with significant energy and thereby will have some sort of beating, distortion, or diurnal

inequalities leading to tidal power variability. Clearly, a full and accurate characterization of the tidal energy resource, including resolution of the intermittency of the power, requires an accurate determination of all the relevant tidal constituents, the amplitudes, and phases. The IEC technical specification for tidal energy resource assessments (IEC 2015) recommends resolving at least the 20 largest constituents. Finally, to maximize the ultimate technical power produced by an individual turbine requires a good understanding of the relationship with the theoretical power through the turbine power coefficient and how this depends on the tidal characteristics such as tidal distortion.

Regional Feasibility Assessments

While performing resource assessments for deployments of individual turbines is possible using the previously described concepts, in practice, resource assessments will be required for projects in which arrays of turbines are deployed. The first step is to identify potential locations for tidal energy projects, performing regional feasibility studies to find areas with strong tidal currents. The particular modeling methodology required for a resource assessment will greatly depend on the specific goals to be accomplished for the study. The IEC technical specification for tidal energy resource assessments (IEC 2015) provides guidance suggesting that feasibility studies may be computed using depth-averaged 2D (or full 3D) models with computational grid point spacing no greater than 500 m.

The tidal current model data from these feasibility studies may be used to identify regions with large enough currents to be of interest for tidal energy production. The predicted velocities from these types of studies may be used to estimate the AEP, although with a high level of uncertainty. However, this type of assessment is insufficient to estimate power potential for projects that have large arrays relative to the channel cross-sectional area. Additionally, Vennell et al. (2015) suggests that any array with total swept area larger than 2–5% of the cross-sectional area may be considered large. For these large arrays, the effect of the turbines slowing down the velocities must be considered.

Therefore, feasibility studies frequently use the data from tidal models in conjunction with theoretical analysis of the maximum extractable power to produce the AEP estimate. These theoretical analyses account for the various effects that the turbines have on the flow field, producing an AEP estimate with less uncertainty than using the undisturbed velocities alone.

Garrett and Cummins (2005) identified the significance of the backflow-induced head differential created by the obstructions in the channel. This backflow effect increases the pressure differential driving the flow and enhances the current velocity. A tidal fence consisting of turbines across the entire cross section of a constricted channel, connecting two large bodies of water in which the tides at both ends are assumed to be unaffected by the currents through the channel, is considered. For this situation, a general formula gives the maximum average power to be

between 20 and 24% of the peak tidal pressure head times the peak of the undisturbed mass flux through the channel, independent of the location of the turbine fences along the channel. The maximum average tidal stream power, P_{max}, for a single sinusoidal constituent is given as

$$P_{max} = \gamma \cdot \rho \cdot g \cdot a \cdot Q_{max} \tag{6}$$

where γ is a parameter representing the 20–24% of the peak tidal pressure head, ρ is the density of seawater, g is acceleration of gravity, a is the amplitude of the tidal water level constituent, and Q_{max} is the maximum corresponding flow rate. For a background friction-dominated, non-sinusoidal (i.e., considering more than one tidal constituent) case, if data for the head and flux in the natural state are available, the maximum average power may be estimated with an accuracy of 10% using $\gamma = 0.22$, without any need to understand the basic dynamical balance (Garrett and Cummins, 2005). A multiplying factor is used to account for additional constituents (a_1, a_2, …) given as

$$1 + \left(\frac{9}{16}\right)(r_1^2 + r_2^2 + \ldots) \tag{7}$$

where $r_1 = \frac{a_1}{a}, r_2 = \frac{a_2}{a} \ldots$ This upper bound on the available power ignores losses associated with turbine operation and assumes that turbines are deployed in uniform fences, with all the water passing through the turbines at each fence.

The validity of the value of γ in Eq. (6) was demonstrated by Sutherland et al. (2007) using numerical simulations of channel-wide energy extraction. However, they did find that for more complex channel geometries such as split channels, Eq. (6) overestimated the maximum power of the free stream by up to 50%, demonstrating one of the limits to the applicability of this method. Recognizing the unlikeliness of installing tidal fences across the full channel, Garrett and Cummins (2007) analyzed partial fences across the channel. Analytically it was found that the resultant maximum power for the partial fence was reduced from the maximum power for the complete fence by a factor of 1/3–2/3.

Further considerations for the effects of partially blocked channels were completed by Vennell (2010, 2011). He found that the power in a channel that is available for generation is maximized through proper tuning of the turbine array. In particular, he found that by adjusting the flow reduction (ratio of the wake velocity to the incoming velocity), the turbine array could be better optimized. The previous work by Garrett and Cummins (2007) had found the optimal limit to be 1/3; however, this assumed that the upstream velocity was unaffected by changes in the turbine drag. Vennell argues that changes to individual turbines will affect the overall array drag and therefore found that by tuning the flow reduction ratio in the ranges from 1/3 to 1, it was possible to exceed the maximum power estimates by Garrett and Cummins (2007). Vennell (2011) also discusses the need to tune multiple rows of turbines "in-concert" because even if rows are widely separated such that the wake sufficiently recovers, they will still have interactions due to the

full array's effect on the overall array drag coefficient. An excellent discussion comparing the results from Garrett and Cummins with the work by Vennell is found in Vennell (2012).

The previously discussed studies generally focused on relatively simple channel geometry; however, tidal estuaries are frequently much more complex where the currents have vertical structure and the estuary may contain multiple channel branches as well as intertidal storage. Under these more complex scenarios, kinetic power density is sometime still used to estimate the resource (e.g., Blunden and Bahaj 2006; Carballo et al. 2009; Iglesias et al. 2012; Polagye and Bedard 2006; Bomminayuni et al. 2012). However, additional work has been completed to extend the analytical approaches above to more complex geometries. Blanchfield et al. (2008) modeled a closed bay and open ocean, which was successfully verified by Yang et al. (2013) numerically. Polagye and Malte (2011) treated tidal networks like electrical circuits and found the most power efficient turbine deployment in networks required equally deploying turbines across sub-channels, or deploying upstream to the channel bifurcation to reduce flow diversion.

An example large-scale feasibility study is the national assessment of tidal stream power resource for the USA (Defne et al. 2012). The Regional Ocean Modeling System (ROMS) was used to generate a geodatabase for tidal constituents for the USA. Regional assessments of tidal stream power resource were carried out by identifying locations with considerably high kinetic power density. This study found that while Alaska has the bulk of the tidal energy power for the USA, Maine in the northeast and Washington in the northwest have significant power as well. In addition, many other states had locations with concentrated power that could potentially be viable for tidal energy extraction.

Project Assessments

Once a project location has been determined, the project design process requires a resource assessment with a much higher degree of scrutiny, including an understanding and quantification of the effects of turbines on the hydrodynamics. These effects can be small scale, where turbines interact with one another directly (i.e., wake effects), or large scale, where the energy extraction from the turbines affects the estuarine scale tidal flows. Vennell et al. (2015) discuss the design process for arrays of tidal turbines and describe these different scales of processes as macro- and micro-effects. They also provide a list of the overall effects from arrays, partially reproduced here:

- Power extraction by an array reduces the free stream flow within a channel.
- Optimally tuned turbines in an array are not constrained by the Betz limit because they are not isolated turbines.
- Adding additional turbines to a single row may either increase or decrease the power depending on the channel characteristics.

- Adding additional rows of turbines to a channel has diminishing returns of power.

As discussed by Vennell (2012), the difference between the behavior of turbines in an array versus in a free stream flow is best illustrated by looking at the source of the array's energy. For a turbine in a free stream velocity, the optimal power is extracted when the flow through the turbines is reduced down to 1/3. However, for an array with significant flow blockage, the source of energy comes from the change in head induced by the flow blockage, therefore allowing the downstream velocity ratio to approach 1. In essence, the difference in behavior is attributed to the difference between extracting potential energy versus extracting kinetic energy.

Due to the complexity of tidal flows on the scale of an array, designing array layouts and performing the associated resource assessment require the use of numerical simulations of the array. Adcock et al. (2015) discuss the broad range of scales which must be resolved, beginning with turbine blade scales (O(cm)) ending with regional or estuary scales (O(100 km)). While it is not possible to resolve all these scales in a single model, it is necessary to resolve a broad range of scales, which is computationally challenging. Resource assessments utilized for siting considerations require a much higher model resolution than feasibility studies. Typical grid resolutions are suggested by the IEC TS (2015) to be less than 50 m to capture the spatial variability of the flow. Adding to the difficulty is the fact that the model domain generally must include the full estuary and even extend out to the continental shelf; therefore, variable grid resolution is generally utilized. This may be accomplished using models with unstructured grids, such as the resource assessment for New Jersey by Tang et al. (2014) and for the Tacoma Narrows by Yang et al. (2014). Another study by Ramos et al. (2014) coupled several structured grids with varying grid resolutions in a relatively simple estuary. In another example, Bomminayuni et al. (2012) used a model with an unstructured grid and therefore higher resolution in the region of interest to simulate the flows in tidal channels near Rose Dhu Island, Georgia. Recently, Lewis et al. (2015) simulated the Irish Sea with a structured grid model and determined that model resolution had a significant effect on the local resource assessment. They demonstrated that higher model resolutions (with grid spacing less than 500 m) are required for siting considerations. The Kennebec River of the central Maine coast was found to contain narrow passages where mean tidal energy capacity is sufficient to meet the consumption needs of about 150 homes (Brooks 2011).

For larger projects, in order to adequately address array effects, numerical simulations of the project site must include quantification of the effects of turbines on the flow field. The IEC TS (2015) puts the threshold for large projects at 10 MW, or 2% of the theoretical resource using the Garrett and Cummings (2005) method. This may be accomplished with high-order computational fluid dynamics (CFD) models resolving both the turbines and the fluid flow (e.g., Jo et al. 2012; Shi et al. 2013) or using actuator disk theory (e.g., Harrison et al. 2010). However, due to the high computational demands and the necessity to include a large domain to capture the far-field effects, simplified approaches to resolving the effect of turbines

are generally utilized. While there are several different options for incorporating the impacts of turbines on the flow field into models, they generally have similar approaches (e.g., Defne et al. 2011; Work et al. 2013; Yang et al. 2013).

One approach for modeling energy extraction incorporates an extra retarding force into the momentum equations. This force $\vec{F}$ may be written as

$$\vec{F} = \frac{1}{2}\rho C_{ext}|\vec{V}|\vec{V} \tag{8}$$

where C_{ext} is an extraction coefficient. It is possible to relate the extraction coefficient to specific turbine parameters including the losses related to the turbine structure as

$$C_{ext} = (A_c C_s + A_s C_t)N_t \tag{9}$$

where A_c is the cross-sectional area of the turbine support structure, C_s is the drag coefficient for the support structure, A_s is the swept area, C_t is the thrust coefficient, and N_t is the number of turbines within the grid cell. After solving the momentum equations with the extra retarding force, the corresponding produced power is then found as

$$P = \frac{1}{2}\rho C_p A_s |\vec{V}|^3 \tag{10}$$

where C_p is the turbine power coefficient.

The application of this type of approach can vary depending on the model resolution. For relatively coarse grid resolution, each grid point where the retarding force is applied may represent multiple turbines and therefore the extraction coefficient can become quite large. A drawback of course is that the turbines within each grid cell cannot be individually tuned, and therefore, the optimal turbine array layout cannot be determined. However, this approach can be beneficial for analyzing far-field effects within the full estuary or bay. Alternatively, for simulations with relatively high grid resolution, a single turbine may be resolved within a grid cell. Obviously, this would be the preferred approach for optimizing the array layout. For 3D model applications in deeper tidal straits, the retarding force may also have a depth dependence where the vertical position of the turbine is resolved, further improving the accuracy of the localized effect of energy extraction.

In addition to the turbines exerting a retarding force on the flow, turbines and their associated structure will have a pronounced effect on the turbulent characteristics of the flow field. In order to account for the change in turbulence produced by tidal turbines, Roc et al. (2013) incorporated modifications to the turbulence closure scheme. One modification includes an added turbulent kinetic energy source term for the grid cells with turbines. Another addition is to include a term accounting for the transfer of large-scale turbulence to smaller-scale turbulence, a short circuiting of the turbulent cascade induced by the interaction of existing

turbulence with the turbine structure. Finally, a term is included to model reduction in the spectrum of the turbulent length scales due to the partial generation of turbulence from the fluid structure interactions.

There have been numerous tidal power assessments performed with the effects of tidal power extraction around the world. The maximum tidal power potential of Johnstone Strait, British Columbia, Canada, was studied by Sutherland et al. (2007) using a 2D finite element model and the maximum extractable power in northwestern Johnstone Strait was estimated. Also, using a 2D model, Polagye et al. (2009) studied and characterized the in-stream tidal energy potential of Puget Sound, Washington, and quantified the far-field, barotropic effects of the energy extraction. The available tidal power from in-stream turbines placed in the Minas Passage of the Bay of Fundy and the Passamaquoddy–Cobscook Bay located near the entrance to the Bay of Fundy has also been examined using 2D models (Karsten et al. 2008, Walters et al. 2013). Recently, Funke et al. (2014) have applied an adjoint method with a 2D shallow water hydrodynamic model for designing tidal turbine layouts. This approach allows for quicker convergence to the optimized turbine array layout, thereby requiring much less computational resources than using a large suite of traditional forward model simulations alone.

Three-dimensional models have also been utilized for simulating the impacts of energy extraction. Tidal stream energy resources in northwest Spain were modeled numerically and the impacts of tidal stream energy were assessed (Ramos et al. 2014). Yang et al. (2013, 2014) used a 3D model applied for an idealized case and for the Tacoma Narrows and showed significant volume flux impacts between the 1D/2D and the 3D simulations. Yang and Wang (2015) evaluated the effect of energy extraction on stratification in an idealized estuary. Hasegawa et al. (2011) applied a model looking at far-field effects from tidal energy extraction in the Bay of Fundy and the Gulf of Maine. Shapiro (2011) used a 3D model to demonstrate a significant decrease in the extractable energy for a given turbine capacity compared to 1D estimates due to flow bypassing the turbine array. Rao et al. (2016) used a 3D model of the Western Passage in Passamaquoddy Bay to optimize the turbine array layout. Hakim et al. (2013) modeled the Muskeget Channel and found modest impacts on the underlying hydrodynamics. Pacheco and Ferreira (2016) designed the optimal location of a turbine array on the coast of Scotland and examined the effect on the hydrodynamics.

When performing resource assessments using numerical models for tidal energy projects, validation of the model is an essential component of the process. The IEC TS for tidal energy resource assessments (IEC 2015) provides guidelines for performing the calibration and validation of the numerical model. Model calibration is the procedure by which model parameters (e.g., bottom friction, turbulence parameters) are adjusted to provide the most accurate match to measured data. The TS recommends comparing the model and measured tidal height data on the basis of harmonic constituents, both the amplitudes and the phases, and adjusting the model parameters as necessary. For calibrating the currents, the TS suggests comparing the model results with mobile current observations that capture spatial

and temporal variability to ensure that the model is able to capture the strongly advective flows as well as refining the grid sufficiently to ensure grid convergence.

Validation is the procedure which is used to ensure that the model simulations have sufficiently low uncertainty for providing reasonable resource assessments. The TS recommends that the AEP be calculated using both direct measurements as well as the model simulations for at least one proposed turbine location. The recommendation is for the uncertainty in the AEP to be less than circa 15%. This comparison can only be accomplished for observations prior to turbine deployments and therefore model simulations in which energy extraction is not included. For large projects in which energy extraction needs to be included in the model for the final resource assessment, the validation of the model is done without energy extraction, because it is not possible to obtain data prior to turbine deployment. The only exception would be if a pilot study in which a small number of turbines are deployed at the project location was done prior to the resource assessment for the full-scale project, then a modeling study including the energy extraction for the pilot study could be used to validate the model.

Case Study

A case study illustrating numerical model-based resource assessments at the turbine, regional feasibility, and project scale based on a site from Defne et al. (2012) is presented in this section. The location is the Piscataqua River on the border between Maine and New Hampshire. For the feasibility study, simulations of the tidal currents were completed using ROMS with the model domain shown in Fig. 1 outlined in blue with grid spacing between 150 and 250 m. The tidal constituents for the currents were calculated based on 32 days of model data for the entire domain. The tidal constituents were then used to compute a one-year time series which in turn was used to compute the magnitude of the mean currents as shown in Fig. 2a. In addition, Eqs. (6) and (7) based on the method from Garrett and Cummings (2005) were used to estimate the theoretical maximum annual average power of 21 MW for the entire estuary. This provides an estimate for the upper bound as to how much power could be extracted from the entire region. The resolution for this grid is sufficient for producing the regional resource assessment; however, it is insufficient for determining the resource for a specific project. The particular tidal energy installation is to be located near Seavey's Island as shown in Fig. 2b, comprised of multiple parallel channels, thereby making application of simple analytical models infeasible for computing the potential resource.

To do a project-scale assessment, Yang and Haas (2015) used grid refinement with a structured grid to produce higher-resolution (25–40 m) model results within the Piscataqua River. Figure 1 shows the child grid (red outline) within the parent grid which focuses on the entrance to the estuary. The mean current magnitudes from the child grid are shown in Fig. 2b. Based on this improved data (the validation is demonstrated in Yang and Haas (2015)), regions of larger currents were

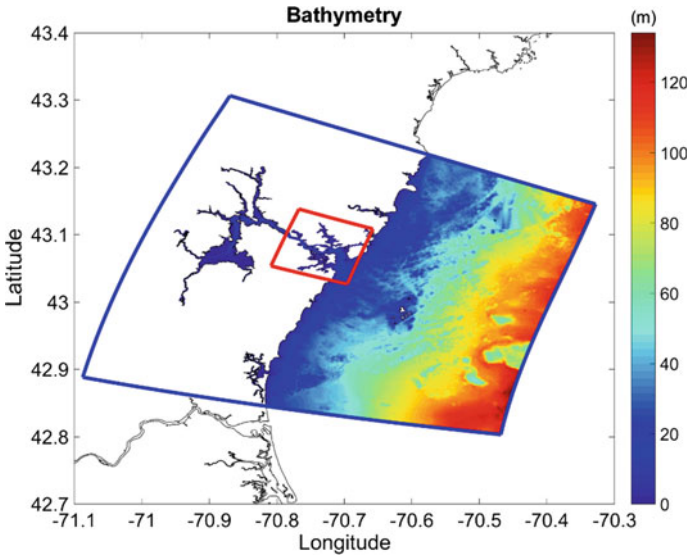

Fig. 1 Bathymetry from the parent grid (*blue outline*) and child grid (*red outline*) for the feasibility study of the Piscataqua River

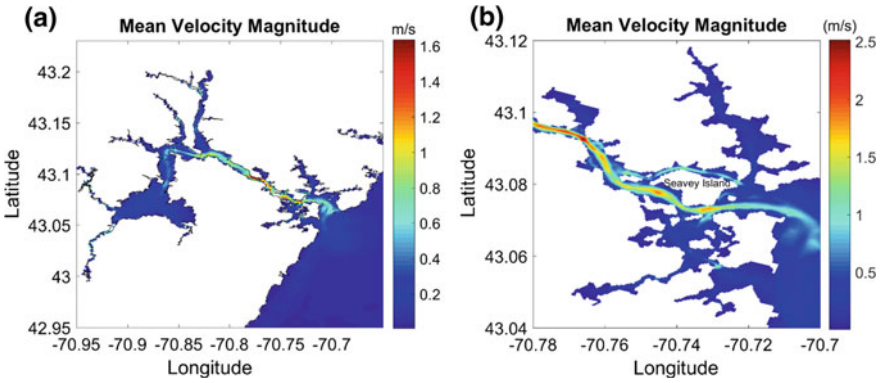

Fig. 2 Color contours of the magnitude for the mean depth average currents for **a** the feasibility study of the Piscataqua River (Defne et al. 2012), serving as the parent grid and **b** the child grid (Yang and Haas 2015)

identified for the Portsmouth Naval Shipyard located on Seavey's Island. The grid refinement capability showed significant advantage over the original simulation results given its relatively low computational expense and high accuracy for the regions with the refined resolution. Of particular interest is the channel on the north side of Seavey's Island (labeled in Fig. 2b), which the parent grid did not resolve.

For a small deployment with little impact on the currents, the technical resource assessment for an individual turbine requires computing the velocity probability distribution shown in Fig. 3a. Using Eq. (4) with the power curve shown in Fig. 3b and taking the swept area to be 20 m^2, the power probability distribution is computed and shown in Fig. 3c. The peak power is under 100 kW, well under the maximum estimated for the full estuary. Finally, the AEP is computed using Eq. (5) as 186 MWhr for this location.

For larger-scale projects which will extract a significant portion of the kinetic energy in the flow, the resource assessment requires the model simulation to include the effect of the turbines on the flow field. Therefore, two new sets of simulations were completed where turbines are modeled using Eq. (8) for grid points in a transect spanning the width of the channel north of Seavey's Island. The coefficient C_{ext} was set equal to 0.05 and 0.2 for the two simulations. The extraction coefficient is formulated using Eq. (9), and the drag and thrust coefficient along with the area associated with each individual turbine stays constant; therefore, the higher extraction coefficient is indicative of a factor-four increase in the number of turbines within the cell.

The tidal constituents were computed from the 32-day simulations and used to compute one-year times series of the velocity for each grid point across the transect. Figure 4 shows the probability distributions for velocity in the center grid cell in the transect for the three cases: C_{ext} equal to 0, 0.05, and 0.2. The effect of energy extraction on the flow field is quickly apparent as the peak velocity weakens and the distribution becomes more narrow. An even clearer example of the effect of energy extraction is shown in Fig. 5 as the spatial distribution of the mean velocity difference between the energy extraction case and the original non-extraction case. The reduction of velocity (negative values) in the channel is more significant, 0.3 versus 0.1 m/s, for the larger extraction cases in Fig. 5b. There is a corresponding

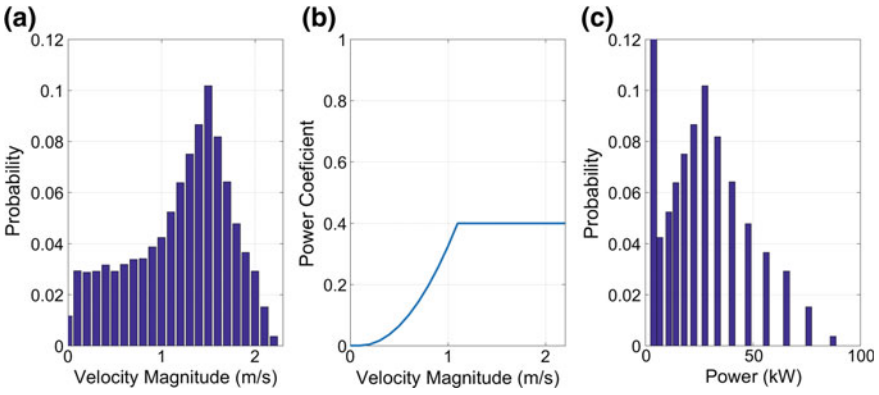

Fig. 3 **a** Velocity probability distribution for a location north of Seavey's Island (43.0841° N 70.7384° W). **b** Example power curve used for computing AEP. **c** Probability distribution of the power for an array of devices with a total capture area of 20 m^2

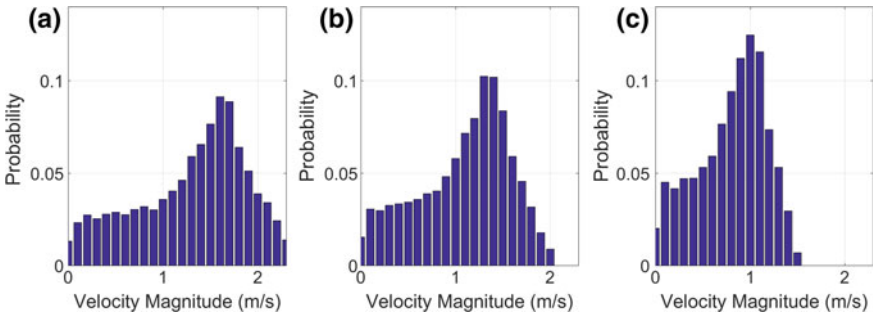

Fig. 4 Mean velocity probability distributions for the center grid cell in the transect north of Seavey's Island (43.0841° N 70.7384° W) for **a** no energy extraction **b** C_{ext} equal to 0.05 and **c** C_{ext} equal to 0.2

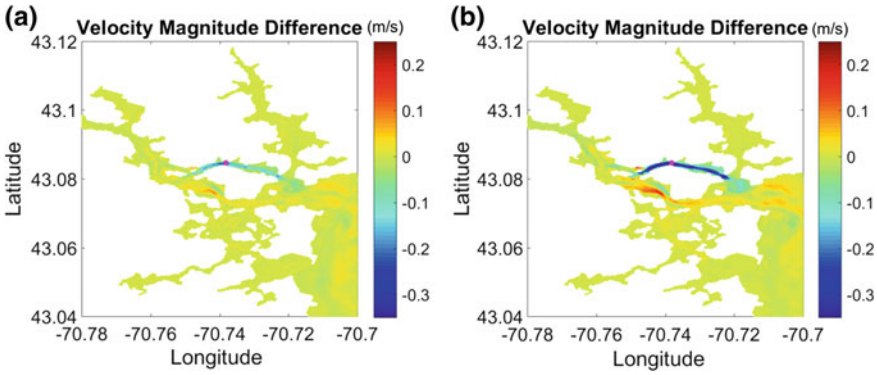

Fig. 5 Color contours of the difference of the depth-averaged velocity magnitude between the energy extraction and original non-extraction cases for **a** C_{ext} equal to 0.05 and **b** C_{ext} equal to 0.2. The magenta dot shows the location of energy extraction

increase in velocity (0.1–0.2 m/s), although not as pronounced, in the main channel south of Seavey's Island. Clearly, the added resistance of the turbines in the north channel is diverting some of the flow to the south channel.

Tidal turbines have backwater effects where the increased dissipation causes the water level to increase behind the turbine which is reflected through the changes in mean water level shown in Fig. 6. In this figure, it is clear that the turbines cause an increase in mean water level on the order of several cm in the north channel. Because of the bidirectionality of the flow, the mean water level increases on both sides of the turbine arrays. There is also a small increase (<1 cm) in water level further upstream in the estuary and a minimal decrease (<0.5 cm) in the south channel.

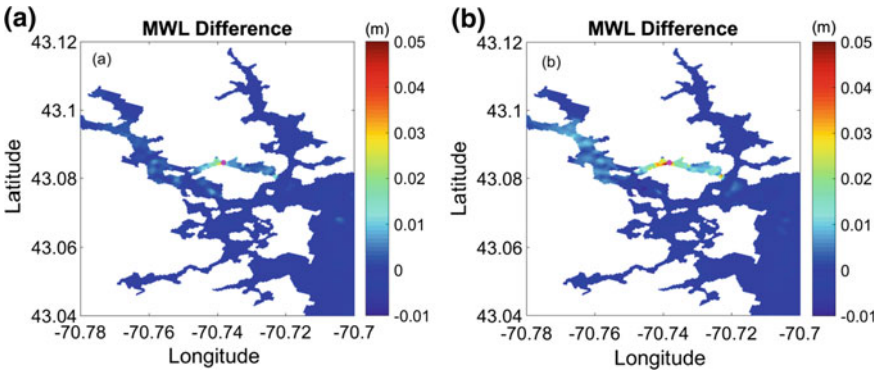

Fig. 6 Color contours of the difference of the mean water level (MWL) between the energy extraction and original non-extraction cases for **a** C_{ext} equal to 0.05 and **b** C_{ext} equal to 0.2. The magenta dot shows the location of energy extraction

The dissipated power (P_{diss}) by the turbines is computed as

$$P_{diss} = C_{ext} \frac{1}{2} \rho V^3 dA \tag{11}$$

where dA is the horizontal surface area of the grid cell with the turbines. Note that this is subtly different than the vertical face generally used for the swept area in Eq. (4). As indicated in Eq. (9), this is the total power dissipated which includes losses from the support structure as well as usable power captured by the turbines.

In addition to calculating the power dissipated by the turbines, it is beneficial to compute both the kinetic and potential energy flux (or power) through the transect and to evaluate how much this changes with the energy extraction. The kinetic energy flux, $P_{kinetic}$, is computed as the sum of I grid cells across the transect written as

$$P_{kinetic} = \sum_{i=1}^{I} \frac{1}{2} \rho |V_i|^3 h_i w_i \tag{12}$$

where h_i and w_i are the water depth and width of each cell across the channel, $|V_i|$ is the depth-averaged velocity for each grid cell. Similarly, the potential energy flux is computed as

$$P_{potential} = \sum_{i=1}^{I} \rho g |V_i| \eta_i h_i w_i \tag{13}$$

where η_i is the sea level fluctuation away from the mean water level.

Figure 7 shows time series of the power dissipated as well as the kinetic and potential energy fluxes both before and after extraction. It is apparent that the

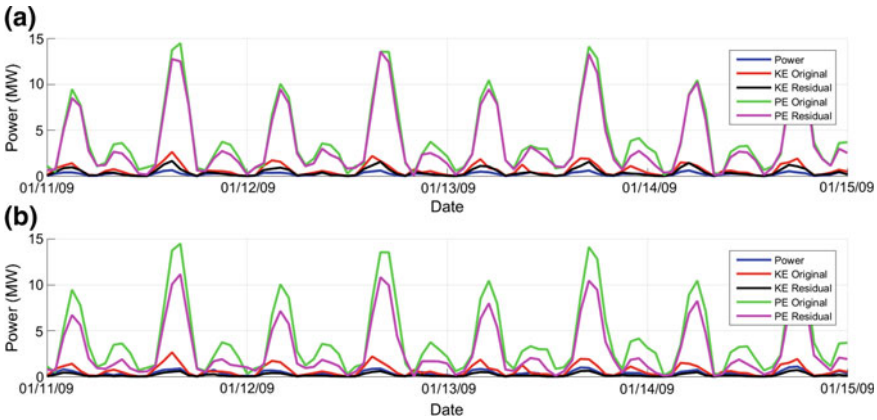

Fig. 7 Time series of the extracted power, the original and residual kinetic power, and the original and residual potential power for the transect on the north side of Seavey's Island (43.0841° N 70.7384° W) for **a** C_{ext} equal to 0.05 and **b** C_{ext} equal to 0.2

potential energy flux is much larger than the kinetic energy flux, close to an order of magnitude difference. The energy extraction has the effect of decreasing both the kinetic and potential energy flux; therefore, it is clear that it is theoretically possible to extract more than 100% of the original kinetic energy flux. For the two cases shown here, the 1-year-averaged original undisturbed kinetic energy flux is 0.43 MW and the mean power dissipated is 0.14 and 0.22 MW which is 33% and 53% of the mean kinetic energy flux, respectively. Because this is a small branch for the estuary, this power is significantly less than the maximum available power according to the Garrett and Cummings estimate of 21 MW. The residual kinetic energy flux is decreased for both cases down to 0.26 and 0.11 MW, respectively. For this site, the total energy flux reduction from both the kinetic and potential energy flux is greater than the rate of dissipation because a portion of the flow is diverted to the southern side of the island. It is also apparent that the loss for both the potential and kinetic energy flux is far greater for the second case with a smaller proportional increase in energy dissipation, indicating less efficient energy extraction for this case.

Finally, the velocity probability distributions are used to produce the corresponding power probability distributions as shown in Fig. 8. The two cases have similar shape for the probability distribution, although the higher extraction case has higher rates of occurrences and higher peak power. The AEP for both cases is calculated using annual probability distributions and Eq. (5) and is found to be 1220 and 1925 MWhr per year, respectively.

This resource assessment is sufficient to provide a general idea of the available power and what could be generated along with the potential channel and estuary scale effects. However, in order to do a full site design including turbine layouts within the array, an even higher grid resolution such that each turbine location is individually resolved would be required. Although the action of the turbines

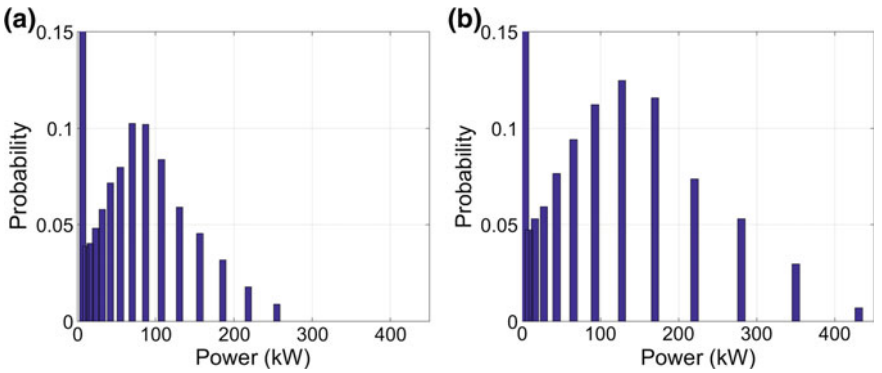

Fig. 8 Probability distribution of the power for the center grid cell for the transect north of Seavey's Island (43.0841° N 70.7384° W) for **a** C_{ext} equal to 0.05 and **b** C_{ext} equal to 0.2

themselves do not necessarily need to be resolved, having the model resolve each turbine location would permit the ability of the model to account for the turbine interactions and permit a sensitivity test for the turbine locations. In addition, for a full hydrokinetic tidal power project design, power intermittency will have to be considered as well; its relative significance depends on individual project needs and available energy storage resources.

Summary

Strong currents resulting from constricted tidal flows are a promising source of hydrokinetic renewable energy. As with any form of energy, resource assessments to determine how much energy is available and ultimately how much electricity can be produced are an essential part of the project planning and design process. While tidal currents have significant spatial and temporal variability, the predictability of tidal flows makes deterministic modeling a suitable methodology for hydrokinetic tidal energy resource assessments.

The scope and scale of the resource assessment determines the basic concepts and methodology to be utilized. In general, resource assessments can provide the theoretical, technical, or practical resource. At the turbine scale, the theoretical power density is computed based on the velocity at the specific turbine location. In order to determine the technical resource, the amount of electricity that a particular turbine would produce at a specific location, various turbine parameters including the power curve are incorporated. The technical resource is frequently quantified as the AEP computed based on the velocity distribution for the specific turbine location along with the turbine properties. The uncertainty associated with the estimates of the AEP is highly dependent on the accuracy of the tidal constituent amplitudes and phases.

Regional resource assessments are used to determine the feasibility of tidal energy for a sizable region, frequently at the scale of an estuary. These assessments generally use numerical models to map out the spatial distribution of the power density. In addition, simplified models or even analytical analysis can be done to produce a regional power estimate. These types of assessments carry a high level of uncertainty due to the simplifications and assumptions required for the computations. However, they can provide an upper bound on the total theoretical energy available at the regional scale.

Resource assessments at the project scale provide both the theoretical and the technical energy. In addition, a project resource assessment can provide the practical energy accounting for many additional constraints, including social, economic, and environmental restrictions, which are beyond the scope of this chapter. The IEC technical specification (IEC 2015) provides the essential guidelines for performing project-scale resource assessments. These guidelines include minimum grid resolution requirements as well as model calibration and validation procedures. In addition, larger projects need to include the effect of energy extraction on the flow field to produce more accurate estimates of velocity probability distributions used for computing the technical resource. The data from these model simulations may also be used for evaluating other constraints for the practical resource assessments such as quantifying the environmental effects.

References

Adcock, T. A., & Draper, S. (2014). Power extraction from tidal channels–multiple tidal constituents, compound tides and overtides. *Renewable Energy, 63,* 797–806.

Adcock, T. A., Draper, S., Houlsby, G. T., Borthwick, A. G., & Serhadlıoğlu, S. (2014). Tidal stream power in the Pentland Firth–long-term variability, multiple constituents and capacity factor. *Proceedings of the Institution of Mechanical Engineers, Part A: Journal of Power and Energy*.

Adcock, T. A., Draper, S., & Nishino, T. (2015). Tidal power generation—A review of hydrodynamic modelling. *Proceedings of the Institution of Mechanical Engineers, Part A: Journal of Power and Energy*.

Arbic, B. K., & Garrett, C. (2010). A coupled oscillator model of shelf and ocean tides. *Continental Shelf Research, 30*(6), 564–574.

Ben Elghali, S. E., Benbouzid, M. E. H., & Charpentier, J. F. (2007). Marine tidal current electric power generation technology: State of the art and current status. *In IEEE International Electric Machines & Drives Conference, 2007 IEMDC'07* (Vol. 2, pp. 1407–1412). IEEE.

Betz, A. (1920). Das maximum der theoretisch möglichen ausnützung des windes durch windmotoren. *Zeitschrift für das gesamte Turbinenwesen, 26*(8), 307–309.

Blanchfield, J., Garrett, C., Wild, P., & Rowe, A. (2008). The extractable power from a channel linking a bay to the open ocean. *Proceedings of the Institution of Mechanical Engineers, Part A: Journal of Power and Energy, 222*(3), 289–297.

Blunden, L. S., & Bahaj, A. S. (2006). Initial evaluation of tidal stream energy resources at Portland Bill. *UK. Renewable Energy, 31*(2), 121–132.

Blunden, L. S., & Bahaj, A. S. (2007). Tidal energy resource assessment for tidal stream generators. *Proceedings of the Institution of Mechanical Engineers, Part A: Journal of Power and Energy, 221*(2), 137–146.

Bomminayuni, S., Bruder, B., Stoesser, T., & Haas, K. (2012). Assessment of hydrokinetic energy near Rose Dhu Island, Georgia. *Journal of Renewable and Sustainable Energy, 4*(6), 063107.

Brooks, D. A. (2011). The hydrokinetic power resource in a tidal estuary: The Kennebec river of the central maine coast. *Renewable Energy, 36*(5), 1492–1501.

Bruder, B., Bomminayuni, S., Haas, K., & Stoesser, T. (2014). Modeling tidal distortion in the Ogeechee Estuary. *Ocean Modelling, 82,* 60–69.

Bruder, B. & Haas, K. (2014). Tidal Distortion as Pertains to Hydrokinetic Turbine Selection and Resource Assessment. *Marine Energy Technology Symposium*, April 2014, Seattle, WA.

Carballo, R., Iglesias, G., & Castro, A. (2009). Numerical model evaluation of tidal stream energy resources in the Ría de Muros (NW Spain). *Renewable Energy, 34*(6), 1517–1524.

Defne, Z., Haas, K. A., Fritz, H. M., Jiang, L., French, S. P., Shi, X., et al. (2012). National geodatabase of tidal stream power resource in USA. *Renewable and Sustainable Energy Reviews, 16*(5), 3326–3338.

Defne, Z., Haas, K. A., & Fritz, H. M. (2011). Numerical modeling of tidal currents and the effects of power extraction on estuarine hydrodynamics along the Georgia coast. *USA. Renewable Energy, 36*(12), 3461–3471.

Funke, S. W., Farrell, P. E., & Piggott, M. D. (2014). Tidal turbine array optimisation using the adjoint approach. *Renewable Energy, 63,* 658–673.

Garrett, C., & Cummins, P. (2005). The power potential of tidal currents in channels. *Proceedings of the Royal Society of London A: Mathematical, Physical and Engineering Sciences. The Royal Society*. *461*(2060), 2563–2572.

Garrett, C., & Cummins, P. (2007). The efficiency of a turbine in a tidal channel. *Journal of Fluid Mechanics, 588,* 243–251.

Gorban, A. N., Gorlov, A. M., & Silantyev, V. M. (2001). Limits of the turbine efficiency for free fluid flow. *Journal of Energy Resources Technology, 123*(4), 311–317.

Gunawan, B., Neary, V. S., & Colby, J. (2014). Tidal energy site resource assessment in the East River tidal strait, near Roosevelt Island, New York, New York. *Renewable Energy, 71,* 509–517.

Hakim, A. R., Cowles, G. W., & Churchill, J. H. (2013). The Impact of Tidal Stream Turbines on Circulation and Sediment Transport in Muskeget Channel, MA. *Marine Technology Society Journal, 47*(4), 122–136.

Harrison, M. E., Batten, W. M. J., Myers, L. E., & Bahaj, A. S. (2010). Comparison between CFD simulations and experiments for predicting the far wake of horizontal axis tidal turbines. *IET Renewable Power Generation, 4*(6), 613–627.

Hasegawa, D., Sheng, J., Greenberg, D. A., & Thompson, K. R. (2011). Far-field effects of tidal energy extraction in the Minas Passage on tidal circulation in the Bay of Fundy and Gulf of Maine using a nested-grid coastal circulation model. *Ocean Dynamics, 61*(11), 1845–1868.

IEC (2013). TS 62600–1:2013 Marine energy—Wave, tidal and other water current converters—Part 1: Terminology.

IEC (2014). TS 62600-200:2014 Marine energy—Wave, tidal and other water current converters —Part 200: Power performance assessment of electricity producing tidal energy converters.

IEC (2015). TS 62600-201:2015 Marine energy—Wave, tidal and other water current converters - Part 201: Tidal energy resource assessment and characterization.

Iglesias, G., Sánchez, M., Carballo, R., & Fernández, H. (2012). The TSE index–a new tool for selecting tidal stream sites in depth-limited regions. *Renewable Energy, 48,* 350–357.

Jo, C., Yim, J., Lee, K., & Rho, Y. (2012). Performance of horizontal axis tidal current turbine by blade configuration. *Renewable Energy, 42,* 195–206.

Joukowsky, N. E. (1920). Windmill of the NEJ type. *Transactions of the Central Institute for Aero-hydrodynamics of Moscow, 1,* 57.

Karsten, R. H., McMillan, J. M., Lickley, M. J., & Haynes, R. D. (2008). Assessment of tidal current energy in the Minas Passage, Bay of Fundy. *Proceedings of the Institution of Mechanical Engineers, Part A: Journal of Power and Energy, 222*(5), 493–507.

Lanchester, F. W. (1915). A contribution to the theory of propulsion and the screw propeller. *Journal of the American Society for Naval Engineers, 27*(2), 509–510.

Lawn, C. J. (2003). Optimization of the power output from ducted turbines. *Proceedings of the Institution of Mechanical Engineers, Part A: Journal of Power and Energy, 217*(1), 107–117.
Lewis, M., Neill, S. P., Robins, P. E., & Hashemi, M. R. (2015). Resource assessment for future generations of tidal-stream energy arrays. *Energy, 83,* 403–415.
Naksrisuk, C., & Audomvongseree, K. (2013). Dependable capacity evaluation of wind power and solar power generation systems. *2013 10th International Conference on Electrical Engineering/Electronics, Computer, Telecommunications and Information Technology (ECTI-CON)* (pp. 1–6). IEEE.
National Research Council (NRC). (2013). An Evaluation of the U.S. Department of Energy's Marine and Hydrokinetic Resource Assessments. The National Academies Press.
Neary, V. S., Gunawan, B., & Sale, D. C. (2013). Turbulent inflow characteristics for hydrokinetic energy conversion in rivers. *Renewable and Sustainable Energy Reviews, 26,* 437–445.
Pacheco, A., & Ferreira, Ó. (2016). Hydrodynamic changes imposed by tidal energy converters on extracting energy on a real case scenario. *Applied Energy, 180,* 369–385.
Polagye, B. & Bedard, R. (2006). Tidal in-stream energy resource assessment for Southeast Alaska. *Electric Power Research Institute*.
Polagye, B. L., Epler, J., & Thomson, J. (2010). Limits to the predictability of tidal current energy. *OCEANS 2010* (pp. 1–9). IEEE.
Polagye, B., Kawase, M., & Malte, P. (2009). In-stream tidal energy potential of Puget Sound, Washington. *Proceedings of the Institution of Mechanical Engineers, Part A: Journal of Power and Energy, 223*(5), 571–587.
Polagye, B. L., & Malte, P. C. (2011). Far-field dynamics of tidal energy extraction in channel networks. *Renewable Energy, 36*(1), 222–234.
Polagye, B., & Thomson, J. (2013). Tidal energy resource characterization: methodology and field study in Admiralty Inlet, Puget Sound, WA (USA). *Proceedings of the Institution of Mechanical Engineers, Part A: Journal of Power and Energy*, 0957650912470081.
Rao, S., Xue, H., Bao, M., & Funke, S. (2016). Determining tidal turbine farm efficiency in the Western Passage using the disc actuator theory. *Ocean Dynamics, 66*(1), 41–57.
Ramos, V., Carballo, R., Álvarez, M., Sánchez, M., & Iglesias, G. (2014). A port towards energy self-sufficiency using tidal stream power. *Energy, 71,* 432–444.
Roc, T., Conley, D. C., & Greaves, D. (2013). Methodology for tidal turbine representation in ocean circulation model. *Renewable Energy, 51,* 448–464.
Shapiro, G. I. (2011). Effect of tidal stream power generation on the region-wide circulation in a shallow sea. *Ocean Science, 7*(1), 165.
Shi, W., Wang, D., Atlar, M., & Seo, K. C. (2013). Flow separation impacts on the hydrodynamic performance analysis of a marine current turbine using CFD. *Proceedings of the Institution of Mechanical Engineers, Part A: Journal of Power and Energy, 227*(8), 833–846.
Stock-Williams, C., Parkinson, S., & Gunn, K. (2013). An investigation of uncertainty in yield prediction for tidal current farms. *10th European wave and tidal energy conference (EWTEC)*.
Sutherland, G., Foreman, M., & Garrett, C. (2007). Tidal current energy assessment for Johnstone Strait, Vancouver Island. *Proceedings of the Institution of Mechanical Engineers, Part A: Journal of Power and Energy, 221*(2), 147–157.
Tang, H. S., Kraatz, S., Qu, K., Chen, G. Q., Aboobaker, N., & Jiang, C. B. (2014). High-resolution survey of tidal energy towards power generation and influence of sea-level-rise: A case study at coast of New Jersey, USA. *Renewable and Sustainable Energy Reviews, 32,* 960–982.
Vennell, R. (2010). Tuning turbines in a tidal channel. *Journal of Fluid Mechanics, 663,* 253–267.
Vennell, R. (2011). Tuning tidal turbines in-concert to maximise farm efficiency. *Journal of Fluid Mechanics, 671,* 587–604.
Vennell, R. (2012). Realizing the potential of tidal currents and the efficiency of turbine farms in a channel. *Renewable Energy, 47,* 95–102.
Vennell, R., Funke, S. W., Draper, S., Stevens, C., & Divett, T. (2015). Designing large arrays of tidal turbines: A synthesis and review. *Renewable and Sustainable Energy Reviews, 41,* 454–472.

Walters, R. A., Tarbotton, M. R., & Hiles, C. E. (2013). Estimation of tidal power potential. *Renewable Energy, 51,* 255–262.

Work, P. A., Haas, K. A., Defne, Z., & Gay, T. (2013). Tidal stream energy site assessment via three-dimensional model and measurements. *Applied Energy, 102,* 510–519.

Yang, X., & Haas, K. A. (2015). Improving assessments of tidal power potential using grid refinement in the coupled ocean-atmosphere-wave-sediment transport model. *Journal of Renewable and Sustainable Energy, 7*(4), 043107.

Yang, Z., & Wang, T. (2015). Modeling the effects of tidal energy extraction on estuarine hydrodynamics in a stratified estuary. *Estuaries and Coasts, 38*(1), 187–202.

Yang, Z., Wang, T., & Copping, A. E. (2013). Modeling tidal stream energy extraction and its effects on transport processes in a tidal channel and bay system using a three-dimensional coastal ocean model. *Renewable Energy, 50,* 605–613.

Yang, Z., Wang, T., Copping, A., & Geerlofs, S. (2014). Modeling of in-stream tidal energy development and its potential effects in Tacoma Narrows, Washington, USA. *Ocean and Coastal Management, 99,* 52–62.

Yuce, M. I., & Muratoglu, A. (2015). Hydrokinetic energy conversion systems: A technology status review. *Renewable and Sustainable Energy Reviews, 43,* 72–82.

Tidal Energy Resource Measurements

Jim Thomson, Brian Polagye and Vincent S. Neary

Introduction

Accurate characterization and assessment of the tidal resource are essential to the design, plan, and development of a tidal energy project. The accuracy is important for both economic (i.e., how much electricity can be produced?) and technical aspects (i.e., will a turbine survive the turbulence at a given site?) of the tidal energy development. This chapter highlights the role of field measurements in characterizing and assessing the tidal resource for the purpose of energy extraction. Such measurements are commonly used in conjunction with numerical models, which is the focus of chapter "Hydrokinetic Tidal Energy Resource Assessments Using Numerical Models." For many tidal energy projects, examination of the resource progresses through stages of reconnaissance, feasibility, and design. Progression through these stages often involves a gradual shift in emphasis from models to measurements.

Standard definitions and best practices for tidal resource characterization and assessment continue to evolve (e.g., IEC 2015), and this chapter presents one distinct approach to these issues. Herein, "resource characterization" is defined as the task of describing the attributes of the resource that relate to a tidal energy conversion, often using a set of metrics or parameters. "Resource assessment" is the appraisal or valuation of a marine resource (national, regional, or site) for the purpose of energy

J. Thomson (✉)
Applied Physics Laboratory and Department of Civil and Environmental Engineering, University of Washington, Seattle, USA
e-mail: jthomson@apl.washington.edu

B. Polagye
Department of Mechanical Engineering, University of Washington, Seattle, USA

V.S. Neary
Sandia National Laboratories, Albuquerque, USA

Z. Yang and A. Copping (eds.), *Marine Renewable Energy*,
DOI 10.1007/978-3-319-53536-4_5

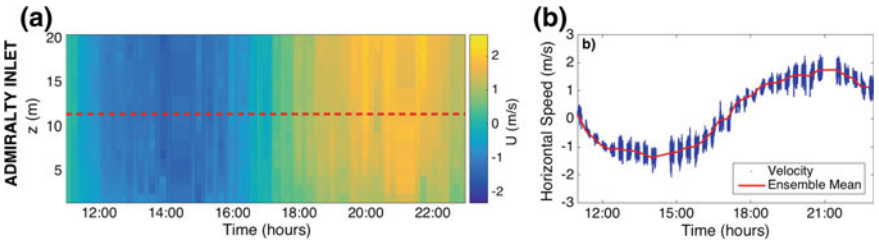

Fig. 1 Example acoustic Doppler current profiler data from Admiralty Inlet. The *left panel* shows the horizontal velocity, as a function of distance above the seabed and time. The *right panel* shows the time series from 11 m above the seabed, with the 10 min means (deterministic) in *red* and 8 Hz raw velocity fluctuations (stochastic) in *blue* (Guerra and Thomson in minor revision)

conversion. Assessment must weigh opportunities for energy extraction against various project risks (those to deployment, operation, survival, etc.). Resource assessments often emphasize the potential for energy production. Following recommendations by the National Research Council (2013), distinctions are made between the theoretical resource (how much energy is recoverable within natural limits of the resource?), the technical resource (how much of the theoretical resource is available based on technology limits, such as turbine efficiency and operational availability), and the practical resource (how much of the technical resource is available after considering social, economic, and environmental constraints?). Both measurements *and* models are combined to accomplish these tasks.

Measurements are typically emphasized during the later stages of development, when the cost of new measurements is justified by a viable resource identified by a model, historical measurements, or local knowledge. Furthermore, information from measurements, though more accurate than most models, may be sparse and localized. Indeed, detailed resource characterization is always site-specific. This chapter reviews the use of measurements in several recent resource assessments and then uses a case study from Admiralty Inlet in Puget Sound, in Washington State (USA), to demonstrate the role of measurements in quantifying the tidal resource.[1] An example of tidal currents measured at this site is shown in Fig. 1.

The Tidal Energy Resource

Tidal motions carry both kinetic and potential energy. Modern approaches to tidal energy conversion use in-stream turbines to extract some portion of the kinetic energy flux, or power density, of the currents, which is given locally by

[1]Several figures, which have not been published previously in academic papers, use data from this case study. The data and more information regarding the case study are available at http://depts.washington.edu/nnmrec/project_meas.html#admiralty.

$$K = \frac{1}{2}\rho u^3$$

where u is the current speed in meters per second, and ρ is the water density. Power density is conventionally expressed in kilowatts per meter squared or in watts per meter squared in tidal turbine applications. A key challenge in quantifying power density throughout a region is the innate richness and complexity of tidal currents. Figure 1 shows an example of these currents, using a subset of acoustic Doppler current profiler (ADCP) measurements collected in Admiralty Inlet, in Washington State (USA). In addition to the regular ebb and flood currents shown in this figure, there are variations across a wide range of scales, including vertical shear (change with depth in the left panel) and turbulent fluctuations (rapid changes in time in the right panel).

In general, the tidal energy resource contains both deterministic characteristics, which are repeatable, and stochastic characteristics, which must be described statistically. The basis for this distinction is the decomposition of the tidal currents as the sum of a mean velocity and turbulent fluctuation

$$u = \overline{u} + u'.$$

By convention, the demarcation between deterministic and stochastic components is on timescales with quasi-stationarity (5–10 min for tidal currents, McCaffrey et al. 2015). A more granular decomposition of the current may explicitly treat wind-generated currents and wave-orbital velocities (Polagye and Thomson 2013), as well as measurement noise and model error.

Table 1 lists the common metrics derived from field measurements of tidal currents, following the framework of deterministic and stochastic characteristics.

Table 1 Tidal resource parameters obtained directly from measurements

Tidal resource parameter	Application
Harmonic constituents	Deterministic predictor of mean currents
Current histograms	Stochastic predictor of mean currents
Power density, K (kW/m^2)	Local kinetic energy flux
Turbine annual energy production (MWh/yr)	Power produced by a turbine in a small, sparse array
Lateral shear (spatial gradients)	Array design/placement
Asymmetry (magnitude and direction)	Turbine design/selection
Peak current (m/s)	Turbine survivability
Turbulence intensity (–)	Stochastic predictor of fluctuations
Turbulence spectra	Scales of fluctuations
Wind/wave conditions	Survivability and operation and maintenance windows

These are useful for site-specific resource assessments, in particular assessments covering small spatial domains. At larger scales, analytic and computational models are needed to compliment the information from the measurements, and the merger of measurements with such models is discussed at the end of the chapter.

Measurements of Deterministic Tidal Resource Characteristics

Tidal currents originate in highly predictable astronomical cycles. As such, field measurements of mean currents can be used as an input to harmonic analysis of the tidal constituents for extrapolation over longer horizons. The result is essentially a model (albeit one with explicit tuning) that can be applied to predict currents indefinitely (Palowicz et al. 2002), though with greater uncertainty than for tidal elevation (Godin 1983). The result is mean currents that are described by a summation of a set of amplitudes and phases, each at known astronomical periods. This method is used to generate tidal and current tables for general use by coastal mariners (e.g., by US National Oceanic and Atmospheric Administration and the UK Admiralty Tide Tables).

The measurements for harmonic analysis are typically collected using ADCPs mounted on or near the seafloor. At least 35 days of site-specific data are required to capture the main tidal constituents, and longer records are essential for predictability of the strongest currents (Polagye and Thomson 2013; Kutney et al. 2013). Figure 2 shows the increased accuracy obtained by using longer measurement records to derive the deterministic parameters of the resource at Admiralty Inlet.

Though widely used, harmonic analysis may not be able to accurately predict currents at locations that have strong ebb/flood asymmetry (Godin 1983) or deterministic, but non-harmonic, large-scale flow features (e.g., eddies resulting

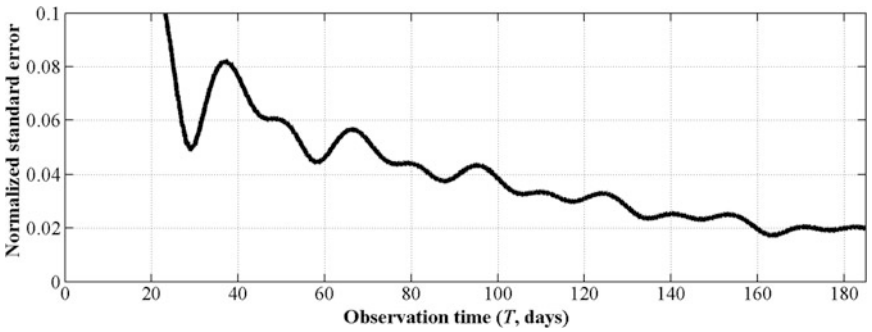

Fig. 2 Normalized error in mean power density versus record length of measurements (Polagye and Thomson 2013)

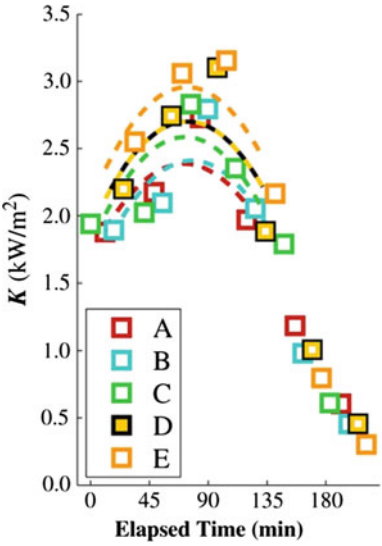

Fig. 3 Variations in local kinetic power density (K) during a partial tidal cycle (0–180 min) from five different locations (indicated by *colors*) separated by less than 250 m and measured simultaneously (Palodichuck et al. 2013)

from bathymetric or topographic features). In such cases, a histogram representation of current speeds from a record of sufficient length may be preferable (Kutney et al. 2013) and can be readily applied to the calculation of annual energy production (AEP). This is an estimate of turbine energy generation obtained by convolving a turbine performance curve (e.g., electrical power as a function of current velocity) with a histogram of current speed for a typical year, as discussed later in this chapter.

The results of harmonic analysis or histograms from field measurements are only strictly applicable at the actual location of the measurements. Many tidal hot-spots are channels with lateral and/or vertical constrictions, where the geometry causes strong gradients in the mean currents. Thus, measurements at one location may not be applicable to other locations, even at ranges on the order of 100 m. A method for characterizing such spatial variations in the deterministic mean currents and power density is given by Palodichuck et al. (2013) and an example of the results from Admiralty Inlet is shown in Fig. 3. This method relies on "station keeping" at a limited number of sites in close proximity over a tidal cycle.

The complex geometries common to tidal energy sites can also cause asymmetries in the direction and strength of the mean currents between ebb and flood. This is of varying importance, depending on the details of a particular turbine design, but it can be significant (Neill et al. 2014; Frost et al. 2015). Some devices yaw to face the principal axes of the currents, while others remain fixed, and this will alter the device efficiency. Figure 4 shows an example of ebb–flood asymmetries in both the direction and magnitude of the mean currents at two locations in Admiralty Inlet.

Finally, vertical shear is common to tidal sites, because currents are reduced through the bottom boundary layer. This may reduce turbine performance lower in

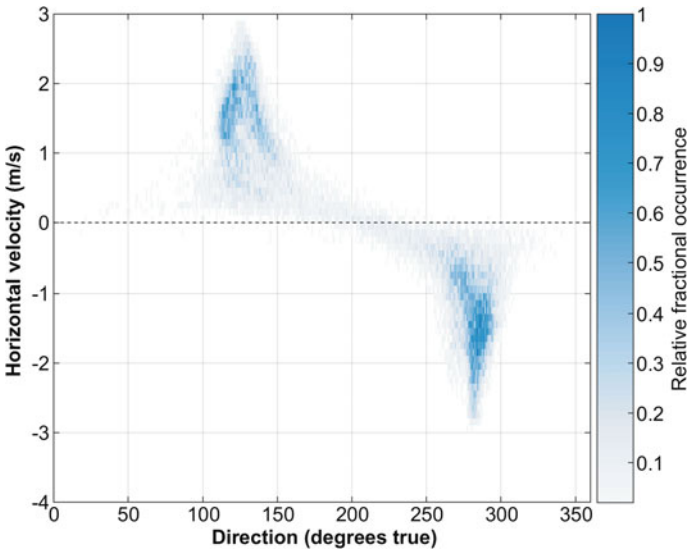

Fig. 4 Example of asymmetry in a joint probability distribution of tidal current and direction from a site in Admiralty Inlet

the water column, or, if vertical shear is significant over the turbine swept area, it can intensify cyclic blade loads and shorten fatigue life. See Fig. 1 for an example of measured shear (increasing current magnitude with distance above the seabed).

Measurements of Stochastic Tidal Resource Characteristics

Given the high Reynolds numbers of the fast currents at tidal energy sites, one can expect strong turbulent fluctuations at these sites. These fluctuations are random and not predictable, and thus their quantification relies on statistical parameters—the most common of which is the turbulence intensity, which is defined as:

$$I_u = \frac{\sigma_u}{\overline{u}}$$

where $\sigma_u = \sqrt{\overline{u'u'}}$ is the standard deviation or root-mean-square velocity. This must be calculated over timescales with stationary statistics (i.e., stable mean). By convention, this is often taken as 5–10 min in a tidal flow. Figure 5 shows an example of measured turbulent intensity, which is approximately 10% at Admiralty Inlet (Thomson et al. 2012). Note that because this metric is normalized by the magnitude of the mean current, it obscures the fact that, in absolute terms, turbulent perturbations increase with increasing mean current. Turbulent stresses and

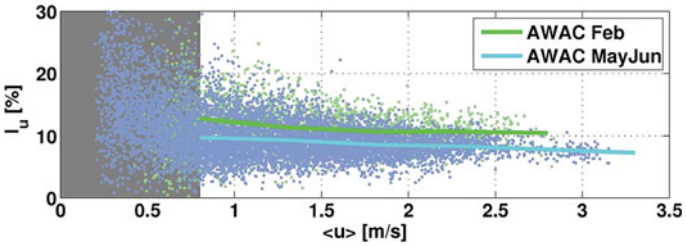

Fig. 5 Raw and bin-averaged turbulence intensities versus mean currents measured in Admiralty Inlet using an ADCP (Thomson et al. 2012)

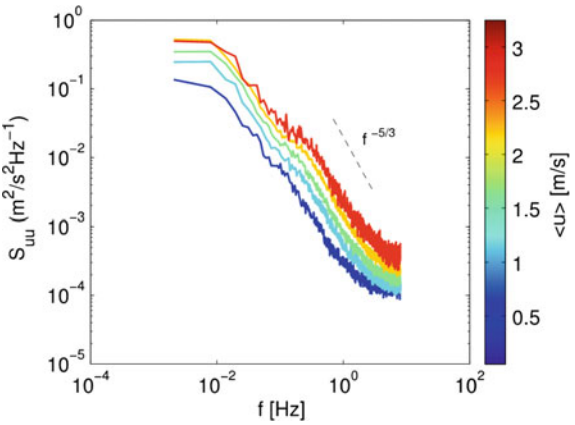

Fig. 6 Frequency spectra of turbulent kinetic energy at different mean currents (*colors*) measured in Admiralty Inlet using an ADV (Thomson et al. 2015)

intensities can vary significantly between flood and ebb tides (Gunawan et al. 2014). Also note that for the ADCP measurements most commonly used at tidal energy sites, an important step in data processing is the removal of variance from Doppler noise when calculating I from the raw velocity data as follows:

$$I_u = \frac{\sigma_u}{\langle u \rangle} = \frac{\sqrt{\langle u'^2 \rangle - n^2}}{\overline{u}},$$

where n is the uncertainty, or "single-ping error," of the raw ADCP data (Thomson et al. 2012).

The Doppler noise contamination is much less severe when using measurements from ADVs, which can be moored at a tidal site for additional measurements of turbulence (Thomson et al. 2015; Kilcher et al. 2016). In particular, the lower noise means that the frequency spectra of turbulent kinetic energy can be observed from ADV measurements. The calculation of spectra partitions the turbulence into discrete scales, which may be useful in predicting the performance and survivability of a particular turbine (based on the scales of motion relative to power performance and structural loading). Figure 6 shows an example of spectra from Admiralty Inlet,

in which there is a classic "cascade" of turbulent energy from large scales (low frequencies) to small scales (high frequencies). The frequency spectra from measurements can also be useful to "seed" a numerical model for the turbulence at a site (e.g., TurbSim; Jonkman and Kilcher 2012).

In addition to affecting turbine performance and structural loads, stochastic turbulence can also affect the AEP (which is captured, in part, by the histogram of current speed). The changes to the AEP are because of the quadratic relationship between current speed and load density, and the cubic relationship between current speed and power density. As a result, turbulent fluctuations that are symmetric about the mean will have non-symmetric effects on the power density.

The average load density over a representative period of record is given by

$$\overline{F} = \frac{1}{2} \cdot \rho \cdot \overline{u^2} = \frac{1}{2} \cdot \rho \cdot \left(1 + I_u^2\right) \cdot \overline{u}^2$$

and the average power density is

$$\overline{K} = \frac{1}{2} \cdot \rho \cdot \overline{u^3} = \frac{1}{2} \cdot \rho \cdot \left(1 + 3I_u^2 + \gamma I_u^3\right) \cdot \overline{u}^3$$

where ρ is water density, u is the instantaneous horizontal current velocity component, and $\gamma = \overline{u'^3}/\sigma^3$ is the skewness coefficient, which is negligible.

These equations show that accurate assessment of the average hydrodynamic force and available power requires resolution of the turbulent fluctuations and turbulence intensity as well as the mean velocity. As an example, if a turbine is responsive to the majority of energy-containing eddies, then turbulence intensity at 20% of hub height would increase the hydrodynamic force and power by 4% and 13%, respectively, relative to steady-state inflow conditions. The effects of turbulence should therefore be considered in the structural design and performance estimates for a tidal turbine. However, non-dimensional measures of turbine performance, such as the coefficient of performance and coefficient of thrust, are weakly influenced by turbulence (Mycek et al. 2014).

Finally, stochastic metrics can also be used to describe non-tidal processes that can affect tidal sites. These may include wind-generated currents and wave-orbital motions at depth that may affect turbine performance and survivability. Similarly, wind and wave conditions at the surface may limit windows for operations and maintenance.

Annual Energy Production

As previously alluded to, annual energy production, AEP, is a commonly used resource assessment metric. AEP can be calculated as deterministic quantity, using the time integral of the power, or it can be calculated as a statistical quantity, using a histogram of the power. As recommended by the International Electrotechnical

Commission (IEC 2015), technical resource AEP is the integration of the product of the turbine power as a function of tidal current and mean current frequency histogram:

$$AEP = (8766)\eta \sum_{i=1}^{n} \overline{P}\left(\overline{U_i}\right) \cdot f_i\left(\overline{U_i}\right)$$

where $f_i\left(\overline{U_i}\right)$ is the frequency of occurrence of a given mean current speed, 8766 is the number of hours in a Julian year (365.25 days), P_i is the turbine power output as a function of current, and η is the assumed operational availability of the technology (i.e., allowances for outages associated with planned and unplanned maintenance). For widely spaced turbines extracting a small fraction of the theoretical resource, the undisturbed velocity distribution at turbine hub height is often a reasonable approximation of U_i. As inter-turbine spacing narrows, U_i must be adjusted to account for wake interactions and, as array size increases, it must also account for "back effects." For this reason, the theoretical resource cannot be estimated as the product of time-average kinetic power density and channel cross-sectional area (Garrett and Cummins 2008).

The adequacy of field measurements to determine AEP depends on record length and localization, because extrapolation beyond the measured data may introduce errors. The adequacy of models to determine AEP depends on model accuracy and resolution, because the currents will vary over a wider range of space and time-scales than models can fully represent.

Large-Scale Resource Assessment and the Merging of Measurements with Models

Large-scale resource assessments often combine information from measurements and models. These assessments typically focus on the deterministic aspects of the tidal currents and target one or more of the three resource categories: theoretical, technical, and practical. However, merely quantifying the kinetic energy density is insufficient at most scales of development.[2] Although tidal turbines are generally considered to harness kinetic energy, the potential energy of the tidal system, which is generally much greater than the kinetic, cannot be ignored at the large-scale levels of resource assessment. At the most basic level, there is no law of "conservation of kinetic energy." Rather energy, in aggregate, is conserved and the act of energy extraction can involve exchange between kinetic and potential. Several theoretical and numerical studies have shown that the "back effects" of energy

[2]Many early tidal resource assessments at the site, regional, and national levels did, however, attempt to do this, prior to the emergence of a better understanding of energy balances in tidal channels.

extraction play an important role in resource assessment (Garrett and Cummins 2005; Blanchfield et al. 2008; Karsten et al. 2008; Polagye et al. 2008; Shapiro 2011; Adcock et al. 2013; Sanchez et al. 2014; Yang and Wang 2015). A number of recent regional and national resource assessments have used an analytical estimate for the theoretical resource, following classic hydraulics, in which total power is derived from the tidal elevation change H and volume flux (Q) in an undisturbed state as

$$P_{\text{total}} \approx \rho g Q H$$

where ρ is water density, g is gravity, and the resulting units are watts. The theoretical resource is a fraction of this quantity, which is on the order of one-quarter for most tidal channels (Garrett and Cummins 2008). For tidal regimes in which a single constituent is dominant (e.g., strongly semidiurnal regimes), H and Q correspond to the amplitude of the natural tidal range and flow rate, with minimal cycle-to-cycle fluctuations. Theoretical annual energy production (AEP) is, therefore, simply the product of P_{total} and the number of hours in a year. In cases of mixed regimes, (e.g., mixed mainly semidiurnal regimes typical of the US West Coast), corrections for multiple tidal constituents are available for some channel geometries (Garrett and Cummins 2005). Further, the analytical relation for P_{total} may not be suitable for networks of tidal channels (Polagye and Malte 2011). Finally, P_{total} corresponds to the total power that can be removed from the system. This includes the energy harnessed for electricity generation, as well as losses from wake mixing and support structures, both of which can be substantial fractions of P_{total} (Garrett and Cummins 2007; Garrett and Cummins 2008). This was the approach used to construct the US tidal resource atlas (Zafer et al. 2012) and is most appropriate for national and regional tidal energy resource assessments, which can cover thousands of square kilometers, with multiple tideways spread over an entire region or nation (e.g., Iyers et al. 2013; Lewis et al. 2015).

Although approximate, the analytical approach is far preferable to taking a spatial integral of the local power densities over the cross-sectional area of a tidal channel, because this entirely ignores the back effects of extraction. As demonstrated by Garrett and Cummins (2008), the spatial integral of local power density is unrelated to the theoretical resource. Deployment of tidal turbines with a projected area greater than a mere 2% of the channel cross section can, in some situations, alter channel hydrodynamics (Vennell et al. 2012). Resource assessments for the purposes of project siting do, however, often rely on estimates of power density in the absence of "back effects" (Goundar and Ahmed 2014; Serhadlıoğlu et al. 2013; Gunawan et al. 2014, Carballo et al. 2009). This is appropriate for identifying areas with high resource intensity, but not for valuation of the theoretical resource.

The obvious alternative to analytical approximations is a numerical simulation that explicitly includes turbine power extraction (e.g., Yang and Wang 2015). In addition to the difficulty of accurately simulating power extraction, the ambient conditions alone at tidal energy sites are challenging to simulate, particularly in regard to power density. Regions with strong tidal currents generally have complex

geometries that drive the dynamics (e.g., Easton et al. 2012) and high spatial heterogeneity in the resulting currents (e.g., Robins et al. 2015). This requires fine spatial resolutions that entail high computational cost over the requisite simulation timescales (e.g., at least a fortnight, in addition to model spin-up time from a quiescent domain). It is essential that models be verified by measurements before they are applied to quantify a tidal resource, and, once validated, that models not be applied for characterization metrics that reach beyond the level of model validation (e.g., investigation of design loads using velocities from a regional simulation at a grid resolution on the order of the turbine diameter).

Using Measurements to Validate Model-Based Resource Assessments

Because of the need to account for back effects, national and regional resource assessments rely on models. In addition, it is often impractical (or impossible) to collect enough data to cover the domain of interest at the reconnaissance stage. Tidal resource values based on the models are, of course, only as accurate as the model itself. This accuracy is particularly sensitive, because errors in the currents are exacerbated when taking the cube of the currents to calculate the tidal resource intensity. In this context, measurements are used to validate and tune the models.

For example, the model used for the US resource atlas grossly underestimated power density relative to in situ measurements at a potential tidal energy site in Admiralty Inlet in Washington State (USA), as shown in Fig. 7. While the model qualitatively captures the amplification of currents by the nearby headland, quantitative agreement is poor; measured power density exceeds model values by a factor of two to three and has a proportional implication for estimates of the cost of energy from tidal current power generation at this site. Models run at much higher resolution can more accurately quantify power density throughout the channel and the effects of the headland (Yang and Wang 2013; Thyng et al. 2013), but this level of detail is often beyond the scope of national reconnaissance activities. In Fig. 8, both models and measurements show strong gradients in the currents at small spatial scales (~100 m), demonstrating the importance of model validation prior to

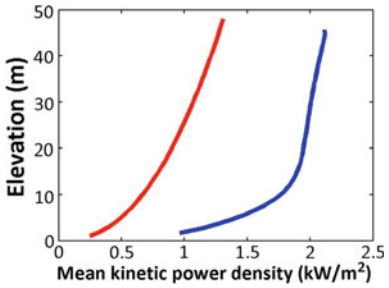

Fig. 7 Comparison of average power density, *K*, measurement with ADCP data (*blue*) and modeled in the US tidal atlas (*red*) for the case study at Admiralty Inlet

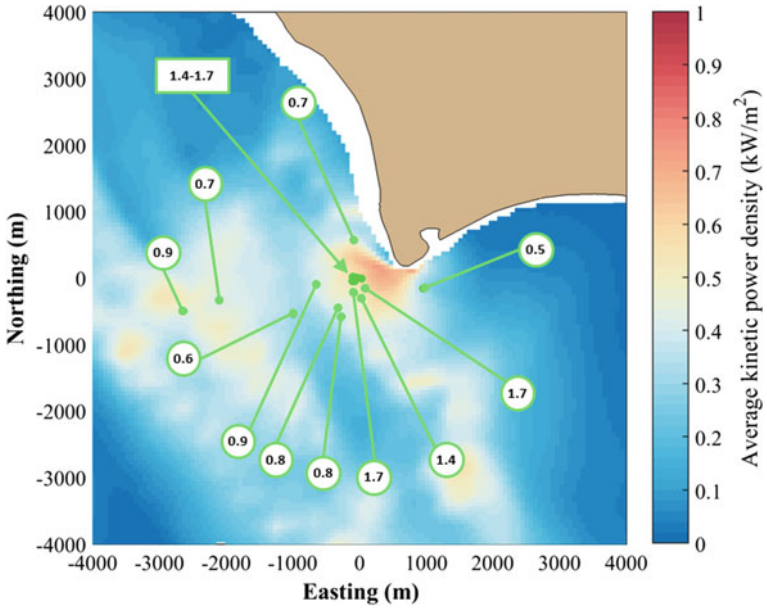

Fig. 8 Comparison of modeled and measured kinetic power density at a tidal energy site in Admiralty Inlet, Washington (USA) at a height of 10 m above the seabed. Model results derived from Thyng (2012). *Color map* denotes modeled kinetic power density. *Circles* denote measurements at specific locations

model application for resource assessment. It also supports the recommendation for site-specific resource characterization based on the field measurements (IEC 2015), because the regional-scale nature of most reconnaissance resource assessments is not well-matched to the small-scale complexity of tidal currents.

The resource assessment conducted by Iyers et al. (2013) for the UK illustrates how theoretical, technical, and practical AEP can be estimated for a large region. This resource assessment was greatly simplified at the outset by limiting tidal energy extraction to first-generation tidal turbine technologies, which requires spring peak currents to be greater than 2.5 m/s and depths between 25 and 50 m. A similar approach was used by Boehme et al. (2006), but with a threshold current of 2.0 m/s and depths between 30 and 50 m. This limited the scope of the assessment to seven locations around the UK. Tidal current time series data from the UK Hydrographic Office Admiralty Chart were used in lieu of current speed data derived from ADCP measurements or a numerical model. These data are generated using a simple model based only on the two dominant tidal harmonic constituents, M2 and S2. Resource assessments that rely on field data are most often applied over small domains (e.g., Fairley et al. 2013). More commonly, resource assessments cover larger domains and rely on realistic circulation models that have been validated to various degrees by field measurements.

One of the key contributions of reconnaissance studies at national scales is the identification of hot spots that have high local power densities and, therefore, high AEP values (e.g., O'Rourke et al. 2010). After hot spots are identified in the reconnaissance phase, feasibility-level assessments are conducted to refine project siting and increase the resolution and accuracy of resource characterization to plan a tidal energy farm. Data sources for feasibility studies often rely heavily on validated model hindcasts, but these should be supplemented with field measurements, such as bottom- and vessel-mounted ADCP measurements. Finally, design-level assessments are conducted at spatial resolutions similar to the size of individual turbines and are best done with fixed field measurements, such as bottom-mounted ADCPs. Moored acoustic Doppler velocimeters (ADVs) can also be used during this stage. These methods are described by the IEC (2015), Neary et al. (2011), Blunden and Bahaj (2007), and Kilcher et al. (2016).

Conclusions

While tidal resource assessment can be limited in scope to an estimate of AEP, this simplification obscures the many complexities of the resource. While the resolution of deterministic components may be adequate for characterizing AEP, both components need to be quantified to determine design loads on tidal energy conversion devices. Large space and time variations are common at most tidal energy sites, and, given the limitations of modeling, site-specific measurements are required to fully characterize such variations. Quantifying a full suite of parameters (i.e., Table 1), as well as AEP, provides a more comprehensive characterization and assessment of the tidal energy resource; one that includes quantification of the risks, as well as opportunities for a tidal energy project. Measurements are a key component of this process. Field measurements must be at high sampling frequencies (~10 Hz), and over long durations (~months) to resolve stochastic and deterministic components occurring over a broad range of temporal scales. While this can be accomplished for a point measurement, it becomes challenging when measuring current speeds and turbulent fluctuations over a profile or cross section. Ongoing improvements in measurement techniques, e.g., Kilcher et al. (2016), and improved current profiler technology, e.g., Guerra and Thomson (in minor revision), will help researchers address these challenges.

The other role of field measurements is to evaluate and validate models. This role is equally important, because models have become a standard tool for high-level resource assessments (e.g., national and regional assessments). Small biases in the currents predicted by models can result in significant changes in the local power density (because of the cubic relation) and thus model accuracy must be confirmed at each level (or resolution) of its application. Furthermore, models often parameterize details of the flow (e.g., turbulence closure schemes) that measurements can provide (Thyng et al. 2013).

Best practices for quantifying the tidal resource are still being actively developed by a large community of researchers. The choice of parameters and approaches depends on study objective and site characteristics, but it is clear that the measurements, combined with models, are essential for capturing the complexity of the tidal resource in sufficient detail to effectively harness the energy.

References

Adcock, T. A., Draper, S., Houlsby, G. T., Borthwick, A. G., & Serhadlıoğlu, S. (2013). The available power from tidal stream turbines in the Pentland Firth. In *Proceedings of the Royal Society A*, *469*(2157), 20130072. The Royal Society.

Blachfield, J., Garrett, C., Rowe, A., & Wild, P. (2008). The extractable power from a channel linking a bay to the open ocean. *Proceedings of IMechE Part A: Journal of Power Energy, 222* (A3), 289–297.

Blunden, L. S., & Bahaj, A. S. (2007). Tidal energy resource assessment for tidal-stream generators. *Journal of Power Energy, 221,* 137–146.

Boehme, T., Taylor, J., Wallace, A. R., & Bialek, J. (2006). *Matching renewable electricity generation with demand*. Edinburgh: The Scottish Executive.

Carballo, R., Iglesias, G., & Castro, A. (2009). Numerical model evaluation of tidal-stream energy resources in the Ría de Muros (NW Spain). *Renewable Energy, 34*(6), 1517–1524.

Defne, Z., Haas, K. A., Fritz, H. M., Jiang, L., French, S. P., Shi, X., et al. (2012). National geodatabase of tidal stream power resource in USA. *Renewable and Sustainable Energy Reviews*, *16*(5), 3326–3338. ISSN 1364-0321. doi:10.1016/j.rser.2012.02.061.

Easton, M. C., Woolf, D. K., & Bowyer, P. A. (2012). The dynamics of an energetic tidal channel, the Pentland Firth, Scotland. *Continental Shelf Research, 48,* 50–60.

Fairley, I., Evans, P., Wooldridge, C., Willis, M., & Masters, I. (2013). Evaluation of tidal stream resource in a potential array area via direct measurements. *Renewable Energy, 57,* 70–78.

Frost, C., Morris, C. E., Mason-Jones, A., O'Doherty, D. M., & O'Doherty, T. (2015). The effect of tidal flow directionality on tidal turbine performance characteristics. *Renewable Energy, 78,* 609–620.

Garrett, C., & Cummins, P. (2005). The power potential of tidal currents in channels. *Proceedings of the Royal Society A*, *461*, 2563–2572.

Garrett, C., & Cummins, P. (2007). The efficiency of a turbine in a tidal channel. *Journal of Fluid Mechanics*, *588*, 243–251.

Garrett, C., & Cummins, P. (2008). Limits to tidal current power. *Renewable Energy, 33,* 2485–2490.

Godin, G. (1983). On the predictability of currents. *International Hydrographic Review, 60,* 119–126.

Goundar, J. N., & Ahmed, M. R. (2014). Marine current energy resource assessment and design of a marine current turbine for Fiji. *Renewable Energy, 65,* 14–22.

Guerra, M., & Thomson, J. (in minor revision). Turbulence measurements from 5-beam ADCPs. *Journal of Atmospheric and Ocean Technology.*

Gunawan, B., Neary, V. S., & Colby, J. (2014). Tidal energy site resource assessment in the East River tidal strait, near Roosevelt Island, New York, New York. *Renewable Energy, 71,* 509–517.

IEC (2015) TS 62600-201:2015 Marine energy—Wave, tidal and other water current converters—Part 201: Tidal energy resource assessment and characterization.

Iyer, A., Couch, S., Harrison, G., & Wallace, A. (2013). Variability and phasing of tidal current energy around the United Kingdom. *Renewable Energy, 51,* 343–357.

Jonkman, J. B., & Kilcher, L. (2012). TurbSim user's guide: Version 1.06. 00, National Renewable Energy Laboratory. Technical report. https://wind.nrel.gov/designcodes/preprocessors/turbsim/TurbSim.pdf.

Karsten, R. H., McMillan, J. M., Lickley, M. J., & Haynes, R. D. (2008). Assessment of tidal current energy in the Minas Passage, Bay of Fundy. *Proceedings of the Institution of Mechanical Engineers, Part A: Journal of Power and Energy, 222*(5), 493–507.

Kilcher, L., Thomson, J., Talbert, J., & deKlerk, A. (2016). Measuring turbulence from moored acoustic Doppler velocimeters: A manual to quantifying inflow at tidal energy sites. NREL technical report TP-5000-62979.

Kutney, T., Karsten, R., & Polagye, B. (2013). Priorities for reducing tidal energy resource uncertainty. In *European Wave and Tidal Energy Conference, Aalborg, Denmark, September 2–5*.

Lewis, M., Neill, S. P., Robins, P. E., & Hashemi, M. R. (2015). Resource assessment for future generations of tidal-stream energy arrays. *Energy, 83*(1), 403–415.

McCaffrey, K., Fox-Kemper, B., Hamlington, P. E., & Thomson, J. (2015). Characterization of turbulence anisotropy, coherence, and intermittency at a prospective tidal energy site: Observational data analysis. *Renewable Energy, 76,* 441–453.

Mycek, P., Gaurier, B., Germain, G., Pinon, G., & Rivoalen, E. (2014). Experimental study of the turbulence intensity effects on marine current turbines behaviour. Part I: One single turbine. *Renewable Energy, 66,* 729–746.

National Research Council. (2013). An evaluation of the U.S. department of energy's marine and hydrokinetic resource assessments. ISBN 978-0-309-26999-5, 114 p.

Neary, V., Gunawan, B., Richmond, M., Durgesh, V., Polagye, B., Thomson, J., Muste, M., & Fontaine, A. (2011). *Field measurements at rivers and tidal current sites for hydrokinetic energy development: best practices manual.* Oak Ridge National Laboratory Technical Manual 2011/419.

Neill, S. P., Hashemi, M. R., & Lewis, M. J. (2014). The role of tidal asymmetry in characterizing the tidal energy resource of Orkney. *Renewable Energy, 68,* 337–350.

O'Rourke, F., Boyle, F., & Reynolds, A. (2010). Tidal current energy resource assessment in Ireland: Current status and future update. *Renewable and Sustainable Energy Reviews, 14,* 3206–3212.

Palodichuk, M., Polagye, B., & Thomson, J. (2013). Resource mapping at tidal energy sites. *Journal of Ocean Engineering*, *38*.

Pawlowicz, R., Beardsley, R., & Lentz, S. (2002). Classical tidal harmonic analysis including error estimates in MATLAB using T_TIDE. *Computers & Geosciences, 28*(8), 929–937.

Polagye, B., & Thomson, J. (2013). Tidal energy resource characterization: Methodology and field study in Admiralty Inlet, Puget Sound, US. *Proceedings of IMechE, Part A: Journal of Power and Energy*, *227*.

Polagye, B. L., & Malte, P. C. (2011). Far-field dynamics of tidal energy extraction in channel networks. *Renewable Energy, 36*(1), 222–234.

Polagye, B., Malte, P., Kawase, M., & Durran, D. (2008). Effect of large-scale kinetic power extraction on time-dependent estuaries. *Proceedings of IMechE, Part A: Journal of Power and Energy*, *222*(5), 471–484.

Robins, P. E., Neill, S. P., Lewis, M. J., & Ward, S. L. (2015). Characterizing the spatial and temporal variability of the tidal-stream energy resource over the northwest European shelf seas. *Applied Energy*, *147*, 510–522.

Sanchez, M., Carballo, R., Ramos, V., Álvarez, M., Vazquez, A., & Iglesias, G. (2014). Impact of tidal stream energy exploitation on estuarine hydrodynamics. *Coastal Engineering Proceedings, 1*(34), 22.

Serhadlıoğlu, S., Adcock, T. A., Houlsby, G. T., Draper, S., & Borthwick, A. G. (2013). Tidal stream energy resource assessment of the Anglesey Skerries. *International Journal of Marine Energy, 3,* e98–e111.

Shapiro, G. I. (2011). Effect of tidal stream power generation on the region-wide circulation in a shallow sea. *Ocean Science*, *7*, 165–174.

Thomson, J., Richmond, M., Polagye, B., & Durgesh, V. (2012). Measurements of turbulence at two tidal energy sites. *Journal of Ocean Engineering*, *37*.

Thomson, J., Talbert, J., de Klerk, A., Zippel, S., Guerra, M., & Kilcher, L. (2015). Turbulence measurements from moving platforms. In *Currents, Waves, and Turbulence Measurements Workshop, St. Petersburg, FL*.

Thyng. (2012). Numerical simulation of admiralty inlet, WA, with tidal hydrokinetic turbine siting application. PhD Thesis, University of Washington.

Thyng, K. M., Riley, J. J., & Thomson, J. (2013). Inference of turbulence parameters from a ROMS simulation using the k-ε closure scheme. *Ocean Modelling, 72,* 104–118.

Vennell, R. (2012). Realizing the potential of tidal currents and the efficiency of turbine farms in a channel. *Renewable Energy, 47,* 95–102.

Yang, Z., & Wang, T. (2013). Tidal residual eddies and their effect on water exchange in puget sound. *Ocean Dynamics, 63,* 995–1009.

Yang, Z., & Wang, T. (2015). Modeling the effects of tidal energy extraction on estuarine hydrodynamics in a stratified estuary. *Estuaries and Coasts, 38*(1 Supplement), 187–202. doi:10.1007/s12237-013-9684-2.

Wave-Tide Interactions in Ocean Renewable Energy

M. Reza Hashemi and Matt Lewis

Introduction

If marine renewable energy is to make a significant contribution to meeting future electricity demand, resilient devices that can operate efficiently in oceanographic conditions typical of marine renewable energy sites need to be manufactured. In the seas of northwest of the European continental shelf, researchers have observed significant wave climates at potential tidal-stream energy sites (e.g., Lewis et al. 2014) and tidal effects to the wave resource (e.g., Hashemi and Neill 2014).

The characterisation of nearshore waves in Scottish waters has been noted to be complicated by strong wave-current interactions in locations such as the Pentland Firth (Gleizon and Woolf 2013). Indeed, wave-tide interaction is a noted effect near sites of potential wave and tidal energy projects in Orkney waters (Saruwatari et al. 2013); hence, dynamically coupled models for resource assessment were used in this region (e.g., Venugopal and Nemalidinne 2014). Further, Guillou et al. (2016) studied the influence of waves in the Fromveur Strait (France) on tidal-stream energy and found waves affected the resource during extreme conditions by 12%, which can have implications for cost-benefit analysis of potential tidal projects in that region.

Wave-tide interaction effects at wave farms have also been investigated in the United Kingdom (UK), and results showed that tidal elevation and currents can have a notable effect on waves and sediment transport processes (Gonzalez-Santamaria et al. 2015). In other regions of the world, potential tide and wave energy sites are in close proximity to one another (e.g., Colombia as shown by Osorio et al. 2016);

M.R. Hashemi (✉)
Department of Ocean Engineering, Graduate School of Oceanography, University of Rhode Island, Narragansett, RI, USA
e-mail: reza_hashemi@uri.edu

M. Lewis
School of Ocean Sciences, Bangor University, Bangor, UK
e-mail: m.j.lewis@bangor.ac.uk

Z. Yang and A. Copping (eds.), *Marine Renewable Energy*,
DOI 10.1007/978-3-319-53536-4_6

therefore, wave-current interaction at marine energy sites needs to be considered for specific regions.

The effect of waves upon the tidal resource, and the effect of tides on the wave resource, needs to be quantified for accurate resource assessment and device design. Wave power is proportional to the square of wave height, and tidal-stream power is proportional to the cube of current speed; therefore, small modulations due to wave-tide interaction could have a large effect on the marine renewable energy resource. Furthermore, during an extreme event, renewable energy devices are likely to go into a shutdown mode to decrease the likelihood of damage; however the conditions for the threshold of device shutdown are unclear and the effect to electricity supply is unquantified.

As a first-order approximation, the wave conditions at potential tidal-stream energy sites, and the tidal conditions at potential wave energy sites are investigated on a global scale to show wave-tide interaction is an important process to consider in marine renewable energy development (see Fig. 1). Tidal constituents were extracted from the FES2012 (Finite Element Solution) data-assimilated global tidal model (Carrère et al. 2012) at 1/16° resolution, with the peak tidal amplitude (associated with tidal elevation) and peak tidal current speeds assumed to be represented by the sum of the four major tidal constituents that describe the majority of the diurnal and semidiurnal tidal movement around the globe (see Pugh 1996; Robins et al. 2015). Global mean daily significant wave heights for a typical year (2014) were extracted from the European Centre for Medium-Range Weather Forecasts (ECMWF) ReAnalysis, ERA-interim product (Dee et al. 2011) at 3/4° resolution (Fig. 1c). Interpolating ETOPO2 (Earth TOPOgraphy) bathymetric data at 1/30° resolution (see Marks and Smith 2006), the ERA-interim wave climate and the FES2012 tidal climate data onto a common grid (the 1/16° FES2012 grid), allows the wave and tidal conditions at potential marine energy sites around the world to be assessed (Fig. 2). The daily mean wave height (averaged for 2014) is likely to be greater than 1 m for the majority of theoretical tidal-stream energy sites when resolved at 1/16° (hence some grey shaded regions that represent unresolved sites; see Fig. 2), and for many potential tidal energy sites (especially second generation sites; Lewis et al. 2015) having a yearly average daily wave height above 3 m (Fig. 2a and b).

Using the global mean daily wave height (H, see Fig. 1) and period (T), theoretical wave energy sites are assumed to be represented by high daily mean wave power estimates, averaged for 2014, with the representative tidal conditions shown in Fig. 2c and d, which reveal tidal currents >0.5 m/s and tidal range >2 m can be expected at potential wave energy sites around the globe.

Although many marine energy sites, such as the wave sheltered tidal-stream energy resource in Puget Sound USA, are unlikely to have significant wave-tide interaction because of their locations, some potential tidal energy sites around the globe will experience significant wave exposure, and conversely may experience strong wave-tide interaction. Nevertheless, the analysis of Figs. 1 and 2 cannot resolve processes below 1/16 spatial resolution (and wave analysis is for 1 year only and thus cannot resolve interannual variability). Hence, specific developments maybe in

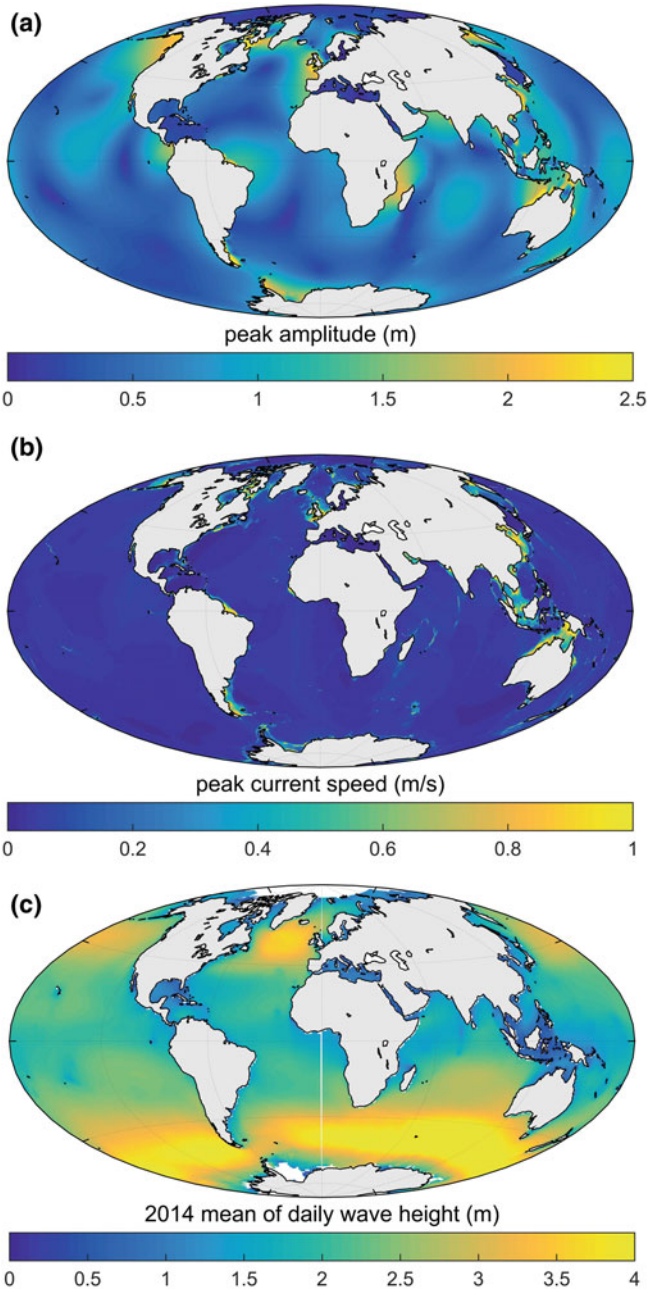

Fig. 1 The global distribution of the tide and wave energy resource (2014). **a** Peak tidal amplitude (associated with tidal elevation) and **b** peak current speed are represented by the sum of K1, O1, S2, and M2 constituents from the FES2012 database, and daily wave height **c** averaged from ERA-interim data for 2014. *Acronyms* FES (Finite Element Analysis); ERA (ECMWF ReAnalysis); ECMWF European Centre for Medium-Range Weather Forecasts

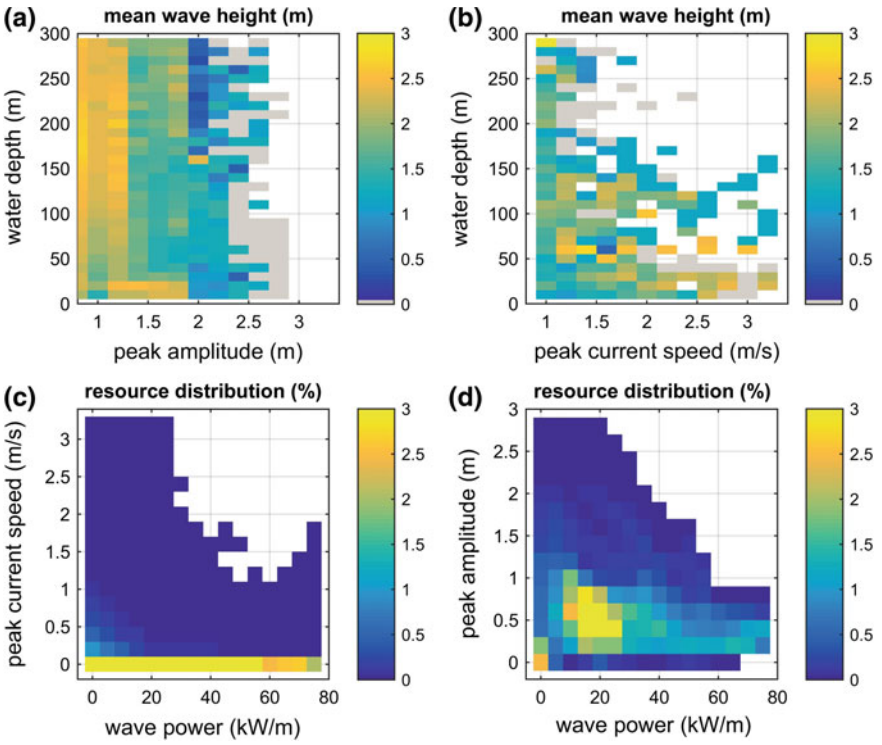

Fig. 2 The 2014 averaged daily wave height conditions at theoretical tidal range **a** and tidal-stream **b** energy sites around the globe, with the corresponding tidal conditions **c** and **d** at theoretical wave energy sites shown as the percentage of the global ocean area (resource distribution) based on Fig. 1

regions of low wave-tide interaction, and yet in many parts of the world (as discussed previously) the influence of waves on tidal energy schemes, and the influence of tides on wave energy schemes, may need to be considered.

To further demonstrate the wave-current interaction problem, Fig. 3 shows that significant wave events were observed over a 5 month period at two UK potential tidal-stream energy sites: the Crown Estates tidal energy demonstration zone in North West Anglesey (Site A, 172 days), and the Pentland Firth (Site B, 182 days). Mean wave conditions during the observation period (see Fig. 1) were 1.50 m and 7.5 s at Site A, and 1.07 m and 5.6 s at Site B. The largest waves of 6.6 m (11 s) and 5.45 m (8.7 s) were observed at Site A (Winter) and Site B (Summer) respectively, and the wave climate was demonstrated by the probability density (% of occurrence in 20 cm and 1 s bin sizes) shown in Fig. 3. Therefore, challenges surrounding waves at tidal-stream energy sites are an important consideration for some regions of the world, and if the true global potential of tidal energy is to be realized then these challenges need to be considered in the design and maintenance of marine renewable devices and associate resource assessment studies.

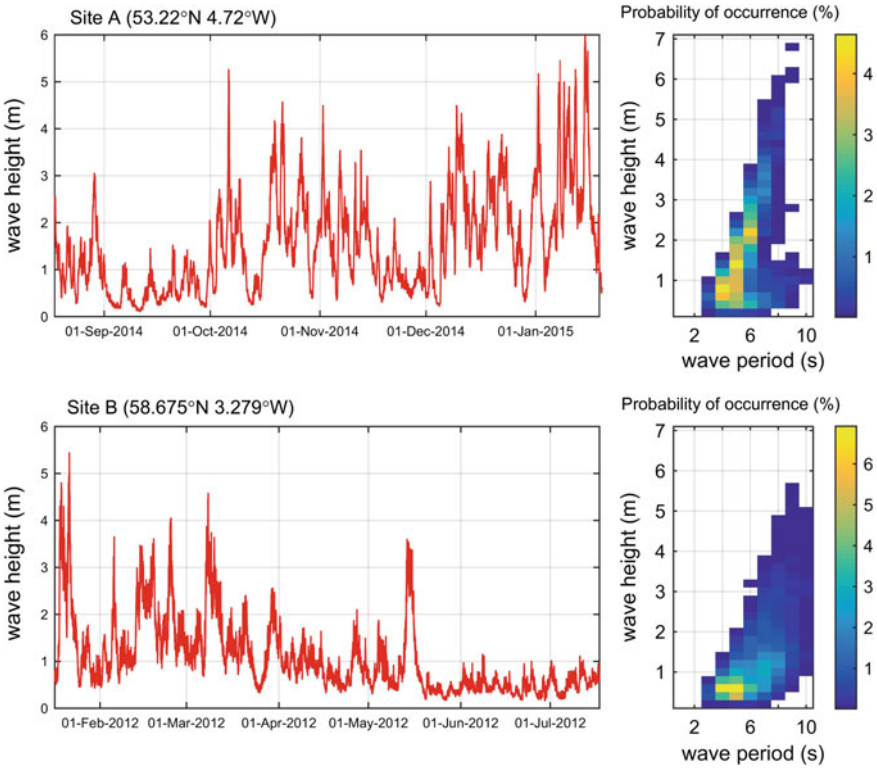

Fig. 3 The observed wave climate at two potential tidal-stream energy sites in the UK; the Crown Estates NorthWest Anglesey Demonstration Zone (*Site A*), and the Pentland Firth (*Site B*)

For resource characterizations, in many modeling studies, the interactions of waves and tides have been ignored by assuming that they are not be significant (e.g., Smith et al. 2013; ABPmer 2008; Neill et al. 2014; Draper et al. 2014) even though this assumption may not be valid in many of the regions (e.g., González-Santamaría et al. 2010; Saruwatari et al. 2013). Further, it is possible to simulate the effect of tides on a wave energy resource or vice versa by employing coupled modeling systems. However, these models are computationally more expensive, and more challenging to develop and validate. Therefore, it is helpful to understand wave-tide interaction processes, and the simple and basic methods that can quantify the importance of these processes, before developing complex numerical models. In observation-based data, which are collected to characterize the marine energy of a site, wave-tide interaction effects are inherently included. However, measurements usually take place during a particular period (e.g., certain wave conditions, facing a certain tidal current), and are usually carried out at specific locations. The concepts discussed in this chapter help understand and generalize measurement results for various locations and other time periods, which may involve different conditions.

This chapter introduces the topic of wave-current interaction within the context of marine renewable energy resource characterization, summarizing current research and discussing simple and advanced techniques for assessing associated impacts. The implications of wave-tide interaction on energy devices is another topic of interest, that needs to be discussed separately because the scale of the processes and tools, and concepts are different. A short discussion about this topic and some references are included.

Introduction to Wave-Tide Interaction

Tides and waves can be regarded as long and short waves that interact in multiple ways. Doppler shift is a clear example in which the frequency of waves changes by ambient current:

$$\omega = \sigma + ku \tag{1}$$

where σ is intrinsic or relative wave frequency (observed in a coordinate system moving with the same velocity as the ambient current), ω is the absolute wave frequency (observed in a fixed frame), u is the ambient current velocity, and k is the wave number. For wave energy development studies, a relevant question is whether the presence of tides and their effect on waves can be significant during various stages of a project such as site characterization, or evaluation of the performance of a wave energy device. In theory, wave energy propagates with group velocity which directly depend on water depth and ambient currents (Dalrymple and Dean 1991):

$$C_g = \frac{\sigma}{k} = \frac{\omega - ku}{k}\{\frac{1}{2}(1 + \frac{2kh}{\sinh 2kh})\} \tag{2}$$

where C_g is the group velocity, and h is the water depth; the angular frequency and wavenumber are related to water depth by the linear dispersion relationship,

$$\sigma^2 = (\omega - uk)^2 = gk\tanh(kh) \tag{3}$$

Because tides change water depth and generate currents, they can change the propagation of wave energy. Further, the magnitude of wave energy is proportional to the wave height squared, which also changes with ambient currents. For instance, currents opposing waves can cause a significant increase in wave height and lead to wave breaking or even complete blockage of wave energy propagation.

Similar issues may arise during tidal-stream project development. In general, waves interact with the shallow water bottom boundary layer, and enhance the bottom roughness. This process, particularly in shallow waters, leads to an increase in the bed shear stress, and consequently, the slowdown of tidal currents. Because tidal power is proportional to velocity cubed, this can have some impact on the tidal energy resource at a site (e.g., see Guillou et al. 2016). Also, wave-induced momentum, caused by wave radiation stresses, can modify the dynamics of tides.

In general, there are two questions about the implication of wave-tide interactions in marine renewable energy studies: When/where can these interactions be ignored? If significant, how can wave-tide interaction effects be included in studies at a reasonable cost? Here, we focus more on site characterization, but the implications for device design could be also important (e.g., Gaurier et al. 2013). We present/review an introduction to simple and advanced techniques for assessing the effects of wave-tide interactions in marine renewable energy studies.

Wave Effects in Tidal Energy Projects

In tidal-stream energy regions that have an influential wave climate (see section "Introduction"), wave effects need to be considered in resource assessment (section "Wave Climate Effects to Resource Assessment", and "Simplified Methods)" as well as planning for maintenance window conditions when conditions are calm enough for device inspection or repair work. Necessary provisions also need to be incorporated in design standards and power curves to account for shutdown limits and maintenance windows of tidal energy devices when they are exposed to waves.

Tidal-stream energy industry is still in its infancy, so consideration of waves in other offshore engineering schemes provides useful concepts to apply here; for example, the extreme wave climate and viability of access for maintenance, both of which could be affected by wave-tide interaction, is considered in most offshore engineering schemes. Current guidelines in the offshore wind industry state that boat access for maintenance programs requires wave heights <2 m (Lewis et al. 2014). Maintenance concerns have been discussed in tidal-stream energy research (e.g., Rourke et al. 2010), hence the concept of maintenance windows (e.g., O'Connor et al. 2013) and the challenges that surround this (e.g., Mueller and Wallace 2008), which should also consider wave-current interaction (e.g., wave steepness and tidally affected wave climates).

Some evidence also suggests the potential impact of tidal-stream energy schemes on sediment transport (Neill et al. 2009) should be considered in the context of the natural variability of the environment due to the wave climate (Robins et al. 2014). However, we concentrate on the effect of waves on resource assessment.

Waves add additional momentum to the tidal flow; for example, in the form of wave orbitals (see Fig. 4), Stokes velocities and radiation forces can also modify the shear stress (associated with vertical velocity profile; Luznik et al. 2013). Therefore, and as summarized in Fig. 4, waves can play an important part in the technical tidal-stream resource assessment (section "Wave Climate Effects to Resource Assessment"), and in tidal-stream energy converter design considerations (section "Wave Considerations in the Design of Tidal Turbines"). Design considerations are included briefly in this chapter because when characterizing the oceanographic conditions for design, feedback into a technical resource assessment needs to be considered (tidal- stream energy device behavior should be considered, such as downtime). Section "Simplified Methods" summarizes the use of depth-averaged models and

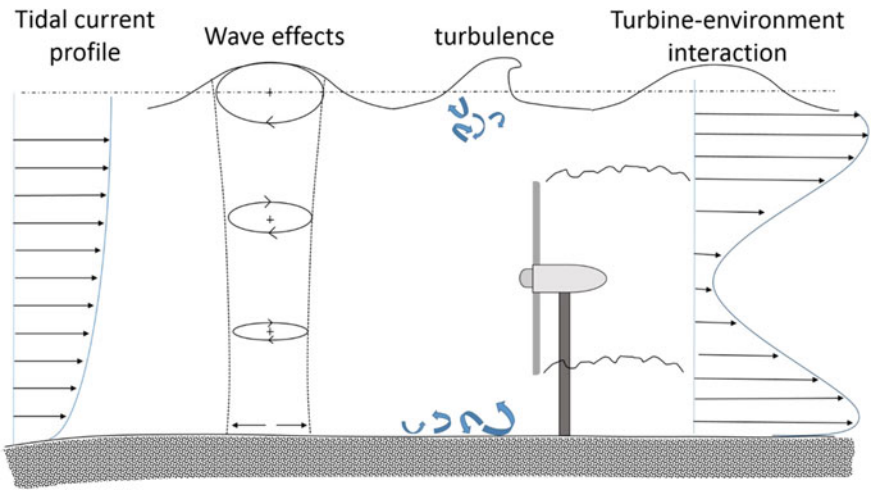

Fig. 4 A diagram of the oceanographic conditions present at a tidal-stream energy site

simplified methods to include wave effects within tidal-stream energy research, but this chapter does not investigate the effect of waves upon tidal-range energy schemes.

Wave Climate Effects to Resource Assessment

Tidal energy convertor devices (e.g., turbines) are likely to be designed to enter a safe mode during extreme wave conditions to reduce the risk of damage. Research is not clear on a safe mode limit because any such wave threshold (i.e., wave height and period) is likely to be dependent on water depth and device characteristics. Nevertheless, practical resource estimates will need to incorporate this shut down limit in their estimation of the resource, and when planning for the distribution of electricity to end-user (e.g., the UK's National Grid).

The presence of waves has been shown to reduce tidal velocities when averaged over a tidal cycle (Wolf and Prandle 1999), and is attributed to the artificial bed roughness (see section "Simplified Methods"). Because power is proportional to the cube of tidal velocity, the presence of waves reduces the power available in the tidal current by 10% per meter of wave height increase—based on an approximate relation proposed by Lewis et al. (2014). However, this relationship is appears to be dependent on water depth and the wave direction (relative to the tidal current) and period, which will vary due to the tide and thus requires a dynamically coupled wave-tide modelling approach, such as COAWST (Coupled Ocean-Atmosphere-Wave-Sediment Transport; Lewis et al. 2014) or TELEMAC-TOMAWAC (Hashemi et al. 2015b). Some simplified approaches for estimating the effect of waves on bottom friction and tidal resources are introduced in section "Simplified Methods". Cou-

pled models that can simulate these processes are discussed in section "Dynamically Coupled Wave-Tide Modeling Systems".

Wave Considerations in the Design of Tidal Turbines

Although this chapter, in general, considers the implications of wave-tide interactions on resource characterization, a brief discussion about devices is provided here. The tools and the concepts for dealing with the effect of waves on tidal devices (or vice versa) are mainly different because of the scale of the processes, and another review is necessary to expand upon this topic in detail. Nevertheless, due to importance and relevance of this topic to this chapter, some previous research are briefly discussed.

The wave climate should be considered when designing and siting tidal-stream energy convertors, because waves are known to modify velocity profile/shear stress, loadings, and fatigue on such tidal energy devices (e.g., Luznik et al. 2013). Surface waves are also known to increase turbulence (Myers and Bahaj 2010; Barltrop et al. 2007), which will affect wake recovery, and thus array configuration design. Furthermore, wave-current interaction may become increasing important in marine renewable energy research if floating tidal-stream energy schemes become viable (Khan et al. 2009; Liu et al. 2011).

Variability of the tidal current in the form of turbulence and shear stress results in cyclic loading to the tidal-stream energy device and support structure that can lead to fatigue and potential failure of the device, it can also effect performance characteristics (Batten et al. 2008; Mason-Jones et al. 2013).

Scaled tank experiments and device scale computer simulations (e.g., Computational Fluid Dynamics (CFD) models) have been used to study the effect of realistic oceanographic conditions on tidal energy convertors (Myers and Bahaj 2010; Afgan et al. 2013; de Jesus Henriques et al. 2016; Bai et al. 2014). CFD methods have been routinely used to simulate the effect of waves on tidal turbines (Tatum et al. 2016; Galloway et al. 2014; Holst et al. 2015). However, the parametrization of oceanographic conditions likely to occur at tidal-stream energy sites, through the use of three-dimensional coupled wave-tide oceanographic models and observations (e.g., Work et al. 2013) is an area of current research. For example, directional misalignment between the wave propagation direction and tidal flow may be present (Lewis et al. 2014), which could affect device performance and resilience (Galloway et al. 2014; Frost et al. 2015). The data used in Fig. 5 are based on hourly averaged data from an RDI 5-beam 600 kHz acoustic Doppler current profiler (ADCP) deployed for a 61 day period (SeptNov 2014) at 53.13° N 4.73° W (a UK tidal-stream energy demonstration zone, see http://www.seacams.co.uk) in 44 m of water where peak spring tidal currents can exceed 2.5 m/s (Lewis et al. 2015). The figure shows the frequent misalignment between wave and tidal current direction at this potential tidal-stream energy site (defined in Fig. 5 as >20° between wave direction and axis of current travel), thereby highlighting the need for further research into the realistic oceanographic conditions at tidal-stream energy sites.

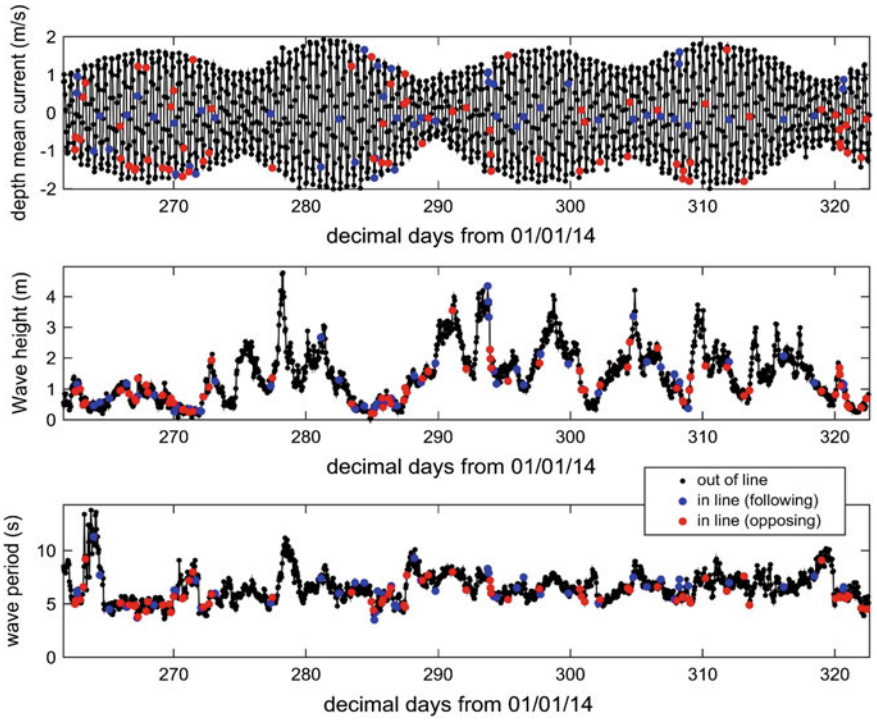

Fig. 5 Observed wave-current misalignment in interaction at a potential tidal-stream energy site in the UK observed with a RDI 5-beam 600 kHz ADCP deployed at 53.13° N 4.73° W

Simplified Methods

As mentioned previously, the interaction of waves with the bottom boundary layer increases the bottom roughness. This effect has been investigated in many studies in the literature (e.g., see Davies et al. 1988; Soulsby et al. 1993; Van Rijn 2007; Soulsby and Clarke 2005); but, research is still in progress in this complex area (Tambroni et al. 2015). Coupled hydrodynamic, wave, and sediment transport models (e.g., Warner et al. 2010), usually incorporate these formulations to compute the increased bottom friction, radiation stress and vortex forces. They also formulate the rate of sediment transport due to combined shear stress induced by waves and currents (e.g., Warner et al. 2010).

A simpler way to estimate this effect is to increase the bed roughness using the wave parameters (Hashemi et al. 2015b). Hydrodynamic models, which are used to simulate the tides, have various options for quantifying bottom friction (Hervouet 2000; Shchepetkin and McWilliams 2005). To approximately account for increased

wave induced roughness, the friction parameters such as the bed roughness length, corresponding to the Nikuradse law of friction, or the bottom drag coefficient, corresponding to quadratic friction law,[1] can be modified using the empirical relations available from the past research. To enhance the bed roughness due to wave-current interaction, Van Rijn (2007) introduced the following relation,

$$k_a = k_s \exp\left(\Gamma \frac{U_w}{u}\right) < 10, \qquad \Gamma = 0.80 + \varphi - 0.3\varphi^2 \tag{4}$$

where k_a and k_s are the apparent and physical roughness, respectively; u is the depth-averaged current velocity (neglecting wave-current interaction) and U_w is near bed wave-induced orbital velocity; φ is the angle between wave direction and current direction in radians. The apparent bed roughness due to waves can be up to an order of magnitude larger than the original physical bed roughness under certain conditions (Van Rijn 2007).

Alternatively, for the drag coefficient, which is more popular in ocean models and is used to compute the bed shear stress, an empirical formulation can be derived based on Soulsby and Clarke (2005) and Soulsby (1997), as follows,

$$\gamma = \frac{C_D^*}{C_D} = \left[1 + 1.2\left(\frac{\lambda}{1+\lambda}\right)^{3.2}\right] < 2.2, \qquad \lambda = \frac{\tau_w}{\tau_c} \tag{5}$$

where C_D is the drag coefficients assuming no waves and C_D^* is the drag coefficients in the presence of waves, averaged over the wave period. τ_c is bed shear stresses due to current alone and τ_w is the bed shear stresses due to waves alone. The current alone shear stress depends on the current velocity and is given by, $\tau_c = \rho C_D u^2$. The wave-induced bed shear stress is a function of the bottom wave orbital velocity (U_w) (Soulsby 1997),

$$\tau_w = \frac{1}{2}\rho f_w U_w^2, \qquad f_w = 0.237\left(\frac{A}{k_s}\right)^{-0.52} \tag{6}$$

where f_w is the wave friction factor, and A is the semi-orbital wave excursion, $A = \frac{U_w T}{2\pi}$. k_s is Nikuradse bed roughness approximately equals to $2.5d50$, and $d50$ is the median grain size at the bottom, if the bed material is sand or gravel. For sites that are on the bedrocks, the physical roughness of the bed rock can be used to determine k_s.

Although wave models, such as SWAN (Simulating WAves Nearshore), can compute wave orbital velocities based on the wave spectrum, simplified equations have been provided in the literature (Soulsby 2006). Wave orbital velocity near the sea bed is a function of the wave height, wave period, and water depth. Based on the linear wave theory, simplified methods for monochromatic waves and irregular (spectral)

[1] Some models use the Chezy coefficient, C_z, which is related to drag coefficients as $C_z = \sqrt{g/C_D}$ (Soulsby 1997).

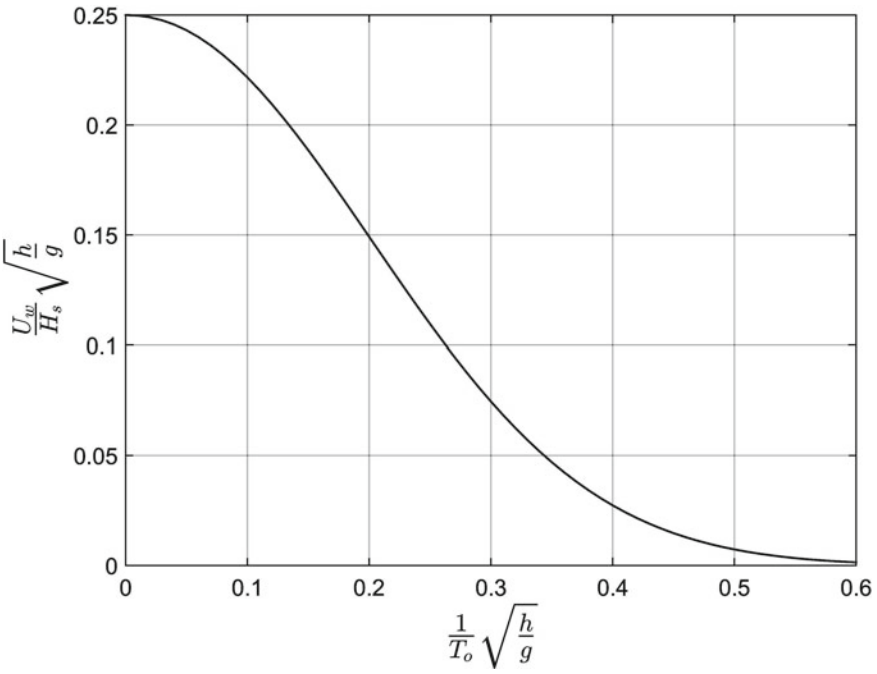

Fig. 6 Relationship of (near bed) wave orbital velocity, significant wave height, water depth, and mean wave period (Soulsby 2006)

waves have been formulated. By considering each wave frequency and its orbital velocity, the room-mean-square wave orbital velocity (U_w) can be approximated as,

$$U_w = \frac{H_s}{4}\sqrt{\frac{g}{h}}\exp\left(-15.16\left\{\frac{1}{T_o}\sqrt{\frac{h}{g}}\right\}^{2.1}\right) \tag{7}$$

where T_o is the mean wave period, and H_s is the significant wave height. The above equation is plotted, using dimensionless variables, in Fig. 6.

Assuming a dominant wave climate for a region, Eq. 5 or Eq. 4 can be used to estimate the effect of waves on the bottom friction, and predict whether the increased bottom friction can significantly reduce the tidal energy resources in a region. The sample graph in Fig. 7 shows the increased drag coefficient assuming various grain roughness, for a current of 1 m/s. In the modeling studies, the enhanced bed roughness or drag coefficient should be implemented in the model domain, for the duration of a simulation. Therefore, depending on the water depth, the stage of tide, and the wave climate of a region, high values of orbital velocities (i.e., >10 cm/s), may occur in the shallow regions of a domain as well as low current values (i.e., <1 m/s) (Wiberg and Sherwood 2008). As a case study, the above method was implemented for Skerries site located at the northwestern headland of Anglesey, UK (Hashemi et al. 2015b). The site has a moderate wave climate. As a result of wave radiation

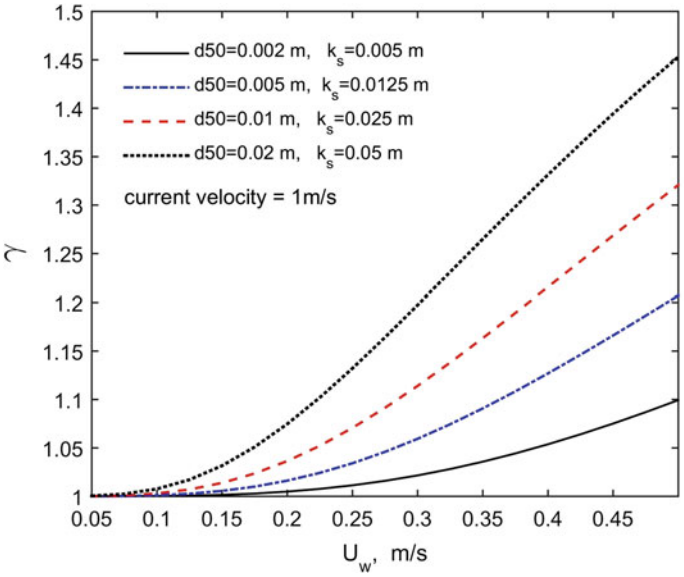

Fig. 7 Enhancement of the drag coefficient due to wave-current interaction for various bottom roughness cases, and assuming a 1 m/s current. U_w is bottom wave orbital velocity and γ is the ratio of drag coefficient in the presence and absence of waves

stresses and enhanced bottom friction, the tidal energy resource was predicted to reduce by up to 20% and 15%, for an extreme and a mean winter wave scenarios, respectively, for this site. Higher effects were predicted for sites exposed to more extreme waves.

Tidal Effects in Wave Energy Projects

As mentioned, strong tides (currents and change in water depth) can affect the wave energy resources of a region, which will be discussed in this section. The implications of tides in the design and the mooring of wave energy converters (WECs) is another topic of interest which is mentioned only briefly, because it is not the focus of this chapter.

Wave Energy Assessment in the Presence of Tides

Wave height and wave group velocity change according to the tides; the former quantifies the magnitude of wave energy, and the latter determines the speed and direction of the wave energy transport. Further, wave properties and processes that control the

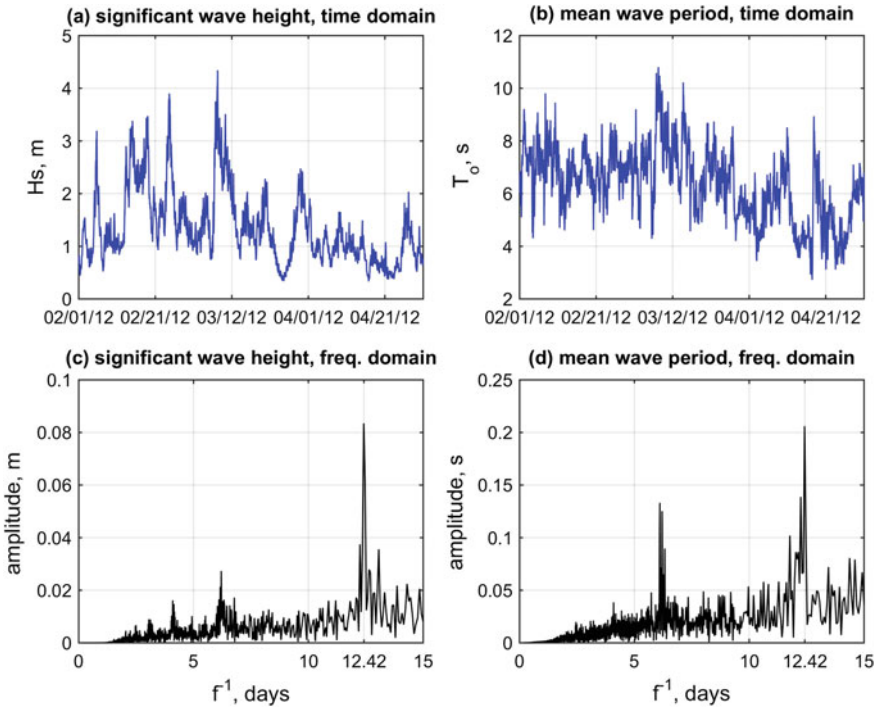

Fig. 8 The modulation of the significant wave height and the mean wave period by tides at a measurement location in Pentland Firth at 58.67° N 3.28° W

propagation of waves such as refraction, breaking, and celerity, in general, are functions of water depth, which is modified by tides. Figure 8 shows how the significant wave height and the mean wave period are modulated by tides at a measurement location in Pentland Firth; by transforming the time series of the significant wave height to the frequency domain, using the fast Fourier transform (FFT; Van Loan 1992; Krauss et al. 1994), the modulation at the frequency of the semidiurnal M2 tide, 12.42 h, and M4 tide at 6.21 h is clearly visible in the signal. Other wave properties such as the wave period, and wave energy are modulated by tides in a similar way.

According to the linear wave theory, the wave energy flux—for a monochromatic wave—averaged over a wave period per unit width of the wave crest is given by (Dalrymple and Dean 1991),

$$P = \left(\frac{1}{8}\rho g H^2\right) C_g = EC_g; \tag{8}$$

where P is the "wave power" or wave energy flux, H is the wave height, C_g is the group velocity, and E is the period-averaged wave energy. For deep water waves which is a good assumption for the majority of wave energy sites (i.e., $kh \geq \pi$), C_g

can be replaced by $gT/(4\pi)$. As mentioned before, one of the important effects of tidal currents on waves is the Doppler shift (Eq. 1), which is the change in the frequency of waves due to ambient currents. Because wave group velocity is $\frac{\partial\omega}{\partial k}$, therefore,

$$C_g^* = C_g + u \;\rightarrow\; EC_g^* = EC_g + uE \tag{9}$$

where C_g^* is the group velocity in the present of ambient currents; EC_g is the wave energy transport by the group velocity, and uE is the wave energy transport by tidal currents. Additionally, when waves propagate in the presence of currents, the wave energy flux is no longer conserved. This is because of the energy exchange between wave and current fields, which is the reason why wave models use the conservation of the wave action (E/σ), rather than wave energy in their formulations (e.g., Booij et al. 2004). In the presence of currents, the total period-averaged energy flux due to waves and currents (or energy transport) is conserved; for monochromatic waves, the conservation of energy can be expressed as follows (e.g., see Longuet-Higgins and Stewart 1960; Whitham 2011; Hashemi et al. 2016),

$$\left[E\,C_g + E\,u\right] + \left\{\frac{1}{2}\rho g h u^3\right\} + \left\{u\left(2\frac{C_g}{C} - \frac{1}{2}\right)E\right\} = \text{cst} \tag{10}$$

where in addition to the terms in Eq. 9, two other terms have been added to the right-hand-side and are interpreted as follows: transport of the kinetic energy of tidal currents, and the work done by the current against the wave radiation stress.

By solving the conservation of the wave action equation and a proper dispersion relation (linear/nonlinear), it is possible to simulate the effect of tidal currents and change in water depth on the wave properties. In wave models such as SWAN, this is usually done by reading the input current and water elevation data or by direct coupling of the wave model and tidal models. Hashemi et al. (2016) presented a simple and quick technique for estimating the effect of opposing or following currents (when waves and tides are aligned with each other) on wave power, using linear wave theory. For linear monochromatic waves, and assuming deep water approximation for the dispersion relation (i.e., $C = g/\omega$), the effect of currents on the wave height can be simply estimated as, (Hashemi et al. 2016)

$$\frac{H^*}{H} = \frac{\sigma}{\omega}\left[\frac{1}{1 + \frac{2u}{C}\frac{\sigma}{\omega}}\right]^{\frac{1}{2}} \tag{11}$$

where H^* is the water depth in presence of currents. This equation shows that opposing currents (i.e., $u < 0$) will increase the wave height. Figure 9 shows how wave height and wave energy flux will change with opposing or following currents based on the cited study. As this figure shows, opposing currents can significantly increase the wave height, and consequently, wave steepness (Fig. 10). This can lead to wave breaking if the wave steepness, kH, approaches 0.6 (Chawla and Kirby 2002). On the other hand, the wave group velocity will decrease by opposing currents. In an

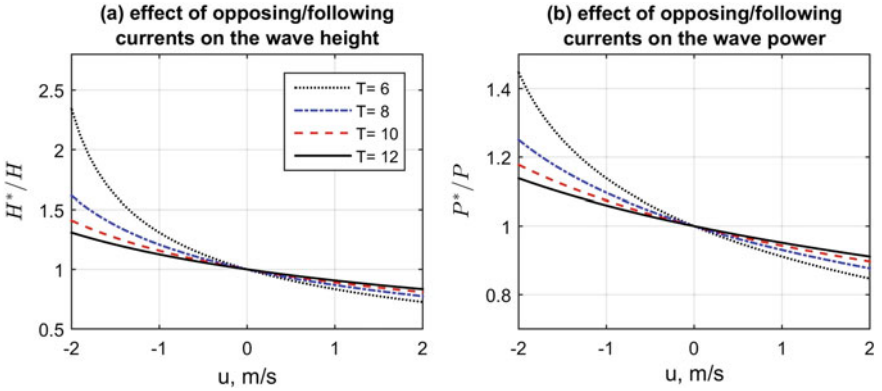

Fig. 9 Effect of currents on wave height and wave power ($EC_g + uE$) when currents and waves are aligned assuming the linear wave theory, and for $kH \ll 0.6$

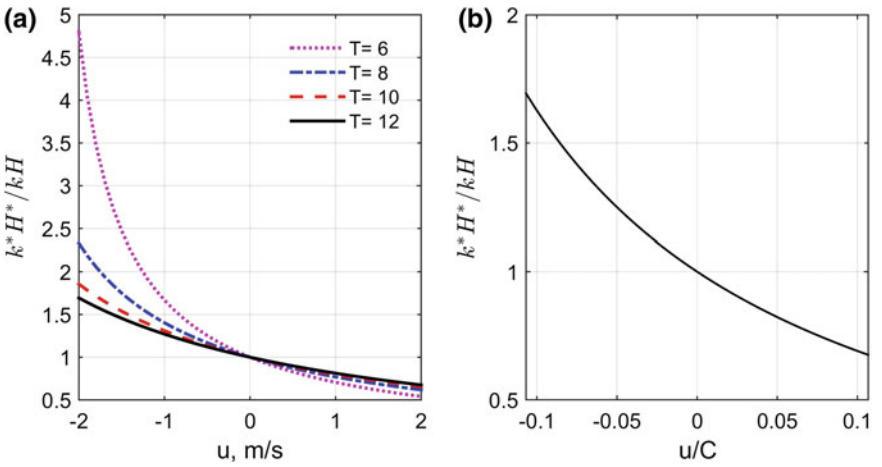

Fig. 10 Effect of opposing/following currents on the wave steepness. **b** shows that if the current velocity is normalized by the wave celerity, all *curves* in (**b**) overlap on *one curve*. The results are valid for $kH \ll 0.6$ where waves have not been broken

extreme case, the transfer of the wave energy can be completely stopped by opposing currents when group velocity approaches zero. The current velocity which can stop the wave energy transfer is estimated by $u = -g/(4\omega)$ (Moreira and Peregrine 2012).

Tidal Effects on Wave Energy Converters

Because WECs are usually moored in relatively shallow waters (compared to offshore structures), tidal currents affect the design and loading of their mooring systems (Johanning et al. 2007). It has been also shown that the performance and energy absorption of WECs can change by tidal depth variations (López et al. 2015; Castellucci et al. 2013). Therefore, the effect of tidal currents/elevations on the mooring and efficiency of a WEC should be assessed, before deploying WECs in regions where tides are significant. This assessment usually is device specific and needs a separate study.

Dynamically Coupled Wave-Tide Modeling Systems

Several suites of free open-source and commercial ocean models offer coupled wave and hydrodynamic modeling, which can be used to include the interactions of waves and tides. In general, these models can be classified into models based on structured and unstructured meshes. Structured models, which are usually based on the finite difference method, need multiple stages of nesting to properly represent a region of interest with a high-resolution grid, while unstructured models, which are based on finite element or finite volume methods, can use a triangular mesh that gradually transitions from low-resolution to high-resolution areas. However, the generation of an unstructured mesh usually needs a considerable time and some skills. Two popular software that are used to generate unstructured triangular meshes are Blue Kenue (free; http://www.nrc-cnrc.gc.ca), and Surface Modeling System (commercial; http://www.aquaveo.com).

The COAWST modeling system has been employed in several studies to assess wave-tide interactions in the context of ocean renewable energy (e.g., Hashemi et al. 2015a; Barbariol et al. 2013; Lewis et al. 2014). COAWST is based on a regular curvilinear grid, and consists of the ocean model ROMS (Regional Ocean Modeling System), the atmospheric model WRF (Weather Research and Forecasting), the wave model SWAN, and the sediment capabilities of the Community Sediment Transport Model. The output data generated by this model is in the Network Common Data Form (NetCDF), which allows for a convenient postprocessing in MATLAB to present wave, tide, and wave-tide interaction parameters (e.g., wave radiation forces). ROMS has been widely applied to a range of scales in shelf sea modelling and renewable energy studies (Neill et al. 2014; Hashemi and Neill 2014; Ramos et al. 2013). The ROMS code is very flexible, and the user is able to compile it for a range of physical and solution algorithms such as momentum equations, pressure gradient, turbulence, open boundary forcing, and wave-current interactions (Warner et al. 2010). TELEMAC is another open access model that is used frequently for tidal energy resource assessment and impact studies (Hashemi et al. 2015b; Robins et al. 2014; Blunden and Bahaj 2006; Burrows et al. 2009; Hashemi et al. 2012). The TELEMAC

modeling system is based on the finite element/volume method. TELEMAC has a spectral wave module TOMAWAC (TELEMAC-based Operational Model Addressing Wave Action Computation) that is coupled with a hydrodynamic module (Villaret et al. 2013; Brown and Davies 2009). Another popular unstructured model is FVCOM (Finite-Volume Community Ocean Model), which in particular, has been used for tidal energy assessment in the Gulf of Maine and Bay of Fundy (Chen et al. 2011; Karsten et al. 2008). FVCOM also has been coupled with SWAN (Qi et al. 2009). A number of commercial models have been also used by the industry, and they can incorporate the interactions of waves and tides. MIKE, developed by the Danish Hydraulic Institute, has been used for resource assessment studies of several sites (e.g., Carr et al. 2016; Kramer and Piggott 2016), and it can simulate some of the wave-current interaction processes (Sabatino et al. 2015). The MIKE model has a user-friendly interface that is attractive especially for commercial purposes.

Limitations, and previous skill assessments of each modeling suite should be considered. Generally, within each model, a user can apply a wide range of simplifications while setting up a model. For instance, a user can choose a uniform (or nonuniform) friction over the entire domain. Two-dimensional (instead of three-dimensional) simulation is another example to simplify a model. These simplifications can lead to unrealistic/inaccurate results. Model resolution is a critical factor that controls the performance of a model for a specific region. Furthermore, many processes have been parameterized in ocean models, and can not be resolved in common resolutions of these models (e.g., turbulence). Therefore, concurrent collection of wave and tide data at a site is essential to validate a coupled model. Simplified analytical methods, can help to interpret the results of these models.

Conclusions

The significance of wave-tide interaction in characterizing the energy resource of marine renewable energy projects is site specific. At a potential wave energy site, where tidal currents are strong, the effect of tides on wave properties such as wave height or wave period can be directly observed by analysis (e.g., FFT) of the measured signals. Unlike tides, waves have a random nature, so many different scenarios of wave-tide interaction can occur: waves can oppose or follow the currents; waves can be inline or oblique to the major axis of tidal currents. Therefore, it is important to understand how wave properties are affected by tides, in order to generalize the resource assessment results. Simplified analytical techniques help to understand these processes, and perform initial estimations. Advanced coupled wave-tide models can incorporate many wave-tide interaction processes; however, due to the scarcity of observational data (i.e., concurrent measurement of tides and waves), validation of wave-tide processes in these models is challenging.

At a potential tidal energy site that has a relatively strong wave climate, tidal currents can be slowed down due to the enhanced bottom roughness and wave forces. During extreme conditions tidal energy devices may go into a shut-down mode to

avoid damage, so the wave climate may have an effect on technical resource assessments. Finally, waves may also play an important role when planning for installation of devices and their maintenance. Therefore, the influence of waves on tidal energy schemes and wave-current interaction may have a significant effect at wave-exposed sites. Although few sites are considered to be wave exposed (such as some UK sites), if marine renewable energy is to make a substantial contribution to meeting carbon emission targets, and to be deployed throughout the world, the challenges associated with waves will need to be understood and overcome.

Acknowledgements M. Lewis wishes to acknowledge the support of the Sêr Cymru National Research Network for Low Carbon, Energy and the Environment (NRN-LCEE) project QUOTIENT, the SEACAMS research project (Sustainable Expansion of the Applied Coastal and Marine Sectors: Grant Number 80366), the Welsh Government, the Higher Education Funding Council for Wales, the Welsh European Funding Office, and the European Regional Development Fund Convergence Programme. Thanks to Simon Neill (Bangor University) and Philippe Gleizon (University of the Highlands and Islands) for providing the wave buoy data at Pentland Firth.

References

ABPmer. (2008). Atlas of UK marine renewable energy resources, Technical report, Department for Business Enterprise & Regulatory Reform.

Afgan, I., McNaughton, J., Rolfo, S., Apsley, D., Stallard, T., & Stansby, P. (2013). Turbulent flow and loading on a tidal stream turbine by LES and RANS. *International Journal of Heat and Fluid Flow*, *43*, 96–108.

Bai, X., Avital, E., Munjiza, A., & Williams, J. (2014). Numerical simulation of a marine current turbine in free surface flow. *Renewable Energy*, *63*, 715–723.

Barbariol, F., Benetazzo, A., Carniel, S., & Sclavo, M. (2013). Improving the assessment of wave energy resources by means of coupled wave-ocean numerical modeling. *Renewable Energy*, *60*, 462–471.

Barltrop, N., Varyani, K., Grant, A., Clelland, D., & Pham, X. (2007). Investigation into wave–current interactions in marine current turbines. *Proceedings of the Institution of Mechanical Engineers, Part A: Journal of Power and Energy*, *221*(2), 233–242.

Batten, W., Bahaj, A., Molland, A., & Chaplin, J. (2008). The prediction of the hydrodynamic performance of marine current turbines. *Renewable energy*, *33*(5), 1085–1096.

Blunden, L. S., & Bahaj, A. S. (2006). Initial evaluation of tidal stream energy resources at Portland Bill, UK. *Renewable Energy*, *31*(2), 121–132.

Booij, N., Haagsma, I., Holthuijsen, L., Kieftenburg, A., Ris, R., Van Der Westhuysen, A., & Zijlema, M. (2004). *SWAN cycle III version 40.41 user manual* (Vol. 115). Delft University of Technology.

Brown, J. M., & Davies, A. G. (2009). Methods for medium-term prediction of the net sediment transport by waves and currents in complex coastal regions. *Continental Shelf Research*, *29*(11), 1502–1514.

Burrows, R., Walkington, I., Yates, N., Hedges, T., Wolf, J., & Holt, J. (2009). The tidal range energy potential of the west coast of the United Kingdom. *Applied Ocean Research*, *31*(4), 229–238.

Carr, D., Gill, L., & McNabola, A. (2016). Development of a high resolution wave climate modelling methodology for offshore, nearshore and onshore locations of interest. *International Journal of Marine Energy*, *16*, 30–40.

Carrère, L., Lyard, F., Cancet, M., Guillot, A., & Roblou, L. (2012). FES2012: A new global tidal model taking advantage of nearly 20 years of altimetry. In *Proceedings of Meeting* (Vol. 20).

Castellucci, V., Waters, R., Eriksson, M., & Leijon, M. (2013). Tidal effect compensation system for point absorbing wave energy converters. *Renewable energy*, *51*, 247–254.

Chawla, A., & Kirby, J. T. (2002). Monochromatic and random wave breaking at blocking points. *Journal of Geophysical Research: Oceans*, *107*(C7).

Chen, C., Huang, H., Beardsley, R. C., Xu, Q., Limeburner, R., Cowles, G. W., et al. (2011). Tidal dynamics in the Gulf of Maine and New England Shelf: An application of FVCOM. *Journal of Geophysical Research: Oceans*, *116*(C12).

Dalrymple, R. A., & Dean, R. G. (1991). *Water wave mechanics for engineers and scientists*. USA: World Scientific.

Davies, A. G., Soulsby, R. L., & King, H. L. (1988). A numerical model of the combined wave and current bottom boundary layer. *Journal of Geophysical Research: Oceans (1978–2012)*, *93*(C1), 491–508.

de Jesus Henriques, T. A., Hedges, T. S., Owen, I., & Poole, R. J. (2016). The influence of blade pitch angle on the performance of a model horizontal axis tidal stream turbine operating under wave–current interaction. *Energy*, *102*, 166–175.

Dee, D., Uppala, S., Simmons, A., Berrisford, P., Poli, P., Kobayashi, S., et al. (2011). The ERA-Interim reanalysis: Configuration and performance of the data assimilation system. *Quarterly Journal of the Royal Meteorological Society*, *137*(656), 553–597.

Draper, S., Adcock, T. A., Borthwick, A. G., & Houlsby, G. T. (2014). Estimate of the tidal stream power resource of the pentland firth. *Renewable Energy*, *63*, 650–657.

Frost, C., Morris, C. E., Mason-Jones, A., O'Doherty, D. M., & O'Doherty, T. (2015). The effect of tidal flow directionality on tidal turbine performance characteristics. *Renewable Energy*, *78*, 609–620.

Galloway, P. W., Myers, L. E., & Bahaj, A. S. (2014). Quantifying wave and yaw effects on a scale tidal stream turbine. *Renewable energy*, *63*, 297–307.

Gaurier, B., Davies, P., Deuff, A., & Germain, G. (2013). Flume tank characterization of marine current turbine blade behaviour under current and wave loading. *Renewable Energy*, *59*, 1–12.

Gleizon, P., & Woolf, D. (2013). Wave energy assessment in Scottish Seas. IN *Proceedings of the 10th European Wave and Tidal Energy Conferences, Aalborg, Denmark*.

Gonzalez-Santamaria, R., Zou, Q.-P., & Pan, S. (2015). Impacts of a wave farm on waves, currents and coastal morphology in South West England. *Estuaries and Coasts*, *38*(1), 159–172.

González-Santamaría, R., Zou, Q., Pan, S., & Padilla-Hernandez, R. (2010). Modelling wave-tide interactions at a wave farm in the southwest of England. *Coastal Engineering*, *2*.

Guillou, N., Chapalain, G., & Neill, S. P. (2016). The influence of waves on the tidal kinetic energy resource at a tidal stream energy site. *Applied Energy*, *180*, 402–415.

Hashemi, M. R., & Neill, S. P. (2014). The role of tides in shelf-scale simulations of the wave energy resource. *Renewable Energy*, *69*, 300–310.

Hashemi, M. R., Grilli, S. T., & Neill, S. P. (2016). A simplified method to estimate tidal current effects on the ocean wave power resource. *Renewable Energy*, *96*, 257–269.

Hashemi, M. R., Neill, S. P., & Davies, A. G. (2015a). A coupled tide-wave model for the NW European shelf seas. *Geophysical & Astrophysical Fluid Dynamics*, *109*(3), 234–253.

Hashemi, M. R., Neill, S. P., Robins, P. E., Davies, A. G., & Lewis, M. J. (2015b). Effect of waves on the tidal energy resource at a planned tidal stream array. *Renewable Energy*, *75*, 626–639.

Hashemi, M. R., Neill, S. P., & Davies, A. G. (2012). A numerical study of wave and current fields around Ramsey Island—Tidal energy resource assessment. In *XIXth TELEMAC-MASCARET User Conference*. Oxford: United Kingdom.

Hervouet, J.-M. (2000). TELEMAC modelling system: An overview. *Hydrological Processes*, *14*(13), 2209–2210.

Holst, M. A., Dahlhaug, O. G., & Faudot, C. (2015). Cfd analysis of wave-induced loads on tidal turbine blades. *IEEE Journal of Oceanic Engineering*, *40*(3), 506–521.

Johanning, L., Smith, G. H., & Wolfram, J. (2007). Measurements of static and dynamic mooring line damping and their importance for floating wec devices. *Ocean Engineering*, *34*(14), 1918–1934.

Karsten, R. H., McMillan, J., Lickley, M., & Haynes, R. (2008). Assessment of tidal current energy in the Minas Passage, Bay of Fundy. *Proceedings of the Institution of Mechanical Engineers, Part A: Journal of Power and Energy*, *222*(5), 493–507.

Khan, M., Bhuyan, G., Iqbal, M., & Quaicoe, J. (2009). Hydrokinetic energy conversion systems and assessment of horizontal and vertical axis turbines for river and tidal applications: A technology status review. *Applied Energy*, *86*(10), 1823–1835.

Kramer, S. C., & Piggott, M. D. (2016). A correction to the enhanced bottom drag parameterisation of tidal turbines. *Renewable Energy*, *92*, 385–396.

Krauss, T. P., Shure, L., & Little, J. N. (1994). *Signal processing toolbox for use with MATLAB*.

Lewis, M., Neill, S., Robins, P., & Hashemi, M. (2015). Resource assessment for future generations of tidal-stream energy arrays. *Energy*, *83*, 403–415.

Lewis, M., Neill, S., Hashemi, M., & Reza, M. (2014). Realistic wave conditions and their influence on quantifying the tidal stream energy resource. *Applied Energy*, *136*, 495–508.

Liu, H.-W., Ma, S., Li, W., Gu, H.-G., Lin, Y.-G., & Sun, X.-J. (2011). A review on the development of tidal current energy in China. *Renewable and Sustainable Energy Reviews*, *15*(2), 1141–1146.

Longuet-Higgins, M. S., & Stewart, R. (1960). Changes in the form of short gravity waves on long waves and tidal currents. *Journal of Fluid Mechanics*, *8*(04), 565–583.

López, I., Pereiras, B., Castro, F., & Iglesias, G. (2015). Performance of owc wave energy converters: Influence of turbine damping and tidal variability. *International Journal of Energy Research*, *39*(4), 472–483.

Luznik, L., Flack, K. A., Lust, E. E., & Taylor, K. (2013). The effect of surface waves on the performance characteristics of a model tidal turbine. *Renewable energy*, *58*, 108–114.

Marks, K., & Smith, W. (2006). An evaluation of publicly available global bathymetry grids. *Marine Geophysical Researches*, *27*(1), 19–34.

Mason-Jones, A., O'Doherty, D. M., Morris, C. E., & O'Doherty, T. (2013). Influence of a velocity profile & support structure on tidal stream turbine performance. *Renewable Energy*, *52*, 23–30.

Moreira, R., & Peregrine, D. (2012). Nonlinear interactions between deep-water waves and currents. *Journal of Fluid Mechanics*, *691*, 1–25.

Mueller, M., & Wallace, R. (2008). Enabling science and technology for marine renewable energy. *Energy Policy*, *36*(12), 4376–4382.

Myers, L., & Bahaj, A. (2010). Experimental analysis of the flow field around horizontal axis tidal turbines by use of scale mesh disk rotor simulators. *Ocean Engineering*, *37*(2), 218–227.

Neill, S. P., Hashemi, M. R., & Lewis, M. J. (2014). The role of tidal asymmetry in characterizing the tidal energy resource of Orkney. *Renewable Energy*, *68*, 337–350.

Neill, S. P., Litt, E. J., Couch, S. J., & Davies, A. G. (2009). The impact of tidal stream turbines on large-scale sediment dynamics. *Renewable Energy*, *34*(12), 2803–2812.

Neill, S. P., Lewis, M. J., Hashemi, M. R., Slater, E., Lawrence, J., & Spall, S. A. (2014). Inter-annual and inter-seasonal variability of the orkney wave power resource. *Applied Energy*, *132*, 339–348.

O'Connor, M., Lewis, T., & Dalton, G. (2013). Weather window analysis of irish west coast wave data with relevance to operations & maintenance of marine renewables. *Renewable energy*, *52*, 57–66.

Osorio, A., Ortega, S., & Arango-Aramburo, S. (2016). Assessment of the marine power potential in colombia. *Renewable and Sustainable Energy Reviews*, *53*, 966–977.

Pugh, D. T. (1996). *Tides, surges and mean sea-level (reprinted with corrections)*. UK: Wiley.

Qi, J., Chen, C., Beardsley, R. C., Perrie, W., Cowles, G. W., & Lai, Z. (2009). An unstructured-grid finite-volume surface wave model (FVCOM-SWAVE): Implementation, validations and applications. *Ocean Modelling*, *28*(1), 153–166.

Ramos, V., Carballo, R., Álvarez, M., Sánchez, M., & Iglesias, G. (2013). Assessment of the impacts of tidal stream energy through high-resolution numerical modeling. *Energy*, *61*, 541–554.

Robins, P. E., Neill, S. P., & Lewis, M. J. (2014). Impact of tidal-stream arrays in relation to the natural variability of sedimentary processes. *Renewable Energy*, *72*, 311–321.

Robins, P. E., Neill, S. P., Lewis, M. J., & Ward, S. L. (2015). Characterising the spatial and temporal variability of the tidal-stream energy resource over the Northwest European shelf seas. *Applied Energy*, *147*, 510–522.

Rourke, F. O., Boyle, F., & Reynolds, A. (2010). Marine current energy devices: Current status and possible future applications in Ireland. *Renewable and Sustainable Energy Reviews*, *14*(3), 1026–1036.

Sabatino, A. D., McCaig, C., Murray, R. O., & Heath, M. R. (2015). Modelling wave-current interactions off the east coast of scotland. *Ocean Science Discussions*, *12*, 3099–3142.

Saruwatari, A., Ingram, D. M., & Cradden, L. (2013). Wave-current interaction effects on marine energy converters. *Ocean Engineering*, *73*, 106–118.

Shchepetkin, A. F., & McWilliams, J. C. (2005). The regional oceanic modeling system (ROMS): A split-explicit, free-surface, topography-following-coordinate oceanic model. *Ocean Modelling*, *9*(4), 347–404.

Smith, H. C., Haverson, D., & Smith, G. H. (2013). A wave energy resource assessment case study: Review, analysis and lessons learnt. *Renewable energy*, *60*, 510–521.

Soulsby, R. L., Hamm, L., Klopman, G., Myrhaug, D., Simons, R. R., & Thomas, G. P. (1993). Wave-current interaction within and outside the bottom boundary layer. *Coastal Engineering*, *21*(1), 41–69.

Soulsby, R. (1997). *Dynamics of marine sands: A manual for practical applications*. UK: Thomas Telford.

Soulsby, R. (2006). *Simplified calculation of wave orbital velocities*.

Soulsby, R., & Clarke, S. (2005) Bed shear-stresses under combined waves and currents on smooth and rough beds. HR Wallingford, Report TR137.

Tambroni, N., Blondeaux, P., & Vittori, G. (2015). A simple model of wave-current interaction. *Journal of Fluid Mechanics*, *775*, 328–348.

Tatum, S., Allmark, M., Frost, C., O'Doherty, D., Mason-Jones, A., & O'Doherty, T. (2016). Cfd modelling of a tidal stream turbine subjected to profiled flow and surface gravity waves. *International Journal of Marine Energy*.

Van Loan, C. (1992). *Computational frameworks for the fast Fourier transform* (Vol. 10). USA: SIAM.

Van Rijn, L. C. (2007). Unified view of sediment transport by currents and waves. i: Initiation of motion, bed roughness, and bed-load transport. *Journal of Hydraulic Engineering*, *133*(6), 649–667.

Venugopal, V., & Nemalidinne, R. (2014). Marine energy resource assessment for orkney and pentland waters with a coupled wave and tidal flow model. In *ASME 2014 33rd International Conference on Ocean, Offshore and Arctic Engineering* (pp. 09–090100909010). American Society of Mechanical Engineers

Villaret, C., Hervouet, J.-M., Kopmann, R., Merkel, U., & Davies, A. G. (2013). Morphodynamic modeling using the Telemac finite-element system. *Computers & Geosciences*, *53*, 105–113.

Warner, J. C., Armstrong, B., He, R., & Zambon, J. B. (2010). Development of a coupled ocean-atmosphere-wave-sediment transport (COAWST) modeling system. *Ocean Modelling*, *35*(3), 230–244.

Whitham, G. B. (2011). *Linear and nonlinear waves* (Vol. 42). USA: Wiley.

Wiberg, P. L., & Sherwood, C. R. (2008). Calculating wave-generated bottom orbital velocities from surface-wave parameters. *Computers & Geosciences*, *34*(10), 1243–1262.

Wolf, J., & Prandle, D. (1999). Some observations of wave-current interaction. *Coastal Engineering*, *37*(3), 471–485.

Work, P. A., Haas, K. A., Defne, Z., & Gay, T. (2013). Tidal stream energy site assessment via three-dimensional model and measurements. *Applied Energy*, *102*, 510–519.

Use of Global Satellite Altimeter and Drifter Data for Ocean Current Resource Characterization

Ruo-Shan Tseng, Yu-Chia Chang and Peter C. Chu

Introduction

Interest in renewable and green energy around the world is burgeoning, especially in countries that have very limited natural resources. Concerns about the depletion of fossil fuel sources, environmental pollution, and climate change are primary motivations in the quest for affordable energy alternatives that have less of a negative impact on the ecosystem than the conventional fossil fuel power plants. The Intergovernmental Panel on Climate Change has identified six alternative energy sources that have promising global potential: bioenergy, direct solar energy, geothermal energy, hydropower, wind energy, and ocean energy (Edenhofer and Kalkuhl 2011). Ocean energy involves a variety of technologies used to extract energy from sources such as waves, tidal streams, ocean currents, ocean thermal energy conversion, and salinity gradients. Although still in the early stages of development, ocean current energy can provide reliable and predictable power and base load supply. This chapter is focused on the characterization of ocean current power generation in the global oceans, particularly in the Pacific Ocean.

Ocean current energy usually refers to the kinetic energy contained in large-scale, open-ocean, near-surface currents. These ocean currents are generally persistent, sustainable, much faster than background ocean currents and exhibit the strongest flows near the ocean surface. Using ocean currents to drive turbines and

R.-S. Tseng (✉)
Department of Oceanography, National Sun Yat-sen University, Kaohsiung, Taiwan
e-mail: rstseng@mail.nsysu.edu.tw

Y.-C. Chang
Department of Marine Biotechnology and Resources, National Sun Yat-sen University, Kaohsiung, Taiwan

P.C. Chu
Department of Oceanography, Naval Postgraduate School, Monterey, USA

Z. Yang and A. Copping (eds.), *Marine Renewable Energy*,
DOI 10.1007/978-3-319-53536-4_7

generate electricity has been studied over the past several decades (Lissaman 1979; Hanson et al. 2010; Duerr and Dhanak 2012; Yang et al. 2014). VanZwieten et al. (2013) provide an initial assessment of kinetic energy flux in the worldwide ocean current systems based on three years (2009–2011) of HYbrid Coordinate Ocean Model (HYCOM) data. Eight regions with time-averaged power densities of at least 500 W/m^2 were compared and discussed along with other factors such as the variability of power density, distances from land, and areas of sea surface with selected average power densities. VanZwieten et al. (2014) further expanded the analysis based on a longer time series of HYCOM data and included current direction variability. Studies to characterize region-specific ocean current resources have been performed for some western boundary currents of the Pacific and Atlantic oceans, especially in the Florida Current of the Gulf Stream system in the USA (Duerr and Dhanak 2012; Yang et al. 2014, 2015a), the Kuroshio Current near Taiwan and Japan (Chen 2010; Chang et al. 2015), and the Agulhas Current off the coast of South Africa (Bryden et al. 2005; Lutjeharms 2006). Duerr and Dhanak (2012) estimate that approximately 25 GW of hydrokinetic power is available in the Florida Current, while Yang et al. (2014) have shown that the average power dissipated ranges between 4 and 6 GW, when considering extraction over a region composed of the Florida Current portion of the Gulf Stream system.

Previous studies that assessed the energy production potential of ocean currents were mostly based on available ocean model data such as the HYCOM, Navy Coastal Ocean Model (NCOM), Regional Ocean Modeling System (ROMS), and in situ-measured data such as those derived from moored Acoustic Doppler Current Profilers (ADCPs). The output data from the archived Global HYCOM normally have a temporal resolution of 1 day and a spatial resolution of 1–7 km, which is insufficient for the prediction of the core location and temporal variability of strong currents. Comparison of HYCOM with in situ ADCP data in two regions, the Florida Strait and the Agulhas Current off the coast of South Africa, indicates that the variability of current speed and the mean current speed was both underpredicted by HYCOM (VanZwieten et al. 2014). This underprediction may result in underestimation of the available power. Despite the lack of exact correlation with measurements, HYCOM still appears to be a useful tool for preliminary identification of areas in which to develop ocean current energy. On the other hand, Chang et al. (2015) employed a different and novel method. They analyzed the historical drifter data set to estimate the mean current and occurrence frequency in $0.25° \times 0.25°$ bins and used this information to select sites for the development of potential ocean current power generation. Due to its accumulated large amount of data over the past several decades and the Lagrangian perspective of flow measurement with drifters drogued at 15 m depth, Chang et al.'s (2015) method provides another interesting view of ocean current characterization. Still another method of observing ocean surface geostrophic current is to use the satellite altimeter. Chang et al. (2013) employed satellite altimeter data for ship navigational use.

Building upon data derived from historical drifters, satellite altimeters, and scatterometers, previous studies have used statistics to determine the flow patterns of global surface currents and mean streamlines (Niiler 2001; Chu 2009;

Maximenko et al. 2009; Lumpkin and Johnson 2013). Knowledge of global surface currents can be used in current power generation, rescue efforts, oil spill response, and ship routing (Ponta and Jacovkis 2008; Davidson et al. 2009; Chang et al. 2013). Strong ocean currents often occur during tropical cyclones or high-wind-speed conditions (Chang et al. 2010, 2012, 2014). A distinct feature of ocean circulation that is driven by surface winds is the so-called intensification of western boundary currents (WBCs). WBCs are formed by the momentum balance of the wind stress, friction, and increase in the Coriolis parameter with latitude. Based on the conservation of mass and potential vorticity, earlier studies (Stommel 1948; Munk 1950) indicated that the WBCs of the subtropical gyre are narrow, strong ocean currents along the western boundaries of the world's major ocean basins. In the WBC regions that have extremely strong flow, such as the Kuroshio Current, ocean currents can potentially provide sufficient, renewable, clean, and possibly cost-effective power.

The purpose of this chapter is to characterize global ocean current resources by analyzing in situ ocean current data from surface drifters and satellite altimeters; provide a complete map of strong currents that have high power densities; and identify possible sites for ocean current power plants in the world's oceans, emphasizing the Pacific Ocean and neighboring marginal seas. The data and analysis method used is described in section "Data and Method". The distribution of the strong ocean currents and their temporal and spatial variations in the global oceans are discussed in section "Strong Ocean Currents and the Seasonal Variation of Current Speeds". The potential sites for ocean current power generation—determined using a criterion that combines several factors, including location and current speed—are given in section "Ocean Current Power Resource", followed by a discussion, summary, and concluding remarks.

Data and Method

In this study, the surface geostrophic currents of 1992–2012, derived from a merged product of ocean Topography Experiment/Poseidon, Jason 1, and European Research Satellite altimeter observations, are used to examine the circulation of the global ocean surface. Produced by the French Archiving, Validation, and Interpolation of Satellite Oceanographic Data (AVISO) project using the mapping method of Ducet et al. (2000), the absolute geostrophic currents can be obtained from the AVISO Web site (http://aviso.altimetry.fr/index.php?id=1271). The optimal interpolation with realistic correlation functions generates a combined map merging measurements from all available altimeter missions (Ducet et al. 2000) to greatly improve the estimation of mesoscale signals. The data are interpolated onto a global grid of 1/3° resolution between 82° S and 82° N and are archived in weekly (7-day) averaged frames. The geostrophic currents are calculated from the absolute dynamic topography (ADT), which consists of a mean dynamic topography and the sea-level anomalies. Rio and Hernandez (2004) have explained in detail the method of estimating the ADT.

The resulting geostrophic currents have been validated by independent drifter data with a root-mean-square difference of about 14 cm/s in the area of the Kuroshio Current (Rio and Hernandez 2004). Readers are referred to Le Traon et al. (2001) and Pascual et al. (2006) for more details on the data analysis method.

Direct velocity measurements in the mixed layer of the ocean are obtained using satellite-tracked Surface Velocity Program (SVP) drifters drogued at a nominal depth of 15 m to reduce the downwind slip. Drifter data are acquired from an enhanced version of the global drifter data set maintained at Atlantic Oceanographic and Meteorological Laboratory, available online at (http://www.aoml.noaa.gov/phod/dac/dacdata.html) (Niiler 2001). Drifter positions are determined every few hours, depending on latitudes, by Doppler ranging with the Argos satellite system. Time series of irregular drifter positions are interpolated to a 6-h interval by Kriging. The estimated accuracy of the velocity measurements in a 10 ms^{-1} wind is 10^{-2} ms^{-1} when the drogue remains attached to the drifter (Niiler et al. 1995). If the drogue is lost, the downwind slip increases to 1–1.5% of the wind speed (Poulain et al. 2009). We only use drogued drifter data collected from 1979 to 2012 in this study.

Data acquired from six high-frequency (HF) radar stations along the east coast of Taiwan over a three-year period (2013–2015) were used to map the sea surface currents and the Kuroshio Current east of Taiwan. These radar stations are operated by the Taiwan Ocean Research Institute. Each station is equipped with a coastal ocean dynamic application radar, long-ranger model, with a practical spatial observation radius of up to 220 km and a horizontal resolution of around 8 km in the radial direction and 2° in azimuth. Detailed analysis of signal processing and noise removal to obtain the sea surface currents can be found in Yang et al. (2015b).

Strong Ocean Currents and the Seasonal Variation of Current Speeds

Maps of the mean absolute geostrophic surface current speeds in the global oceans based on analysis of 21 years of AVISO data averaged in 1/3° × 1/3° bins (Fig. 1) clearly show the subtropical gyre in the Northern Hemisphere associated with the intensification of WBCs. Note that all WBCs feature maximum current speeds in excess of 0.6 ms^{-1} can be clearly identified in each major ocean basin. These WBCs are the South Equatorial Current (SEC), Gulf Stream (GS), North Brazil Current, and Brazil Current of the Atlantic Ocean; the SEC, North Equatorial Counter Current, Kuroshio Current (KC), Mindanao Current (MC), and East Australian Current of the Pacific Ocean; and the Agulhas Current (AC), Mozambique Current, and Antarctic Circumpolar Current of the Indian Ocean. Hsin et al. (2013) used mean shipboard-ADCP (Sb-ADCP)-derived depth-averaged current (0–150 m) between 1991 and 2005 to verify AVISO absolute geostrophic velocity at the region of the KC east of Taiwan. Their results indicated that the mean AVISO

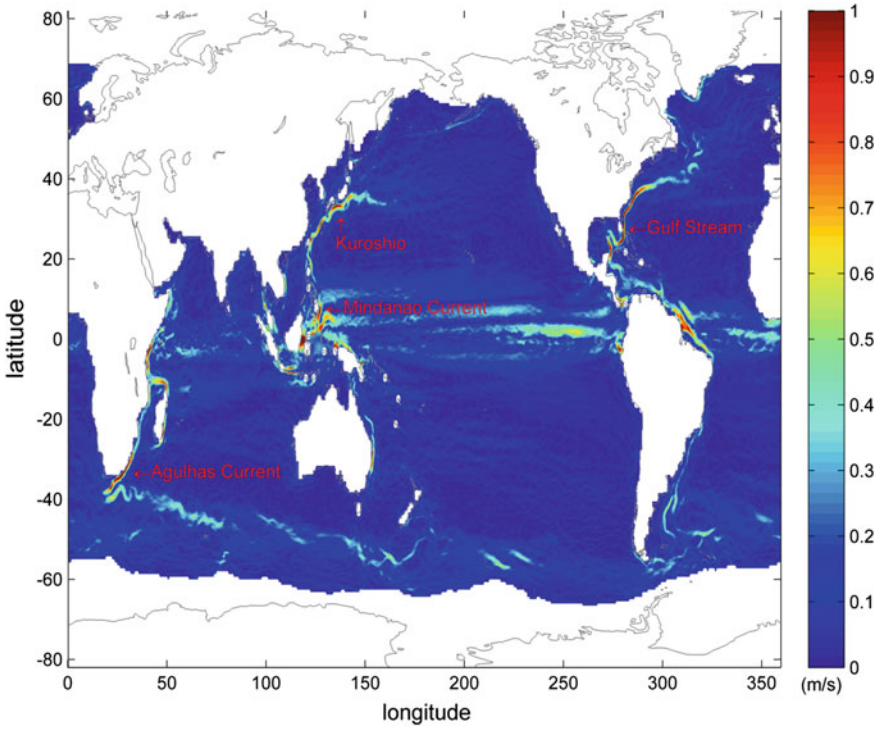

Fig. 1 Averaged near-surface geostrophic current speeds in 1/3° × 1/3° bins of the world oceans from the AVISO satellite altimeter data of 1992–2012

absolute geostrophic velocities are smaller than the mean velocities derived using the Sb-ADCP, but the overall flow pattern of the KC is similar.

Historical SVP drifter data from 1979 to 2012 (34 years) were also processed by the ensemble average method (Centurioni et al. 2004) in 1/3° × 1/3° bins to display the mean near-surface current field of the world oceans, as shown in Fig. 2. The number of independent observations of SVP drifters is shown in Fig. 3. More drifter data can be found in the eastern, western boundaries, and the equatorial waters of the North Pacific Ocean as well as the North Atlantic Ocean. Overall, drifter data about the world oceans are sufficient, which greatly improves the quality of our estimates. A comparison between Figs. 1 and 2 finds mostly similar features, further supporting the well-known results for global upper-ocean circulation as well as the location and speed of the strong flows derived from two independent data sets. Note that the 6-h drifter-measured data can reveal details of small length scale (e.g., small-scale eddy) and short timescale (e.g., tidal current) components of ocean currents, and the weekly averaged altimeter-observed data can yield underestimation of maximum currents and smooth out spatial and temporal variabilities. Also note that the drifter-measured velocity at the 15 m depth might be somewhat different than satellite-measured absolute geostrophic velocity at the sea surface.

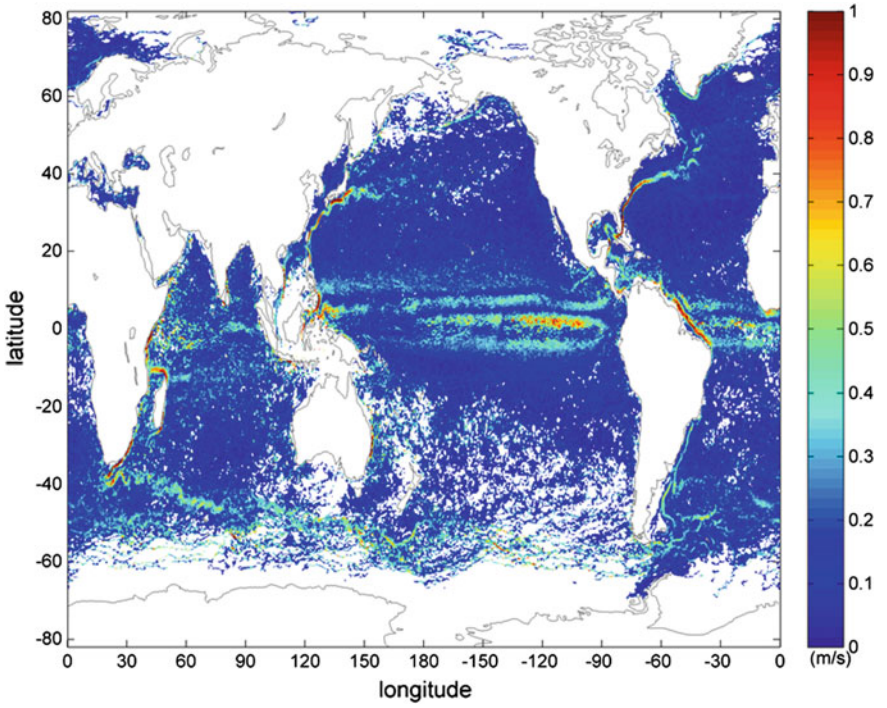

Fig. 2 Averaged near-surface current speeds in 1/3° × 1/3° bins of the world oceans from the global drifter climatology of 1979–2012

A comparison between the drifter-observed current velocities and HF radar-mapped surface current velocities east of Taiwan averaged over three years (2013–2015) was also conducted during this study. Our results (not depicted here) show that the flow patterns of the KC in this region derived from the two data sets are similar. However, the drifter-observed currents are slightly higher than the HF radar-mapped currents.

Among the global ocean currents, the four WBCs that are most prominent have a 21-year mean speed (1992–2012) at a certain grid point (1/3° × 1/3°) greater than 1 ms^{-1}, as can be clearly seen from both satellite altimeter and drifter observations. These four fast currents are the AC (Indian Ocean), GS (Atlantic Ocean), MC (Pacific Ocean), and KC (Pacific Ocean). Figures 4 and 5 show the enlarged plots of these four WBCs derived from satellite altimeter and drifter observations, respectively. The maximum of the mean surface speeds of the AC, GS, MC, and KC based on altimeter data are 1.41, 1.32, 1.12, and 1.01 ms^{-1}, respectively. The locations of maximum speeds for the AC, GS, MC, and KC are near Port Elizabeth in South Africa (26.3° E, 34.5° S), Miami in the USA (79.7° W, 26.9° N), Caraga in the Philippines (126.7° E, 6.6° N), and Higashimuro in Japan (134.7° E, 33.9° N), respectively, as shown in the magenta triangles in Fig. 4. Bryden et al.

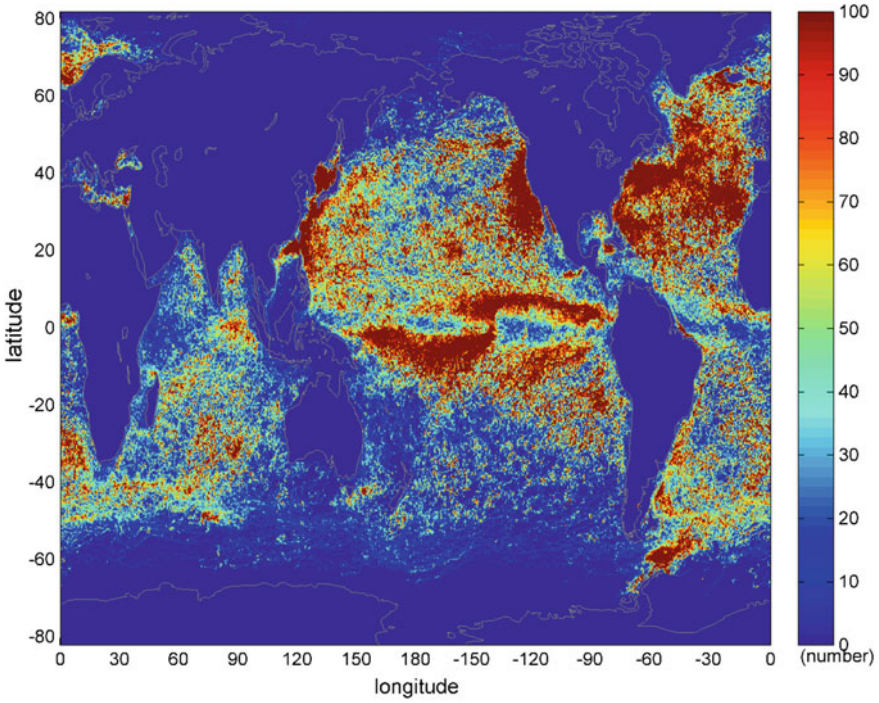

Fig. 3 Numbers of drifter data point in 1/3° × 1/3° bins

(2005) indicated that the transport of the AC is larger than that of either the GS or KC at comparable latitudes (24–32° N and 24–32° S). The net transports of the AC, GS, MC, and KC are estimated to be 70, 30, 33, and 22 Sv (1 Sv = 10^6 m^3 s^{-1}) at 31° S, 27° N, 5.5° N, and 24° N, respectively (Lukas et al. 1991; Stramma and Lutjeharms 1997; Johns et al. 2001; Bryden et al. 2005). The present study shows that the AC, with a maximum of mean surface speed of 1.4 ms^{-1}, is stronger than the GS (1.3 ms^{-1}) and KC (1.0 ms^{-1}), which suggests that the AC is the strongest WBC in the world oceans in terms of maximum current speeds and volume transport.

Monthly averaged surface geostrophic current speeds and the number of data points from satellite altimeter measurements for the AC, GS, KC, and MC at the respective locations of their maximum current speeds are plotted in Fig. 6. Except for the MC, which is at around 5.5° N, the other three WBCs all show clear seasonal variations with higher current speeds occurring in the summer (August for the GS and KC in the Northern Hemisphere and February for the AC in the Southern Hemisphere) and lower speeds occurring in the winter. In terms of mean maximum current speeds, the AC is the strongest WBC, followed by the GS, MC, and KC. Note that the KC and AC have more marked interannual variations, which are represented by the larger error bars in Fig. 6.

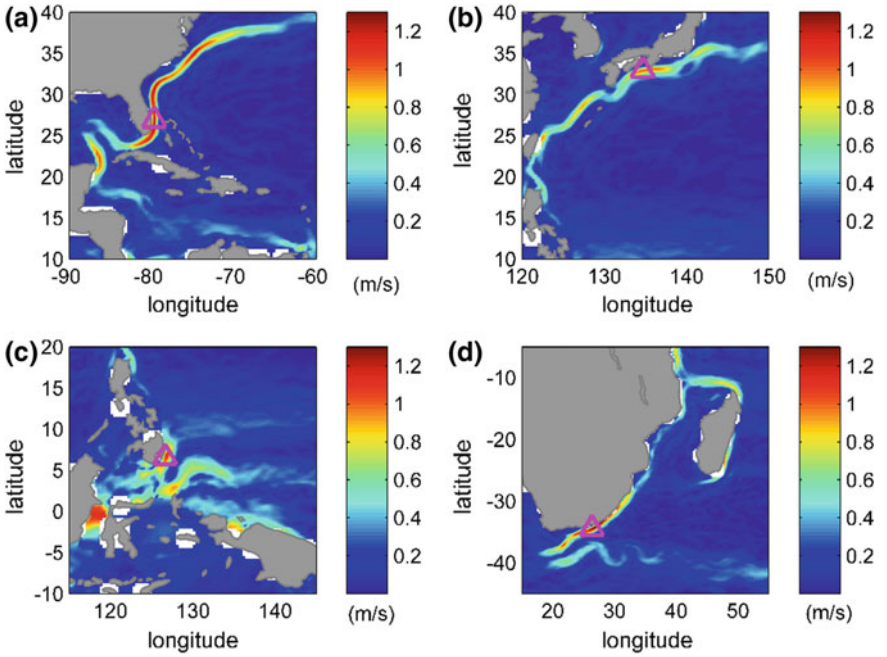

Fig. 4 The four WBCs of the **a** Gulf Stream, **b** Kuroshio Current, **c** Mindanao Current, and **d** Agulhas Current from the AVISO satellite altimeter data. The *magenta triangles* marked in each panel are locations of maximum current speeds and are used in Fig. 6

The mechanisms that cause the variability of the velocity and transport of WBCs have been studied by a number of researchers. For instance, Johns et al. (2001) showed that the instantaneous maximum surface velocities of the KC reach extreme values of 2.0 ms^{-1} and typical values of 1.5 ms^{-1}, based on data derived from a moored current meter array off northeastern Taiwan. On seasonal timescales, Hsin et al. (2013) indicated that the KC off the eastern coast of Taiwan tends to migrate inshore and have a smaller volume transport in winter and to shift offshore and have a larger transport in summer. Results from recent, intensive three-year observations off eastern Taiwan by multiple platforms (Sb-ADCP, Seagliders, SVP drifters, HF radars, and numerical models) reveal new insights into the mean structure and variability of the KC (Yang et al. 2015b). On the interannual timescale, the KC has a weaker volume transport during El Niño years (Kashino et al. 2009; Qiu and Chen 2006).

Ocean Current Power Resource

To curb global warming, many developed countries have devoted large efforts to reducing greenhouse gas emissions and developing devices to harness renewable energy. A 2006 report from the US Department of the Interior indicated that the

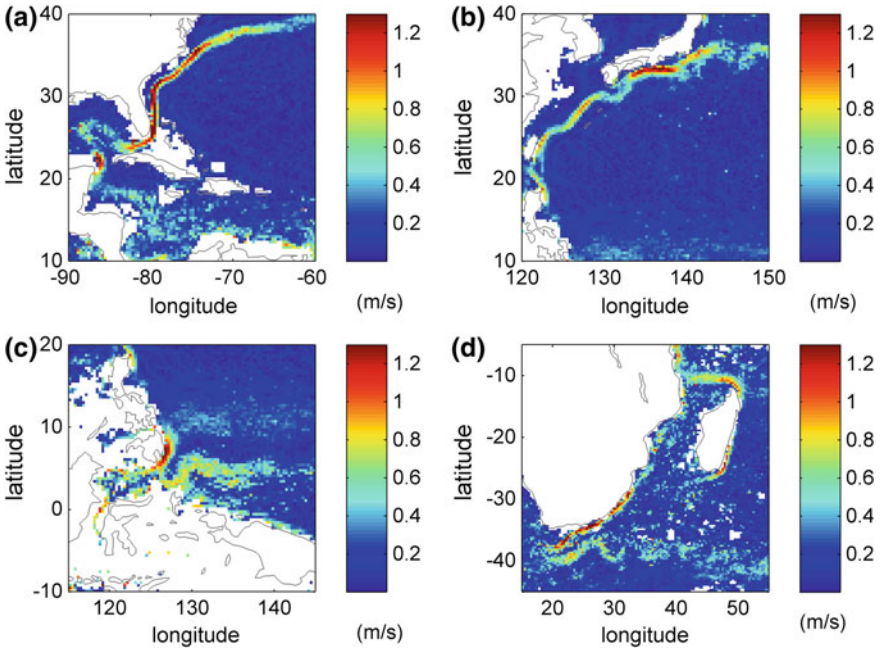

Fig. 5 The four WBCs of the **a** Gulf Stream, **b** Kuroshio Current, **c** Mindanao Current, and **d** Agulhas Current from the drifter climatology. A comparison between Figs. 4 and 5 finds mostly similar features, further supporting the location of the strong flows derived from two independent data sets

total worldwide power contained in ocean currents has been estimated to be about 5,000 GW (http://www.e-renewables.com/documents/Ocean/Ocean%20Current%20Energy%20Potential.pdf). The ocean current power P_o (Wm^{-2}) from a generator is given by (Twidell and Weir 2006; Bahaj 2011):

$$P_o = \frac{1}{2}\rho A U^3 \tag{1}$$

where ρ is the density of seawater (~1023 kg m^{-3}), A is the cross-sectional area of the rotor under consideration, and U is the ocean current speed. Note that actual recoverable energy will be much lower than ocean current power P_o because of turbine and transmission efficiency, backwater effect, etc. Devices that extract power from a fluid's momentum only can realistically reach an efficiency of about 50% (Chang et al. 2015). Figure 7 shows the average marine surface current power in the world oceans including the current speed obtained from satellite observations. The available power density from the four WBCs has values ranging from 500 to 1400 Wm^{-2}. Note that these values are based on mean surface current speed, so they only represent the power level at the surface. The power level throughout the water column will be smaller than these values, considering the typical velocity

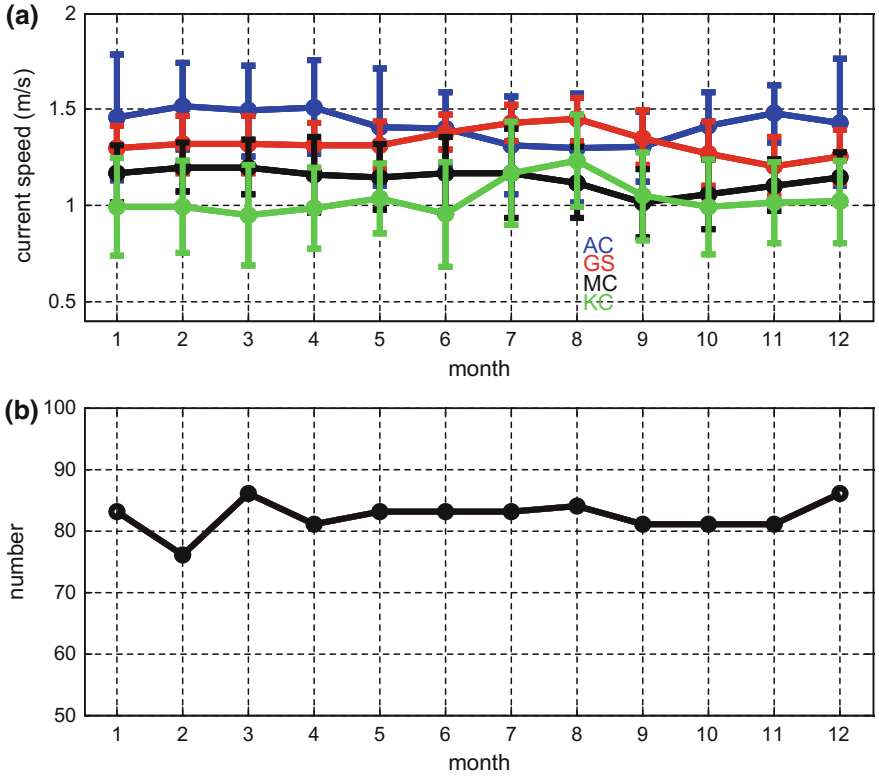

Fig. 6 **a** Monthly mean current speeds of the Agulhas Current, Gulf Stream, Mindanao Current, and Kuroshio Current from altimeter measurements at the locations marked as *magenta triangles* in Fig. 4. The *error bars* represent one standard deviation, and **b** is the monthly number of data points

profiles of decreasing velocities away from the sea surface. The largest current power of 1403 Wm^{-2} is found for the AC, and its core position (magenta triangles) is near Port Elizabeth, South Africa. This provides a global statement from a very limited location. Other estimated current power densities for the GS, MC, and KC are approximately 1124, 681, and, 512 Wm^{-2} near Miami in the USA, Caraga in the Philippines, and Higashimuro in Japan, respectively. VanZwieten et al. (2013) also computed the time-averaged power density for various regions of the world oceans at a depth of 50 m based on three-year HYCOM results. Eight areas that might be minimally eligible for consideration of ocean current turbines' production sites were identified by VanZwieten et al. (2013), and each had a power density greater than 500 Wm^{-2}. Our results are largely consistent with those of VanZwieten et al.'s (2013), but ours show a more detailed distribution of power density in various regions. Note that current speed is not the only factor considered when determining suitable locations for power plants. Other factors, such as the

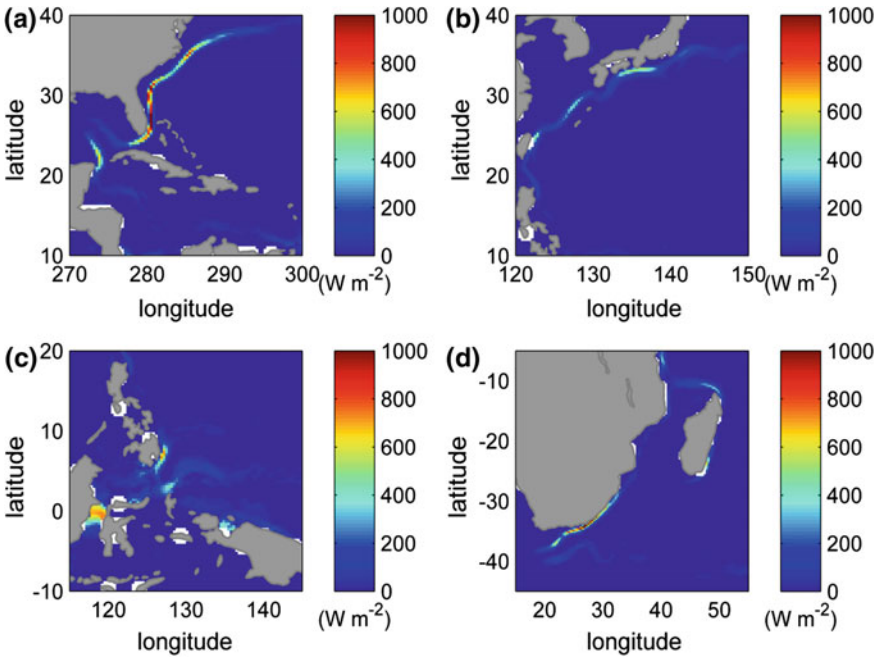

Fig. 7 Average ocean current power (Wm^{-2}) of **a** Gulf Stream, **b** Kuroshio, **c** Mindanao Current, and **d** Agulhas Current from the AVISO satellite altimeter data

water depth, distance from the shore, and stability of currents, should also be considered. For instance, there are two modes of the KC path off southern Japan—the large meander path and the non-large meander path (Kawabe 2005). If turbine generators are to be set up near the coast, the speed of ocean current could become substantially weaker during the large meander path period.

Site Selection for Ocean Current Power Generation

Selection of a potential site for ocean current power generation can be achieved by considering various factors, such as the maximum average power density, distances from land, areas of sea surface with selected average power densities, depth of seafloor, and flow direction variability (VanZwieten et al. 2013, 2014). More recently, Chang et al. (2015) used an index *I*, which is based on four factors (distance to the coast, water depth, mean flow speed, and maximum flow speed), to determine potential sites for ocean current power generation. Using the mean current speed derived from a long, historical drifter data set (1985–2009), Chang et al. (2015) found several suitable sites in the strong ocean currents of the East Asia, i.e., the KC in the northwestern Pacific Ocean south of Japan, east of Taiwan,

and northeast of Luzon; and the coastal jets east of Vietnam in the South China Sea. In this chapter, we use the same index *I*, but a different data set of surface geostrophic currents derived from satellite altimeters, to find some potential sites for ocean current power generation. A comparison between the analyzed results from the two different data sets is made and discussed.

Index *I* is expressed as the summation of four subindices, *Ii*, multiplied by each of their respective weights, *Wi* (Chang et al. 2015), i.e.,

$$I = \sum_{i=1}^{4} W_i I_i, \tag{2}$$

where $I_1 = [1 - (L/50\,\text{km})]$, $I_2 = [1 - (D/1000\,\text{m})]$, $I_3 = P$, and $I_4 = U/1.4$ ms^{-1}. Here, L is the shortest distance to a power station; D is the water depth; P is the percentage of current speed greater than 1 ms^{-1}; and U is the current speed. The choice of constants ($L = 50$ km, $D = 1000$ m, and $U = 1.4$ ms^{-1}) is based on the results of several earlier studies (Finkl and Charlier 2009; Chen 2010; Chang et al. 2015). Each of these indices was weighted to reflect its impact on revenue, capital costs, maintenance costs, etc. According to the financial analysis of the capital cost, operational expenses, and sales income of a 30-MW pilot plant assuming a lifetime of 20 years, percentages of expenditure and income can be estimated to be 31% and 69%, respectively (Chen 2010; Chang et al. 2015). I_1 and I_2 reflect the impact on expenditure, while I_3 and I_4 reflect the impact on revenue. Assuming a 50/50 equivalent weighting, w_1 and w_2 are each set to be 15.5%, and w_3 and w_4 are each set to be 34.5% (Chang et al. 2015). Note that the results of site selection will be very dependent on the choice of the subindices and their respective weights. Some sort of sensitivity test will need to be performed on the chosen values for w_i in future research. In this study, we followed the same approach and analysis of Chang et al. (2015).

The depth (D) and the shortest distance from shore (L) for any point in the world oceans can be calculated from coastline data, which can be downloaded from the National Oceanic and Atmospheric Administration–National Geophysical Data Center Web site. With the available topographic data and the mean surface geostrophic current averaged from 21 years of AVISO data, the index *I* of the global oceans can be computed according to Eq. (2). Variations of the index *I* are shown in Figs. 8 and 9 for East Asia and Southeast Asia and Oceania, respectively. Note that the higher the index value is, the more suitable the site is for ocean current power generation. In East Asia, our results indicate that there are more ocean surface areas near the coast of Japan that have index values greater than 0.3, followed by the regions off the Philippines, Vietnam, Taiwan, South Korea, and China (Fig. 8). Some sites that have particularly high index values, ranging between 0.3 and 0.5, are within the KC south of Japan, the upstream KC northeast of Taiwan, the coastal jet off eastern Vietnam, and the upstream KC and MC off the Philippines.

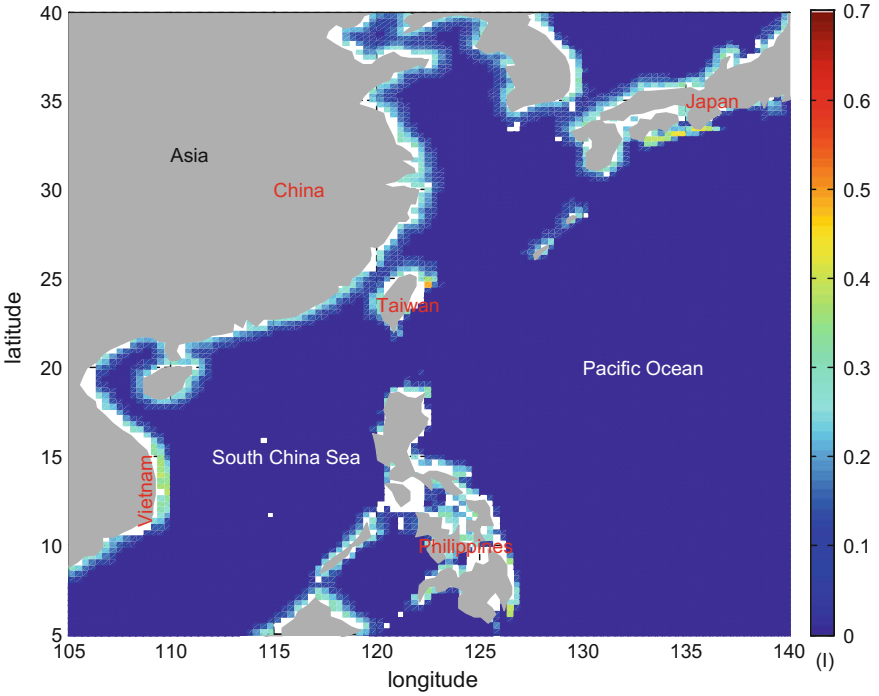

Fig. 8 Enlargement of index *I* and suitable ocean current power generation sites in East Asia

A comparison between the estimated index values, using mean surface currents from historical drifter data (Fig. 10) and using surface geostrophic currents from satellite altimeters (Fig. 8), shows mostly similar results. Figures 8 and 10 both suggest that the most suitable region to develop for ocean current power generation is the shallow coastal water near Japan, Taiwan, Vietnam, and the Philippines. Furthermore, the present results can reveal more detailed features of *I* and its spatial distribution because the AVISO surface geostrophic current data have more comprehensive coverage globally than the drifter data. For example, there are no or very few drifter data available for the coastal waters of the East China Sea and South China Sea. As the conditions of subindices become harsher, the number of sites selected becomes smaller (Fig. 11). Nevertheless, it should be noted that the AVISO weekly data on surface geostrophic currents may underestimate the current speed and thus the power potential. Figure 9 shows that in Southeast Asia and Oceania, more ocean surface areas near the coasts of Indonesia have the largest index values, ranging between 0.3 and 0.65, followed by Malaysia, Papua New Guinea, and Australia.

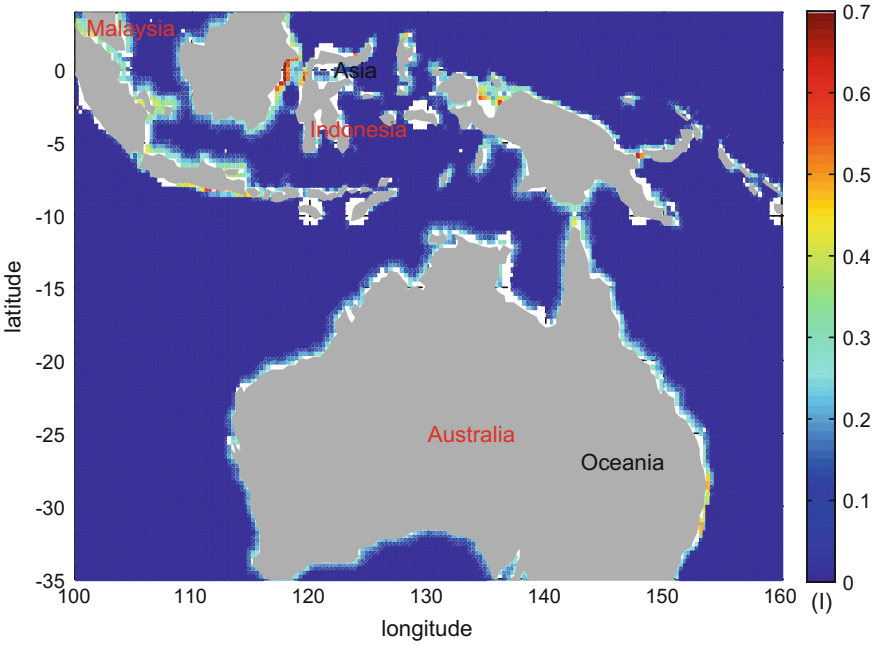

Fig. 9 Enlargement of index *I* and suitable ocean current power generation sites in Southeast Asia and Oceania

Discussion and Conclusions

This study has illustrated flow patterns of strong near-surface currents in the western boundaries of world oceans by analyzing two relatively long data sets of velocity measurements derived from satellite altimeters and SVP drifters. Current speeds in excess of 1.0 ms^{-1} were observed in the four strongest WBCs, and the 21-year averaged velocity maximums were 1.4, 1.3, 1.1, and 1.0 ms^{-1} for the AC, GS, MC, and KC, respectively. The locations of maximum velocities for these four WBCs are near Port Elizabeth in South Africa (26.3° E, 34.5° S), Miami in the USA (79.7° W, 26.9° N), Caraga in the Philippines (126.7° E, 6.6° N), and Higashimuro in Japan (134.7° E, 33.9° N), respectively. Temporal variability of the WBCs is significant at the seasonal timescale, which is influenced by the monsoon winds, and at the interannual timescale, which is connected to the El Niño–Southern Oscillation phenomenon.

The maximum available mean, undisturbed current power from these four WBCs is 1403, 1124, 681, and 512 Wm^{-2}, respectively, for the AC, GS, MC, and KC. Assessment of ocean current energy in previous studies was mostly based on numerical ocean calculation models (HYCOM, NCOM, JPL ROMS, etc.). In this study, the selection of sites for ocean current power generation in the Pacific Ocean and South China Sea is done by calculating the index values in each grid. Doing so

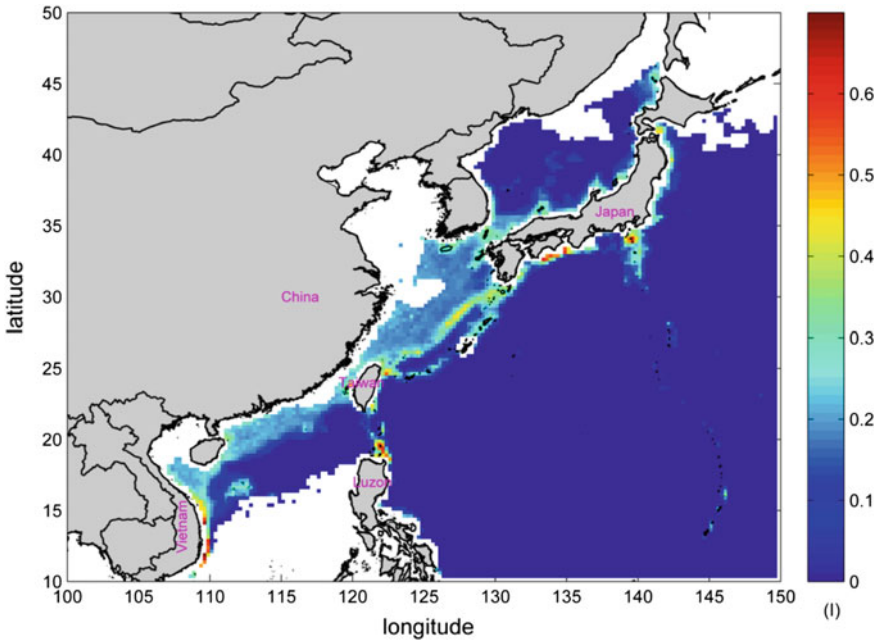

Fig. 10 Distribution of index I in East Asia from drifter-derived mean surface current. *Reproduced from* Chang et al. (2015)

depends on four factors: the frequency with which currents occur, the magnitudes of their speed, the depth at which they occur, and their distance from the shore. In situ near-surface current data from SVP drifters and AVISO satellite altimeters are used. Our results indicate that Japan, Taiwan, Vietnam, the Philippines, Malaysia, Papua New Guinea, and Australia have promising potential for the development of ocean current power generation.

One factor we have ignored in the estimation of maximum available power is the backwater effect, including turbine and transmission efficiencies, losses from supporting structures, and wake interference. This is a practical issue of concern for ocean current power engineering design and has received attention recently (Garrett and Cummins 2007, 2008; Yang et al. 2013). Numerical modeling results from the recent studies indicate that the maximum extractable energy strongly depends on the turbine hub height in the water column, and there is a limit to the available power because too many turbines will merely block the flow. Further investigation is suggested to be pursued along this line.

Further analysis is also required relative to Eq. (2) for the index calculation. "P" and "U" in this equation are two interdependent parameters; a higher value of P will result in a higher value of U. Thus, more justification is needed to choose a best value. Some sort of sensitivity test relative to the values of the weights w_i will be performed in the future.

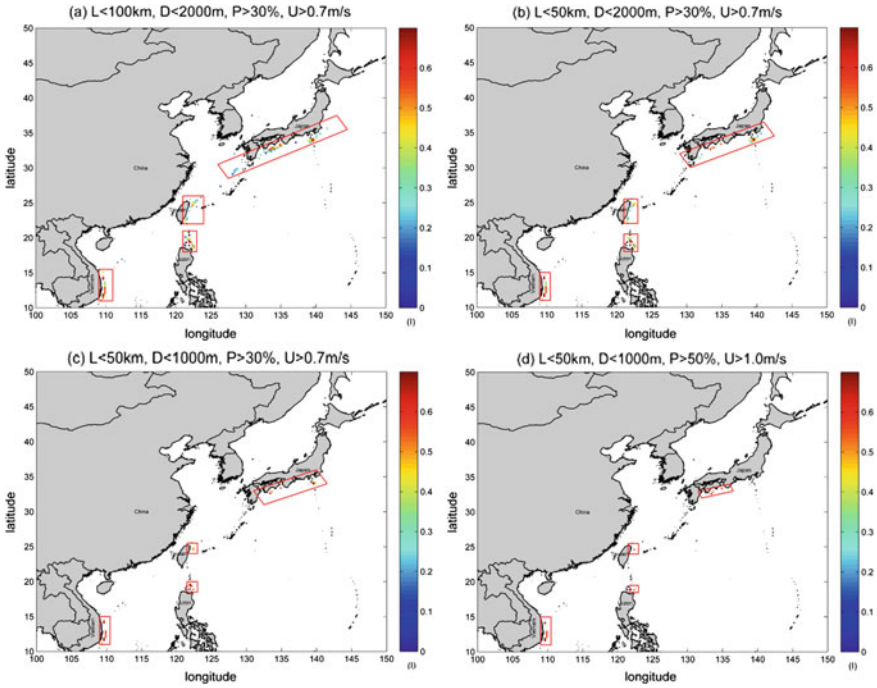

Fig. 11 Selected sites in conditions of **a** L < 100 km, D < 2000 m, P > 30%, and U > 0.7 ms^{-1}; **b** L < 50 km, D < 2000 m, P > 30%, and U > 0.7 ms^{-1}; **c** L < 50 km, D > 1000 m, P > 30%, and U > 0.7 ms^{-1}; and **d** L < 50 km, D < 1000 m, P > 50%, and U > 1.0 ms^{-1}. *Reproduced from* Chang et al. (2015)

Finally, other factors are potentially important and might need to be included in the index determination—factors such as sea state condition (rough vs. calm, this will have a huge impact on the engineering design and installation and maintenance cost), marine environment consideration (whether the sea area is a protected natural reserve), and socioeconomic factors (levelized cost of energy, which also depends on environmental concerns, permitting challenges, and comparisons between the cost of energy for non-renewable sources vs. renewable sources of power and timeline under consideration). These are some important tasks to be completed in the future.

Acknowledgements This research was completed with grants from the Ministry of Science and Technology of Taiwan, the Republic of China (MOST 104-2611-M-10-008). Peter C. Chu was supported by the Naval Oceanographic Office. We are grateful for the comments of anonymous reviewers. We thank Luca Centurioni of Scripps Institution of Oceanography for providing drifterdata.

References

Bahaj, A. S. (2011). Generating electricity from the oceans. *Renewable and Sustainable Energy Reviews, 15,* 3399–3416.

Bryden, H., Beal, L. M., & Duncan, L. M. (2005). Structure and Transport of the Agulhas current and its temporal variability. *Journal of Oceanography, 61,* 479–492.

Centurioni, L. R., Niller, P. P., & Lee, D.-K. (2004). Observations of inflow of Philippine sea surface water into the South China Sea through the Luzon Strait. *Journal of Physical Oceanography, 34,* 113–121.

Chang, Y.-C., Tseng, R.-S., & Centurioni, L. R. (2010). Typhoon-induced strong surface flows in the Taiwan Strait and Pacific. *Journal of Oceanography, 66,* 175–182.

Chang, Y.-C., Chen, G.-Y., Tseng, R.-S., Centurioni, L. R., & Chu, P. C. (2012). Observed near-surface currents under high wind speeds. *Journal Geophysical Research, 117,* C11026. doi:10.1029/2012JC007996.

Chang, Y.-C., Tseng, R.-S., Chen, G.-Y., Chu, P. C., & Shen, Y.-T. (2013). Ship routing utilizing strong ocean currents. *Journal of Navigation, 66,* 825–835.

Chang, Y.-C., Chu, P. C., Tseng, R.-S., & Centurioni, L. R. (2014). Observed near-surface currents under four super typhoons. *Journal of Marine Systems, 139,* 311–319.

Chang, Y.-C., Tseng, R.-S., & Chu, P. C. (2015). Site selection of ocean current power generation from drifter measurements. *Renewable Energy, 80,* 737–745.

Chen, F. (2010). Kuroshio power plant development plan. *Renewable and Sustainable Energy Reviews, 14,* 2655–2668.

Chu, P. C. (2009). Statistical characteristics of the global surface current speeds obtained from satellite altimeter and scatterometer data. *IEEE Journal of Selected Topics in Applied Earth Observations and Remote Sensing, 2*(1), 27–32.

Davidson, F. J. M., Allen, A., Brassington, G. B., Breivik, Ø, Daniel, P., Kamachi, M., et al. (2009). Applications of GODAE ocean current forecasts to search and rescue and ship routing. *Oceanography*, *22 (3)*, 176–181.

Ducet, N., Le Traon, P.-Y., & Reverdin, G. (2000). Global high resolution mapping of ocean circulation from TOPEX/Poseidon and ERS-1 and -2. *Journal Geophysical Research, 105,* 19477–19498.

Duerr, A. E. S., & Dhanak, M. R. (2012). An assessment of the hydrokinetic energy resource of the Florida Current. *IEEE Journal of Oceanic Engineering, 37*(2), 281–293.

Edenhofer, O., & Kalkuhl, M. (2011). When do increasing carbon taxes accelerate global warming? A note on the green paradox. *Energy Policy, 39,* 2208–2212.

Finkl, C. W., & Charlier, R. (2009). Electrical power generation from ocean currents in the Straits of Florida: Some environmental considerations. *Renewable and Sustainable Energy Reviews, 13,* 2597–2604.

Garrett, C., & Cummins, P. (2007). The efficiency of a turbine in a tidal channel. *Journal of Fluid Mechanics, 588,* 243–251.

Garrett, C., & Cummins, P. (2008). Limits to tidal current power. *Renewable Energy, 33,* 2485–2490.

Hanson, H. P., Skemp, S. H., Alsenas, G. M., & Coley, C. E. (2010). Power from the Florida Current a new perspective on an old vision. *Bulletin of the American Meteorological Society, 91,* 861–866.

Hsin, Y.-C., Qiu, B., Chiang, T.-L., & Wu, C.-R. (2013). Seasonal to interannual variations in the intensity and central position of the surface Kuroshio east of Taiwan. *Journal Geophysical Research, 118,* 4305–4316.

Johns, W. E., Lee, T. N., Zhang, D., Zantopp, R., Liu, C.-T., & Yang, Y. (2001). The Kuroshio east of Taiwan: Moored transport observations from WOCE PCM-1 array. *Journal of Physical Oceanography, 31,* 1031–1053.

Kashino, Y., Espana, N., Syamsudin, F., Richards, K. J., Jensen, T., Dutrieux, P., et al. (2009). Observations of the North Equatorial Current, Mindanao Current, and the Kuroshio Current

system during the 2006/07 El Nino and 2007/08 La Nina. *Journal of Oceanography, 65,* 325–333.

Kawabe, M. (2005). Variations of the Kuroshio in the southern region of Japan: Conditions for large meander of the Kuroshio. *Journal of Oceanography, 61,* 529–537.

Le Traon, P.-Y., Dibarboure, G., & Ducet, N. (2001). Use of a high-resolution model to analyze the mapping capabilities of multiple-altimeter missions. *Journal of Atmospheric and Oceanic Technology, 18,* 1277–1288.

Lissaman, P. B. S. (1979). The Coriolis program. *Oceanus, 22,* 23–28.

Lukas, R., Firing, E., Hacker, P., Richardson, P. L., Collins, C. A., Fine, R., et al. (1991). Observations of the Mindanao current during the western equatorial Pacific Ocean circulation study. *Journal Geophysical Research, 96*(C4), 7089–7104.

Lumpkin, R., & Johnson, G. C. (2013). Global ocean surface velocities from drifters: Mean, variance, El Niño-Southern Oscillation response, and seasonal cycle. *Journal of Geophysical Research: Oceans, 118*(6), 2992–3006.

Lutjeharms, J. R. E. (2006). *The Agulhas Current* (1st ed.). Berlin: Springer.

Maximenko, N., Niiler, P., Centurioni, L., Rio, M.-H., Melnichenko, O., Chambers, D., et al. (2009). Mean dynamic topography of the ocean derived from satellite and drifting buoy data using three different techniques. *Journal of Atmospheric and Oceanic Technology, 26*(9), 1910–1919.

Munk, W. H. (1950). On the wind-driven ocean circulation. *Journal of Meteorology, 7,* 79–93.

Niiler, P. P. (2001). The world ocean surface circulation. *International Geophysics, 77*, 193–204. In G. Siedler, J. Church & J. Gould (Eds.), *Ocean circulation and climate: Observing and modeling the global ocean.* San Diego, Calif: Academic Press.

Niiler, P. P., Sybrandy, A. S., Bi, K., Poulain, P. M., & Bitterman, D. (1995). Measurements of the water following capability of holey-sock and TRISTAR drifters. *Deep-Sea Research, 42A,* 1951–1964.

Pascual, A., Faugere, Y., Larnicol, G., & Le Traon, P.-Y. (2006). Improved description of the ocean mesoscale variability by combining four satellite altimeters. *Geophysical Research Letters, 33,* L02611. doi:10.1029/2005GL024633.

Ponta, F. L., & Jacovkis, P. M. (2008). Marine-current power generation by diffuser-augmented floating hydro-turbines. *Renewable Energy, 33*(4), 665–673.

Poulain, P.-M., Gerin, R., Mauri, E., & Pennel, R. (2009). Wind effects on drogued and undrogued drifters in the eastern Mediterranean. *Journal of Atmospheric and Oceanic Technology, 26,* 1144–1156. doi:10.1175/2008JTECHO618.1.

Qiu, B., & Chen, S. (2006). Decadal variability in the large-scale sea surface height field of the South Pacific Ocean: Observations and causes. *Journal of Physical Oceanography, 36*(9), 1751. doi:10.1175/JPO2943.1.

Rio, M.-H., & Hernandez, F. (2004). A mean dynamic topography computed over the world ocean from altimetry, in situ measurements, and a geoid model. *Journal Geophysical Research, 109,* C12032. doi:10.1029/2003JC002226.

Stommel, H. (1948). The westward intensification of wind-driven ocean currents. *Transactions American Geophysical Union, 29,* 202–206.

Stramma, L., & Lutjeharms, J. (1997). The flow field of the subtropical gyre of the South Indian Ocean. *Journal Geophysical Research, 99,* 14053–14070.

Twidell, J., & Weir, A. (2006). *Renewable energy resources*. Taylor and Francis.

VanZwieten Jr., J. H., Duerr, A. E. S., Alsenas, G. M., & Hanson, H. P. (2013). Global ocean current energy assessment: An initial look. In *Proceedings of the 1st Marine Energy Technology Symposium (METS13), April 10–11, Washington D.C.*

VanZwieten, J. H., Meyer, I., & Alsenas, G. M. (2014). Evaluation of HYCOM as a tool for ocean current energy assessment. In *Proceedings of the 2nd Marine Energy Technology Symposium (METS14) April 15–18, 2014, Seattle, WA*.

Yang, X., Haas, K. A., & Fritz, H. M. (2014). Evaluating the potential for energy extraction from turbines in the gulf stream system. *Renewable Energy*, 12–21.

Yang, X., Haas, K. A., Fritz, H. M., French, S. P., Shi, X., Neary, V. S., et al. (2015a). National geodatabase of ocean current power resource in USA. *Renewable and Sustainable Energy Reviews, 44,* 496–507.

Yang, Y. J., Jan, S., Chang, M.-H., Wang, J., Mensah, V., Kuo, T.-H., et al. (2015b). Mean structure and fluctuations of the Kuroshio east of Taiwan from in-situ and remote observations. *Oceanography, 28*(4), 74–83.

Yang, Z., Wang, T., & Copping, A. E. (2013). Modeling tidal stream energy extraction and its effects on transport processes in a tidal channel and bay system using a three-dimensional coastal ocean model. *Renewable Energy, 50,* 605–613.

Mapping the Ocean Current Strength and Persistence in the Agulhas to Inform Marine Energy Development

I. Meyer, L. Braby, M. Krug and B. Backeberg

Introduction

Renewable energy technology has undergone tremendous development over the last three decades and has found great commercial success in the onshore and offshore wind, solar, and biomass spheres. Of the renewable energy technologies, ocean energy technology is the least developed, and due to the vastness of the resource, many facets are yet to be fully understood. Energy in the world's oceans is found in either kinetic (i.e. waves, tides, or currents) or potential (i.e. thermal or salinity gradients) forms, and all forms are being investigated to generate useful electric power.

I. Meyer (✉)
Centre for Renewable and Sustainable Energy Studies,
Stellenbosch University, Stellenbosch, South Africa
e-mail: imke.meyer90@gmail.com; imke@sun.ac.za

M. Krug
Earth Observations, Natural Resources and the Environment,
CSIR, Stellenbosch, South Africa
e-mail: mkrug@csir.co.za

B. Backeberg
Coastal Systems, Natural Resources and the Environment,
Council for Scientific and Industrial Research, Stellenbosch, South Africa
e-mail: bbackeberg@csir.co.za

L. Braby · M. Krug · B. Backeberg
Nansen-Tutu Centre for Marine Environmental Research,
Department of Oceanography, University of Cape Town,
Cape Town, South Africa
e-mail: laurabraby@gmail.com

B. Backeberg
Nansen Environmental and Remote Sensing Center, Bergen, Norway

Z. Yang and A. Copping (eds.), *Marine Renewable Energy*,
DOI 10.1007/978-3-319-53536-4_8

The focus of this study is ocean current energy, the kinetic energy available in large-scale open-ocean geostrophic surface currents, and specifically the Agulhas Current. Western boundary ocean currents have become an area of focus (Duerr and Dhanak 2012; Chang et al. 2015), and the Agulhas Current is of specific interest in the Southern Hemisphere (Meyer et al. 2014; VanZwieten et al. 2014, 2015). Each ocean current has its own features but most western boundary currents have similar characteristics. Western boundary currents are narrow, intense, flow poleward, and are driven by the zonally integrated wind stress curl of the adjacent basins (Lutjeharms 2006).

Western boundary currents generally exhibit their strongest flow near the ocean's surface. In recent years, interest in these currents has evolved closer to commercial development, so the physical characteristics of the currents and their possible impacts on power generation need to be identified and fully understood. Ocean current resource characterisation studies have been performed for the Gulf Stream in the United States (Duerr and Dhanak 2012; Haas et al. 2013) and the Kuroshio Current near Japan and Taiwan (Chen 2010). Studies of the Agulhas Current on the East Coast of South Africa (e.g. Lutjeharms 2006; Beal and Bryden 1999; Bryden et al. 2005) have focused predominantly on understanding open-ocean oceanographic and climate-related processes. Few studies focus on characterising the Agulhas Current for ocean energy extraction technologies; in particular, the ocean current dynamics near the continental shelf region where technology deployment is possible are poorly understood.

Western boundary currents have the potential to be more reliable sources of energy than erratic winds because of their inherent reliability, persistence, and strength. Further, water is approximately 1,000 times denser than air resulting in high energy density in the oceans. Recent investigations by Haas et al. (2013) have shown that the Gulf Stream could potentially have an average power dissipation of 18.6 GW or 163 TWh/yr (serving the electricity needs of approximately 16 million households). According to the Ocean Energy Council, "Ocean currents are one of the largest untapped renewable energy resource on the planet. Preliminary surveys show a global potential of over 450,000 MW, representing a market of more than US$550 billion" (Renewable Energy Caribbean 2014).

The Agulhas Current flows southward along South Africa's East Coast, as a fast and narrow stream, and transports on average 70 million cubic metres of water per second (Bryden et al. 2005). Studies of the northern extent (north of 35ºS) of the current have shown that its course closely follows the narrow continental shelf (Gründlingh 1983), meandering less than 15 km from its mean path, and that the core of the current lies within 31 km from the coast almost 80% of the time (Bryden et al. 2005). The intensity of the current, its close proximity to the coast, and its relative stability make the Agulhas Current one of the more attractive ocean currents in the world to exploit for energy extraction.

However, the stable trajectory of the current is intermittently interrupted by perturbations known as Natal Pulses—large solitary meanders that form at the Natal Bight, a region between 29 and 30°S, and propagate downstream in the Agulhas Current at ±10 km/day (Lutjeharms and Roberts 1988). Fluctuations in the Agulhas

Current path associated with these meanders do not display the same frequency characteristics at all latitudes (Rouault and Penven 2011), because of the dissipation mechanisms of the Natal Pulses as they propagate downstream. Variability in the current and its velocities occurs across of a range of temporal and spatial scales (Lutjeharms 2006), and understanding, monitoring, and predicting these are vital for the effective use of the Agulhas Current as a renewable energy resource.

One of the most effective ways to monitor ocean currents over large spatial areas at a relatively high temporal frequency is through the use of satellite measurements. While ocean currents cannot be directly measured from space at present (Dohan and Maximenko 2010), surface current information can be derived from a range of remotely sensed observations to study and monitor the ocean circulation. At the larger scales (tens of kilometres), geostrophic currents, which occur as a result of pressure and Coriolis forcing, often drive most of the circulation. Wind stress at the ocean's surface also drives transport that can be estimated using the Ekman theory (Ekman 1905). Satellite observations of ocean surface winds and sea surface height (SSH) have therefore widely been used over the last two decades to study and monitor ocean circulation (Robinson 2004). Other remote-sensing observations such as Sea Surface Temperature (SST) and sea surface roughness can also be used routinely and systematically to derive ocean current information. The Agulhas Current is associated with strong signatures in SSH, SST, and sea surface roughness, all of which have been exploited successfully to study the variability of the Agulhas Current as demonstrated by Rouault et al. (2010), Rouault and Penven (2011), and Krug and Tournadre (2012). When used in synergy with the global network of in situ surface drifters, satellites can provide improved global observations of the sea surface velocity.

However, satellite measurements are limited to the surface and for the purpose of marine energy extraction, it is important to have information about the vertical structure of the water column. Measurements of the vertical structure of the ocean are even sparser. To deal with the spatially and temporally incoherent observations of the oceans, we use numerical models combined with observations through a process called data assimilation. Realistic simulations of the Agulhas system are complicated by the highly nonlinear nature of the mesoscale variability governing the Agulhas Current (Biastoch et al. 2008). Even if a model is capable of representing the mean circulation and variability of the region, inaccuracies in the initial state estimate inhibit the forecast skill of the model up to the decadal time scale (Meehl et al. 2009). Data assimilation provides the means to estimate a physically consistent three-dimensional (3D) estimate of the ocean state, combining a dynamical forecast model and observations together with their relative errors. Due to inaccurate numerics and boundary conditions, model solutions are imperfect. By repeatedly assimilating data, models may be constrained to provide a more realistic estimate of the ocean state. Such data-assimilative models of the ocean play a vital role in predicting ocean currents as well as in understanding the 3D structure and its variability.

By combining state-of-the-art satellite remote-sensing observations with data-assimilative (predictive) ocean models, this study aims to identify areas of energetic flow along South Africa's East Coast for the purpose of marine energy

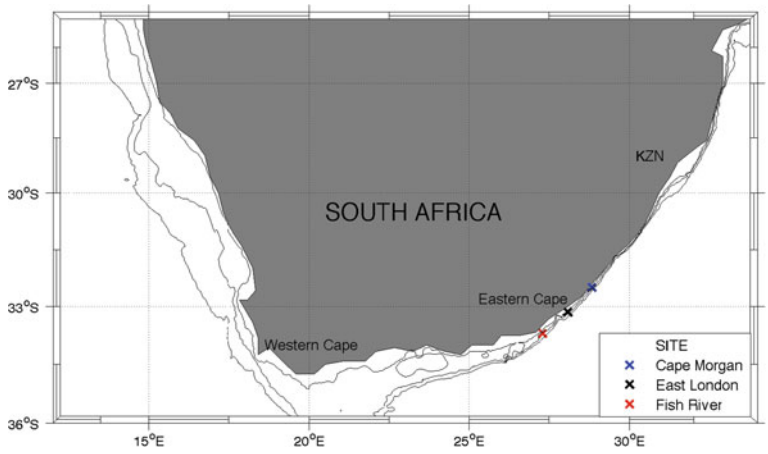

Fig. 1 Position of ADCP deployments with 100, 200, and 500 m isobaths

extraction and to examine the associated current characteristics. The ability and usefulness of the satellite remote-sensing observations and predictive models to monitor and predict current velocities and their variability will be assessed by comparing them with in situ velocity measurements from Acoustic Doppler Current Profilers (ADCPs) for the period from 2009 to 2010. In doing so, the impact of the current behaviour on the potential power production will be quantified, and the present day state-of-the-art tools used to accurately monitor and predict fluctuations in the Agulhas Current that affect power production will be critically examined.

The focus area for the analysis lies between the latitudes of 31 and 34°S as indicated in Fig. 1. The coastal proximity and strength of the Agulhas Current in the southeast Agulhas Current region make it the most suitable region for energy exploitation. Farther south, the Agulhas Current flows too far from the coast to allow for efficient energy recovery. Farther north, the current strength is decreased.

This chapter examines the Agulhas Current characteristics and attempts to quantify how its behaviour will affect potential power production. In the following section, the available data and data types are described, followed by an investigation of current strength and variability, the usefulness of the various data sets, and the implications for possible energy production. The technical, environmental, and social impacts of harnessing energy from the Agulhas Current are also considered.

Data and Methods

The data sets described in the following sections are used to determine the physical characteristics of the Agulhas Current. The sections also address the relative usefulness of each data set towards reducing the barriers of entry into the ocean current energy market.

GlobCurrent Data Set

In this study, we use the combined 15-m-depth GlobCurrent Version 2 product, which is available from the GlobCurrent project (http://www.globcurrent.org/). This data set consists of 13 years of global gridded ocean current fields and is provided at a 0.12° spatial resolution and 3-hour time interval. The combined current in the GlobCurrent data set is computed as the sum of the geostrophic and Ekman components of the flow. In the GlobCurrent product, geostrophic currents are derived from satellite observations of SSH from multiple altimeters, while the Ekman currents (driven by local wind forcing) are estimated using Lagrangian ocean current information collected from surface drifters and Argo floats. A detailed description of the method used to derive the GlobCurrent geostrophic and Ekman ocean currents is provided by Rio et al. (2014).

Confirming the validity of using satellite data to monitor the behaviour of the Agulhas Current is crucial to reducing the costs of monitoring the operations of a potential ocean current plant as well as monitoring upstream events that can affect the potential power output of a plant.

Global Hybrid Coordinate Ocean Model

3D ocean forecast data from a global Hybrid Coordinate Ocean Model (HYCOM) are used in this study. These data are freely available from the HYCOM consortium (hycom.org), a multi-institutional effort sponsored by the National Ocean Partnership Program, as part of the U.S. Global Ocean Data Assimilation Experiment, to develop and evaluate a data-assimilative hybrid isopycnal-sigma-pressure (generalised) coordinate ocean model.

The numerical model is configured for the global ocean, and computations are carried out on a Mercator grid between 78°S and 47°N at 1/12° (± 7 km) resolution. There are 32 vertical layers, and the model's bathymetry is derived from a quality-controlled Naval Research Laboratory Digital Bathymetry Data Base 2-minute resolution data set. Surface forcing data are from the Navy Operational Global Atmospheric Prediction System and include wind stress, wind speed, heat flux (using bulk formula), and precipitation.

The data assimilation scheme used is the Navy Coupled Ocean Data Assimilation system (Cummings 2005), which uses the model forecast as a first guess in a Multi-Variate Optimal Interpolation scheme and assimilates available along-track satellite altimeter observations (obtained via the NAVOCEANO Altimeter Data Fusion Center), satellite and in situ SST as well as available in situ vertical temperature and salinity profiles from Expendable BathyThermographs, ARGO floats, and moored buoys. The surface measurements are projected to the model interior using the Modular Ocean Data Assimilation System (Fox et al. 2002).

On a daily basis, 5-day hindcasts and 5-day forecasts are produced. The raw data are interpolated to 33 fixed horizontal levels, which are 0, 10, 20, 30, 50, 75, 100, 125, 150, 200, 250, 300, 400, 500, 600, 700, 800, 900, 1,000, 1,100, 1,200, 1,300, 1,400, 1,500, 1,750, 2,000, 2,500, 3,000, 3,500, 4,000, 4,500, 5,000, and 5,500 m.

U- and v-component velocities from 1 December, 2009 to 31 January, 2013 were downloaded and subset to 25–35ºE and 27–36ºS. The data were generated by two experiments. The first experiment (expt_90.8) ended on 2 January, 2011, after which expt_90.9 was used. The two experiments are subtly different in that the top layer in expt_90.9 was 1 m thick (as opposed to 3 m in expt_90.8). This difference is not expected to affect our analysis.

The ability to predict the behaviour of the Agulhas Current will be advantageous for the integration of any future power plants into the national power pool. Accurate forecasts at a high temporal resolution will ensure the maximum utilisation of an ocean current power plant.

Acoustic Doppler Current Profilers

Between 2005 and 2010, the South African electricity utility, Eskom, conducted a series of in situ current measurements along the eastern shores of South Africa as part of a preliminary assessment of the Agulhas Current as a source of energy. The in situ ocean currents were measured using moored ADCPs at selected sites along the continental shelf and in water depths ranging from 96 to 60 m. All ADCPs sampled ocean current velocities throughout the water column in 2-m-high vertical bins. Bins from different deployments were concatenated by linking together measurements from the closest bin (nearest bin approach). A summary of this ADCP data is provided in Table 1.

It is observed that the ADCP measurements (Table 1) were taken at the periphery of the current. Rouault and Penven (2011) found that near the location of the East London, the landward edge of the Agulhas Current is generally lies 20 km from the shore and above the 100 m isobath. Note that the dates on which each data set was recorded do not coincide and this can possibly lead to a bias towards one site.

Between 2012 and mid-2013, an additional two ADCPs were deployed at a mid-shelf and offshore location and resulted in an 18-month period of continuous data in the region of 28.8°E and 32.5°S. The details of the captured data are outlined in Table 2. The data were collected using Teledyne RDI ADCPs with a 60-min temporal resolution. Viable data for the mid-shelf location range from 84 to 10 m below the sea surface and for the offshore location, and from 238 to 22 m below the sea surface.

Table 1 Details of in situ ADCP measurements

ADCP site name	Instrument type	Longitude (E)	Latitude (S)	Water depth (m)	Record length	Sampling interval (h)
Cape Morgan CM305	RDI 300	28.83183	32.50733	89	2009/12/05-2010/03/03	1
Cape Morgan CM306	RDI 300	28.83179	32.50725	87	2010/03/03-2010/09/13	1
Fish River FR308	RDI 300	27.29750	33.70335	88	2009/12/04-2010/03/04	1
Fish River FR309	RDI 300	27.29745	33.71332	91	2010/03/04-2010/09/03	1
East London EL314	RDI 300	28.00866	32.15145	82	2009/12/04-2010/03/03	1
East London EL315	RDI 300	28.08651	33.15140	85	2010/03/03-2010/09/13	1

Table 2 Deployment series 2: details of available ADCP data

Location	ADCP type/bin resolution (m)	Distance from shore (km)	Time period	Sounding depth (m)
Mid-shelf	RDI 300/2	14	2012/01/24-2013/06/30	91
Offshore (edge of shelf)	RDI 150/6	18	2012/01/24-2013/06/30	255

Current Strength and Variability

Comparison GlobCurrent, HYCOM, ADCPs

To compare the three ocean velocity products, Principal Component Analysis (PCA) was applied to the ADCP velocity data as well as the GlobCurrent and HYCOM data at the same locations (Cape Morgan, East London, and Fish River) and depths. PCA decomposes data in terms of orthogonal basis functions to find time series and spatial patterns (Wold et al. 1987). The two eigenvectors contain most of the details about the data. They were computed and plotted as 95% confidence interval ellipses in Fig. 2 and represent the two dominant directional modes of the measured current velocities at the three selected locations, indicating the dominant current direction as well as its lateral variation.

Figure 2 provides a good overview of the Agulhas Current time-averaged strength as well as its overall variability. Comparisons between the in situ satellite and numerical model output data sets show distinct differences. From the in situ

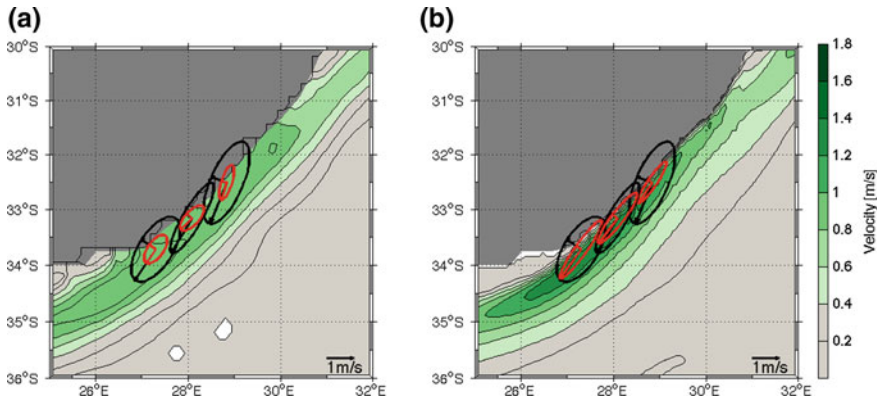

Fig. 2 **a** Map of Agulhas time-averaged currents from the GlobCurrent product with overlaid current ellipses from ADCP data (*black*, at 20 m or in the upper layer best suited for energy production) and GlobCurrent data (*red*, at 15 m depth), and **b** map of Agulhas time-averaged currents from the HYCOM product with overlaid current ellipses from ADCP data (*black*, at 20 m or in the upper layer best suited for energy production) and HYCOM data (*red*, at same depth as ADCPs)

ADCP data, it is seen that the Cape Morgan location is the most energetic and has the strongest major velocity component. This finding is reiterated by the GlobCurrent data but not by the HYCOM data.

Comparing the ADCP and GlobCurrent ellipses (Fig. 2a, black and red, respectively), it is evident that although the direction of flow is similar, there are significant differences between the two data sets at all three locations. The ADCP data indicate a much stronger south-westward flowing velocity component with larger lateral variations compared to the GlobCurrent data.

The HYCOM velocity map (Fig. 2b) indicates that the data-assimilative modelling system is able to produce high mean velocities, and comparing the HYCOM ellipses to the ADCP ellipses suggests that the mean south-westward component is better represented than in GlobCurrent, but the lateral variability seems to be reduced in HYCOM.

In agreement with the current ellipses (Fig. 2a), the major and minor velocity components summarised in Table 3 confirm that the GlobCurrent data underestimate the ADCP measured current velocity by ±60%. While there is a slight improvement in HYCOM, the data-assimilative modelling system still underestimates the measured ADCP velocities (Table 4). It is important to note the differences between satellites remotely sensed, modelled, and in situ observed data because these differences could lead to incorrect site selection and evaluations for energy production. Further, if the HYCOM data set is used as a first step towards identifying energetic regions prior to deploying in situ measurement devices, this data set would lead to incorrect assumptions about the most energetic region. Further, the significant under prediction seen in the GlobCurrent data set can result in termination of further exploration.

Table 3 Details of the time-averaged velocity vector lengths of the GlobCurrent and ADCP measurements

Site name	ADCP data		GlobCurrent	
	Major component (m/s)	Minor component (m/s)	Major component (m/s)	Minor component (m/s)
CM	1.6710	0.6850	0.6815	0.2377
EL	1.5496	0.3959	0.6475	0.2769
FR	1.4216	0.6997	0.6564	0.3251

Table 4 Details of the time-averaged velocity vector lengths of the HYCOM and ADCP measurements

Site name	ADCP data		HYCOM	
	Major component (m/s)	Minor component (m/s)	Major component (m/s)	Minor component (m/s)
CM	1.6710	0.6850	0.9794	0.1918
EL	1.5496	0.3959	1.2333	0.2542
FR	1.4216	0.6997	1.3730	0.2443

The observed underestimation of both GlobCurrent and HYCOM may have to do with the temporal averaging of the data in their generation. The regularly gridded satellite data (GlobCurrent) are produced using optimal interpolation and merging techniques to fill the gaps between spatially sparse satellite ground tracks. This merging process results in the smoothing of the data in both space and time (Ducet et al. 2000) and the underestimation of the ocean current velocities. The underestimation observed in HYCOM may be associated with the combined effect of the model itself underestimating the currents in addition to the assimilation of satellite products into the model.

The impact of spatial and temporal smoothing is examined below, by performing a spectral analysis (Fig. 3), whereby the dominant frequencies of variability in the three data sets are compared. Then, temporal smoothing (daily, weekly, 10-daily, and monthly) is applied to the ADCP data and plotted in a Taylor Diagram (Fig. 4), which is a way to graphically summarise how closely a set of data matches a reference data set (in this case the hourly ADCP data).

A spectral analysis essentially transforms magnitude—time data into variance—frequency space. Figure 3 shows the spectra from the ADCP data (a), GlobCurrent data (b), and HYCOM data (c) for the Cape Morgan and East London locations.

Variability in the Agulhas Current can occur at a number of time scales, which is evident from examining the ADCP data. Some examples of variability include tides, sub-mesoscale and mesoscale eddies, Natal Pulses, seasonal variations in current velocities (Krug and Tournadre 2012), and longer term variations associated with climate modes such as the El Niño Southern Oscillation and gyre circulation changes. The ADCP spectra were compared with the GlobCurrent and HYCOM

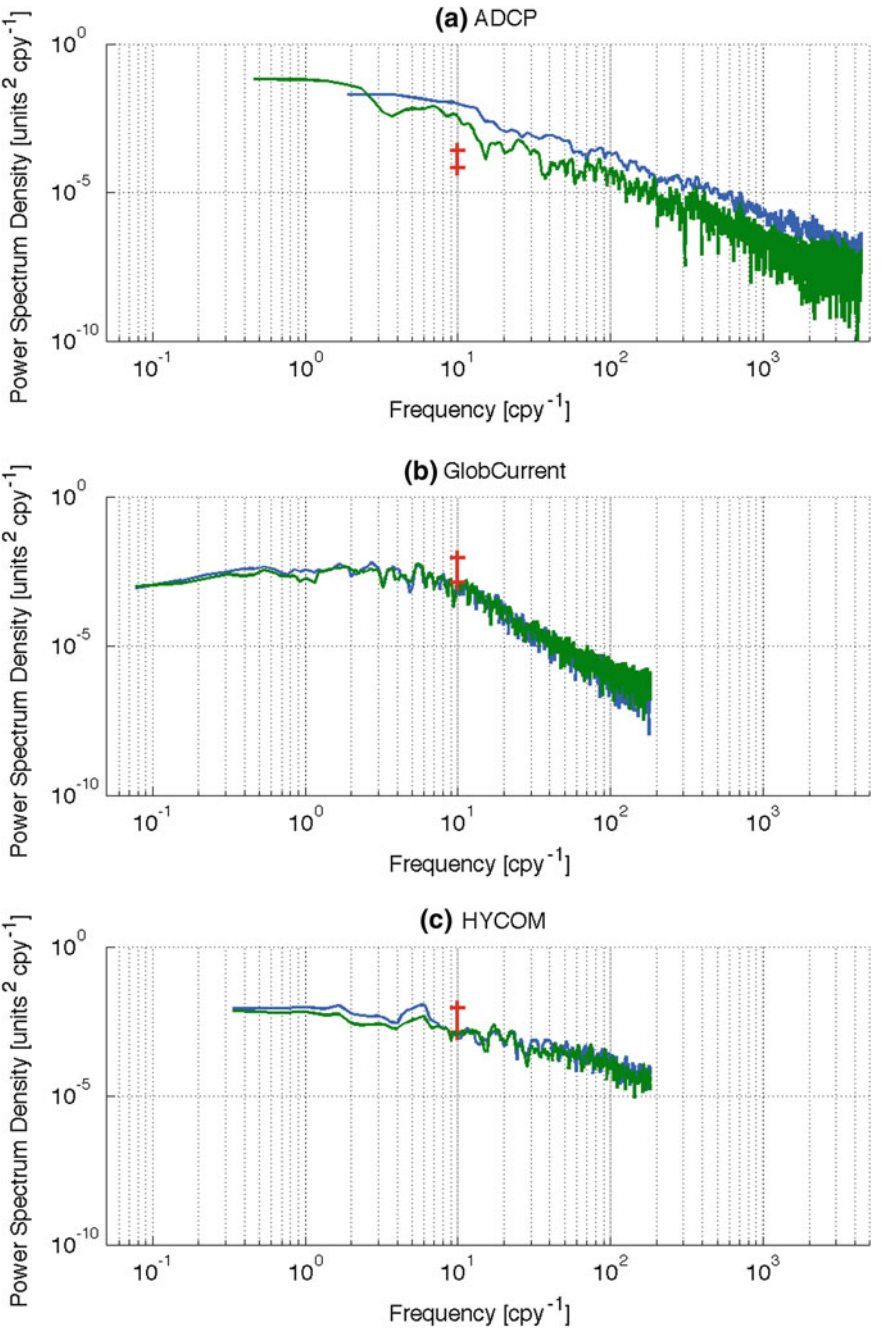

Fig. 3 Spectra at selected sites—Cape Morgan (*green*) and East London (*blue*)—using **a** ADCP data for record data lengths of 193 days (*green*) and 137 days (*blue*), **b** GlobCurrent data for a record data length of 14 years, and **c** HYCOM data for a record data length of 3 years. The *red* line indicates the 95% significance level

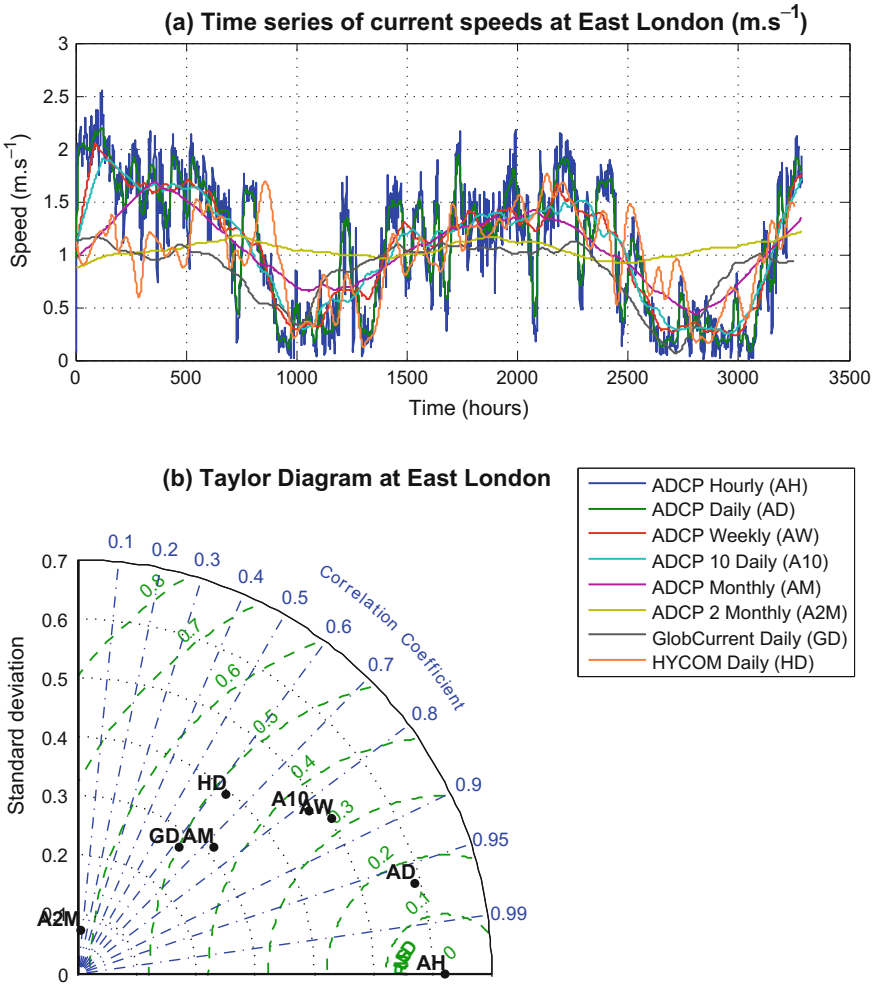

Fig. 4 **a** A time series of Agulhas Current speeds (m/s) at East London using hourly, daily, weekly, 10-daily, monthly, and 2-monthly ADCP data as well as daily GlobCurrent and HYCOM data at the same location. **b** A Taylor Diagram showing the standard deviation, correlation, and centred root-mean-square difference of the same data sets at East London

spectra to evaluate the accuracy of the modelled and satellite-derived velocities with respect to these modes of variability.

Comparing the three data sets, it is evident that there is very little difference between the Cape Morgan and East London spectra in the GlobCurrent and HYCOM data sets. The ADCP data set, however, shows a higher spectrum density at the East London location. This suggests that there are slightly higher levels of variability at East London compared to Cape Morgan, which is in agreement with the PCA analysis (Fig. 2).

To determine the frequency of the dominant mode of variability, one evaluates where the strongest change in the slope of the spectra occurs. The x-axis of Fig. 3 represents frequency, where 100 is 1 cycle per year. Each successive vertical grid line to the right is one additional cycle per year. Thus, the GlobCurrent data indicate a predominant mode of variability of six cycles per year (two-monthly), which may be related to the passage of Natal Pulses or other Agulhas Current meanders. This two-monthly cycle is also present in HYCOM, but the change in slope is much weaker, and therefore, the signal is not significant. The lengths of the ADCP time series (193 days at Cape Morgan, 137 days at East London,) are too short to confidently confirm the two-monthly dominant mode of variability.

Typically, spectra of ocean processes should have steep slopes, which signify an inverse cascade of energy from low frequencies to high frequencies (e.g. hourly to monthly) (Scott and Wang 2005). The slopes in the spectra of the ADCP and GlobCurrent data sets are in good agreement with each other, indicating a rapid decay in the ocean current energy towards high frequency. At higher frequencies (101–102), the HYCOM data set has more energy compared to the ADCP and GlobCurrent data sets, but the slope is flatter indicating that all frequencies have similar levels of energy, which is indicative of white noise. The flatter slope in the HYCOM data set shows that energy decay in the model is inadequately simulated and that in the assimilated model output, there are no coherent processes producing an inverse energy cascade. The fact that the slopes of the inverse energy cascade in the spectra of GlobCurrent and the ADCP data agree indicates that both data sets are able to capture the larger (meso) scale processes that dominate the energy spectra. Comparatively, the higher frequency variability is relatively less important, as is evident in the flattening of the slope.

Figure 4a shows the time series of the hourly ADCP data, the daily, weekly, 10-daily, monthly, and 2-monthly averaged ADCP data, as well as the GlobCurrent and HYCOM daily data for East London. The comparison highlights the impact of temporally averaged data as well as the variability captured by the temporally smoothed ADCP data and the daily satellite and modelled data products. The correlation coefficient, standard deviation, and root-mean-square difference (RMSD) of the temporally averaged ADCP data together with the GlobCurrent and HYCOM data are summarised in the Taylor Diagram (Fig. 4b).

As expected, the correlation coefficient and standard deviation decrease, concurrently with increasing RMSD when the ADCP is averaged over increasingly longer time periods (i.e. hourly to daily to weekly to monthly to two-monthly).

Using the hourly ADCP data as a reference, and comparing the respective daily, weekly, 10-daily, monthly, and 2-monthly averaged ADCP data to the daily GlobCurrent and HYCOM data, suggests that HYCOM and GlobCurrent are only able to accurately represent variability occurring at the monthly time scale. This is indicated by the fact that the monthly ADCP data and the GlobCurrent and HYCOM daily data are clustered around similar correlation coefficients, standard deviations, and RMSDs.

These results have significant implications for the ability to use state-of-the-art satellite remotely sensed and assimilative modelling products when determining

potential energy extraction sites. Furthermore, the ability to use these tools to predict variability in the Agulhas Current is questionable at this stage, and this highlights the need for further development and improvement of these products. Nevertheless, in the absence of a spatial and temporally coherent ocean observing system for the Agulhas Current, these data provide useful insights into the modes of variability of the Agulhas Current and their implications for energy production.

Implications for Energy Production

For resource measurements to be useful in monitoring or predicting behaviour, the temporal resolution of the data used in the prediction need to be able to capture the temporal variability associated with the ocean processes to be predicted. For example, if significant variability is seen at an hourly resolution, then the monitoring equipment needs to be able to accurately capture this variability to be able to successfully control a potential ocean current power plant. As noted in the above analysis, in situ ADCP data are the only data at present that can accurately capture the full variability of the Agulhas Current, but deploying and managing ADCP devices are costly and spatially limiting. In the absence of ADCP data, the only alternative data sources are those derived from satellite remote-sensing measurements and data-assimilative predictive models. In the previous section, it is shown that the correlation between data obtained from the ADCPs and those obtained from the Globcurrent and HYCOM products only compare well on a monthly scale and thus have limited use in assisting in monitoring and predicting the shorter time scales of variability in the Agulhas Current. Additionally, satellite remote-sensing observations are limited to the surface level, so it is important to note that there is a need for the characteristics throughout the depth of the water column to characterise to be useful in monitoring and predicating energy output from this resource.

Figure 5 shows time series ADCP data plots of velocity versus depth highlighting the variability of the Agulhas Current. The presence of major events of variability—a Natal Pulse—is recognised as a drop in the current speed to near zero throughout the water column for longer than 10 continuous days. This indicates that the current core has been displaced seaward from its original course by the Natal Pulse meander. All measurements taken at different latitudes have been plotted on the same temporal axis so that the propagation of a Natal Pulse southward along the coastline can be identified.

In Fig. 5a, the presence of four Natal Pulses, which occurred in Nov 09, Mar 10, May 10, and Aug 10 and each persisted for at least 20 days, is seen from November 2009 to September 2010. In Fig. 5c, it is seen that the Natal Pulses of November 2009–September 2010 in Fig. 5b did not dissipate as they travelled southward, and the presence of these pulses is seen in the data set in Fig. 5c.

Each of these pulses takes approximately 15–20 days to travel down the coast between the two locations. Similarly, the Natal Pulse that occurred in July 2008 travelled down the coast; the Pulse is first seen in the data set captured in Fig. 5a,

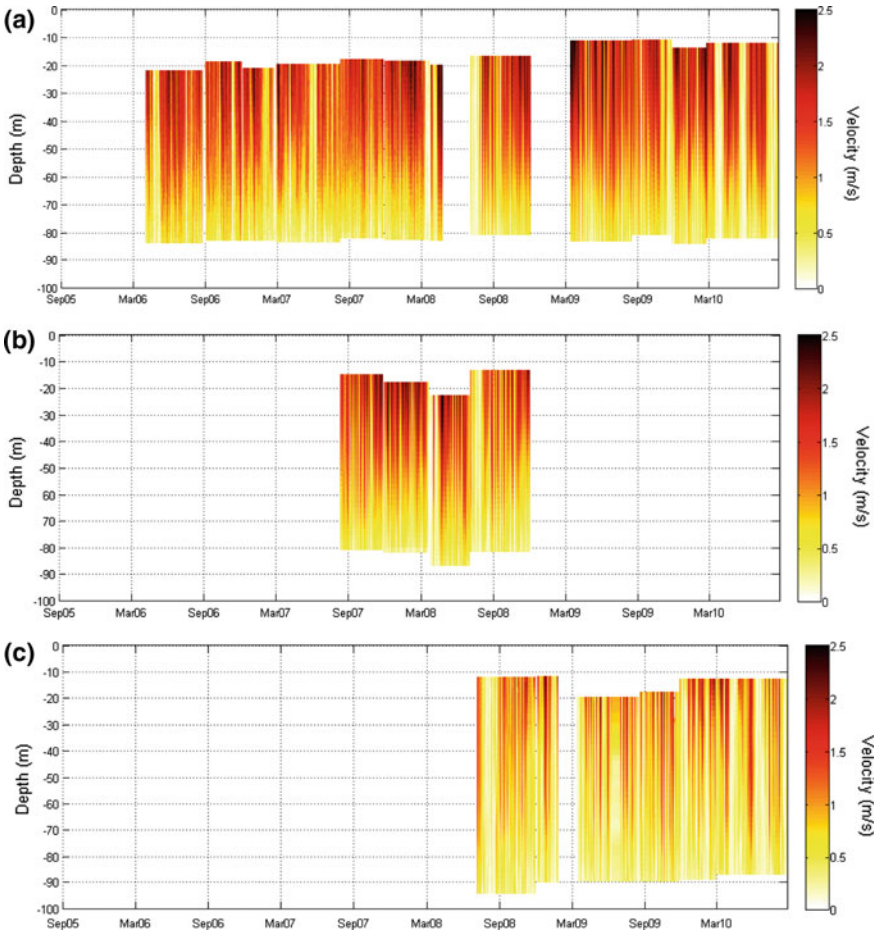

Fig. 5 Temporal plots of velocity magnitude versus depth at **a** Cape Morgan, **b** East London, and **c** Fish River

then again in the Fig. 5b data set, and lastly in the Fig. 5c data set. This Natal Pulse also takes approximately 15 days to arrive at the location plotted in Fig. 5c from the location plotted in Fig. 5a. The fact that the Natal Pulse took a fortnight to travel ~200 km is a testament to the sluggish velocity magnitude at which such pulses propagate.

Figure 5a, shows the results from two deployed ADCPs, one deployed from April 2006 to May 2008 and another from March 2009 to September 2010. When the two time periods are compared, the 24-month period from April 2006 to May 2008 only sees three pulses of approximately 10-days duration whereas during the 17-month period from March 2009 to September 2010 four Natal Pulses are observed. The difference in the occurrence of Natal Pulses at the same location over

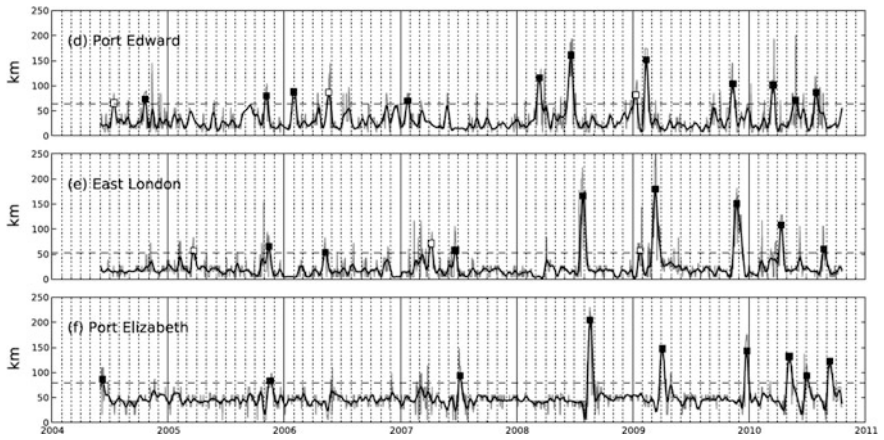

Fig. 6 Position of the Agulhas Current used to identify the presence of Natal Pulses. Natal Pulses are indicated by black squares, adapted from Fig. 5 in Rouault and Penven (2011)

different time periods shows the erratic and unpredictable nature of this phenomenon and emphasises the importance of anticipating such events.

The results found in the temporal velocity magnitude plots compare well with the results found by Rouault and Penven (2011). Figure 6 shows the position of the Agulhas Current inshore front relative to the shore at three locations along the coastline in order to determine the presence and propagation of Natal Pulses. It is promising to see the correlation between the in situ data presented in Fig. 5a and the satellite data used to plot Fig. 6e. From Fig. 6, it is seen that the occurrence of the four Natal Pulses from November 2009 to September 2010 is abnormally high; Rouault and Penven (2011) found the average to be 1.6 pulses a year when considering a 20-year period. Further, the same propagation trend down the coastline that was found in Fig. 5 is shown in Fig. 6.

The lag between the locations shows the sluggish nature of the phenomenon but can be used to the advantage of plant operators. If an ocean current power plant were to be installed in the energetic region of 32.5°S and the behaviour of the Agulhas Current were tracked further up the coast around 31.2°S, the presence of an approaching Natal Pulse could be predicted approximately two weeks in advance. Such tracking may be done using a remote-sensing technique, but the reduced correlation between in situ and satellite data at the weekly to 10-day time scale (Figs. 5 and 6) may hamper this ability.

A timely warning of the occurrence of Natal Pulses is critical, however, and will allow power grid operators to plan to use the period when a Natal Pulse is present for maintenance of the ocean current power plant. Furthermore, grid planners can mobilise other capacity to ensure the demand of the country is met. However, other available capacity may not be available during winter months when demand is high, and because there is no seasonal trend in the occurrence of Natal Pulses, there is risk related to the firm capacity of an ocean current power plant. The lengthy

presence of a pulse (~20 days) in one location is a concern for the technically possible capacity factor and the capability of ocean current energy to supply a reasonably uninterrupted supply of power to off-takers..

Characteristics of Energetic Region

From the analysis in current strength and variability section, of the data collected along the South African East Coast, the energetic region lies in the region of 28.8 E and 32.5 S (Cape Morgan location). This location has favourable velocities and because of the bathymetry in the region the current core lies in close proximity to the coast. The following analysis presents the physical characteristics of a mid-shelf and offshore site in this region.

Current Magnitude

Figure 7 shows the current velocity magnitude versus depth. A minimum, 75% exceedance, 50% exceedance, 15% exceedance, and the current maximum are plotted.

When comparing the two sites, the presence of the Agulhas core is seen clearly at the offshore location, where at water depths of 50 and 30 m the mean velocity magnitude is 1.49 and 1.59 m/s, respectively. For the mid-shelf deployment, the mean current velocity magnitude is 1.00 and 1.34 m/s at water depths of at 50 and 30 m, respectively. The mid-shelf mooring is thus placed at the core's edge. At the 30 m water depth, the offshore current velocity magnitude is 1.2 times greater than the mid-shelf velocity magnitude, which is when the cubed relationship between velocity magnitude and power is considered, results in a significant difference. The 75% exceedance values at the 30 m depth are 1.0 and 1.29 m/s for the mid-shelf and offshore deployments, respectively; the 75% exceedance values at the 50 m depth are 0.69 and 1.17 m/s for the respective deployments. A similar trend is seen for the 15% exceedance plot; values for the respective mid-shelf and offshore deployments at the 30 m depth are 1.91 and 2.16 m/s and at the 50 m depth they are 1.45 and 2.06 m/s. These ranges indicate that a turbine that is deployed in the Agulhas Current will need to operate at speeds between 0.6 and 2 m/s.

Figures 8 and 9 are temporal time series plots of time versus depth in which the colour scale indicates the current velocity magnitude for each location. These plots highlight the variability of the current velocity magnitude and show the erratic presence of day-long eddies and Natal Pulses. The distinct presence of a Natal Pulse is seen during April 2013, as indicated by the entire water column velocity magnitude dropping to near zero. The size of these meanders are realised because both sites are affected by this occurrence. Figures 8 and 9 show how problematic the presence of this phenomenon will be to potential power production from a turbine

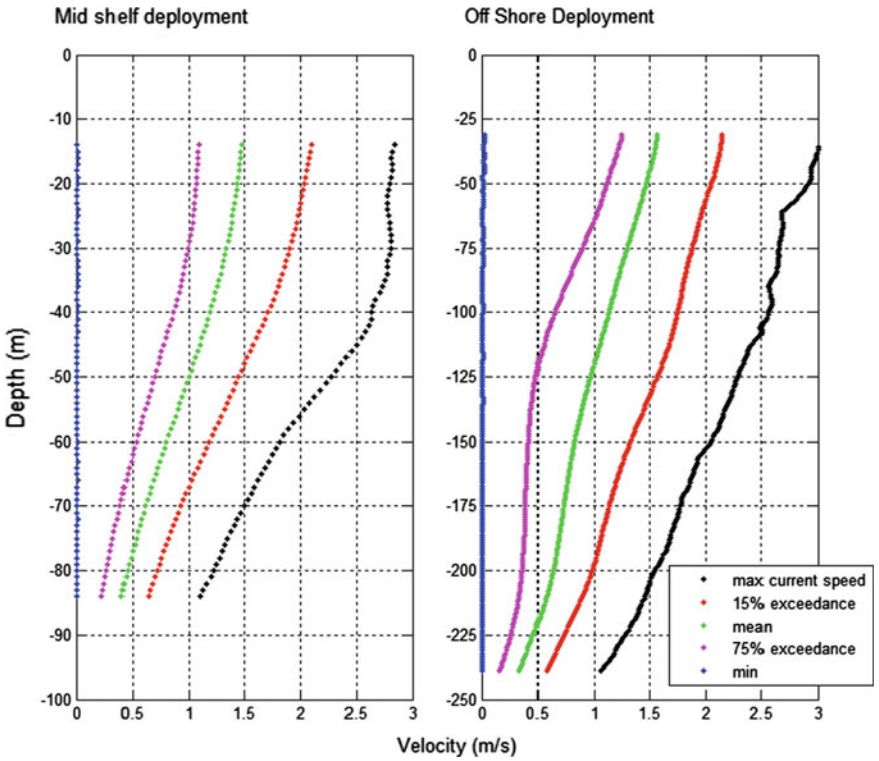

Fig. 7 Current velocity magnitude (m/s) ADCP minimum (*blue*), 75% (*magenta*), mean (*green*), 15% (*red*), and maximum (*black*) flow speeds at the mid-shelf (*left-hand* figure) and offshore (*right-hand* figure) locations (Meyer and Van Niekerk 2016)

array because all power production will stop during the presence of a Natal Pulse. Three other time periods of low velocity magnitude seen in these figures indicate the presence of eddies in the current core—during February 2012, May 2012, and October 2012. These eddies did not persist as long as the occurrence in April 2013, but such events add to the variability of the current and lower the availability of the current.

Rouault and Penven (2011) found an average of 1.6 Natal Pulses travel down the East Coast of South Africa annually. The data set evaluated here is 18 months long and has only one distinct occurrence present that can result in a more optimistic capacity factor for this period than in an average year. This shows that the measured in situ data sets cannot be used in isolation to quantify the performance of the current, but need to be compared to data sets that cover a longer period of time (10 years or more) to ensure correct trends are observed, and this can be achieved by using remote-sensing data.

Figures 10 and 11 show the velocity magnitude distribution and cumulative frequency of occurrence at the 30 and 50 m depths for each of the locations. In both

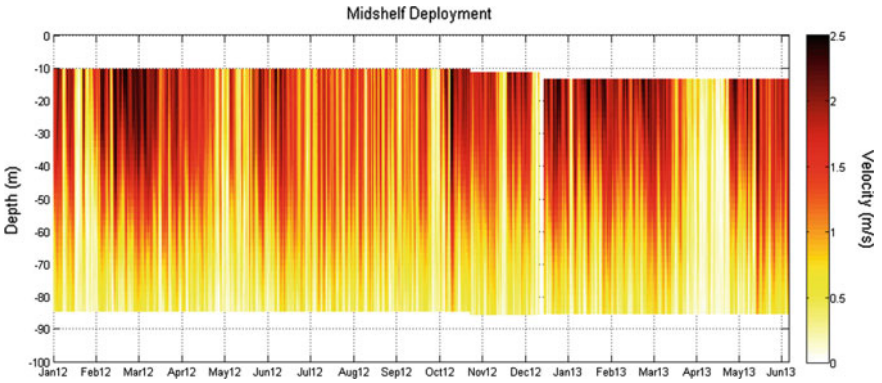

Fig. 8 Temporal plot at the mid-shelf location. Time versus depth with the colour scale indicating current speed (m/s) (Meyer and Van Niekerk 2016)

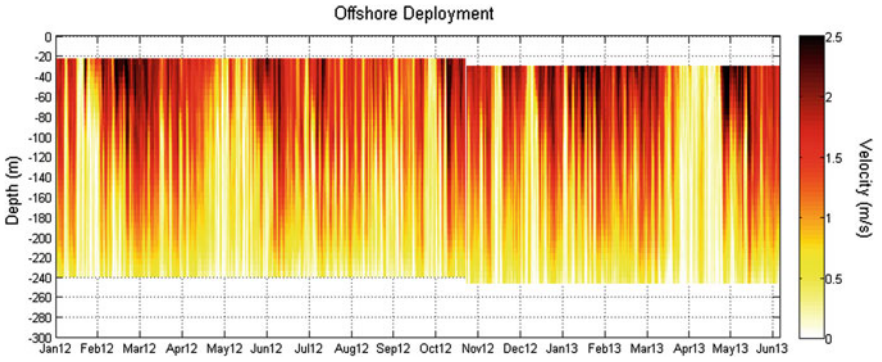

Fig. 9 Temporal plot at the offshore location. Time versus depth with the colour scale indicating current speed (m/s) (Meyer and Van Niekerk 2016)

Figs. 10 and 11, in the Frequency of Occurrence plot, two distinct peaks are seen: the first is low velocity magnitude peak, indicating the velocity magnitude distribution during the presence of a Natal Pulse or weekly eddies, and the second occurs when no such phenomena are present. The second peak tends to the bell shaped curve of a normal distribution curve, but is skewed to the left by low velocity magnitude values. This observed distribution must be noted when the mean velocity magnitude or mean power density is evaluated throughout the water column, because if the periods when Natal Pulses are present are treated as maintenance periods and are thus excluded, then the average velocity magnitude or power density will be higher than represented. However, as seen in Figs. 10 and 11, there are periods of low velocity magnitude that do not persist as long as Natal Pulses, but they will negatively affect potential power production and cannot be discounted.

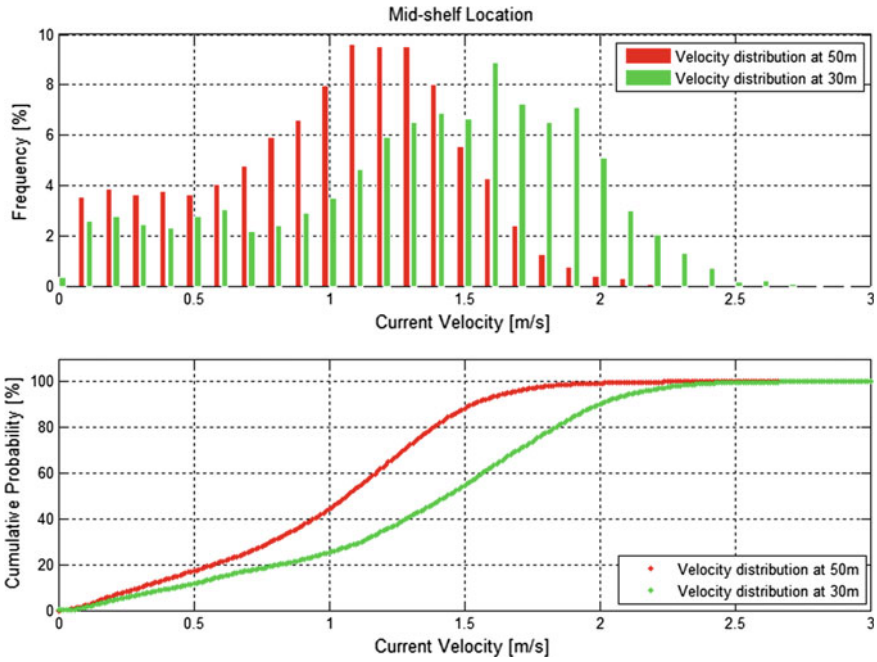

Fig. 10 Velocity magnitude distribution at the mid-shelf location (Meyer and Van Niekerk 2016)

The typical cut-in speed of marine turbines is between 0.5 and 1.0 m/s (Meyer and Van Niekerk 2016). If the velocity magnitude distribution is compared to these velocity magnitude values for both the mid-shelf and offshore location, one notes that the low velocity magnitude peak present in the full distribution curve will result in non-operational turbines.

In Figs. 10 and 11, the shift in the histogram bars towards the higher velocities for the shallower measurement highlights the difference in velocity magnitude seen at the 30 m depth compared to the 50 m depth. There is less of a difference between the velocities at the 30 and 50 m depths at the offshore location due to the deeper penetration of the current core at this site and lesser impact of seabed drag on the current. Furthermore, velocities at a 60 m water depth at the offshore location are comparable to the velocities at a 20 m depth at the mid-shelf location. This is important to note because deploying and mooring a turbine array at a sea bed depth of 255 m may prove to be challenging. Figure 8 through Fig. 11 reiterate the importance of mooring the turbine array as close to the surface as possible for maximum power output.

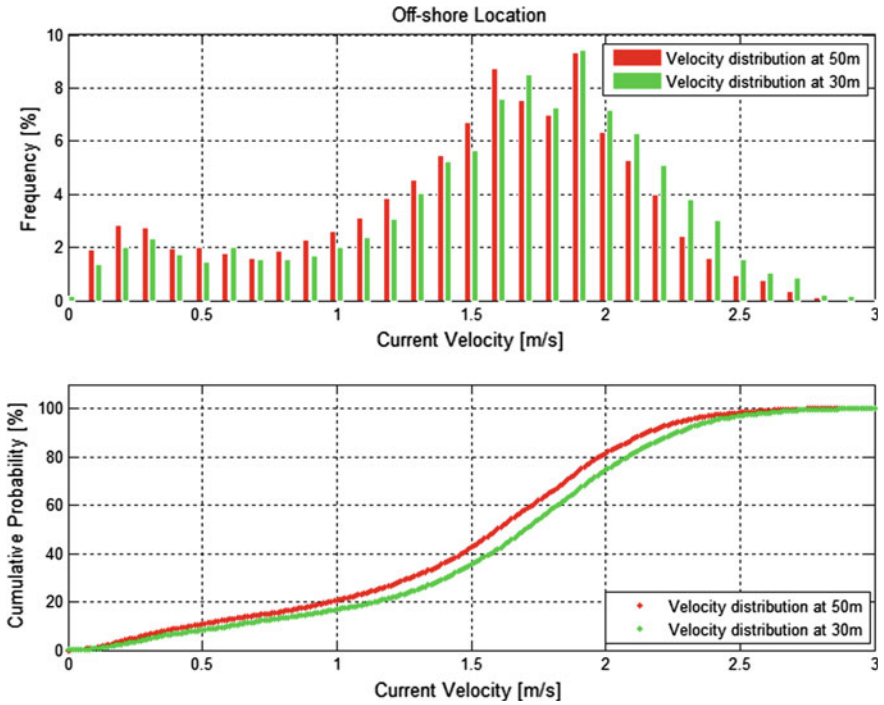

Fig. 11 Velocity magnitude distribution at the offshore location (Meyer and Van Niekerk 2016)

Power Density

The power density of a fluid stream across a unit cross section is given by:

$$P = \rho \frac{1}{2} v_{ins}^3 \tag{1}$$

where ρ is the density of the fluid and v_{ins} is the instantaneous velocity magnitude of the fluid stream.

The mean power density versus depth is plotted in Fig. 12. As noted in the velocity magnitude analysis, the power density at 20 m at the mid-shelf deployment (2,265 W/m^2) is similar to that at 60 m at the offshore deployment (2,180 W/m^2). At the 30 m water depth, the mean power density is 1,857 and 2,866 W/m^2 at the mid-shelf and offshore locations, respectively. The power density at the offshore location is 1.5 times greater than the power density at the mid-shelf location at the 30 m water depth. At the 50 m water depth, the mean power density is 813.6 and 2,440 W/m^2 at the mid-shelf and offshore locations, respectively. This results in the power density at the offshore location being three times larger than that of the mid-shelf deployment at the 50 m water depth. When comparing these values with

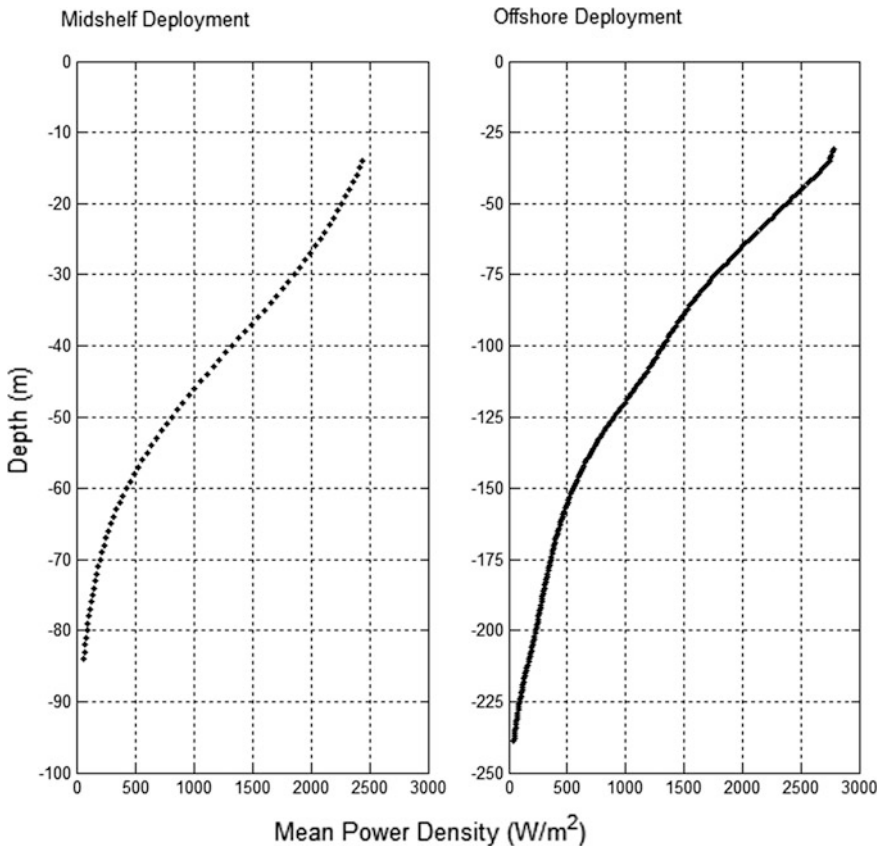

Fig. 12 Mean power density (W/m^2) (Meyer and Van Niekerk 2016)

the current velocity magnitude at the same depths, the cubed relationship between power and velocity magnitude is highlighted.

Directional Analysis

The current direction at each location is described using directional roses plotted at depths of 80, 50, and 30 m in Fig. 13. When the mid-shelf and offshore locations are compared a slight shift in the predominant current direction is seen as the current approaches the shore.

At the offshore location, the predominant current direction is approximately 195° from North where at the mid-shelf location, the predominant current direction is 210° from North. This directionality shows that the current flows in a general south-westerly direction with onshore components.

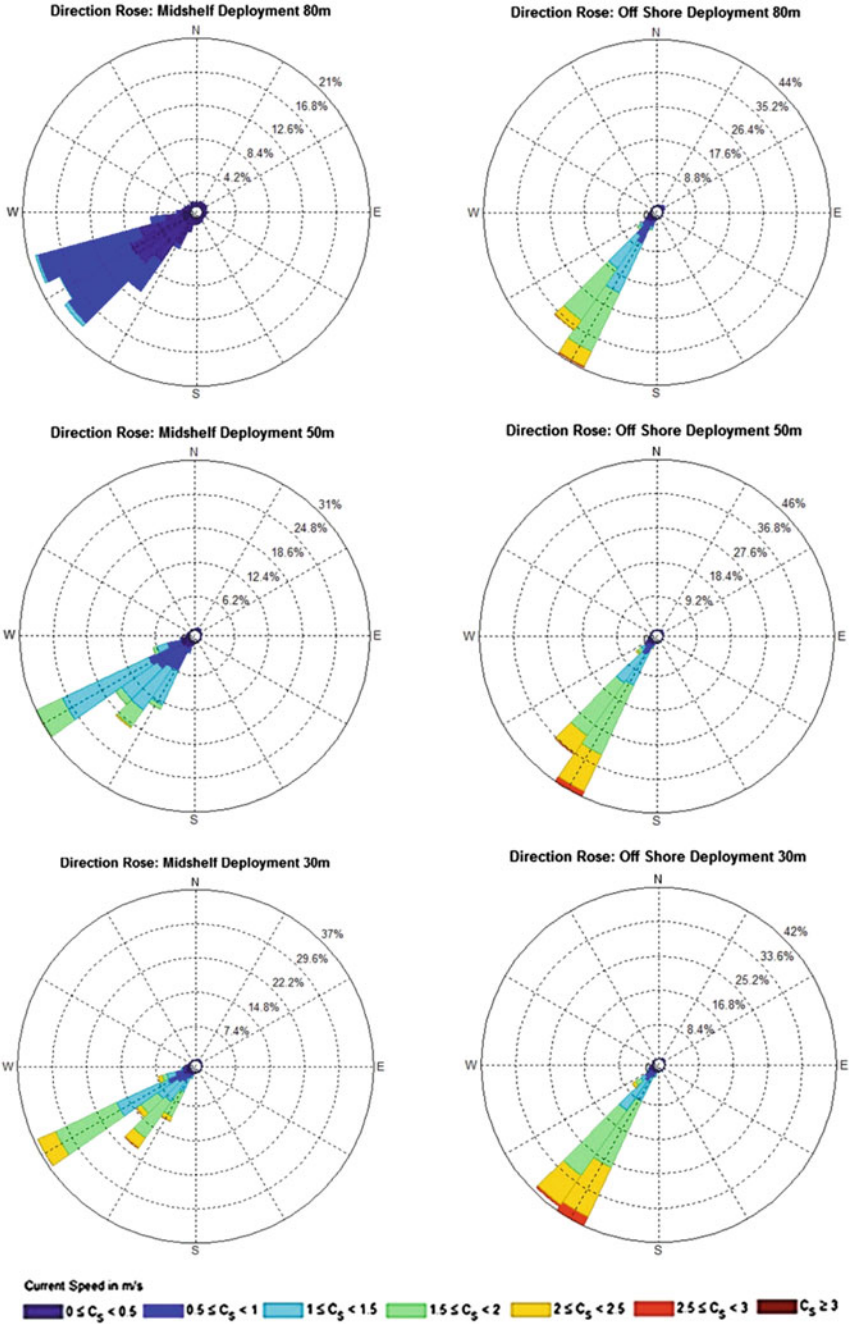

Fig. 13 Mid-shelf location (*left*) and offshore location (*right*): current directional roses at the 80 m (*top*), 50 m (*centre*), and 30 m (*bottom*) water depths (Meyer and Van Niekerk 2016)

At the mid-shelf location, at the 80 m water depth, onshore directional tendencies are seen, whereas at the 50 and 30 m water depths, the directionality ranges between 195° and 210° from North. The current directionality is more constant at the offshore location where only two predominant directions are seen, namely 195° and 200° from North, compared to the mid-shelf deployment that possesses five distinct directional components. This indicates the presence of the core at the offshore location, where the more swift flowing waters reduce the variability in the direction of the current.

The directional roses do not show directionality when the velocity magnitude is zero, but the near-zero velocity magnitude components can be seen to ring the centre of the rose, indicating that during eddies or Natal Pulses the directionality of the current is no longer in the south-westerly direction and current reversals take place.

Figure 14 illustrates the relationship of the standard deviation of direction and the percentage of current reversals with depth below the sea surface. The standard

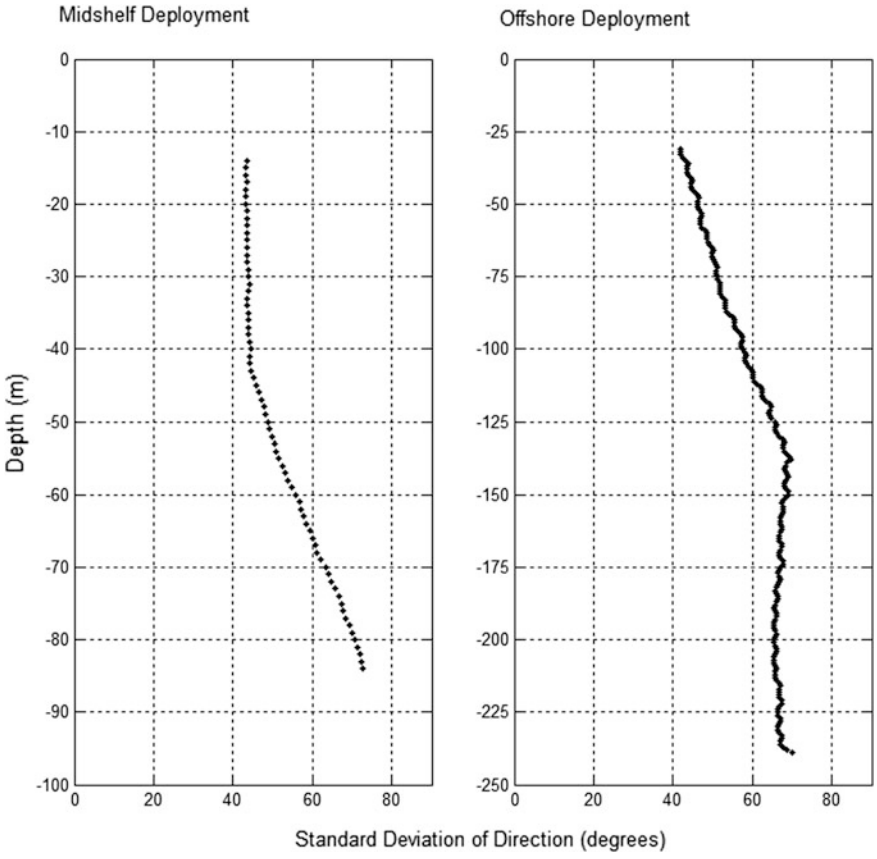

Fig. 14 Standard deviation of flow direction in degrees (Meyer and Van Niekerk 2016)

deviation of the current's direction increases with depth in the upper water column as seen in both mid-shelf and offshore locations. In the offshore location, the variability stabilises below a depth of 137 m. At the 30 m depth, the standard deviation is 43.98° and 40.08° for the mid-shelf and offshore locations, respectively. At a depth of 50 m, the standard deviation is 48.66° and 44.85° for the mid-shelf and offshore locations, respectively. This variability shows that the chosen turbine must be able to adapt to the change in flow direction in order to achieve a maximum power output.

Technical and Environmental Considerations

Technology Considerations

The magnitude of practically extractable power depends on the technology used to harness the current's energy and the power density at which this technology can be deployed. The ocean energy industry as a whole is still immature; ocean current energy technology readiness levels range between TRL 1 and TRL 5 (Mofor et al. 2014). At the time of this study, no ocean current turbines are operating at a commercial scale for energy extraction.

From the results of the current magnitude and directional analysis, it is established that the required technology needs to operate in a flow range of 0.6 and 2 m/s with the mean velocity magnitude occurring between 1 and 1.5 m/s. Further, this technology must be adaptable to change in current direction and must be able to survive the presence of a Natal Pulse that results in a period of zero velocity magnitude.

Of the technology developers developing turbines for tidal applications, Minesto, has expressed interest in adapting the Deep Green 500 kW turbine for ocean current applications with a specific focus on the Gulf Stream (reNews 2014). The Minesto technology holds promise with a design that accelerates the flow velocity through the use of relative motion as the turbine flies through the water in a figure eight pattern. The Minesto Deep Green 500 kW turbine is a tethered turbine with a rated operating speed of 1.6 m/s, cut-in speed of 0.5, and cut-out speed of 2.5 m/s (Minesto 2015). These parameters indicate the suitability of the Minesto Deep Green turbine for deployment in the Agulhas Current.

Another tethered turbine, the Aquantis 2.5 MW C-Plane, has been specially designed to operate in ocean currents (specifically the Gulf Stream) and has a rated speed of 1.6 m/s, which indicates the potential suitability of this device for deployment in ocean current applications (Ecomerit Technologies 2012). However, at the time of this study, no sea trials have been carried out on the C-Plane, so the success of the device is still to be verified. Similarly, IHI Corporation and Toshiba are currently developing a tethered turbine for deployment in the Kuroshio Current.

This device is still in the simulation phase and construction is yet to begin (IHI Corporation 2015).

To compare the variability of the Agulhas Current to other renewable energy resources, a suitable turbine is selected and a capacity factor is obtained from the practically extractable power. Array configuration and spacing are not considered in this research and the capacity factor of a single turbine is presented. The capacity factor is described by the following expression:

$$C_f = \frac{\sum_{i=1}^{N} Powerproduced}{\sum_{i=1}^{N} Turbineratedpower} \tag{2}$$

where N is the total number of time steps over which the capacity factor is calculated.

The theoretical power produced by the turbine is found by using the published power curve (found in Minesto 2011); a polynomial equation is developed to follow this power curve of the turbine using instantaneous velocity magnitude as the input and instantaneous power as the output. For the Minesto turbine that travels through a range of depths, this calculation method makes use of the instantaneous velocity magnitude at one depth, and thus, with the observed decreasing vertical velocity magnitude profile, this method of calculation has the potential to overestimate the total energy output from the system. Furthermore, as outlined by Haas et al. (2013), a single turbine has little to no effect on the upstream characteristics of the current, but a large number of devices can block the flow and reduce the current velocity, and hence reduce the generated power from each device. Thus, it is noted that this methodology cannot be extrapolated to an array of turbines, but rather can be used as a comparative method to identify an energetic site.

The theoretical capacity factors at the mid-shelf and offshore location for the deployment of one Minesto Deep Green 500 kW turbine is presented in Table 5. Table 6 presents the findings from the 500 kW Deep Green turbine that has a rated speed of 1.6 m/s and an optimal operating range of 1.4–2.2 m/s. Similar to the wind turbine industry, the economics of the availability of power versus the magnitude of the power produced must be weighed against one another to find the best-suited turbine. Table 6 shows the theoretical power output and specific yield from the 500 kW Minesto turbine.

Upon examination of Table 5, the capacity factor for the offshore location is significantly higher than the mid-shelf location; there is only a 6% drop in capacity

Table 5 Found capacity factor for the Minesto 500 kW turbine

Minesto 500 kW deep green rated speed of 1.6 m/s		
Depth (m)	Mid-shelf location (%)	Offshore location (%)
30	62	74
50	37	68

Table 6 Theoretical power output at the 30 m depth

	Minesto 500 kW deep green rated speed of 1.6 m/s	
	Annual yield (MWh/annum) (MWh)	Specific yield (kWh/yr-kW installed) (kWh/kW)
Mid-shelf location	2,708	5,416
Offshore location	3,258	6,515

factor between the 30 and 50 m deployment depths. At the mid-shelf location, a 25% drop in capacity factor is seen between the 30 and 50 m deployment depths. Because the mid-shelf location is situated at the edge of the Agulhas Current, the core does not penetrate as deeply as at the offshore location, which results in a drop in velocity that is amplified by the cubed power velocity relation and the subsequent drop in capacity factor.

When comparing the found capacity factors at both locations to the values of other renewable energy resources, the Agulhas Current fairs well. Desktop analysis by Kritzinger (2015), in collaboration with the South African Department of Energy's Independent Power Producer office, approved for publication in 2014, found that for the South African wind resource, the capacity factor for the under-construction or installed wind farms greater than 80 MW ranges from 30 to 45%. If the turbines are installed at 50 m or shallower depths, the found capacity factors are greater than those generated by wind farms for both analysed turbines. A typical capacity factor found for tidal energy extraction ranges from 20 to 30%, and for wave energy extraction devices, it ranges from 15 to 22% (Boyle 2012). The found capacity factors of the Agulhas Current point to a more constant resource in comparison to other renewable energy resources, which indicates a possible contribution to the base-load supply of electricity.

For the 500 kW turbine, the annual electricity production at the offshore location is 3.26 GWh and at the mid-shelf location it is 2.71 GWh. Although the capacity factor and the specific yield of the offshore site is higher than that of the mid-shelf location, the economics of the longer sea cable and increased mooring challenges must be taken into consideration when deciding on an optimal deployment location.

The closest developed technology to that of ocean current turbines is the technology developed to harness tidal stream energy. The rated operating speed of the stationary (gravity or pile mounted) horizontal axis turbines is greater than 2.5 m/s, so these turbines will perform poorly if deployed in the Agulhas Current. Further, the pile mounting or gravity base will prove problematic due to the mooring depth at energetic ocean current sites. Tethered turbines still require development to be optimally deployed in the Agulhas Current; however, Minesto has gained support from the Welsh government and plans to deploy a 10 MW array by 2019 at Holyhead Deep off the coast of Anglesey (Minesto 2015), which indicates progress towards a commercial industry. The turbines used in the analysis are designed

specifically for tidal applications, so the turbine chosen for the Agulhas Current conditions will need to be optimised to maximise the turbine capacity factor and produced energy.

The practically extractable power depends not only on the selected power take-off technology and resource velocity magnitude and directionality, but also is on a number of other factors, as discussed below.

Geotechnical and Mooring Considerations

With respect to current magnitude and direction, the study results indicate that a strong and constant flow of seawater takes place at deeper locations because the current core lies approximately above the 200 m bathymetry line at 28.831 E and 32.507 S. However, the deeper the sounding depth, the larger will be the concerns surrounding the mooring challenges and the drag forces on the turbine tether in order to moor the turbine hub at 30 m below the surface. A stronger and more advanced mooring system will be required at deeper locations, and the economics of higher power production versus the cost of a more robust mooring system must be considered.

Most experience in such applications is related to the mooring of tidal energy extraction devices and this mooring takes place in water depths of less than 100 m. Because there is no oil drilling activity in the area off the eastern South African coast, practical engineering experience gained from working in the required water depths is lacking. When working in water depths of 100 m or less some of the lessons learned from the tidal industry will be transferable, but when working in a tidal resource there is a period of slack water as the tide changes between ebb and flow. The constant flow of the current may prove to be challenging during the deployment and maintenance of ocean current power plants.

To ensure the successful mooring of turbines within the Agulhas Current, the engineering constraints related the environment need to be well understood. For example, the sedimentary and geotechnical properties of the seabed relative to mooring need to be considered. Limited information is available about these characteristics and properties of the subsurface ocean. Documentation of ocean bed topography along the southeast coast of South Africa occurred in the late 1970s and the information presented here is based on the associated maps and findings.

Figure 15 shows a schematic diagram of the shelf section between the latitudes of 28 and 34 S. The region of focus (Sections B and C in Fig. 15) is the outer-shelf region that is dominated by the current. The Agulhas Current dictates the sedimentary transport in this region. Here, the presence of shifting subaqueous dunes and relict gravels is seen. Dune heights of up to 8 m, lengths of 200 m, and dune field widths of a minimum of 10 km have been recorded. The outer-shelf gravels consist of relict sediments produced during the early Flandrain transgression by reworking of fossil algal reef bioherms (Flemming 1978). There is a distinct change in bed form type between the inner shelf and outer shelf, which consist of relict

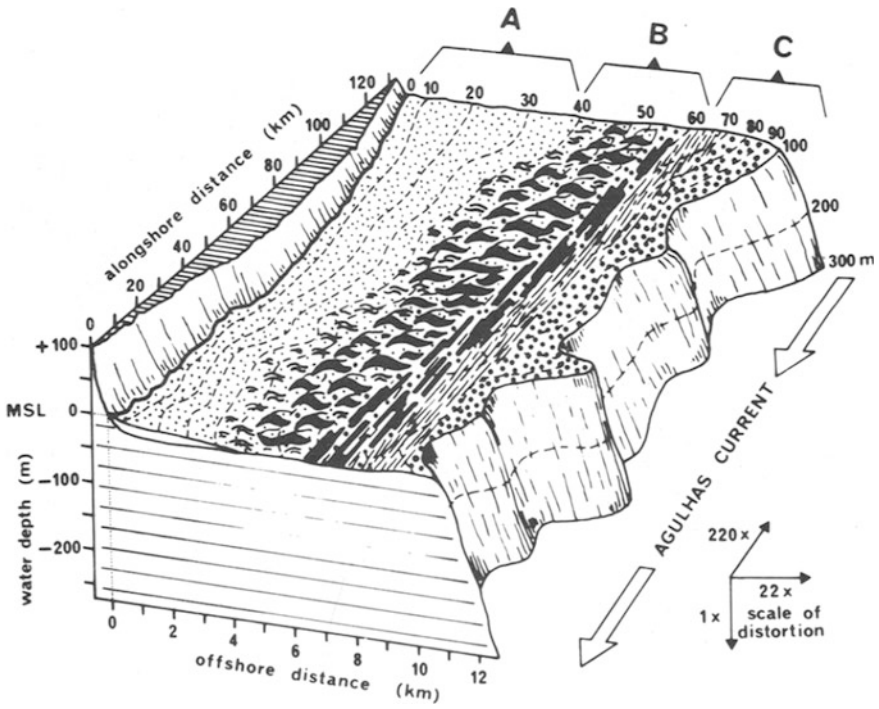

Fig. 15 Schematic block diagram of the shelf section summarising the sedimentary and structural characteristics of the ocean floor topography (Flemming 1980)

carbonate facies. The continental shelf has a very steep slope (~12° gradient) and is dissected by numerous submarine canyons. The outer-shelf region consists of current-generated bed forms such as sand streamers, dunes, and an exposed gravel pavement (Flemming 1980).

The shifting dunes can be problematic because cabling running ashore can be exposed, thereby increasing the risk of scour and requiring more frequent maintenance of the cabling. The presence of the dunes will also increase the amount of dredging that has to be done before bedrock is reached. These dunes are a continuous feature along the southeast margin of the African continent and thus will be encountered continuously along the coast.

An array of turbines will be tethered and anchored to the sea bed. The concerns surrounding this mooring method will be similar to those in other unidirectional currents that have one main loading direction where vortices and vortex shedding may be problematic. The device will have to be robust and designed to withstand geological and environmental extremes while keeping the sophisticated equipment afloat, thus the anchoring foundation must be designed for dynamical loading. The anchors must be designed to resist high cyclic lateral loads and have good scour protection on the tethering cable (Dean 2010).

Another phenomenon within the Agulhas Current is the presence of "Giant Waves" that are unpredictable and have the ability to break large ships in two (Lutjeharms 2006). These waves occur in the core of the current at the landward border, the same position being investigated for device deployment. Although the energy extraction devices will be located at least 20 m below the surface, such extreme conditions must be taken into account when addressing maintenance concerns and the fatigue loading in the device and mooring system.

Very little experience has been gained with respect to mooring considerations in this region, so extensive geotechnical surveys will have to be carried out if ocean current energy becomes a reality.

Commercial Fishing Activities

Figure 16 shows areas of importance to the fisheries industry. The map shows a cost–benefit analysis indicating the zones of high yield. The area of interest for current turbine development lies between East London and Port St John's, and from Fig. 16, it can be seen that this is not a prime area for fishing. This finding is positive because placing a turbine array in this area will help unlock the economic potential of the ocean in this region without interfering with other economic activities or ocean users. This is a preliminary finding; the site-specific effect of the turbine array on commercial and subsistence fish farmers will need to be determined by conducting an environmental impact assessment.

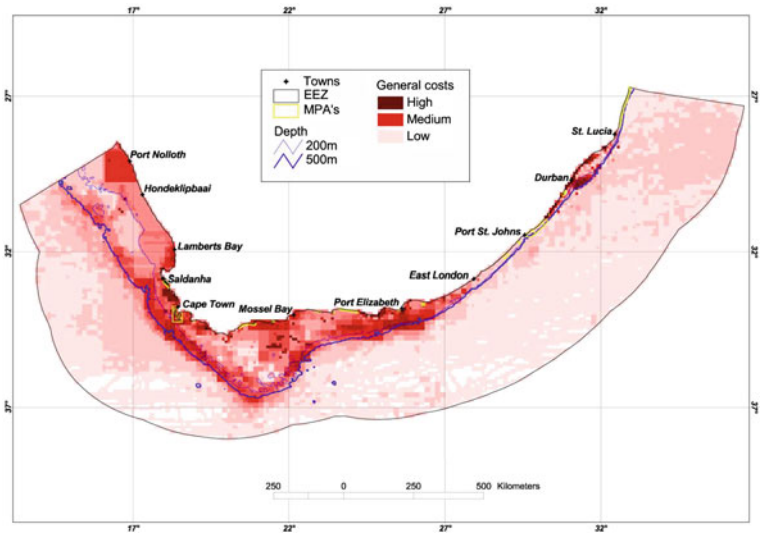

Fig. 16 Map showing the cost benefit to the fisheries industry. The darker areas are of greater importance to the industry in both benthic and pelagic respects (Sink et al. 2011)

Shipping Routes

The shipping route down the east coast of South Africa is an important trade route as illustrated in Fig. 17 by the number of journeys made during a one-year period. The establishment of a turbine array must not hinder this economic activity, and the appropriate depth below the surface must be established. Although the deployment depth of the turbines will take heed of ship wakes, exclusion zones may have to be considered with respect to ship anchoring concerns in the region of turbine deployment.

Existing Infrastructure that Can Consume the Generated Energy

A schematic of the existing Eskom substations is seen in Fig. 18, which indicates the distances from the ADCP deployment locations (mid-shelf and offshore locations indicated by white circles). The mid-shelf site is located 14 km from the shore and 30 km from the nearest medium voltage station. The offshore site is 18 km from shore and 30 km from the nearest medium voltage station. This indicates that there is existing infrastructure to make use of the generated electricity, but an economic analysis must be carried out to determine whether the increased power generated at the offshore location justifies the increase in sea cabling length.

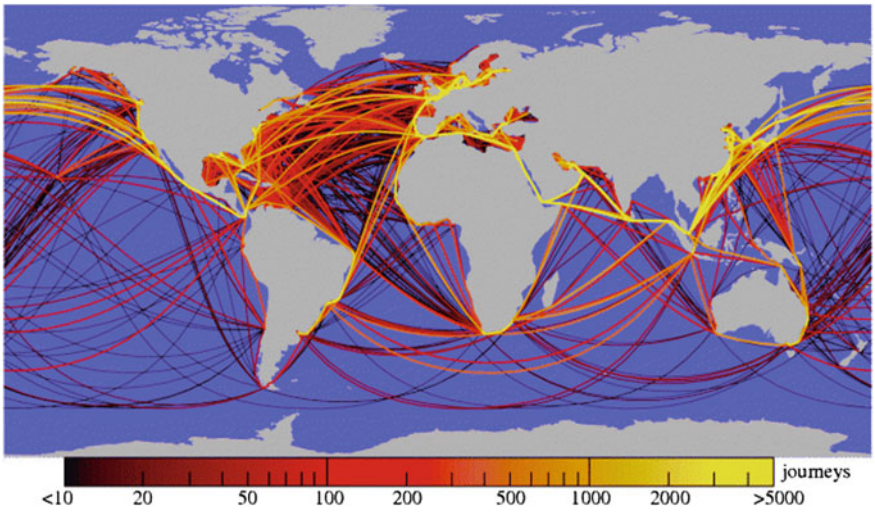

Fig. 17 Trajectories of all cargo ships bigger than 10,000 GT during 2007 (Kaluza et al. 2010)

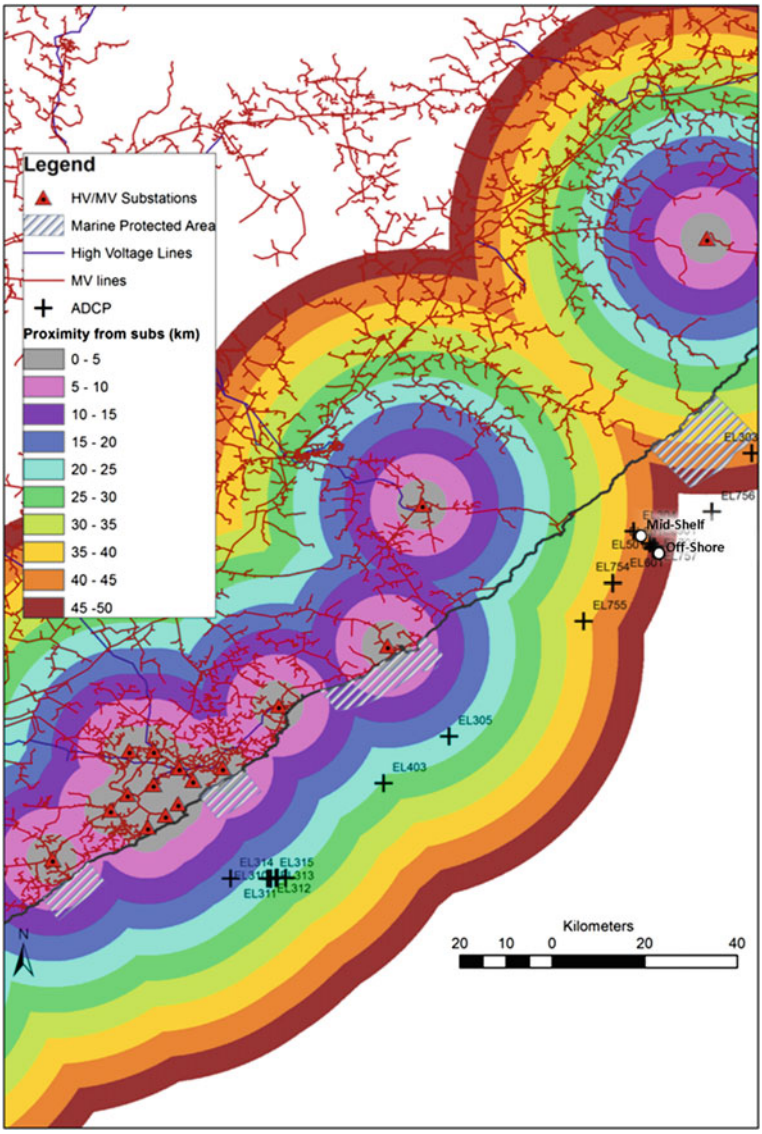

Fig. 18 Position of existing Eskom substations in the region of interest (Meyer et al. 2013)

The distances from the deployment sites to the nearest substation are significantly longer than those seen for tidal sites, but are comparable to offshore wind sites. For offshore wind sites, subsea AC cabling is used for projects located up to approximately 60 km offshore (Norton et al. 2011).

Environmental Impact

The closest existing marine protected area lies 15 km north of the analysed sites. No marine protected areas lie between the selected sites and the closest harbour located on the coast is Port Elizabeth, 350 km southwest of the chosen sites. The positions of the existing and proposed marine protected areas along the South African coastline are seen in Fig. 19. The closest economic hub in this area is East London, which lies south of the analysed sites; thus, no cabling or vessels required for the deployment and maintenance of the devices will pass through marine protected areas. It is also encouraging to notice that the proposed marine protected areas will not cause obstacles in this regard. Furthermore, the chosen turbines are shrouded, which decreases the impact of these devices on marine mammals.

On a larger scale, the environmental impact on the meridional overturning circulation of placing turbines that extract energy from the Agulhas Current has not yet been investigated and the maximum size of a potential power plant is yet to be established. In 2007, the Bureau of Ocean Energy Management published an Environmental Impact Statement (U.S. Department of the Interior Minerals Management Service 2007) in which the effects of deployment of ocean current turbines in the Gulf Stream are considered. The impacts will depend on the technology and array configuration chosen, but typical impacts include reduction in current velocity and energy and possible reduction in wave height in the vicinity of the devices (U.S. Department of the Interior Minerals Management Service 2007). Reduction of wave height will be localised, but the reduction in current energy can affect larger

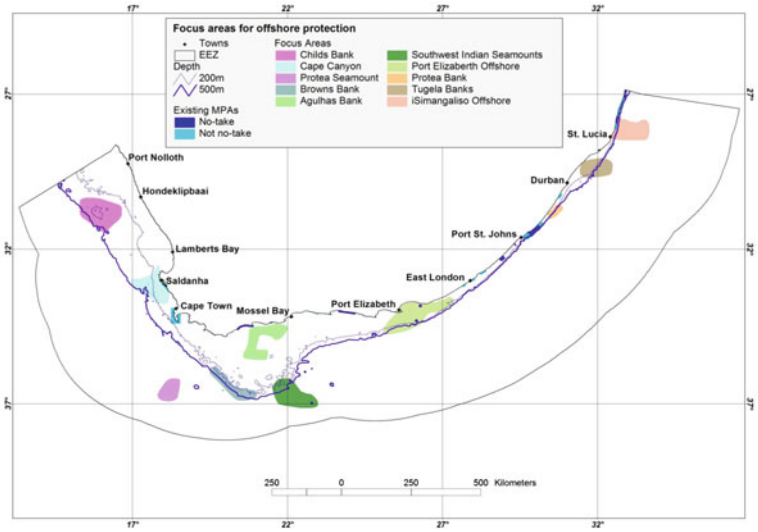

Fig. 19 Existing and proposed marine protected areas around the South African coast (Sink et al. 2011)

systems—namely weather patterns and the interactions of current with nearshore waters.

Using a depth-averaged 2D equation model, Haas et al. (2013) examined the effects of placing an array of turbines in the Gulf Stream. For a limited turbine array, the impact of turbines was found to be primarily confined in the turbine regions with negligible far-field effects. However, as the turbine region increases the region with reduced flow grows accordingly and leads to a reduced flow rate. If the turbine region extends across the core of the Gulf Stream, the energy extraction from the turbines can slow the flow universally across the entire basin. Such impacts within the Agulhas Current will need to be determined through large-scale ocean modelling. The impacts of ocean current turbine systems can be limited by restricting the quantity of energy extracted from the current and maximising the efficiency of the systems deployed. If such mitigations are put in place, this environmental challenge should not result in the discontinuation of ocean current projects.

Regulatory Environment

South Africa has a well-established National Environmental Management: Integrated Coastal Management Act (2008) (ICMA) that regulates the activities along its coastline. Prior to any construction on the coastline, an environmental impact assessment will need to be carried out in accordance with this Act. However, there is a lack of Marine Spatial Planning (MSP) within the Exclusive Economic Zones of South Africa to regulate marine usage by the various stakeholders in the marine environment. The launch of Operation Phakisa has seen the establishment of a formal MSP process for South Africa. The MSP focus areas are aquaculture, mining, shipping, fisheries, and conservation (Marine Protection Services and Governance 2014). Renewable energy has been excluded from this plan, and this can result in uncertainty surrounding the consenting process for marine renewable energy projects.

Other formal permits that will need to be considered in order to obtain consent for a marine renewable energy project include those associated with the National Environmental Management Biodiversity Act, Sea Birds and Seals Protection Act, and National Energy Regulator of South Africa Electricity Regulation Act. This is not necessarily a comprehensive list because each project's permitting will need to be approached on a site-by-site basis.

From the preliminary analysis of other contributing factors, no one factor will cause such a project to be a no-go. The economics of such an endeavour are still a challenge and the environmental concerns will need to be addressed so that renewable energy stakeholders become well-established and welcomed users of the marine environment.

Conclusion About the Best Site

Through the analysis of ADCP, GlobCurrent, and HYCOM data sets along the eastern South African coastline, an area of swift, stable flow in the Agulhas Current has been identified. This area is approximately 100 km northeast of East London, the closet economic hub. One mid-shelf and one offshore site in this area were analysed, and the offshore site was found to be more energetic with higher velocities and reduced directional variability. The mean velocity found at the 30 m depth at the offshore location is 1.59 m/s, and the mean velocity at the mid-shelf location is 1.34 m/s. Ideally, a turbine will operate at a rated speed within this velocity magnitude range.

Unique challenges for exploiting this resource for energy generation exist, including the irregular occurrence of large Agulhas Current meanders (known as Natal Pulses). The comparison between GlobCurrent and HYCOM data and in situ ADCP data was used to determine if this variability can be captured remotely. PCA showed that the GlobCurrent product shows a weaker Agulhas Current with less variability than indicated by the in situ data, and the HYCOM product shows more accurate Agulhas Current velocities but very little variability in the current. Comparison of the ADCP, GlobCurrent, and HYCOM data spectra indicates that the satellite-derived product is able to capture the correct levels of variability in terms of the inverse energy cascade of processes in the ocean, while the modelled data show some limitations in this regard. However, upon closer examination, it is evident that both GlobCurrent and HYCOM data sets only adequately represent scales of variability at the monthly time scale. This latter fact places a significant limiting factor on using these data for prediction to inform stakeholders and highlights the need for further development and improvement of these products.

Nevertheless, in the absence of a spatial and temporally coherent ocean observation system for the Agulhas Current, these data provide useful insights into the modes of variability in the Agulhas Current and their implications for energy production. With the aid of satellite measurements, the presence of Natal Pulses have been found to be predicted approximately 15 days prior to their occurrence at the identified energetic site if tacked from a location higher up the coast. It should be noted, however, that the reduced correlation between in situ and satellite data at the weekly to 10-day time scale may decrease the accuracy of such predications. This prediction will help in minimising the effects of this phenomenon because such periods of no production can be used for scheduled maintenance, and grid planners will have warning enough to mobilise other forms of power generation.

To reduce the barrier of entry into the ocean energy market in South Africa, the challenges facing remote-sensing and assimilative modelling data need to be addressed. There is a critical need for the predictive ocean modelling and satellite remote-sensing community to develop the capabilities to resolve the high spatial–temporal resolution processes needed for accurate characterisation of ocean current energy potential. The new Sentinel series satellites recently launched by the European Space Agency may provide the high-resolution data satellite required.

Regional modelling and data assimilation efforts such as those detailed by Backeberg et al. (2014) are critical for achieving improved predictive skill in the Agulhas Current in particular. The open access nature of these data sets is instrumental in opening the market to future developers as well as in reducing future monitoring and operational costs. If the region of interest is accurately mapped at a high resolution, this knowledge can be used to inform MSP policies so that marine energy extraction activities can be taken into consideration and further advance the industry.

Although a number of engineering and financial issues challenge deployment of a turbine array in the Agulhas Current, if the resource is paired with the correct turbine, the estimated capacity factors compare well with other renewable energy resources; thus, this current holds potential to make a significant contribution to the South African electricity grid.

Acknowledgements The authors would like to acknowledge the South African national utility Eskom for making available the data, without which this research would not have been possible. Dr Backeberg acknowledges joint support from the Nansen-Tutu Centre for Marine Environmental Research, Cape Town, South Africa; the Nansen Environmental and Remote Sensing Center, Bergen, Norway; and the South African National Research Foundation through the Grants 87698 and 91426. This work has also received a grant for computer time from the Norwegian Program for supercomputing (NOTUR project number nn2993 k). Special thanks to Dr Julie Deshayes for her input and guidance in analyzing the spectra. Both the GlobCurrent and HYCOM data used in this study are freely available online at http://www.globcurrent.org and hycom.org, respectively. GlobCurrent products are available for free thanks to European Space Agency funding under GlobCurrent DUE project A0/1-7472/13/I-LG.

References

Backeberg, B. C., Counillon, F., Johannessen, J. A., et al. (2014). *Ocean Dynamics, 64,* 1121. doi:10.1007/s10236-014-0717-6.

Beal, L. M., & Bryden, H. L. (1999). The velocity and vorticity structure of the Agulhas Current at 32 S. *Journal of Geophysical Research, 104*(C3), 5151–5176.

Biastoch, A., Lutjeharms, J. R. E., Böning, C. W., & Scheinert, M. (2008b). Mesoscale perturbations control inter-ocean exchange south of Africa. *Geophysical Research Letters*, *35* (L20602).

Boyle, G. (2012). *Renewable energy* (3rd ed.). Oxford: Oxford University Press.

Bryden, H. L., Beal, L. M., & Duncan, L. M. (2005). Structure and transport of the Agulhas Current and its temporal variability. *Journal of Oceanography, 61,* 479–492.

Chang, Y.-C., Chu, P. C., & Tseng, R.-S. (2015). Site selection of ocean current power generation from drifter measurements. *Renewable Energy*, *80*, 737–745. doi:10.1016/j.renene.2015.03.003.

Chen, F. (2010). Kuroshio power plant development plan. *Renewable and Sustainable Energy Reviews*, *14*(9), 2655–2668. doi:10.1016/j.rser.2010.07.070.

Cummings, J. A. (2005). Operational multivariate ocean data assimilation. *Quarterly Journal* of the *Royal Meteorological Society*, *Part C*, *131*, (613), 3583–3604.

Dean, E. (2010). *Offshore geotechnical engineering*. London: Thomas Telford Limited.

Dohan, K., & Maximenko, N. (2010). Monitoring ocean currents with satellite sensors. *Oceanography, 23*(4), 94–103. doi:10.5670/oceanog.2010.08.

Ducet, N., Le Traon, P.-Y., & Reverdin, G. (2000). Global high-resolution mapping of ocean circulation from TOPEX/Poseidon and ERS-1 and -2. *Journal Geophysical Research, 105,* 19477–19498.

Duerr, A. S., & Dhanak, M. R. (2012). An assessment of the hydrokinetic energy resource of the Florida current. *IEEE Journal of Oceanic Engineering, 37*(2), 281–293.

Ecomerit Technologies. (2012). Aquantis [Online]. http://www.ecomerittech.com/aquantis.php. [2015, February 7].

Ekman, V. W. (1905). On the influence of the Earth's rotation on ocean currents. *Archives of Mathematics, Astronomy, and Physics, 2*(11), 1–52.

Flemming, B. (1978). Underwater Sand Dunes along the Southeast African continental Margin-Observations and implications. *Marine Geology, 26,* 177–198.

Flemming, B. (1980). Sand transport and bedform patterns on the continental shelf between Durban and Port Elizabeth (Southeast African Continental Margin). *Sedimentary Geology, 26,* 179–205.

Fox, D. N., Teague, W. J., Barron, C. N., Carnes, M. R., & Lee, C. M. (2002). The modular ocean data assimilation system (MODAS). *Journal of Atmospheric and Oceanic Technology, 19,* 240–252.

Gründlingh, M. L. (1983). On the course of the Agulhas Current. *South African Geographical Journal, 65,* 49–57.

Haas, K., et al. (2013). Assessment of Energy Production Potential from Ocean Currents along the United States Coastline, Atlanta.

IHI Corporation, Power Generation Using the Kuroshio Current. (n.d.). Retrieved November 26, 2015 from http://www.ihi.co.jp/var/ezwebin_site/storage/original/application/149ee9de3149aba2e1215fd5f9cd46ec.pdf.

Kaluza, P., Kolzsch, A., Gastner, M. T., & Blasius, B. (2010). The complex network of global cargo ship movements. *Journal of the Royal Society, 7,* 1093–1103.

Kritzinger, K. (2015). Personal Communication. 23 February, Stellenbosch.

Krug, M. J., & Tournadre, J. (2012). Satellite observations of an annual cycle in the Agulhas Current. *Geophysical Research Letters, 39,* L15607.

Lutjeharms, J. (2006). *The Agulhas Current*. Berlin: Springer.

Lutjeharms, J. R. E., & Roberts, H. R. (1988). The natal pulse: An extreme transient on the Agulhas Current. *Journal Geophysical Research, 93,* 631–645.

Marine Protection Services and Governance. (2014). *Unlocking the economic potential of South Africa's Oceans*. Durban: Operation Phakisa.

Meehl, G. A., Goddard, L., Murphy, J., Stouffer, R. J., Boer, G., Danabasoglu, G., et al. (2009). Decadal prediction. *Bulletin of the American Meteorological Society*, *90*, 14671485.

Meyer, I., & Van Niekerk, J. L. (2016). International Journal of Marine Energy Towards a practical resource assessment of the extractable energy in the Agulhas ocean current. *International Journal of Marine Energy*, *16*, 116–132. doi:10.1016/j.ijome.2016.05.010.

Meyer, I., Reinecke, J., Roberts, M., & van Niekerk, J. L. (2013). *Assessment of the ocean energy resources off the South African coast*. Stellenbosch: Centre for Renewable and Sustainable Energy Studies, Stellenbosch University.

Meyer, I., Reinecke, J., & Van Niekerk, J. L. (2014). Resource assessment of the Agulhas Current for the purpose of marine energy extraction. In *5th International conference on ocean energy*. Halifax.

Minesto. (2011). DG-12 *Technical Specifications*. Sweden: Minesto.

Minesto. (2015). Minesto—Power from Tidal and Ocean Currents, (n.d.). Retrieved November 23, 2015 from http://minesto.com/.

Mofor, L., Goldsmith, J., & Jones, F. (2014). Ocean *energy: technology readiness, patents, development status and outlook*. Bonn: International Renewable Energy Agency [Online]. http://www.irena.org/DocumentDownloads/Publications/IRENA_Ocean_Energy_report_2014.pdf. [2015, February 10].

Norton, M., Mansoldo, A., & Rivera, A. (2011). Offshore *grid study: analysis of the appropriate architecture of an irish offshore network*. Dublin: EirGrid Plc [Online]. http://www.eirgrid.com/media/2257_Offshore_Grid_Study_FA.pdf. [2015, June 20].

Renewable Energy Caribbean. (2014). Ocean Current Energy, an Untapped Resource. https://renewableenergycaribbean.com/2014/09/01/the-potential-of-ocean-current-energy/.

reNews. (2014). Minesto heading for Florida. http://renews.biz/68909/minesto-heading-for-florida/.

Rio, M.-H., Mulet, S., & Picot, N. (2014). Beyond GOCE for the ocean circulation estimate: Synergetic use of altimetry, gravimetry, and in situ data provides new insight into geostrophic and Ekman currents. *Geophysical Research Letters*, *41*. doi:10.1002/2014GL061773.

Robinson, I. S. (2004). *Measuring the oceans from space*. Berlin: Springer.

Rouault, M. J., & Penven, P. (2011). New perspectives on the natal pulse from satellite observations. *Journal of Geophysical Research, 116,* C07013.

Rouault, M. J., Mouche, A., Collard, F., Johannessen, J. A., & Chapron, B. (2010). Mapping the Agulhas Current from space: An assessment of ASAR surface current velocities. *Journal of Geophysical Research, 115,* C10026.

Scott, R. B., & Wang, F. (2005). Direct evidence of an oceanic inverse kinetic energy cascade from satellite altimetry. *Journal of Physical Oceanography, 35,* 1650–1666.

Sink, K. Sink, K. J., Attwood, C. G., Lombard, A. T., Grantham, H., Leslie, R., et al. (2011). *Spatial planning to identify focus areas for offshore biodiversity protection in South Africa: Final report for the offshore marine protected area project*. Cape Town: South African National Biodiversity Institute.

U.S. Department of the Interior Minerals Management Service. (2007). *Programmatic environmental impact statement for alternative energy development and production and alternate use of facilities on the outer continental shelf: Final environmental impact statement*. USA: Bureau of Ocean Energy Management.

Van Zwieten, J. H., et al. (2014). Evaluation of HYCOM as a tool for ocean current energy assessment.

Van zwieten, J. H., et al. (2015). SS marine renewable Energy—Ocean current turbine mooring. In *Offshore technology conference*. Houston.

Wold, S., Esbensen, K., & Geladi, P. (1987). Principal component analysis. *Chemometrics and Intelligent Laboratory Systems, 2,* 37–52.

Ocean Current Energy Resource Assessment for the Gulf Stream System: The Florida Current

Kevin Haas, Xiufeng Yang, Vincent Neary and Budi Gunawan

Introduction

Ocean currents are the continuous flow of ocean water in persistent directions with a variety of driving forces, spatial locations, and temporal and spatial scales. The major driving forces for large scale currents (on the order of 1000-km-length scale) are the wind stress and density gradients from temperature and salinity variations. At the mesoscale (on the order of 100-km-length scale), ocean currents are also driven by tides, river discharge, and pressure gradients (generated by sea surface slope set up by coastal long waves, for example). However, among these drivers, only astronomical tidal forcing is deterministic. As a result, stochastic types of forecasting are required for ocean current resource assessments.

Ocean basin-wide surface currents are generally wind driven and develop their typical clockwise spirals in the northern hemisphere and counterclockwise rotation in the southern hemisphere because of the imposed wind stresses. The Gulf Stream System (see Fig. 1) is an example of a circulation system driven by the trade winds in the northern hemisphere. These trade winds are caused by a combination of convection air currents and the Earth's rotation. Atmospheric circulation cells observed in both hemispheres are generated by greater atmospheric heating over the Equator relative to northern and southern latitudes; including Hadley cells between the Equator and 30° latitude, and Ferrel cells between 30° latitude and 60° latitude. The surface air currents within these circulation cells are deflected by the Coriolis

K. Haas (✉)
Georgia Institute of Technology, Atlanta, USA
e-mail: khaas@gatech.edu

X. Yang
Chevron Energy Technology Company, Houston, USA

V. Neary · B. Gunawan
Sandia National Laboratories, Albuquerque, USA

Z. Yang and A. Copping (eds.), *Marine Renewable Energy*,
DOI 10.1007/978-3-319-53536-4_9

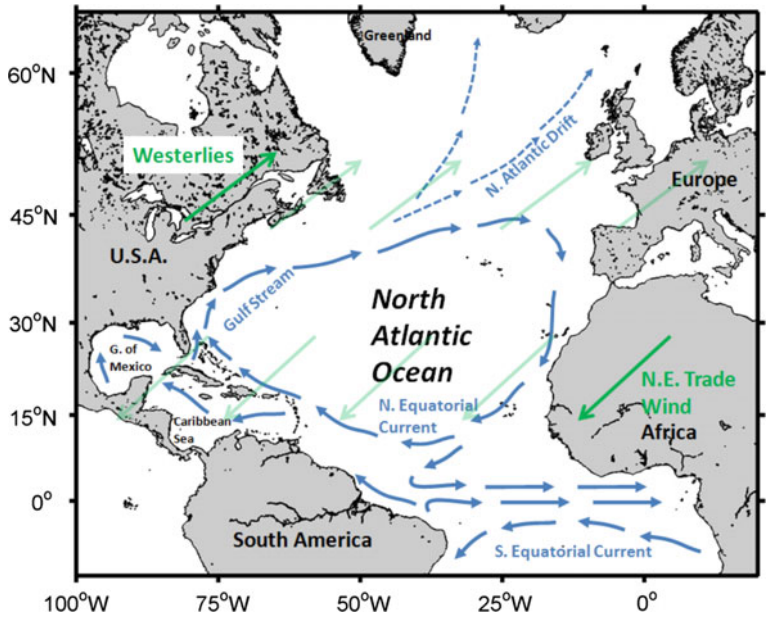

Fig. 1 Schematic of the North Atlantic surface ocean circulation

effect, or the spin of the Earth. The resulting Northeast trade winds and Westerlies in the northern hemisphere drive the ocean current circulation pattern observed in the North Atlantic shown in Fig. 1. The Coriolis effect also intensifies currents at the western boundary of the North Atlantic Ocean.

Beginning in the Caribbean and ending in the northern North Atlantic, the Gulf Stream current is one of the world's most intensely studied current systems. On average, the Gulf Stream current is broad, O(10–100 km), and deep, O(100–1000 m). The current speed is fastest near the surface, with the maximum speed typically exceeding 2 m/s (Stommel 1965; Richardson 1985; Fratantoni 2001). The Gulf Stream System's water volume transport varies seasonally (stronger in the fall and weaker in the winter) and weekly (Kelly and Gille 1990; Zlotnicki 1991; Hogg and Johns 1995). Intra-seasonal variability can account for more than twice that of seasonal transport variability (Schott et al. 1988; Halkin and Rossby 1985). High frequency transport variability on scales from days to weeks appears correlated with wind stress from frontal passages (Mooers and Fiechter 2005). Seasonal variability in the Florida Straits has been shown to be similar to the along channel wind stress as well as the wind stress curl forcing upstream over the Caribbean (Baringer and Larsen 2001).

An ocean current energy converter extracts and converts the kinetic energy in the current into a transmittable energy form such as electricity. A variety of conversion devices have been proposed. Most of these are axial-flow turbines that are analogous to horizontal axis wind turbines. Similar to wind turbines, they can be

designed with large swept areas as ocean depths are on the order of hundreds of meters. Ocean turbines, with diameters on the order of tens of meters and installed capacities up to 1 MW, can be mounted on glider platforms moored to the sea bed, e.g., the US Department of Energy's RM4 device (Neary et al. 2014), or from moored buoys, e.g., (Shirasawa et al. 2016). The available in-stream power per unit area, or power density P_t, is calculated using the equation

$$P_t = \frac{1}{2}\rho V^3 \tag{1}$$

where ρ is the density of the fluid and V is the flow speed. The available power density can be converted to the available energy for a particular device by multiplying by the device rotor swept area.

The total power extraction potential from ocean currents, however, does not simply correspond to the superposition of the power densities from multiple devices. The dynamics of ocean circulation and accumulative effects of converters need to be considered. Various ocean current energy assessments have been performed for the Gulf Stream System with the earliest systematic studies dating back to the 1970s. A research project named "Coriolis Program" predicted about 10 GW of hydrokinetic power could be extracted from the Gulf Stream using turbines (Lissaman 1979). A more conservative prediction suggested up to 1 GW of kinetic energy can be extracted from the Gulf Stream without seriously disrupting climatic conditions (Von Arx et al. 1974). However, neither study provided details of their resource estimates. Hanson et al. (2010) provides an interesting historical overview of assessments and project developments related to Gulf Stream energy extraction.

This chapter focuses on assessing the potential for generating energy from the Gulf Stream System. The overall characteristics related to the energy potential of the Gulf Stream are described. This is followed by several different levels of resource assessment: from the assessment of the undisturbed currents, to idealized modeling of energy extraction, to a full three-dimensional ocean circulation model including energy extraction.

Gulf Stream Characteristics

This section describes the characterization of ocean currents from a probabilistic perspective with an emphasis on the energetic portions of the Gulf Stream System. There have been numerous characterizations of these flows from an oceanographic as well as a hydrokinetic energy perspective using observational as well as numerically modeled data. The main consideration for extracting energy from western boundary currents is that, while the overall volume transport is persistent, the specific location of the flow can be quite variable. Thus for the Gulf Stream System, the practical locations for energy extraction are likely those where variability in the

Gulf Stream position is minimal. Therefore, the two most likely locations are the Florida Straits and offshore of Cape Hatteras, N.C.

The Gulf Stream transports a huge volume of water mass and heat. It starts from the Gulf of Mexico, flows as the Florida Current, and leaves the east coast of the US near Cape Hatteras. The specific point of departure from the coast is constantly changing in time, usually shifting north in the fall and south in the winter (Auer 1987). The volume transport in the Gulf Stream increases from about 30 Sv (1 Sv = 10^6 m^3/sec) in the Florida Current to a maximum of about 150 Sv at approximately 45 W (Larsen and Sanford 1985; Hogg and Johns 1995). The increase in volume transport in the downstream direction is theorized to be from the current speed increase in the deep water, which is due to deep ocean circulation (Hall and Fofonoff 1993; Johns et al. 1995). The Gulf Stream has variations both in space and in time, with fluctuations of transport as large as 30% of the mean observed with different time scales (Greatbatch et al. 1995). The Gulf Stream transport has a strong seasonal variation, strongest in summer and weakest in winter (Niiler and Richardson 1973; Baringer and Larsen 2001). This fluctuation is mostly within the upper 300 m of the ocean and is partly due to seasonal heating and expansion of the surface water (Hogg and Johns 1995). Other variabilities at shorter periods can be attributed to lateral meanders and local wind forcing, among others (Duing 1975; Lee and Williams 1988).

A comprehensive study by Yang et al. (2015) performed a detailed assessment for the Florida Current portion of the Gulf Stream System in the context of utilization for energy extraction. Similar to Duerr and Dhanak (2012), this study primarily relies on numerically modeled data providing high spatial and temporal resolution as well as statistically significant duration (~7 years). Several different ocean model data from various sources were obtained and compared with ocean surface drifter data in terms of their statistical agreement. The data with the highest statistical agreement with surface drifter data were selected for each area. The method and procedure of model selection are documented in great detail in Haas et al. (2013). Of all the data sources evaluated, a combination of the Hybrid Coordinate Ocean Model (HYCOM) and Navy Coastal Ocean Model (NCOM) data had the statistically best agreement with the drifter data and therefore was selected for this study. A total of 7 years of model data were utilized. The validation of the model used a combination of in situ and remote sensing data and is documented by Neary et al. (2012) and Yang et al. (2015).

The spatial variation of the Florida Current is demonstrated through the distribution of the annual mean and standard deviation (STD) of the current speed on the ocean surface as well as in a vertical cross-section plane shown in Figs. 2 and 3. The core of the current where the flow is the strongest is concentrated within about 100 m of the surface layer and spans about half of the channel width. The core of the Florida Current is slightly offset westwards of the channel centerline (Figs. 2a and 3a) reducing the potential cost of transmitting extracted power to shore, assuming extraction devices are likely to be deployed close to the core of the current flow. Figures 2b and 3b show the level of variability of the current speed at each location within the region. The highest temporal variability in the Florida

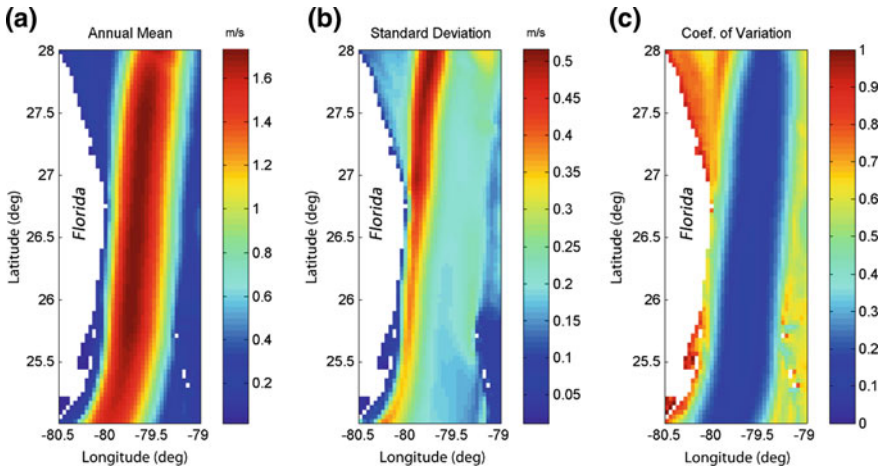

Fig. 2 Florida Current: **a** annual mean surface current speed, **b** standard deviation, **c** coefficient of variation (ratio of the standard deviation to the mean)

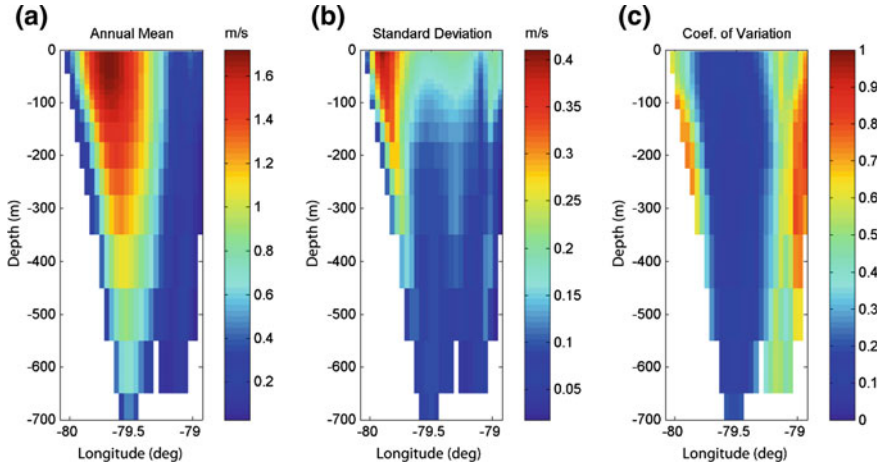

Fig. 3 Cross-sectional distribution of **a** the annual mean current speed, **b** the standard deviation, **c** coefficient of variation (ratio of the standard deviation to the mean) in the Florida Current at the latitude of 26.6264 N

Current is located on the edge of the strongest current facing the Florida shoreline. The variability of the core of the current is relatively weak relative to the mean as seen from the coefficient of variation in Figs. 2c and 3c. Comparing daily and monthly snapshots of the current speed distribution shows that high variation usually occurs near the edge as a direct result of the meandering and seasonal broadening of the core of the current flow.

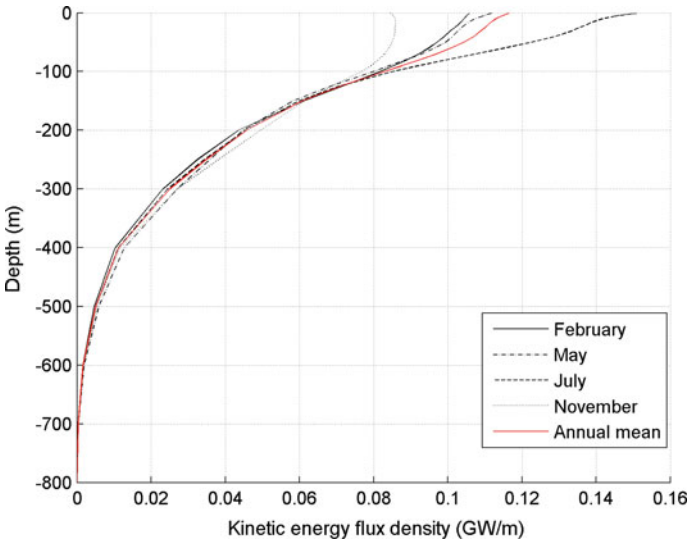

Fig. 4 The vertical kinetic energy flux density in the Florida Current for arbitrary months (Feb., May, Jul., and Nov.) and the annual mean

The kinetic energy flux is a primary indicator of the undisturbed hydrokinetic energy reserve in ocean currents and is computed as the area integral of the power density across the full channel. The mean energy flux in the Florida Current calculated from 7 years of model data is approximately 22.6 GW with variability at multiple time scales from weeks to years. The vertical structure of the energy flux is computed by integrating the energy flux density across the channel width but not over depth. Figure 4 shows the kinetic energy flux density (GW/m) as a function of the depth for 4 different months and the annual mean. These months include the minimum and maximum conditions (November and July). The general shape of different curves in Fig. 4 is similar to the vertical profile of the current speed, strongest near the surface and weakest near the bottom. Interestingly, more than half of the total kinetic energy flux is concentrated in the upper 200 m of the water column in the Florida Current. Monthly variability becomes negligible below 100 m water depth, implying that the monthly variability mostly results from seasonal variation of surface momentum flux such as surface wind stress. The summer season features the highest level of energy flux while winter has the lowest. February and May have flux levels comparable to the annual mean.

Yang et al. (2015) used the 30 years of volume flux data available from the telecommunication cables running almost perpendicularly across the Florida Strait from West Palm Beach, FL to Eight Mile Rock, Grand Bahamas Island (http://www.aoml.noaa.gov/phod/floridacurrent/) to create a longer record of the daily kinetic energy flux. This required the development of an empirical relationship between the volume flux and the kinetic energy flux using the 7 years of overlap between the cable and model data. The predicted mean kinetic energy flux from

30 years of cable data is approximately 22.8 GW, and the standard deviation is approximately 5.4 GW.

Figure 5 shows both monthly and yearly variations of the mean kinetic energy flux computed based on 30 years of data. The 95% confidence interval for the monthly mean energy flux is also plotted in Fig. 5a as error bars to resolve the uncertainty. The mean kinetic energy flux is the highest in the summer, particularly in July when the peak occurs (~25.57 GW). The lowest mean energy flux occurs in November (~20.30 GW), which is in agreement with previous findings. The kinetic energy flux also shows very strong year-to-year variability as seen in Fig. 5b. The annual mean power reaches a high 27 GW in 2002, and a low 18 GW in 1991.

A recent review by Bane et al. (2016) characterized ocean western boundary currents with a particular focus on the Gulf Stream on the South Atlantic Bight where it passes relatively close to shore near Cape Hatteras, NC. Using a combination of observations from a moored acoustic Doppler current profiler (ADCP) and numerical simulations using ROMS, they estimated the mean current to be on the order of 1 m/s. However, there were significant fluctuations on the order of ±1 m/s with time scales of days due to meanders of the Gulf Stream. There were also fluctuations of similar magnitudes with time scales of several weeks due to large along-stream scale shifts of the full current. Using six years of model simulations, they also demonstrated that for fixed locations, there were substantial interannual variations due to year-to-year changes in the level of meandering and shifting of the Gulf Stream. Hanson (2014) looked at the Gulf Stream as it flowed northeast of Cape Hatteras and attributed the increase in volume flux due to energy sources beyond just the winds driving the subtropical gyre. However, the challenges for energy extraction for locations this deep and far offshore are perhaps insurmountable. Hanson et al. (2011) discussed several issues related to the potential for energy extraction from the Florida Current using a variety of data sources including acoustic Doppler current profiler data which showed variability of the current with time scales of days.

Resource Assessment

There are many different types and methods for performing resource assessments for ocean energy projects. To help clarify the types of resource assessments, the International Electrotechnical Commission (IEC) defined a conceptual framework for assessing marine hydrokinetic resources (IEC 2013) which the US Department of Energy (DOE) has adopted (The National Research Council 2013). The overall assessment process is considered in three stages: theoretical, technical, and practical. The theoretical resource consists of the hydrokinetic energy available for conversion without consideration of any turbine properties. In essence, this is the power within the undisturbed flow field. The technical resource is the amount of power that can be generated considering the particular technology to be utilized. This resource assessment incorporates turbine efficiencies and interactions with the

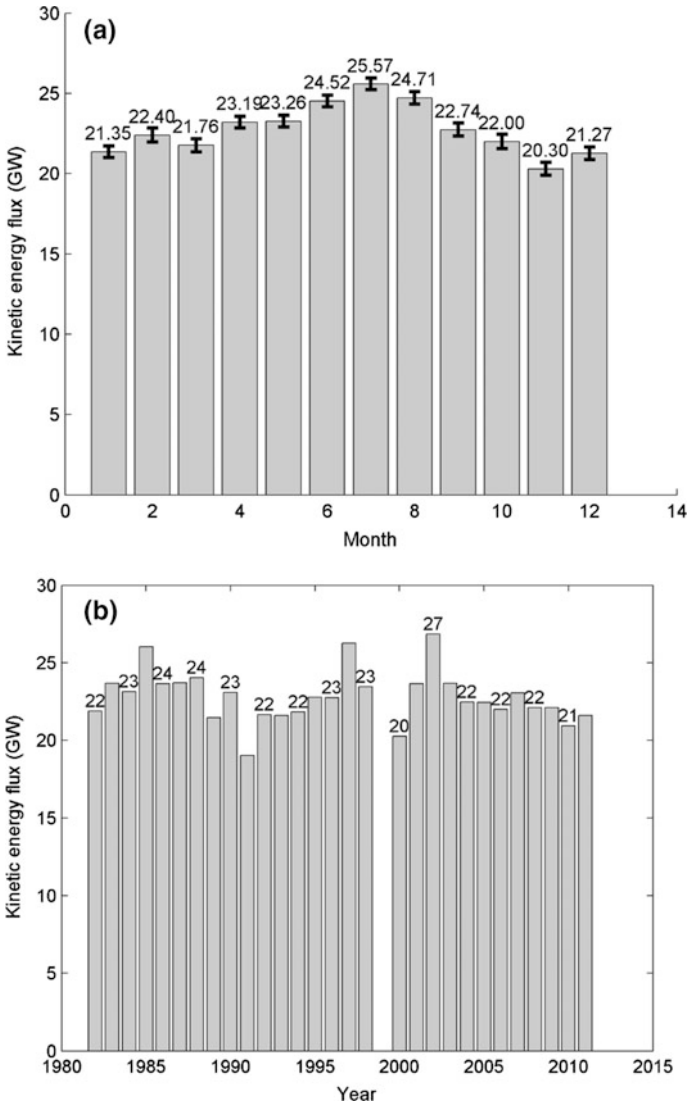

Fig. 5 **a** Monthly (1-Jan, 2-Feb, etc.) variation of mean kinetic energy flux with a 95% confidence interval based on projected 30 years of kinetic energy flux. **b** Yearly variation of mean kinetic energy flux in the Florida Current based on projected 30 years of kinetic energy flux (cable data in the year of 1999 is missing)

flow field and is a fraction of the theoretical resource. Finally, the practical resource includes the additional constraints of turbine operation such as regulatory, environmental, economic, and life cycle constraints.

Undisturbed Flow Assessments

A study by Duerr and Dhanak (2012) considered a fraction of the undisturbed kinetic power density in the Gulf Stream as equivalent to the available power potential. They estimated approximately 20–25 GW of available hydrokinetic power in the Florida Current based on the computer model Hybrid Coordinate Ocean Model (HYCOM) data. Duerr and Dhanak (2012) further stated that the power potential reduces to 1–4 GW if the analysis is limited to a realistic deployment region with consideration of operational constraints such as the array packing density and turbine availability.

From a practical point of view, it is helpful to quantify the undisturbed kinetic power in terms of hypothetical turbine arrays. Although this approach neglects the effects from extraction, it represents an upper bound estimate and helps to determine the approximate size and capacity of turbine arrays necessary to extract a certain amount of power. Yang et al. (2015) assumed that turbines are uniformly deployed 50 m below the sea surface in the Florida Current and used the monthly means of modeled current velocities to calculate the power. The principle velocity component in the Florida Current is northward along the channel, and the undisturbed kinetic power (P_k) from this turbine array is estimated using

$$P_k = \Sigma \frac{1}{2} \rho |V|^3 E_f A_s A_c N \tag{2}$$

where V is the velocity at the assumed turbine depth, ρ is the water density (1025 kg/m^3), E_f is the assumed efficiency (40%), A_s is the swept area of device (1600 m^2), A_c is the surface area of computation cell (~16 km^2), and N is the assumed number of devices per unit surface area (1/4 km^2) corresponding to 2 km spacing between devices. This equation does not account for operational availability or downtime for maintenance and repairs. Also, it is assumed herein that the energy extraction plane of the turbine always orients itself perpendicular to the current so that the velocity is the current speed.

The turbine region is specified within a box area covering the water area between Florida and the Bahamas shown in Fig. 6a; turbines are assumed to be uniformly deployed in this area where the current speed exceeds 1 m/s. The surface area of the turbine region is the area marked by black dots shown in Fig. 6a (approximately 2.0×10^4 km^2). Figure 6b shows the average monthly variation of the power generation from this hypothetical turbine array with error bars representing the level of uncertainty. The peak power is shown to occur in July and reaches almost 7 GW, and the lowest power occurs in November and is about 4.3 GW. The annual mean kinetic power from this hypothetical turbine array is about 5.2 GW corresponding to a mean power per device of approximately 1.1 MW based on approximately 4500 devices installed.

However, the estimate of P_k carries uncertainty and could be varied significantly by adjusting turbine parameters. In addition, the estimate of P_k based on

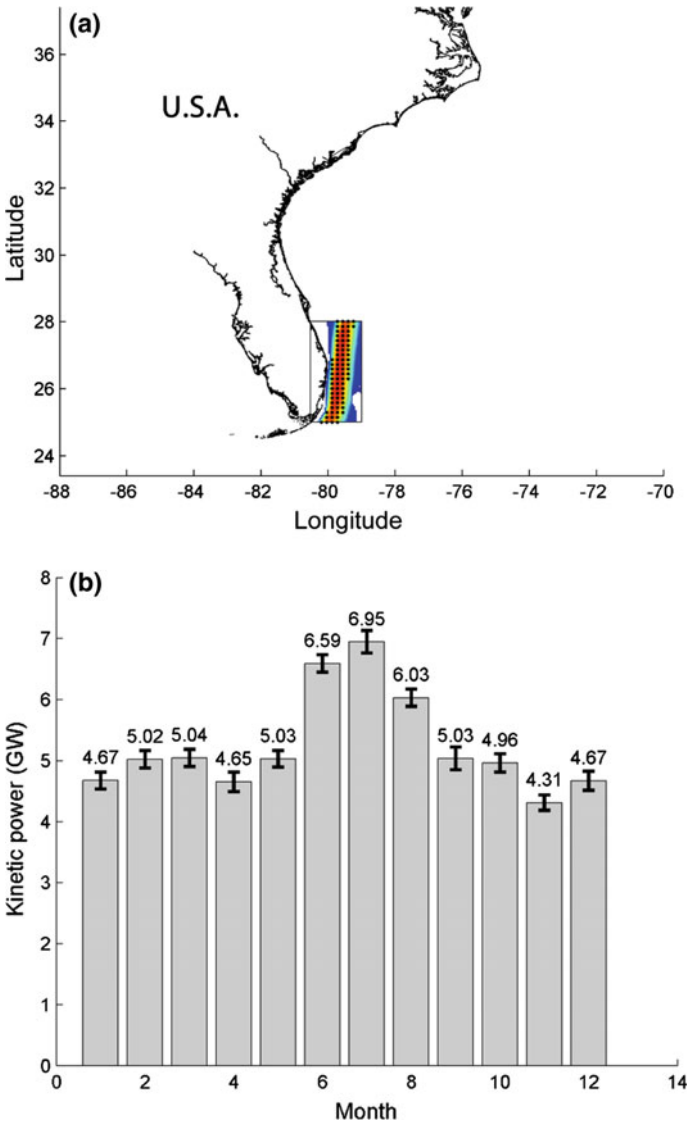

Fig. 6 **a** Map with the box showing the original turbine area and *black dots* representing the area with mean current speed exceeding 1 m/s. **b** Monthly variation of total kinetic power in the Florida Current with 95% confidence intervals

undisturbed power density is only meaningful when the accumulative effect of power extraction on the flow field is relatively small. The current speed is reduced as an increasing amount of energy is extracted and consequently a larger number of turbines are needed to extract the same amount of power. Therefore, the estimate of P_k based on the undisturbed velocity field is only useful for providing an order of

magnitude of available power for the number of devices and is not recommended to be used solely for determining the maximum available power.

Idealized Ocean Model Assessments

While power density is a good indication of the transport of kinetic energy, it is not equivalent to the generation rate of energy. Energy extraction from ocean currents using turbines can be viewed as additional energy dissipation. Therefore, it is helpful to first understand the energy balance in the ocean circulation system. The total energy dissipation from the western boundary currents in the North Atlantic Ocean was predicted to be around 70 GW (Csanady 1989). Another study considered the energy balance between atmosphere and the ocean and estimated about 20 GW of energy from atmospheric wind that drives the circulation in the Atlantic (Wunsch 1998). However, the undisturbed natural dissipation provides limited insight for total possible energy dissipation by additional turbines since these turbines will modify the circulation and hence the natural dissipation as well.

A recent study provided a simple and novel approach of assessing the theoretical energy potential from the ocean circulation by studying the dominant dynamics of the primarily wind-driven circulation system (Yang et al. 2013). This simplified ocean circulation model was based on the Stommel (1948) model, which only considered surface wind stress, Coriolis force, hydrostatic pressure gradient, and friction in the momentum balance. The extractable power from the addition of turbines is estimated through the incorporation of extra energy dissipation by uniform turbine drag. The model was solved analytically, and it was found that a peak power of about 44 GW can be removed from the circulation with the additional turbine drag. This is the maximum extra rate of energy dissipation that the system can support without any consideration of additional constraints such as the number or locations of turbines. It was also found that turbine drag can have a significant impact on the residual volume and energy fluxes in the circulation. The turbine drag may also change the sea level, possibly resulting in a slight sea level rise in offshore Florida and a slight sea level drop in the Bahamas.

Realistically, turbines will only be present in the Gulf Stream System at locations with the strongest currents such as in the Florida Current, as opposed to being applied to the entire domain for the sake of simple analytical solutions. In order to improve the assessment, the model was modified by Yang et al. (2014) to only include localized turbine drag in the central region of the western boundary layer (i.e., the Florida Current) and solved numerically. The quasi-geostrophic shallow water governing equations of the steady state circulation include the two momentum equations and the continuity equation

$$-fv = -g\frac{\partial \eta}{\partial x} - \frac{C_{\text{total}}(x,y)}{H}u - \frac{\tau_0}{\rho H}\cos\left(\frac{\pi}{b}y\right) \tag{3}$$

$$fu = -g\frac{\partial \eta}{\partial y} - \frac{C_{\text{total}}(x,y)}{H}v \tag{4}$$

$$\frac{\partial u}{\partial x} + \frac{\partial v}{\partial y} = 0 \tag{5}$$

where ρ is the constant water density, b is basin width in the meridional (y) direction, H is the water depth, f is the Coriolis parameter, u and v are two velocity components in zonal (x) and meridional (y) directions, η is the sea surface level, C_{total} is the spatially varying drag coefficient associated with natural friction and turbulence (C_d) and turbines (C_t) as $C_{\text{total}} = C_d + C_t$, and τ_0 is the maximum wind stress. These equations use the shallow water approximation (no variations in the vertical direction) and assume hydrostatic pressure. These assumptions are reasonable given the small ratio of ocean depth (on the order of 1 km) to its horizontal extensions (on the order of 1000 km). Non-linear terms in the governing equations are neglected given the small Rossby number for the large scale circulation in the ocean (Vallis 2006). The Coriolis parameter is approximated as $f = f_0 + \beta y$ by adopting the β plane approximation. These equations can be combined and solved by introducing a stream function. Because of the spatially varying drag coefficient, the stream function governing equation is solved using a finite difference scheme described in Yang et al. (2014). Finally, the equation is calibrated such that the model produces reasonable volume and energy flux for the undisturbed flow conditions without turbines, matching the mean conditions from the seven years of HYCOM data.

To realistically represent the scenario of extracting power from the fastest western boundary currents, the turbine drag coefficient profile is specified as

$$C_t(x,y) = C_{t0}e^{-\frac{\left(x^2 + \left(y - \frac{1}{2}b\right)^2\right)}{\epsilon}} \tag{6}$$

where C_{t0} is the peak value of the turbine drag coefficient, and ϵ is a parameter controlling the approximate area of the turbine region. Five different scenarios of localized turbine dissipation are formed using different values of ϵ. Figure 7a shows the approximate areas of localized turbine regions (boundaries defined as contour lines of 50% of the peak drag coefficient) for 5 different scenarios, ranging from about 0.1% (scenario A) to approximately 23% (scenario E) of the entire basin area. Different scenarios can be related to different realistic spatial coverage. For example, scenario A has an approximate area of 2×10^4 km^2, which is similar to the actual surface area of the Florida Strait. Scenario C has an area of approximately 1.7×10^5 km^2, which is similar to the surface area of the Gulf Stream along the US east coast extending from Florida to Cape Hatteras. The sensitivity of energy dissipation by turbines to the peak turbine drag coefficient C_{t0} is shown in Fig. 7b.

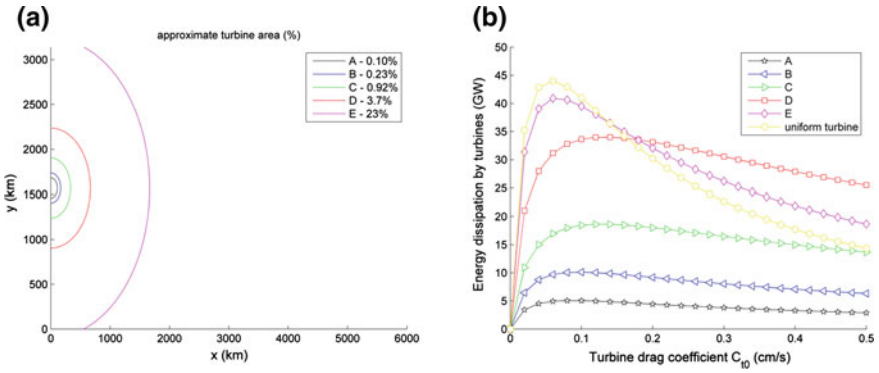

Fig. 7 **a** Approximate areas of turbine regions for 5 different scenarios, **b** energy dissipation by turbines as a function of the peak turbine drag coefficient C_{t0} for 5 different scenarios

For different scenarios, the energy dissipation from localized turbines with respect to different levels of turbine drag coefficients all share similar trends. As the turbine drag coefficient increases from zero, the energy dissipation by turbines increases until it reaches its peak. Beyond the peak, further increasing the turbine drag coefficient reduces the total energy dissipation from turbines. As the area of the turbine region increases from scenario A to scenario E, the peak energy dissipation by turbines increases accordingly and approaches an upper bound corresponding to the uniform turbine drag coefficient. The peak power removal from the flow by turbines is found to be about 5.1 GW, occurring at $C_{t0} = 0.08$. The peak power removal increases to approximately 10.1 GW in scenario B and 18.6 GW in scenario C. In scenario D, the turbine area covers almost the entire western boundary (3.7% of the basin area) with fast currents, and the peak power removal reaches about 34 GW at $C_{t0} = 0.14$. In scenario E, the turbine area covers almost the entire western quarter of the basin (23% of the basin area), and the peak energy removal rate (40.9 GW) is very close to the case with uniform turbine drag coefficient (44 GW).

In Yang et al. (2014), this simplified model was also used to evaluate the effects of the energy extraction on the hydrodynamics of the entire Gulf Stream System. It was found that the localized turbine drag significantly reduces the meridional velocity component of ocean currents in the turbine region. The additional turbine drag also modifies the zonal velocity component in the turbine region, primarily changing its direction, resulting in redirection of the Gulf Stream flow. The net result is reduced flow in the turbine area while the core of the current shifts further offshore to avoid the region of high resistance. A significant sea surface drop is observed in the turbine region due to modification of the local pressure gradient force, which is accompanied by a negligible sea surface rise in the rest of the basin. Localized turbine drag significantly reduces residual kinetic energy flux in the circulation. However, its influence on the residual volume flux depends on the size the turbine region.

Numerical Ocean Model Assessment

Large scale energy extraction from the Gulf Stream will affect the natural flow condition and therefore have an impact on the background flow. The idealized approach in the previous subsection provides guidance as to the impacts of the energy extraction, based on the bulk flow; however, this simplification makes it difficult to include the impact of the actual bottom topography and forcings on the currents. Therefore, a model with a more realistic representation of the Gulf Stream System using a full numerical simulation of the North Atlantic circulation can provide a higher quality resource assessment. In addition, more detailed evaluations of the large scale impacts of energy extraction can be evaluated.

In Haas et al. (2014), simulations of the full Northern Atlantic Ocean using the model HYCOM were performed including the effect of energy extraction from turbines. The additional momentum sink by the turbines is included in the governing equations as an extra retarding force within the computational cells where conversion devices are located. The retarding force per unit volume in the i direction (F_i) is

$$F_i = \frac{1}{2}\frac{\rho C_{\text{ext}}}{\Delta h}|\vec{V}|V_i \tag{7}$$

where C_{ext} is an extraction coefficient, $\vec{V}$ is the velocity in the computational cell, and Δh is the model layer thickness, which varies with depth and location. The total extracted power is found as the sum

$$P = \sum_{i,j,l}\frac{1}{2}\rho C_{\text{ext}}|V_{i,j}|^3\Delta x_{i,j,l}\Delta y_{i,j,l} \tag{8}$$

where i and j are the horizontal computation indices, l is the computational layer, and $\Delta x_{i,j,l}\Delta y_{i,j,l}$ are the horizontal grid spacings.

In this study, three different turbine distribution cases were utilized: 1—turbines uniformly distributed throughout the Florida Current between 50 and 200 m depth, 2—turbines uniformly distributed in a single array across the Florida Strait between 60 and 100 m depth, and 3—turbines uniformly distributed between 60 and 100 m depth along the center line of the Florida Current with the same surface area as case 2. The model is forced with the monthly climatology from the Levitus and Boyer (1994) climatology files. The model is spun up for 6 years without extraction, 3 months with extraction and then a further 3 years with extraction, which is averaged together to give a "typical" year.

The additional turbine drag slows down the current flow through the Florida Strait channel and causes reduction in the residual kinetic energy flux in the channel. Figure 8 shows the original kinetic energy flux in the Florida Current together with the residual energy flux for the 3 extraction cases. The power dissipation by turbines from the three cases is also shown in Fig. 8. It is shown that the residual energy flux and the power dissipation do not add up to the original energy

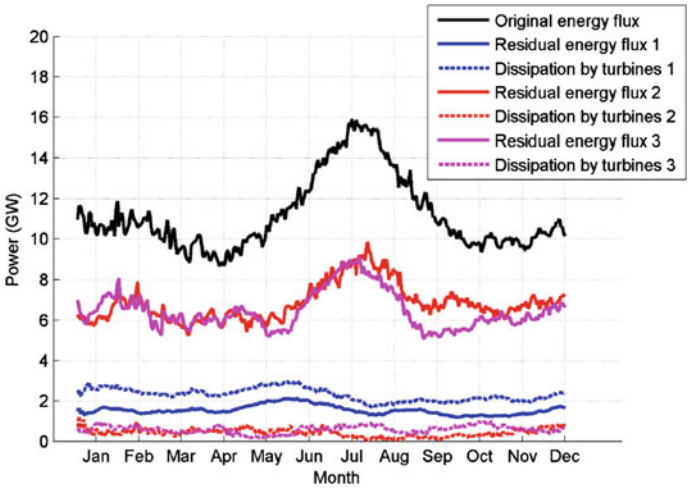

Fig. 8 The 3-year mean kinetic energy flux and power dissipation by turbines for the different cases

flux, indicating a net kinetic energy loss in the Florida Current due to the diversion of the course of the current flow. It is interesting to note that when the energy flux is the strongest in summer time, the power extraction is not necessarily the strongest due to higher bypassing occurring in summer leading to lower energy extraction.

The effect of power extraction on the hydrodynamics of the flow field is analyzed through the change of surface current magnitude. Figure 9a shows the difference of the mean surface current speed between case 1 and the baseline. The rerouting of the surface current flow is very obvious in this case. The mean current speed in the Florida Strait drops by up to 1 m/s. As the upper portion of the waterway in the Florida Strait is partially blocked by the presence of the turbines, the surface flow entering the Florida Strait changes direction and moves toward the southeast to go through the channel between Cuba and the Bahamas. Further downstream it flows along the east coast of the Bahamas to the north and merges back with the original Gulf Stream. The ocean current speed increase on the east of the Bahamas due to the rerouting can be as high as 0.8 m/s. Therefore, the current exiting from the Florida Strait slows down, and the newly formed strong flow occurs to the east, resulting in a slight shift of the path of the Gulf Stream to the east.

For cases 2 and 3, due to the lower strength of power extraction, a prominent rerouting of the surface ocean current does not occur (Fig. 9b, c). The effect of the power extraction has a smaller spatial extent, and most of the flow modification is located in the vicinity of the turbine region. The location immediately downstream of the turbine region exhibits the greatest current speed drop of about 0.6–0.7 m/s. The surface current speed downstream of the turbine region to the east of the Gulf Stream path increases as a result of the flow redirection. The current speed increases on both sides of the turbine area as the flow seeks to bypass the area with high turbine resistance.

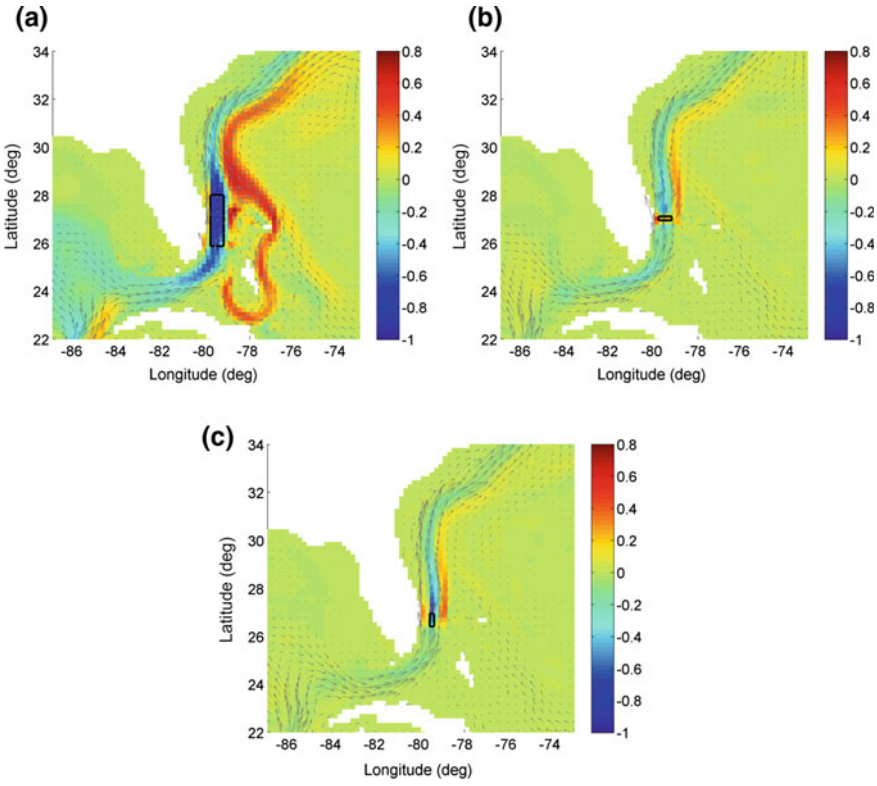

Fig. 9 Change in mean surface current speed for **a** case 1, **b** case 2, and **c** case 3. The turbine regions are highlighted with a *black box*

The effect of power extraction on the hydrodynamics of the flow field is also demonstrated by the mean water level change. As additional turbine drag changes the local momentum balance, the pressure gradient is modified accordingly, which in turn leads to modified sea surface height (SSH). The maps of water level difference between the undisturbed case and three cases with power extraction are shown in Fig. 10 with arrows showing the current directions. As turbine drag is added in the Florida Current in case 1, we observe a significant water level drop in the vicinity of the turbine region, and the maximum water level drop is approximately 0.5 m. Furthermore, a general water level rise along the coast of the Gulf of Mexico and Florida is also seen. The greatest water level increase could reach as high as 0.2 m. For cases 2 and 3, since power is extracted from a much smaller area of the Florida Current, the effect in terms of water level change is of similar nature but relatively weaker than in case 1. The area downstream of the turbine region with significant water level drop becomes smaller. The greatest water level rise occurs along the Florida coast upstream of the turbine region. Similarly, a water level rise

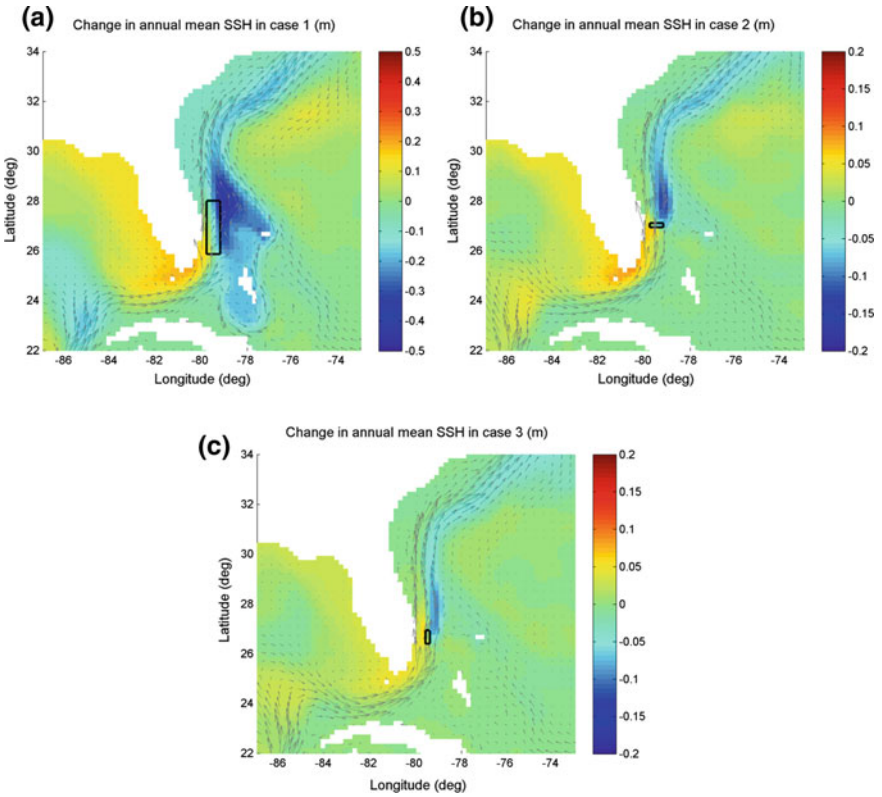

Fig. 10 Change in mean sea surface height for **a** case 1, **b** case 2, and **c** case 3. The turbine regions are highlighted with a *black box*

is seen along the most of the Gulf coast. Generally, the turbine arrangement in case 2 is shown to have greater impact on the SSH than in case 3 due to relatively greater turbine cross-sectional area in the flow direction.

Summary

The Gulf Stream System provides a viable renewable energy source, although regionally concentrated, such as the portion (Florida Current) constrained in the Florida Strait. The overall characteristics related to the energy potential of the Gulf Stream have been described based on 7 years of model simulations and 30 years of volume flux observations. Within the Florida Current portion of the Gulf Stream System, the mean kinetic power was found to be over 22 GW with a standard deviation near 6 GW. Although the largest currents and hence higher energy are near the surface, the majority of the variability was found to be contained within the

top 100 m of the water column. Therefore, turbine deployment schemes will need to take this into consideration.

Assessments based on the undisturbed flow indicated that deployment on the order of 4500 turbines could average over 5 GW of power. Obviously, larger and more efficient turbines than assumed here would result in much fewer turbines to extract the same amount of power. The drawback of this assessment method is that the deployment of such a large number of turbines would undoubtedly have an impact on the flow. Therefore, in order to quantify the effects of the energy extraction on the circulation to obtain a better estimate of the available power, idealized and realistic modeling of the ocean circulation were presented. The idealized model indicates that a mean of 5 GW of power could be dissipated within the Florida Straits, with much more power dissipated if broader regions are considered for energy extraction.

These assessments all provide the theoretical energy that could be generated. The technical resource assessment would determine the electricity that could be generated based on technology efficiencies. However, technical resource assessments are hampered by uncertainties in technology performance and lack of deployment and operational experience.

Taking this another step further, practical resource assessments which account for all other factors involved in quantifying the amount of electricity that could be produced are hampered by uncertainties determining social, economic, and environmental constraints. The practical constraints on ocean current energy extraction, such as the acceptable range of impacts on the flow as was shown with the realistic 3D ocean model simulation, lead to a reduction in the assessment of the power available. While it is not feasible at this time to quantify all the possible constraints even if only 30% of the estimated 5 GW of kinetic power is recovered, the power generation from this completely renewable energy source is more than that from a typical nuclear power plant, enough to support a million homes.

References

Auer, S. (1987). Five-year climatological survey of the Gulf Stream System and its associated rings. *Journal of Geophysical Research, 92,* 11709–11726.

Bane, J. M., He, R., Muglia, M., Lowcher, C. F., Gong, Y., & Haines, S. M. (2016). Marine hydrokinetic energy from western boundary currents. *Annual Review of Marine Science*, *9*(1).

Baringer, M. O., & Larsen, J. C. (2001). Sixteen years of Florida Current transport at 27N. *Geophysical Research Letters, 28*(16), 3179–3182.

Csanady, G. T. (1989). Energy-dissipation and upwelling in a western boundary current. *Journal of Physical Oceanography, 19,* 462–473.

Duerr, A. E. S., & Dhanak, M. R. (2012). An assessment of the hydrokinetic energy resource of the Florida Current. *IEEE Journal of Oceanic Engineering, 37,* 281–293.

Duing, W. (1975). Synoptic studies of transients in the Florida Current. *Journal of Marine Research, 33,* 53–73.

Fratantoni, D. M. (2001). North Atlantic surface circulation during the 1990's observed with satellite-tracked drifters. *Journal of Geophysical Research Oceans, 106,* 22067–22093.

Greatbatch, R., Lu, Y., DeYoung, B., & Larsen, J. (1995). The variation of transport through the straits of Florida: A barotropic model study. *Journal of Physical Oceanography, 25*(1), 2726–2740.

Haas, K., Fritz, H., French, S., & Neary, V. (2013). Assessment of energy production potential from ocean currents along the United States coastline. doi:10.2172/1093367.

Haas, K., Yang, X., & Fritz, H. (2014). Modeling impacts of energy extraction from the Gulf Stream System. Marine Energy Technology Symposium, April 2014, Seattle WA.

Hall, M., & Fofonoff, N. (1993). Downstream development of the Gulf Stream from 68 to 55W. *Journal of Physical Oceanography, 23*(C1), 225–249.

Halkin, D., & Rossby, T. (1985). The structure and transport of the Gulf Stream at 73° W. *Journal of Physical Oceanography, 15,* 1439–1452.

Hanson, H. P. (2014). Gulf Stream energy resources: North Atlantic flow volume increases create more power. *Ocean Engineering, 87,* 78–83.

Hanson, H. P., Skemp, S. H., Alsenas, G. M., & Coley, C. E. (2010). Power from the Florida Current: A new perspective on an old vision. *Bulletin of the American Meteorological Society, 91*(7), 861.

Hanson, H. P., Bozek, A., & Duerr, A. E. (2011) The Florida Current: A clean but challenging energy resource. *Eos Transactions AGU*, *92*(4).

Hogg, N. G., & Johns, W. E. (1995). Western Boundary Currents. *Reviews of Geophysics, 33,* 1311–1334.

IEC (2013). TS 62600-1:2013 Marine energy—Wave, tidal and other water current converters - Part 1: Terminology.

Johns, W. E., Shay, T. J., Bane, J. M., & Watts, D. R. (1995). Gulf Stream structure, transport, and recirculation near 68w. *Journal Geophysical Research, 100*(C1), 817–838.

Kelly, K. A., & Gille, S. T. (1990). Gulf-Stream surface transport and statistics at 69-Degrees-W from the geosat altimeter. *Journal of Geophysical Research Oceans, 95,* 3149.

Larsen, J. C., & Sanford, T. B. (1985). Florida Current volume transports from voltage measurements. *Science, 227*(4684), 302–304.

Lee, T., & Williams, E. (1988). Wind-forced transport Fluctuations of the Florida Current. *Journal of Physical Oceanography, 18,* 937–946.

Lissaman, P. B. S. (1979). Coriolis Program. *Oceanus, 22,* 23–28.

Levitus, S., & Boyer, T. (1994). World ocean atlas 1994. Tech. rep., NOAA Atlas NESDIS, NOAA, Silver Spring, Md.

Mooers, C. N., & Fiechter, J. (2005). Numerical simulations of mesoscale variability in the Straits of Florida. *Ocean Dynamics, 55*(3–4), 309–325.

National Research Council (NRC) (2013). An Evaluation of the U.S. Department of Energy's Marine and Hydrokinetic Resource Assessments. The National Academies Press.

Neary, V. S., Gunawan, B., & Ryou, A. S. (2012). Performance evaluation of HYCOM-GOM for hydrokinetic resource assessment in the Florida Strait, Technical Report: ORNL/TM-2012/221 Available at: https://wiki.ornl.gov/sites/publications/Files/Pub36784.pdf, Oak Ridge National Laboratory, Oak Ridge, TN, 2012.

Neary, V. S., Previsic, M., Jepsen, R. A., Lawson, M., Yu, Y., Copping, A. E. et al. (2014). Methodology for design and economic analysis of Marine Energy Conversion (MEC) technologies. SAND2014-9040, Sandia National Laboratories, March 2014. 261 pages.

Niiler, P., & Richardson, W. (1973). Seasonal variability of the Florida Current. *Journal of Marine Research, 31,* 144–167.

Richardson, P. L. (1985). Average velocity and transport of the Gulf-Stream near 55w. *Journal of Marine Research, 43,* 83–111.

Schott, F. A., Lee, T. N., & Zantopp, R. (1988). Variability of structure and transport of the Florida Current in the period range of days to seasonal. *Journal of Physical Oceanography, 18*(9), 1209–1230.

Shirasawa, K., Tokunaga, K., Iwashita, H., & Shintake, T. (2016). Experimental verification of a floating ocean-current turbine with a single rotor for use in Kuroshio currents. *Renewable Energy*, *91*, 189–195.

Stommel, H. (1948). The westward intensification of wind-driven ocean currents. *Transactions American Geophysical Union, 29,* 202–206.

Stommel, H. (1965). *The Gulf Stream: A physical and dynamical description* (2nd ed.). Berkeley, CA: University of California Press.

Vallis, G. (2006). *Atmospheric and oceanic fluid dynamics: fundamentals and large-scale circulation*, Cambridge University Press.

Von Arx, W., Stewart, H., & Apel, J. (1974). The Florida Current as a potential source of usable energy. In *Proceedings mac arthur workshop feasibility of extracting usable energy from the Florida Current* (pp. 91–101).

Wunsch, C. (1998). The work done by the wind on the oceanic general circulation. *Journal of Physical Oceanography, 28,* 2332–2340.

Yang, X., Haas, K., & Fritz, H. (2013). Theoretical assessment of ocean current energy potential for the Gulf Stream System. *Marine Technological Society Journal*, *47*(4).

Yang, X., Haas, K., & Fritz, H. (2014). Evaluating the potential for energy extraction from turbines in the Gulf Stream System. *Renewable Energy, 72,* 12–21.

Yang, X., Haas, K., Fritz, H., French, S., Shi, X., Smith, B., et al. (2015). National geodatabase of ocean current power resource in USA. *Renewable and Sustainable Energy Reviews, 44,* 496–507.

Zlotnicki, V. (1991). Sea-level differences across the Gulf-Stream and Kuroshio Extension. *Journal of Physical Oceanography, 21,* 599–609.

Marine Hydrokinetic Energy in the Gulf Stream Off North Carolina: An Assessment Using Observations and Ocean Circulation Models

Caroline F. Lowcher, Michael Muglia, John M. Bane, Ruoying He, Yanlin Gong and Sara M. Haines

Introduction

Marine hydrokinetic (MHK) energy, the kinetic energy in moving seawater, is one potential renewable energy source for electricity generation. Almost all MHK energy is in ocean surface waves, tidal motions, and large-scale (non-tidal) currents. In this chapter, we consider the potential for harvesting MHK energy from

C.F. Lowcher (✉)
Scripps Institution of Oceanography, University of California,
San Diego, La Jolla, CA 92093, USA
e-mail: clowcher@ucsd.edu

M. Muglia
University of North Carolina Coastal Studies Institute,
Wanchese, NC 27891, USA
e-mail: Muglia@csi.northcarolina.edu

J.M. Bane · S.M. Haines
Department of Marine Sciences, University of North Carolina,
Chapel Hill, NC 27599, USA
e-mail: bane@unc.edu

S.M. Haines
e-mail: sarahaines@unc.edu

R. He · Y. Gong
Department of Marine, Earth, and Atmospheric Sciences,
North Carolina State University, Raleigh, NC 27695, USA
e-mail: rhe@ncsu.edu

Y. Gong
e-mail: ygong3@ncsu.edu

Z. Yang and A. Copping (eds.), *Marine Renewable Energy*,
DOI 10.1007/978-3-319-53536-4_10

large-scale ocean currents to generate electricity using moored submarine turbines. A worldwide survey of ocean currents using Hybrid Coordinate Ocean Model (HYCOM) simulations shows that the western boundary currents (WBCs) in the wind-driven subtropical gyres are essentially the only large-scale currents with flow speeds sufficiently fast to be considered for commercial installation of electricity-generating turbines (VanZwieten et al. 2013; Bane et al. 2017). These WBCs include the Gulf Stream, Kuroshio Current, North Brazil Current, Agulhas Current, Somali Current, and East Australian Current (Imawaki et al. 2013).

We provide herein an assessment of the MHK energy and power density in the Gulf Stream offshore of North Carolina in the region of the Carolina Capes (Cape Hatteras, Cape Lookout, and Cape Fear), based on direct observations of ocean currents and ocean circulation model simulations. Our study region off North Carolina is one of the two locations along the Gulf Stream off the southeastern US coast where the Gulf Stream flows close to the coastline (Fig. 1). The other location is within the Florida Straits (see Haas et al. chapter "Ocean Current Energy Resource Assessment for the Gulf Stream System: The Florida Current" in this volume). The proximity of the Gulf Stream to the shoreline and coastal population centers in these areas, and its limited meandering relative to the rest of the southeastern US coast, makes these two locations desirable for possible future commercial development. Chapter "Ocean Current Energy Resource Assessment for the Gulf Stream System: The Florida Current" by Haas et al. in this volume provides a model-based assessment of MHK energy in the Florida Current, which is the portion of the Gulf Stream within the Florida Straits.

To examine the power (kinetic energy per unit time) in the Gulf Stream flow off North Carolina, we use current observations from moored and boat-mounted acoustic Doppler current profilers (ADCPs) and ocean surface-current radars, and simulations of ocean currents by a regional ocean circulation model. This model-data approach gives estimates of how much power is available for the resource in this region, delineates how the power varies in space and time, and will help determine which areas off North Carolina are optimal for future deployments of MHK devices. This approach also provides for model-observation comparisons of current speed and power, thereby revealing the confidence that may be placed in model predictions of ocean power at times and at locations where observations are unavailable. In the following discussion, we present the characteristics of Gulf Stream power. The engineering, environmental, legal, financial, and other use considerations that will likely affect the development of commercial MHK energy harvesting facilities are not our focus here and thus are not discussed. Details about these subjects may be found in other publications, for example, Boehlert and Gill (2010), Neary et al. (2014), Brown et al. (2015), and Li et al. (2017). In the next section, we describe pertinent aspects of MHK energy, and in section "The Gulf Stream", we give a description of the Gulf Stream off the southeastern US coast. Section "Assessing MHK Energy and Power Density" presents the available data sets to determine MHK energy, and section "MHK Energy from the Gulf Stream Along North Carolina" discusses the speed and power at particular locations off the coast of North Carolina, including their temporal and spatial variations.

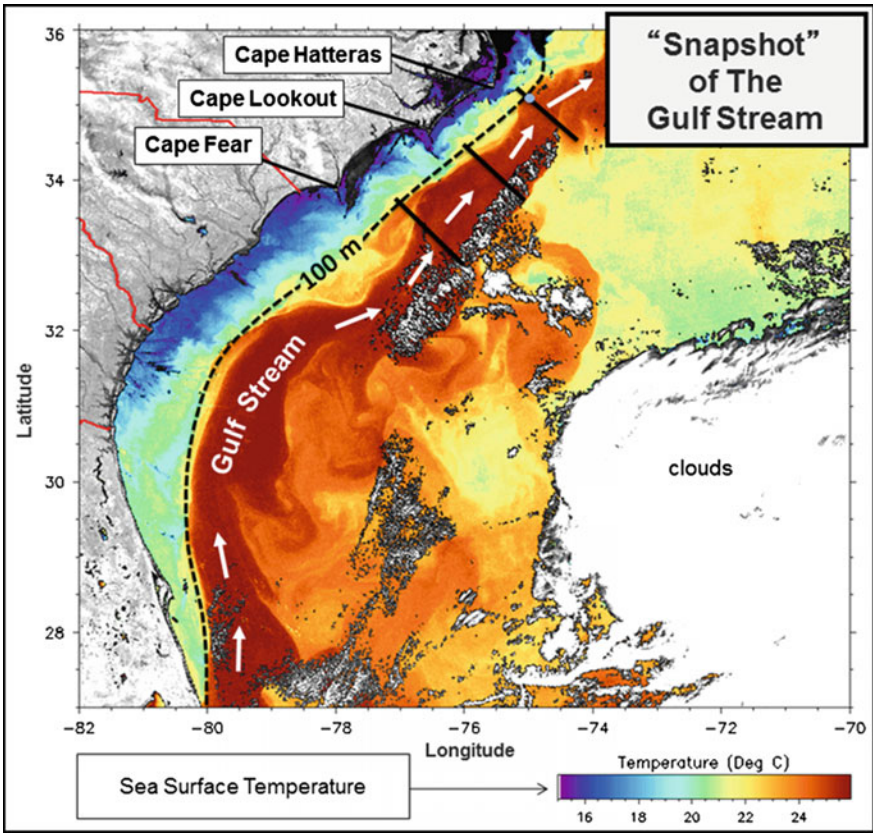

Fig. 1 A sea surface temperature "snapshot" showing the warm Gulf Stream flowing poleward along the southeastern US coastline in March 2008. Note the wavelike meandering of the path of the Gulf Stream, especially noticeable north of 32° N latitude. Raleigh Bay is located between Cape Hatteras and Cape Lookout, and Onslow Bay is between Cape Lookout and Cape Fear. The three cross-isobath transects that have been studied in detail are shown as *solid black lines* orthogonal to the coastline. The Gulf Stream is closest to the coastline off Cape Hatteras, North Carolina, and within the Florida Straits, south of 27.5° N latitude, where the continental shelf is relatively narrow. The 100-m isobath (the seaward edge of the continental shelf) is denoted by the *dashed black line*

MHK Energy and Power Density

Harvesting the Gulf Stream's MHK energy with moored submarine turbines is a type of "in-stream" power generation, meaning it does not use water impoundment like a hydroelectric power plant that stores water behind a dam (VanZwieten et al. 2014). Kinetic energy flux in an oceanic current is the amount of MHK energy that flows through a unit cross-sectional area oriented perpendicular to the current

direction per unit time. Kinetic energy flux is equivalent to the power density, P (in W m^{-2}), of the current, and it is given by

$$P = 1/2\,\rho S^3$$

where ρ is the density of seawater (taken to be 1025 kg m^{-3} in our power assessment) and S is the current speed (in m s^{-1}). The total power in the current flowing past a submarine turbine is P integrated over the surface area, A, swept by the turbine blades (the "blade circle"). For a current speed that is non-varying across the cross-sectional area swept by the turbine blades, the total power is P times A. To address the Gulf Stream's power density off the North Carolina coastline, we must know the current speed, and in this chapter, this is provided by the ADCP measurements and the numerical model simulations.

Submarine electricity-generating turbines are basically underwater versions of wind turbines used for electrical power generation, which would likely be moored to the ocean bottom using anchor lines (e.g., Corren et al. 2013) as opposed to solid masts like those used for wind turbines. Although there are presently no large size submarine turbines that would be appropriate for commercial use in large-scale ocean currents, smaller versions are presently operating in many locations in inshore and estuarine waters (e.g., www.verdantpower.com). Neary et al. (2014) present a model study of a submarine turbine that has a rotor diameter of 33 m and a 1 MW power rating. The pertinent operational characteristics of this model turbine (Fig. 2) are start-up speed = 0.5 m s^{-1} (no power generated if the current speed is below this), maximum-rotation-rate speed = 1.7 m s^{-1} (maximum power of 1 MW generated if the current speed exceeds this), and maximum rotor power coefficient = 0.48 (power harvested from the current is 48% of the current's power density times the blade circle area).

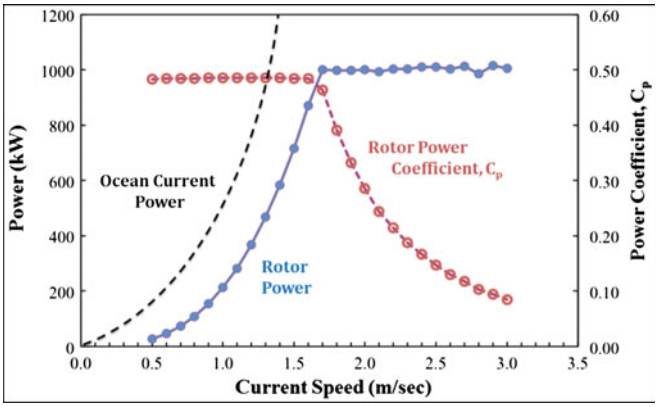

Fig. 2 Ocean current power, rotor power, and power coefficient versus current speed for the rotor on the model submarine turbine presented by Neary et al. (2014). This is a 33-m-diameter, three-blade rotor. (Figure from Bane et al. 2017, adapted from Neary et al. 2014)

Siting an array of subsurface turbines off North Carolina will take into account the power available at the site (section "MHK Energy from the Gulf Stream Along North Carolina"), ecological and bottom geological properties, proximity of the array to the coastline (for cable connections from the turbine array to shore), and onshore electrical grid connection locations. The array site would likely be on the upper portion of the continental slope, as shown in Fig. 3, because this positions the turbines relatively close to shore, in water depths that will allow reasonable mooring design, and near the high-speed core of the Gulf Stream current. Turbines will need to be positioned so that all hardware is at least 30 m or so below the surface in order to keep the machinery out of the active surface wave zone and below surface ship traffic.

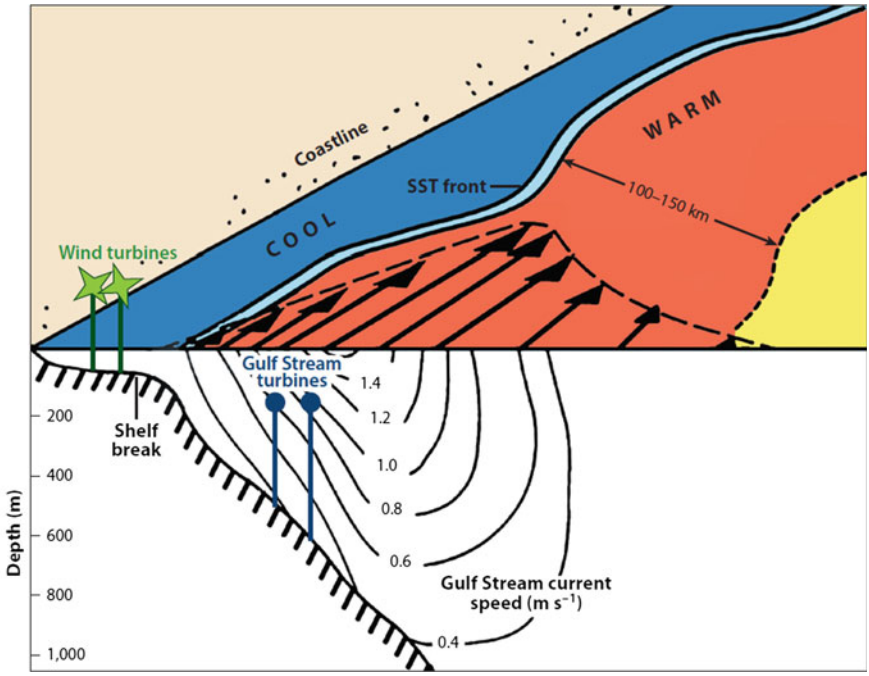

Fig. 3 A schematic of the Gulf Stream current off the southeastern US coastline. The inshore edge of the Stream, indicated by the sea surface temperature (SST) front, is typically located near the shelf break (~40 km from the coastline near Cape Hatteras, ~100 km from the coastline off Georgia, and a few kilometers from the coastline off southeast Florida). The main Gulf Stream jet meanders as it flows over the continental slope, seaward of the shelf break. Surface-current arrows are drawn with a typical profile showing the lateral current shear. The lengths of the arrows and the subsurface isotach curves show the fastest speed at the surface in the core of the current. These speeds diminish in the *horizontal* and *vertical* directions away from the surface-current maximum. Subsurface current turbines (*blue circles*) are shown moored on the upper portion of the continental slope. For reference, offshore wind turbines might be moored on the shallower continental shelf, where current speeds are much lower than in the Gulf Stream. (Figure from Bane et al. 2017.)

The Gulf Stream

The Gulf Stream, like most WBCs, is a narrow (~100 km in width), deep (~1 km in vertical extent) jetlike flow that has a maximum surface-current speed often in excess of 2 m s^{-1} (Imawaki et al. 2013). Current speed decreases in any direction away from this surface maximum. These characteristics are shown schematically in Fig. 3. Off Cape Hatteras, the inshore edge of the Gulf Stream is approximately 40 km (~25 miles) from shore, where surface-current speeds along the edge are roughly 0.2 m s^{-1}. To reach the core, where the fastest speeds can be found, is an additional 30–40 km. This is based on the cross-current extent of the Stream, and the fact that its cyclonic shear zone is roughly the inner third of the Gulf Stream and the anticyclonic shear zone is the other two-thirds, thus leading to an asymmetry in the current's jetlike shape. Cape Hatteras is the closest location to the Gulf Stream along the US east coast north of the Florida Straits where it is only several km from Fort Lauderdale. The volume transport in the Straits is approximately 30 Sv (Barringer and Larsen 2001), and the transport off Cape Hatteras is typically about 90 Sv (Halkin and Rossby 1985) (1 Sv = 10^6 m^3 s^{-1}). Another apparent feature in Figs. 1 and 3 is the wavelike, meandering path of the Stream (Webster 1961). This meandering pattern propagates poleward, and each meander wave has an alongshore wavelength between 100 km and a few hundred km (Tracey and Watts 1986). At a fixed location, it will take from around 3 days to as many as 20 days for one meander wavelength to propagate past (the "meander period") (Bane et al. 1981). This means that the Gulf Stream jet will move closer to shore for about half of the meander period, then move offshore again for the next half-period. This lateral meandering motion of the Stream's narrow jet will cause the current speed at a fixed turbine location to increase and decrease with a meander's period. Another type of motion that the path of the Gulf Stream undergoes from time to time is a longer term lateral shift of the jet's path (Bane and Dewar 1988; Quattrocchi et al. 2012). This can move the Stream laterally relative to a moored turbine site, either decreasing or increasing the power generated by that turbine for weeks to months (Bane et al. 2017). In section "MHK Energy from the Gulf Stream Along North Carolina", we show observed and modeled power variations at a fixed turbine site that are caused by meanders and path shifts. These Gulf Stream motions will be the dominant causes for power generation variations over time.

Assessing MHK Energy and Power Density

Our study region is over the outer continental shelf and continental slope from 32.5° N to 36° N and 73.5–77° W, and we focus on three cross-isobath transects within this area (Fig. 4). At one location along the northern transect, we make comparisons between simulations from a regional ocean circulation model and ADCP observations. Each transect covers most of the average Gulf Stream's cyclonic and

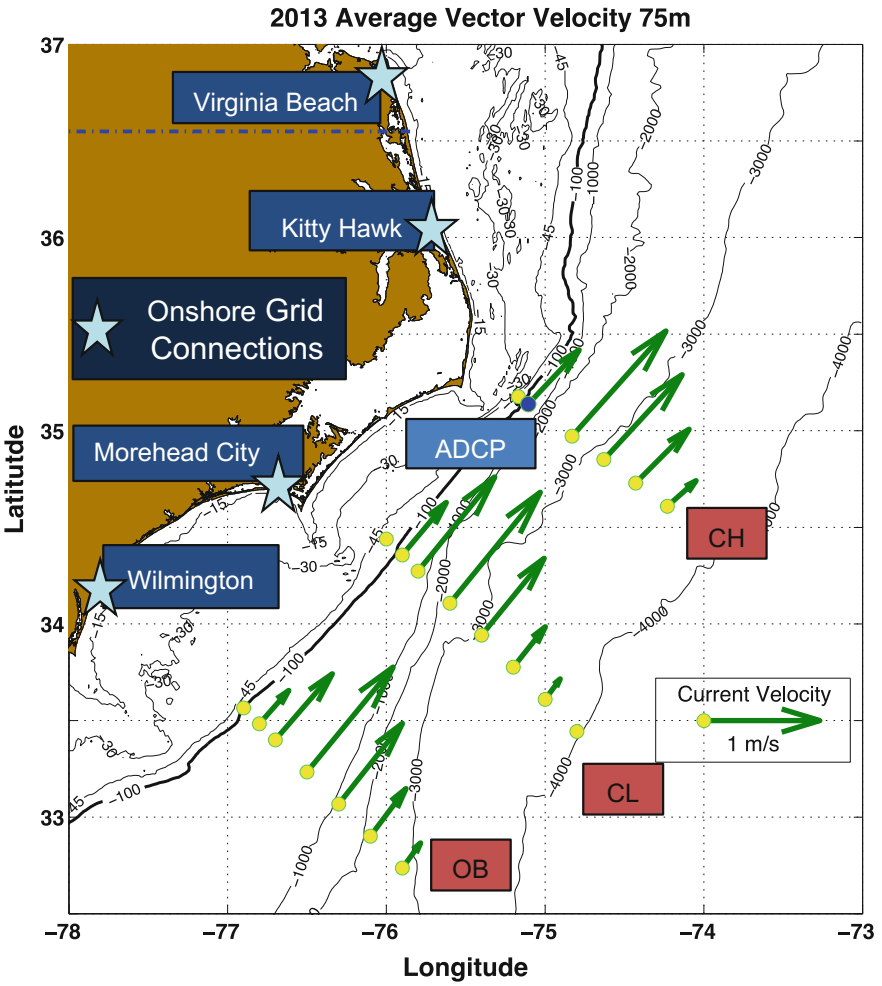

Fig. 4 2013 average current velocities at 75 m overlying a North Carolina base map. Stations in the cross-isobath transects are shown by *yellow circles* with both model and observational data at the *blue circle*. The transects are labeled CH for Cape Hatteras, CL for Cape Lookout, and OB for Onslow Bay. *Green arrows* show the current velocity. Isobaths are the *black contour lines*, and the 100-m isobath is in bold. The *four blue stars* show the locations of the cities Virginia Beach, Kitty Hawk, Morehead City, and Wilmington—the sites where MHK energy from the Gulf Stream can be connected to the power grid

anticyclonic shear zones. The northernmost transect, the Cape Hatteras (CH) transect, is located southwest of a bathymetric feature known commonly as The Point. The Point is offshore of Cape Hatteras at the location where the 100-m isobath crosses 35.5° N. This is where the shelf break changes from a northeastward to a more northward orientation. The Gulf Stream typically separates from its flow

along the upper continental slope near The Point and begins its transit into the deeper water of the open Atlantic.

There are 33 stations total from which we have gathered model data, 21 of these are displayed in Fig. 4. Of these displayed, 6 of which are shown along the CH transect as 5 yellow circles and one blue circle. These have been selected to cover the span of the average Gulf Stream. The geographical coordinates and total water depth for each station on the CH transect are listed in Table 1. The bottom-moored 150 kHz ADCP lies on the CH transect at the blue circle in Fig. 4. The middle transect (Cape Lookout = CL) is positioned in Raleigh Bay just off Cape Lookout, and the southernmost transect (Onslow Bay = OB) is in Onslow Bay. Tables 2 and 3 in the Appendix give the position and water depth of each station along these transects. Blue stars in Fig. 4 denote four sites where the present-day grid is substantial enough for MHK energy harvested from the Gulf Stream to be introduced. The sites are at Virginia Beach, Kitty Hawk, Morehead City, and Wilmington. Our power assessment for MHK energy in the Gulf Stream focuses on a depth of 75 m below the surface, given consideration of MHK device operating depths, turbine technology, commercial shipping interests, and surface wave influences on turbines and their moorings.

The Gulf Stream power assessment presented here uses data sets from two different sources. One is the Regional Ocean Model System (ROMS) that has been run for an area that encompasses the Cape Hatteras region. The other is a 150 kHz ADCP that was moored on the ocean floor on the upper continental slope off Cape Hatteras. Each data source is described below.

Table 1 Cape Hatteras (CH) transect stations

Cape Hatteras			
Stations	Latitude (°)	Longitude (°)	Depth (m)
CH 1	35.18	−75.17	62
CH 2	35.16	−75.13	102
CH 3	35.14	−75.11	222
CH 4	35.13	−75.10	271
CH 5	35.14	−75.09	315
CH 6	35.12	−75.08	376
CH 7	35.12	−75.07	460
CH 8	35.11	−75.06	614
CH 9	35.11	−75.05	695
CH 10	35.10	−75.05	884
CH 11	35.10	−75.04	1058
CH 12	35.09	−75.03	1265
CH 13	34.97	−74.83	2779
CH 14	34.85	−74.63	3107
CH 15	34.73	−74.43	3276
CH 16	34.61	−74.23	3548

ROMS Model

Simulated ocean currents were generated by a regional ocean circulation model implemented for the Mid-Atlantic Bight (MAB) and South Atlantic Bight (SAB), hereafter MABSAB, covering the area between 81.8–69.8° W and 28.4–41.8° N (Bane et al. 2017). The model is based on the ROMS (Shchepetkin and McWilliams 2005), a free-surface, terrain-following, primitive equations ocean model in widespread use for estuarine, coastal, and basin-scale applications. The horizontal resolution of this model is 2 km, sufficient to resolve the Gulf Stream's variability. Model bathymetry was interpolated from the National Geophysical Data Center (NGDC) 2-Minute Gridded Global Relief Data. Vertically, there are 36 terrain-following layers that have high resolution near the surface and bottom in order to better resolve ocean boundary layers. Momentum advection equations were solved using a third-order upstream bias scheme for three-dimensional (3D) velocity and a fourth-order centered scheme for two-dimensional (2-D) transport, whereas tracer (temperature and salinity) advections were solved with a third-order upstream scheme in the horizontal direction and a fourth-order centered scheme in the vertical direction. The horizontal mixing for both the momentum and tracer used the harmonic formulation with 100 and 20 $m^2\ s^{-1}$ as the momentum and tracer mixing coefficients, respectively. Turbulent mixing for both momentum and tracers was computed using the Mellor/Yamada Level-2.5 closure scheme (Mellor and Yamada 1982). For open boundary conditions, the model was nested inside the 1/12 degree global data assimilative HYCOM/Navy Coupled Ocean Data Assimilation (Chassignet et al. 2007; Gong et al. 2015) output superimposed with tidal forcing of 6 major tidal constitutes (M2, S2, N2, O1, K1, and Q1) derived from an Advanced Circulation (ADCIRC) tidal model (Luettich et al. 1991) simulation of the western Atlantic. The MABSAB hindcast ran from January 1, 2009 through December 31, 2014, and it did not incorporate the observations from the ADCP into the model computations of currents. Hourly model output was used for this study.

Moored ADCP Measurements

The moored 150 kHz ADCP location was selected based on its position within a region where Gulf Stream meanders have relatively low lateral amplitudes (Miller 1994). Higher power density levels at a fixed location tend to result from less lateral movements of the Stream. The ADCP was deployed for nine months, from August 1, 2013 through May 29, 2014. It was deployed in a water depth of 228 m at 35.1° N and 75.1° W. The instrument measures currents from 9 m above the bottom to 30 m below the surface with 4 m vertical resolution every 10 min. Measurements within 30 m of the surface are unreliable because of overwhelming acoustic reflection from the air–sea interface. The ADCP pod also contained a conductivity, temperature, and depth sensor.

Additional Observations

In addition to the moored ADCP measurements, hourly high-frequency (HF) radar surface-current measurements were collected, and sporadic (as weather allowed) vessel-mounted ADCP current measurements were made with downward-looking ADCPs along the CH transect. As these data get processed and analyzed, future studies will be able to make model comparisons with them in order to improve the spatial coverage for power density computations. As confidence is gained in the quality of the radar surface currents and their ability to accurately determine the variability in Stream location, they will serve as a valuable tool to infer MHK energy variability in this region. Because the structure of the Gulf Stream jet is remarkably consistent (Halkin and Rossby 1985), surface currents alone may provide accurate inferences about the MHK resource beneath them.

HF Radar Surface Currents

A network of land-based 5 MHz HF radars made consistent hourly (3 h averaged) surface-current measurements with 6 km^2 spatial resolution (Fig. 5). During the moored ADCP time frame, an additional radar was added to the network on Core Banks to enhance spatial coverage of the Gulf Stream. Currents were measured within the Cape Hatteras MHK Gulf Stream focus area. The radars are essential because they provide consistent hourly estimates of the Gulf Stream location previously not available from other historical methods such as satellite sea surface temperatures (SST) and altimetry. The primary cause of variability in Gulf Stream power density at a given location is the variability in Gulf Stream position caused by the Stream's meanders and path shifts. Thus, we are endeavoring to develop methods to determine the hourly Gulf Stream location using the radar network. These methods use the hourly location of the landward Gulf Stream edge from HF surface currents to identify the maxima in the relative vorticity in the surface currents and determine the maximum gradients in radial velocities (relative to individual radars). A demonstration of this method is shown in Fig. 6.

ADCP Vessel Transects

Currents have been measured along the shoreward portion of the CH transect (Fig. 4) on several occasions from a small vessel and from the Research Vessel (RV) Neil Armstrong. The small vessel has a downward-looking 300 kHz ADCP that measures currents in the top 100 m of the water column with 4 m resolution. Thirteen transects have been conducted during the 2013–2016 period along the inshore side of the CH transect, extending 14 km from the 100–1000-m isobaths.

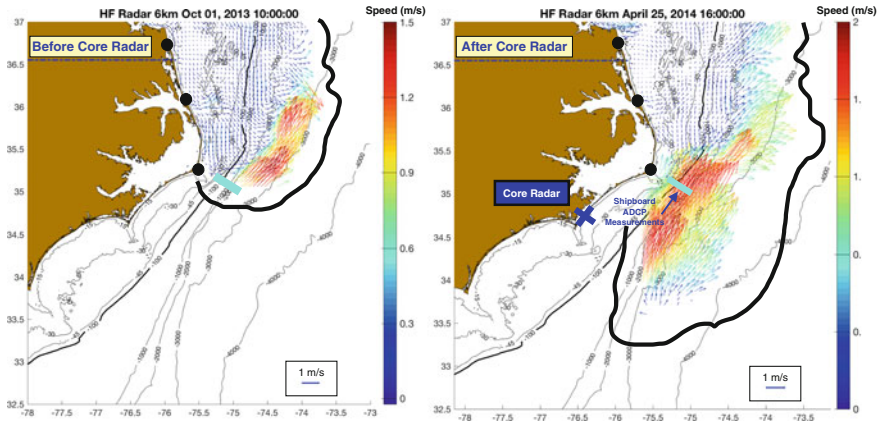

Fig. 5 The Gulf Stream MHK energy program added a radar to the southern extent of network coverage in 2013 to expand surface-current coverage over the area being considered for harvesting energy (*black dots* are the locations of preexisting Coastal Ocean Dynamics Applications Radar and *blue* "x" is the recently added radar on Core Banks). The *blue line* is the cross-shelf ADCP boat transect within the focus area that crosses the ADCP mooring. The boat transect is along the shoreward portion of the CH transect

The RV Armstrong is a research vessel that has three downward-looking ADCPs at three different frequencies: 38, 150, and 300 kHz. The Armstrong measured currents along the CH transect in April 2016 (Fig. 7). The 70-km transect started at the 100-m isobath in the cyclonic shear zone of the Gulf Stream and extended offshore through the anticyclonic shear zone. The cross-stream current measurements are valuable for observing the variability in MHK resource with depth along the CH transect, and for examining shears in the water column that are important engineering considerations for the development of energy extraction devices. In Fig. 7, the canonical velocity structure indicative of the Stream off Cape Hatteras is apparent in the top 1000 m. The notable counter flow below the Stream hugging the shelf slope is likely Upper Labrador Sea Water (e.g., Richardson 1977).

MHK Energy from the Gulf Stream Along North Carolina

Average Currents

The average model current velocities from 2013 at 75-m depth are displayed in Fig. 4. The average Gulf Stream jet is apparent in this figure; the inshore edge of the average jet is roughly along the 100-m isobath, while the offshore edge of the

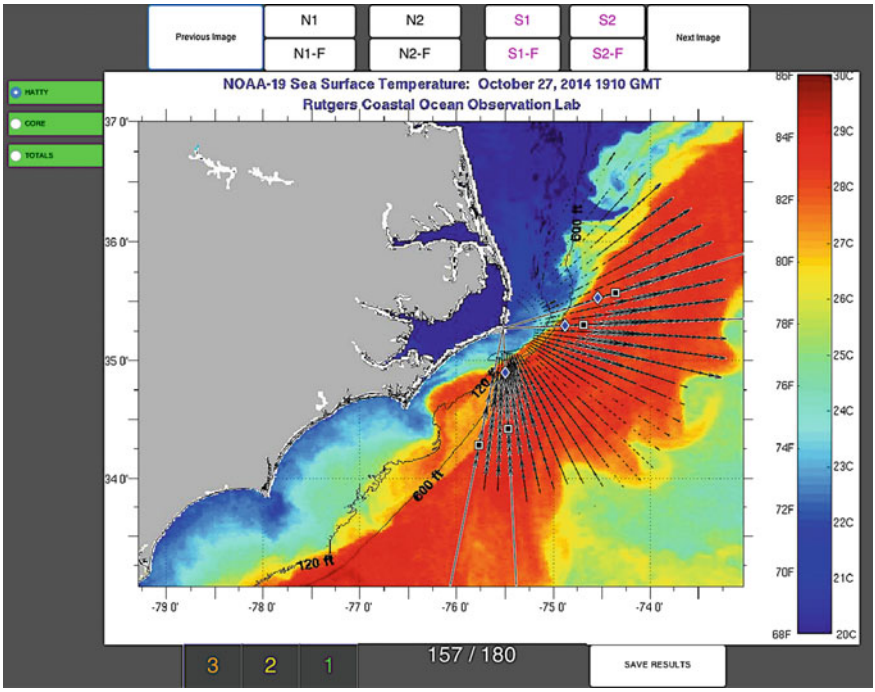

Fig. 6 An example of a graphical user interface developed for radar/SST edge detection comparison to evaluate the efficacy of radar Gulf Stream edge detection methods. *Four lines* radiating from the Buxton, North Carolina HF radar site are the four bearings selected for edge detection by the radar; the max surface velocity gradients (*blue diamonds*) and max surface velocity (*black squares*) are overlaid on a high-quality SST image

Stream is close to the 4000-m isobath. Near the center of each of the CH, CL, and OB transects, average 75 m velocities are slightly greater than 1 m s^{-1}. Average velocities diminish toward either edge of each transect.

Figure 8 shows a 3D view of model currents in the upper 1000 m on November 1, 2013, that agrees well with Gulf Stream structure from vessel transect observations. The Stream's jetlike structure is apparent on each transect. White arrows are the surface currents, red arrows are the wind stress, and the magenta X is the ADCP mooring location. The dark red core of the current meanders along the North Carolina continental slope as seen by its differing location on each of the transects. The core of the current is farthest offshore in the CH transect, and closer to shore in the CL and OB transects. This model day coincides with an occurrence when the Stream location was away from the shelf break near Cape Hatteras. Such offshore movement of the Stream occurs because of meandering and longer term path shifts. These lateral meanderings are described in greater detail in the next sections.

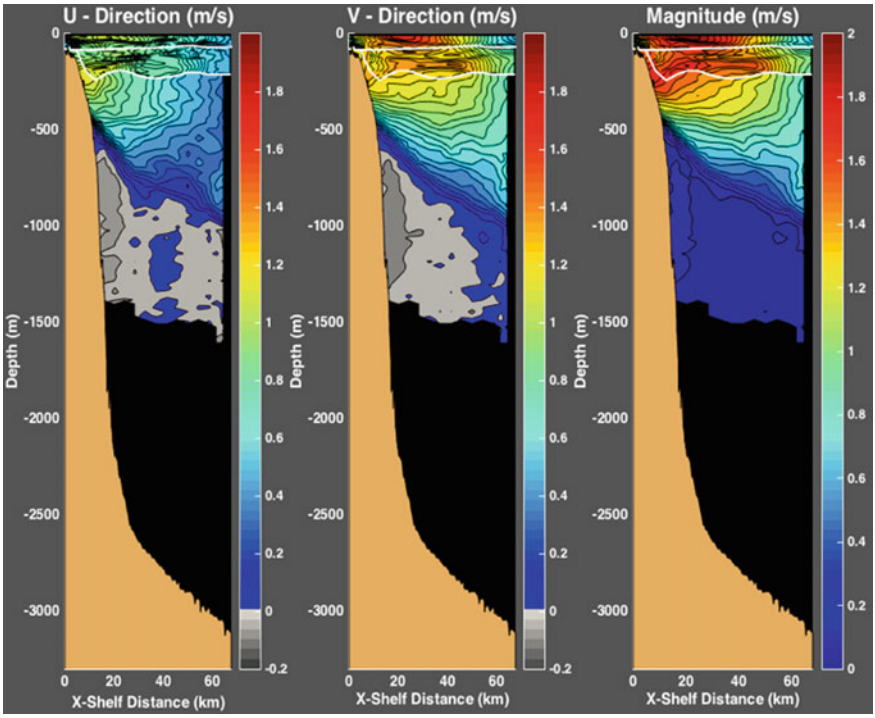

Fig. 7 Cross-stream measurements made by the three RV Armstrong ADCPs in April 2016. The *white curves* delineate the depths to which currents were measured at the 300 and 150 kHz frequencies (respectively). The 38 kHz ADCP measured to approximately 1500 m depth. Some discontinuity exists along current contours due to varying resolution at differing frequencies of the three instruments. Water below the ADCP range is *black*, and the *brown* is the ocean bottom measured from the onboard multibeam system

Current Speed and Power Density Time Series

Figure 9 shows the current speed time series computed by the model (red time series) and observed by the moored ADCP (blue time series) from August 1, 2013 to April 28, 2014 at 75 m below the surface at the ADCP site. During this time period, the ADCP and model each had average current speeds of 0.94 m s^{-1} (black horizontal line in Fig. 9). The maximum observed current speed was just above 2 m s^{-1}, while the model speed maximum was 2 m s^{-1}. Current speeds fluctuate with periods that range from semi-daily (tidal) to multi-monthly (Gulf Stream path shifts). There are times when the model speeds are generally slower than the observed speeds, such as from August through mid-October and from the latter half of March to the end of April. In general, the model underestimates many of the higher frequency speed fluctuations seen in the ADCP observations, but successfully captures the lower frequency changes. It is notable that in November, both the

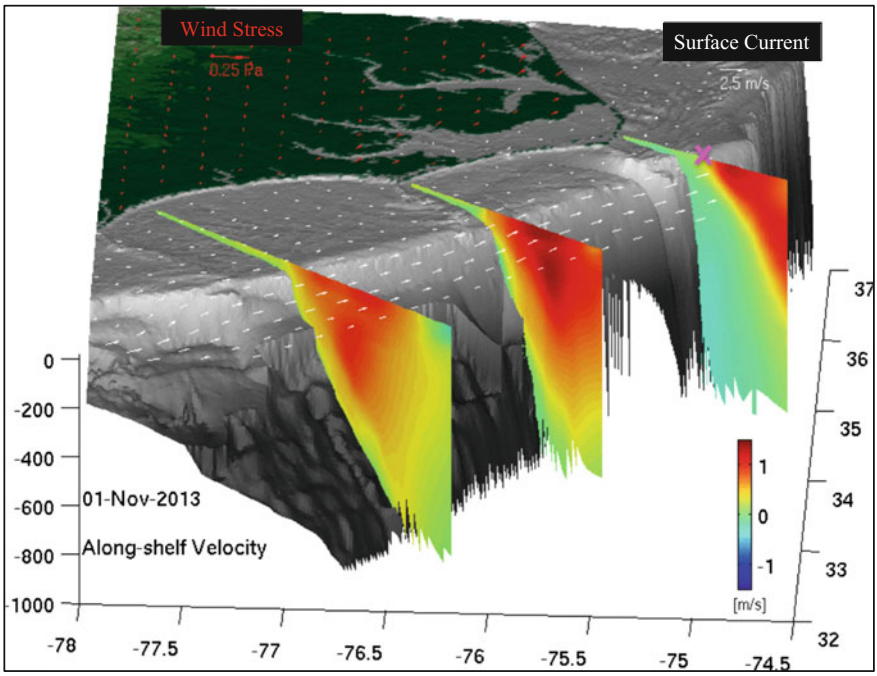

Fig. 8 Snapshot of the vertical slices at the three cross-isobath transects on November 1, 2013, constructed using model data. The core of the current is shown in *dark red*, *white arrows* show the surface currents, and *red arrows* show the wind stress. This is a frame from a movie that shows the model speeds at the transects from August 1, 2013 through April 28, 2014

model and observed current speeds decreased to near zero for almost 3 weeks before rapidly increasing to 1.5 m s^{-1} in the model and 1.8 m s^{-1} in the ADCP observations. During this time, a large Gulf Stream meander propagated through the area, causing the Stream's core to be farther offshore and weaker current speeds over the ADCP site.

Time series of power density from the ADCP (blue time series) and model (red time series) is shown in Fig. 10. Unlike the close agreement in speed averages (Fig. 9), the ADCP has an average power density of 798 W m^{-2} (blue horizontal line in Fig. 10), while the model has an average power density of 641 W m^{-2} (red horizontal line). The observed average power density is 24% higher than the model's, due mostly to the model's tendency to have smaller amplitude speed peaks (primarily from Gulf Stream meanders) than the ADCP. Because power density is proportional to speed cubed, pronounced differences in speed (where the ADCP observations have higher amplitudes than the model, such as August 1 through mid-October 2013) result in even greater differences in the power density. During November, the current speeds (and hence power density values) decreased to near zero. With the Stream positioned farther offshore during this time, the ADCP location was no longer within the jet and measured very weak flow speeds.

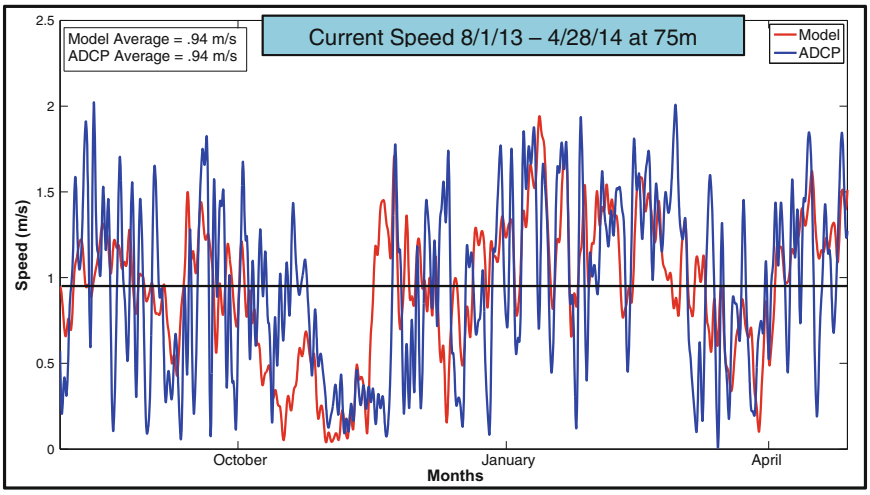

Fig. 9 Time series of the current speed at 75 m from August 1, 2013 through April 28, 2014. Model speeds are shown in *red* and moored ADCP speeds in blue. The *horizontal black bar* is the model and ADCP average speed of 0.94 m s^{-1}

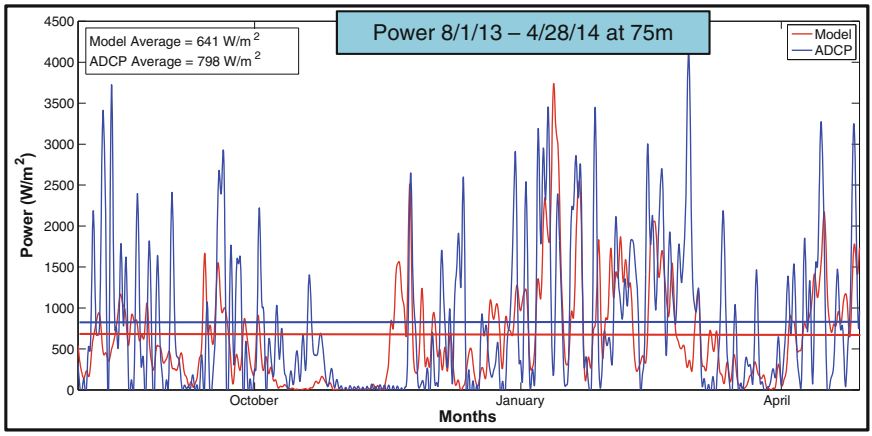

Fig. 10 Time series of the power density at 75 m from August 1, 2013 through April 28, 2014. Model time series is shown in red and ADCP time series in *blue*. The *red horizontal bar* shows the model power density average of 641 W m^{-2}, and the *blue horizontal bar* shows the ADCP power density average of 798 W m^{-2}

Year-to-Year Power Variations

Reasonably good agreement between the model and ADCP observations supports using the model to compute annual-average power levels at all of our stations off North Carolina. The colored vertical bars in Figs. 11, 12, and 13 are the average

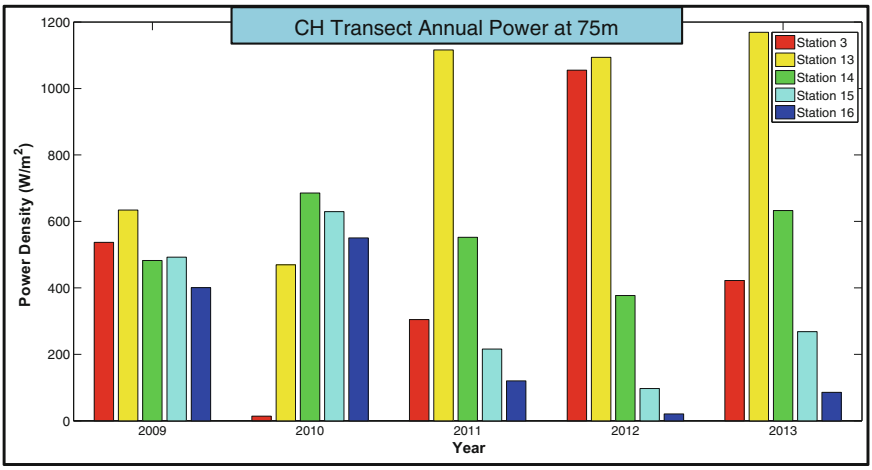

Fig. 11 Five-year model annual power density averages from 2009–2013 at 75 m at multiple stations in the Cape Hatteras transect. Red vertical bars represent the ADCP location. The stations presented above are the same stations in the Cape Hatteras transect shown in Fig. 4 for average current velocities

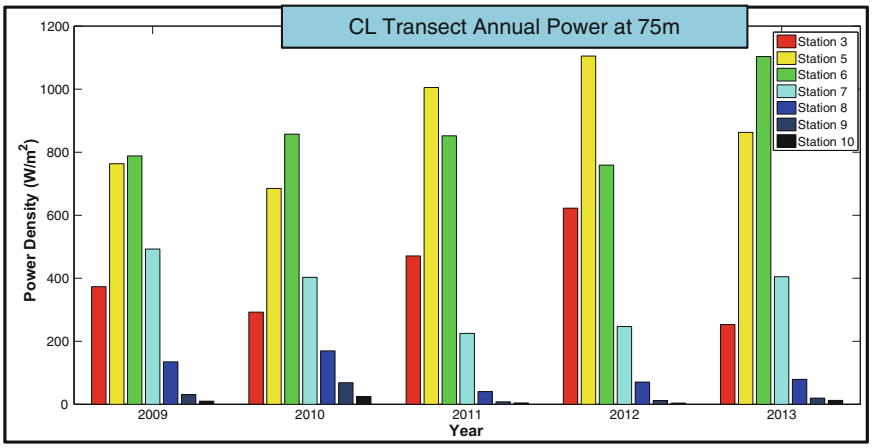

Fig. 12 Five-year model annual-average power densities from 2009 through 2013 at 75 m at stations in the Cape Lookout transect. These stations are shown in the Cape Lookout transect in Fig. 4

power densities from 2009 through 2013 for the stations in Fig. 4. The red vertical bars in Fig. 11 are the model's annual power averages at the ADCP location (blue circle on CH transect). At this location, the 2010 annual average of 14 W m^{-2} is very low compared to the subsequent years, and is 3% of the 5-year average (467 W m^{-2}) and only 1% of the power in 2012 (1055 W m^{-2}). Meanwhile, the

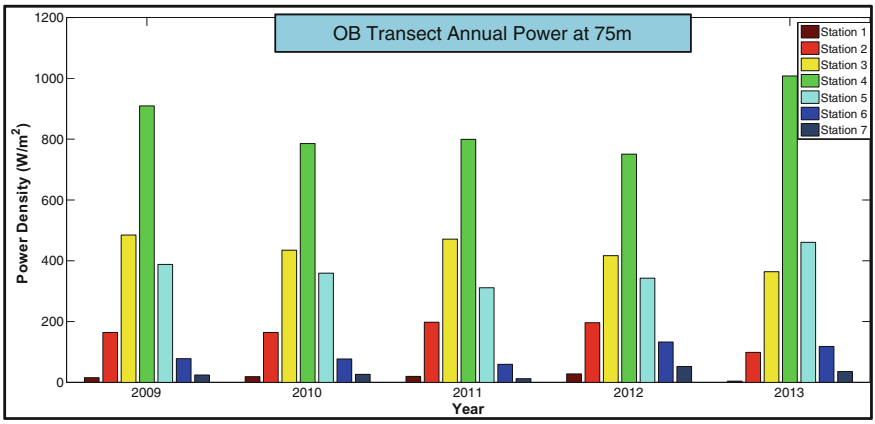

Fig. 13 Five-year model annual power density averages from 2009 through 2013 at 75 m at multiple stations in the Onslow Bay transect. These are the same stations in the Onslow Bay transect with average current velocities shown in Fig. 4 for average current velocities

average power in 2012 is 230% of the overall average. In 2010, the Gulf Stream path had a long-term shift offshore of the ADCP location that produced much lower averaged current speeds. Two years later, the Stream had shifted onshore and was positioned against the continental shelf break with the core of the current over the ADCP site and hence greater speeds. For both of these years, it appears that the current had long-term lateral shifts in the Stream's path that produced large fluctuations in available power. The other 3 years—2009, 2011, and 2013—had averages close to the 5-year average. This was likely a result of the Gulf Stream's path staying over the ADCP location for much of the year, with minimal long-term lateral shifts in the Stream's path.

The maximum power density reached at the Cape Hatteras transect (Fig. 11) during these 5 years is 1,169 W m^{-2} at Station 13 (yellow bar) in 2013. In 2009, there is small lateral variation in power density, with greater lateral variation in the subsequent 4 years. The greatest annual-average power density is at Station 13 for most of the years. In 2011–2013, the power density peaks are greater and more pronounced, while stations not within the peaks experienced much less power and greater horizontal current shear. Comparing our ADCP location in 2010 to the other stations in the transect, we note that the ADCP station lies along the inshore flank of the Gulf Stream, within its cyclonic shear zone, and greater power is found at more offshore stations. Again in 2012, the Gulf Stream had shifted onshore as indicated by the skewed power envelope of the annual averages, the result being much higher power at the ADCP station.

The same analysis of the CL and OB transects is shown in Figs. 12 and 13. The maximum power density at the CL transect is 1,105 W m^{-2} at Station 5 in 2012. The distribution is skewed more landward. The power peak for each year fluctuates between Stations 5 and 6—the yellow and green bars. These stations both have a

5-year average of about 875 W m^{-2}, and lie over depths of approximately 500 and 2800 m. This is important to note considering the costs of cabling and hardware required to reach greater power availability in the Stream at locations farther offshore. A depth of 2,800 m presents significant challenges for mooring turbines to capture power and then transporting the power back to shore over longer distances.

On the OB transect, the maximum power is 1,008 W m^{-2} at Station 4 in 2013. The annual OB transect power is more uniform and consistent throughout the 5 years. The lateral shear is apparent, and the greatest available power is at Station 4. The water depth at Station 4 is 654 m, presenting potential engineering challenges. In 4 of the 5 years, Station 3 has the second greatest power with a 5-year average of about 400 W m^{-2} and a water depth of 334 m. This is much shallower than the depths of Stations 5 and 6 in the CL transect, and based on its consistent power density over these 5 years, this suggests it would be a viable turbine location.

Current Directions

Current roses in Figs. 14 and 15 were constructed from ADCP observations and model currents at a depth of 75 m from August 1, 2013 to April 28, 2014. They are binned in 0.5 m s^{-1} speed and 15° directional increments. The Stream almost always flows northeastward for the time period considered. The flow direction is 45° about 70% of the time for the model and about 60% of the time for the observed currents. There are also a few instances on both roses when the current reverses to flow toward the southwest. Reversal speeds are small and occur less than 2% of the time. These flow reversals are likely caused by frontal filaments or cold-core eddies propagating along the cyclonic edge of the current (e.g., Bane et al. 1981). Flow of the Gulf Stream at the ADCP site is nearly unidirectional at about 45°. While there

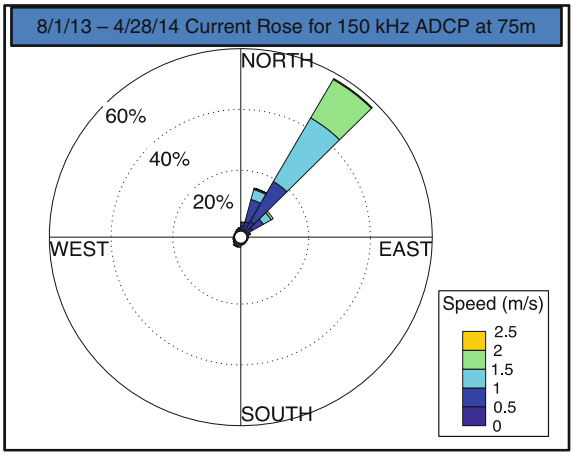

Fig. 14 Moored ADCP current rose from August 1, 2013 through April 28, 2014 at 75 m. Percentages show the time spent in a given direction

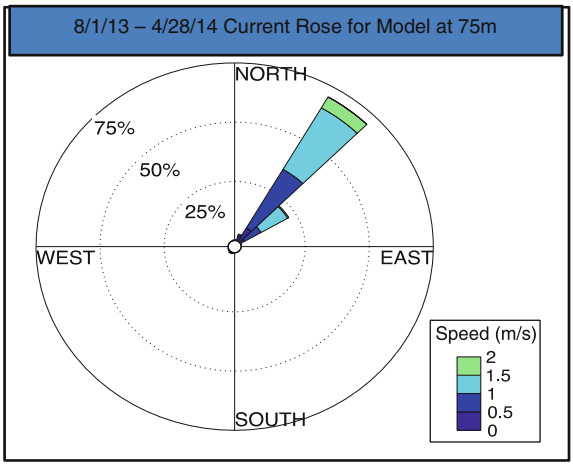

Fig. 15 Model current rose from August 1, 2013 through April 28, 2014 at 75 m at the ADCP location. Percentages show the time spent in a given direction

are lateral meanders of the Gulf Stream in which the whole current shifts onshore and offshore, the direction of flow within the current has small variation. This agrees with Kabir et al. (2015) who also found current direction to be quite uniform in the northeastward direction.

Discussion

In this chapter, we have presented an observation-and model-based assessment of MHK energy in the Gulf Stream off the coast of North Carolina, as well as demonstrated the additional available observations from land-based HF radars and shipboard ADCPs that will be included in future studies. Data from a moored 150 kHz ADCP and a ROMS model were analyzed. At a depth of 75 m at the ADCP location, the ADCP data and model data yield the same 9-month speed average of 0.94 m s^{-1}, and a fairly uniform 45° current direction. The power density time series shows that the ADCP observations occasionally reach 4,500 W m^{-2} with an average of nearly 800 W m^{-2}. Recent offshore wind studies in North Carolina have demonstrated that winds produce an average hub-height power density of 600–800 W m^{-2}, close to the ADCP power density average of 798 W m^{-2}. This suggests that Gulf Stream subsurface turbines may become viable as turbine and mooring technology develop.

Kabir et al. (2015) used HYCOM and a grid bounded by 34.9° N to 35.2°N and 74.9–74.5°W to find that more than 50% of the days from November 2003 through December 2012 at 20 m depth exhibit a power density of 500 W m^{-2} or greater. This coincides with the offshore end of the CH transect near Station 14. From Fig. 10 it can be seen that approximately 48% of the time both the model and ADCP site yield power densities greater than or equal to 500 W m^{-2}. Figure 10 and Kabir et al. (2015) use different models to conclude that nearly the same power

densities of 500 W m^{-2} are available for the same percentage of the time. The small difference between the two percentages is likely due to the analyzed model grid location being farther offshore than the ADCP site.

Yang et al. (2014) define the recoverable resource as the amount that can be extracted within current technological limits. Given the present uncertainty in underwater turbine technology and engineering capabilities, it is difficult to provide with confidence a determination of the recoverable energy resource available from the Gulf Stream. However, here, we have provided a view into the energy resource available and demonstrated its spatial and temporal variations along the North Carolina continental slope. Quantifying the Gulf Stream power characteristics is an essential step for the development of ocean current energy in this region. Accurate approximations of the energy resource and ocean environment will lay the foundation for extracting Gulf Stream energy in the future. As society continues to exploit fossil fuels and non-renewable resources at great cost to the environment, renewable energy increasingly becomes a more attractive long-term alternative. In helping to reach the goal of 80% of US electricity generation from renewable energy resources by 2050 (National Renewable Energy Laboratory 2012), ocean energy can be an essential component of a renewable energy portfolio that takes advantage of continuing technological advances in resource characterization, turbine design, mooring technology, and ocean engineering.

Acknowledgements We gratefully acknowledge funding from the North Carolina Renewable Ocean Energy Program for continued support of MHK energy research off North Carolina. We also appreciate Joe DeCarolis, Billy Edge, Mo Gabr, Harvey Seim, and Jim VanZwieten for their suggestions. Thank you to Patterson Taylor for supplying Fig. 6 and to Zhaoqing Yang and Kevin Haas for their comments that helped improve this chapter.

Appendix

Tables list geographical position and depth for each model station in the Cape Hatteras (CH), Cape Lookout (CL), and Onslow Bay (OB) transects.

Table 2 Cape Lookout (CL) transect stations

Cape Lookout			
Stations	Latitude (°)	Longitude (°)	Depth (m)
CL 1	34.44	−76.00	53
CL 2	34.40	−75.95	80
CL 3	34.36	−75.90	174
CL 4	34.32	−75.85	268
CL 5	34.27	−75.80	488
CL 6	34.11	−75.60	2775
CL 7	33.94	−75.40	3031
CL 8	33.78	−75.20	3316
CL 9	33.61	−75.00	3617
CL 10	33.44	−74.80	3904

Table 3 Onslow Bay (OB) transect stations

Onslow Bay			
Stations	Latitude (°)	Longitude (°)	Depth (m)
OB 1	33.57	−76.90	96
OB 2	33.48	−76.80	212
OB 3	33.40	−76.70	374
OB 4	33.23	−76.50	654
OB 5	33.07	−76.30	1076
OB 6	32.90	−76.10	2147
OB 7	32.74	−75.90	2800

References

Bane, J. M., Brooks, D. A., & Lorenson, K. R. (1981). Synoptic observations of the three-dimensional structure and propagation of Gulf Stream meanders along the Carolina continental margin. *Journal of Geophysical Research, 86,* 6411–6425.

Bane, J. M., & Dewar, W. K. (1988). Gulf Stream bimodality and variability downstream of the Charleston bump. *Journal of Geophysical Research, 93,* 6695–6710.

Bane, J. M., He, R., Muglia, M., Lowcher, C. F., Gong, Y., & Haines, S. M. (2017). Marine hydrokinetic energy from western boundary currents. *Annual Review of Marine Science*. doi:10.1146/annurev-marine-010816-060423. Invited Paper.

Barringer, M. O., & Larsen, J. C. (2001). Sixteen years of Florida current transport at 27° N. *Geophysical Reseach Letters, 28,* 3179–3182.

Boehlert, G. W., & Gill, A. B. (2010). Environmental and ecological effects of ocean renewable energy development: a current synthesis. *Oceanography, 23,* 68–81.

Brown, A., Beiter, P., Heimiller, D., Davidson, C., Denholm, P, Melius, J., et al. (2015). *Estimating renewable energy economic potential in the United States: methodology and initial results.* Tech. Rep. NREL/TP-6A20-64503, Natl. Renew. Energy Lab, Golden, CO.

Chassignet, E. P., Hurlburt, H. E., Smedstad, O. M., Halliwell, G. R., Hogan, P. J., Wallcraft, A. J., et al. (2007). The HYCOM (Hybrid Coordinate Ocean Model) data assimilative system. *Journal of Marine Systems, 65,* 60–83.

Corren, D., Hughes, S., Paquette, J., Sotiropoulos, F., & Calkins, J. (2013). *Improved structure and fabrication of large, high-power KHPS rotors*. Tech. Rep. DOE/GO18168, Verdant Power, New York, NY.

Gong, Y., He, R., Gawarkiewicz, G. G., & Savidge, D. K. (2015). Numerical investigation of coastal circulation dynamics near Cape Hatteras, North Carolina, in January 2005. *Ocean Dynamics, 65,* 1–15.

Halkin, D., & Rossby, T. (1985). The structure and transport of the Gulf Stream at 73° W. *Journal of Physical Oceanography, 15,* 1439–1452.

Imawaki, S., Bower. A., Beal, L., & Qiu, B. (2013). Western boundary currents. In G. Siedler., S. M. Grifies., J. Gould & J. A. Church (Eds.), *Ocean Circulation and Climate*: *A 21st Century Perspective,* 2nd ed. (pp. 305–38).Oxford, UK: Academic.

Kabir, A., Lemongo-Tchamba, I., & Fernandez, A. (2015). An assessment of available ocean current hydrokinetic energy near the North Carolina shore. *Renewable Energy*. http://dx.doi.org/10.1016/j.renene.2015.02.011.

Li, B., Bane, J., DeCarolis, J. F., Neary, V., de Queiroz, A. R., & Keeler, A. G. (2017). The economics of ocean current energy: a Gulf stream case study. Submitted to *Nature Energy*.

Luettich, R. A., Birkhahn, R. H., & Westerink, J. J. (1991). Application of ADCIRC-2DDI to Masonboro Inlet, North Carolina: A brief numerical modeling study, Contractors Report to the US Army Engineer Waterways Experiment Station, August 1991.

Mellor, G. L., & Yamada, T. (1982). Development of a turbulence closer model for geophysical fluid problems. *Reviews of Geophysics, 20,* 851–875.

Miller, J. L. (1994). Fluctuations of Gulf Stream frontal position between Cape Hatteras cand the Straits of Florida. *Journal Geophysical Research, 99,* 5057–5064.

National Renewable Energy Laboratory. (2012). Renewable Electricity Futures Study. Hand, M. M., Baldwin, S., DeMeo, E., Reilly, J. M., Mai, T., Arent, D., Porro, G., Meshek, M., Sandor, D. (Eds.), 4 vols. NREL/TP-6A20-52409. Golden, CO: National Renewable Energy Laboratory.

Neary, V. S., Previsic, M., Jepsen, R. A., Lawson, M. J., Yu, Y.-H., et al. (2014). Reference model 4 (RM4): ocean current turbine. In V. Neary, M. Previsic, R. A. Jepsen, M. J. Lawson, Y.-H. Yu, et al. (Eds.), *Methodology for Design and Economic Analysis of Marine Energy Conversion (MEC) Technologies* (pp. 180–228). Albuquerque, NM: Sandia Natl. Lab.

Quattrocchi, G., Pierini, S., & Dijkstra, H. A. (2012). Intrinsic low-frequency variability of the Gulf Stream. *Nonlinear Processes in Geophysics, 19,* 155–164.

Richardson, P. L. (1977). On the crossover between the Gulf Stream and the Western Boundary Undercurrent. *Deep Sea Research, 24,* 139–159.

Shchepetkin, A. F., & McWilliams, J. C. (2005). The regional ocean modeling system (ROMS): a split-explicit, free-surface, topography-following-coordinate oceanic model. *Ocean Modelling, 9,* 347–404.

Tracey, K. L., & Watts, D. R. (1986). On Gulf Stream meander characteristics near Cape Hatteras. *Journal Geophysical Research, 91,* 7587–7602.

VanZwieten, J. H., Duerr, A. E. S., Alsenas, G. M., & Hanson, H. P. (2013). Global ocean current energy assessment: an initial look. In *Proceedings of the 1st Marine Energy Technology Symposium, April 10–11, Washington, DC*. http://www.globalmarinerenewable.com/images/global%20ocean%20current%20energy%20assessment%20an%20initial%20look.pdf.

VanZwieten, J., McAnally, W., Ahmad, J., Davis, T., Martin, J., Bevelhimer, M., et al. (2014). In-stream hydrokinetic power: review and appraisal. *The Journal of Energy Engineering, 141,* 04014024.

Webster, F. (1961). A description of Gulf Stream meanders off Onslow Bay. *Deep Sea Research, 9,* 130–143.

Yang, X., Haas, K. A., & Fritz, H. M. (2014). Evaluating the potential for energy extraction from turbines in the Gulf Stream system. *Renewable Energy, 72,* 12–21.

Effects of Tidal Stream Energy Extraction on Water Exchange and Transport Timescales

Zhaoqing Yang and Taiping Wang

Introduction

Tidal stream energy is one of the most attractive marine renewable energy resources because tidal currents are highly predictable. Rapid development of tidal stream device technologies has occurred to maximize energy extraction. However, tidal stream energy development is heavily constrained by the environmental concerns, at both local and system-wide spatial scales, as well as at short-term and long-term temporal scales. During the past decade, numerous studies have investigated the upper limit of theoretical extractable energy and exploited the tidal energy resource in coastal waters around the world using analytical methods and numerical models (Garrett and Cummins 2005; Myers and Bahaj 2005; Bryden et al. 2007; Garrett and Cummins 2007; Sutherland et al. 2007; Polagye et al. 2009; Vennell 2010; Defne et al. 2011; Karsten et al. 2013; Venugopal and Nemalidinne 2014; Yang et al. 2014; Evans et al. 2015; Lo Brutto et al. 2016; Rao et al. 2016). One of the major barriers to tidal stream energy development is the potential environmental impact of deployment and operation of tidal energy converters (TECs) on marine systems. Compared to tidal energy resource characterization and assessment, assessments of environmental impacts as a result of tidal stream energy extraction have been limited, partially due to the complex relationships between energy extraction and many environmental variables, challenges in field observations related to environmental impacts, as well as high uncertainties associated with the assessment of environmental effects.

Z. Yang (✉) · T. Wang
Pacific Northwest National Laboratory, 1100 Dexter Ave North, Suite 400, Seattle, WA 98109, USA
e-mail: zhaoqing.yang@pnnl.gov

Z. Yang and A. Copping (eds.), *Marine Renewable Energy*,
DOI 10.1007/978-3-319-53536-4_11

Environmental effects due to TECs can be largely grouped into two categories: effects on marine life and habitats, such as turbine collision risks, fish migration, seabird population (Ward et al. 2010; Furness et al. 2012; Alexander et al. 2013; Criales et al. 2013; Miller et al. 2013; Schlezinger et al. 2013; Benjamins et al. 2015; Hammar et al. 2015; Copping et al. 2016; Gove et al. 2016), and effects on physical and biogeochemical transport processes, such as hydrodynamics, underwater acoustics, sediment transport, and water quality (Shields et al. 2011; Kadiri et al. 2012; Nash et al. 2014; Martin-Short et al. 2015; VanZwieten et al. 2015; Long et al. 2016; Roche et al. 2016; Williamson et al. 2016). To date, most of the existing studies of physical effects have been based on the characterization of the influence of tidal energy extraction on the volume flux across a TEC farm, i.e., the changes in hydrodynamics alone (Polagye et al. 2008; Hasegawa et al. 2011; Shapiro 2011; Thiebot et al. 2015; Yang and Wang 2015). Although velocity field or tidal volume flux is the most direct physical property to be affected by TECs, the most critical environmental concerns about tidal stream energy development are closely related to biogeochemical transport processes driven by the flow field, such as sediment erosion and transport, mixing and water exchange, and changes in water quality in marine systems (Neill et al. 2009; Nash et al. 2014; Wang et al. 2015; van der Molen et al. 2016). One parameter that closely links tidal volume flux, or tidal prism, to the biogeochemical transport processes in coastal and estuarine systems is flushing time (Dyer 1973; Officer 1976), which has been widely used as the transport timescale to represent the overall flushing capability of an aquatic system.

This chapter explores the flushing time approach for assessing the system-wide effect of tidal stream energy extraction on the physical marine environment. The flushing time concept and tidal prism theory are presented first, followed by a detailed review of the analytical methods and numerical models, from simplified one-dimensional (1-D) to advanced three-dimensional (3-D) models, which are used for characterizing the theoretical tidal energy resource and evaluating the impacts on tidal flows. Finally, two case studies using a 3-D model and tidal flushing time method are given to illustrate the flushing time approach for assessing the impacts of TECs on physical systems.

Definition and Calculation Methods of Flushing Time

Flushing time is one of the most widely used transport timescales for describing the rate of water exchange in a waterbody. The flushing time concept was first introduced by Dyer (1973) and Officer (1976) to quantify the time required for flushing existing water out of an estuary or coastal embayment as a function of freshwater discharge and tidal prism. It is generally regarded as a bulk or integrative property that describes the overall exchange/renewal capability of a waterbody. Its calculation methods are described below.

Tidal Prism Method

Dyer (1973) and Officer (1976) defined flushing time as a function of freshwater discharge R and tidal prism P, which is the volume of water in an estuary or bay between high tide and low tide. The tidal prism method has been widely used to estimate flushing time T_f. The most common and simplest tidal prism model has the following form (Dyer 1973; Wang et al. 2004):

$$T_f = \frac{V+P}{Q+R} \tag{1}$$

where $Q = P/T$ is the tidal volume flux in and out of the bay, V is the volume of the bay at low tide, and T is the tidal period. Equation 1 does not consider the effect of the return flux of tracer and net inflow. Several modifications were made on the simple tidal prism model to include the effect of return flux and the influence of net inflow on tidal prism (Wood 1979; Kuo and Neilson 1988; Sanford et al. 1992; Luketina 1998). Based on Luketina (1998), the governing equation for the rate of change of a conservative trace concentration $c(t)$ is described as follows:

$$\frac{dc(t)}{dt} = -\left[\frac{(1-b)\frac{P}{T} + (1+b)\frac{R}{2}}{V+P}\right] c(t) \tag{2}$$

where t is time and b is the return factor in the range of 0–1. Solving Eq. 2 for an initial condition problem with $c(0) = c_0$ yields $c(t) = c_0\, exp\left(-t/T_f\right)$ with the flushing time T_f defined as follows (Sanford et al. 1992; Luketina 1998):

$$T_f = \frac{V+P}{(1-b)Q + (1+b)R/2} \tag{3}$$

Clearly, T_f is the time required for the tracer concentration to drop to e-fold of the initial concentration ($c_o/e = 0.3679 \cdot c_o$), also called the e-folding time. Note that Eq. 3 is slightly different from Eq. 1 even when the return flux factor is not considered ($b = 0$). This discrepancy is due to the consideration of the effect of net inflow on tidal prism (Luketina 1998). Equation 3 reduces to the classical form $T_f = (V+P)/R$ when river flow is dominant over tidal volume flux ($R >> Q$). For cases in which river flow can be neglected and the return flux factor is not considered ($b = 0$), Eq. 3 is identical to Eq. 1.

Numerical Simulation

The tidal prism method for estimating flushing time assumes the tracer concentration in the bay is fully mixed and controlled by volume exchange, which

typically is not the case under real-world conditions. A more accurate method for estimating the system-wide flushing timescale is based on numerical simulations of tracer transport in the bay. Assuming the system-wide averaged tracer concentration follows an exponential decay relationship with a decay rate K,

$$\frac{dc(t)}{dt} = -Kc(t) \tag{4}$$

Similar to Eq. 2, the solution of Eq. 4 has the following form:

$$c(t) = c_o e^{-Kt} \tag{5}$$

and the e-folding flushing time T_f is given by:

$$T_f = \frac{1}{K} \tag{6}$$

The flushing time then can be calculated based on Eq. 6 by fitting Eq. 5 to the model results and determining the decay rate K. The accuracy of this method depends on the characteristics of the coastal bay and the accuracy of the model results. Therefore, model validation against observations is an important first step in calculating the flushing time.

Effects of TECs on Flows—Analytical and Numerical Approaches

Significant efforts have been made in developing analytical and numerical models to evaluate the effects of tidal stream energy extraction on the hydrodynamics and transport processes in marine systems. This section provides a detailed review of different methods for assessing the maximum extractable tidal energy and its associated effect on volume flux across a tidal channel.

Analytical and 1-D Models

One-dimensional models, especially analytical models, are useful for providing fundamental understanding of the effects of tidal stream energy extraction. Many studies have been conducted to determine the upper limit of extractable tidal stream energy and the effects on flow fields based on 1-D governing equations. Bryden et al. (2004) first examined the potential extractable energy in a natural channel with uni-directional flow using a steady-state 1-D momentum equation. An approximate linear relationship was found between the reduction in flow speed and the extracted energy

across the channel when a maximum extraction of 20% of natural energy flux was considered. Their results showed that extraction of 10% of the energy flux would cause a 3% reduction in the flow speed in the channel. In their pioneering work on the theoretical extractable energy in a tidal channel, Garrett and Cummins (2005) developed a formula for the maximum tidally averaged extractable power P_{max} as a function of the maximum volume flux Q_{max} in the channel based on a 1-D model:

$$P_{max} = \gamma \rho g a Q_{max} \tag{7}$$

where ρ is water density, a is the amplitude of the tidal height difference across the channel, g is the gravity acceleration, and γ is a coefficient varying from 0.20 to 0.24. Equation 7 has been validated by others using two-dimensional (2-D) and 3-D model simulations (Sutherland et al. 2007; Hasegawa et al. 2011; Yang et al. 2013), and applied for large-scale regional resource assessment as a first-order approximation (Defne et al. 2012). A relationship between potential extractable power P and volume flux Q was also established with added tidal turbines in the tidal channel, as shown by Garrett and Cummins (2005) and Sutherland et al. (2007):

$$\frac{P}{P_{max}} = \left(\frac{3^{\frac{3}{2}}}{2}\right)\left(\frac{Q}{Q_{max}}\right)\left[1 - \left(\frac{Q}{Q_{max}}\right)^2\right] \tag{8}$$

Clearly, the normalized power P/P_{max} is a nonlinear function of the normalized volume flux Q/Q_{max} (Fig. 1). A similar distribution pattern was found between extracted power and flow speed in a study by Bryden and Couch (2007).

To evaluate the effect of power extraction on the volume flux reduction, the relative volume flux reduction is introduced: $\Delta Q_r = (1 - Q/Q_{max})$. Equation 8 can be rearranged as follows:

$$\frac{P}{P_{max}} = \left(\frac{3^{\frac{3}{2}}}{2}\right)\left(2\Delta Q_r - 3\Delta Q_r^2 + \Delta Q_r^3\right) \tag{9}$$

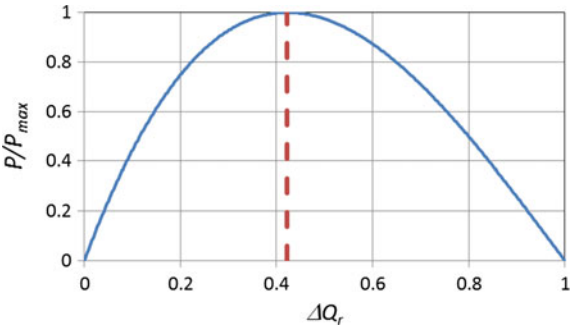

Fig. 1 Relative power as a function of volume flux reduction ΔQ_r

Equation 9 shows that the relative extractable power is a third-order polynomial function of the relative volume flux reduction ΔQ_r. Taking the derivative of P/P_{max} with respect to ΔQ_r, the maximum power ($P/P_{max} = 1$) can be determined when $\Delta Q_r = 0.423$, which indicates that the extractable power has a diminished return when the volume flux Q is reduced by approximately 42%, as shown by the red dashed line in Fig. 1.

Figure 1 also shows that a substantial percentage (44.5%) of energy can be extracted from the tidal channel with a 10% reduction in volume flux. Assuming that no more than a 10% reduction in volume flux would be acceptable for environmental concerns, dropping the higher order terms in Eq. 8 yields a linear approximation for reductions up to 10%:

$$\frac{P}{P_{max}} = 3^{3/2}\Delta Q_r = 5.2 \cdot \Delta Q_r \tag{10}$$

Equation 10 shows that if a fraction of the volume flux reduction is acceptable in a tidal channel, the percentage of extractable energy is about five times the volume flux reduction. Conversely, extraction of 10% of the maximum theoretical energy will only result in a 2% volume flux reduction. This sounds very promising as far as environmental impacts are concerned, because tidal energy extraction at specific real-world sites will likely be within 10% of the maximum theoretical energy in the system. However, because Eq. 10 is derived based on a 1-D model, which could be overly simplified for any real-world conditions, it must be used with caution in applications to real project sites considering its high uncertainty.

Following the work by Garrett and Cummins (2005), a number of studies were conducted to extend the analytical solution to various conditions. Garrett and Cummins (2007) further examined the maximum power for the condition in which a partial tidal turbine fence is placed across the tidal channel. Blanchfield et al. (2008) showed that Eq. 7 is also suitable for a tidal channel linking to a coastal bay, when a is defined as the tidal amplitude outside of the channel and γ equals 0.22. Solving a similar 1-D model with turbine effect, Vennell (2010) showed that the potential power production depends on the tidal farm's configuration and channel geometry. Tidal turbine arrays must occupy the largest fraction of a channel's cross section in order to reach maximum turbine efficiency. Polagye and Malte (2011) developed a 1-D model for channel networks to investigate the tidal energy resource and far-field effects in the channel networks. Specifically, effects on tidal amplitude, transport, kinetic power density, and frictional power dissipation were quantified.

2-D and 3-D Models

While analytical solutions and 1-D models are useful for determining the upper limit of the resource and providing insight into the fundamental relationship

between tidal energy resource and far-field effects on hydrodynamics, high uncertainties exist in resource estimates because of assumptions and simplification applied to the governing equations. It is also impossible to use analytical solutions and 1-D models to quantify the spatial (both horizontal and vertical) variability of far-field effects due to TECs deployment. To accurately assess tidal energy potential and far-field effects in real-world sites, advanced 2-D or 3-D numerical models are required.

Sutherland et al. (2007) applied a depth-averaged 2-D model to simulate the tidal energy potential in multiple tidal channels in the Johnstone Strait near Vancouver Island, Canada. By increasing the bottom drag in the model to represent the turbine power dissipation, they found that the modeled volume flux reduction corresponding to the maximum extractable power in all of the channels agreed very well with the analytical solution (Eq. 7) developed by Garrett and Cummins (2005), with a discrepancy of ~1% of volume flux reduction. Using the similar approach of representing energy extraction by increasing of bottom drag, Karsten et al. (2008) applied a coastal Finite Volume Community Ocean Model (FVCOM; Chen et al. 2003) to estimate the maximum theoretical tidal energy of Minas Passage in the Bay of Fundy. The authors found their model results were in a good agreement with the analytical solution (Eq. 7) when it was extended to the case of a channel connecting to a tidal basin, assuming a in Eq. 7 is the amplitude of the tidal forcing. Their model results showed that the maximum extractable power of 7,000 MW in the Minas Passage corresponded to 40% flow reduction through the passage.

Nash et al. (2014) conducted a comprehensive modeling study to evaluate the impacts of tidal stream energy extraction on tidal regimes, intertidal zones, and flushing time in the Shannon Estuary in Ireland using a depth-averaged 2-D hydrodynamic and water quality model. The effect of a tidal farm was simulated based on the Linear Momentum Actuator Disc Theory (LMADT) (Draper et al. 2010; Roc et al. 2014). Averaged residence time was estimated by simulating tracer distribution and was used to evaluate the effect of tidal energy farms on the flushing timescale in the estuary. Nash et al. (2014) found that the normalized tracer concentration in the estuary followed the exponential decay curve, and the residence time for the high-density turbine farm scenario increased approximately 70% due to the blockage effect of the tidal turbine farm. Their model results also indicated that over 30% of the intertidal zone could be lost because some intertidal areas became permanently wet or dry due to distortion of the tidal regime caused by high-density tidal turbine farms.

The horizontal 2-D modeling approach assumes that turbines are able to capture tidal energy throughout the entire water column. This assumption is not realistic because tidal turbines are typically deployed at a specific level in the water column (called the "hub height"). Therefore, 3-D models are necessary to accurately simulate the energy extraction by TECs. Shapiro (2011) first quantified the back effect of tidal stream energy extraction on ocean currents and alterations in regional-scale residual currents and passive tracers in the Celtic Sea using a 3-D ocean circulation model. A kinetic energy loss (sink) term in the 3-D model was introduced to represent the energy dissipation by tidal turbine farms. Shapiro (2011) found that in

the case of a high-power turbine farm, the kinetic energy of currents can be altered significantly. Furthermore, model simulations suggested that at a high level of energy extraction, the currents tended to bypass the tidal turbine farms; therefore, the increase in extracted energy is much smaller than the increase in the rated power capacity of farms. The effect of tidal energy extraction on passive tracers was evaluated using neutral buoyant drifter simulations. Simulated Lagrangian trajectories indicated that the effects of tidal energy extraction on passive tracers vary significantly in the horizontal domain; the effects range from 13 to 238% and are extremely sensitive to the drifter release locations.

A number of 3-D model applications have been conducted to assess tidal stream resource potential and far-field effects since the initial work performed by Shapiro (2011) (Hasegawa et al. 2011; Hakim et al. 2013; Work et al. 2013; Yang et al. 2013; Roc et al. 2014; Yang et al. 2014; Pacheco and Ferreira 2016; Rao et al. 2016; van der Molen et al. 2016). In a 3-D modeling study for an idealized tidal channel linked to a bay, Yang et al. (2013) examined the theory of maximum extractable power developed by Garrett and Cummins (2005) and Blanchfield et al. (2008). A tidal turbine module was implemented in FVCOM using the momentum sink approach. Yang et al. (2013) found that the estimated maximum extractable power based on 2-D simulations matched the analytical solution (Eqs. 7 and 8) very well. However, model results from 3-D simulations showed that the volume flux reduction corresponding to the maximum power extraction was much lower than the analytical solution of 42%, and it varied significantly from 23 to 36% when turbine hub height increases near the bottom to the mid-layer of the water column. They found that the maximum extractable power and turbine farm efficiency (power/turbine) were sensitive to the hub height, and that the maximum extractable power occurs near the mid-layer of the water column. Yang et al. (2013) also evaluated the effect of energy extraction on flushing time in the bay connecting to tidal channel based on model simulations of tracer transport.

In recent years, coupled hydrodynamic and biogeochemical models have been used to directly simulate the effect of tidal stream energy extraction on biogeochemical processes. For example, Wang et al. (2015) developed a 3-D biogeochemical model coupled with FVCOM to assess the effects of tidal energy extraction on water quality in an idealized coastal bay. They found that the responses of water quality variables to tidal energy extraction, such as dissolved oxygen, depended highly on the decrease in flushing time in the bay and increase in vertical mixing in the tidal channel. van der Molen et al. (2016) applied a 3-D coupled hydrodynamic-biogeochemical model to investigate the large-scale environmental impact of tidal energy generation in the Pentland Firth. Simulated biogeochemical variables include suspended sediment, silicate, chlorophyll a, and nitrate. Their model results suggested that realistic scale power generation from the tidal stream has minor effects on tidal circulation and undetectable effects on biogeochemical processes. However, large-scale tidal energy extraction of 8 GW such as that proposed in Pentland Firth would result in up to 10% changes in marine environmental variables.

Case Studies for Assessing the Effects on Flushing Time

Idealized Channel Linking to a Bay

Yang et al. (2013) simulated the effects of tidal energy extraction on volume flux and tracer flushing time in a tidal channel connecting to a bay. The tidal channel is 30 km long, 6 km wide, and 60 m deep. The semi-enclosed bay is 150 km long, 30 km wide, and 100 m deep. The detailed model setup was described by Yang et al. (2013). The change in tracer concentration in the bay was simulated with initial conditions of unity concentration in the bay and clean water in the tidal channel and coastal ocean. Figure 2 shows the simulated surface distribution of tracer concentration after 5 days of initial tracer release inside the bay. Strong lateral mixing induced by tidal vortexes and tidal intrusion of coastal water are clearly seen from the tracer distribution.

The flushing time of the bay was estimated based on the numerical simulations, as well as Eqs. 5 and 6. Changes in the flushing time in the bay were determined as a function of volume flux reduction through different turbine farms occupying the tidal channel. Results showed the increased flushing time in the semi-enclosed bay roughly follows an exponential distribution as a function of the volume flux

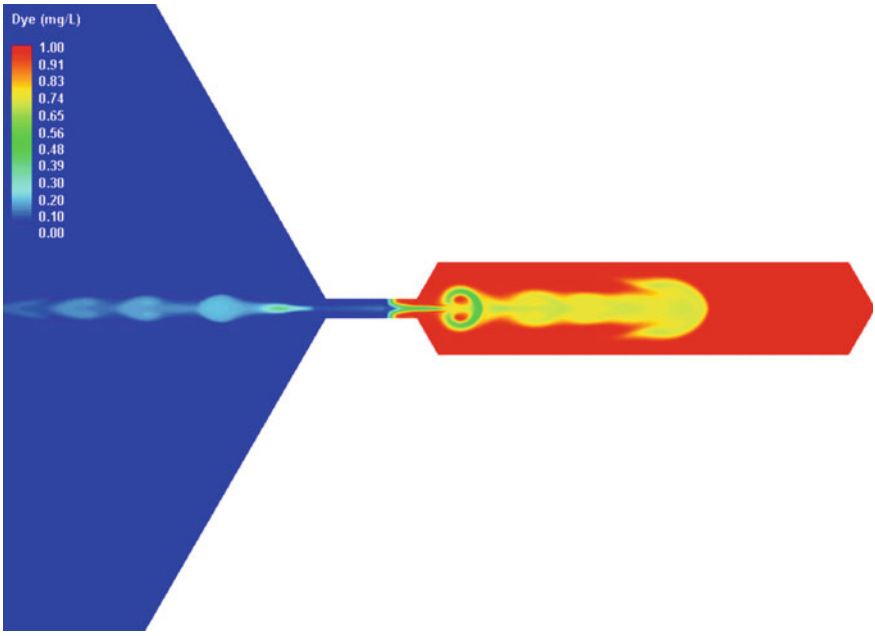

Fig. 2 Simulated tracer concentration in a tidal basin connecting to a tidal channel occupied by turbines after 5 days of tidal flushing. The *red color* represents unit tracer concentration and the *blue* represents zero concentration (clean water) in the open ocean

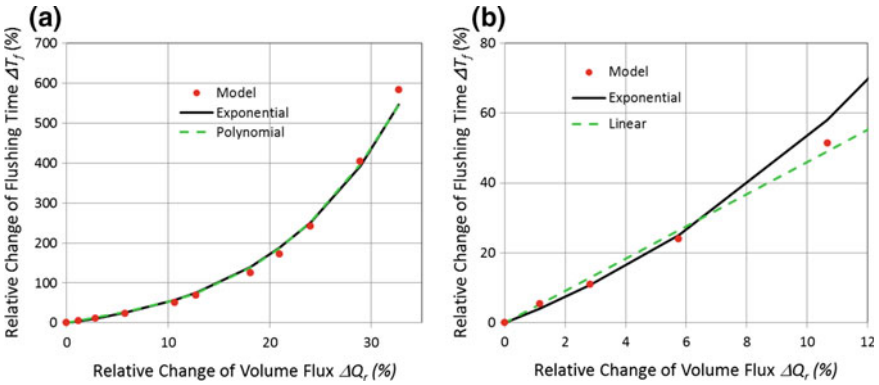

Fig. 3 **a** Simulated relative change in the flushing time ΔT_f (%) as a function of relative volume flux reduction ΔQ_r (%) (*red circle*), exponential fit (*solid black line*), and third-order polynomial fit (*dashed green line*); **b** change in ΔT_f (%) in the small range of ΔQ_r (%). The *dashed green line* represents linear regression

reduction (Fig. 3a). Applying exponential or third-order polynomial regressions to the model results (red circle) in Fig. 3 shows the following:

$$\Delta T_f = \begin{cases} 43 \cdot \ \exp(0.08\,\Delta Q_r); & \textit{Exponential Fit} \\ 5 \cdot \Delta\, Q_r - 0.1181 \cdot \Delta Q_r^2 + 0.0145 \cdot \Delta Q_r^3; & \textit{Polynomial Fit} \end{cases} \tag{11}$$

The comparison of changes in flushing time calculated from model simulation (red circle), the exponential fit (black line), and the polynomial fit (dashed green line) is presented in Fig. 3a. Clearly, both the exponential and the third-order polynomial regression formulas match the model results well. As discussed in the previous section, practical power extraction is likely being constrained by the concerns of environmental impacts, such as an upper limit of 10% charge in volume flux. Re-plotting Fig. 3a for a small range of ΔQ_r (%) indicates the relative change in flushing time ΔT_f (%), and volume flux reduction ΔQ_r (%) approximately follows a linear relationship (Fig. 3b):

$$\Delta T_f = \beta \cdot \Delta Q_r \tag{12}$$

where $\beta = 4.6$, which is close to the linear coefficient of 5.0 in the polynomial regression (Eq. 11). Equation 12 shows that the effect of tidal energy extraction on flushing time is several times greater than its effect on volume flux. This result suggests that if flushing time is used as an environmental impact indicator and a 10% change is the acceptable upper limit, the 10% change in volume flux may not be a good reference for environmental impact assessment.

Tacoma Narrows in Puget Sound

A case study at a real-world site, Tacoma Narrows in Puget Sound, Washington State, USA, was conducted to demonstrate that flushing time is a unique indicator for assessing the impacts of tidal energy extraction on transport processes. Puget Sound is a large estuarine system that is identified as one of the top potential sites for tidal energy development in US coastal waters (Kilcher et al. 2016). Tacoma Narrows is a narrow and shallow channel that, as a glacial sill, separates the south Puget Sound (South Sound) from the rest of the waterbodies in Puget Sound (Fig. 4). Tacoma Narrows has an average length of 9,000 m, width of 2,000 m, and water depth of 35 m. Tidal currents in Tacoma Narrows are extremely strong because of the narrow channel and strong tidal forcing, which makes the site ideal for exploring tidal stream energy production (Polagye et al. 2009; Kilcher et al. 2016).

The 3-D coastal hydrodynamic model used in the present study was based on a previously validated Puget Sound model (Yang and Khangaonkar 2010), which was further refined by Yang et al. (2014) to estimate the practical extractable power with a relatively small number of turbines (<100) and evaluate the effects of TECs

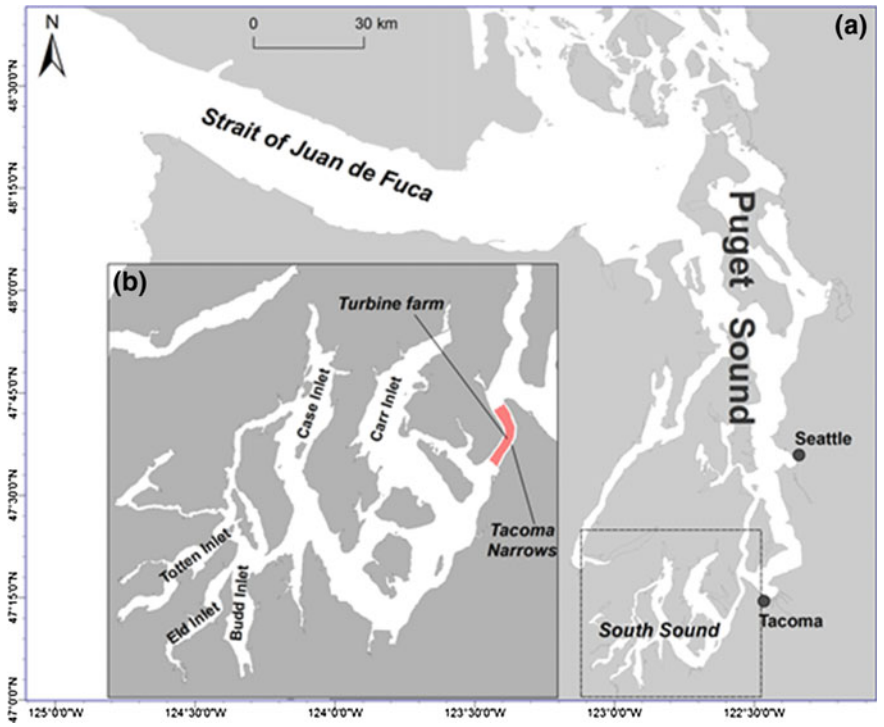

Fig. 4 Puget Sound (**a**) and the study site of Tacoma Narrows and South Sound (**b**). The location of turbine farm is located in the central area of Tacoma Narrows, as marked in *red* in (**b**)

on the flow field and bottom shear stress in Tacoma Narrows. In the present study, hypothetical tidal turbine farms were simulated with turbine density ranging from 17- to 2-rotor-diameter spacing. Tidal turbines were uniformly distributed in the entire central deep region of Tacoma Narrows (Fig. 4b) where water depth is mostly greater than 30 m. The turbine diameter was 10 m, and the hub height was specified at 15 m from the sea bed. The turbine thrust coefficient was specified as 0.9, the same value used in the previous study (Yang et al. 2014). Because the primary focus of this study was to quantify the impact of tidal energy extraction on tidal flux and water exchange, the hydrodynamic model was run in the barotropic mode, i.e., temperature and salinity were not simulated. In addition, river discharge and meteorological forcing were not included as a simplification. The rest of the model configuration remained the same as that used by Yang et al. (2014).

All simulations were conducted for a period of 125 days, and the first 5 days represented the model spin-up time. The simulated changes in volume flux corresponding to different energy extraction scenarios in Tacoma Narrows are presented in Fig. 5a. The average extractable power was calculated based on a 120-day period. While the distribution of extractable power as a function of volume flux reduction in Tacoma Narrows is similar to the results from analytical solutions (Garrett and Cummins 2005; Sutherland et al. 2007), the volume flux reduction corresponding to the maximum extractable power of 130.5 MW is only about 10.8%, which is much smaller than the theoretical value of 42% derived by Garrett and Cummins (2005). The discrepancy was noted by Yang et al. (2013) in their study that assessed the impact of tidal energy extraction in an idealized tidal channel using a 3-D model. One of the shortcomings of 1-D and depth-averaged 2-D models is the assumption that tidal energy is extracted through the entire water column of the channel cross section. In real-world applications, TECs only extract energy at a water depth around the hub height, and therefore water flow can bypass the turbine farms above and below the turbines. Yang et al. (2013) found that the volume flux corresponding to the maximum extractable power in the idealized channel was only reduced by 23% when the

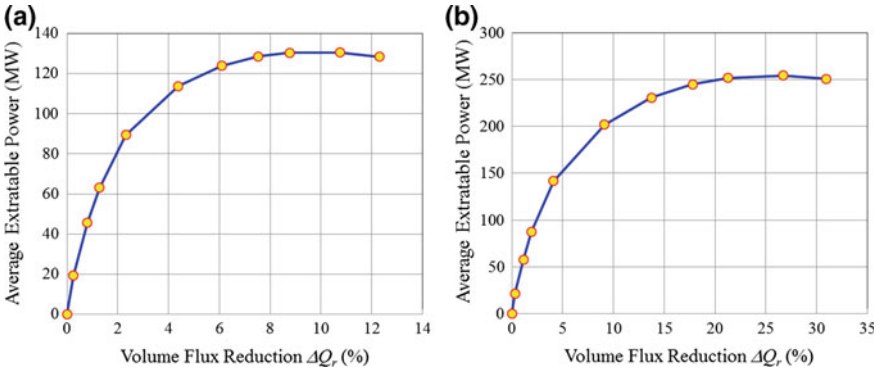

Fig. 5 Average extractable power versus volume flux reduction in Tacoma Narrows. **a** Results from 3-D model simulations. **b** Results from depth-averaged 2-D model simulations

turbine hub height was specified to be near the bottom of the water column. Karsten et al. (2013) combined LMADT with volume flux to assess the extractable tidal energy and effect of turbine fence blockage ratios in Minas Passage, in the Bay of Fundy. They found that the maximum extractable power became much smaller and the corresponding flow reduction was less than 10% when small turbine blockage ratios were considered. Hasegawa et al. (2011) investigated the far-field hydrodynamic impacts of tidal energy extraction in Minas Passage using a 3-D coastal circulation model and showed that the volume flux reduction corresponding to the maximum power output was only about 10% when energy was extracted from the lower water column, and over 38% when energy was extracted from the whole water column, which is much closer to the theoretical value of 42% given by Garrett and Cummins (2005).

To illustrate the difference between 2-D and 3-D modeling approaches for assessing extractable tidal energy in Tacoma Narrows, model simulations were conducted for the same tidal turbine farms (as shown in Fig. 5a), but in a depth-averaged 2-D mode such that tidal energy was extracted from the entire water column. Simulated average extractable power versus volume flux reduction from the 2-D model runs is presented in Fig. 5b. The simulated maximum extractable power from 2-D model simulation increased from 130.5 MW (3-D result) to 254.4 MW, which was very close to the theoretical extractable power of 248 MW derived by Yang et al. (2014) based on a modified form of Eq. 7 using amplitudes of eight tidal constituents (S_2, M_2, N_2, K_2, K_1, P_1, O_1, and Q_1) at the entrance of Tacoma Narrows. The relative volume flux reduction corresponding to maximum extractable power increased from 10.8% in 3-D mode to 26.7% in 2-D mode. Polagye et al. (2009) applied a 1-D model to investigate the far-field effects of tidal stream energy extraction in Puget Sound. They found that a 5% reduction in volume flux would correspond to 120 MW of power dissipation by TECs in Tacoma Narrows. Their findings were similar to the results of the present study, as shown in Fig. 5. It should be noted that the estimated maximum extractable power highly depends on the turbine farm configurations and the exact values should be used as general guidance.

Tracer transport simulations were conducted in 3-D mode to estimate the flushing time in the South Sound, a sub-basin connected to the main basin of Puget Sound through Tacoma Narrows. The initial tracer concentration was specified as 1.0 inside the South Sound and zero in Tacoma Narrows and the rest of Puget Sound. Figure 6a shows the depth-averaged instantaneous tracer concentration distribution for the baseline condition after 100 days of tracer release. It can be seen that for most areas of the South Sound, tracer concentration has decreased to less than 0.5 or 50% of the initial value. As expected, higher tracer concentrations are restricted to upstream tributaries that are relatively far away from Tacoma Narrows, e.g., Case Inlet and Carr Inlet. Figure 6b shows the tracer concentration difference between the scenario with 63 MW averaged power extraction and the baseline condition. Positive values occurred in most areas of the South Sound with highest concentration differences (>0.06) in Case Inlet. This suggests that extracting tidal power from Tacoma Narrows will reduce tidal flushing in tidal basins behind the

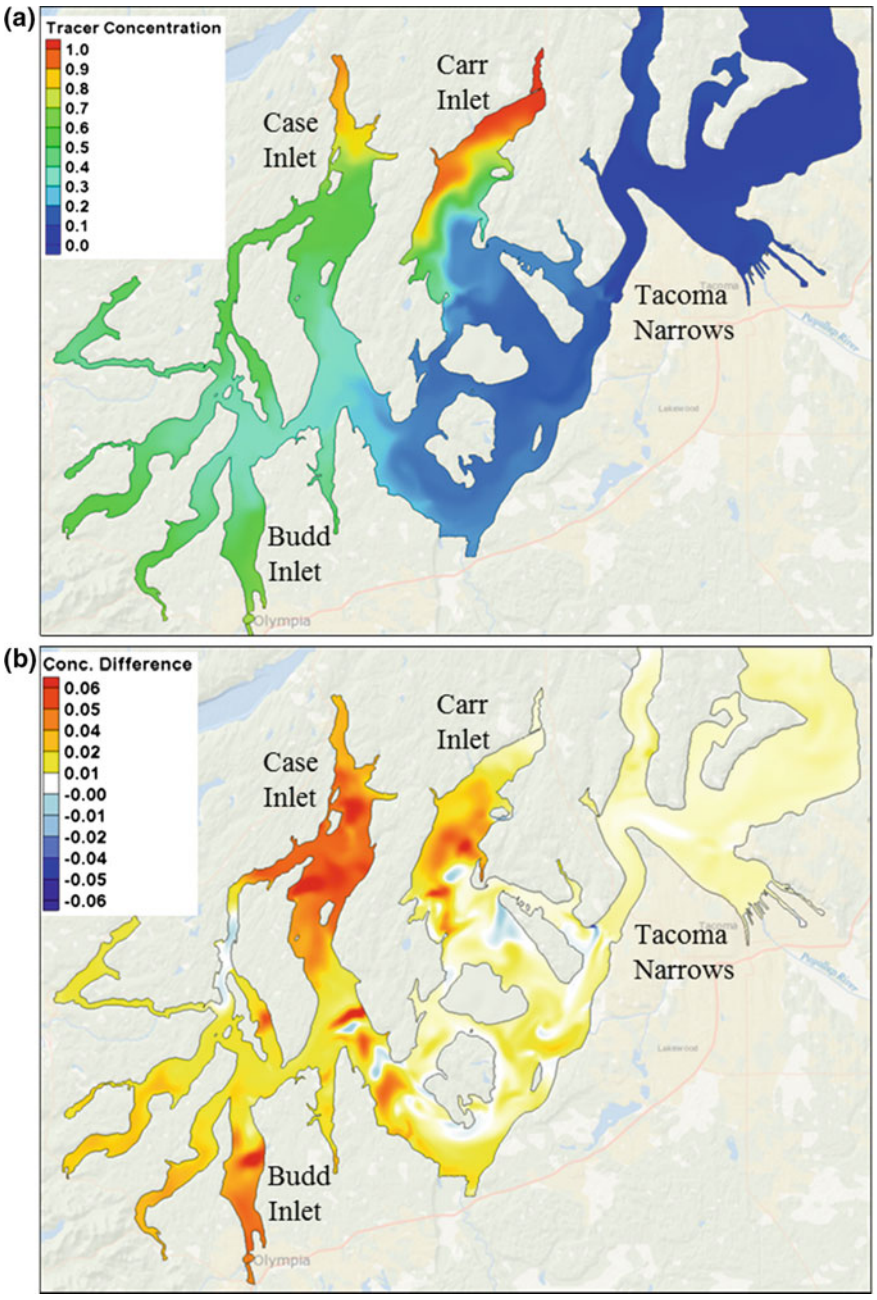

Fig. 6 **a** Simulated instantaneous tracer concentration for the baseline condition (without tidal turbine) in Tacoma Narrows of Puget Sound. **b** Difference in tracer concentrations between 63 MW power and baseline condition in the South Sound sub-basin. Tidal turbines were specified in Tacoma Narrows of Puget Sound

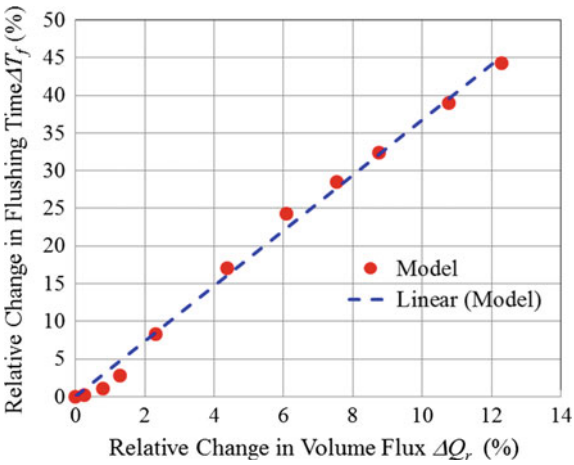

Fig. 7 Simulated change in flushing time (%) versus volume flux reduction caused by tidal stream energy extraction in Tacoma Narrows of Puget Sound. Simulations were conducted in 3-D mode and turbine configurations are the same as Fig. 5a

strait. The maximum impact is likely to occur in Case Inlet, potentially as a result of its relative deep depth and far distance from Tacoma Narrows.

Assuming the spatially averaged tracer concentration in the South Sound follows an exponential distribution after the initial release, as described by Eq. 5, the decay rate K can be determined by an exponential regression to spatial-average tracer concentration simulated by the model. The flushing time in the South Sound then can be estimated based on Eq. 6 for the baseline condition and all tidal farm configurations. The relative change in flushing time as a function of volume flux reduction is presented in Fig. 7. As can be seen, there is an approximate linear relationship between change in flushing time and volume flux reduction, similar to the idealized case study results (Fig. 3b). Applying the linear regression of Eq. 12 to the model results yields $\Delta T_f = 3.7 \cdot \Delta Q_r$, which indicates that the effect of tidal energy extraction in Tacoma Narrows on flushing time is several times greater than the effect on the volume flux. As a result, the potential impact on key physical and biogeochemical processes such as sediment transport and primary productivity should be much greater than that indicated by the change in volume flux alone. This suggests that care should be taken when harnessing more energy from a tidal system because the potential environmental impact could increase more rapidly.

Summary

The effects of TECs on physical processes in marine systems, such as far-field hydrodynamics and transport processes, are one of the environmental concerns in tidal stream energy development. Due to spatial and temporal limitations of field measurements, numerical models are useful tools for assessing tidal energy resources and evaluating the impacts of energy extraction on physical systems, such

as circulation and transport processes. This chapter provides a detailed review of various methods, including simple 1-D models and analytical solutions to advanced 3-D models for assessing the theoretical extractable tidal energy across a tidal channel and the effects of energy extraction on far-field hydrodynamics and transport processes. Examples based on an idealized tidal channel linking to a coastal bay and a realistic site—Tacoma Narrows—illustrate the use of numerical models for evaluating the effects of tidal energy extraction on volume flux and transport processes. Specifically, the flushing time concept was used to quantify the impact of TECs on the change in transport timescale. The flushing time of a coastal bay was calculated using an exponential decay formula based on tracer simulations from a 3-D hydrodynamic and transport model. One of the key findings from this study is that if a 10% change in flushing time is the acceptable upper limit for the concern of environmental impact due to TECs, a smaller percentage reduction in volume flux must be considered because the change in flushing time is several times greater than the change in volume flux.

While analytical solutions or 1-D models are useful for estimating the upper limit of theoretical extractable power, they should be used with caution when applied to real-world sites because of the strict assumptions underlying the governing equations. Results derived from the case studies for idealized tidal channel connecting to a coastal bay and Tacoma Narrows in Puget Sound suggest that the maximum extractable power and the corresponding volume flux reduction in a real-world site could be much smaller than those derived from idealized conditions, because in reality flow can bypass tidal turbines in both the horizontal and vertical planes. The impact of tidal energy extraction on volume flux and flushing timescales is a 3-D problem, which highly depends on the turbine hub height in the vertical water column as well as on the horizontal array layout. Study results indicate that, within a small range of volume flux reduction (less than 10%), the change in flushing time is approximately linearly proportional to the volume flux reduction but shows a greater rate of change. Therefore, flushing time in a coastal bay or estuary system is a better parameter for quantifying the impact of tidal energy extraction on the transport processes in the physical system.

To improve the accuracy of environmental impact assessments associated with the installation and operation of TECs, it is necessary to include these physical variables and processes in the model simulations, especially in an estuarine system like Puget Sound where density-driven two-layer circulation is evident (Yang and Wang 2015). The present study also suggests that unless tidal farms consist of high densities of turbines, the volume flux across Tacoma Narrows will be restricted to less than a few percent. Therefore, available marine space may become a bigger factor than the system-wide impact in decision making for practical energy extraction (Polagye et al. 2009; Nash et al. 2014). Environmental impact assessments for tidal energy extraction should be combined with marine spatial planning analysis and focus on tidal farms with reasonable turbine densities that are not limited by marine space. In the present study, river inflows and baroclinic effects due to temperature and salinity gradients were not considered in the circulation and transport simulations.

References

Alexander, K. A., Potts, T., & Wilding, T. A. (2013). Marine renewable energy and Scottish west coast fishers: Exploring impacts, opportunities and potential mitigation. *Ocean and Coastal Management, 75,* 1–10.

Benjamins, S., Dale, A. C., Hastie, G., Waggitt, J. J., Lea, M. A., Scott, B., et al. (2015). Confusion reigns? A review of marine megafauna interactions with tidal-stream environments. *Oceanography and Marine Biology: An Annual Review, 53*(53), 1–54.

Blanchfield, J., Garrett, C., Wild, P., & Rowe, A. (2008). The extractable power from a channel linking a bay to the open ocean. *Proceedings of the Institution of Mechanical Engineers Part a-Journal of Power and Energy, 222,* 289–297.

Bryden, I. G., & Couch, S. J. (2007). How much energy can be extracted from moving water with a free surface: A question of importance in the field of tidal current energy? *Renewable Energy, 32,* 1961–1966.

Bryden, I. G., Couch, S. I., Owen, A., & Melville, G. (2007). Tidal current resource assessment. *Proceedings of the Institution of Mechanical Engineers Part a-Journal of Power and Energy, 221,* 125–135.

Bryden, I. G., Grinsted, T., & Melville, G. T. (2004). Assessing the potential of a simple tidal channel to deliver useful energy. *Applied Ocean Research, 26,* 198–204.

Chen, C. S., Liu, H. D., & Beardsley, R. C. (2003). An unstructured grid, finite-volume, three-dimensional, primitive equations ocean model: Application to coastal ocean and estuaries. *Journal of Atmospheric and Oceanic Technology, 20,* 159–186.

Copping, A., Sather, N. H. L., Whiting, J., Zydlewski, G., Staines, G., Gill, A., et al. (2016). Annex IV 2016 state of the science report: Environmental effects of marine renewable energy development around the world. *Ocean Energy Systems*, Seattle WA, USA.

Criales, M. M., Zink, I. C., Haus, B. K., Wylie, J., & Browder, J. A. (2013). Effect of turbulence on the behavior of pink shrimp postlarvae and implications for selective tidal stream transport behavior. *Marine Ecology Progress Series, 477,* 161–176.

Defne, Z., Haas, K. A., & Fritz, H. M. (2011). Numerical modeling of tidal currents and the effects of power extraction on estuarine hydrodynamics along the Georgia coast, USA. *Renewable Energy, 36,* 3461–3471.

Defne, Z., Haas, K. A., Fritz, H. M., Jiang, L. D., French, S. P., Shi, X., et al. (2012). National geodatabase of tidal stream power resource in USA. *Renewable and Sustainable Energy Reviews, 16,* 3326–3338.

Draper, S., Houlsby, G. T., Oldfield, M. L. G., & Borthwick, A. G. L. (2010). Modelling tidal energy extraction in a depth-averaged coastal domain. *IET Renewable Power Generation, 4,* 545–554.

Dyer, K. R. (1973). *Estuaries: A Physical Introduction*. New Yrok: Wiley.

Evans, P., Mason-Jones, A., Wilson, C., Wooldridge, C., O'Doherty, T., & O'Doherty, D. (2015). Constraints on extractable power from energetic tidal straits. *Renewable Energy, 81,* 707–722.

Furness, R. W., Wade, H. M., Robbins, A. M. C., & Masden, E. A. (2012). Assessing the sensitivity of seabird populations to adverse effects from tidal stream turbines and wave energy devices. *ICES Journal of Marine Science, 69,* 1466–1479.

Garrett, C., & Cummins, P. (2005). The power potential of tidal currents in channels. *Proceedings of the Royal Society a-Mathematical Physical and Engineering Sciences, 461,* 2563–2572.

Garrett, C., & Cummins, P. (2007). The efficiency of a turbine in a tidal channel. *Journal of Fluid Mechanics, 588,* 243–251.

Gove, B., Williams, L. J., Beresford, A. E., Roddis, P., Campbell, C., Teuten, E., et al. (2016). Reconciling biodiversity conservation and widespread deployment of renewable energy technologies in the uk. *PLoS One 11*.

Hakim, A. R., Cowles, G. W., & Churchill, J. H. (2013). The impact of tidal stream turbines on circulation and sediment transport in muskeget channel, MA. *Marine Technology Society Journal, 47,* 122–136.

Hammar, L., Eggertsen, L., Andersson, S., Ehnberg, J., Arvidsson, R., Gullstrom, M., et al. (2015). A probabilistic model for hydrokinetic turbine collision risks: Exploring impacts on fish. *PLoS One 10*.

Hasegawa, D., Sheng, J. Y., Greenberg, D. A., & Thompson, K. R. (2011). Far-field effects of tidal energy extraction in the Minas Passage on tidal circulation in the Bay of Fundy and Gulf of Maine using a nested-grid coastal circulation model. *Ocean Dynamics, 61,* 1845–1868.

Kadiri, M., Ahmadian, R., Bockelmann-Evans, B., Rauen, W., & Falconer, R. (2012). A review of the potential water quality impacts of tidal renewable energy systems. *Renewable and Sustainable Energy Reviews, 16,* 329–341.

Karsten, R. H., McMillan, I. M., Lickley, M. J., & Haynes, R. D. (2008). Assessment of tidal current energy in the Minas Passage, Bay of Fundy. *Proceedings of the Institution of Mechanical Engineers Part a-Journal of Power and Energy, 222,* 493–507.

Karsten, R., Swan, A. & Culina, J. (2013). Assessment of arrays of in-stream tidal turbines in the Bay of Fundy. *Philosophical Transactions of the Royal Society A-Mathematical Physical and Engineering Sciences 371*.

Kilcher, K., Thresher, R. & Tinnesand, H. (2016). Marine Hydrokinetic Energy Site Identification and Ranking Methodology Part II: Tidal Energy. NREL/TP-5000-66079. National Renewable Energy Laboratory, Golden, CO.

Kuo, A. Y., & Neilson, B. J. (1988). A modified tidal prism model for water-quality in small coastal embayments. *Water Science and Technology, 20,* 133–142.

Lo Brutto, O. A., Nguyen, T., Guillou, S. S., Thiebot, J., & Gualous, H. (2016). Tidal farm analysis using an analytical model for the flow velocity prediction in the wake of a tidal turbine with small diameter to depth ratio. *Renewable Energy, 99,* 347–359.

Long, W., Jung, K. W., Yang, Z. Q., Copping, A., & Deng, Z. D. (2016). Coupled modeling of hydrodynamics and sound in coastal ocean for renewable ocean energy development. *Marine Technology Society Journal, 50,* 27–36.

Luketina, D. (1998). Simple tidal prism models revisited. *Estuarine, Coastal and Shelf Science, 46,* 77–84.

Martin-Short, R., Hill, J., Kramer, S. C., Avdis, A., Allison, P. A., & Piggott, M. D. (2015). Tidal resource extraction in the Pentland Firth, UK: Potential impacts on flow regime and sediment transport in the Inner Sound of Stroma. *Renewable Energy, 76,* 596–607.

Miller, R. G., Hutchison, Z. L., Macleod, A. K., Burrows, M. T., Cook, E. J., Last, K. S., et al. (2013). Marine renewable energy development: Assessing the Benthic footprint at multiple scales. *Frontiers in Ecology and the Environment, 11,* 433–440.

Myers, L., & Bahaj, A. S. (2005). Simulated electrical power potential harnessed by marine current turbine arrays in the Alderney Race. *Renewable Energy, 30,* 1713–1731.

Nash, S., O'Brien, N., Olbert, A., & Hartnett, M. (2014). Modelling the far field hydro-environmental impacts of tidal farms—A focus on tidal regime, inter-tidal zones and flushing. *Computers and Geosciences, 71,* 20–27.

Neill, S. P., Litt, E. J., Couch, S. J., & Davies, A. G. (2009). The impact of tidal stream turbines on large-scale sediment dynamics. *Renewable Energy, 34,* 2803–2812.

Officer, C. B. (1976). *Physical Oceanography of Estuaries (and Associated Coastal Waters)*. New York: Wiley.

Pacheco, A., & Ferreira, O. (2016). Hydrodynamic changes imposed by tidal energy converters on extracting energy on a real case scenario. *Applied Energy, 180,* 369–385.

Polagye, B., Kawase, M., & Malte, P. (2009). In-stream tidal energy potential of Puget Sound, Washington. *Proceedings of the Institution of Mechanical Engineers Part a-Journal of Power and Energy, 223,* 571–587.

Polagye, B. L., & Malte, P. C. (2011). Far-field dynamics of tidal energy extraction in channel networks. *Renewable Energy, 36,* 222–234.

Polagye, B., Malte, P., Kawasel, M., & Durran, D. (2008). Effect of large-scale kinetic power extraction on time-dependent estuaries. *Proceedings of the Institution of Mechanical Engineers Part a-Journal of Power and Energy, 222,* 471–484.

Rao, S., Xue, H. J., Bao, M., & Funke, S. (2016). Determining tidal turbine farm efficiency in the western passage using the disc actuator theory. *Ocean Dynamics, 66,* 41–57.

Roc, T., Greaves, D., Thyng, K. M., & Conley, D. C. (2014). Tidal turbine representation in an ocean circulation model: Towards realistic applications. *Ocean Engineering, 78,* 95–111.

Roche, R. C., Walker-Springett, K., Robins, R. E., Jones, J., Veneruso, G., Whitton, T. A., et al. (2016). Research priorities for assessing potential impacts of emerging marine renewable energy technologies: Insights from developments in Wales (UK). *Renewable Energy, 99,* 1327–1341.

Sanford, L. P., Boicourt, W. C., & Rives, S. R. (1992). Model for estimating tidal flushing of small embayments. *Journal of Waterway Port Coastal and Ocean Engineering-Asce, 118,* 635–654.

Schlezinger, D. R., Taylor, C. D., & Howes, B. L. (2013). Assessment of zooplankton injury and mortality associated with underwater turbines for tidal energy production. *Marine Technology Society Journal, 47,* 142–150.

Shapiro, G. I. (2011). Effect of tidal stream power generation on the region-wide circulation in a shallow sea. *Ocean Science, 7,* 165–174.

Shields, M. A., Woolf, D. K., Grist, E. P. M., Kerr, S. A., Jackson, A. C., Harris, R. E., et al. (2011). Marine renewable energy: The ecological implications of altering the hydrodynamics of the marine environment. *Ocean and Coastal Management, 54,* 2–9.

Sutherland, G., Foreman, M., & Garrett, C. (2007). Tidal current energy assessment for Johnstone Strait, Vancouver Island. *Proceedings of the Institution of Mechanical Engineers Part A—Journal of Power and Energy, 221,* 147–157.

Thiebot, J., du Bois, P. B., & Guillou, S. (2015). Numerical modeling of the effect of tidal stream turbines on the hydrodynamics and the sediment transport—Application to the Alderney Race (Raz Blanchard), France. *Renewable Energy, 75,* 356–365.

van der Molen, J., Ruardij, P., & Greenwood, N. (2016). Potential environmental impact of tidal energy extraction in the Pentland Firth at large spatial scales: Results of a biogeochemical model. *Biogeosciences, 13,* 2593–2609.

VanZwieten, J., McAnally,W., Ahmad, J., Davis, T., Martin, J., Bevelhimer, M., et al. (2015). In-stream hydrokinetic power: review and appraisal. *Journal of Energy Engineering 141*.

Vennell, R. (2010). Tuning turbines in a tidal channel. *Journal of Fluid Mechanics, 663,* 253–267.

Venugopal, V. & Nemalidinne, R. (2014). Marine energy resource assessment for orkney and pentland waters with a coupled wave and tidal flow model. *33rd International Conference on Ocean, Offshore and Arctic Engineering, 2014* (Vol. 9b).

Wang, C. F., Hsu, M. H., & Kuo, A. Y. (2004). Residence time of the Danshuei River estuary. *Taiwan. Estuarine Coastal and Shelf Science, 60,* 381–393.

Wang, T. P., Yang, Z. Q., & Copping, A. (2015). A modeling study of the potential water quality impacts from in-stream tidal energy extraction. *Estuaries and Coasts, 38,* S173–S186.

Ward, J., Schultz, I., Woodruff, D., Roesijadi, G. & Copping, A. (2010). Assessing the effects of marine and hydrokinetic energy development on marine and estuarine resources. *Oceans 2010*.

Williamson, B. J., Blondel, P., Armstrong, E., Bell, P. S., Hall, C., Waggitt, J. J., et al. (2016). A Self-Contained subsea platform for acoustic monitoring of the environment around marine renewable energy devices-field deployments at wave and tidal energy sites in Orkney, Scotland. *IEEE Journal of Oceanic Engineering, 41,* 67–81.

Wood, T. (1979). Modification of existing simple segmented tidal prism models of mixing in estuaries. *Estuarine and Coastal Marine Science, 8,* 339–347.

Work, P. A., Haas, K. A., Defne, Z., & Gay, T. (2013). Tidal stream energy site assessment via three-dimensional model and measurements. *Applied Energy, 102,* 510–519.

Yang, Z. Q., & Khangaonkar, T. (2010). Multi-scale modeling of Puget Sound using an unstructured-grid coastal ocean model: From tide flats to estuaries and coastal waters. *Ocean Dynamics, 60,* 1621–1637.

Yang, Z. Q., & Wang, T. P. (2015). Modeling the effects of tidal energy extraction on estuarine hydrodynamics in a stratified estuary. *Estuaries and Coasts, 38,* S187–S202.

Yang, Z. Q., Wang, T. P., & Copping, A. E. (2013). Modeling tidal stream energy extraction and its effects on transport processes in a tidal channel and bay system using a three-dimensional coastal ocean model. *Renewable Energy, 50,* 605–613.

Yang, Z. Q., Wang, T. P., Copping, A., & Geerlofs, S. (2014). Modeling of in-stream tidal energy development and its potential effects in Tacoma Narrows, Washington, USA. *Ocean and Coastal Management, 99,* 52–62.

The Impact of Marine Renewable Energy Extraction on Sediment Dynamics

Simon P. Neill, Peter E. Robins and Iain Fairley

Introduction

Previously identified research priorities on the environmental impacts of marine renewable energy (MRE) extraction have focused on issues that do not directly affect the resource, such as the collision risk of marine mammals and the effects of underwater noise generated by turbines (e.g. Aquatera Ltd and Marine Space 2015). However, apart from the direct feedback of energy extraction on the resource itself (e.g. Adcock et al. 2013), it is primarily impacts on sediment dynamics and associated morphodynamics that will significantly affect the resource and hence alter the environment in which devices operate (Neill et al. 2009). Of the potential impacts of MRE electricity generation on the marine environment, the impact on sediment transport pathways, and its effect on associated morphodynamic features, such as offshore sand banks, is probably the most easily quantified (Shields et al. 2011), particularly since the transport of sediments can be described by a defined set of equations (Soulsby 1997) that can readily be incorporated into regional hydrodynamic models (e.g. Neill et al. 2007). However, field data are important for parameterising and tuning such sediment transport models, because the models are sensitive to a range of variables, including sediment grain size distribution and the underlying hydrodynamic flow field (e.g. Camenen and Larroudé 2003). In addition, it is essential that the natural variability of sedimentary systems (pre-construction) is fully understood, so that impacts attributed to energy extraction can be quantified (Robins et al. 2014).

S.P. Neill (✉) · P.E. Robins
School of Ocean Sciences, Bangor University, Bangor, UK
e-mail: s.p.neill@bangor.ac.uk

I. Fairley
College of Engineering, Swansea University, Swansea, UK

Z. Yang and A. Copping (eds.), *Marine Renewable Energy*,
DOI 10.1007/978-3-319-53536-4_12

Developers seek highly energetic tidal stream and wave sites, because the theoretical resource at such sites is generally considered to lead to the highest electricity yield. It is often assumed that the seabed sediment is composed exclusively of bedrock or cobbles at such high-energy sites, but that is rarely the case. Even in extremely energetic sites such as the Pentland Firth in Scotland (Fig. 1), the bedrock will be overlain with a veneer of mobile sediment (e.g. Evans 1990), and predominant bedrock will be interspersed with regions of sand (e.g. Easton et al. 2011; Robins et al. 2014; Fairley et al. 2015). Such pockets of mobile sediment are important habitats for fisheries, and important repositories of sediment that exchange material with neighbouring beaches over a range of timescales (Neill et al. 2008). Further, although many of the high-energy wave sites are located in regions where the coastline is rocky, these regions of rocky intertidal and cliffs are punctuated by pocket beaches; for example, the Outer Hebrides of Scotland, and in particular the Isle of South Uist (V gler et al. 2011). Many of the beaches in such regions that are adjacent to proposed wave energy arrays will be characterised by sub-tidal sand bars, which exhibit strong seasonal variability (Gallagher et al. 1998). In addition,

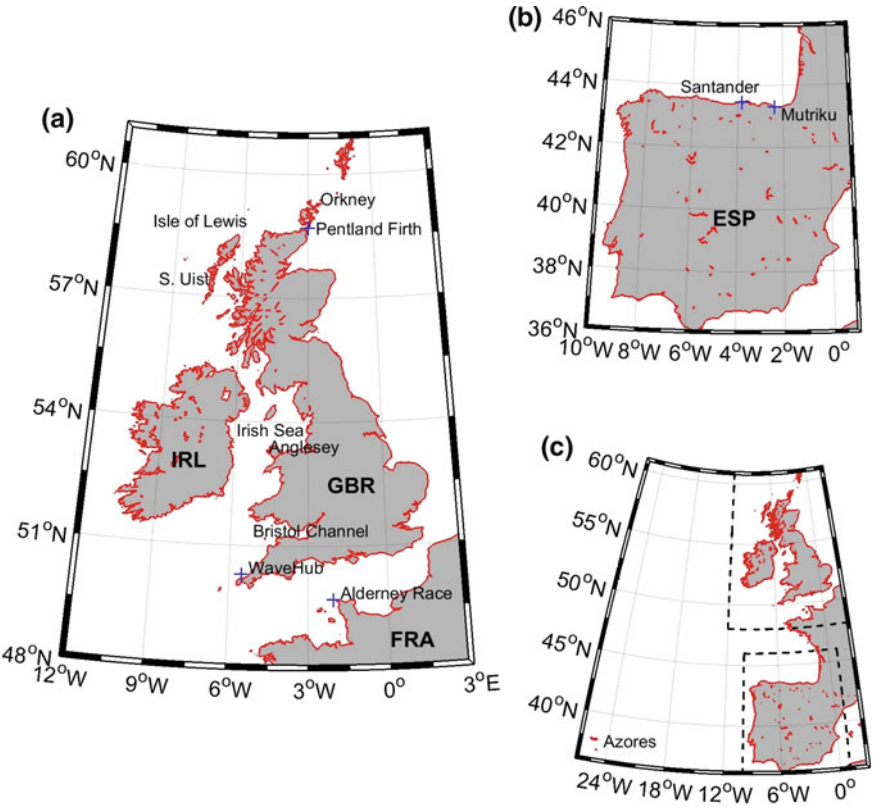

Fig. 1 Key locations referred to throughout this article

such high-energy wave and tidal sites may not be representative of the global MRE resource, which is likely to be characterised by lower tidal streams and less energetic wave conditions (Lewis et al. 2015b). Many of the high-energy sites, for example in the north-west of Scotland, are far from population centres and so remote from regions of high electricity demand; hence, the development of less energetic sites could be advantageous from a transmission perspective. Development of lower tidal energy sites also has the added advantage of offering more phase diversity than the development of high tidal energy sites alone (Iyer et al. 2013; Neill et al. 2014, 2016). Therefore, a wide range of sedimentary regimes should be reviewed when considering the wider topic of the impacts of MRE schemes on sediment dynamics.

The Transport of Sediment in the Marine Environment

Sediment transport in the marine environment is a combination of tide- and wave-induced bedload and suspended load,[1] and it occurs over a range of time-scales from a single wave orbital excursion of order seconds to semi-diurnal and storm events extending to seasonal, interannual, and decadal variability. Sediment spans a wide range of sizes, from clay (grain size less than 0.002 mm) through silt (0.002–0.06 mm), sand (0.06–2 mm), and up to cobbles and boulders (Fig. 2). The most commonly used measure of sediment grain size is the median grain size (d_{50}) —the grain size at which 50% of particles, by mass, are smaller. Although the transport of sediments includes both fine (cohesive) and coarse (non-cohesive) materials, here we consider only coarse material, i.e. sand and gravel, because such non-cohesive material will generally be representative of sediment that is available for transport at high-energy wave and tidal sites (Neill et al. 2012).

Sediment Transport Due to Tides

Tidal currents are capable of stirring up sediments from the seabed and transporting them instream with the tidal flow direction—a process known as bedload transport. Hence, any net tidal transport is likely to determine the net direction of sand transport, subject to other forces such as wave stirring (see the section "Sediment Transport Due to Waves"). In high-energy environments, coarse sands and gravel move along the seabed via bedload transport if the tidal currents are strong enough

[1]Although sediment transport can also be induced by storm surge and ocean currents, it is generally dominated by wave and tidal processes.

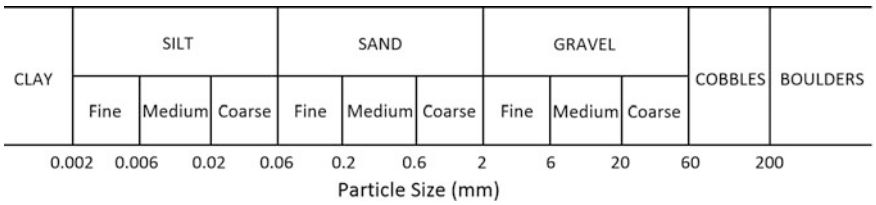

Fig. 2 Particle size ranges

to exceed the threshold of motion, above which the friction on the seabed—the bed shear stress—is large enough to force sediment from its resting position. The rate of bedload transport can be expressed in SI units as volume (m^3) per unit time (s) per unit width of bed (m), i.e. $m^2\ s^{-1}$ (Soulsby 1997). A number of competing formulae have been proposed to calculate the bedload transport rate. Most of them are a function of the bed shear stress (τ_0), expressed in dimensionless form as the Shields parameter, defined by (Soulsby 1997):

$$\theta = \frac{\tau_0}{g(\rho_S - \rho)d}$$

where g is the acceleration due to gravity, ρ is the density of sea water, ρ_s is the density of sediment grains, and d is the diameter of sediment grains. The bed shear stress can be expressed as $\tau_0 = \rho C_D \overline{U}^2$, where C_D is the drag coefficient and $\overline{U}$ is the depth-averaged flow speed. The threshold flow speed (U_{cr}), above which transport occurs, has been experimentally calculated for coarse sediments by Soulsby (1997):

$$\overline{U_{cr}} = 8.5 d_{50}^{0.6} \log_{10}(4h/d_{90}), \text{ for } 500 \leq d_{50} \leq 2000\,\text{mm}$$

where h is the water depth and d_{50} and d_{90} represent the median and 90% (of particles finer than) grain sizes, respectively. Where sediment has accumulated, the seabed will invariably be formed of sand ripples or dunes, conveniently represented by the total roughness length z_0, which can be used to calculate the total drag coefficient and bed shear stress (Soulsby 1997).

Non-linear tidal propagation in shallow shelf seas has been shown to control patterns of bedload transport over long timescales and with distinct zones of bedload divergence, transport, and convergence (e.g. Pingree and Griffiths 1979). Additional non-linear interactions of tidal motions and geomorphology can generate eddy systems (e.g. Neill 2008; Neill and Scourse 2009) and constricted currents (e.g. Brown and Davies 2009), which can further modify bedload transport in areas where tidal energy extraction may occur, such as the Bristol Channel (Neill et al. 2009) and the Orkney archipelago (Scotland; Martin-Short et al. 2015).

Sediment transport is typically subdivided into bedload and suspended load transport. Suspended load transport consists of lighter material that is entrained in the water column once current speeds are significantly above the threshold of

motion and carried over large spatial and temporal scales at the speed of the ambient currents. For material to remain in suspension, its settling speed must be less than the upward turbulent motion (Soulsby 1997). There are numerous methods of calculating the threshold of suspension and sediment settling speed, which are determined by the sediment grain size and density, and the viscosity of the water. Most of these methods are described in detail by Soulsby (1997).

For tidal current speeds that significantly exceed the threshold of suspension, strong tidal dissipation can generate regions of turbidity maxima, which are characterised by high concentrations of suspended material such as fine (mineral) sediments and organic particulate matter such as detritus, zooplankton, and fish early-life stages (Bowers et al. 2005). Turbidity maxima are important ecologically at the shelf scale; these regions of highly concentrated suspended material enhance nutrient supply for marine species, thereby serving as critical nursery areas and increasing secondary production (Ellis et al. 2008; Robins et al. 2014). They also mediate marine population dynamics (e.g. Morgan et al. 1997) and potentially species connectivity across shelf regions. However, the associated turbid waters can have a negative ecological impact, because they reduce solar input at depth (Robins et al. 2014).

By their very nature, some regions of highly concentrated suspended material or turbidity maxima are also regions of interest for tidal stream energy extraction. One important example is the Anglesey Turbidity Maxima in the Irish Sea (Bowers et al. 2002; Ellis et al. 2008)—a region of strong tidal currents that is also a region of interest for tidal stream MRE developers (Lewis et al. 2015b). Hence, the impact of tidal stream arrays on the turbidity maxima, and conversely the impact of the suspended material on the devices and the resource itself, is of obvious concern. From an initial study of the impact of energy extraction on suspended sediment concentrations, Robins et al. (2014) concluded that tidal energy converter (TEC) arrays of order <100 MW were unlikely to affect the suspended sediment concentrations beyond natural levels of variability—a criterion that could be applied to environmental impact assessments for MRE schemes elsewhere.

Sediment Transport Due to Waves

In sufficiently shallow water ($h < L/2$; where L is the wavelength), wave motion extends to the seabed. This oscillatory motion leads to the generation of a wave-induced bed shear stress, which acts on seabed sediments. The threshold, or incipient, motion of seabed sediment is primarily controlled by the amplitude of the bottom orbital velocity, in conjunction with sediment grain size and (relative) sediment density. For linear, or Airy, waves (i.e. sinusoidal waveforms), the oscillatory motion over each half of a wave cycle is symmetrical, so there is no net sediment motion. However, when waves are non-linear, for example when relatively steep waves propagate in shallow water, there is increased sediment motion beneath the wave crest compared to the sediment motion that occurs beneath the

wave trough. This leads to asymmetry in sediment transport and net transport in the direction of wave propagation, in the absence of a tidal mechanism.

Sediment Transport Due to Combined Tides/Waves

Waves provide a stirring mechanism that keeps sediment grains in suspension. The tidal current adds to this stirring, but also provides a mechanism for net sediment transport (Soulsby 1997), which is particularly important in the case of linear (Airy) waves. Although marine sediment is transported as both bedload and suspended load, it is generally the *total sediment transport rate* that is required for addressing practical applications such as the morphodynamic response of coastal regions to engineering structures (Soulsby 1997). Although many competing formulae are used to quantify total load transport by waves plus currents, one of the most popular methods is Soulsby–Van Rijn formula, particularly because this method is very easy to embed within hydrodynamic models or apply to the outputs of such models as an offline post-process (e.g. Neill et al. 2007, 2012). Neglecting bed slope, total load sediment transport rate q_t is given by

$$q_t = A_s \overline{U} \left[\left(\overline{U}^2 + \frac{0.018}{C_D} U_{rms}^2 \right)^{1/2} - \overline{U}_{cr} \right]^{2.4} \tag{1}$$

where $\overline{U}$ is the depth-averaged current speed, C_D is the drag coefficient due to the current alone, U_{rms} is the root-mean-square-wave orbital velocity, $\bar{U}_{cr}$ is the threshold current speed, and

$$A_s = A_{sb} + A_{ss}$$

where

$$A_{sb} = \frac{0.005h(d_{50}/h)^{1.2}}{[(s-1)gd_{50}]^{1.2}}$$
$$A_{ss} = \frac{0.012d_{50}D_*^{-0.6}}{[(s-1)gd_{50}]^{1.2}}$$

and s is the relative density of sediment and D_* is the dimensionless grain size, given by

$$D_* = \left[\frac{g(s-1)}{\nu^2} \right]^{1/3} d_{50}$$

where ν is the kinematic viscosity of water.

Morphodynamics

Morphodynamics describes the study of changes in the shape of the seabed over time. When the morphodynamic change is a result of an object or structure, the process is referred to as scour. For the MRE industry, morphodynamics and scour are important for determining scales and rates of accretion and erosion as a direct result of any device, array, or tidal range scheme development. This is achieved by means of the sediment budget equation, which can be written for one-dimensional (x) applications over large distances (e.g. 100 m) and times as (Soulsby 1997):

$$\frac{\partial \zeta}{\partial t} = -\frac{1}{1-\varepsilon}\left(\frac{\partial q_t}{\partial x}\right)$$

where ζ = bed-level change, t = time, ε = porosity of the bed, and q_t = volumetric total (bedload + suspended load) transport rate in the x-direction.

Using the sediment budget equation, in conjunction with sediment transport methods such as the Soulsby–Van Rijn formula (Eq. 1), coastal morphodynamic models can be used to compute the distribution of erosion and accretion over the coastal model domain (e.g. De Vriend 1993). Presently, morphodynamic models are computationally expensive compared to hydrodynamic-only models, meaning that long-term (e.g. decadal) simulations are challenging, particularly if feedback between the evolving morphodynamics and hydrodynamics are included. One way around this problem is to use make use of a "morphological factor", for example, where a short-term simulation of bed-level change over one tidal cycle is scaled-up by a factor of n to represent n tidal cycles of morphological change (e.g. Roelvink 2006; McCann 2011). Care must be given to the magnitude of the factor n. While values of 100 or greater have been shown to produce reasonable results (e.g. Dissanayake et al. 2009), appropriate values depend upon both the situation being modelled and the properties of the model grid (Ranasinghe et al. 2011).

Natural Variability

Offshore sand banks are important natural systems that protect coastal communities from the impact of storm waves, and they can be important nursery grounds for fisheries (Neill 2008). Sand banks can be generated and maintained by strong tidal currents and bathymetric irregularities (see Huthnance 1982) and are generally found in or near regions that are suitable for tidal energy extraction (e.g. Neill et al. 2012). Strong tidal flow past a headland leads to the generation of large eddy systems, which are characterised by an opposite sense of vorticity between the flood and ebb phases of the tide (Robinson 1981). The outward-directed centrifugal force within each transient eddy system is balanced by the inward-directed pressure gradient, and because the centrifugal force is weaker at the seabed (as a result of bed friction),

this leads to the inward movement of relatively coarse sediment at the bed (Pingree 1978). Hence, the interaction between pressure gradient forces, centrifugal forces, and friction results in the convergence of sand and the formation and maintenance of headland sand banks (Bastos et al. 2002).

The morphology (and hence volume) of offshore sand banks is affected by a variety of processes that occur over a range of timescales, such as long-term sediment supply and sea-level rise (Lewis et al. 2015a). Shorter timescale processes that influence sand banks include storm wave events (e.g. Fairley et al. 2016) and semi-diurnal tidal currents (Neill et al. 2007). During storms, near-bed wave orbital velocities from waves can greatly exceed the critical speed of sediment motion, even in water depths of 10s of metres (Mitchell et al. 2012). This short-term (relative to the action of tidal currents) wave-induced sediment transport can affect the evolution and maintenance of an offshore sand bank (Van de Meene and Van Rijn 2000). Therefore, the frequency and intensity of storm wave events between each year (i.e. the interannual variability of the storm wave climate) may be an important process affecting sand bank evolution over decadal timescales. However, the role of the annual storm wave climate, within the interannual variability of offshore sand bank morphology, is unclear (Lewis et al. 2015a).

Beach profile variability is often considered on a seasonal basis and features distinct summer and winter profiles (Fig. 3). Summer profiles are accretive profiles that are characterised by steeper gradients and the presence of a high-tide berm; such profiles are formed under low-energy conditions. Winter profiles typically have shallower gradients, and one or more offshore bars may be present caused by accumulation of sediment under the break point of storm waves. Such break point bars are beneficial, because they dissipate some of the wave energy prior to its reaching the shoreline. The transition from summer and winter conditions can occur rapidly over the course of one storm event, but the transition between winter and summer is a more gradual process. On coastlines in areas that experience little seasonality, similar profiles may be termed pre- and post-storm profiles.

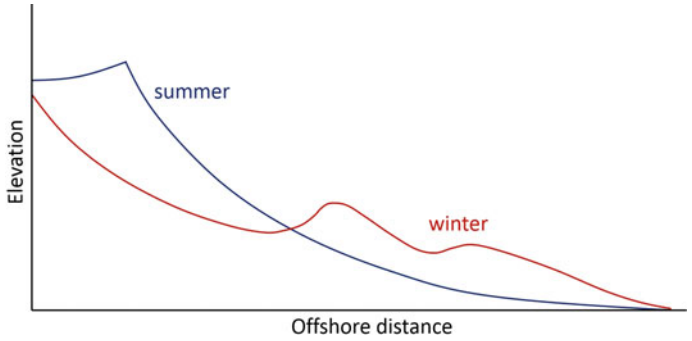

Fig. 3 Illustrative beach profiles for a sandy beach. A schematic example summer profile is shown in *blue* and a winter profile in *red*

While storm-induced intertidal change is relatively well understood, the processes and timescales involved with storm recovery are still an ongoing research area.

Interannual variability can be related to larger scale atmospheric processes such as the North Atlantic Oscillation (Masselink et al. 2014; Vespremeanu-Stroe et al. 2007) or El Nino/La Nina (Ruggiero et al. 2005; Barnard et al. 2015). The frequency of occurrence of storm events has been linked to these cycles.

The rate of profile variability can also be linked to the region of the beach profile. Intertidal areas vary on daily timescales or less. Timescales of variability increase further offshore in deeper water depths (Ruggerio et al. 2005).

Impact of Marine Energy Devices on Sediment Dynamics

Extracting energy from the marine environment will clearly alter local, and possibly regional, hydrodynamics. Although, for most extraction scenarios, the influence on tidal currents and wave properties is likely to be very small, the influence on bed shear stress will be greater, because bed shear stress is quadratically related to tidal currents and wave orbital velocities. Further, the transport of sediments is a function of tidal current and wave orbital velocity cubed. Therefore, even small changes in the flow field caused by tidal or wave array operation could lead to significant impacts on regional sediment dynamics.

Individual Tidal Stream Devices

Turbulence produces a net upward flux of sediment that is balanced by the tendency of the sediment to settle back towards the bed. The vertical distribution of sediment in the water column can be described using a Rouse profile (e.g. Neill 2009):

$$\frac{C}{C_a} = \left[\frac{h-z}{h-a}\frac{a}{z}\right]^{w_s/\kappa u*}$$

where C is the concentration of sediment, C_a is the reference concentration at level $z = a$, h is the water depth, and $w_s/\kappa u*$ is the Rouse parameter, where w_s is the settling velocity, κ is Von Karman's constant (=0.41), and $u*$ is the frictional velocity. Taking a range of settling velocities and corresponding sediment grain sizes, we can calculate theoretical sediment concentration profiles at a typical tidal energy site with an assumed peak depth-averaged current speed of 2.5 m/s (Fig. 4).

The Rouse profiles in Fig. 4 demonstrate two important features of sediment concentrations in relation to tidal stream turbines. First, the finer sediments have a higher concentration in the water column. Second, because of the higher Rouse parameter associated with higher settling velocities, the coarser sediments are

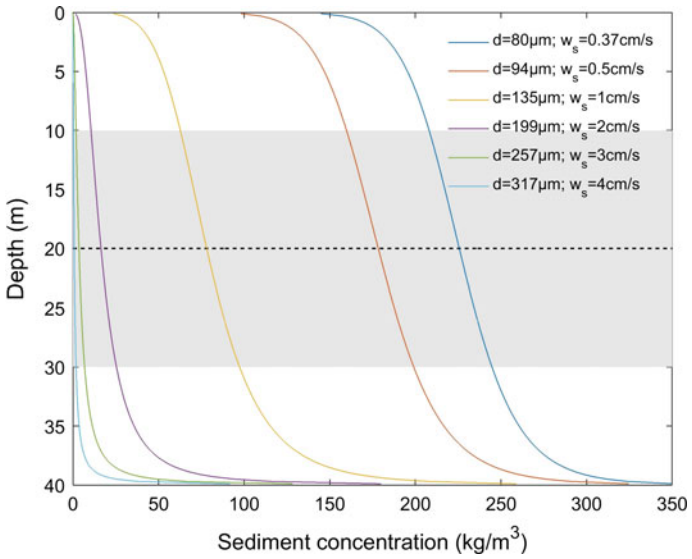

Fig. 4 Calculated sediment concentration profiles for a range of sediment grain sizes (d) (with corresponding settling velocities w_s) and depth-averaged current speed of 2.5 m/s in 40 m water depth. The horizontal *dashed line* is (mid-depth) hub height, and the *grey shaded area* is the swept area for a turbine diameter of 20 m

confined to the lower part of the water column, whereas it is only the finer sediments that have a substantial concentration higher in the water column, particularly with respect to device hub height and the turbine-swept area. In the example shown in Fig. 4, sediment grain sizes of <135 μm (fine sand; see Fig. 2) have an appreciable concentration at hub height, whereas medium sands (257 and 317 μm) have minimal concentrations either at hub height or over the swept area of the turbine. Because the seabed at the majority of tidal energy sites will be characterised by medium/coarse sands and gravels, sediment concentrations are not likely to impose significant loadings on turbine blades; however, in some regions where there is a localised source of finer sediment, or energy extraction leads to a change in the sediment regime in favour of finer sediments, consideration should be given to the possible impact of finer sediments on the wear of hub bearings and turbine blades.

A single TEC, for example of the horizontal axis configuration, is composed of a support structure and a rotor. The support structure alone will generate a wake, possibly characterised by eddy shedding, analogous to the flow past a bridge pier or a small island (e.g. Neill and Elliott 2004a, b). Flow past the support structure will influence sediment dynamics in two ways. First, localised scouring will occur in regions of strong tidal flow (Den Boon et al. 2004), and for this reason, when installing turbines in regions that have a sufficient local source of mobile sediment, developers will need to consider providing scour protection, e.g. rock armour, to prevent undermining of foundations. Second, wakes lead to a winnowing of sediments (Wolanski et al. 1984), where the fine component of an initially poorly sorted

(well-graded) sediment is removed and the coarser fraction remains. This could result in the wake zone being characterised by well-sorted (poorly graded) sediment, leading to further erosion problems associated with a less stable sedimentary structure. Further, and in contrast to obstacles placed in a riverine environment, such processes will be bidirectional in the case of tidal turbines, so scouring and winnowing will occur alternately on opposite sides of the support structure during either the flood or ebb phases of the tidal cycle. However, of even more interest, and a topic that is considerably under-researched, is the influence of the turbine rotor on sediment dynamics, particularly because the rotor is a dynamical component of the turbine, in contrast to the static nature of the support structure.

Figure 5 shows the main influence of tidal turbine rotors on the velocity profile. Because the depth of energy extraction spans only a portion of the water column, energy extraction over the depth of the rotor will be accompanied by an increase in flow speed (a bypass) both above and below the rotor, in addition to a velocity deficit over the height of the rotor (e.g. Yang et al. 2014). Of greatest significance to sediment dynamics, the near-bed bypass will lead to increased bed shear stress, so it will enhance the transport of sediments, particularly bedload and the near-bed component of the suspended load. Therefore, studies that have used depth-averaged terms to account for energy extraction (e.g. Neill et al. 2012; Robins et al. 2014) are likely to underestimate the impacts of arrays on sediment dynamics.

Arrays of Tidal Stream Devices

Although the impact of single turbines will be localised (<1 km), it is when devices are arranged in arrays, providing the potential for significant scales of electricity

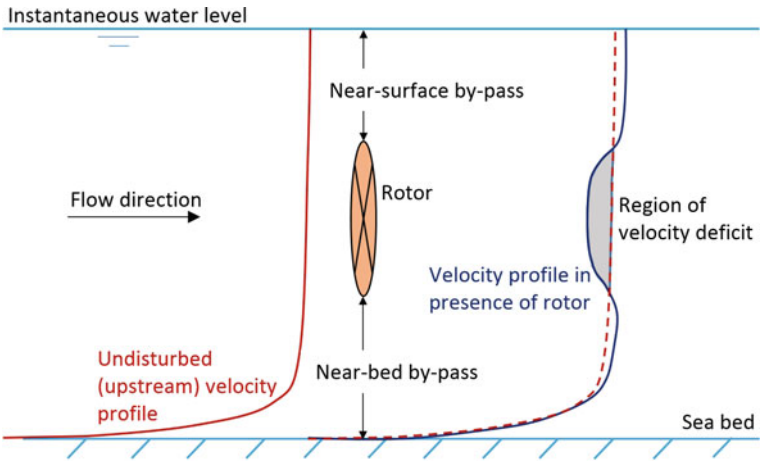

Fig. 5 Influence of tidal turbine rotor on velocity profile

generation, the impacts on regional (1–10 km) and far-field (>10 km) sediment dynamics could become important (e.g. Neill et al. 2009, 2012; Ahmadian et al. 2012). Tidal stream energy extraction tends to reduce the bedload transport rate and deflect the sediment fluxes (e.g. Fig. 6). One obvious concern about TEC array development is the arrays' potential near-field and far-field influence on the natural range of seasonal and interannual variability of sand features such as offshore sand banks (Neill et al. 2012). Therefore, when developers are planning the micro-siting of an array within an area, the device layout within the array, and the design of the devices, they should give careful consideration not only to the potential economic yield, but also to minimising the impact on the sedimentary environment. This is a crucial step in any site-specific micro-siting of TEC arrays. For example, energy extraction from regions that exhibit significant tidal asymmetry, such as in tidal channels or near headlands or islands, is likely to have a far greater impact on sedimentary systems than energy extraction in regions of tidal symmetry (Neill et al. 2009). Even regions of minimal sediment accumulation, such as bedload parting (divergence) zones, could in theory accumulate sediment over long time-scales because of the influence of a TEC array on the hydrodynamic flow field (Neill et al. 2009).

Morphodynamic model simulations provide the only realistic means for achieving economic–environmental optimisation of TEC arrays prior to their deployment and to aid in the assessment of environmental impacts. But there are several shortcomings of state-of-the-art morphodynamic applications relevant to such studies. At the regional scale, TEC array energy extraction is commonly represented in models as a momentum sink term distributed across the block array area (e.g. Neill et al. 2012; Robins et al. 2014; Thiébot et al. 2015). Such a

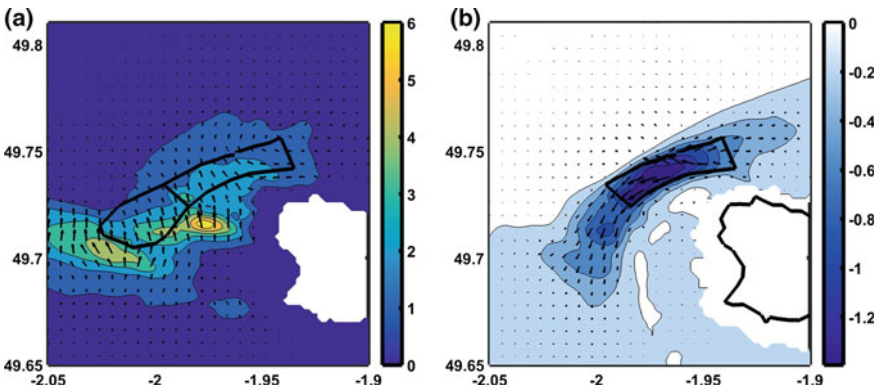

Fig. 6 Changes in bed shear stress (in pascals) as a result of a 290 MW tidal energy array in the Alderney Race. **a** Mean stress exceedance magnitude and mean direction of the exceedance for the baseline case and **b** mean changes induced by a tidal array sited within the enclosed region offshore. The *arrows* represent the direction of the perturbation. Results correspond to a sediment grain size of 3.8 mm. Results are averaged over 1 month (Thiébot et al. 2015, reproduced with kind permission from Elsevier)

methodology does not account for detailed internal array configuration or design, which can have important implications for the resulting hydrodynamic flow field (e.g. Ahmadian and Falconer 2012). Another limiting issue at present appears to be a general lack of knowledge of the sedimentary environment (and hence, spatial variability in sediment sources and bed roughness) at high-flow speed sites such as the Alderney Race (Thiébot et al. 2015) and the Pentland Firth (Fairley et al. 2015; Martin-Short et al. 2015). This means that it is both difficult to parameterise and validate models of sediment transport. At a more fundamental level, there is presently a lack of universal formulation within models of several processes, such as sediment transport rates, sediment trapping, and sediment sorting mechanisms. Furthermore, it remains a considerable computational task to simulate morphological change over the decadal timescales that are necessary to capture interannual variability, without approximating such timescales using a morphological factor. Orthogonal model mesh configurations cannot scale up from array to regional scales without resort to nesting, which potentially introduces errors propagating from nesting boundaries and may not account for feedback between the inner and outer nest. Rather, unstructured grids are preferred for array- to regional-scale morphodynamic modelling.

Nevertheless, apparent development of scientific consensus seems to suggest that siting TEC arrays farther offshore has several resource and environmental advantages. For example, farther offshore, the tidal stream resource capacity, and its temporal variability are likely reduced, and the currents are often more rectilinear and symmetrical (Robins et al. 2015; Lewis et al. 2015b), potentially leading to reduced sedimentary impacts (Neill et al. 2009, 2012; Robins et al. 2014). On the other hand, wave heights (and hence, wave-induced bed shear stress) farther offshore are typically greater (Lewis et al. 2015b). An important consideration for sedimentary environmental impact assessments is that the potential impact of energy extraction at a TEC site should fall within the natural levels of seasonal and interannual variability in bed shear stress—a proxy for sediment transport that can easily be quantified by numerical simulations (Robins et al. 2014). Under such a condition, it is theoretically possible to calculate the threshold TEC array size for any region, using tide wave-coupled model simulations. In such simulations, it will be vital to capture the natural variability of extremes in surge and wave–tide interactions. A positive result for the MRE industry, from some initial case studies of sedimentary impacts, suggests that small- to medium-sized TEC arrays (on the order of 10–100 MW) will not significantly affect the surrounding morphology in relation to natural variability (e.g. Robins et al. 2014; Fairley et al. 2015).

Wave Energy Arrays

Wave energy converters (WECs) extract energy from a wave field, thereby leading to a reduction in wave height in their lee. Depending on the device type, there is the

potential for wave reflection and local wave focusing. WECs can be grouped based on deployment area: shore-attached, nearshore, and offshore.

Shore-attached WECs are predominantly built into breakwaters, hard rock cliffs, or other such structures where the quantity of mobile sediment is limited. Mobile sediment coastlines typically have shallower seabed gradients, where greater wave energy dissipation would occur prior to reaching the WEC, and the abundance of mobile sediment would accelerate wear on devices via abrasion. Examples of early shore-attached WECs include the Pico Oscillating Water Column in the Azores and the Mutriku wave energy plant in the Basque Country. While there may be some scouring of the seabed seaward of such structures, the impact on wider field sediment transport and morphology will likely be minimal. If shore-attached devices were deployed in series on mobile sediment coasts, they might act to alter longshore sediment transport, similar to a groyne field (e.g. Schoonees et al. 2006), with accretion on the updrift side and erosion on the downdrift side.

Most prevalent of the specifically nearshore designs is the oscillating surge converter. These devices are typically deployed in 15–30 m water depths. The motion of a surface-piercing flap around a bottom-mounted hinge can be used to pump water ashore and then through generator turbines or to directly generate energy. The impact of such devices is discussed in the section "Nearshore Devices".

Offshore devices are deployed in deeper water, and the range of technology types is diverse. Offshore wave energy devices have been the most intensively studied from a morphodynamic perspective by the academic community. Impacts can be categorised as either near field or far field, both of which are considered in the section "Offshore Devices".

Nearshore Devices

Nearshore oscillating surge converter devices such as the Aquamarine Oyster or the Resolute Marine Energy SurgeWEC, being situated close to the shoreline, have the potential to have greater impact on shoreline dynamics than devices located farther offshore. However, as far as the authors are aware, little academic research has considered the impact of these devices on nearshore morphodynamics. A report about coastal processes for the proposed Outshore Point wave farm in Orkney (Xodus Group Ltd. 2012) likens the probable impact of nearshore devices such as the Oyster to the impact of detached breakwaters. Detached breakwaters typically cause accumulation of sediment at the shoreline in the lee of the structure (Fig. 7). The type of accumulation depends on the abundance of sediment, the distance of the structure from the shore, the length of the structure, the transmission coefficient of the structure, the gap distance, and the incident wave climate. Shoreline responses typically vary from no response, via the formation of a salient, to the extreme case of a tombola, where sediment accumulation reaches the breakwater because of combined refraction and diffraction processes. Similar impacts might be expected for nearshore WECs, but one aspect is different: the active back and forth

Fig. 7 Beach response to detached breakwaters at Sea Palling, UK. Accretion of the shoreline towards the structure can be observed

movement of the paddle may lead to a different dynamical response near the device, in contrast to a passive breakwater.

Offshore Devices

Near-field effects of offshore devices can be split between localised scour effects and the impact of reduced wave climate on regional sediment dynamics. Harris et al. (2011) considered the scour associated with offshore wind installations and raised the importance of scour to wave energy developments. As far as the authors are aware, no work has been conducted on scour attributed to WECs explicitly, although there is a significant body of work on marine scour (e.g. Whitehouse 1998). Scour must be considered both from the perspective of an environmental impact assessment and to ensure the integrity of the installation, which may require scour protection measures.

A regional-scale study by Gonzalez-Santamaria et al. (2011) showed that impacts on sediment dynamics are larger in the far-field than in the near-field vicinity of the WEC arrays. Early work that considered the far-field impact of WEC arrays on sediment dynamics assessed the suitability of WECs as a form of coastal defence—both for a hypothetical scenario (Zanuttigh et al. 2010) and the case study of Milano Marittima, Italy (Ruol et al. 2011). The presence of WECs was also shown to reduce the net volume of longshore sediment transport, and it is postulated that intelligent control of WECs could be used to mitigate coastal erosion. Similarly, Mendoza et al. (2014) considered different types of WECs at two locations: Santander (Spain) and Las Glorias (Mexico). A wave model was used to transform waves inshore in the absence and presence of WECs. Device specifics and array layouts both affected morphological change. For the case study at Santander, farm implementation led to shoreline accretion in all cases, while at Las Glorias, erosion was predicted for some locations. Due to lack of calibration, only the ratio of protected to unprotected cross-shore change was of relevance (Fig. 8). The region $-1 < X_p/X_u < 1$ on the vertical axis of the figure indicates levels at which change caused by WECs is less than the baseline change. At the extremities of the beach,

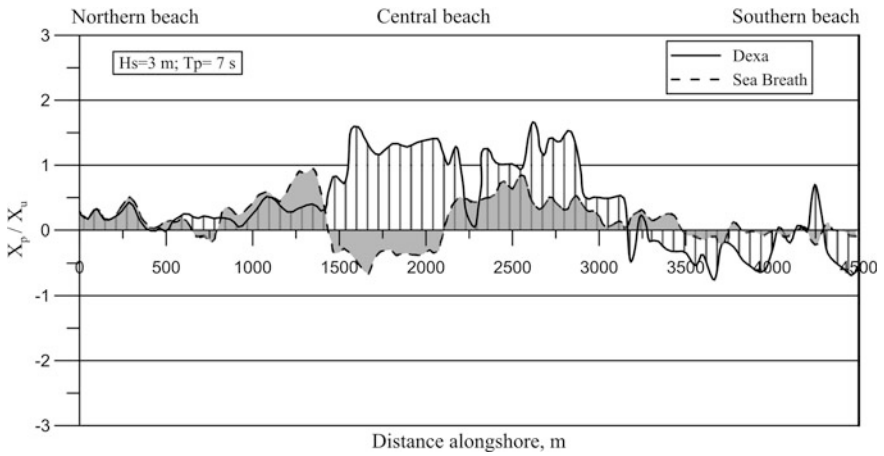

Fig. 8 Predicted shoreline response at Las Glorias, Mexico, for two different types of wave energy converter (reproduced from Mendoza et al. 2014 with permission from Elsevier)

the impact is similar for both types of devices and is less than the baseline case. In the centre, behind the farm, device type has a large impact on morphological response.

A large amount of work has focused on the WaveHub site in the United Kingdom (UK). The WaveHub is a facility for the demonstration of full-scale wave energy devices; it is fully consented, its subsea cables are already installed, and it has a capacity of 30 MW. Gonzalez-Santamaria et al. (2011, 2015) considered regional-scale impact, while Abanades et al. (2014a, b, 2015a, b) focused on the nearshore and intertidal regions for hypothetical deployments close to the WaveHub site. Gonzalez-Santamaria et al. (2011) used a two-way coupled ROMS-SWAN (Regional Ocean Modeling System Simulating Waves Nearshore) modelling system to investigate the impact of energy extraction at the WaveHub site. Wave–current interaction, sediment transport, and morphological change in the region were all considered. Importantly, inclusion of currents altered wave direction, which magnified the impact of the wave farm in this case; this suggests that fully coupled numerical models including waves, hydrodynamics, and sediment transport may be required to accurately simulate morphological change.

Abanades et al. (2014a) considered the impact that deployment of an 11-device farm might have on the two-dimensional cross-shore profile evolution at a beach adjacent to the WaveHub. Storm conditions were tested, and wave height reductions of up to 3.3% were observed due to WEC array operation. Farm implementation led to reduction in erosion over the tested profiles, in particular at the beach face and over the subtidal bar. However, the scale of these impacts may be overstated, because WEC devices would not generally be expected to generate electricity during storm events when they would enter “survival mode” and become passive. The case study was extended to three dimensions, and similar results were found (Abanades et al. 2014b). The greatest reduction in erosion was predicted at

the dune toe, and significant modification of sediment transport pathways was observed. Abanades et al. (2015a) assessed the role of coast-to-farm distance; unsurprisingly, they found that farms deployed farther offshore had less impact on shoreline morphodynamics. Consideration has also been given to the modal beach state at Perranporth (Abanades et al. 2015b). The conceptual beach model of Masselink and Short (1993) was used, and the study concluded that changes in wave height led to a shift in beach state from reflective towards dissipative. Consideration of changes in the modal beach state is likely to prove fruitful from a management perspective, because it provides a simplistic descriptor of change.

The work described thus far in this section has considered the impact of WECs on largely sandy coastlines. In the UK, the west coast of Orkney (Scotland) could be one of the early areas to be affected by large-scale wave energy conversion; similarly, interest is focused on the west coast of the Isle of Lewis (Scotland). Neither location conforms to the previously examined sandy environments. Instead, the coastlines consist of hard rock cliffs, boulder and cobble foreshore, and embayed sandy beaches. These more complex environments, which both are geologically controlled and have limited sediment supply, are more challenging to model. Fairley and Karunarathna (2014) used the commercially available MIKE 3 software to set up a fully coupled coastal area model (spectral waves, hydrodynamics, and morphological change) to investigate morphological impacts at the Bay of Skaill (west coast of Orkney). The Bay of Skaill is important because of the presence of Skara Brae, a Neolithic village, and UNESCO World Heritage Site. It consists of an embayed beach, constrained by rocky headlands to the north and south, a cobble back beach, and a bedrock subtidal region (Fig. 9). Only in the intertidal region of the embayment is mobile sediment present, although farther

Fig. 9 Survey work at the Bay of Skaill, Orkney. The cobble back beach and hard rock headland can both be seen. The hard rock lower intertidal region can be observed behind the surveyor as it is exposed by the receding tide

offshore sand dominates. Model results were compared to measured cross-shore profiles with limited success. It was postulated that the sparsity of sediment and the dominance of swash zone transport were the main reasons for poor model performance. Although this represents an isolated case, such atypical environments are likely to be common in regions of wave energy development, so it is important to have confidence in the assessment of potential impacts. Where impacts on complex environments are critical, a combination of measurement campaigns and expert opinion may be more fruitful than numerical modelling.

Long-Term Variability

To better understand the potential long-term (decadal and climatic) impact of tidal stream and wave energy extraction on regional-scale morphology, we need to first understand natural levels of morphodynamic variability, at a site-specific level and without MRE development; i.e. the variabilities and recent trends (last 50 years) in bedload transport rates (Van Landeghem et al. 2012), offshore sand bank formation and maintenance (e.g. Neill 2008; Neill and Scourse 2009), and beach profiles (e.g. Neill et al. 2008; Ruggiero et al. 2009). This requires long-term monitoring strategies (see the section "Long-Term Variability"), as well as validated morphodynamic model simulations. Then, morphodynamic models can be applied to simulate projected variability over longer timescales—either the expected lifespan of an MRE device or array (e.g. 25 years) or over timescales of relevance to climate change (50–100 years). Next, long-term energy extraction scenarios can be performed to determine rates of change, relative to the baseline (environment unmodified by MRE development), and to quantify their impacts. However, large model uncertainties currently exist, both in simulating transport and morphology accurately and in representation of energy extraction (e.g. see the section "Arrays of Tidal Stream Devices").

For different potential MRE regions, the relative controls on sediment transport and morphology need to be quantified. For example, the influence of wave-induced bed shear stress is larger in shallow waters than in deeper waters and, of course, in more exposed regions where wave heights are typically greater. Likewise, in high-flow speed regions, strong tidal currents likely control transport magnitude/direction and morphology, rather than waves. In addition, local sediment types and geophysics will influence the patterns of transport and morphology. The relative influences on bedload transport of tidal variability (e.g. transport during spring tides in comparison with neap tides) and of storm surges and storm waves are also poorly understood. It is therefore important to assess the role effect extreme (e.g. storm) events have on net sediment dynamics.

Monitoring

Monitoring of the impact of the first MRE arrays on mobile sediment regions will be vital to better understand the likely impacts of future arrays. Because of the interannual and intra-annual variability of morphodynamic behaviour (section "Natural Variability"), baseline studies of sufficient duration should be performed prior to device deployment. Monitoring of intertidal regions is relatively inexpensive (compared to offshore bathymetry surveys), and hence, it is viable to expect surveys to be conducted with some regularity. Traditionally, monitoring of intertidal change has relied on repeated measurement of defined cross-shore profiles, often based on data collected by local authorities for coastal management purposes. In some areas, profile records are available for many decades, although repeatability varies due to changing measurement technology (Harley et al. 2011). Initially, profiles were measured using the emery board technique (Emery 1961); more recently, theodolites and real-time kinematic global positioning system (RTK-GPS) surveys have been used. A key issue with profiles collected by local authorities is the temporal frequency of collection, which is often conducted on an annual or 6-monthly summer–winter basis (e.g. Neill et al. 2008). This is not only insufficient temporal resolution to define intra-annual changes, but the timing of surveys relative to storm events (and associated coastal recession) can obscure actual trends in the morphological evolution of beaches. Ideally, higher temporal resolution, e.g. monthly, is recommended, to ensure seasonal changes are captured. Additional surveys may be collected before and after storms to capture changes under high-energy conditions.

As technology progresses, intertidal surveys have gone beyond two-dimensional profiles to the creation of full three-dimensional digital terrain maps of intertidal regions. These are typically created from RTK-GPS surveys, which for efficiency may be conducted on a quad bike or similar device.

Novel monitoring techniques have also been applied, for example Argus video systems. Such video systems have been deployed at beaches in the lee of the WaveHub site in the UK for many years, which ensures that when devices are deployed, any impacts on morphodynamics can be compared to a long-term morphological record (Poate et al. 2012, 2014). This type of monitoring is advantageous because the video data are collected every day and analysis frequency is user-dependent. Similarly, X-band radar can be used to remotely monitor shorelines (Bell et al. 2016).

Multibeam echosounder (MBES) systems have revolutionised offshore bathymetric surveys. Although MBES surveys are relatively expensive, they represent an accurate technique that can be used to rapidly survey large areas of seabed to investigate local and regional seabed features (e.g. Robins et al. 2014). However, MBES surveys should be supplemented by seabed grab samples and subsequent particle size analysis to provide validation of seabed type and to fully characterise seabed sediments. Although MBES surveys provide a snapshot of the seabed, it is important for monitoring purposes to repeat such surveys over appropriate and

regular time intervals if possible, for example, to determine the influence of storm events on morphodynamics and to monitor the natural variability of systems such as offshore sand banks (e.g. Schmitt and Mitchell 2014).

Tidal Lagoons/Barrages

Where tidal ranges are large enough, there is potential for tidal barrages[2] and tidal lagoons[3] to contribute to substantial renewable energy generation. For example, tidal barrages and/or lagoons could contribute at least 10% to the UK's electricity demand, 5% of which could come from the Severn Estuary alone (Burrows et al. 2009). However, several barrage proposals have failed to gain governmental support to date, in part because of opposition due to significant environmental implications and high capital cost (e.g. Kirby and Shaw 2005). Lagoons are coastal or enclosed walled embayments typically several kilometres in circumference that create an artificial tidal phase difference and head difference between the body of water within and outside the lagoon. The water-level difference between the ocean and the lagoon (called the head of water) drives flow through turbines using various strategies such as ebb tide-only generation, or two-way (flood and ebb tide) generation, among more complex designs (Prandle 1984; Ahmadian et al. 2010; Kadiri et al. 2012; Cornett et al. 2013). Two-way generation turbines have been shown to generate power for a greater proportion of the tidal cycle (e.g. Zhou et al. 2014), thereby reducing intermittency in electricity supply.

An obvious impact of lagoon structures will be a markedly reduced energetic environment within the lagoon walls, especially during the water-holding periods (Cornett et al. 2013; Angeloudis et al. 2015). Weaker tidal currents and vertical mixing will reduce suspended sediment concentrations (Wolf et al. 2009; Ahmadian et al. 2012). By concentrating turbines and sluices in one section of the lagoon wall (sometimes called the powerhouse), counter-rotating eddies may form in the turbine wake (Falconer et al. 2009; Wolf et al. 2009; Cornett et al. 2013; Angeloudis et al. 2016), resulting in localised sediment resuspension and scour. Evenly spacing turbines throughout the lagoon structure would reduce this impact (Falconer et al. 2009). In practice, this may be difficult to achieve because of bathymetric or other practical constraints, in addition to increased cost, but could have a role in influencing design.

Outside the lagoon, the alteration of the natural physical environment will depend on the regional hydrodynamics and atmospheric conditions, local topography and bathymetry, the design of the lagoon, and the operational specifications of the lagoon (Angeloudis et al. 2015). Processes that are particularly vulnerable are

[2]A tidal range power plant that spans the entire width of a channel with turbines embedded in the retaining wall.

[3]In contrast to a tidal barrage, this is a tidal range power plant that is enclosed.

scour near the lagoon walls, sediment supply to neighbouring beaches and sand banks, and wave reflection/diffraction processes. Reduced or altered sediment supply to sand banks and to neighbouring beaches may affect the ability of these features to absorb wave energy from winter storms, hence making the coast more vulnerable to erosion (Neill et al. 2012; Robins et al. 2014). Considering a two-way (flood and ebb) generation regime, Angeloudis et al. (2016) suggest that the loss of intertidal regions can be minimised, which is a major source of concern with regard to ebb generation operation.

In light of these potential impacts, lagoon optimisation will be an important task; e.g. the lagoon shape and the number and position of turbines and sluices can be optimised to maximise energy yield and minimise environmental impacts. Numerical models that include a variety of lagoon designs and turbine parameterisation options are being developed (e.g. Cornett et al. 2013). The tidal and wave resource near potential lagoon sites needs to be better characterised, including the interactions of the resource with proposed lagoons and their surrounding environment, e.g. wave and storm climates and natural variability, sediment transport pathways, and turbulent mixing rates (inside lagoons), with particular attention paid to extreme events and climate change.

Summary and Conclusions

There is a growing body of research into the impact of wave and tidal stream devices on sediment dynamics. The research generally reports that it is only at large scales of electricity generation (e.g. >100 MW) that the impacts could exceed natural variability, but this "rule of thumb" will vary depending on site conditions and the sensitivity of a region. However, consistent monitoring pre- and post-construction is necessary to ascertain the range of natural variability, so that any post-construction impacts can be quantified. Further, before arrays are installed in the marine environment, much reliance is placed on numerical modelling, yet few of these sediment transport and morphodynamic models have been validated.[4] An important step towards reducing model uncertainty is to calibrate and validate the regional sediment transport models. This again comes back to the collection and integration of models with field data collected over appropriate timescales. In addition, it is important to ensure that arrays are correctly and consistently represented in two- and three-dimensional regional hydrodynamic models. Finally, many uncertainties about the implications of tidal lagoons relative to sedimentary processes remain. Consensus is needed how we represent lagoons in hydrodynamic models before the impacts of tidal lagoons on sediment dynamics and morphodynamics can be estimated with any certainty.

[4]In contrast, the underlying hydrodynamic flow fields tend to be well validated.

Acknowledgements S. Neill and P. Robins acknowledge the support of the Sêr Cymru National Research Network for Low Carbon, Energy and the Environment (NRN-LCEE). I. Fairley acknowledges the support of the Engineering and Physical Sciences Research Council Terawatt project (EP/J010170/1). Thanks to Jerome Thiébot and Edgar Mendoza for providing high-resolution figures. We also thank the reviewers and editors for their constructive comments on an earlier version of the manuscript.

References

Abanades, J., Greaves, D., & Iglesias, G. (2014a). Wave farm impact on the beach profile: A case study. *Coastal Engineering, 86,* 36–44.

Abanades, J., Greaves, D., & Iglesias, G. (2014b). Coastal defence through wave farms. *Coastal Engineering, 91,* 299–307.

Abanades, J., Greaves, D., & Iglesias, G. (2015a). Coastal defence using wave farms: The role of farm-to-coast distance. *Renewable Energy, 75,* 572–582.

Abanades, J., Greaves, D., & Iglesias, G. (2015b). Wave farm impact on beach modal state. *Marine Geology, 361,* 126–135.

Adcock, T. A. A., Draper, S., Houlsby, G. T., Borthwick, A. G. L., & Serhadlıoğlu, S. (2013). The available power from tidal stream turbines in the Pentland Firth. *Proceedings of the Royal Society of London A: Mathematical, Physical and Engineering Sciences, 469,* 2157.

Ahmadian, R., & Falconer, R. A. (2012). Assessment of array shape of tidal stream turbines on hydro-environmental impacts and power output. *Renewable Energy, 44,* 318–327.

Ahmadian, R., Falconer, R., & Bockelmann-Evans, B. (2012). Far-field modelling of the hydro-environmental impact of tidal stream turbines. *Renewable Energy, 38,* 107–116.

Ahmadian, R., Morris, C., & Falconer, R. (2010). Hydro-environmental modelling of off-shore and coastally attached impoundments off the north wales coast. In *First IAHR European Congress, Edinburgh (UK), 4–6 May 2010*.

Angeloudis, A., Ahmadian, R., Bockelmann-Evans, B., & Falconer, R. A. (2015). Numerical modelling of a tidal lagoon along the North Wales coast. In C. G. Soares (Ed.), *Renewable energies offshore* (pp. 139–145).

Angeloudis, A., Ahmadian, R., Falconer, R. A., & Bockelmann-Evans, B. (2016). Numerical model simulations for optimisation of tidal lagoon schemes. *Applied Energy, 165,* 522–536.

Aquatera Ltd and Marine Space. (2015). ORJIP ocean energy—The forward look; an ocean energy environmental research strategy for the UK. Report No. P627, Version 3, July 2015, 62 pp.

Barnard, P. L., Short, A. D., Harley, M. D., Splinter, K. D., Vitousek, S., Turner, I. L., et al. (2015). Coastal vulnerability across the Pacific dominated by El Nino/Southern oscillation. *Nature Geoscience, 8*(10), 801–807.

Bastos, A. C., Kenyon, N. H., & Collins, M. (2002). Sedimentary processes, bedforms and facies, associated with a coastal headland: Portland Bill, Southern UK. *Marine Geology, 187,* 235–258.

Bell, P., Bird, C., & Plater, A. (2016). A temporal waterline approach to mapping intertidal areas using X-band marine radar. *Coastal Engineering, 107,* 84–101.

Bowers, D., Gaffney, S., White, M., & Bowyer, P. (2002). Turbidity in the southern Irish Sea. *Continental Shelf Research, 22,* 2115–2126.

Bowers, D. G., Ellis, K. M., & Jones, S. E. (2005). Isolated turbidity maxima in shelf seas. *Continental Shelf Research, 25,* 1071–1080.

Brown, J. M., & Davies, A. G. (2009). Methods for medium-term prediction of the net sediment transport by waves and currents in complex coastal regions. *Continental Shelf Research, 29,* 1502–1514.

Burrows, R., Yates, N. C., Hedges, T. S., Li, M., Zhou, J. G., Chen, D. Y., et al. (2009). Tidal energy potential in UK waters. *Proceedings of the ICE-Maritime Engineering, 162,* 155–164.

Camenen, B., & Larroudé, P. (2003). Comparison of sediment transport formulae for the coastal environment. *Coastal Engineering, 48,* 111–132.

Cornett, A., Cousineau, J., & Nistor, I. (2013). Assessment of hydrodynamic impacts from tidal power lagoons in the Bay of Fundy. *International Journal of Marine Energy, 1,* 33–54.

De Vriend, H. J. (Ed.). (1993). Coastal morphodynamics: Processes and modelling. *Coastal Engineering*, *21*(1–3).

Den Boon, J. H., Sutherland, J., Whitehouse, R., Soulsby, R., Stam, C. J. M., Verhoeven, K., et al. (2004). Scour behaviour and scour protection for monopile foundations of offshore wind turbines. In *Proceedings of the European Wind Energy Conference* (Vol. 14).

Dissanayake, D. M. P. K., Roelvink, J. A., & van der Wegen, M. (2009). Modelled channel patterns in a schematized tidal inlet. *Coastal Engineering, 56,* 1069–1083.

Easton, M. C., Harendza, A., Woolf, D. K., & Jackson, A. C. (2011). Characterisation of a tidal energy site: Hydrodynamics and seabed structure. In *Proceedings of the 9th European Wave and Tidal Energy Conference, Southampton, UK*.

Ellis, K., Binding, C., Bowers, D. G., Jones, S. E., & Simpson, J. H. (2008). A model of turbidity maintenance in the Irish Sea. *Estuarine, Coastal and Shelf Science, 76,* 765–774.

Emery, K. O. (1961). A simple method for measuring beach profiles. *Limnology and Oceanography, 6,* 90–93.

Evans, C. D. R. (1990). *United Kingdom offshore regional report: The geology of the western English Channel and its western approaches*. London: HMSO for the British Geological Survey. 93 pp.

Fairley, I., & Karunarathna, H. (2014). The morphodynamics of a beach in the lee of wave energy converter arrays. In *EIMR (Environmental Impacts of Marine Renewables) Conference*, April 30–May 1, 2014, Stornoway, UK.

Fairley, I., Masters, I., & Karunarathna, H. (2015). The cumulative impact of tidal stream turbine arrays on sediment transport in the Pentland Firth. *Renewable Energy, 80,* 755–769.

Fairley, I., Masters, I., & Karunarathna, H. (2016). Numerical modelling of storm and surge events on offshore sandbanks. *Marine Geology, 371,* 106–119.

Falconer, R. A., Xia, J., Lin, B., & Ahmadian, R. (2009). The Severn barrage and other tidal energy options: Hydrodynamic and power output modeling. *Science in China Series E: Technological Sciences, 52,* 3413–3424.

Gallagher, E. L., Elgar, S., & Guza, R. T. (1998). Observations of sand bar evolution on a natural beach. *Journal of Geophysical Research, 103,* 3203–3215.

Gonzalez-Santamaria, R., Zou, Q. P., & Pan, S. (2011). Two-way coupled wave and tide modelling of a wave farm. *Journal of Coastal Research, 64,* 1038–1042.

Gonzalez-Santamaria, R., Zou, Q. P., & Pan, S. (2015). Impacts of a wave farm on waves, currents and coastal morphology in South West England. *Estuaries and Coasts, 38,* S159–S172.

Harley, M. D., Turner, I. L., Short, A. D., & Ranasinghe, R. (2011). Assessment and integration of conventional RTK-GPS and image derived beach survey methods for daily to decadal coastal monitoring. *Coastal Engineering, 58,* 194–205.

Harris, J. M., Whitehouse, R. J. S., & Sutherland, J. (2011). Marine scour and offshore wind—Lessons learnt and future challenges. In *30th International Conference on Ocean, Offshore and Arctic Engineering* (Vol. 5, pp. 849–858).

Huthnance, J. M. (1982). On one mechanism forming linear sand banks. *Journal of Estuarine and Coastal Marine Science, 14,* 19–99.

Iyer, A. S., Couch, S. J., Harrison, G. P., & Wallace, A. R. (2013). Variability and phasing of tidal current energy around the United Kingdom. *Renewable Energy, 51,* 343–357.

Kadiri, M., Ahmadian, R., Bockelmann-Evans, B., Rauen, W., & Falconer, R. (2012). A review of the potential water quality impacts of tidal renewable energy systems. *Renewable and Sustainable Energy Reviews, 16,* 329–341.

Kirby, R., & Shaw, T. L. (2005). Severn barrage, UK—Environmental reappraisal. *Proceedings of the ICE-Engineering Sustainability, 158,* 31–39.

Lewis, M. J., Neill, S. P., & Elliott, A. J. (2015a). Inter-annual variability of two contrasting offshore sand banks in a region of extreme tidal range. *Journal of Coastal Research, 31,* 265–275.

Lewis, M. J., Neill, S. P., Robins, P. E., & Hashemi, M. R. (2015b). Resource assessment for future generations of tidal-stream energy arrays. *Energy, 83,* 403–415.

Martin-Short, R., Hill, J., Kramer, S. C., Avdis, A., Allison, P. A., & Piggott, M. D. (2015). Tidal resource extraction in the Pentland Firth, UK: Potential impacts on flow regime and sediment transport in the Inner Sound of Stroma. *Renewable Energy, 76,* 596–607.

Masselink, G., Austin, M., Scott, T., Poate, T., & Russell, P. (2014). Role of wave forcing, storms and NAO in outer bar dynamics on a high-energy, macro-tidal beach. *Geomorphology, 226,* 76–93.

Masselink, G., & Short, A. D. (1993). The effect of tide range on beach morphodynamics and morphology—A conceptual beach model. *Journal of Coastal Research, 9,* 785–800.

McCann, D. (2011). Long-term morphological modelling of tidal basins. Doctoral dissertation, Bangor University.

Mendoza, E., Silva, R., Zanuttigh, B., Angelelli, E., Lykke Andersen, T., Martinelli, L., et al. (2014). Beach response to wave energy converter farms acting as coastal defence. *Coastal Engineering, 87,* 97–111.

Mitchell, N. C., Huthnance, J. M., Schmitt, T., & Todd, B. (2012). Threshold of erosion of submarine bedrock landscapes by tidal currents. *Earth Surface Processes and Landforms, 38,* 627–639.

Morgan, C. A., Cordell, J. R., & Simenstad, C. A. (1997). Sink or swim? Copepod population maintenance in the Columbia River estuarine turbidity-maxima region. *Marine Biology, 129,* 309–317.

Neill, S. P. (2008). The role of Coriolis in sandbank formation due to a headland/island system. *Estuarine, Coastal and Shelf Science, 79,* 419–428.

Neill, S. P. (2009). A numerical study of lateral grain size sorting by an estuarine front. *Estuarine, Coastal and Shelf Science, 81,* 345–352.

Neill, S. P., & Elliott, A. J. (2004a). Observations and simulations of an unsteady island wake in the Firth of Forth, Scotland. *Ocean Dynamics, 54,* 324–332.

Neill, S. P., & Elliott, A. J. (2004b). In situ measurements of spring-neap variations to unsteady island wake development in the Firth of Forth, Scotland. *Estuarine, Coastal and Shelf Science, 60,* 229–239.

Neill, S. P., & Scourse, J. D. (2009). The formation of headland/island sandbanks. *Continental Shelf Research, 29,* 2167–2177.

Neill, S. P., Elliott, A. J., & Hashemi, M. R. (2008). A model of inter-annual variability in beach levels. *Continental Shelf Research, 28,* 1769–1781.

Neill, S. P., Hashemi, M. R., & Elliott, A. J. (2007). An enhanced depth-averaged tidal model for morphological studies in the presence of rotary currents. *Continental Shelf Research, 27,* 82–102.

Neill, S. P., Hashemi, M. R., & Lewis, M. J. (2014). Optimal phasing of the European tidal stream resource using the greedy algorithm with penalty function. *Energy, 73,* 997–1006.

Neill, S. P., Hashemi, M. R., & Lewis, M. J. (2016). Tidal energy leasing and tidal phasing. *Renewable Energy, 85,* 580–587.

Neill, S. P., Jordan, J. R., & Couch, S. J. (2012). Impact of tidal energy converter (TEC) arrays on the dynamics of headland sand banks. *Renewable Energy, 37,* 387–397.

Neill, S. P., Litt, E. J., Couch, S. J., & Davies, A. G. (2009). The impact of tidal stream turbines on large-scale sediment dynamics. *Renewable Energy, 34,* 2803–2812.

Pingree, R. D., & Griffiths, D. K. (1979). Sand transport paths around the British Isles resulting from M2 and M4 tidal interactions. *Journal of the Marine Biological Association of the United Kingdom, 59,* 497–513.

Pingree, R. D. (1978). The formation of the shambles and other banks by tidal stirring of the seas. *Journal of the Marine Biological Association of the United Kingdom, 58,* 211–226.

Poate, T., Masselink, G., & Russell, P. E. (2012). Assessment of potential morphodynamic response to wave hub. In *Fourth International Conference on Ocean Energy, Dublin*.

Poate, T. G., Masselink, G., Russell, P., & Austin, M. (2014). Morphodynamic variability of high-energy macrotidal beaches, Cornwall, UK. *Marine Geology, 320,* 97–111.

Prandle, D. (1984). Simple Theory for Designing Tidal Power Schemes. *Advances in Water Resources, 7,* 21–27.

Ranasinghe, R., Swinkels, C., Luijendijk, A., Roelvink, D., Bosboom, J., Stive, M., et al. (2011). Morphodynamic upscaling with the MORFAC approach: Dependencies and sensitivities. *Coastal Engineering, 58,* 806–811.

Robins, P. E., Neill, S. P., & Lewis, M. J. (2014). Impact of tidal-stream arrays in relation to the natural variability of sedimentary processes. *Renewable Energy, 72,* 311–321.

Robins, P. E., Neill, S. P., Lewis, M. J., & Ward, S. L. (2015). Characterising the spatial and temporal variability of the tidal-stream energy resource over the northwest European shelf seas. *Applied Energy, 147,* 510–522.

Robinson, I. S. (1981). Tidal vorticity and residual circulation. *Deep-Sea Research, 28,* 195–212.

Roelvink, J. A. (2006). Coastal morphodynamic evolution techniques. *Coastal Engineering, 53,* 277–287.

Ruggiero, P., Kaminsky, G. M., Gelfenbaum, G., & Voigt, B. (2005). Seasonal to interannual morphodynamics along a high-energy dissipative littoral cell. *Journal of Coastal Research, 21,* 553–578.

Ruggiero, P., Walstra, D. J. R., Gelfenbaum, G., & Van Ormondt, M. (2009). Seasonal-scale nearshore morphological evolution: Field observations and numerical modeling. *Coastal Engineering, 56,* 1153–1172.

Ruol, P., Zanuttigh, B., Martinelli, L., Kofoed, J. P., & Frigaard, P. (2011). Near-shore floating wave energy converters: Applications for coastal protection. In *Proceedings of the 32nd International Conference on Coastal Engineering, Shanghai*,

Schmitt, T., & Mitchell, N. C. (2014). Dune-associated sand fluxes at the nearshore termination of a banner sand bank (Helwick Sands, Bristol Channel). *Continental Shelf Research, 76,* 64–74.

Schoonees, J. S., Theron, A. K., & Bevis, D. (2006). Shoreline accretion and sand transport at groynes inside the Port of Richards Bay. *Coastal Engineering, 53,* 1045–1058.

Shields, M. A., Woolf, D. K., Grist, E. P., Kerr, S. A., Jackson, A. C., Harris, R. E., et al. (2011). Marine renewable energy: The ecological implications of altering the hydrodynamics of the marine environment. *Ocean and Coastal Management, 54,* 2–9.

Soulsby, R. (1997). *Dynamics of marine sands: A manual for practical applications*. Thomas Telford, 272 pp.

Thiébot, J., Bailly du Bois, P., & Guillou, S. (2015). Numerical modeling of the effect of tidal stream turbines on the hydrodynamics and the sediment transport—Application to the Alderney Race (Raz Blanchard), France. *Renewable Energy, 75,* 356–365.

Van de Meene, Y. W. H., & Van Rijn, L. C. (2000). The shoreface-connected ridges along the central Dutch coast—part 2: Morphological modelling. *Continental Shelf Research, 20,* 2325–2345.

Van Landeghem, K. J., Baas, J. H., Mitchell, N. C., Wilcockson, D., & Wheeler, A. J. (2012). Reversed sediment wave migration in the Irish Sea, NW Europe: A reappraisal of the validity of geometry-based predictive modelling and assumptions. *Marine Geology, 295,* 95–112.

Vespremeanu-Stroe, A., Constantinescu, S., Tatui, F., & Giosan, L. (2007). Multi-decadal evolution and North Atlantic Oscillation influences on the dynamics of the Danube Delta shoreline. *Journal of Coastal Research, 50,* 157–162.

V gler, A., Christie, D., Lidster, M., & Morrison, J. (2011). Wave energy converters, sediment transport and coastal erosion. In *ICES Annual Science Conference, 19–23 September 2011, Gdańsk, Poland*.

Whitehouse, R. (1998). *Scour at marine structures: A manual for practical applications*. London: Thomas Telford. 198 p.

Wolanski, E., Imberger, J., & Heron, M. L. (1984). Island wakes in shallow coastal waters. *Journal of Geophysical Research: Oceans, 89,* 10553–10569.

Wolf, J., Walkington, I. A., Holt, J., & Burrows, R. (2009). Environmental impacts of tidal power schemes. *Proceedings of the Institution of Civil Engineers-Maritime Engineering, 162,* 165–177.

Xodus Group Ltd. (2012). Impact of the Outshore Point wave farm on local coastal processes, report for Brough head wave farm, report no: BHWFSD.PR.EU.UK.ORKB.06REP0001.

Yang, Z., Wang, T., Copping, A., & Geerlofs, S. (2014). Modeling of in-stream tidal energy development and its potential effects in Tacoma Narrows, Washington, USA. *Ocean and Coastal Management, 99,* 52–62.

Zannughti, B., Martinelli, L., Castagnetti, M., Ruol, P., Kofoed, J. P., & Frigaard, P. (2010). *Integration of wave energy converters in coastal protection schemes*. Bilbao: Proccedings of third International conference on ocean enery.

Zhou, J., Pan, S., & Falconer, R. A. (2014). Optimization modelling of the impacts of a Severn Barrage for a two-way generation scheme using a Continental Shelf model. *Renewable Energy, 72,* 415–427.

Assessing the Impacts of Marine-Hydrokinetic Energy (MHK) Device Noise on Marine Systems by Using Underwater Acoustic Models as Enabling Tools

Paul C. Etter

Introduction

This chapter describes the use of underwater acoustic models for the evaluation of marine-system noise impacts associated with the installation and operation of marine-hydrokinetic energy (MHK) devices, particularly in coastal oceans. Selection guidance is provided for the current inventory of propagation and noise models. Where available, case studies are examined to illustrate the use of acoustic models for the assessment of MHK device impacts on marine mammals and fish.

Background

Over the past several decades, the soundscape of the marine environment has responded to changes in both natural and anthropogenic influences. A soundscape is a combination of sounds that form, or arises from, a vast environment. The study of a soundscape is sometimes referred to as acoustic ecology. Soundscape refers to both the natural acoustic environment (consisting of natural sounds, including animal vocalizations, the sounds of weather, and other natural elements), and anthropogenic sounds (created by humans), including sounds of mechanical origin associated with the use of industrial technology. The disruption of the natural acoustic environment results in noise pollution.

The soundscape baseline is defined by ambient noise, which is the prevailing, background of sound at a particular location in the ocean at a given time of the year. For acoustic-signal processing, it is the background of noise, typical of the time,

P.C. Etter (✉)
Northrop Grumman Corporation, P.O. Box 1693, Baltimore, MD 21203, USA
e-mail: paul.etter@ngc.com

Z. Yang and A. Copping (eds.), *Marine Renewable Energy*,
DOI 10.1007/978-3-319-53536-4_13

location and depth against which an acoustic signal must be detected. Natural noise sources include surface weather (wind and rain noise). Anthropogenic activity can include naval-sonar systems, seismic-exploration activity, merchant shipping, fishing vessels, marine-hydrokinetic energy devices, and wind-farm development. Even noise from low-flying coastal aircraft can couple into the water column and add to the background noise field.

Organization of Chapter

Building upon the brief background presented in section "Introduction," section "Evolving Trends and Challenges" addresses evolving trends and challenges. Section "Noise Sources" discusses noise sources, emphasizing marine kinetic energy activity such as tidal turbines and wave-energy devices. Section "Mitigation and Monitoring" reviews mitigation and monitoring. Section "Underwater Acoustic Modeling Techniques as Enabling Tools" reviews the utility of underwater acoustic modeling techniques as enabling tools. Section "Summary" summarizes the notable advances in underwater acoustic modeling that support analyses of noise effects on physical systems due to the deployment of marine renewable energy devices. References and an appendix containing definitions of abbreviations and acronyms are also included.

Evolving Trends and Challenges

Evolving trends and challenges related to the assessment of the impacts of MHK device noise on marine systems are best set in the context of the coastal environments in which such devices may be deployed. Then, an assessment of the associated biological noise impacts, enabling technologies, and emerging solutions can be examined.

Coastal Environments

Coastal environments are generally characterized by high spatial and temporal variabilities. When coupled with attendant acoustic spectral dependencies of the surface and bottom boundaries, these natural variabilities make coastal regions very complex acoustic environments. Changes in the temperature and salinity of coastal waters affect the refraction of sound in the water column. These refractive properties have a profound impact on the transmission of acoustic energy in a shallow-water waveguide that has an irregular bottom and a statistically varying sea

surface. Thus, accurate modeling and prediction of the acoustic environment is essential to understanding the prevailing noise fields in coastal oceans.

Physical processes controlling the hydrography of shelf waters often exhibit strong seasonal variations. Episodic passages of meteorological fronts from continental interiors affect the thermal structure of the adjacent shelf waters through intense air–sea interactions. River outflows create strong salinity gradients along the adjacent coast. Variable bottom topographies and sediment compositions with their attendant spectral dependencies complicate acoustic bottom boundary conditions. At higher latitudes, ice formation complicates acoustic surface boundary conditions near the coast. Waves generated by local winds under fetch-limited conditions, together with swells originating from distant sources, conspire to complicate acoustic surface boundary conditions and also create noisy surf conditions. Marine life, which is often abundant in nutrient-rich coastal regions, can generate or scatter sound.

Biological Noise Impacts

Underwater noise is now classed as pollution in accordance with the European Union's Marine Strategy Framework Directive (Directive 2008/56/EC dated 17 June 2008). Noise from shipping is a major contributor to the ambient-noise levels in the ocean, particularly at low (<300 Hz) frequencies. Copping and O'Toole (2010) noted that the effects of underwater noise from MHK devices on receptors such as marine mammals and fish include physical auditory damage, behavioral changes, avoidance of area, chronic stress, altered acoustic sensitivity, and mortality.

Enabling Technologies and Emerging Solutions

Underwater acoustic models are viewed as enabling tools for evaluating marine-system impacts arising from noise associated with the installation and operation of marine renewable (hydrokinetic) energy devices. Broadly defined, modeling is a method for organizing knowledge accumulated through observation or deduced from underlying principles. Modeling applications fall into two basic categories: prognostic and diagnostic. Prognostic applications include prediction and forecasting functions for which future oceanic conditions or acoustic sensor performance must be anticipated, such as selection of sites for future MHK device installations. Diagnostic applications include system-design and analysis functions typically encountered in engineering trade-off studies involving the interpretation of sparse measurements of sounds produced by marine-energy converters.

Farcas et al. (2016) emphasized that the underwater acoustic models that are presently used in environmental impact assessments (EIAs) consider only the sound-pressure component of sound, which is the means by which marine

mammals hear; however, the primary mechanism by which fish and invertebrate species detect sound is through the particle-motion component of sound.

For the period 1996–2015, Finneran (2015) reviewed progress in the methods employed by research groups conducting marine-mammal temporary threshold shift (TTS) experiments. (TTS refers to a temporary increase in the threshold of hearing; i.e., the minimum intensity needed to hear a sound at a specific frequency, but which returns to its pre-exposure level over time.) Specifically, he summarized the relationships between the experimental conditions, the noise-exposure parameters, and the observed TTS. An attempt was made to synthesize the major findings across experiments to provide the current state of knowledge for the effects of noise on marine-mammal hearing. The most critical gaps involved the manner in which exposure frequency affects the resulting patterns of TTS growth and recovery. TTS growth curves at various frequencies are needed for representative species so that effective weighting functions can be developed to predict the onset of TTS and establish upper safe limits to prevent permanent threshold shift (PTS) for various noise frequencies. The noise sources of greatest concern, such as military sonar systems and seismic air guns, involve acute exposures to high-intensity, intermittent sounds; however, significant questions remain regarding the rate of TTS growth and recovery after exposure to intermittent noise and the effects of single and multiple impulses. At present, data are insufficient to construct generalized models for recovery or to determine the time necessary to treat subsequent exposures as independent events. More information is needed about the relationship between auditory evoked potentials and behavioral measures of TTS for various stimuli. Finally, data on noise-induced threshold shifts in marine mammals are available for only a few species, and for only few individuals within these species. Questions still remain about the most appropriate methods for extrapolation to other species.

Noise Sources

To form a more complete portrait of the prevailing noise fields composing the soundscape, this section describes the background noise fields arising from natural as well as anthropogenic noise sources. The noise fields associated with MHK devices, as well as wind-farm noise, are also described.

Natural Background Noise

As summarized in Table 1, the background of natural noise comprises seismo-acoustic noise, bioacoustic noise, wind and rain noise, surf noise, and (where appropriate) Arctic ambient noise.

Table 1 Summary of natural background noise sources

Noise source	Comments
Seismo-acoustic noise	Seismo-acoustics refers to low-frequency (<3 Hz) noise signals originating in Earth's interior and the oceans (Orcutt 1988)
Bioacoustic noise	Marine bioacoustic signal sources are typically transient in nature and exhibit diverse temporal, spatial, and spectral distributions. The main contributors to bioacoustic signals include certain shellfish, fish, and marine mammals. Of the marine mammals, whales are the most notable contributors (see Etter 2013)
Wind and rain noise	Ambient noise correlates well with wind speed in the frequency band 500 Hz–25 kHz, but correlates poorly with significant wave height. The poor correlation with wave height can be attributed to the disproportionate effect of swell on the frequency of breaking waves, which are considered the primary source of wind-dependent noise in the ocean (Felizardo and Melville 1995). The underwater noise spectrum generated by rain has a unique spectral shape that is distinguishable from other noise sources by a broad peak at about 15 kHz; moreover, the relationship between spectral level and rate of rainfall is quantifiable (Scrimger et al. 1987)
Surf noise	Ambient noise in the surf zone in the frequency range 120 Hz–5 kHz is dominated by breaking waves (Bass and Hay 1997)
Arctic ambient noise	Although it is unlikely that large-scale MHK devices would initially be deployed in Arctic regions, they may be used to power autonomous sensor systems and, consequently, it is useful to note that the noise environment under, or near, the Arctic ice is different from that of any other ocean area. Shipping noise is extremely low due to the lack of surface traffic. The ice cover itself affects the ambient-noise field significantly: It can decouple the water from the effects of the wind and produce ambient-noise conditions that are much quieter than a corresponding sea-state zero in the open ocean. The ice itself may produce noises as wind, waves, and thermal effects act on it (see Etter 2013)

Anthropogenic Background Noise

As summarized in Table 2, the three principal sources of anthropogenic noise of interest include seismic sources, shipping traffic, and environmental phenomena of human origin that contribute to the background noise levels. Additional sources of anthropogenic noise may derive from a new generation of multistatic naval sonar systems.

MHK Device and Wind-Farm Noise

This section addresses available observations of the noise fields associated with the installation and operation of MHK devices and wind farms in the context of marine renewable energy (MRE). A discussion of wind-farm noise is included because there is a relative abundance of acoustic data collected on the installation and

Table 2 Summary of anthropogenic background noise sources

Noise source	Comments
Seismic sources	Marine seismic surveys are used to assess the location of hydrocarbon resources, including gas and oil. Acoustic models have been used to estimate marine-mammal sound-exposure levels generated in geophysical surveys by multi-beam echo sounders, side-scan sonar systems, subbottom profilers, and seismic boomers (Zykov 2013)
Shipping traffic	Noise from distant shipping generally occupies the frequency band 20–500 Hz (Carey and Evans 2011). A comparison of time-series measurements of ocean ambient noise over two periods (1963–1965 and 1994–2001) revealed that noise levels from the latter period exceeded those of the earlier period by about 10 dB in the frequency ranges of 20–80 Hz and 200–300 Hz, and by about 3 dB at 100 Hz. The observed increase was attributed to increase in shipping (Andrew et al. 2002). Ambient-noise measurements collected at the same site but separated by an interval of nearly 40 years (1964–1966 and 2003–2004) revealed an average noise increase of 2.5–3 dB per decade in the frequency band 30–50 Hz (McDonald et al. 2006, 2008)
Environmental phenomena	Climate change also affects the ocean soundscape. The emission of carbon into the atmosphere through the effects of fossil-fuel combustion and industrial processes increases atmospheric concentrations of carbon dioxide (CO_2). Ocean acidification, which occurs when CO_2 in the atmosphere reacts with water to create carbonic acid (H_2CO_3), is increasing. The attenuation of low-frequency sound in the sea is pH-dependent; specifically, the higher the pH, the greater the attenuation. Thus, as the ocean becomes more acidic (lower pH) due to increasing CO_2 emissions, the attenuation will diminish and low-frequency sounds will propagate farther, effectively making the ocean noisier (see Etter 2013)

operation of such devices; these data may have direct application to the estimation of MHK device noise fields.

Deployment of MHK devices is still in the early stages, and a substantial database is not yet available regarding the impacts of MHK noise on the environment. Only a limited understanding of the environmental impacts has been achieved to date because few of these projects are presently operational. Therefore, it is important to note that much of the following discussion describes results that precede recent published work on the characterization of sound generated by operational MHK devices.

The topic of uncertainty is included here to raise awareness of inherent limitations in the fidelity of model outputs.

Tidal Turbines

Lloyd et al. (2011) modeled underwater noise sources associated with horizontal-axis tidal turbines and their potential impact on shallow-water marine environments. The requirement for device-noise prediction as part of environmental

impact assessment was considered in light of the limited amount of measurement data available. Noise sources included self-noise, interaction noise, and hydroelastic noise. In future studies, machinery (generator) noise and cavitation noise also need to be considered. The dominant flow-generated noise sources were modeled using empirical techniques. The predicted sound-pressure level due to inflow turbulence for a typical horizontal-axis tidal turbine was estimated to generate 1/3-octave-bandwidth pressure levels of 119 dB re 1 μPa at 20 m from the turbine at individual frequencies. This preliminary estimate revealed that this noise source alone would not be expected to cause either a PTS or TTS in typical marine animals of the North Sea including cod, harbor seal, and harbor porpoise.

Li and alişal (2010) presented a preliminary study of four principal characteristics of tidal-current turbines: power output, torque, induced velocity, and acoustic emission. Numerical models were developed to predict these characteristics for tidal-current turbines. It was proposed that these same models could also be used to develop standards for tidal-current turbines. The resulting hydrodynamic noise intensity (acoustic emission) was evaluated at three locations downstream from the subject turbine. The frequencies corresponding to the first peak (main noise frequency) at the three locations were all around 4 Hz. Successively smaller amplitude peaks were also observed at 18 Hz and at 31 Hz.

Wave-Energy Devices

Austin et al. (2009) provided wave-energy developers in Oregon with fundamental information about the principles, methods, and equipment involved in conducting environmental noise assessments related to the permitting of such projects. In the absence of any documented ambient-noise measurements for the near-shore environment off the Oregon coast, characterizations of the environmental components that contribute to the overall ambient-noise field were provided instead. The marine operations noise model (MONM) computed transmission losses for arbitrary three-dimensional, range-varying acoustic environments using a parabolic-equation (PE) solution to the acoustic wave equation. The modeling took into account a number of environmental parameters including bathymetry, sound-speed profile in the water column, and geoacoustic properties of the seafloor.

Ikpekha et al. (2014) developed a computer model that simulated low-frequency (<1000 Hz) acoustic signals produced by a wave-energy device in coastal environments. They analyzed these signals with the aid of marine-mammal audiograms of the harbor seal. This enabled them to estimate the levels of acoustic noise experienced by marine mammals due to the presence of ocean-deployed devices. Propagation of the underwater acoustic signals was modeled using the finite-element (FE) method with appropriate boundary conditions at the sea surface and the seafloor. Based on an audiogram of the harbor seal, it was deduced that animals at least 51 m distant from the sound source would not be affected.

Wind-Farm Noise

A wind farm, which is a group of wind turbines in the same location used for production of electric power, may be located offshore. The installation of ocean wind farms requires medium water depths (<30 m) and construction logistics such as access to specialized vessels to install the turbines. Economic wind generators require wind speeds of 16 km/h or greater (Etter 2013).

One of the most significant activities during MHK device and wind-farm construction is foundation installation, during which dredging, rock laying, and pile driving may be undertaken Activities include scour protection, cable protection, and modifying non-ideal bathymetry. Other construction activities include cable laying, turbine and turbine-tower installation, and ancillary structure installation (such as offshore transformers). Additional noise sources include industrial traffic associated with transporting workers, materials, and hydrokinetic energy devices to offshore sites (Etter 2013).

Uncertainty

Uncertainty has been defined as a quantitative measure of our lack of complete knowledge of the sound-speed field and boundary conditions constituting the waveguide information necessary for simulation of the acoustic field (Finette 2005). This uncertainty is distinct from any errors related to numerical solution of the wave equation. Existing simulation methods typically solve a deterministic wave equation separately over many realizations, and the resulting set of pressure fields is then used to estimate statistical moments of the field. Proper sampling may involve the computation of thousands of realizations to ensure convergence of the statistics.

A study of the impacts of uncertainty in the modeling of anthropogenic noise impacts suggested a precautionary approach to regulation (Lawson 2009): Due to the complex patterns of sound propagation encountered in diverse shelf regions, some marine mammals may not necessarily encounter the average sound-exposure conditions predicted for any given impact scenario.

In practice, noise modeling efforts in support of EIAs are often carried out using simplistic underwater acoustic models, with limited environmental data, and with little or no field measurements to ground-truth the model predictions. In some cases, practitioners have developed proprietary models, the inner workings of which are not disclosed to regulators. This presents regulatory decision-makers with considerable uncertainty regarding the prediction of possible impacts; moreover, this uncertainty is often not apparent. In an effort to better inform regulators, stakeholders, and developers of the factors that may lead to uncertainty in noise assessments, Farcas et al. (2016) provided concrete examples of how different modeling procedures can affect predictions. Raising awareness of these issues can help promote best practice in noise-impact assessments and enable better-informed EIA processes for noise-generating developments. To further explore this aspect, Farcas et al. (2016) used measurements of impact pile-driving noise that were made

simultaneously at two locations in the Cromarty Firth, Scotland. Different acoustic models were then used to calculate the source level of pile-driving noise. This exercise served to illustrate that, although there is considerable uncertainty about the relationship between noise levels and impacts on aquatic species, the science underlying noise modeling appears to be well understood. Farcas et al. (2016) further observed that underwater acoustic models that are currently applied in EIAs consider only the sound-pressure component of sound, which is the means by which marine mammals hear; however, the primary mechanism by which fish and marine invertebrate species detect sound is through the particle-motion component of sound.

Mitigation and Monitoring

In the present context, mitigation refers to the administrative, procedural, legal, and technical aspects of reducing or eliminating sources of noise that might be potentially harmful to marine life, especially marine mammals. Monitoring indicates connections between identified environmental impacts, measurement indicators, detection limits, and the thresholds that will signal the need for corrective action. This section is divided into three parts: (1) mitigation measures and monitoring; (2) passive acoustic technologies; and (3) underwater acoustic networks.

Mitigation Measures and Monitoring

The Committee on Potential Impacts of Ambient Noise in the Ocean on Marine Mammals was charged by the Ocean Studies Board of the U.S. National Research Council to assess the state of our knowledge of underwater noise and recommend research areas to assist in determining whether noise in the ocean adversely affects marine mammals (National Research Council 2003). One of the findings of this committee was that models describing ocean noise are better developed than those describing marine-mammal distribution, hearing, and behavior. The biggest challenge lies in integrating the two types of models. The National Research Council (2005) further examined what constitutes biologically significant in the context of level B harassment as used in the latest amendments to the U.S. Marine Mammal Protection Act (MMPA). The MMPA separates harassment into two levels. Level A harassment is defined as "any act of pursuit, torment, or annoyance which has the potential to injure a marine mammal or marine mammal stock in the wild." Level B harassment is defined as "any act of pursuit, torment, or annoyance which has the potential to disturb a marine mammal or marine mammal stock in the wild by causing disruption of behavioral patterns, including, but not limited to, migration, breathing, nursing, breeding, feeding, or sheltering." Enacted in 1972, the MMPA was the first legislation that called for an ecosystem approach to natural-resource

management and conservation; it specifically prohibited the *take* (i.e., hunting, killing, capture, and/or harassment) of marine mammals.

Todd et al. (2015) described noise-reduction methods and associated acoustic-mitigation devices. Noise-reduction methods included acoustic-isolating materials and bubble curtains (or screens) that reduced initial sound output or reduced sound intensity along a propagation path. Acoustic-mitigation devices included acoustic-harassment devices (or pingers) that encouraged animals to move away from high-risk operational areas.

Ramp-up (or soft-start) procedures employ a gradual increase in the source level in order to mitigate the effects of sonar transmissions on marine mammals. Von Benda-Beckmann et al. (2014) investigated the effectiveness of ramp-up procedures in reducing the area within which changes in hearing thresholds in marine mammals can occur. The effectiveness of the ramp-up procedure depended strongly on the assumed response threshold of the marine mammals and differed with ramp-up duration.

Passive Acoustic Technologies

Fixed autonomous passive acoustic arrays can sample continuously for prolonged periods of time in all weather conditions, thereby allowing for assessments of seasonal changes in both the distribution and acoustic behavior of individual animals without the disturbance of survey vessels or aircraft. Autonomous underwater vehicles and gliders can serve as adjuncts to ship-based hydrographic casts, towed sensors, and satellite-based sensors. Underwater acoustic networking is the enabling technology for these applications.

Underwater Acoustic Networks

To collect data about noise emitted from MHK devices, it may be necessary to deploy seafloor-mounted and autonomous-drifting hydrophones to monitor noise levels before, during, and after testing of wave-energy and tide-energy conversion devices.

A model of the ocean medium between acoustic sources and receivers is called a *channel model*, and it may be digital or analog. In an oceanic channel, characteristics of the acoustic signals change as they travel from transmitters to receivers. These characteristics depend upon the acoustic frequency, the distances between sources and receivers, the paths taken by the signals, and the prevailing ocean environment in the vicinity of the paths. Properties of received signals can be derived from those of the transmitted signals using *channel models* (Etter 2013).

Underwater Acoustic Modeling Techniques as Enabling Tools

This section summarizes the modeling techniques that can be employed to predict and assess the acoustic impacts of MHK device installation and operation, with particular emphasis on propagation and noise models.

Propagation Models

As sound propagates through the ocean, the effects of spreading and attenuation diminish its intensity. Spreading loss includes spherical and cylindrical spreading losses in addition to focusing effects. Attenuation loss includes losses due to absorption, leakage out of ducts, scattering, and diffraction. Propagation losses increase with increasing frequency due largely to the effects of absorption. Sound propagation is also affected by the conditions of the surface and bottom boundaries of the ocean as well as by the vertical and horizontal distribution of sound speed within the ocean volume. Sound-speed gradients introduce refractive effects that may focus or defocus the propagating acoustic energy.

Formulations of acoustic propagation models generally begin with the three-dimensional, time-dependent wave equation. For most applications, a simplified linear, hyperbolic, second-order, time-dependent partial differential equation is used:

$$\nabla^2 \Phi = \frac{1}{c^2} \frac{\partial^2 \Phi}{\partial t^2} \tag{1}$$

where $\nabla^2 = (\partial^2/\partial x^2) + (\partial^2/\partial y^2) + (\partial^2/\partial z^2)$ is the Laplacian operator, Φ is the potential function, c is the speed of sound, and t is the time.

Subsequent simplifications incorporate a harmonic (single-frequency, continuous-wave) solution in order to obtain the time-independent Helmholtz equation. Specifically, a harmonic solution is assumed for the potential function Φ:

$$\Phi = \phi \, e^{-i\omega t} \tag{2}$$

where ϕ is the time-independent potential function, ω is the source frequency ($2\pi f$), and f is the acoustic frequency. Then the wave Eq. (1) reduces to the Helmholtz equation:

$$\nabla^2 \phi + k^2 \phi = 0 \tag{3}$$

where $k = (\omega/c) = (2\pi/\lambda)$ is the wavenumber and λ is the wavelength. Equation (3) is referred to as the time-independent (or frequency-domain) wave equation; in

cylindrical coordinates, it is commonly referred to as the elliptic-reduced wave equation

Propagation models of potential interest to MHK acoustic assessments can be reduced to three techniques (Etter 2013): **ray-theoretical models** calculate propagation loss on the basis of ray tracing; **normal-mode solutions** are derived from an integral representation of the elliptic-reduced wave equation; and **parabolic approximation approaches** replace the elliptic-reduced wave equation with a PE.

Each of these three techniques has a unique domain of applicability that can be defined in terms of acoustic frequency and environmental complexity (for more details, refer to Etter 2013). These domains are determined by the assumptions invoked in deriving each solution from the wave equation. **Ray-theoretical models** invoke the geometrical acoustics approximation, which effectively limits the ray-theoretical approach to the high-frequency domain: $f > 10\ c/H$, where f is the frequency, H is the duct depth, and c is the speed of sound. **Normal-mode solutions** compute eigenvalues (or characteristic values) that represent the discrete set of values for which solutions of the normal-mode functions exist; the number of modes increases with increasing frequency, which makes this approach more viable at lower frequencies. **Parabolic approximation approaches** can be numerically solved using marching solutions when the initial field is known; although this approach is also more viable at lower frequencies, the computational advantage lies in the fact that a parabolic-differential equation can be marched in the range dimension, whereas the normal-mode approach must be numerically solved in the entire range-depth region simultaneously.

A further division can be made according to range-independent (1D—depth-dependence only) or range-dependent environmental specifications, where environmental range-dependence can be 2D (depth and range) or 3D (depth, range, and azimuth). Hybrid formulations obtained by combining two or more different techniques are often developed to improve domain robustness.

The Ocean Acoustics Library (OALIB) (http://oalib.hlsresearch.com) (last accessed August 24, 2016) provides access to selected stand-alone propagation models of potential interest to MHK acoustic assessments. This access is provided directly to downloadable software or indirectly by reference to other authoritative Web sites. Candidate models derived from the OALIB are summarized in Table 3. A more extensive list of underwater acoustic propagation models is presented by Etter (2013).

Some applications, such as work related to acoustic impacts on marine mammals, do not require extremely high-fidelity model outputs. Transmission losses averaged over depth, for example, are often adequate. An approach referred to as *energy-flux* (Weston 1971, 1980a, b) is useful for the rapid calculation of transmission losses where the propagation conditions are dominated by numerous boundary-reflected multipaths, and when only the coarse characteristics of the acoustic field are needed. In specific configurations, especially at long ranges in shallow-water environments, the transmitted field can be viewed as being composed of many paths propagating by successive reflections from the surface and bottom boundaries. Here, the acoustic energy will remain trapped between these two

Table 3 Summary of candidate underwater acoustic propagation models that are accessible on the OALIB Web site (http://oalib.hlsresearch.com). (Acronyms are defined in Appendix A. Also see Etter 2013 for more details regarding these and other propagation models.)

Technique	Candidate models
Ray theory	BELLHOP HARPO TRIMAIN TV-APM
Normal mode	COUPLE KRAKEN MOATL WKBZ
Parabolic approximation	FOR3D PDPE PECan RAM/RAMSURF UMPE

boundaries. Furthermore, if the acoustic frequency is high enough that the field oscillations can be considered to be random, then an average intensity can be calculated using simple algebraic formulas. This concept can be extended to ocean environments where the sound speed is not constant, or where there are slight losses at the boundaries. In such cases, the transmitted field cannot be taken as a volumetric average. Rather, it has to be decomposed into its angular components and the cyclic characteristics of the various beams must be detailed (Lurton 1992, 2002).

Noise Models

Noise is the prevailing, unwanted background of sound at a particular location in the ocean at a particular time. The local noise field is thus characterized by temporal, spatial, and spectral variabilities. The noise generated by both natural and anthropogenic point sources is diminished by the effects of spreading and attenuation, which are quantified by propagation models. Ambient-noise models are applicable over a broad range of frequencies and consider noise originating from surface weather, biologics, shipping, and other commercial activities.

One example of a noise model with potential application to MHK acoustic research is ESME (effects of sound on the marine environment). This is a multidisciplinary research and development effort to explore the interactions between anthropogenic sounds, the acoustic environment, and marine mammals (Shyu and Hillson 2006; Siderius and Porter 2006). The ESME workbench models the entire sound path including the sound sources, the medium (water column and seafloor), and the TTS models of the marine mammals. The goal is to predict impacts of anthropogenic sounds on marine mammals. This entails three elements: accurate estimates of the sound field in the ocean, accurate estimates of the cumulative sound exposure of the marine mammals, and reliable predictions of the incidence of TTS for the species of interest given the estimated cumulative exposure. A more extensive list of underwater acoustic noise models is presented by Etter (2013).

Summary

This chapter describes the use of underwater acoustic models for the evaluation of marine-system noise impacts associated with the installation and operation of MHK devices, particularly in coastal oceans. This review is placed in the context of an underwater soundscape, which is a combination of sounds that characterize, or arise from, an ocean environment. Disruption of the natural acoustic environment results in noise pollution. The field of underwater acoustics enables us to observe and predict the behavior of this soundscape and the response of the natural acoustic environment to noise pollution. Specifically, underwater acoustic models can serve as enabling tools for assessing noise impacts on marine systems through the generation of analytical metrics useful in resource management.

Marine-mammal protection research has focused on simulating anthropogenic sound sources, which derive in part from seismic-exploration activity, merchant shipping traffic, and a new generation of multistatic naval sonar systems. Additional sources derive from MRE resources, including the deployment of wind farms, tidal turbines, and wave-energy devices.

One of the most significant activities during MHK device construction is foundation installation, which may involve dredging, rock laying, and pile driving. Other construction activities could include cable laying, turbine and turbine-tower installation, and ancillary structure installation (such as offshore transformers). Additional noise sources include industrial traffic associated with transporting workers, materials, and hydrokinetic energy devices to offshore sites. Knowing the length of time the marine environment is exposed to an underwater noise source is useful when assessing environmental effects.

A review of the methods employed in conducting marine-mammal TTS experiments indicates that (1) existing data are insufficient to construct generalized models for recovery, and (2) existing models cannot determine the time necessary to treat subsequent exposures as independent events. More information is needed about the relationship between auditory evoked potentials and behavioral measures of TTS for various stimuli. Data on noise-induced threshold shifts in marine mammals are available for only a few species, and for only a few individuals within these species. Questions still remain about the most appropriate methods for extrapolation to other species. A study of the impacts of uncertainty in the modeling of anthropogenic impacts suggested a precautionary approach to regulation based on modeling results; specifically, due to the complex patterns of sound propagation encountered in diverse shelf regions, some marine mammals may not necessarily encounter the average sound-exposure conditions predicted for any given impact scenario.

Mitigation refers to the administrative, procedural, legal, and technical aspects of reducing or eliminating sources of noise that might be harmful to marine life, especially marine mammals. Monitoring indicates connections between identified environmental impacts, measurement indicators, detection limits, and the thresholds that will signal the need for corrective action. Noise-reduction methods include

acoustic-isolating materials and bubble curtains (or screens) that reduce initial sound output or reduce sound intensity along a propagation path. Acoustic-mitigation devices include acoustic-harassment devices (or pingers) that encourage animals to move away from high-risk operational areas.

Applied underwater acoustic modeling technologies (specifically, propagation and noise models) have evolved over the past several years in response to new regulatory initiatives that place restrictions on uses of sound in the ocean. The mitigation of marine-mammal endangerment is now an integral consideration in acoustic-system design, installation, and operation. Additional advances have been achieved using energy-flux techniques that can simplify the interpretation of sound-channel models. To assist researchers and practitioners in the proper usage of underwater acoustic models, updated summaries are provided for the existing inventory of propagation and noise models, tailored to potential MHK applications. Additional guidelines are provided to assist users in the selection and utilization of the most appropriate models for any given impact scenario. Where available, case studies are examined to illustrate the use of acoustic models for the assessment of MHK device impacts. It is important to note that many underwater acoustic models currently used in EIAs consider only the sound-pressure component of sound, which is the means by which marine mammals hear; however, the primary mechanism by which fish and invertebrate species detect sound is through the particle-motion component of sound. Consequently, this aspect warrants further development and refinement of the existing model inventory.

Finally, it should be stressed that the deployment of MHK devices is still in the early stages, so a substantial database is not yet available regarding the impacts of MHK noise on the environment. Only a limited understanding of the environmental impacts has been achieved to date because few of these projects are presently operational. This situation creates an opportunity for numerical modelers to generate prognostic indicators of MHK noise impacts to guide resource planners in the selection of sites suitable for MHK installations.

Appendix A—Abbreviations and Acronyms

1D	One-dimensional
2D	Two-dimensional
3D	Three-dimensional
BELLHOP	Gaussian-Beam, Finite-Element, Range-Dependent Propagation Model
CO_2	Carbon dioxide
COUPLE	Coupled Mode Model
dB	Decibel(s)
EIA	Environmental impact assessment
ESME	Effects of sound on the marine environment
FE	Finite element

FOR3D	Finite Difference Methods, Ordinary Differential Equations, and Rational Function Approximations to Solve the LSS 3D Wave Equation
h	Hour(s)
HARPO	Hamiltonian Acoustic Raytracing Program—Ocean
Hz	Hertz (cycles per second)
kHz	Kilohertz
km	Kilometer(s)
KRAKEN	Adiabatic/Coupled Normal Mode Model
LSS	Lee-Saad-Schultz Method
m	Meter(s)
MHK	Marine-hydrokinetic
MMPA	Marine Mammal Protection Act
MOATL	Modal Acoustic Transmission Loss Model
MONM	Marine Operations Noise Model
MRE	Marine renewable energy
OALIB	Ocean Acoustics Library
PDPE	Pseudo-Differential PE
PE	Parabolic equation
PECan	Canadian Parabolic Equation
pH	Scale used to specify the acidity or basicity of an aqueous solution
PTS	Permanent threshold shift
RAM	Range-Dependent Acoustic Model
RAMSURF	RAM Rough Surface
TRIMAIN	Range-Dependent Acoustic Propagation Model Based on Triangular Segmentation of the Range-Depth Plane
TTS	Temporary threshold shift
TV-APM	Time-Variable Acoustic Propagation Model
UMPE	University of Miami PE
WKBZ	Adiabatic Normal Mode Model

References

Andrew, R. K., Howe, B. M., Mercer, J. A., & Dzieciuch, M. A. (2002). Ocean ambient sound: Comparing the 1960s with the 1990s for a receiver off the California coast. *Acoustic Research Letters Online, 3*(2), 65–70.

Austin, M., Chorney, N., Ferguson, J., Leary, D., O'Neill, C., & Sneddon, H. (2009). Assessment of underwater noise generated by wave energy devices. Prepared by JASCO Applied Sciences on behalf of Oregon Wave Energy Trust. Technical Report, P001081-001, Version 1.0.

Bass, S. J., & Hay, A. E. (1997). Ambient noise in the natural surf zone: Wave-breaking frequencies. *IEEE Journal of Oceanic Engineering, 22,* 411–424.

Carey, W. M., & Evans, R. B. (2011). *Ocean ambient noise: Measurement and theory*. New York: Springer.

Copping, A. E., & O'Toole, M. J. (2010). OES-IA annex IV: Environmental effects of marine and hydrokinetic devices. In *Experts' Workshop, September 27th–28th 2010, Clontarf Castle, Dublin, Ireland*. Pacific Northwest National Laboratory, PNNL-20034. Prepared for the US Department of Energy under Contract DE-AC05-76RL01830, 64 pp.

Etter, P. C. (2013). *Underwater acoustic modeling and simulation* (4th ed.). Boca Raton, Florida, USA: CRC Press.

Farcas, A., Thompson, P. M., & Merchant, N. D. (2016). Underwater noise modelling for environmental impact assessment. *Environmental Impact Assessment, 57,* 114–122. doi:10.1016/j.eiar.2015.11.012.

Felizardo, F. C., & Melville, W. K. (1995). Correlations between ambient noise and the ocean surface wave field. *Journal of Physical Oceanography, 25,* 513–532.

Finette, S. (2005). Embedding uncertainty into ocean acoustic propagation models. *The Journal of the Acoustical Society of America, 117,* 997–1000.

Finneran, J. J. (2015). Noise-induced hearing loss in marine mammals: A review of temporary threshold shift studies from 1996 to 2015. *The Journal of the Acoustical Society of America, 138,* 1702–1726.

Ikpekha, O. W., Soberon, F., Daniels, S. (2014). Modelling the propagation of underwater acoustic signals of a marine energy device using finite element method. In *International Conference on Renewable Energies and Power Quality (ICREPQ'14), Cordoba, Spain*.

Lawson, J. W. (2009). *The use of sound propagation models to determine safe distances from a seismic sound energy source*. Department of Fisheries and Oceans, Canadian Science Advisory Secretariat, Res. Doc. 2009/060.

Li, Y., & alişal, S. M. (2010). Numerical analysis of the characteristics of vertical axis tidal current turbines. *Renewable Energy, 35,* 435–442. doi:10.1016/j.renene.2009.05.024.

Lloyd, T. P., Turnock, S. R., & Humphrey, V. F. (2011). Modelling techniques for underwater noise generated by tidal turbines in shallow waters. In *Proceedings of 30th International Conference on Ocean, Offshore and Arctic Engineering (OMAE2011), Rotterdam, The Netherlands* (pp. 1–9).

Lurton, X. (1992). The range-averaged intensity model: A tool for underwater acoustic field analysis. *IEEE Journal of Oceanic Engineering, 17,* 138–149.

Lurton, X. (2002). *An introduction to underwater acoustics: Principles and applications*. New York: Springer.

McDonald, M. A., Hildebrand, J. A., & Wiggins, S. M. (2006). Increases in deep ocean ambient noise in the Northeast Pacific west of San Nicolas Island California. *The Journal of the Acoustical Society of America, 120,* 711–718.

McDonald, M. A., Hildebrand, J. A., Wiggins, S. M., & Ross, D. (2008). A 50 year comparison of ambient ocean noise near San Clemente Island: A bathymetrically complex coastal region off Southern California. *The Journal of the Acoustical Society of America, 124,* 1985–1992.

National Research Council. (2003). *Ocean noise and marine mammals*. Washington: The National Academies Press.

National Research Council. (2005). *Marine mammal populations and ocean noise: Determining when noise causes biologically significant effects*. Washington, DC: The National Academies Press.

Orcutt, J. A. (1988). Ultralow- and very-low-frequency seismic and acoustic noise in the Pacific. *The Journal of the Acoustical Society of America*, *84*(1), S194.

Scrimger, J. A., Evans, D. J., McBean, G. A., Farmer, D. M., & Kerman, B. R. (1987). Underwater noise due to rain, hail, and snow. *The Journal of the Acoustical Society of America, 81,* 79–86.

Shyu, H.-J., & Hillson, R. (2006). A software workbench for estimating the effects of cumulative sound exposure in marine mammals. *IEEE Journal of Oceanic Engineering, 31,* 8–21.

Siderius, M., & Porter, M. B. (2006). Modeling techniques for marine-mammal risk assessment. *IEEE Journal of Oceanic Engineering, 31,* 49–60.

Todd, V. L. G., Todd, I. B., Gardiner, J. C., & Morrin, E. C. N. (2015). *Marine mammal observer and passive acoustic monitoring handbook*. Exeter, UK: Pelagic Publishing.

von Benda-Beckmann, A. M., Wensveen, P. J., Kvadsheim, P. H., Lam, F.-P. A., Miller, P. J. O., Tyack, P. L., et al. (2014). Modeling effectiveness of gradual increases in source level to mitigate effects of sonar on marine mammals. *Conservation Biology, 28*(1), 119–128. doi:10.1111/cobi.12162.

Weston, D. E. (1971). Intensity-range relations in oceanographic acoustics. *Journal of Sound and Vibration, 18,* 271–287.

Weston, D. E. (1980a). Acoustic flux formulas for range-dependent ocean ducts. *The Journal of the Acoustical Society of America, 68,* 269–281.

Weston, D. E. (1980b). Acoustic flux methods for oceanic guided waves. *The Journal of the Acoustical Society of America, 68,* 287–296.

Zykov, M. (2013). Underwater sound modeling of low energy geophysical equipment operations. JASCO Document 00600, Version 2.0. Prepared by JASCO Applied Sciences for CSA Ocean Sciences Inc.

Challenges to Characterization of Sound Produced by Marine Energy Converters

Brian Polagye

Introduction

Concerns about the effects of anthropogenic noise on marine animals have risen over the past decades (Williams et al. 2015). This has motivated interest in understanding of the sound that could be produced by marine energy converters (MECs) while they are in early development. Here, we concern ourselves with two types of MEC: those that convert surface waves to electrical power (Wave Energy Converters, or WECs) and those that convert fast moving tidal or ocean currents (collectively, current turbines).

In doing so, it is first helpful to consider these concerns in context. MECs primarily produce continuous sound at relatively low, time-varying intensity, in comparison to impulsive, high-intensity sound associated with naval sonars and seismic exploration. For MECs, radiated sound is a by-product of harnessing power available from waves and currents and, consequently, bounded by the power absorbed by the device. For an idealized source enclosed by a sphere with a diameter of one meter, source power, in Watts, is given as

$$\mathrm{SL}\ [\mathrm{W}] = 4\pi \frac{\left(10^{-6} x 10^{(\mathrm{SL[dB]}/20)}\right)^2}{\rho c}$$

B. Polagye (✉)
Department of Mechanical Engineering, University of Washington, Seattle, WA, USA
e-mail: bpolagye@uw.edu

Z. Yang and A. Copping (eds.), *Marine Renewable Energy*,
DOI 10.1007/978-3-319-53536-4_14

where SL [dB] is the broadband sound pressure at a range of 1 m from the source in units of dB re 1 μPa, ρ is the density of water, and c is the sound speed (Bassett et al. 2012). Note also that the term in the parentheses has units of Pa-m. A Panamax vessel injects approximately 45 MW of mechanical power into the water column to overcome drag (MAN Diesel 2009), producing a broadband source level on the order of 180 dB re 1 μPa (Bassett et al. 2012). If one assumes that a MEC absorbing approximately 1 MW of mechanical power emits a similar proportion of acoustic power, then this suggests that broadband source levels for MECs are unlikely to exceed 165 dB re 1 μPa. Consequently, while this sound is likely to be audible to marine life, it is unlikely to cause acoustic injury. Interpretation of potential behavioral effects of these types of low-intensity sounds is a complicated problem, since marine animal reaction to sound is context-dependent (Ellison et al. 2012). While large vessels are likely to have higher source levels than MECs, MEC sound will be more persistent at a given location, though modulated by the intensity of the wave or current forcing.

The sound emitted by tidal and ocean current turbines is likely to consist of mechanical noise associated with rotating generators, gearboxes, pitch servomotors, yaw servomotors, support structure vibration, and blade vibration as a consequence of turbulent loading. Unlike the propellers on vessels, cavitation is unlikely, since this would significantly reduce the hydrodynamic efficiency of the rotor and damage blade surfaces. The sound emitted by wave energy converters is more heterogeneous, given the wider range of concepts and can include the sound from moorings, generators, gearboxes, and pumps, as well as sound produced by waves breaking on surface-piercing structures. A recent summary of measurements and simulation of MECs is presented in Copping et al. (2016). While limited, these agree with the analytical argument that single device demonstrations are unlikely to cause acoustic injury and may, at most, produce behavioral modification through avoidance or attraction (e.g., attraction of a predator to fish around an artificial reef established on the MEC foundation). While there are significant differences in the frequency content of sound produced by various MECs, in general they produce sound up to tens of kHz, with the highest intensity sound at frequencies below one kHz. For example, a spectrogram and annotated periodogram of drifting measurements made in close proximity to a WEC are shown in Fig. 1.

Given these results, questions remain about the environmental effects of arrays of MECs intended to produce utility-scale power (i.e., installations producing, on average, hundreds of MW of electrical power in comparison to single MECs producing less than one MW). If the acoustic characteristics of MECs are well-understood, then array scale-up (or, at a minimum, bounding the effect of array scale-up) is relatively straightforward through acoustic modeling.[1] However, the

[1]This does, however, require considerable information about the acoustic environment, including parameters that may not be readily available, such as the seabed composition. Examples of the consequences of environmental parameter uncertainty on transmission loss are discussed in Farcas et al. (2016).

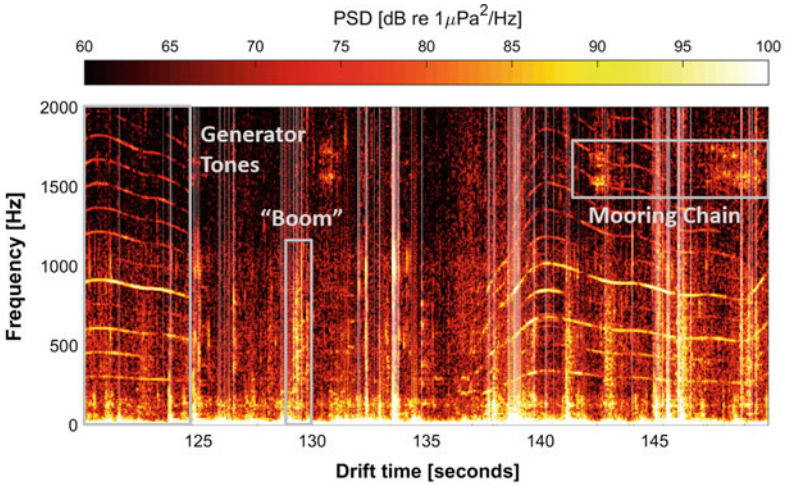

(a) Annotated spectrogram of Azura WEC over a 30 s period. Transparent white overlays have been classified as containing significant flow-noise or self-noise.

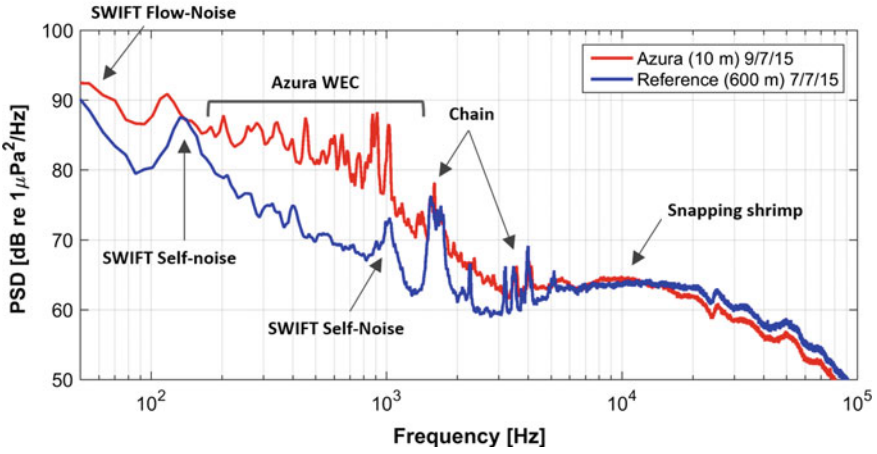

(b) Annotated periodogram of Azura WEC compared to a reference periodogram obtained beyond the acoustic influence of the WEC.

Fig. 1 Spectrogram and periodogram from a WEC at the US Navy Wave Energy Test Site illustrating the type of sounds that can be produced by a WEC. Measurements obtained by a hydrophone mounted to a SWIFT buoy (Thomson 2012)

present understanding of MEC sound is incomplete. Here, three challenges to comprehensive characterization of MEC sound are discussed: (1) the influences on sound generation by a MEC, (2) identification of MEC sound amidst other sources of ambient noise, and (3) masking of MEC sound during measurements by flow-noise. Each of these challenges is typified by the representative case in Fig. 1 (i.e., How would the Azura WEC periodogram change in a different sea state? What sound is produced by the Azura below 200 Hz where measurements are dominated by flow-noise and self-noise? Are the tonals from chain noise associated with the Azura or another mooring in the general area?). This chapter discusses each of the challenges in sequence. In several cases, there exists no generally accepted practice to completely addressing a particular challenge. In such cases, known problems with conventional approaches are presented, along with potential solutions that await more thorough testing and verification in the field.

In addition to these challenges, most measurements have been obtained from MEC prototypes that are likely to undergo modification prior to array-scale deployment and may not be operating in the same manner as in a utility-scale array. Further, the cost of acoustic characterization remains an important consideration. Accurate measurements must be made in challenging metocean conditions at sufficiently low cost to be of practical use to the emerging marine renewable energy industry. Readers interested in general best practices for accurate measurement of underwater sound are referred to the presentation in Robinson et al. (2014).

Influences on Sound Generation by Marine Energy Converters

Given experience with other sources of sound in the ocean (e.g., vessel traffic, McKenna et al. 2013) and air (e.g., wind turbines, Hubbard and Shepherd 1991), it is reasonable to hypothesize that the sound produced by MECs is likely to vary with their operating state. This suggests that the characteristics of sound produced by current turbines will likely be a function of the current speed, while the sound produced by wave energy converters (WECs) will likely be a function of sea state (i.e., wave height and period). Further, sound characteristics will likely depend on how the MEC is being controlled (e.g., different levels of power generation or shaft rotation are possible for a single environmental forcing).

For reasons discussed later in this chapter, WEC observations are typically made using fixed instrumentation (attached to the seabed or moored) while current turbine observations are typically made using drifting instrumentation. In theory, one could evaluate all currents that will ever be experienced by a tidal turbine during a single perigean spring tide. In practice, logistical constraints may dictate that observations be conducted over several tidal cycles. For ocean current turbines, observations

would need to be spread across seasonal variations in resource intensity (Yang et al. 2015). However, for WECs, making observations over all possible sea states is challenging. As for international standards for power performance characterization (IEC 2012), acoustic measurements over at least half a year may be required to characterize sound produced during the majority of sea states. This is still not daunting for cabled observations (though, to date, no cabled observations of WEC sound have been reported in the literature), but for autonomous systems, data collection over these time scales can be prohibitively expensive. This is particularly the case if spatially distributed observations are required, as would be the case if one wished to investigate whether WEC sound directivity is a function of operating state.

Identification of Marine Energy Converter Sound

Given a measurement of sound at some distance from a MEC, a requirement for extrapolating to the sound produced by an array is to identify the frequencies at which MEC sound exceed ambient levels. For example, if sediment-generated noise (Bassett et al. 2013) masks current turbine sound over some frequencies, then these sounds should not be included in the source term for a current turbine in an acoustic model. Initially, it may appear attractive to collect pre-installation "baseline" measurements and compare post-installation measurements against these. Such a method has been used, with good effect, to identify the sound associated with pile driving (e.g., Bailey et al. 2010). However, in the case of pile driving, the signal-to-noise ratio is high and observations of ambient noise are often temporally adjacent to observations including the sound produced by pile driving. For MECs, if the ambient and operating cases are temporally remote and MEC sound is only marginally higher than ambient, then matching the acoustic spectrum from an operating MEC to the appropriate ambient baseline may be deceptively complicated.

Consider, as an example, measurement of sound around a WEC. The first criterion for equivalence would be the sea state between ambient and operating measurement. Second, precipitation rates and wind speeds (Ma et al. 2005) should also be equivalent, as both contribute to the ambient soundscape. Consequently, in addition to ambient noise measurements by a hydrophone, one would also need co-temporal observations of sea state, precipitation, and wind speed at the site. These can be obtained, but at increased cost to the measurement program. Third, the sound speed profile between the source and receiver should be equivalent, which would require temporally resolved sound speed profiles during baseline and post-installation measurements. While the water column is relatively well-mixed at current energy sites, sound speed variations of a few m/s over the upper 30 m of the water column are possible at wave energy sites (unpublished data). Further, there

should be equivalent anthropogenic noise, which could be achieved by limiting comparison to cases in which no vessels are present within a given range (say, within 10 km of the WEC). This would require an Automatic Identification System (AIS) receiver station for large vessels (e.g., Merchant et al. 2012) and radar or optical camera for vessels not equipped with AIS beacons. Lastly, one would need to establish equivalence for biological sources, such as snapping shrimp (Au and Banks 1998) and low-frequency cetacean vocalizations (Richardson et al. 2013), which can be an important contributor to ambient noise at wave energy sites (Haxel et al. 2013). This is difficult, if not impossible, to achieve in practice as the position, orientation, and intensity of biological sources cannot be easily quantified or easily distinguished from WEC sound when signal-to-noise ratios are low.

Three caveats to these concerns are warranted. First, not all factors may be relevant at all sites (e.g., received levels may be relatively insensitive to the sound speed profile for some arrangements of sources and receivers). Second, these factors are easier to control in observations of current turbines, given the more limited duration of required measurements (on the order of several hours over a period of a few days) and the opportunity for continuous observations of acoustic co-variates by human observers. Third, this challenge does not obviate the value of baseline acoustic observations. They are, indeed, invaluable if one seeks to understand how the presence of a MEC will affect the soundscape. For example, given a statistical distribution of pre-installation noise levels, a statistical distribution of MEC source levels, and a propagation model, it is possible to estimate changes in ambient noise statistics at various ranges from the MEC.

The differentiation between MEC sound and ambient noise is an active area of research, but several strategies have been proposed. One possibility is to decouple the MEC from its environmental forcing. For current turbines, this could be achieved by feathering blades (pitch control) or yawing the rotor out of the flow (yaw control). For WECs, this decoupling can be more complicated, since disengaging or locking the power take-off may not significantly attenuate sound production. A second possibility is to make co-temporal measurements around the MEC and at a reference location beyond the acoustic extent of MEC sound. This can be challenging because the acoustic extent of a MEC may not be known a priori, and it may be difficult to conclusively identify a site that would have a sufficiently similar ambient soundscape, without the presence of a MEC. Third, drifting measurements have been proposed as a mechanism to identify range-dependent portions of the acoustic spectra. This could also be done with fixed measurements of WECs, but at increased cost due to the number of required sensors and deployment platforms. Finally, directional arrays of receivers could be used to identify sounds originating from the known bearing of a MEC using time-delay-of-arrival methods (Spiesberger and Fristrup 1990), though this may be complicated by reflection of MEC sound from adjacent structures and the seabed. While there are many potentially viable options, none have been conclusively demonstrated for a range of MECs and sites.

Masking by Flow-Noise

In addition to the possibility of MEC sound being masked by other sources of ambient noise, MEC sound can be masked by flow-noise. Flow-noise is a consequence of non-propagating pressure fluctuations experienced by a hydrophone associated with turbulence advected across the element or shed by the element. This is distinct from self-noise originating from aspects of the measurement system (e.g., a rattle from a loose component on a drifting hydrophone system).

The intensity and frequency extent of flow-noise scale with current velocity relative to the receiver (Wenz 1962; Strasberg 1979; Bassett et al. 2014). As relative velocity increases from quiescent conditions, flow-noise first becomes apparent at the lowest frequencies and can extend to several hundred Hz for relative velocities of a few m/s; this is likely to mask ambient noise at these frequencies (Bassett et al. 2014). Flow-noise can be mistaken as low-frequency sound that shows a dependence on current velocity. While this is sometimes hypothesized to be the sound produced by ambient turbulence at significant range from the receiver, this is incorrect because, as turbulence is a quadrupole source (Urick 1975; Dowling and Ffowcs Williams 1983), it is a weak radiator of acoustic noise in underwater environments and unlikely to generate appreciable propagating sound relative to sound produced by a MEC.

For this reason, drifting systems that minimize the relative velocity at a hydrophone are recommended for acoustic characterization of current turbines (Polagye and Murphy 2015). However, in doing so, care must be taken to avoid inadvertently producing relative velocity, as can be caused if a hydrophone is suspended from a drifting surface vessel that experiences significantly different forcing than the hydrophone element due to winds, waves, or vertical shear in currents.

Flow-noise can also be encountered in measurements at wave energy sites obtained from fixed platforms, which are generally recommended to achieve a duration of measurements that covers the majority of sea states, while minimizing human safety risks associated with deployment and recovery of drifting systems in high sea states. Wave orbital velocities can, however, produce significant flow-noise. Figure 2 shows sound recorded at a wave energy site with a depth of approximately 30 m (the hydrophone is located 0.9 m above the sea floor) during a sea state with a significant wave height of 3.4 m and energy period of 12 s. Elevation of low-frequency sound is apparent twice per wave period, while tonals associated with the WEC power take-off are visible between 200 and 250 Hz.

Several approaches have been proposed to mitigate flow-noise, but none have been proven. One is time domain processing for multi-element receivers that can recover the coherent portion of the acoustic signal, if the signal-to-noise ratio of the coherent portion is high enough (Chung 1977; Buck and Greene 1980). This is, however, often not the case for high-amplitude flow-noise encountered at marine renewable energy sites. A second is the use of flow-shields (Lee et al. 2011), common in naval applications (Urick 1975), which creates a quiescent envelope

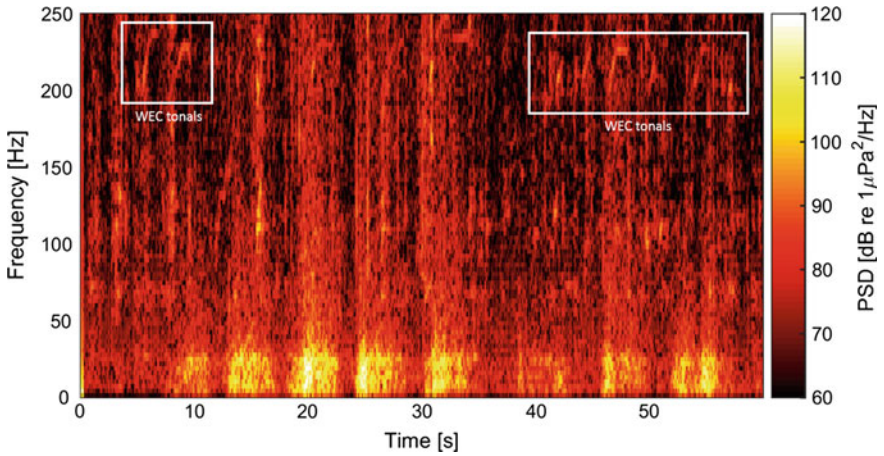

Fig. 2 Spectrogram from a WEC at the US Navy Wave Energy Test Site showing flow-noise contamination for a fixed hydrophone at a depth of 30 m (unpublished data). The energy period is 12 s and significant wave height is 3.4 m

around the hydrophone and average pressure fluctuations over a larger surface. The size of flow-shields can be an issue, as can attenuation of higher frequencies. Finally, drifting systems can minimize relative velocities (Wilson et al. 2013), but because of vertical shear and system inertia, relative motion remains possible and can be difficult to quantify.

Conclusions

There are three primary challenges to comprehensive acoustic characterization of marine energy converters (MECs): (1) temporal variability in the sound produced by a MEC, (2) identification of MEC sound amidst other sources of ambient noise, and (3) masking of MEC sound by flow-noise. The sound produced by current turbines will likely be primarily a function of water current speed, while the sound produced by wave energy converters (WECs) will likely be a function of sea state (i.e., wave height and period). Several mechanisms to differentiate between MEC sound and ambient noise have been proposed (e.g., directional arrays of receivers to identify sound originating from the known location of a MEC using time-delay-of-arrival methods), but all require further testing and verification. In any measurement, mitigation of flow-noise will be necessary and might be achieved by several methods (e.g., flow-shields), all of which also require further testing and verification.

While this discussion focuses on the difficulties of comprehensive acoustic characterization of MECs, this is not intended to discourage such activities. Rather,

it is intended to emphasize that this is a challenging problem, worthy of pursuit, provided that one is cognizant of the pitfalls. Certainly, any improved, albeit imperfect, understanding of the sound produced by MECs represents tangible progress in this area.

Acknowledgements Many thanks to Chris Bassett for reviewing an early draft of the chapter and providing helpful comments, as well as subsequent comments from three anonymous reviewers. Thanks also to Paul Murphy for the example of flow-noise from a bottom-mounted hydrophone at the US Navy wave energy Test Site.

References

Au, W. W., & Banks, K. (1998). The acoustics of the snapping shrimp *Synalpheus parneomeris* in Kaneohe Bay. *The Journal of the Acoustical Society of America, 103*(1), 41–47.

Bailey, H., Senior, B., Simmons, D., Rusin, J., Picken, G., & Thompson, P. M. (2010). Assessing underwater noise levels during pile-driving at an offshore windfarm and its potential effects on marine mammals. *Marine Pollution Bulletin, 60*(6), 888–897.

Bassett, C., Polagye, B., Holt, M., & Thomson, J. (2012). A vessel noise budget for Admiralty Inlet, Puget Sound, Washington (USA). *The Journal of the Acoustical Society of America, 132* (6), 3706–3719.

Bassett, C., Thomson, J., & Polagye, B. (2013). Sediment-generated noise and bed stress in a tidal channel. *Journal of Geophysical Research: Oceans, 118*(4), 2249–2265.

Bassett, C., Thomson, J., Dahl, P. H., & Polagye, B. (2014). Flow-noise and turbulence in two tidal channels. *The Journal of the Acoustical Society of America, 135*(4), 1764–1774.

Buck, B. M., & Greene, C. R. (1980). A two-hydrophone method of eliminating the effects of nonacoustic noise interference in measurements of infrasonic ambient noise levels. *The Journal of the Acoustical Society of America, 68*(5), 1306–1308.

Chung, J. Y. (1977). Rejection of flow noise using a coherence function method. *The Journal of the Acoustical Society of America, 62*(2), 388–395.

Copping, A., Sather, N., Hanna, L., Whiting, J., Zydlewski, G., Staines, G., et al. (2016). Annex IV 2016 State of the Science Report: Environmental Effects of Marine Renewable Energy Development Around the World. pp. 224.

Dowling, A. P., & Ffowcs Williams, J. E. (1983). *Sound and sources of sound*. New York, NY, USA: Wiley.

Ellison, W. T., Southall, B. L., Clark, C. W., & Frankel, A. S. (2012). A new context-based approach to assess marine mammal behavioral responses to anthropogenic sounds. *Conservation Biology, 26*(1), 21–28.

Farcas, A., Thompson, P. M., & Merchant, N. D. (2016). Underwater noise modelling for environmental impact assessment. *Environmental Impact Assessment Review, 57,* 114–122.

Haxel, J. H., Dziak, R. P., & Matsumoto, H. (2013). Observations of shallow water marine ambient sound: the low frequency underwater soundscape of the central Oregon coast. *The Journal of the Acoustical Society of America, 133*(5), 2586–2596.

Hubbard, H. H., & Shepherd, K. P. (1991). Aeroacoustics of large wind turbines. *The Journal of the Acoustical Society of America, 89*(6), 2495–2508.

International Electrotechnical Commission (IEC). (2012). Marine energy—Wave, tidal and other water current converters—Part 100: Electricity producing wave energy converters—Power performance assessment. *IEC TS, 62600–100,* 2012.

Lee, S., Kim, S. R., Lee, Y. K., Yoon, J. R., & Lee, P. H. (2011). Experiment on effect of screening hydrophone for reduction of flow-induced ambient noise in ocean. *Japanese Journal of Applied Physics*, *50*(7S), 07HG02.

Ma, B. B., Nystuen, J. A., & Lien, R. C. (2005). Prediction of underwater sound levels from rain and wind. *The Journal of the Acoustical Society of America, 117*(6), 3555–3565.

MAN Diesel (2009). *Propulsion trends in container vessels*. MAN Diesel A/S, Copenhagen.

McKenna, M. F., Wiggins, S. M., & Hildebrand, J. A. (2013). Relationship between container ship underwater noise levels and ship design, operational and oceanographic conditions. *Scientific reports*, *3*.

Merchant, N. D., Blondel, P., Dakin, D. T., & Dorocicz, J. (2012). Averaging underwater noise levels for environmental assessment of shipping. *The Journal of the Acoustical Society of America*, *132*(4), EL343–EL349.

Polagye, B. L., & Murphy, P. G. (2015). Acoustic characterization of a hydrokinetic turbine. In *Proceedings of the 11th European Wave and Tidal Energy Conferenc*e. Nantes, France, September 5–11.

Richardson, W. J., Greene Jr, C. R., Malme, C. I., & Thomson, D. H. (2013). *Marine mammals and noise*. Academic press.

Robinson, S. P., Lepper, P. A., & Hazelwood, R. A. (2014). Good practice guide for underwater noise measurement, National Measurement Office, Marine Scotland, The Crown Estate, NPL Good Practice Guide No. 133, ISSN: 1368-6550.

Spiesberger, J. L., & Fristrup, K. M. (1990). Passive localization of calling animals and sensing of their acoustic environment using acoustic tomography. *American Naturalist*, 107–153.

Strasberg, M. (1979). Nonacoustic noise interference in measurements of infrasonic ambient noise. *The Journal of the Acoustical Society of America, 66*(5), 1487–1493.

Thomson, J. (2012). Wave breaking dissipation observed with "SWIFT" drifters. *Journal of Atmospheric and Oceanic Technology, 29*(12), 1866–1882.

Urick, R. J. (1975). *Principles of underwater sound*. New York: McGrawHill.

Wenz, G. M. (1962). Acoustic ambient noise in the ocean: spectra and sources. *The Journal of the Acoustical Society of America, 34*(12), 1936–1956.

Williams, R., Wright, A. J., Ashe, E., Blight, L. K., Bruintjes, R., Canessa, R., et al. (2015). Impacts of anthropogenic noise on marine life: Publication patterns, new discoveries, and future directions in research and management. *Ocean and Coastal Management, 115,* 17–24.

Wilson, B., Benjamins, S., & Elliott, J. (2013). Using drifting passive echolocation loggers to study harbour porpoises in tidal-stream habitats. *Endangered Species Research, 22*(2), 125–143.

Yang, X., Haas, K. A., Fritz, H. M., French, S. P., Shi, X., Neary, V. S., et al. (2015). National geodatabase of ocean current power resource in USA. *Renewable and Sustainable Energy Reviews, 44,* 496–507.

Planning and Management Frameworks for Renewable Ocean Energy

Anne Marie O'Hagan

Introduction

Maritime Spatial Planning (MSP) is a relatively new approach to planning where and when human activities occur in marine spaces. Countries are at differing stages of implementing MSP: in some places, this is a response to competition for space, and in other cases, it is a legal requirement. In the European Union (EU), a Directive establishing a framework for MSP (2014/89/EU) was adopted in July 2014 requiring Member States to have maritime spatial plan(s) in place by 2021 at the latest.

MSP can cover specific uses or more strategic objectives in order to achieve ecological, economic, and social objectives. There are many definitions of MSP, and the terms "marine" and "maritime" spatial planning appear to be used synonymously (see Hildebrand and Schröder-Hinrichs 2014). One of the most widely cited definitions of MSP is that of UNESCO (2009), which defines MSP as "a public process of analysing and allocating the spatial and temporal distribution of human activities in marine areas to achieve ecological, economic, and social objectives that usually have been specified through a political process. Characteristics of MSP include ecosystem-based, area-based, integrated, adaptive, strategic, and participatory". The United Kingdom's Department of Environment, Food and Rural Affairs describes MSP as "strategic, forward-looking planning for regulating, managing, and protecting the marine environment, including through allocation of space, that addresses the multiple, cumulative, and potentially conflicting uses of the sea" (Tyldesley 2004; Meaden et al. 2016). For the purposes of this chapter, MSP is taken to be a strategic planning process, carried out through a consistent and agreed-upon framework, which may or may not be legally binding, that enables

A.M. O'Hagan (✉)
MaREI Centre, Environmental Research Institute, University College Cork, Beaufort Building, Haulbowline Road, Ringaskiddy, Country Cork, Ireland
e-mail: A.OHagan@ucc.ie

Z. Yang and A. Copping (eds.), *Marine Renewable Energy*,
DOI 10.1007/978-3-319-53536-4_15

integrated, future-looking, sustainable, and consistent decision-making on spatial uses of the sea.

The desire to develop a clean, secure, and indigenous energy supply has prompted governments to publish dedicated marine renewable and/or ocean energy strategies mapping out the potential development path for the sector in their countries. Other actors, such as the European Commission together with Ocean Energy Europe, the European trade association, have also been in the vanguard of promoting ocean energy. In 2014, the European Commission published a two-phase action plan. The first phase saw the creation of a dedicated Ocean Energy Forum comprised of three work streams focusing on environment and consenting, finance, and technology. The three work streams work to build consensus on specific topics and enable pragmatic solutions to the identified issues to be developed. This culminated in the publication of an Ocean Energy Strategic Roadmap (Ocean Energy Forum 2016); which forms the second phase of the action plan. Such initiatives and strategies represent an important policy context and can prompt further development and growth. Planning, regulatory, and management systems which apply to ocean energy can derive from several sources. National, or domestic, legislation incorporates broader international obligations and, in the EU, also includes EU objectives—all of which reflect the rights and duties of coastal States as recognised by international law. Because the wave and tidal energy sector is still at a pre-commercial stage of development, the consenting of such projects tends to be subject to the same legislation and administrative procedures governing other forms of marine development, though in many countries this situation is evolving as experience grows. The term "consenting" is used generically in this chapter to capture the various consents, permissions, licences, concessions, and leases necessary to undertake development. Consenting processes reflect numerous aspects of development, including the occupation of sea space (seabed leasing), environmental impacts, terrestrial planning, grid/electrical connection, and decommissioning (O'Hagan 2012, 2015). As more integrated marine governance continues to be advocated by a wide diversity of international and regional sources, MSP is continually promoted as one of the cross-cutting tools that is capable of delivering integrated governance.

MSP does not replace single-sector planning or management but has a number of advantages that may benefit the development of the renewable ocean energy sector. In this context, "ocean energy" is taken to include wave and tidal energy sources. The term "marine renewable energy" (MRE) is more expansive and includes ocean energy and offshore wind. MSP can provide greater certainty to the private sector in planning new investments and should reduce conflicts between incompatible users and activities. It should also promote more efficient use of marine resources and space, indicate opportunities for coexistence of activities, and facilitate the implementation of a streamlined permitting process for marine activities. In some locations around the world, the development of offshore wind energy in particular has driven the development and subsequent implementation of MSP. In many northern

European countries, such as Germany, the Netherlands, and Belgium, specific zones have been allocated for offshore wind development. Similarly, in other locations worldwide, specific ocean energy test sites have been established for the testing and demonstration of those technologies. Whilst such sites do not represent marine planning zones, they operate with some of the same features; for example, they can be planned through a participatory process, operated with and through exclusion zones (where necessary), and have environmental monitoring programmes in place to minimise negative environmental effects and be adapted accordingly if required. MSP should ideally set the framework for planning decisions, which become operational through the granting of various consents. Under EU law and the recently adopted EU MSP Directive, all maritime spatial plans developed will be subject to a Strategic Environmental Assessment (SEA) because they may have significant environmental effects. Environmental Impact Assessment (EIA) applies at the site/project level.

This chapter presents descriptions of consenting systems for ocean renewable energy in countries around the world. Consenting is one of the most important, time-consuming, and resource-intensive category of legal considerations encountered by a project developer. It is also one of the most significant threats to the financial viability of a project because of the inherent "regulatory risk" (O'Hagan 2014). Given the development status of these technologies, which ranges from research and development to the prototype stage and to the pre-commercial stage, it is not possible to define what constitutes "best practice" in terms of consenting. A key focus is placed on MSP systems in this chapter in an effort to highlight how this new approach to managing marine activities may influence the development of offshore renewable energy both currently and in the future. The content is derived from relevant external documentary sources and supplemented with findings from a questionnaire completed by all International Energy Agency–Ocean Energy Systems (IEA-OES) Annex IV participant countries for the OES Annex IV State of the Science report (Copping et al. 2016). In the IEA-OES, each country is represented by a Contracting Party, which nominates participants that can be from government departments, national energy agencies, research or scientific bodies, and academia. Currently, there are 13 participating countries in Annex IV.[1] The questionnaire was conducted with the Contracting Party representatives. It included questions about whether the needs of the ocean renewable energy sector were included in MSP, how this was achieved, how scientific information is used, how cumulative impacts are addressed, how conflicts are managed, how other stakeholders are involved, and if there are limitations to implementing MSP currently or likely to be as the sector becomes more established. The information is presented alphabetically by country.

[1]The Annex IV participant countries are Canada, China, Ireland, Japan, New Zealand, Nigeria, Norway, Portugal, South Africa, Spain, Sweden, the UK, and the USA.

Canada

The Department of Natural Resources Canada leads a Marine Renewable Energy Enabling Measures programme that is active in developing a policy framework for administering MRE activities in the federal offshore. Maritime jurisdiction in Canada is complex: under the Constitution, provincial jurisdiction generally ends at the low-water mark, but in Newfoundland and Labrador, it extends to the 3-mile territorial sea limit, and in British Columbia, the waters between Vancouver Island and the mainland are considered provincial waters. Consents required before a MRE project is approved involve those related to land use, project operation, electricity transmission, health and safety, environmental protection, and navigation. A Marine Renewable Energy Technology Roadmap was prepared by Natural Resources Canada with industry collaboration through the Ocean Renewable Energy Group and outlines a technology development strategy to facilitate progress (Natural Resources Canada 2011). This prioritised Environmental Assessment (EA) with the intention of streamlining permitting procedures in the longer term. Whilst there is no one legislative instrument at the federal level that applies to marine energy, certain provinces have been active in better tailoring their legislation to the requirements of marine energy. Nova Scotia, for example, has been particularly progressive in this regard, given the huge potential for tidal energy in the Bay of Fundy and consequent publication of the province's Marine Renewable Energy Strategy in 2012, which contained broad policy, economic, and legal conditions for MRE projects and technologies in expectation of commercial-scale development (Province of Nova Scotia 2012). The legal aspects of the Strategy have since been taken forward via the enactment of a dedicated Marine Renewable Energy Act in 2015. This covers wave, tidal range, in-stream tidal, ocean currents, and offshore wind technologies in designated areas of the Nova Scotia offshore.

The priority areas designated under the Act are the Bay of Fundy and Cape Breton Island's Bras d'Or Lakes. The effect of this is that MRE projects cannot be permitted in these areas without approval from the Nova Scotia Minister of Energy. The Act defines "marine renewable energy resources" as "ocean waves, tides and currents and winds blowing over marine waters, and any other source prescribed by the regulations" (Section 3(1)(n), Marine Renewable Energy Act of 2015). Within these priority areas, the province may designate smaller areas for project development known as "Marine Renewable Electricity Areas" (MREAs). The purpose of an MREA is to identify the best possible locations to develop MRE projects and to provide clarity about the use of this marine space. MREAs will only be identified after significant research and consultation has taken place, and under the 2015 Act four of these have been designated—namely the Fundy Ocean Research Center for Energy site, Digby Gut, Grand Passage, and Petit Passage MREAs—for in-stream tidal energy converter deployments. Any developer proceeding in a priority area without an approval will be in violation of the Act. A licence will allow a project developer to carry out the business of extracting energy within an MREA using a single device or an array of multiple devices. A permit will be issued for the

temporary deployment of a device for the purposes of testing and demonstration. This system will ensure projects proceed only after undergoing a thorough review by Government and subject to effective Government oversight and monitoring. The creation of MREAs must be completed in consultation with the province's Department of Natural Resources and the Department of Fisheries and Aquaculture. The federal Government must also be consulted in relation to commercial fisheries and maritime transportation concerns. There is also the duty to consult the Aboriginal community about the designation process, but they do not hold any veto power.

A second aspect of the Marine Renewable Energy Strategy was the establishment of a Statement of Best Practices for In-Stream Tidal Energy Development (Nova Scotia Department of Energy 2014), which provides guidance for the development and operations of in-stream tidal energy. The Statement is a tool that can be used by industry, Government, and other key stakeholders to harmonise development with environmental interests and ensure that the industry grows in an environmentally and socially responsible manner. It follows a sequence of essential steps in planning, deployment, operation, and decommissioning of an in-stream tidal energy project. This also covers the regulatory aspects of in-stream tidal energy development and establishes a hierarchy of federal and provincial environmental regulatory review requirements according to three different generation outputs of devices: 50 MW or more; 2–50 MW; and less than 2 MW (Nova Scotia Department of Energy 2014). As a result of the need for multiple consents administered by both the federal and provincial governance levels, the province of Nova Scotia has established a Federal/Provincial One-Window Standing Committee for Tidal Power projects (OWC). This is broadly similar to the "one-stop-shop" approach popular in parts of Europe, the rational being that it can streamline and more effectively coordinate developer applications and associated consents for in-stream tidal energy projects in Nova Scotia.

Strategic planning approaches have also implemented in Canada. In Nova Scotia, for example, an SEA for tidal energy was conducted in 2008 of the Bay of Fundy area (OEER 2008). This was forward-looking and highly participatory, and it culminated in a number of recommendations related to the creation of more specific policies and legislation on tidal energy, the promotion of demonstration projects, continuing engagement and participation, and an incremental approach to tidal energy development based on adaptive management. The Statement of Best Practices captures many of these recommendations and contains principles to be applied in their application (Nova Scotia Department of Energy 2014). Canada has a comprehensive framework for oceans management through the Oceans Act (1997), complemented by Canada's Oceans Strategy in 2002. The country's approach to ocean management is based on the principle of integrated management (IM), which seeks to establish decision-making structures that consider both the conservation and protection of ecosystems, whilst at the same time providing opportunities for creating wealth in oceans-related economies and communities. The IM planning process is described in the Policy and Operational Framework for

Integrated Management of Estuarine, Coastal and Marine Environments in Canada and involves six interrelated stages (Fisheries and Oceans Canada 2002):

- defining and assessing a management area;
- engaging affected interests;
- developing an Integrated Management Plan;
- endorsement of plan by decision-making authorities;
- implementing the plan; and
- monitoring and evaluating outcomes.

The implementation of the above framework has occurred since 2005 through a Large Ocean Management Areas (LOMA) pilot-based approach. Whilst these are not strictly maritime spatial plans per se, the impacts are broadly similar. Currently, there are Integrated Management Plans for five areas: Placenta Bay and Grand Banks, the Scotian Shelf, the Gulf of St Lawrence, the Beaufort Sea, and the Pacific North Coast. The plans take a risk-based management approach to identifying and prioritising key management themes derived from the interactions of marine activities with the ecosystems. The plans operate within existing jurisdictional landscapes and regulatory authorities at different levels of governance and are responsible for implementation of plan goals through management policies and measures under their remit. The creation of the LOMAs began with an assessment of the biophysical elements within each planning area, but the need to understand and incorporate social, economic, and cultural aspects to inform sound management decisions has since been brought into the planning process through a Social, Economic and Cultural Overview and Assessment (SECOA) carried out for a defined area. The Eastern Scotian Shelf Integrated Management Plan, for example, was one of the first large plans to be developed though it focuses entirely on offshore areas, beyond 12 nautical miles, and is not formally linked with any adjoining terrestrial plans (Fisheries and Oceans Canada 2007). The LOMAs are hundreds of square kilometres in size and typically host a range of marine activities. Each LOMA identifies management objectives to ensure the health of the ecosystem, and these are accompanied with socioeconomic objectives, based on the SECOA.

MRE is not mentioned in the majority of the LOMA plan areas. The Pacific North Coast Integrated Management Area Plan (Fisheries and Oceans Canada 2013), which incorporates waters from the north Canadian border with Alaska to Vancouver Island where there is a MRE resource, has representatives from both the wind energy representative group and ocean energy sector representatives on its Integrated Oceans Advisory Committee. On the East Coast, the Eastern Scotian Shelf Integrated Management Plan, published in 2008, was evaluated in 2013 and recognised the opportunities for new marine activities within that LOMA (McCuaig and Herbert 2013). The Eastern Scotian Shelf LOMA includes Nova Scotia, where the Department of Energy has designated areas for tidal energy development. This enables the designation of consecutively smaller areas where development may occur until the individual site licence level is reached, as mentioned above.

The effectiveness of the LOMA plans is monitored and evaluated over time and can be adapted to reflect new scientific information or changing circumstances. The evaluation of the Eastern Scotian Shelf Integrated Ocean Management Plan in 2013 identified limitations in relation to boundaries, whereby coastal regions of Nova Scotia were excluded from the plan and this limited the involvement of certain other relevant sectors. Strategic management objectives in the plan were not always accompanied by explicit timelines and commitments for implementation, and this resulted in inaction on plan implementation and loss of trust amongst stakeholders (McCuaig and Herbert 2013).

Provincially, Nova Scotia is relatively data-rich with respect to marine activities and environments. No singular coordinating body is driving the development of MSP which could be a limitation to its implementation. Most would consider the Department of Fisheries and Oceans Canada the lead for MSP, but that Department is currently resource strained. To date, in Nova Scotia, scientific information about where and how to site MRE projects is largely directed by the Department of Fisheries and Oceans Canada, the Canadian Hydrographic Service, and the Geological Survey of Canada. Data are based on surveys and information collected from fisheries activities.

China

The National Energy Administration is developing a Renewable Energy Development Plan that will cover the period from 2016 to 2020 and include an Ocean Energy Development Strategy developed by the National Ocean Technology Centre and the State Oceanic Administration (SOA). This follows the amendment and subsequent enactment of legislation in 2010 on Renewable Energy in the People's Republic of China, which sought to accelerate and promote the development of renewable energy projects. Contemporaneously, a special funding programme for MRE projects was launched by the Ministry of Finance and is now in its third round. The programme is intended to support the demonstration of key technologies and their progress in reaching industrial scale, the construction of platforms, scaled development, and integrated utilisation of renewable energy and new energy technologies. There appears to be some inconsistencies surrounding what the term "marine renewable energy" comprises in Chinese policy. Xu et al. (2014) quoted an MRE survey organised by the SOA, as encompassing wind, tidal current, and wave resources. Earlier marine energy utilisation zones covered only wave and tidal resources. The terms utilised in this section are taken directly from the overarching policies, unless otherwise stated. Feng et al. (2016) state that by the end of 2011, China had five operational offshore wind farms and 14 more under construction. One tidal energy plant is in operation (Jiangxia Experimental Tide Power Plant). Two wave energy plants are in operation (Xiaomaidao 8 kW Pendulum Wave Power Plant and Daguandao 30 kW Pendulum Wave Power Plant), as well as two tidal projects (Daishan Guishan Waterway Experimental 70 kW-floatage Tidal

Current Power Plant and Daishan Gaoting "WANXIANG-II" Experimental 40 kW Tidal Current Power Plant), but all of these are at the demonstration and pilot stages, so they are not commercial ventures (Feng et al. 2016).

In terms of planning and consenting, China has been implementing the Marine Functional Zoning (MFZ) since it was proposed in 1988. This involved a nationwide, comprehensive investigation of China's coastal zone and tidal flat resources to help develop a zoning plan for those areas in terms of their future utilisation. This comprises the development of an all-inclusive and binding document covering marine development and its regulation and management. The zoning plan is the basis for marine management and divides the sea space into different types of functional zones according to criteria related to geographical and ecological features, natural resources, current usage, and socioeconomic development needs. The Law on the Management of Sea Use, enacted in 2001, requires that all uses of sea areas must comply with approved MFZ schemes (Fang et al. 2011). MFZ covers marine development planning, marine resource management, and the establishment of marine nature reserves. Accordingly, marine activities occur in a series of "rounds" determined by the SOA for coastal provinces, autonomous regions, and municipalities. The national MFZ scheme in 2002 divided sea areas under national jurisdiction into 10 types of functional zones: 941 port and shipping zones, 1,888 fishing and fishery resource conservation zones, 202 mining zones, 452 tourism and recreation zones, 319 sea water use zones, 60 ocean energy use zones, 449 construction use zones (the subzone for submerged pipeline, reclamation, shore protection, bridge, and others), 285 marine protected areas, 309 special use zones, and 451 reserved areas (Zhang 2003). This approach was later identified as being outdated, overly simplistic, and insufficient in some areas. In relation to marine energy, for example, Feng et al. (2016) state that the marine energy utilisation zones, which covered tidal energy, tidal current energy, wave energy, and thermal energy, were "overly detailed as well as incomplete" but ignored the offshore wind energy zone. The national MFZ covers internal waters, the territorial sea, contiguous zone, exclusive economic zone, and continental shelf.

A third and new round of MFZ took place between 2009 and 2012. This round was advanced jointly with relevant authorities and coastal Local Governments in accordance with the Sea Area Use Administration Law, the Law on Marine Environmental Protection, and the Sea Island Protection Law. In March 2012, the State Council approved this latest round of national MFZ. A special functional zone was created for MRE. According to the Technical Guidelines for Marine Functional Zoning and the Technical Requirements for Provincial Marine Functional Zoning,[2] all sea areas of China area divided into eight Class I functional zones and 22 Class II functional zones. The MRE zone is a subzone under the Class I zone, i.e. the "mines and energy zone". Sea areas that have rich and exploitable MRE (wave, tidal current and tidal energy, salinity and temperature gradient energy) are

[2]Available in Chinese only: http://www.tsinfo.js.cn/inquiry/gbtdetails.aspx?A100=GB/T%2017108-2006.

categorised as renewable energy areas. Because offshore wind energy is different from the other sources and the resource is larger, its development is viewed as compatible with some other sea uses and no special basic functional zone is defined for it. The Technical Guidelines list all of the data and materials required for the zoning and the methods used. Base maps, remotely sensed imagery, and satellite imagery are all used as a basis for the maps produced. Accompanying documents detail the area's socioeconomic characteristics and existing marine activities. These documents also include an assessment of the physical environment, possible future plans for sea use, environmental protection requirements, commercial fisheries, and marine reclamation to present as comprehensive and detailed a basis for future zoning as possible. These documents can be accessed by the public on the associated information management system via the Internet.

One of the main purposes of MFZ is to allocate the most suitable sea areas for specific activities and thus avoid conflicts. In areas designated as an "agriculture and fishing zone", no industrial development involving marine reclamation can take place. Similarly, in a "port shipment zone" no activities that would adversely affect shipping can take place. When applying to use an area of sea space, an EIA and justification for that use are required so that it can be demonstrated that the new use conforms with the requirements of the MFZ. With respect to project consenting, this varies according to whether the project is funded by the Government or by private sources. A range of consents is required for projects funded by the Government. These include an initial approval from the Department of Development and Reform, a pre-examination and an EIA from the Land Resources Department and Environmental Protection Department, planning permission from the Urban Planning Department, as well as a formal land use approval granted by the Land Resources Department. For the water-based elements of the project, a certificate of right to use sea areas from the SOA or the maritime administrative department of Local Government is required. A different permitting procedure applies to the power production and grid connection elements of the project, which involves the utility distribution grid operator. The variety of consents required involves a number of different authorities which also vary according to the source of the funding.

Ireland

Ireland has a huge potential MRE resource, primarily for wind and wave energy (DCENR 2014). The Marine and Renewable Energy Test Site in Galway Bay is a quarter-scale test site that is fully operational. A second full-scale, grid-connected test site, the Atlantic Marine Energy Test Site, on the west coast is at the advanced planning stage, and onshore works are underway. The Irish Government's Department of Communications, Energy and Natural Resources (DCENR), published an Offshore Renewable Energy Development Plan (OREDP) in February 2014 (DCENR 2014). The plan highlights the potential opportunities for the

country relative to MRE at low, medium, and high levels of development to reflect the findings of the SEA of the plan carried out prior to plan publication (SEAI 2010). As a policy document, the OREDP sets out key principles, specific actions, and enablers needed to deliver Ireland's significant potential in this area. Accordingly, the OREDP is seen as providing a framework for the development of the sector. The implementation of the OREDP is coordinated by the DCENR, and an Offshore Renewable Energy Steering Group (ORESG) has been created to oversee the implementation. The ORESG consists of members of the main Government departments with roles and responsibilities related to energy and the marine environment, developers, and broader interest and user groups when necessary. The work of the ORESG, and hence the implementation of the OREDP, is organised according to three work streams: environment, infrastructure, and job creation. Under the environment work stream, the Group is tasked with ensuring that the needs of the marine energy industry are reflected in the ongoing reform of the foreshore and marine consenting process. Actions and recommendations derived from the SEA and Appropriate Assessment (specific to the conservation objectives of the site in question) of the OREDP are also taken forward by this group.

The consenting process for MRE incorporates occupation of sea space, electrical generation aspects, environmental impacts, and terrestrial planning requirements. The key legislative instrument governing offshore development is the Foreshore Act, 1933, as amended. Under the provisions of that Act, a project proponent requires a foreshore consent, in the form of a licence and/or lease, to develop in the foreshore area. The foreshore is legally defined as the area between mean high water and the 12 nautical mile territorial sea limit. Currently, foreshore consenting for marine renewables is administered by the Department of Housing, Planning, Community and Local Government (DHPCLG). The Department realises that the nature, scale, and impact of MRE developments can vary considerably but states that all require foreshore consent (1) to investigate/survey the site, (2) to construct the development (and cabling), and (3) to occupy the property.[3] A foreshore licence is required for activities that are not permanent or that do not require sole occupation of the foreshore such as site investigation works and studies relating to EIA. Subsequent to this, a developer may apply for a foreshore lease to undertake further development activities that require exclusive use of the foreshore or longer occupation of the area. It is not possible to obtain a foreshore lease unless the aforementioned preliminary work has been completed, but successful completion of site investigation works does not automatically entitle a developer to a foreshore lease. A lease is generally granted for 35 years and is subject to regular review, on a 5-year basis, by the competent authority. The Minister has the right to reject any application for a foreshore licence or lease, modify the area sought under licence, or allow others to simultaneously investigate the suitability of the licence area (Simas et al. 2015).

Along with the foreshore consents, MRE developments are subject to the requirements of the Electricity Regulation Act, 1999, because MRE devices qualify

[3]See http://www.environ.ie/planning/foreshore/offshore-renewable-energy-projects.

as electricity-generating stations under that legislation. The procedures for electricity authorisations are complex and based on installed capacity (O'Hagan and Lewis 2011). Essentially, a developer must have a licence to generate and a licence to construct or reconstruct a generating station. The applications can be made separately or jointly and, where applicable, must be accompanied by an Environmental Impact Statement (EIS). An EIS, a term used in Irish law, is prepared by the developer and contains an analysis of the likely positive and negative effects a proposed development may have on the environment. Subsequently, the appropriate competent authority then conducts an "assessment" of the EIS, which is then taken into account before consent is granted. Ireland has a significant number of designated coastal conservation areas under EU and national legislation. For EU Special Areas of Conservation designated under the EU Habitats Directive and Special Protection Areas designated under the EU Birds Directive, collectively known as Natura 2000 sites, if a development is likely to affect such a site an Appropriate Assessment (AA) may be required. The AA is specific to the conservation objectives of the site in question. The competent authorities will accept an integrated EIA/AA submission because both relate to the site though the purposes of the assessments differ. Onshore Planning Permission/Exemption for any associated onshore works is required from the adjoining planning authority, or equivalent, depending on the project proponent. A grid connection offer from the relevant operator and a Power Purchase Agreement is also required and operates under a separate administrative process.

A new system for foreshore consenting is currently under development. The development commenced with a comprehensive public consultation on the new process in January 2013 and was followed by the publication of a draft Maritime Area and Foreshore (Amendment) Bill 2013 in October of that year (DECLG 2013). The new legislation seeks to better align the foreshore consenting system with the terrestrial planning system and will also introduce a planning system for marine developments in the exclusive economic zone (EEZ) and on the continental shelf. As a result of the entry into force of the MSP Directive in the EU (and consequently Ireland) as well as a general election in Ireland in 2016, which resulted in a reorganisation of government departments, progress of the Bill through the legislative process has stalled. One impact of the EU MSP Directive is that Member States are required to have maritime spatial plans in place by 31 March 2021. Because this will possibly present a new approach to planning marine activities, it will be intrinsically linked to any consenting processes in operation, and for that reason, it would seem sensible for Ireland and its competent authorities to advance both elements in parallel. At the time of this writing, however, Ireland has no formal MSP system in place. Draft regulations to transpose the provisions of the EU's MSP Directive into Irish law were published in April 2016, subject to a public consultation exercise until May 2016 and enacted into law as the EU (Framework for Maritime Spatial Planning) Regulations 2016 by the Government in June 2016.

A national Integrated Marine Plan, called Harnessing Our Ocean Wealth, is already in place, and it sets out the Government's vision, goals, and "enabling" actions needed to realise the maritime potential of Ireland (Government of Ireland 2012). An appropriate MSP framework for Ireland in the short to medium term was identified as being needed in the plan. A dedicated Enablers Task Force, appointed by the Government's Marine Coordination Group in December 2012, was asked to advise on the development of an MSP framework, and their findings were published in July 2015 (Enablers Task Force 2015). The Task Force recommended a national, strategic marine spatial plan for Ireland's marine waters, and more detailed plans to be developed at a later stage to cover the subnational level as required. The Task Force has specified that MSP will require the enactment of primary legislation, establishment of a lead responsible authority, and a plan-making framework. In the interim period, it is suggested that a multidisciplinary MSP body be created to begin the various processes and actual plan development. The Task Force estimated that a national plan could be adopted within 4 years (Enablers Task Force 2015).

In terms of data and information necessary to undertake MSP and forward planning of MRE projects, Ireland has a considerable amount of data collected by different regulatory bodies, private enterprises, and researchers. These data were collected for other purposes originally and include a marine atlas developed to comply with the EU's Marine Strategy Framework Directive requirements,[4] a seabed survey of the country's entire EEZ area and seabed mapping of the inshore areas,[5] and a range of marine and terrestrial data for various sectoral SEAs. As part of the OREDP, an ocean energy portal covering various aspects of ocean energy development was also created.[6] This information is all freely available and could be used to inform the future development of marine spatial plans. There is also strong scientific and technical research capacity in both MSP and MRE in many universities and third-level institutions. Though no specific zones have been allocated for MRE development, an SEA of the OREDP indicates the areas of highest environmental sensitivity and, whilst these areas do not preclude development of marine energy, there may be additional regulatory requirements for consenting a project in those areas. As part of the implementation of the OREDP, the DCENR has convened an Environmental Working Group that is overseeing the preparation of guidance for EISs and Natura Impact Statements (Appropriate Assessment) as they relate to marine renewables, guidance on environmental monitoring of MRE projects, and a report on environmental, social, and economic data sources and availability and associated data gap analysis. This guidance was published for public consultation in December 2016.

[4] http://atlas.marine.ie/.

[5] http://www.infomar.ie/data/.

[6] http://oceanenergyireland.ie/.

Japan

MRE is at the very early stages of development in Japan. Wind turbines have been incorporated into certain specific locations such as at ports, but there is no clear way in which MSP includes the needs of the MRE sector. Japan has had a Basic Act on Ocean Policy since 2007 that does not prescribe any formal approach to MSP, but it does provide a legal basis for the integrated management of coastal areas and river basins. Under the Basic Act, a policy for the promotion of development of ocean renewable energy was developed which recognises the huge potential of offshore renewable energy generation for the country. Specifically, in relation to offshore wind, the policy states that efforts should be made to reduce implementation costs, resolve technological problems related to durability, and establish methods for assessing environmental impacts (Headquarters for Ocean Policy 2013). Concerning wave and tidal power generation, the policy recognises that Japan is already lagging behind other countries with respect to these technologies and states that basic research for improving efficiency and economic potential should be promoted with due consideration of the special features of seas around Japan. In 2012, the Headquarters for Ocean Policy began working on an action plan for the promotion and utilisation of offshore renewable energy (Headquarters for Ocean Policy 2012). The purpose of the policy was to establish operational demonstration sites in Japanese waters and to coordinate the use of sea areas with local stakeholders. Two or more demonstration sites were to be selected by the end of 2012 in accordance with a specially developed site selection methodology, the requirements for their operation (cables, operation and maintenance requirements, etc.), financial viability, and necessary Government support schemes.

The involvement of stakeholders in planning activities at sea is given high priority under the action plan. The action plan proposes a coordination mechanism that would involve local governments in order to decide upon the most appropriate methods for building consensus with stakeholders, by examining social conditions associated with the use of sea areas from the perspectives of users such as those involved in maritime transportation, the fishing industry, and natural conservation areas. Given the economic significance of commercial fisheries to the economy of Japan, it is the sector most likely to potentially conflict with offshore renewable energy. As a result, MRE developers meet frequently with representatives of the fisheries sector. There is no structured mechanism for doing this as of yet, but the action plan suggested as an underlying principle that a win-win relationship was necessary. This would be accomplished, for example, by involving the fisheries sector representatives in the actual MRE project or giving them priority access to electricity in emergency situations, rather than solely depending on a resolution based on compensation, which is common in relation to public works (Headquarters for Ocean Policy 2012). In some locations, movies based on in situ observation data and numerical simulations have been used to explain the operating principles and effects of MRE devices on the environment to local residents, fishermen, and other marine users.

The action plan called for an examination of the legal issues that might surround the development of MRE projects, specifically in relation to long-term use of sea areas of the territorial waters and the EEZ (Headquarters for Ocean Policy 2012). It was anticipated that this type of legal analysis would help to ensure the safety of offshore structures and power generation equipment through compliance with existing safety standards such as those deriving from the International Electrotechnical Commission, the International Organisation for Standardisation (ISO), and the International Maritime Organisation (IMO). Part of the work on legal issues also focused on the administration of consenting so as to refine and streamline the procedures, perhaps through the application of a one-stop-shop approach. No further details about how these actions have progressed is currently available as the Ocean Policy is updated every 5 years with the next update due in 2017.

Whilst there are no absolute exclusion areas for MRE development in Japan, it is difficult to develop these types of projects in areas used for military training or in nature reserves. Generally, fisheries zones can be adjusted to accommodate different marine activities, but this is not usually achievable within marine protected areas. In terms of data and information that could be used for both site selection and marine planning more broadly, an open-access marine cadastre has been developed and can be accessed by the public and other stakeholders. The cadastre is a direct output from the Basic Act on Ocean Policy in 2007, which called for the development of a system that integrated and provided marine-related information that was dispersed across various regulatory agencies. By developing the cadastre, the information became organised in a more efficient, rational, and user-friendly manner, which could then contribute to the development of marine industry to promote marine-related activities and implement sustainable marine governance (Headquarters for Ocean Policy 2013).

New Zealand

The New Zealand Government has a target of 90% of electricity generation from renewable sources by 2025 (Ministry of Economic Development 2011). The current version of the energy strategy refers to the potential of marine energy for the country, but recognises marine energy is at an early stage of development in New Zealand and states that the Government will encourage it, as appropriate (Ministry of Economic Development 2011). New Zealand has a huge EEZ but no holistic approach to MSP. Marine planning is implemented in a regional manner under the provisions of the Resource Management Act (RMA) 1991 and the coastal plans developed thereunder. When enacted in 1991, the RMA replaced or amended more than 50 pieces of other legislation related to planning and resource management. The rationale for the new legislation was to help achieve a more coordinated, streamlined, and comprehensive approach to environmental management. Under the RMA, regional coastal plans are developed by regional councils and unitary authorities. These plans include objectives, policies, and rules for the activities that

are permitted, controlled, or prohibited within the plan area. The plans operate in a nested way in that they must be consistent with the national New Zealand Coastal Policy Statement (NZCPS) (New Zealand Department of Conservation 2010). The Policy Statement and plans made under the RMA have a seaward limit of 12 nautical miles and an inland scope that varies according to the local geography.

The most recent NZCPS dates from 2010. Like the energy strategy, the NZCPS also acknowledges the potential for the country to generate electricity from offshore wind, wave, and tides in the future, and this is reflected in a number of the policy objectives, specifically those related to activities in the coastal environment. The NZCPS also emphasises the need for coordinated management across council boundaries as well as land and sea. The RMA is complemented by the Exclusive Economic Zone and Continental Shelf (Environmental Effects) Act 2012, which seeks to promote the sustainable management of the natural resources of the EEZ and the continental shelf and manage the environmental effects of permitted and non-permitted activities. It does not equate to MSP, but rather focuses on the planning and management of individual uses. The potential of MSP to assist in planning and managing large marine spaces has been recognised in many parts of New Zealand, and recently, the focus has centred on developing a dedicated marine spatial plan for the Hauraki Gulf–Tikapa Moana region, which covers an area of 1.3 million hectares of ocean. In this area, a preliminary review of MSP initiatives and their possible application to that region highlighted the role of science and the possibility of formalising a Hauraki Gulf Science Advisory Group to oversee any necessary scientific work (Hauraki Gulf Forum 2011). The Hauraki Gulf is one of New Zealand's most intensively used marine areas and was designated as the country's first marine park in 2000. A marine spatial plan is being developed using a bottom-up approach involving central and local government and the *mana whenua* (the Māori who have tribal links to the area), and it is managed by a Stakeholder Working Group. The plan is non-statutory but is intended to provide clarity and certainty to people using the marine space.

The marine spatial plan for Hauraki Gulf could be expanded to incorporate sustainable energies, but it does not specifically include marine energy at this time. This could change as MRE technologies reach commercial maturity. In relation to the aquaculture sector, for example, resource consent applications for marine farms can only be made within aquaculture management areas identified in regional coastal plans. Consents for MRE deployments are evaluated and approved by regional councils in relation to offshore activities and those that straddle land and sea. District and city councils issue land use permits for onshore activities. Alternatively, if a project is deemed to be of national significance, the RMA 1991 prescribes a separate process for such decisions, which is administered by the New Zealand Environmental Protection Authority. To be a nationally significant proposal, it must be considered by the Minister to have national importance or effect in some way. For land-based proposals, this responsibility lies with the Minister for the Environment, and for coastal proposals, it lies with the Minister of Conservation. If a proposal straddles both areas, the Ministers must work collaboratively. When making a decision about whether a proposal is of national significance, a

Minister can consider the level of public concern about the proposal, the impacts the proposed development would have on the environment, the technology, and processes or methods that are new to New Zealand and that may affect its environment and whether the impacts are likely to be experienced in more than one district/region (Environmental Protection Authority 2013). These considerations are derived from Part 6AA of the RMA 1991.

In New Zealand, conflicts between different marine users have already been experienced. Consenting processes are based on specific sectoral activities rather than MSP-based activities, which could increase the possibility of conflict. The Environmental Protection Authority recently declined several high-profile applications where marine mining, environmental protection, and aquaculture activity came into conflict; e.g. Chatham Rock Phosphate Limited was refused a marine consent to mine phosphorite nodules in Chatham rise because it would have adverse environmental effects on benthic communities and potentially existing aquaculture operations in the area.[7] In September 2014, the New Zealand Government launched the Sustainable Seas national science challenge to enhance utilisation of the country's marine resources within biological and environmental constraints. The Sustainable Seas initiative will look at frameworks for assisting the Māori and stakeholders to navigate conflicting uses including trade-offs, mitigation measures, and negotiated accommodations (Ministry of Business, Innovation and Employment 2015). This situation arose from the specific rights of the Māori as a partner to the Treaty of Waitangi that, in some instances, have led to conflicts between the multiple economic, cultural, spiritual, and recreational uses of the marine environment and have the potential to impede development of the marine economy.

Further offshore in the EEZ, certain activities are restricted because of the presence of sensitive ecosystems and because there may be disturbances to local economic activities and Māori interests. The highest level of marine protection applies to marine reserves, and currently, there are 44 reserves in the territorial waters around New Zealand. Marine reserves can be established where there is typical, beautiful, or unique underwater scenery, natural features, or marine life of such distinctive quality that their preservation is in the national interest. Under the Marine Reserves Act 1971, a number of activities can be specifically managed, controlled, or excluded from marine reserves. These activities include marine farming, fishing, extraction, anchoring, point discharges, and research. Strict rules govern the removal or disturbance of marine habitats and life within the boundaries of a marine reserve. Permits are required for monitoring or research within a marine reserve if the activity could potentially cause damage under the Marine Reserves Act. There are also Cable Protection Zones (CPZs) protecting high-value electricity cables for the provision of hydroelectricity. The Submarine Cables and Pipelines Protection Act 1996, the associated Submarine Cables and Pipeline Protection Order 2009, and subsequent amendments legally protect the submarine cables laid

[7] http://www.epa.govt.nz/EEZ/chatham_rock_phosphate/Pages/default.aspx.

within the CPZ. None of these instruments currently impinge upon MRE because there are only a limited number of MRE deployments at sea.

The present marine development consenting system works effectively in a regional context, but there can be very different outcomes depending on where an activity takes place. Generally, the New Zealand planning process is highly participatory. The Environmental Protection Authority and the RMA have an open process and solicit public views. The implementation plan for the NZCPS has a dedicated "engagement" stream for district and regional councils to ensure they are well informed about the requirements and statutory obligations of the policy and are supported to implement its policies (Department of Conservation 2011). The engagement stream is supported by a range of specific actions designed to engage with different stakeholder groups, both regulatory and non-regulatory. A proposal for a marine energy test site off the Wellington coast involved the local council along with Grow Wellington, an economic development agency within the region, though this is still in the planning stage (IEA-OES 2015).

Nigeria

The Nigerian Government has been focusing on studying the feasibility of Ocean Thermal Energy Conversion (OTEC). The respondent to the OES Annex IV questionnaire stated that a preliminary analysis suggests that Nigeria could develop over 10 separate multi-product OTEC plants each generating 100-500 MW, along the coastal shores of the country on an incremental basis if funding permits. A consortium comprising FOT-K and the Nigerian Institute for Oceanography and Marine Research (NIOMR) received Government endorsement, and the first phase of feasibility studies is under way.[8] These studies are expected to identify the most suitable sites for OTEC plants in Nigerian waters. Further offshore, on the continental shelf, the economic viability of OTEC plants is also being explored. The federal Government of Nigeria is deliberating on the creation of a Centre for Ocean Renewable Energy Resources to be co-located within NIOMR in Lagos. The idea is that it would oversee all OTEC initiatives from research and feasibility/development studies to the conceptual design, engineering, and deployment of the integrated OTEC facilities, including connection to the national grid and facility management. In addition, Nigeria has a tidal resource but currently insufficient data to determine whether it would be sufficient for commercial-scale development. NIOMR collects oceanographic data in Nigerian waters, but the temporal scale of the data is not always consistent and the spatial scale is limited to the Lagos area and its environs.

No formal MSP system exists in Nigeria, and marine governance could be described as fragmented with multiple authorities having legal remits and responsibilities. The main authorities include the Nigerian Navy, the Nigerian Maritime

[8] http://www.niomr.gov.ng/OTEC%20page.php.

Administration and Safety Agency, the Nigerian National Petroleum Corporation, and NIOMR, all of whom also collect various types of marine data that could be used for MSP purposes in the future. Because feasibility studies are currently under way for OTEC, it and other types of marine energy do not have a sufficient presence as of yet to be taken seriously in planning policy and processes. The same could be said of MSP because no Government department or agency is designated as being responsible for MSP. Marine scientific data, usually tidal observations, have been collected since 2003, but there is currently no central portal or planning data set into which this information can be fed. This means no strategic approach is taken to data collection, which could limit the use of the data in any future marine planning system. When NIOMR is conducting research in the territorial sea, it must have permission from the NigerianNavy because they are the responsible entity. No allocated or restricted zones exist in Nigerian waters at this time, but it is unclear who would have authority to allocate marine space for offshore energy deployments if such an activity was proposed. The overlapping mandates of various Government departments and agencies have been a key contributory factor to existing conflicts between marine users. Marine developments tend to be planned and managed on a single-use basis with little or no involvement of the public. In cases where cumulative impacts have arisen, these were also managed independently, depending on who has the applicable data and information.

Norway

Ocean energy is generally included in renewable energy policies in Norway. In terms of consenting, a dedicated Offshore Energy Act was enacted in 2010 and it fits into a wider planning framework. The Planning and Building Act, for example, governs planning to one nautical mile from the baseline (low-water mark or straight baseline) and facilitates the preparation of local, inter-municipal, and regional plans for these areas though they tend to cover only land-based activities. From one nautical mile to the limit of the EEZ, there is no explicit legislation for MSP, but the Norwegian Marine Resources Act 2009 (*Havressursloven*) enables the development of Integrated Management Plans, which are accompanied by a series of Government declarations and related parliamentary reports. Originally, the legislation was drafted to protect against biodiversity loss; consequently, planning and management decisions are made with this central objective in mind. The Ministry of the Environment has lead authority for national goals, management systems, and performance monitoring and also plays a key role in coordinating the efforts of other entities that have marine remits (Norwegian Ministry of the Environment 2009).

Integrated Management Plan development began in 2001: the first one in 2006 covered the Barents Sea and was revised in 2011; followed by the Norwegian Sea plan in 2009; and the North Sea and Skagerrak plan in 2013. The plans are advisory and do not detail how to manage particular marine activities. Sectoral ministries and

other regulatory agencies retain the responsibility for management of their sectors, but management must be conducted in a way that is consistent with the overarching plan. The plans cover all existing economic sectors in the plan areas. With respect to renewable ocean energy, the various plans recognise the potential operation of this sector but as of yet renewable ocean energy does not have a commercial-scale presence. The Integrated Marine Plan for the Norwegian Sea states that MRE production will be facilitated but should take into account environmental considerations and other activities (Norwegian Ministry of the Environment 2009). The Barents Sea–Lofoten Integrated Management Plan acknowledges that theoretically there is substantial potential for MRE production (Norwegian Ministry of the Environment 2011), and it tasked a dedicated working group, composed of all the relevant regulatory authorities, with identifying the "best" areas for offshore wind energy in 2010. Subsequent to these impact assessments, the Water Resources and Energy Directorate advised that five of the areas should be given priority—the total area being up to 750 km^2, assuming a turbine size of 5 MW (Norwegian Ministry of the Environment 2013). Two prototype tidal plants currently operate within the Barents Sea–Lofoten management area (Norwegian Ministry of the Environment 2011).

The Offshore Energy Act provides a framework for regulating offshore renewable energy production, and as a general rule, it applies beyond the baselines and on the continental shelf. It can also apply inside the baselines. Under the provisions of the Act, an EIA must be conducted prior to an area being opened for licence applications. Section 2.3 of the Act provides that production areas may only be created after the regulatory authorities have opened specific geographical areas for licence applications. The rationale was that the authorities would adopt a spatial planning process whereby the most appropriate sites were selected in areas where the potential for conflict was as low as possible. Local and regional authorities can participate in this process but more as consultees than as participants. The Integrated Management Plans enable all activities that fall with the geographic scope of the plan to be managed within a single context, so the total environmental pressure from activities should not threaten the ecosystems. Cumulative impacts are explicitly dealt with in the plan documents by detailing the existing cumulative impacts, their assessment, and the effects expected over the longer term. This practice then provides a basis for an overall assessment of the need for measures and tools that are presented later in plan.

Due to the environmental premise of the Integrated Management Plans, substantial amounts of scientific data and information have been integrated into the plans and their supporting documents. These are accompanied by sector-specific scientific reports that describe the data and analyses used. The sector-specific reports may also be used to guide local planning and management decisions. This practice has been supplemented in more recent years through national programmes such as Mareano,[9] which maps bathymetry, topography, sediment composition,

[9]http://mareano.no/en/start.

biodiversity, habitats, and biotopes as well as pollution in the seabed in Norwegian offshore areas. The information derived from such programmes is used in policy- and decision-making for fisheries, hydrocarbons, etc. There is no single geographic information system (GIS) for each of the plan areas but an online state of the environment website hosts a range of thematic information and maps.[10] Due to the extensive maritime area of Norway, over 2 million km^2, significant resource challenges exist for mapping, analyses, plan implementation, and review. Trans-boundary issues, given Norway's proximity to EU countries, also necessitate joint action on certain topics. At a local level, coastal municipalities also need to develop greater capacity for planning and data gathering. All reports and other documents related to the Integrated Management Plans are available through the Internet, and stakeholders are encouraged to participate in the process. Public meetings are often hosted by industry representatives and non-governmental organisation (NGO) groups. In inshore waters, the Planning and Building Act prescribes the rules for public participation including public hearings, contributions, and meetings.

Sectoral interactions and conflicts are comprehensively included in each of the three plans. Because ocean energy currently has no large presence in Norwegian waters, the plans deal only with offshore wind in the North Sea plan area. The North Sea and Skagerrak plan states that there will be spatial overlaps between offshore wind farms and maritime transport activities, and certain petroleum exploration activities and fishing, which have the potential to lead to conflict if activities are not adequately planned and mitigated (Norwegian Ministry of the Environment 2013). The North Sea and Skagerrak plan proposes suitable mitigation measures such as amending shipping lanes and removing certain navigation aids where there could be conflicts with shipping; reducing the size of the area for offshore wind development where it could overlap with petroleum exploration activities; and early engagement with fisheries representatives so as to avoid important fishery grounds (Norwegian Ministry of the Environment 2013). In internal waters, close to shore, conflicts tend to occur between fishing and aquaculture activities (e.g. Narvik); platforms and vessels with conservation sites, landscape, and recreation (e.g. Masfjorden, Rossfjorden/Lyngdal); and decommissioning of oil platforms with spawning grounds (Vindafjord).

Portugal

Portugal has been developing a MSP system for a number of years and was the first country within the EU to transpose the requirements of the EU MSP Directive into national law in 2015. The Basic Law for Planning and Management of the National Maritime Space was enacted in April 2014 (Law No. 17/2014 of April 10) and

[10]See http://www.environment.no/Interactive-map/?lang=en&extent=-138770|6733674|809030|7275274&layers=77:100;106:70;&basemap=KART&opacity=70&saturation=100.

covers the Portuguese maritime area from the baselines to the outer limit of the continental shelf beyond 200 nautical miles. This law is a framework instrument and accordingly does not specify how it will be implemented or operate in practice. According to the legislation, the ecosystem approach and adaptive, integrated, and transboundary management are principles that should be observed. This resulted in two types of legally binding national instruments for MSP for private and public entities. Article 7 describes Situation Plans (*Planos de situação*) and Allocation Plans (*Planos de afetação*). The Situation Plan identifies the protection of historical and archaeological sites, preservation of the marine environment/biodiversity, and the spatial and temporal distribution of current and future uses and resources. The Allocation Plan identifies and allocates areas for new uses, not included in the Situation Plan, but once approved, the Allocation Plans are automatically integrated into the Situation Plan.

The framework law was given substantive legal effect under Decree-Law No. 38/2015 in March 2015. This Decree-Law is organised around four main sections: the legal framework for national MSP instruments; the legal framework for private use of national maritime space and associated financial regime; monitoring and technical assessment instruments; and the legal framework for private use of transitional water resources for aquaculture (Article 1). If a marine activity requires a certain spatial area or certain volume of marine space that is greater than that of a "common use",[11] then a title for its use is assigned in one of three ways. The assignments are dependent on the nature and duration of the proposed private use under Article 48:

1. Concession: where the use of the area is continuous (over the entire year) up to a maximum duration of 50 years (Articles 52–53);
2. Licence: for intermittent (or temporary/seasonal) use(s) of the marine area for periods of less than 1 year and up to a maximum of 25 years (Articles 54–56);
3. Authorisation: limited to scientific research projects and/or pilot projects involving new technologies or non-commercial uses with a maximum duration of 10 years (Article 57).

Any such title obliges the holder to comply with broader requirements including the achievement of Good Environmental Status under the Marine Strategy Framework Directive and Good Ecological Status for coastal and transitional waters. Where a proposed use is already included in the Situation Plan, the proposer of the project can request an appropriate title for that use. In contrast, if the use is not yet included in the Situation Plan, the granting of a title for use is dependent on the approval of an Allocation Plan (Article 50). The Situation Plan is still under development, but it will be based on a preliminary map of existing uses, which has already been compiled for the Portuguese coastal area. On this map, two types of areas have been assigned to wave energy: priority areas with a high wave energy resource and a reduced level of other uses; and secondary areas with a wave

[11]A common use could refer to leisure uses, for example.

resource that is still interesting for exploitation but in areas where conflicts with other marine uses may arise.

Chapter 4 of Decree-Law No. 38/2015 covers the fees payable for a private use of national maritime space. This "utilisation tax" (*Taxa de Utilização Privativa do Espaço Marítimo* [TUEM]) aims to compensate for private use of "common" marine space and to cover the administrative costs associated with planning and management and any possible environmental costs associated with impacts deriving from the activity operating. Private uses permitted under authorisations do not have to pay the tax because they are deemed to be non-commercial. Under Article 76(2), this tax exemption extends to uses that involve the development and use of geological and energy resources. The major share (75%) of the tax goes to the authority responsible for granting the title for private use (i.e. the Natural Resources, Security and Maritime Services Directorate-General, (*Direção-Geral de Recursos Naturais, Segurança e Serviços Marítimos* [DGRM]), but 25% goes towards the adjoining state or autonomous region.

In association with the private use title, a developer of a MRE project also has to apply for a power production licence, administered by the Energy and Geology Directorate-General (*Direcção Geral de Engenharia e Geologia* [DGEG]), the entity that coordinates all licensing processes (including the marine space licence), operating as a one-stop shop. The power production licence encompasses a production permit and an operation permit. If the project is to be grid-connected, the procedure starts with a request for a power supply reservation from the public electrical network from a given point and may also necessitate the submission of an EIA, if the project, or parts of it, is located in or near a national ecological reserve, a Natura 2000 site, and/or the national network of protected areas (Decree-law 215B/2012). Depending on the project's dimension and characteristics, the Commission for Coordination and Regional Development (CCDR, *Comissão de Coordenação e Desenvolvimento Regional*) or the Environmental Portuguese Agency (larger projects) oversees the EIA process. Outside of protected areas and if the project is not covered by national EIA legislation, the CCDR must return a finding of no significant impacts to the DGEG. The EIA procedure for offshore energy projects (except wind farms with 20 or more turbines for which a full EIA is required) follows a simplified procedure, led by the CCDR of the area in which the project is to be located. This is usually quicker and has a specified time frame. Onshore work associated with offshore renewable energy development requires approval from the local planning authority. A specially designed online system (Article 58 of Decree-Law No. 38/2015) is under development to facilitate coordination and communication during the licensing process (of all activities subject to approval in the marine space). The legislation also provides that where other consents are required for a particular activity, they can be viewed simultaneously on the electronic portal and administered centrally from there (Article 62).

South Africa

A national MSP system is in the early stages of development in South Africa. It is not yet operational and consequently any marine and coastal developments generally fall within the scope of the Integrated Coastal Management (ICM) Act 2008 and associated National Coastal Management Programme (NCMP). The current programme runs from 2013 to 2017 and seeks to resolve existing user conflicts and other management issues. The ICM Act defines the coastal zone as the area comprising coastal public property, the coastal protection zone, coastal access land and coastal protected areas, the seashore, coastal waters, and the EEZ and includes any aspect of the environment on, in, under, and above such areas. Arguably, it already provides a basis for marine and coastal spatial planning. The NCMP states that spatial planning in the coastal zone seaward of the high-water mark at this time remains largely sectoral and hence planning processes still principally take place independently from each other (DEA 2014). The overarching Act provides for the strengthening of partnerships between authorities that work in the marine area through the creation of Memoranda of Understanding particularly in relation to activities in the coastal zone that do not currently fall within the scope of the ICM Act. This could include, for example, mining, infrastructure development, fisheries and marine aquaculture, MRE, state assets, shipping, oil and gas, and biodiversity and protected areas.

Research surveys of the Agulhas Current on the east coast of South Africa and of wave energy have proved the technical feasibility of extracting significant large-scale renewable energy from the Agulhas Current and waves (Government Communications 2015). Whilst there are no active MRE deployments in South African waters at this time, any prospective deployments would be subject to a number of different legislative instruments administered by different competent authorities. All renewable energy developments are governed by the National Energy Act 2008. These developments may also be covered by more general legislation such as EIAs and SEAs. The Department of Environmental Affairs (DEA) is currently working on an SEA of wind and solar photovoltaic (PV) energy though it is for land-based developments. If a power generation plan is greater than 100 kW, a power generator licence needs to be obtained from the National Energy Regulator of South Africa when the plant is to be connected to the national grid. South Africa's National Utility provider (ESKOM) is responsible for granting Independent Power Producer access to the national grid. Both of these applications are granted at the discretion of each of the responsible entities. There are no timelines associated with the granting of the consents.

The development of a more integrated approach to ocean governance has been put forward by the South African Government through the Operation Phakisa initiative, which has as its key objectives the establishment of MSP and development of a national ocean and coastal information system. Originally, there was a target of delivering a national MSP framework by December 2015, to be accompanied by a regional framework and more detailed small-scale marine spatial plans that would

enable the transition to a sustainable ocean economy (Marine Protection Services and Governance 2014). A draft Marine Spatial Planning Framework was published by the DEA in August 2016, and though this does not include ocean energy as a current use, it does recognise the sector as an emerging use once an economic and reliable technology is available (DEA 2016). MSP would complement the ICM Act and associated management structures within the territorial sea (12 nautical miles). A dedicated, cross-sectoral Oceans Secretariat is to be established to launch processes and structures to clarify legislation, processes, and responsibilities related to ocean resources for multiple users, including the coordination of timelines for decision-making and facilitation of trade-off discussions between potentially competing industries. The Secretariat would be comprised of three units with functions related to research and data management, permitting and authorisation, and enforcement and compliance (Marine Protection Services and Governance 2014). The permitting and authorisation unit is intended to coordinate the various departments involved to ensure permits and authorisations are processed within predetermined timelines, facilitate cross-departmental discussions if conflict arises between consenting authorities, and to provide a platform for streamlining processes.

Though there are no planned or operational offshore energy projects and no predetermined zones or sites for such developments, a number of protected areas exist along the coastline where development will be prohibited. Section 56 of the Integrated Coastal Management Act of 2008 also provides for the demarcation of coastal planning schemes for specific purposes and activities, or prohibition of certain purposes and activities in the coastal zone or coastal management area, under certain conditions. With changes in marine management expected, it is difficult to say with certainty how future marine activities will be administered. An EIA will remain a requirement for marine developments, and though its completion is dependent on the project's electrical output, the spatial area covered, and the technology to be used, there is an obligation to consult with the public. Public consultation usually takes place via stakeholder meetings at which members of the public can raise their concerns. Generally, development in marine space has not been a priority in the past because the focus has been on conservation activities rather than development of economic activities. Vast areas of land are available for energy development, and the sea shelf around South Africa has a steep gradient that could place a technical constraint on the future development of offshore energy projects.

Spain

In 2010, as part of Spain's transposition of the EU's Marine Strategy Framework Directive, the Spanish Protection of the Marine Environment Act entered into force. This Act contains principles and processes for planning in the marine area and covers internal waters, the territorial sea, the EEZ, the fisheries protection zone in the Mediterranean, and as far as the continental shelf. No other MSP system is operational, though research projects have explored the potential use of MSP for

specific developments, such as the siting of wave energy devices on the Basque continental shelf (Galparsoro et al. 2012). This involved the development of a Suitability Index for wave energy converters that incorporates the technical, environmental, and socioeconomic constraints to deployment. The information generated was combined with the accessible energy potential and the technically exploitable wave energy potential to enable wave energy developers and regulators to identify the most suitable sites for subsequent surveys and studies. This approach was used to select the Basque Marine Energy Platform (*bimep*) site, where 17 data layers covering 10 technical, 4 environmental, and 3 socioeconomic factors were included in a dedicated GIS.

No dedicated consenting process for ocean energy projects exists in Spain, but several legal instruments apply to the development of a project. The Ministry of Industry acts as a coordinator for the various consents required and passes the applications on to other regulatory authorities for comment. Those authorities then return their comments to the Ministry of Industry which decides whether or not to grant consent. An authorisation for occupation of the maritime area is required from the Ministry of Agriculture, Food and Environment. EIA legislation (Royal Decree 1/2008) provides that a developer must submit an initial document outlining the project and its expected environmental impacts. The competent authority analyses the initial document in the light of submissions made by other marine entities and determines whether a full EIA is needed. If approved, the Environmental Authority will grant the Environmental Authorisation and attach project-specific conditions. A simplified process for marine energy projects was introduced in 2013 and is administered by the Ministry of Agriculture, Food and the Environment. The streamlined process was an attempt to address recognised delays in the consenting process with respect to the time taken to get approval. Under the new system, a defined time frame of no more than four months, or six months if there are exceptional circumstances, is necessary (Simas et al. 2015).

Along with meeting the above requirements, MRE development also requires a number of consents related to electrical generation. Royal Decrees 1955/2000 and 1028/2007 govern energy development and the procedure for authorising electricity-generating stations in the territorial sea, respectively. Royal Decree 1028/2007 was originally drafted for offshore wind but has since been expanded to cover ocean energy technologies. The construction, extension, modification, and exploitation of electrical installations require the following:

1. Request for Administrative Authorisation: a technical document related to the project's installation plan;
2. Project Execution Approval (AEP): relates to the commissioning of the project and enables the developer to start construction; and
3. Exploitation Authorisation: once constructed, this allows the development to be "switched on" and proceed to commercial production.

The Ministry of Industry is the competent authority for the Administrative Authorisation. Regional Governments may be involved if the project is located in

internal waters. If an offshore energy development is likely to affect maritime safety or navigation, the Directorate-General of the Merchant Navy, part of the Ministry of Development, will be contacted for input. Where a project requires onshore work, an additional consent from the Port Authorities is needed if such work incorporates the occupation of public ports.

The Ministry of Industry, Energy, and Tourism conducted an SEA of offshore wind in 2009 (Ministerio de Industria, Energía y Turismo 2009) to determine areas of the public maritime domain that had favourable conditions, including little or no expected environmental effects, for the installation of offshore wind farms. The SEA categorised areas according to their suitability including unsuitable or "exclusion zones" and areas that may be suitable, though subject to additional requirements or conditions. Over 60% of the area included in the SEA was considered unsuitable (Ministerio de Industria, Energía y Turismo 2009). This finding was attributed to the fact that there was potential for conflict with other priority marine uses or there was an increased likelihood of significant environmental impacts. There is no provision within any of the legal instruments or administrative processes for dealing with conflicts. Previously, conflicts have been dealt with on a case-by-case basis and have focused on the provision of monetary compensation to those most affected; for example, financial compensation was given to fishermen who lost access to their fishing grounds as a result of MRE development.

It is not yet clear whether additional legislation will be necessary to transpose the requirements of the EU MSP Directive or whether an amendment to existing legislation would suffice. The lack of coordination between administrative entities that have a marine remit at national and local levels remains problematic. During the development of the *bimep* test site, for example, administrative complexities created difficulties during consenting because both national and local administrations were involved as a result of a complex separation of powers between central government, provinces, and autonomous communities. The public can be consulted during all or some of the individual consenting processes, primarily through informal public events. There is also a legal requirement for consultation as part of the EIA process, usually when the EIS has been submitted to the competent authority and before a final assessment is made.

Sweden

The Swedish Agency for Marine and Water Management (SwAM) has been working on the development of maritime spatial plans for three areas: the Gulf of Bothnia, the Baltic Sea, and the Skagerrak and Kattegat. The plans cover both the territorial seas and the EEZ of each area. SwAM is the lead agency for plan development, but activities are planned in association with county administrative boards and coastal municipalities as well as environmental NGOs and the public. Plan development was preceded by the addition of dedicated MSP legislation to the Environmental Code in 2014 (Ordinance 2015:400). This Ordinance recognises the

Government's view that MSP is a necessary tool for the conservation of marine areas and for enabling cohesive marine management. The Ordinance contains provisions for the geographical boundaries of MSP, plan content, and the responsibility for preparation, consultation, and cooperation in the proposal process, and monitoring and review. The plans are non-statutory but operate as guidance documents that should be taken into account when making decisions related to the sea. The Government has authority to adopt binding regulations to fulfil the objectives of the plans, if that is deemed necessary. Under the Planning and Building Act, Swedish municipalities have planning responsibility for Swedish territory, which is taken to include internal waters and the territorial sea. Accordingly, there are 65 municipalities where the responsibilities of the municipality and the State overlap with respect to the territorial sea.

No single legal instrument governs ocean energy in Sweden; rather, the consenting process applied is broadly similar to that for wind energy. It falls within the scope of the Swedish Environmental Code—framework legislation that covers water-based activities such as hydropower and bridge development and not ocean energy per se. No special rules apply to ocean energy. A developer initially has a meeting with the adjoining regional authority, who normally administers the consenting process, and discusses the proposed project, the other authorities that need to be involved, and the EIA process. This information may also be captured in a document that can be used at a later stage for consultation purposes and as a basis for EIA-related work. The developer commences EIA baseline studies after this pre-consent consultation and conducts public meetings about the proposed development. This is all documented and submitted to the regional authority. An approved EIA is a prerequisite for making an application for consent to the Environmental Court. The Environmental Court makes the final decision about whether a permit will be granted. It is at this stage that supplementary information may be requested. If a permit is granted, it usually will have specific terms and conditions attached to it based on the findings of the EIA.

As part of the marine plan development process, the Swedish Energy Agency has declared specific areas for offshore wind where a significant physical wind resource is available. These areas are designated as being in the "national interest" and accordingly are protected under the Swedish Environmental Code in that such areas are protected from measures that may damage their value. In 2013, 27 such offshore wind areas were designated, encompassing an approximate total sea area of 4,000 km^2 (SwAM 2014). As of yet no areas of national interest have been allocated for wave energy development, though it is recognised that this could be important for commercial development in the future. Two test sites, one for wave energy demonstration in Lysekil and one for marine currents research in Söderfors, are currently operational. These sites are operated and managed by Uppsala University. No nationwide resource assessment and mapping exercise has been conducted to inform future site selection and investigation for wave energy development according to the current status report (SwAM 2014). The supporting documentation for MSP development explores the possible conflicts between the various marine sectors, including offshore wind primarily with nature conservation

and defence activities. The marine plans developed are anticipated to propose possible solutions for such conflicts. Certain nature reserves currently preclude the development and operation of ocean energy devices, but these activities usually are decided upon on a case-by-case basis by the regional authority.

United Kingdom

The United Kingdom (UK) comprises England, Wales, Scotland, and Northern Ireland. The latter three may be referred to as devolved administrations because each has its own government or executive branch and legislature. England is governed directly by the UK Government and Parliament on all issues. In Wales, Scotland, and Northern Ireland, certain responsibilities have been retained by the UK Government and are known as "reserved" matters. These vary by administration: in Scotland, "energy" is a reserved matter, and in Northern Ireland, the "foreshore, sea bed, and subsoil and their natural resources" are a reserved matter. In effect, this means that for certain policy areas, the UK Government in Westminster makes the policy and/or legislation, which is then applied in the devolved administrations by their authorities. The UK enacted the Marine and Coastal Access Act in 2009, and this forms the legal basis for marine planning. Under Section 44 of that Act, the UK Government published the Marine Policy Statement, which establishes the framework for preparing marine plans and conducting decision-making in the marine environment (HM Government 2011). In the devolved administrations, this Statement has either been applied in its entirety or supplemented with additional administration-specific legislation for the area.

The Crown Estate is a UK entity that manages lands held by the Crown as sovereign including the foreshore and seabed, usually out to 12 nautical miles and as landowner in the EEZ out to 200 nautical miles. The Crown Estate has legal authority to alienate property through granting a right in the seabed or foreshore to a third party for specific purposes such as mineral extraction, fish farming, or MRE generation. In relation to MRE, it is The Crown Estate that issues leases for renewable energy, depending on the site and technology. The Crown Estate has run six offshore wind leasing rounds since 2000. This leasing activity specified the type and scale of the project, commencing with projects of 30 turbines during Round 1 (2000), larger projects further offshore in Round 2 in 2003, and most recently Round 3 in 2009 during which sites were selected after the completion of an SEA. During this process, project proponents bid for exclusive rights to develop offshore wind farms within the round areas or "zones". The procedures that apply following a successful bid are complex and detailed elsewhere (The Crown Estate 2014; O'Hagan 2015). Currently, there are no absolute prohibitions on siting of ocean energy projects in the UK, but additional requirements may apply if a project is to be located within a designated conservation site or a site of special scientific interest. This can also be the case if a project is to be sited near military grounds. The Crown Estate operates in waters all around the UK, but a consultation on

proposals to establish an interim body to manage The Crown Estate assets in Scotland post-devolution is currently under way (The Scottish Government 2016a). The situation in Northern Ireland is also uncertain given complex jurisdictional issues with the Republic of Ireland.

The UK Government retains responsibility for decommissioning offshore renewable devices under Sections 105–114 of the Energy Act 2004. The Department of Energy and Climate Change (DECC) administers this process and has published guidance notes for developers that apply to territorial waters in or adjacent to England, Scotland, and Wales (between the mean low-water mark and the 12 nautical mile territorial sea limits) and to waters in the UK Renewable Energy Zone (including the part adjacent to Northern Ireland territorial waters). The scheme does not apply to the territorial or internal coastal waters of Northern Ireland because of uncertainties surrounding the ownership of the seabed. Neither does it apply to inter-tidal areas (between the high-water mark and the low-water mark) of any of the other administrations. The guidance applies to all forms of offshore renewable energy devices regardless of the scale of the deployment or whether it is a commercial or demonstration project (DECC 2011). Usually during the pre-application consultation phase, developers will be made aware of the need to discuss their decommissioning plan with the DECC. When a developer has obtained one or more of the required consents (e.g. a marine licence), the Secretary of State will issue a notice requiring the developer to submit a decommissioning programme. This will be drafted by the developer and contain information about what parts and how the project will be decommissioned, an EIA/Habitats Regulations Assessment if necessary and measures to mitigate impacts on the marine environment, stakeholder consultation, anticipated costs and financial security, seabed clearance, and any necessary post-decommissioning monitoring. To align with international law, particularly the Law of the Sea Convention, IMO standards, and the OSPAR Convention, there is a presumption in favour of complete removal of the installation. Exceptions may also be considered under extenuating circumstances, such as unacceptable risk to human safety or the marine environment (DECC 2011). Each administration of the UK is dealt with separately below.

The Marine Policy Statement covers a host of aspects relevant to the implementation of marine planning in the UK. Specifically, Section 2.3.1.6 states that "Marine Plans should provide for continued, as well as new, uses and developments in appropriate locations. They should identify how the potential impacts of activities will be managed, including cumulative effects. Close working across plan boundaries will enable the marine plan authority to take account of the cumulative effects of activities at plan boundaries. The consideration of cumulative effects alongside other evidence may enable limits or targets for the area to be determined in the marine plan, if it is appropriate to do so" (HM Government 2011). In practice, cumulative impacts are more difficult to quantify because there can be a lack of appropriate data; however, the process of developing marine plans on a regional basis has enabled the collection of additional data as well as comprehensive stakeholder input, which in turn identifies areas that are either sensitive to cumulative impacts or areas that are currently very busy. At the industry level, the largest

renewable energy trade association in the UK, RenewableUK, has issued guidelines on cumulative impact assessment for offshore wind farms. The development of guidelines was driven by delays—up to 42 months—experienced in the consenting process for offshore wind farms (RenewableUK 2013).

A strong focus has been placed on engaging with stakeholders during marine plan development. This is intended to give those tasked with writing the plan a greater depth of knowledge about the region in question, but it also seeks to decrease the likelihood of conflicts between different marine sectors in UK waters, which have been known to occur previously. The process of marine planning aims to work through conflict and maintain stakeholder engagement throughout the process. Provision of information is also a key part of the process, and most of the devolved administrations have their own approaches to addressing this (see below). The Marine Policy Statement and the approach taken by those writing the marine plans are guided by the high-level marine objectives (HM Government 2009) that mirror the full range of the UK Government and devolved administrations' marine policies rather than the priorities of any one government department. The marine plans are there to aid decision-makers during the licence application process, at an operational level. It should be noted that according to the Marine Policy Statement, in England and Wales, consents for Nationally Significant Infrastructure Projects (NSIPs), including the larger offshore renewable energy and port developments, must be determined in accordance with the UK Planning Act 2008.

England

The Marine and Coastal Access Act 2009 (MCAA) provides a legal framework for marine planning and the creation of the Marine Management Organisation (MMO), which is responsible for marine planning in English inshore and offshore areas. The boundaries of English marine plan areas were identified after receiving stakeholder and expert input and resulted in 11 plan areas and 10 marine plans (in the north-west, one marine plan covers both the inshore and the offshore regions). In each marine plan region, the priorities and directions for future development within the plan area are outlined and this information is used to inform marine users about the more suitable locations for their activities and where new developments may be sited. The Marine Policy Statement states that marine plans should take account of and identify potential areas for the deployment of different renewable energy technologies (HM Government 2011). At this time, offshore wind is more commercially mature than wave or tidal technologies, and accordingly, it features most prominently in the published marine plans for English waters. In the East Inshore and East Offshore Marine Plans, for example, offshore wind is considered to be one of two transformational sectors over the 20-year vision of the plan, and therefore, there are two dedicated wind policies within the plan area (DEFRA 2014).

The MMO's marine planning team has engaged the public through workshops and public consultation throughout the planning process. For each plan area, a

Statement of Public Participation describing how and when the MMO would provide people with opportunities to get involved in the preparation of marine plans for areas in which they live, work, or have an interest, and how this information is then used, has to be produced in a dedicated report. Information about current marine uses and activities is presented in a Marine Information System[12] (MIS), developed by the MMO, as an interactive Web-based GIS tool to aid implementation and use of adopted marine plans. The evidence base for marine planning is also available via a Marine Planning Portal[13] that is used throughout the plan development process. Both of these tools have been created to increase awareness and support for the marine plans and their development. The Crown Estate also has a decision-support system called Marine Resource System (MaRS),[14] which is GIS-based and can be used to identify areas suitable for offshore energy development based on a number of spatial data sets that have been incorporated into the system. The latter is currently offline to facilitate a planned redevelopment of the system, which can then be used for Round 3 developers and future customers.

MRE projects are primarily consented under the provisions of the Planning Act 2008 and Marine and Coastal Access Act 2009. This varies according to the overall capacity to be generated by the MRE installations. Projects over 100 MW capacity are considered NSIPs and require consent under the Planning Act 2008. NSIPs must be approved by the Planning Inspectorate in a six-stage process. First, there is a pre-application consultation during which the Planning Inspectorate screens and scopes the project and the applicant consults with other relevant statutory consultees, local authorities, communities, or any affected person. After this consultation, the Planning Inspectorate will accept or refuse the project in principle. If the Planning Inspectorate accepts the project, they have 28 days to decide whether the application meets the application standards and consultation requirements before progressing to examination. Prior to examination, public notices must be published by the developer to enable all interested parties to register for involvement in the examination process. During the examination phase, an inspector or panel of inspectors is appointed as an examining authority who then examines the application, in accordance with the Marine Policy Statement, for a period of up to six months. During this period, the examining authority will prepare recommendations for the Secretary of State. The Secretary of State then has three months to issue a decision on the proposal. Post-decision, there is a six-week period during which the decision can be legally challenged in the High Court. Under Sections 98 and 107 of the Planning Act, the total process from the examination to determination phases should not exceed nine months.

The Planning Act 2008 attempted to streamline the consenting process because the development consent granted under it now replaces the previous consents required under Section 36 of the Electricity Act 1989, planning permissions, and

[12] http://mis.marinemanagement.org.uk/.

[13] https://planningportal.marinemanagement.org.uk/.

[14] http://www.thecrownestate.co.uk/mars-portal-notice/.

related environmental approvals (Planning Act, Section 33). Consents or permissions related to navigation risks, safety zones, and the statutory decommissioning scheme are required from the DECC. Projects under 100 MW capacity are subject to the provisions of the Marine and Coastal Access Act 2009 and are administered by the MMO in English waters. The MCAA consolidated six consents into one marine licence. The pre-application stage of the process can be completed online, and applicants can request screening and scoping opinions as well as reviews of their Environmental Statement (ES, the term used in UK law). The MMO will decide whether an EIA is required based on the individual case, consultation with the applicant, and criteria specified in Annex 2 of the Marine Works (EIA) Regulations 2007 or Schedule II of the Electricity Act (EIA) (England and Wales) Regulations 2000. When a full EIA is requested, the applicant must submit an ES incorporating the information set forth in Schedule 3 of the Marine Works (EIA) Regulations 2007. At this stage, the applicant will also submit a Section 36 Electricity Act application form, a Marine Licence application form, the ES, and/or an assessment under the Habitats Regulations (to comply with EU Habitats Directive provisions) online. Unlike other countries, the MMO manages consultation with other public authorities, agencies, and interested parties before providing a final decision. One possible weakness of the MCAA process is that there is no defined time frame for making a final decision though DEFRA guidance contains estimated timescales for dealing with each aspect of a marine licence application (DEFRA 2011).

Wales

The Welsh Government is currently developing the Welsh National Marine Plan (WNMP), which will cover Welsh inshore and offshore waters in a single plan. Public consultation on a proposed approach to marine planning in Wales was conducted during the first quarter of 2011 (Welsh Assembly Government 2011). Two central aims of the WNMP are to promote suitable marine opportunities and to sustainably manage existing and future marine activities. The WNMP will also provide a policy framework for informing marine licensing decisions. A range of supporting work has been conducted in support of plan development. A Strategic Scoping Exercise was carried out to review and analyse the available evidence for Welsh waters (Welsh Government 2015), and a number of research projects to fill specific evidence gaps, such as those related to aquaculture, seascapes, and recreational fishing, have also been commissioned (Welsh Government 2015). A dedicated portal for marine data and information has also been developed as part of this process.[15]

Projects over 100 MW in the Welsh territorial sea and the EEZ are processed according to the NSIP scheme, outlined in the England section (above).

[15]See http://lle.gov.wales/apps/marineportal/#lat=52.5145&lon=-3.9111&z=8.

Responsibilities for consenting MRE projects under 100 MW in Welsh inshore waters (up to 12 nautical miles) are devolved to the Welsh Ministers. The operation of marine licensing was delegated to Natural Resources Wales in April 2013. Because Natural Resources Wales follows the scheme prescribed in the Marine and Coastal Access Act 2009, it operates in a way similar to that outlined for England but with a different competent authority. The Marine Licensing Team in Natural Resources Wales acts as a one-stop shop for marine licensing and is also responsible for EIA and Habitats Regulations Assessment aspects. Like in England, developers of small-scale projects must already have a seabed lease from The Crown Estate. Consents related to navigational safety and decommissioning remain the responsibility of the DECC. Developments that necessitate onshore work may require terrestrial planning permission under the Town & Country Planning legislation, administered by adjoining local authorities.

Scotland

The Marine (Scotland) Act was enacted in 2010 and is similar to the MCAA in that it provides for marine planning and licensing, marine conservation, seal conservation, and enforcement. A new marine management authority for Scottish waters, Marine Scotland, was also created under the Act. Its Marine Licensing Operations Team (MS-LOT) is responsible for all marine licensing functions. A National Marine Plan (NMP) for Scotland was adopted on 25 March 2015 and laid before Parliament on 27 March 2015 (The Scottish Government 2015a). It is a wide-ranging document that covers all current Scottish marine sectors and includes overarching environmental objectives such as those contained in the EU's Marine Strategy Framework Directive. The NMP is accompanied by an interactive Website where Marine Scotland hosts all of its data.[16] The high-level marine objectives of the plan are to achieve a sustainable marine economy; to ensure a strong, healthy and just society; to live within environmental limits; to promote good governance; and to use sound science responsibly (The Scottish Government 2015b). The plan also outlines key objectives for the offshore wind and ocean energy sectors in Scotland, spanning planning and licensing aspects as well as maximising benefits from development of the sector at regional level (Scottish Government 2015b). The NMP will be supported by regional marine plans covering 11 marine regions as far as the territorial sea limit (12 nautical miles). The regional marine plans will be developed by local Marine Planning Partnerships that include representatives from local authorities, inshore fisheries groups, and local coastal partnerships. The Marine Planning Partnerships have delegated powers from Scottish Ministers, and the plans developed will reflect local issues and needs in each region. The partnerships do not have consenting or licensing powers. The first two regional plans

[16]See http://www.gov.scot/Topics/marine/seamanagement/nmpihome.

will cover the Shetland Isles and Clyde area.[17] To complement the NMP and regional plans, sectoral marine plans for offshore wind, wave, and tidal energy sources have also been published and built upon to create separate Regional Locational Guidance documents for offshore wind, wave, and tidal energy (The Scottish Government 2012a, b, and c, respectively).

Any gaps identified during the processes listed above have informed the prioritisation of research and consequently wider national marine planning. To date, work has focused on the uncertainties related to interactions between wave and tidal energy and the marine environment, including potential impacts of MRE on seabirds, marine mammals and habitats, as well as generic research into the potential effects of devices on the marine environment. A dedicated Marine Mammal Scientific Support Research Programme focuses on marine mammal interactions with MRE devices, unexplained seal deaths, and the decline in common seal numbers—the results of which will inform Scottish marine policy and wider marine mammal management and conservation (The Scottish Government 2012d). Marine Scotland has been innovative in licensing offshore energy projects by implementing a risk-based approach through its "Survey, Deploy and Monitor" policy (The Scottish Government 2016b). This approach informs site characterisation survey requirements in the pre-consenting period by enabling EIA requirements to be adjusted at the scoping stage, thereby potentially reducing the burden of collecting survey data to inform EIAs on small-scale projects or projects of low environmental risk. The duration of site characterisation surveys and the level of monitoring are determined by the overall risk profile of the project, based on the environmental sensitivities of the area, the scale of development, and the specificities of the device. These factors are scored and combined to provide an overall risk profile expressed as low, medium, or high. Two years of site characterisation data are required for projects that score "high", whereas for a project with a "medium" score, 2 years of data may also be requested, but monitoring requirements may be relaxed by Marine Scotland on the basis of the monitoring results. Small-scale projects located in areas of low environmental sensitivities may require only 1 year of site characterisation data.

Under the provisions of the Marine (Scotland) Act, offshore licensing is devolved to the Scottish Ministers in Scottish inshore waters (up to 12 nautical miles) and offshore waters (12–200 nautical miles). MS-LOT acts as a one-stop shop for all aspects of marine licensing. With respect to MRE, prospective developers must firstly apply for a marine licence to occupy part of the Scottish marine area (territorial sea). Consent under Section 36 of the Electricity Act 1989 is required for the construction and operation of offshore generating stations that have an overall capacity higher than 1 MW but lower than 50 MW in Scottish waters. Like in England and Wales, the need for an EIA is decided on a case-by-case basis. Additional requirements such as a Habitats Regulations Assessment (Appropriate Assessment under the Habitats Directive) are also administered by Marine Scotland where projects are likely to affect certain species or habitats included in the Habitats

[17]See http://www.gov.scot/Topics/marine/seamanagement/regional.

Directive. The nine-stage procedure to be followed is broadly similar to that of England and Wales:

- pre-screening consultation with MS-LOT;
- environmental screening and scoping;
- consultation on screening and scoping, managed by MS-LOT;
- preparation of documents and pre-application;
- MS-LOT gate checking of documentation;
- submission of applications;
- consultation stage;
- determination [of consent]; and
- monitoring and post-consent actions.

MS-LOT manages consultation with statutory and non-statutory consultees to determine whether an EIA and/or AA is required.

If an EIA or AA is required, the developer may request a formal scoping opinion by submitting a scoping report to Marine Scotland along with a cover letter. MS-LOT will then issue a copy of the scoping report to each of the statutory and non-statutory consultees with a cover letter and advise them of a three-week consultation period. Subsequent to this period, MS-LOT will issue a formal scoping opinion. Under the EIA Regulations, a scoping opinion must be provided in nine weeks. After the screening and scoping stage, the pre-application phase begins with the applicant preparing all of the relevant documents, public notices, and application forms. The ES, a non-technical summary of the Marine Licence application form, the Section 36 licence application form, and other required documents must go through a three-week gate-checking process whereby MS-LOT confirms whether all of the documentation fulfils the requirements of the legislation. If no issues arise, the developer can then submit a formal application, pay the application fee, and publish the public notices. MS-LOT will proceed to administer the application and consultation procedures. According to the Licensing Manual, applications for marine licences only should be dealt with in 8–12 weeks, upon receipt of payment, and provided there are no objections or complex issues (The Scottish Government 2012e). Marine Scotland aims to make a decision on Section 36 applications within nine months of receipt of the application. The timescales for decision-making may vary if developers are requested to provide additional information during the consultation stage, because this will require further consultation and public notices. If an application is refused, MS-LOT will explain the reasons for refusal to the developer and provide advice about a way forward and a new submission, if applicable. Consents granted by MS-LOT may be accompanied by various terms and conditions that are enforceable by MS-LOT, which has statutory power to ensure compliance (The Scottish Government 2012e). One obligation is for developers to submit regular monitoring results, which may result in a change to subsequent monitoring programmes.

Northern Ireland

The Marine (Northern Ireland) Act entered into force in 2013 and has a structure similar to those outlined above. The Act covers the Northern Ireland inshore region, marine conservation zones, and reform of marine licensing for certain electricity work. The Northern Ireland inshore region is defined as the territorial sea and the seabed adjacent to Northern Ireland out to 12 nautical miles, though jurisdictional issues in the border bays with the Republic of Ireland persist. In those areas, a separate North South Implementation Body, the Foyle Carlingford and Irish Lights Commission, has responsibility for promoting and developing both Loughs for commercial and recreational purposes related to marine, fishery, and aquaculture matters. The Northern Ireland Department of Agriculture, Environment, and Rural Affairs (DAERA, formerly the Department of Environment) is the competent authority for MSP and is continuing to work on the Northern Ireland Marine Plan. The plan will cover the Northern Ireland inshore region, out to 12 nautical miles, and the offshore region, beyond 12 nautical miles, in a single document. The Marine Plan Team published a Statement of Public Participation in June 2012, which was subsequently reviewed and updated in May 2013 (DOENI 2013). The draft marine plan is currently undergoing a Sustainability Appraisal, and once this has been completed, both will be issued for public consultation, subject to Northern Ireland Executive and Secretary of State for the Environment approvals, because the draft marine plan includes reserved matters (DAERA 2015).

The Marine and Fisheries Division of DAERA carries out licensing and enforcement functions in Northern Ireland territorial waters, under Part 4 of the Marine and Coastal Access Act 2009. The process follows a similar format to that of Scotland, England, and Wales and consists of the following stages:

- pre-screening consultation with the Marine and Fisheries Division;
- formal EIA screening and scoping (if applicable);
- Habitats Regulations Assessment screening and submission (if applicable);
- preparation of documentation, e.g. ES;
- formal application;
- consultation, feedback, and mediation;
- licence determination and issuing of licence(s) (if needed);
- management of returns, e.g. monitoring reports; and
- decommissioning (if required).

Applicants may request a screening opinion under the Marine Works (EIA) Regulations 2007 (as amended) to determine whether an EIA is required. At this stage, the Marine and Fisheries Division will consult with whomever it deems appropriate before issuing a screening opinion. Consultees are allowed one month (28 days) to respond. Once that decision is made, it will be communicated to the applicant and other relevant consultees and it will appear on the Marine and Fisheries Division's public register. The same procedure and timelines apply to scoping. After screening and scoping, an applicant can make a formal application

for a marine licence. No statutorily defined time frames exist for processing an application, but there is a policy target of processing the application within four months of having received all of the necessary information (DAERA 2016). The consultation phase of the consenting process is managed by the Marine and Fisheries Division. This includes ensuring that the applicant addresses the concerns raised by the stakeholders.

The electrical elements of an MRE project are consented under Section 39 of the Electricity (Northern Ireland) Order. Section 39 consents are granted by the Department for the Economy (formerly the Department of Enterprise, Trade and Investment [DETI]) for offshore generating stations whose capacity exceeds 1 MW. Under the Marine Act (Northern Ireland) 2013, Marine Licences and Section 39 consents can be dealt with simultaneously. If an MRE development requires the construction of onshore works, these may require planning permission. Responsibility for terrestrial works is shared by the Department for Infrastructure and 11 local authorities (Councils). If a development is deemed to be regionally significant, an application can be made directly to the Department for Infrastructure which is responsible for regional development, regionally significant projects, and planning legislation. In some instances, all three consents (marine licence, Section 39 Electricity Order consent, and planning permission) will require the submission of an ES. Prior to Government reorganisation in May 2016, a memorandum of understanding between the DOENI (now DAERA) and DETI (now Department for the Economy) had created a framework for streamlining planning, licensing, and consent application processes, which allowed for the submission of a single ES for all three consents. Prior to any form of new MRE project, the developer must already have a seabed lease from The Crown Estate. Two 100 MW tidal energy projects are currently in an advanced planning stage, having already secured development rights from The Crown Estate in 2012.

United States of America

In the USA, the term marine and hydrokinetic (MHK) energy is used more commonly than MRE. Consenting of projects in the USA is largely determined by location, according to the separation of powers between state and federal authorities and jurisdictions. This has created difficulties for the implementation of a national MSP system. Given the diverse range of political barriers and the multi-jurisdictional and sector-specific nature of jurisdictions over marine space, a comprehensive, country-wide, and prescriptive approach to MSP is probably unrealistic. To date, efforts have focused primarily on coordinating activities between states and federal agencies and promoting greater consistency in their respective endeavours. An Executive Order from the Office of the President led to the release of the National Ocean Policy (NOP) Implementation Plan in 2013 (National Ocean Council 2013). This plan describes particular actions that federal agencies will take to address key ocean challenges. The NOP divided the USA into nine regions and encouraged the

creation of a Regional Planning Body (RPB), composed of the federal, state, local, and Native American Tribal representatives from that area. These bodies are supported in each region by staff from the National Oceanic and Atmospheric Administration (NOAA) in an effort to place science at the centre of marine planning processes and resultant decision-making. Each RPB is in a different stage in implementing marine planning.[18] It should be noted that the RPB has no regulatory authority; federal and state agencies retain these responsibilities.

The Bureau of Ocean Energy Management (BOEM), under the aegis of the US Department of the Interior, is the federal agency responsible for regulating MRE development on the Outer Continental Shelf (OCS, 3–200 nautical miles offshore) and issuing leases for energy development. BOEM has been instrumental in the creation of State-level Renewable Energy Task Forces. The Task Forces can coordinate local, State, and federal efforts to explore and enable MRE development. So far, Task Forces are operational all along the East Coast and in Oregon, California, and Hawaii.[19] In some areas, their work has resulted in the identification of potential Wind Energy Areas, which can later form a BOEM lease area. Independently of this process, many states are also using MSP to guide marine activities and conservation. Washington, Oregon, California, Rhode Island, and Massachusetts had developed state-level marine plans, prior to the publication of the NOP. Washington State completed its first round of MSP in 2013. This effort incorporated data and capacity analysis, education and outreach, creation of data management and display tools, and stakeholder meetings. Though the Washington State Legislature endorsed continued funding for marine and coastal planning activities ($3.7 million USD for the current biennium starting July 1, 2013), state actions have currently stalled as state agencies and the Governor determine a path forward (Van Cleve and Geerlofs 2013).

Though some states (e.g. Massachusetts) are moving towards the designation of specific zones for MRE development, such activity will have to coexist with already established marine uses and the legal protections they might have. National Marine Sanctuaries, for example, are created by statute under the Ocean Sanctuaries Act, as amended, and prohibit activities that would alter the seabed or subsoil or potentially affect environmental conditions within the sanctuary. Shipping lanes and marine protected areas also tend to be excluded from project development activities. Areas identified and used by the Department of Defense may make development at those sites more difficult or at least require an additional level of consultation before any lease could be issued. In Massachusetts, siting and development standards for special, sensitive, or unique (SSU) marine and estuarine life and habitat and for commercial fishing, recreational fishing, and areas of concentrated recreational activity "direct development away from high-value resources and concentrations of existing water-dependent uses" (Commonwealth of Massachusetts 2015).

[18]Links to all regional bodies and their plans can be found on http://cmsp.noaa.gov/activities/index.html.

[19]See http://www.boem.gov/Renewable-Energy-State-Activities/.

Within SSU areas, the Massachusetts plan adopts a precautionary set of standards. Johnson (2014) states that the permitting agency "shall presume that the location of a project outside an SSU area represents a less environmentally damaging practicable alternative than a location within an SSU area". Conflicts experienced to date have tended to materialise when incumbent ocean users or agencies perceive risks to their interests as a result of proposed new uses or protection of ocean resources. The primary solution to address such conflicts has been negotiation between the (potentially) affected stakeholders and the responsible state or federal authorities, depending on the activity concerned.

The Federal Energy Regulatory Commission (FERC) exercises regulatory jurisdiction over MRE projects on navigable waters within 3 nautical miles of the shore and on any projects with an onshore grid connection under an amendment to the Federal Power Act. FERC powers do not extend to OTEC projects, which are under the remit of NOAA following the provisions of the OTEC Act 1980. Due to the fact that the USA has not signed the United Nations Law of the Sea Convention, its definition and interpretation of the term "continental shelf" is different than elsewhere and is understood to include all submerged lands, subsoil, and seabed between the seaward extent of the states' jurisdiction, usually 3 nautical miles, to the limit of federal jurisdiction of 200 nautical miles. In effect, this means that BOEM is responsible for granting the lease if a project located on the OCS produces, transmits, or transports energy and incorporates the temporary or permanent attachment of a structure or device to the seabed. The construction and operation of an MRE device on the OCS will also require a licence from FERC. In an effort to clarify the complex jurisdictional issues that surround authority and responsibilities in marine areas, FERC and BOEM published wide-ranging Guidelines on Regulation of Marine and Hydrokinetic Energy Projects on the OCS in 2012 (BOEM/FERC 2012).

Under the Guidelines, three types of leases can be granted by BOEM for MHK projects (BOEM/FERC 2012):

1. A commercial lease is required for a commercial project.
2. A research lease is issued to federal agencies or states only for renewable energy research activities that support the future production, transportation, or transmission of renewable energy.
3. A limited lease applies to projects of limited scope, normally where the activities associated with project are limited to 5 years and the power generated by the project is also restricted (e.g. 5 MW), both of which are specified in the terms and conditions attached to the lease.

BOEM often assists states in the development of their MRE resource, through specific development proposals and the Task Forces established for that purpose. All lease applications submitted to BOEM are considered on a case-by-case basis but in collaboration with other regulatory and state agencies. A project can be developed with a BOEM lease and without a FERC licence if the technology is experimental, the deployment is temporary, or where it is for educational purposes

and the power generated is not transmitted to the grid. In circumstances outside of these, FERC has the power to grant licence waivers or exemptions. To come under an exemption, a project must be small, short-term, located outside a sensitive area (in FERC's own opinion), removable and capable of shut down at short notice, removed before the end of the licence period, and initiated by a draft application with relevant supporting environmental information capable of analysis by FERC (BOEM/FERC 2012).

Leasing occurs via competitive rounds initiated by BOEM and developers can then respond. Alternatively, a developer can submit an unsolicited application to BOEM stating their interest in obtaining a lease for a specific OCS location, outlining the area concerned, the project proposed, and available resource and environmental data. Applicants must demonstrate that they are qualified to hold a lease in compliance with the Code of Federal Regulations. If there are no competing applications, the developer will then be requested to provide a Site Assessment Plan detailing environmental surveys and resource assessment studies to support the planned project (BOEM/FERC 2012). This does not apply if the proposed project does not involve the installation of bottom-founded facilities. Once a developer has concluded the required documentation and made payment, BOEM will issue a lease to the successful developer. A finalised Site Assessment Plan must be submitted within six months of receiving the lease. The lease does not extend to generation of power, which can only occur once a FERC licence has been obtained. The guidelines specify that the applications for a BOEM lease and FERC licence can be made together, but this is dependent on the type of licence concerned and whether the project is in response to a competitive leasing round or is an unsolicited application.

FERC licensing may follow one of three different forms: an Integrated Licensing Process (ILP), a Traditional Licensing Process, or an Alternative Licensing Process (ALP) (BOEM/FERC 2012). The ILP is the most common process and involves a pre-application stage, during which any necessary studies are conducted and a licence application is prepared, and a post-application stage, when the application is reviewed, an environmental document is compiled, and a decision about licensing is made. FERC coordinates the input of stakeholders during various stages of the process. The process may take up to 2.5 years when in response to a competitive leasing round. Unsolicited applications usually take less time, but this depends on the complexity of the proposed project. FERC licence applications take approximately 1 year, but again this can vary according to the licence type and area concerned. Pilot project licences from FERC take 6 months from the date of submission of the application. The lifespan of the BOEM lease also varies by type: commercial leases are generally issued for 25 years and limited leases for 5 years. Research leases are decided on a case-by-case basis through negotiation with BOEM personnel, federal, or state agencies. FERC licences can be issued for up to 50 years, which can be extended for a further 30–50 years. Pilot licences from FERC tend to be granted for a 5-year period given the early stage of the technology and the scale of the deployment. The BOEM/FERC (2012) guidelines include hybrid projects that are defined as projects that include technologies that generate electricity from more than one form of renewable energy, one of which is a MHK

technology (e.g. wind- and wave-generation) under the same lease. Such projects require both a BOEM lease and a FERC licence.

Projects that straddle the boundary dividing state waters and OCS waters are also covered by the guidelines. In these situations, a developer is required to obtain a lease from BOEM for the OCS part of the project and a licence from FERC for both the OCS and state waters parts. In such cases, FERC prefers to administer the project as one complete project, which is feasible provided the developer consults with FERC, BOEM, the adjoining state authorities, and stakeholders at a sufficiently early stage of the project planning process. When a structure is to be deployed in navigable waters, an authorisation from the US Army Corps of Engineers is required under the Section 10 of the Rivers and Harbors Appropriations Act. If the laying of seabed cables and anchors requires dredging, a permit under the Clean Water Act (Section 404) may be necessary. Any devices that have the potential to obstruct navigation must be clearly marked by navigational aids, but these require a Private Aid to Navigation Permit administered by the US Coast Guard under Title 33 of the Code of Federal Regulations Part 66 (33 CFR Part 66).

With respect to environmental effects, the regulatory framework is also intricate. The National Environmental Policy Act (NEPA) provides a framework for identifying and assessing environmental effects. Under NEPA, the federal agency will first determine whether the project can be excluded from a comprehensive environmental review, termed a "categorical exclusion" (CX).[20] If this is not the case, then an EA will be prepared by the federal agency. The EA document will contain sufficient information to conclude whether an EIS is necessary. If no significant effects are identified during the EA, a Finding of No Significant Impact will be made by federal agency officials coupled with the appropriate supporting documentation. If significant environmental impacts are anticipated, an EIS will be produced with the assistance of other regulatory agencies and stakeholders. A range of additional regulatory authorities may be involved at this stage, each operating under its own governing legislation specific to a range of topics. Specifically, these cover impacts on endangered species and habitats (Endangered Species Act), marine mammals (Marine Mammal Protection Act), migratory birds (Migratory Bird Treaty Act), fisheries and fish habitats (Magnuson-Stevens Fishery Conservation Act), and historic resources (National Historic Preservation Act). The effects on air and water and state coastal zone management policies are also governed by separate legislative instruments.

Given the range of regulatory agencies and topics to be considered prior to project approval, the availability of data and information is a central consideration in MRE development. There are a host of state initiatives for data provision. At the federal level, marine data can be found in a dedicated Marine Cadastre,[21] developed

[20]Broadly equivalent to the "screening" stage in the EU.

[21]See http://marinecadastre.gov/, an integrated marine information system that provides data, tools, and technical support for ocean and Great Lakes planning. It was designed specifically to support renewable energy siting on the US Outer Continental Shelf but is also used for other ocean-related efforts.

in partnership between NOAA's Office for Coastal Management and BOEM. GIS-based tools are favoured and have been developed by federal and state agencies in an effort to provide tools that can handle complexity, uncertainty, and temporal data more effectively. The US Department of Energy, NOAA, and the BOEM funded a team comprising Parametrix, Oregon State University, Robust Decisions, and The Nature Conservancy to develop a tool using Bayesian logic, called a Bayesian Analysis of Spatial Siting (BASS). BASS can integrate disparate data in a manner such that the uncertainty of the data is known and the user can see the risks associated with making certain decisions. The BASS tool is building on a previous Oregon Wave Energy Trust effort involving many of the same partners to assess cumulative effects, potential impacts, and benefits of various MRE scenarios (Van Cleve and Geerlofs 2013). BOEM has also published a range of guidance documents on different types of environmental information including spatial data for site characterisation; avian survey information; geological, geophysical, and hazard information; fisheries survey information; benthic habitat information; and marine mammal and sea turtle information.[22]

A small number of open-water test centres are currently under development in US waters, including the Pacific Marine Energy Centre–South Energy Test Site (PMEC-SETS) and the Hawaii Wave Energy Test Site, operated by the US Navy. It is unlikely that these will be pre-consented because there does not appear to be any provision in US law to facilitate such a process. Commercial-scale projects are planned but not yet functioning. Decommissioning of MRE installations is not yet an issue; however, these aspects are governed by 30 CFR Part 285, which provides that all facilities, including pipelines, cables, and other structures and obstructions must be removed once they are no longer operational. Removal must occur no later than 2 years after the termination of the related lease (30 CFR 285.902). This could be problematic in the future for large projects because the 2-year time frame applies regardless of the size of the project (Kaiser and Snyder 2010). According to Section 6.2 of the BOEM/FERC guidelines (2012), developers are required to provide a decommissioning bond or other acceptable form of financial assurance as part of their BOEM lease and/or FERC licence. Under the terms of a commercial lease, a developer must submit a Construction and Operations Plan (COP) for OCS renewable energy activities under 30 CFR Part 585. The COP describes all of the facilities that are constructed and used for the project, including a conceptual decommissioning plan for each of the planned elements, including onshore and support facilities (US Department of the Interior 2016).

[22]See http://www.boem.gov/National-and-Regional-Guidelines-for-Renewable-Energy-Activities/.

Conclusions

Based on the descriptions of the countries' practices described in the previous sections, it is evident that approaches to MSP are at the very nascent stage of development and implementation. This makes a comprehensive analysis of its impact on the future planning and existing management of MRE projects difficult to state with any kind of certainty. From the information obtained from questionnaire respondents, and also from documentary sources, it appears that great hopes still persist about how MSP could improve planning and management of marine energy developments, and how it could enable more integrated and cohesive marine governance. Like the "developing" status of MSP, MRE can also be described as "developing" in the majority of nations included in this chapter. There are some obvious leaders in terms of commercial-scale development, but for a significant proportion of the countries considered, the presence of MRE devices in waters is almost exclusively limited to projects related to research, further testing, and refinement of technologies. In certain countries, there is little demand for marine space, so MRE development and implementation of MSP are low on the political agenda. The status of the MRE sector can mean that regulatory authorities are not yet overly concerned with the operation of their consenting system. In some jurisdictions, the need for a process for approving the deployment of an ocean energy device has yet to arise. Conversely, countries in which the MRE resource has been mapped and quantified are more likely to have sectoral policy objectives for this emerging sector, and the preparation of those policies often raises awareness of the need to streamline consenting processes or develop new systems.

Jurisdictional boundaries in sea spaces appear to be a key factor that is determining how consenting operates in practice: different zones are subject to different legal instruments and the substance of those instruments is often administered by different authorities responsible for different jurisdictional zones. In the USA, for example, authority for the regulation of ocean space is fragmented and spread across a number of state and federal agencies, divided both spatially and by sector. MRE developments incorporate a wide variety of regulated activities, and accordingly, it is somewhat inevitable that the consenting system governing such development is convoluted and ad hoc in many places. The number and types of different consents required make it difficult to streamline efforts under either one consent or one administrator. The number of regulatory authorities with a marine remit and the levels of interaction and communication between them is a key concern within the MRE developer community internationally. One possible impact of this is uncertainty for the developer and their investors, but at a societal level, it could have weighty implications for achievement of goals related to greater renewable energy production, more efficiency, and cost reduction (Dubbs et al. 2013). The UK, Norway, and parts of Canada have endeavoured to address the issues of multiple consents and authorities through the enactment of legislation that either reforms marine management completely or addresses ocean energy specifically. In some cases, this might be the most preferable option, but for the majority

of countries, it could be regarded as an extreme solution that would require considerable political commitment as well as human and financial resources.

Most land use decisions are devolved to local decision-makers, and certain actors question how a more centralised approach to MSP could affect the ability of local authorities and communities to influence how coastal and marine spaces are used. Despite MSP being advocated as a process that is participatory and stakeholder-driven, currently it is difficult to identify successful examples of MSP at a national scale, given the varying stages of MSP implementation. The reality of the land–sea divide presents a challenge not only to those trying to develop projects in a specific marine space, but also to those trying to better integrate and implement strategic marine governance and the processes it entails. Existing planning and management systems might apply to land only or extend to coastal plans that have a narrow geographical scope, maybe 1 mile from the shoreline. In countries that have no formalised approach to MSP, coastal and regional planning tools are cited as providing a sufficient basis for strategic planning. MSP is perceived to be a tool that can bring land and sea planning systems closer together, but this is very much dependent on how a country chooses to implement MSP. Existing examples tend to consist of a high-level national plan under which objectives pertaining to the important maritime sectors taking priority. In some instances, this has led to criticism of the marine plans developed—opponents say MSP is too focused on economic development and that it ignores environmental and social objectives, whilst advocates are delighted that their sector features in a strategic policy. Whilst the legal basis for harnessing MRE is well established, the procedures involved are multifaceted and often challenging. It is probable that this situation will change as the number of operational MRE projects increases, but in the short-term efforts should concentrate on delivering a process that is both effective and proportionate to the types of development that are presently being installed, namely small-scale, time-limited deployments.

Whilst MSP is intended to deliver sustainable development through the definition of economic, social, and environmental objectives, the material presented in this chapter would suggest that the extent to which this is reflected in existing systems varies by location. In countries such as Canada, Norway, and parts of the UK, MSP processes are founded on a strong environmental component with a concerted effort to plan future activities around the physical realities of their particular marine space. This helps to sustain an environmental focus in MSP as implementation progresses. In consenting processes applicable to MRE developments, the environment is considered formally through the EIA process and to a lesser extent in the SEA, the latter not always being applied to MRE plans and programmes as of yet. Where there are designated conservation sites, these can trigger additional assessment such as the Appropriate Assessment in the EU. The fact that environmental effects are considered only in an EIA may be problematic given the formulaic approach taken for conducting such assessments, which is becoming more apparent. There is little or no consistency in the methodologies applied to the study of specific parameters, which limits the ability to draw inferences, identify trends, and increase knowledge about environmental effects because

different methodologies may produce different results. Scientists need to be able to compare data and results across project sites to build knowledge, increase expertise, and thereby advance learning about these new technologies and the marine environment that can then be used in the development of MSP systems. For a new industrial sector like MRE, it is essential for regulators, developers, and the public more generally to understand the interactions of devices with the marine environment and vice versa. The level of understanding necessary cannot be delivered solely by EIAs and requires a more strategic approach to researching environmental effects as well as more robust monitoring programmes. In situations where consents have taken significant time to obtain, they delay can often be attributed to inadequate environmental information. Uncertainty surrounding actual effects is also a major issue and may be a result of a lack or poor level of knowledge about both the baseline conditions of the receiving environment and the impacts of technologies on each individual environmental receptor. In some instances, the key issue may be getting the scientific information to the decision- and policy-makers.

Not surprisingly, data to support MSP and site-level consenting are said to be frequently lacking in many of the countries examined herein. The scientific data needed to support planning of marine and coastal uses needs strengthening, and the data to support decisions on MRE projects appear to be limited to the availability of the physical resource. In parts of the UK, for example, insufficient data exist to enable an understanding of natural variability and interconnections coupled with changing pressures related to levels of human activities and climate change. Planning decisions, however, continue to be based on fixed lines on a map, and this cannot reflect physical, biological, and social realities. Cumulative impacts remain problematic with no agreed-upon methodology for how to address them using MSP or indeed decision-making systems. Lack of knowledge about interactions with the marine environment coupled with strongly sectoral-based management of marine activities has the potential to increase the likelihood of conflict between different sectors and within local communities. In all of the planning systems featured in this chapter, situations where conflicts have arisen have been dealt with on a case-by-case basis, with no prescribed process for such eventualities addressed in management frameworks. Acceptance of any form of development is neither automatic nor unconditional. Habitually, the involvement of the public in decision-making was almost totally limited to the consultation phase of the EIA process, which resulted in frustration amongst stakeholders in terms of both how they were involved in project planning and their ability to influence the outcome. The strong participatory feature of MSP seeks to limit the possibility of conflict by ensuring each sector is better understood by both other competing sectors and the public. It is also through efforts like this that opportunities for coexistence may be explored, but examples of these are exceptional currently. Zoning for specific marine uses is implemented in some countries, but does not appear to be a commonly used approach, particularly for MRE where dedicated zones are relatively rare. Restrictions to siting development do occur, particularly in areas of high conservation value and also in areas of military use.

At this juncture, arguably, MSP does not feature as prominently as expected in the planning and management of MRE. The implementation of MSP has been limited by technical, political, and resource aspects, which vary by country; yet its implementation could provide an opportunity to improve consenting of all forms of marine developments by increasing transparency and providing greater certainty for developers and their investors, regulators, and all stakeholders. The existing marine spatial plans and related coastal plans tend to focus on existing uses of marine spaces, giving with less consideration to new or innovative marine activities. There is an aspiration across all stakeholders for "good practice" examples of MSP and empirical evidence of how MSP has improved marine governance. In theory, MSP can balance precaution and risk to provide flexibility in decision-making but within a framework that is predicable, consistent, and transparent to those involved. The highly adaptive nature of MSP makes it an approach that is capable of responding to changing circumstances. As such, it should be ideal for the realities of the MRE sector where substantial development potential remains and a large amount of learning needs to occur. In conclusion, MSP offers a range of strengths and opportunities for MRE, but bringing MRE to fruition is entirely dependent on the approach taken to its implementation and enforcement in each country.

Acknowledgements The author would like to thank the international IEA-OES Annex IV Participant Country Representatives for taking the time to complete the questionnaire and garnering additional input from their colleagues. This material is based on work supported by Science Foundation Ireland (SFI) through MaREI, the SFI Centre for Marine and Renewable Energy (12/RC/2302). The support of the Sustainable Energy Authority of Ireland (SEAI) is also acknowledged.

References

BOEM/FERC (Bureau of Ocean Energy Management and Federal Energy Regulatory Commission). (2012). BOEM/FERC Guidelines on Regulation of Marine and Hydrokinetic Energy Projects on the OCS. Version 2, 19 July 2012. http://www.ferc.gov/industries//hydropower/gen-info/licensing/hydrokinetics/pdf/mms080309.pdf.

Commonwealth of Massachusetts. (2015). Massachusetts Ocean Management Plan. Volume 1: Management and Administration. http://www.mass.gov/eea/waste-mgnt-recycling/coasts-and-oceans/mass-ocean-plan/2015-final-ocean-plan.html.

Copping, A., Sather, N., Hanna, L., Whiting, J., Zydlewski, G., Staines, G., et al. (2016). Annex IV 2016 State of the Science Report: Environmental Effects of Marine Renewable Energy Development Around the World. http://tethys.pnnl.gov/publications/state-of-the-science-2016.

DAERA (Department of Agriculture, Environment and Rural Affairs). (2015). A Report by the Department of the Environment on the Marine Plan Process in Northern Ireland. https://www.daera-ni.gov.uk/sites/default/files/publications/doe/marine-report-plan-process-in-ni-oct-2015.pdf.

DAERA (Department of Agriculture, Environment and Rural Affairs). (2016). Northern Ireland Guidance on Marine Licensing Overview and Process, Under Part 4 of the Marine and Coastal Access Act 2009 (May 2016 version). https://www.daera-ni.gov.uk/sites/default/files/

publications/doe/marine-licensing-guidance-overview-and-process-under-part-4-marine-and-coastal-access-act-2009-may-2016.pdf.

DCENR (Department of Communications, Energy and Natural Resources). (2014). Offshore Renewable Energy Development Plan. Department of Communications, Energy & Natural Resources, Dublin. http://www.dcenr.gov.ie/NR/rdonlyres/836DD5D9-7152-4D76-9DA0-81090633F0E0/0/20140204DCENROffshoreRenewableEnergyDevelopmentPlan.pdf.

DEA (Department of Environmental Affairs). (2014). South Africa's National Coastal Management Programme. Cape Town, South Africa. https://www.environment.gov.za/sites/default/files/docs/nationalcoastal_managementprogramme.pdf.

DEA (Department of Environmental Affairs). (2016). Draft Marine Spatial Planning Framework. Government Gazette No. 40219, 19 August, 2016, 41 pages. https://www.greengazette.co.za/notices/draft-marine-spatial-planning-framework-published-for-public-comment_20160819-GGN-40219-00936.pdf.

Department of Conservation. (2011). New Zealand Coastal Policy Statement 2010: National Implementation Plan. Prepared by the NZCPS 2010 Implementation Steering Group. July 2011. http://www.doc.govt.nz/Documents/conservation/marine-and-coastal/coastal-management/nz-coastal-policy-final-implementation-plan.pdf.

Department of Conservation/NZCPS. (2010). Implementation Steering Group. 2011. New Zealand Coastal Policy Statement 2010-National Implementation Plan. http://www.doc.govt.nz/Documents/conservation/marine-and-coastal/coastal-management/nz-coastal-policy-final-implementation-plan.pdf.

DECC (Department of Energy and Climate Change). (2011). Decommissioning of offshore renewable energy installations under the Energy Act 2004: Guidance notes for industry. DECC, London, UK. https://www.gov.uk/government/uploads/system/uploads/attachment_data/file/80786/orei_guide.pdf.

DECLG (Department of Environment, Community and Local Government). (2013). Maritime Area and Foreshore (Amendment) Bill 2013. DECLG, Dublin, Ireland. http://www.environ.ie/planning/foreshore/general-scheme-maritime-area-and-foreshore-amendment-bill.

DEFRA (Department for Environment, Food and Rural Affairs). (2011). Guidance on Marine Licensing under Part 4 of the Marine and Coastal Access Act 2009. DEFRA, London, England. https://www.gov.uk/government/uploads/system/uploads/attachment_data/file/330849/Guidance_RFI_6666.pdf.

DEFRA (Department for Environment, Food and Rural Affairs). (2014). East Inshore and East Offshore Marine Plans. DEFRA, London, England. https://www.gov.uk/government/uploads/system/uploads/attachment_data/file/312496/east-plan.pdf.

DOENI (Department of the Environment Northern Ireland). (2013). Northern Ireland Marine Plan Statement of Public Participation. DOENI, Belfast, Northern Ireland. https://www.daera-ni.gov.uk/publications/marine-plan-statement-public-participation.

Dubbs, L., Keeler, A. G., & O'Meara, T. (2013). Permitting, risk and marine hydrokinetic energy development. *Electricity Journal, 26,* 64–74. doi:10.1016/j.tej.2013.11.002.

Enablers Task Force. (2015). Enablers Task Force on Marine Spatial Planning—Report to the Inter-Departmental Marine Coordination Group. http://www.ouroceanwealth.ie/publications.

Environmental Protection Authority/Te Mana Rauhī Taiao. (2013). What makes a proposal nationally significant? http://www.epa.govt.nz/Publications/EPA_Fact_Sheet_What_makes_a_proposal_nationally_significant.pdf. (Factsheet)

Fang, Q. H., Zhang, R., Zhang, L. P., & Hong, H. S. (2011). Marine functional zoning in China: Experience and prospects. *Coastal Management, 39*(6), 656–667.

Feng, R., Chen, X., Li, P., Zhou, L., & Yu, J. (2016). Development of China's marine functional zoning: A preliminary analysis. *Ocean and Coastal Management, 131,* 39–44. doi:10.1016/j.ocecoaman.2016.08.011.

Fisheries and Oceans Canada. (2002). Canada's Oceans Strategy Our Oceans, Our Future: Policy and Operational Framework for Integrated Management of Estuarine, Coastal and Marine Environments in Canada. Published by Fisheries and Oceans Canada, Oceans Directorate, Ottawa, Ontario, Canada. http://waves-vagues.dfo-mpo.gc.ca/Library/264678.pdf.

Fisheries and Oceans Canada. (2007). Eastern Scotian Shelf Integrated Ocean Management Plan. http://www.dfo-mpo.gc.ca/Library/333115.pdf.

Fisheries and Oceans Canada. (2013). Draft Pacific North Coast Integrated Management Area Plan. http://www.pncima.org/media/documents/pdf/draft-pncima-plan-may-27–2013.pdf.

Galparsoro, I., Liria, P., Legorburu, I., Bald, J., Chust, G., Ruiz-Minguela, P., et al. (2012). A Marine Spatial Planning approach to select suitable areas for installing wave energy converters on the Basque continental shelf (Bay of Biscay). *Coastal Management, 40,* 1–19.

Government Communications. (2015). South Africa Yearbook 2014/2015. Chapter 8: Energy, edited by E. Tibane and M. Honwane. pp. 135–152. http://www.gcis.gov.za/sites/www.gcis.gov.za/files/docs/resourcecentre/Energy2015.pdf.

Government of Ireland. (2012). Harnessing Our Ocean Wealth—An Integrated Marine Plan for Ireland Roadmap. http://www.ouroceanwealth.ie/about-plan.

Hauraki Gulf Forum. (2011). Spatial Planning for the Gulf: An international review of marine spatial planning initiatives and application to the Hauraki Gulf. http://www.aucklandcouncil.govt.nz/SiteCollectionDocuments/aboutcouncil/committees/haurakigulfforum/meetings/haurakigulfforumagitem15att20110411.pdf.

Headquarters for Ocean Policy. (2012). Policy on Initiatives to Promote the Use of Maritime Renewable Energy. http://www.kantei.go.jp/jp/singi/kaiyou/energy/torikumihousin.pdf. (in Japanese).

Headquarters for Ocean Policy. (2013). Basic Plan on Ocean Policy. http://www.kantei.go.jp/jp/singi/kaiyou/kihonkeikaku/130426kihonkeikaku_e.pdf (English translation).

HM Government (Her Majesty's Government). (2009). Our seas: a shared resource, high level marine objectives. https://www.gov.uk/government/uploads/system/uploads/attachment_data/file/182486/ourseas-2009update.pdf.

HM Government (Her Majesty's Government). (2011). UK Marine Policy Statement. HM Government, Northern Ireland Executive, Scottish Government, Welsh Assembly Government. https://www.gov.uk/government/publications/uk-marine-policy-statement.

Hildebrand, L. P., & Schröder-Hinrichs, J.-U. (2014). Maritime and marine: synonyms, solitudes or schizophrenia? *WMU Journal of Maritime Affairs, 13*(2), 173–176. doi:10.1007/s13437-014-0072-y.

IEA-OES. (2015). Ocean Energy Systems Annual Report 2015. https://report2015.ocean-energy-systems.org/.

Johnson, C. B. (2014). Advances in marine spatial planning: zoning earth's last frontier. *Journal of Environmental Law and Litigation*, *29*, 191.

Kaiser, M. J., Snyder, B. (2010). Offshore Wind Energy Installation and Decommissioning Cost Estimation in the U.S. Outer Continental Shelf. U.S. Dept. of the Interior, Bureau of Ocean Energy Management, Regulation and Enforcement, Herndon, VA. TA&R study 648. 340 pp. http://www.bsee.gov/uploadedfiles/bsee/research_and_training/technology_assessment_and_research/648aa.pdf.

Marine Protection Services and Governance/Republic of South Africa. (2014). Unlocking the Economic Potential of South Africa's Oceans—Operation Phakisa. Executive Summary. http://www.operationphakisa.gov.za/operations/oel/pmpg/pages/default.aspx?RootFolder=%2Foperations%2Foel%2Fpmpg%2FMarine%20Protection%20and%20Govenance%20Documents%2FMarine%20Protection%20and%20Govenance&FolderCTID=0x012000B556B9080C268C42BB547329B73E455D&View={4C717C55-EF8E-4D10-AD93-DBCE4099650F}.

McCuaig, J., Herbert, G. (Eds.). (2013). Review and Evaluation of the Eastern Scotian Shelf Integrated Management (ESSIM) Initiative. Can. Tech. Rep. Fish. Aquat. Sci. 3025: xii + 95p.

Meaden, G. J., Aguilar-Manjarrez, J., Corner, R., O'Hagan, A. M., & Cardia, F. (2016). *Marine spatial planning for the Gulf (RECOFI) area*. FAO, Rome, Italy: FAO Fisheries and Aquaculture Technical Paper.

Ministerio de Industria, Energía y Turismo. (2009). Estudio Estratégico Ambiental del Litoral Español para la Instalación de Parques Eólicos Marinos. Ministerio de Industria, Energía y Turismo, Madrid. http://www.aeeolica.org/uploads/documents/562-estudio-estrategico-ambiental-del-litoral-espanol-para-la-instalacion-de-parques-eolicos-marinos_mityc.pdf.

Ministry of Business, Innovation and Employment/New Zealand. (2015). Sustainable Seas *Ko ngā moana whakauka*: National Science Challenge. Sustainable Seas National Science Challenge presentation from the New Zealand Marine Sciences conference, 9 July 2015. http://www.niwa.co.nz/static/media/assets/Sustainable_Seas_NZMSS_July_2015.pdf.

Ministry of Economic Development. (2011). New Zealand Energy Efficiency and Conservation Strategy 2011–2016. New Zealand Government, Wellington, New Zealand. https://www.eeca.govt.nz/assets/Resources-EECA/nz-energy-strategy-2011.pdf.

National Ocean Council. (2013). National Ocean Policy Implementation Plan. https://www.whitehouse.gov/sites/default/files/national_ocean_policy_implementation_plan.pdf.

Natural Resources Canada. (2011). Charting the Course: Canada's Marine Renewable Energy Technology Roadmap. http://www.marinerenewables.ca/wp-content/uploads/2012/09/MRE_Roadmap_e.pdf.

New Zealand Department of Conservation. (2010). New Zealand Coastal Policy Statement 2010. Department of Conservation, Wellington, New Zealand. http://www.doc.govt.nz/Documents/conservation/marine-and-coastal/coastal-management/nz-coastal-policy-statement-2010.pdf.

New Zealand Department of Conservation. (2011). New Zealand Coastal Policy Statement 2010: National Implementation Plan. Prepared by the NZCPS 2010 Implementation Steering Group. July 2011. http://www.doc.govt.nz/Documents/conservation/marine-and-coastal/coastal-management/nz-coastal-policy-final-implementation-plan.pdf.

Norwegian Ministry of the Environment. (2009). Integrated Management of the Marine Environment of the Norwegian Sea. Report No.37 (2008–2009) to the Storting. https://www.regjeringen.no/en/dokumenter/report-no.-37-to-the-storting-2008-2009/id560159/. (English version).

Norwegian Ministry of the Environment. (2011). First update of the Integrated Management Plan for the Marine Environment of the Barents Sea – Lofoten Area. Meld. St. 10 (2010–2011) Report to the Storting (White Paper). [English version]. http://www.miljodirektoratet.no/Global/Havforum/Meld.%20St.10%20(2010-2011)%20Report%20to%20the%20Storting%20(white%20paper)%20First%20update%20of%20the%20Integrated%20Management%20Plan%20for%20the%20Marine%20Environment%20of%20the%20Barents%20Sea-Lofoten%20Area.pdf.

Norwegian Ministry of the Environment. (2013). Integrated Management of the Marine Environment of the North Sea and Skagerrak (Management Plan). Meld. St. 37 (2012–2013) Report to the Storting (White Paper). http://www.miljodirektoratet.no/Global/Havforum/Meld.%20St.37%20(2012-2013)%20Report%20to%20the%20Stortinng%20(white%20paper)%20Integrated%20Management%20of%20the%20Marine%20Environment%20of%20the%20North%20Sea%20and%20Skagerrak.pdf. (English version).

Nova Scotia Department of Energy and Marine Renewables. (2014). Statement of best practices for in-stream tidal energy development and operation: standards and practices for in-stream tidal energy. http://energy.novascotia.ca/sites/default/files/files/Statement%20of%20Best%20Practices%20Booklet.pdf.

Ocean Energy Forum. (2016). Ocean Energy Strategic Roadmap 2016, building ocean energy for Europe. https://webgate.ec.europa.eu/maritimeforum/en/frontpage/1036

OEER. (2008). Fundy Tidal Energy Strategic Environmental Assessment Final Report. Prepared by the OEER Association for the Nova Scotia Department of Energy. Submitted April, 2008. http://www.oera.ca/wp-content/uploads/2013/06/FINAL-SEA-REPORT.pdf.

O'Hagan, A. M., & Lewis, A. W. (2011). The existing law and policy framework for ocean energy development in Ireland. *Marine Policy, 35*(6), 772–783. doi:10.1016/j.marpol.2011.01.004.

O'Hagan, A. M. (2012). A review of international consenting regimes for marine renewables: are we moving towards better practice? In *4th International conference on ocean energy*, 17 October 2012, Dublin, Ireland.

O'Hagan, A. M. (2014). Consenting and environmental challenges for ocean energy. Presentation made to the European Commission's Ocean Energy Forum, Dublin, 11 June 2014.

O'Hagan, A. M. (2015). Chapter 18: Regulation of marine renewable energy. In R. Warner & S. Kaye (Eds.) *Routledge handbook of maritime regulation and enforcement*. Routledge, UK. ISBN 9780415704458.

Province of Nova Scotia. (2012). Nova Scotia Marine Renewable Energy Strategy. http://energy.novascotia.ca/sites/default/files/Nova-Scotia-Marine-Renewable-Energy-Strategy-May-2012.pdf.

RenewableUK. (2013). Cumulative Impact Assessment Guidelines: Guiding Principles for Cumulative Impacts Assessment in Offshore Wind Farms. http://www.renewableuk.com/en/publications/index.cfm/cumulative-impact-assessment-guidelines.

Simas, T., O'Hagan, A. M., O'Callaghan, J., Hamawi, S., Magagna, D., Bailey, I., et al. (2015). Review of consenting processes for ocean energy in selected European Union Member States. *International Journal of Marine Energy, 9,* 41–59. doi:10.1016/j.ijome.2014.12.001.

Sustainable Energy Authority of Ireland (SEAI). (2010). Strategic Environmental Assessment (SEA) of the Offshore Renewable Energy Development Plan (OREDP) in the Republic of Ireland. Environmental Report. Produced for SEAI by AECOM, Metoc and CMRC. http://www.seai.ie/Renewables/Ocean_Energy/Offshore_Renewable_SEA.

Swedish Agency for Marine and Water Management (SwAM). (2014). Marine spatial planning - Current status 2014 National planning in Sweden's territorial waters and Exclusive Economic Zone (EEZ). Version from March 2014 (now updated). https://www.havochvatten.se/download/18.44319c4a145d364b807436c/1448618458195/marine-spatial-planning-current-status-2014-english.pdf.

The Crown Estate. (2014). The Crown Estate Role in Offshore Renewable Energy Developments: Briefing (January 2014 version). http://www.thecrownestate.co.uk/media/5411/ei-the-crown-estate-role-in-offshore-renewable-energy.pdf.

The Scottish Government. (2012a). Offshore Wind Energy in Scottish Waters - Draft Regional Locational Guidance. Parts 1–11. August 2012. The Scottish Government, Edinburgh, Scotland. http://www.scotland.gov.uk/Topics/marine/marineenergy/Planning/windrlg.

The Scottish Government. (2012b). Offshore Wave Energy in Scottish Waters—Draft Regional Locational Guidance. Parts 1–6. August 2012. The Scottish Government, Edinburgh, Scotland. http://www.scotland.gov.uk/Topics/marine/marineenergy/Planning/waverlg.

The Scottish Government. (2012c). Offshore Tidal Energy in Scottish Waters - Draft Regional Locational Guidance. Parts 1–7. August 2012. The Scottish Government, Edinburgh, Scotland. http://www.scotland.gov.uk/Topics/marine/marineenergy/Planning/tidalrlg.

The Scottish Government. (2012d). Development of Offshore Renewable Energy in Scotland's Seas - Research Implementation Strategy. http://www.gov.scot/Topics/marine/marineenergy/ris.

The Scottish Government. (2012e). Marine Scotland Licensing and Consents Manual, covering Marine Renewables and Offshore Wind Energy Development. http://www.gov.scot/Resource/0040/00405806.pdf.

The Scottish Government. (2015a). Scotland's National Marine Plan (NMP)—A Single Framework for Managing Our Seas. The Scottish Government, Edinburgh, Scotland.

The Scottish Government. (2015b). Scotland's National Marine Plan—A Single Framework for Managing Our Seas. A Summary of Objectives and Policies. The Scottish Government, Edinburgh, Scotland.

The Scottish Government. (2016a). Marine Scotland: Crown Estate—Consultation on Proposals for Establishing the Interim Body to Manage the Crown Estate Assets in Scotland Post-Devolution. http://www.gov.scot/Resource/0050/00502476.pdf.

The Scottish Government. (2016b). Survey, Deploy and Monitoring Licensing Policy Guidance (Version 2, 4 April 2016). http://www.gov.scot/Topics/marine/Licensing/marine/Applications/SDM.

Tyldesley, D. (2004). coastal and marine spatial planning framework for the Irish Sea Pilot Project. Report to the Joint Nature Conservation Committee. UK: DEFRA http://jncc.defra.gov.uk/pdf/Tyldesley%20Marine%20spatial%20planning.pdf.

UNESCO: Ehler, C., & Douvere, F. (2009). Marine Spatial Planning: a step-by-step approach toward ecosystem-based management. Intergovernmental Oceanographic Commission and Man and the Biosphere Programme. IOC Manual and Guides No. 53, ICAM Dossier No. 6. UNESCO, Paris, France.

United States Department of the Interior. (2016). Guidelines for Information Requirements for a Renewable Energy Construction and Operations Plan (COP). Office of Renewable Energy Programs, Bureau of Ocean Energy Management. Version 3.0, April 7, 2016. http://www.boem.gov/COP-Guidelines/.

Van Cleve, F. B., & Geerlofs, S. H. (2013). Engagement in Coastal and Marine Spatial Planning Activities in Support of Offshore Wind and Marine and Hydrokinetic Energy Deployment. Final Report. Prepared for the U.S. Department of Energy under Contract DE–AC05–76RL01830, Pacific Northwest National Laboratory, Richland, Washington, U.S.A.

Welsh Assembly Government. (2011). Consultation Document Sustainable Development for Welsh Seas: Our Approach to Marine Planning in Wales. http://gov.wales/docs/desh/consultation/110216marineconsultationen.pdf.

Welsh Government. (2015). Marine Planning section on Welsh Government website: http://gov.wales/topics/environmentcountryside/marineandfisheries/marine-planning/?lang=en. Last updated on 25 April 2015, Accessed 19 June 15.

Xu, W., Li, F., & Xia, D. (2014). Review of China policy of OED sea use management. *Ocean and Coastal Management, 88,* 38–42. doi:10.1016/j.ocecoaman.2013.11.011.

Zhang, H. S. (2003). *Summary of the national marine functional zoning scheme*. Beijing, China: Ocean Press.

Index

Z. Yang and A. Copping (eds.), *Marine Renewable Energy*,
DOI 10.1007/978-3-319-53536-4